NASA Reference Publication 1060

Subsonic Aircraft: Evolution and the Matching of Size to Performance

Laurence K. Loftin, Jr.

CASE FILE COPY

AUGUST 1980

NASA

NASA Reference Publication 1060

Subsonic Aircraft: Evolution and the Matching of Size to Performance

Laurence K. Loftin, Jr.
Langley Research Center
Hampton, Virginia

National Aeronautics
and Space Administration

**Scientific and Technical
Information Branch**

1980

CONTENTS

	Page
I - INTRODUCTION	1
II - DEVELOPMENT AND DESIGN FEATURES OF JET TRANSPORT AIRCRAFT	7
III - SIZING OF JET-POWERED CRUISING AIRCRAFT	99
IV - APPLICATION OF SIZING METHOD FOR JET-POWERED CRUISING AIRCRAFT . .	175
V - DEVELOPMENT AND DESIGN FEATURES OF PROPELLER-DRIVEN AIRCRAFT . . .	227
VI - SIZING OF PROPELLER-DRIVEN AIRCRAFT	315
VII - APPLICATION OF SIZING METHOD FOR PROPELLER-DRIVEN AIRCRAFT	389
APPENDIX A - ESTIMATION OF OVERALL PROPULSION-SYSTEM EFFICIENCY	435
APPENDIX B - ESTIMATED AERODYNAMIC PARAMETERS	438

I - INTRODUCTION

Methods for estimating the size, weight, and power of aircraft intended to meet specified performance requirements and for studying the effects of changes in requirements and configuration variables on these characteristics are of great importance in the aircraft design process. The major aircraft manufacturers utilize elaborate computer programs for such aircraft sizing studies. These programs, which require the use of complex high-speed computing equipment, yield results of great accuracy and are an important factor in insuring the development of highly refined and useful aircraft. These methods, although extremely important and useful, do require availability of the necessary and very costly computing equipment. Furthermore, the physical interrelationships between the various design parameters, and the influence of these parameters on aircraft characteristics, may sometimes tend to be obscured in the complex and automatic computing process.

A number of years ago, the author undertook a study with the objective being to define quick, simple, physically interpretable methods for roughly estimating the physical characteristics required of an aircraft in meeting desired performance goals without the need for complex, expensive computing equipment. Such methods were intended to provide a means for rapid sizing studies and evaluations which could be readily undertaken at home, on a desk at the office, or even while traveling. The methods which evolved from these studies make extensive use of correlations of the characteristics of existing aircraft in terms of well-known aircraft design parameters. The methods are simple and require only the use of a pocket computer for rapid application to specific sizing problems. The physical relationships between the various design parameters and their influence on aircraft characteristics are also easily understood. The procedures and methods are only approximate but will yield results of acceptable accuracy for many purposes.

The rapid sizing methods just discussed have served as the basis of a course in aircraft design which has been taught by the author for several years at the Joint Institute for the Advancement of Flight Sciences.[1] On the basis of the favorable reaction of these classes and at the urging of a number of staff members of the Langley Research Center, the present publication presenting the methods and procedures developed, as well as example applications, has been prepared in the belief that students and small design groups may find them both useful and interesting. The methods presented may be of particular interest to those seeking a fundamental understanding of the airplane sizing process, since the effects of changes in individual performance and configuration parameters on the size, weight, and power of the aircraft are readily apparent.

---

[1]Cosponsored by the George Washington University and the Langley Research Center of the National Aeronautics and Space Administration located at Hampton, Virginia.

The material describing and illustrating the methods for sizing aircraft to meet specified performance objectives is presented in chapters 3 and 4 for jet-powered cruising aircraft and in chapters 6 and 7 for propeller-driven aircraft. The basic sizing procedures are developed in chapters 3 and 6. Application of the methods is illustrated by means of sizing studies of a series of aircraft with varying design constraints in chapters 4 and 7. The chapters on jet and propeller-driven aircraft are, in most respects, independent of each other. Accordingly, chapters 6 and 7 on propeller-driven aircraft can be read with only an occasional reference to derivations given in the earlier chapters on jet aircraft.

In addition to the chapters on aircraft sizing, some aspects of the technical development history of jet-powered cruising aircraft and propeller-driven aircraft are briefly discussed in chapters 2 and 5, respectively. The material in these two chapters has been found useful in providing students and other interested persons an insight into the technical developments which have influenced aircraft design over the years and some of the advantages and disadvantages of different design concepts. These chapters can be read independently; however, the overall picture of aircraft development can perhaps be seen in better perspective by first reading chapter 5 on propeller-driven aircraft.

A few comments regarding the method of presentation in the subsequent chapters are warranted. For each chapter, a detailed table of contents appears at the beginning, and the reference and symbol lists appear at the end. In all numbered items, such as figures, equations, tables, and references, the first number preceding the period is the chapter number. Thus, reference 5.20 indicates reference 20 in chapter 5. Because some form of Standard Atmosphere is needed in making aircraft sizing and performance studies, a simple one-page tabulation, taken from reference 1.1, was used for all calculations contained herein and, for convenience, is reproduced as table 1.I.

Finally, U.S. Customary Units are used throughout this publication since most of the data on the older aircraft are presented in this form in the reference documents. In chapters 2, 3, and 4 distances and velocities are given in nautical miles and knots; in chapters 5, 6, and 7 these quantities are expressed in statute miles and statute miles per hour. This difference exists because the preponderance of the reference data on jet aircraft use the nautical mile and most of the data for propeller-driven aircraft, particularly the older aircraft, are expressed in terms of the statute mile. For convenience, factors for rapid conversion of the various aircraft design and performance quantities from U.S. Customary Units to SI Units, based on reference 1.2, are contained in table 1.II.

The author wishes to express his appreciation for the assistance provided by many people at the NASA Langley Research Center in the preparation of this publication. In particular, the helpful comments and suggestions of John E. Duberg, Mark R. Nichols, and Thomas A. Toll, all of whom reviewed the entire manuscript, are gratefully acknowledged. Others who reviewed individual chapters and offered useful comments are William J. Alford, Jr., John P. Campbell, Donald L. Loving, Robert O. Schade, and John P. Reeder. The author would also like to thank Dr. Jan Roskam, University of Kansas, for his help and encouragement. W. E. Farrar of Lockheed, H. B. Favre of McDonnell Douglas, L. T. Goodmanson of Boeing, H. O. Nay of Cessna, R. R. Tumlinson of Beech, and

P. C. Boisseau of the Langley Research Center were most helpful in providing the photographs used in chapters 2 and 5. Finally, thanks are gratefully extended to Frances M. Arnn who typed several drafts of the text.

REFERENCES

1.1 The Staff of Ames 1- by 3-Foot Supersonic Wind-Tunnel Section: Notes and Tables for Use in the Analysis of Supersonic Flow. NACA TN 1428, 1947.

1.2 Anon.: Standard for Metric Practice. E 380-76, American Soc. Testing & Mater., 1976.

TABLE 1.I.- PROPERTIES OF THE STANDARD ATMOSPHERE

[From reference 1.1, p. 73]

h, ft	t, °F	t, °C	a/a_{SL}	a, ft/sec	a, mph	p/p_{SL}	p, lb/ft^2	p, mb	$\sigma = \rho/\rho_{SL}$	ρ, slugs/ft^3	$\sigma^{1/2}$	$\mu \times 10^7$, slugs/ft-sec	$\nu \times 10^4$, ft^3/sec	q/M^2, lb/ft^2
0	59.00	15.00	1.0000	1117	761.6	1.0000	2116.2	1013.2	1.0000	0.002378	1.0000	3.719	1.564	1481.3
1,000	57.44	13.02	.9966	1113	759.0	.9644	2040.9	977.1	.9711	.002310	.9854	3.699	1.602	1428.6
2,000	51.87	11.04	.9931	1109	756.3	.9298	1967.7	942.1	.9428	.002242	.9710	3.679	1.641	1377.4
3,000	48.31	9.06	.9896	1105	753.7	.8963	1896.7	908.1	.9152	.002177	.9566	3.659	1.681	1327.7
4,000	44.74	7.08	.9862	1102	751.0	.8637	1827.7	875.1	.8881	.002112	.9424	3.639	1.723	1279.4
5,000	41.18	5.10	.9827	1098	748.4	.8321	1760.8	843.0	.8617	.002049	.9283	3.618	1.766	1232.6
6,000	37.62	3.12	.9792	1094	745.7	.8014	1696.0	812.0	.8359	.001988	.9143	3.598	1.810	1187.2
7,000	34.05	1.14	.9756	1090	743.0	.7717	1633.0	781.8	.8107	.001928	.9004	3.577	1.855	1143.1
8,000	30.49	-.84	.9721	1086	740.4	.7428	1571.9	752.6	.7860	.001869	.8866	3.557	1.903	1100.3
9,000	26.92	-2.82	.9686	1082	737.7	.7148	1512.8	724.3	.7620	.001812	.8729	3.536	1.951	1059.0
10,000	23.36	-4.80	.9650	1078	734.9	.6877	1455.4	696.8	.7395	.001756	.8594	3.515	2.002	1018.8
11,000	19.80	-6.78	.9614	1074	732.2	.6614	1399.8	670.2	.7156	.001702	.8459	3.495	2.054	979.9
12,000	16.23	-8.76	.9579	1070	729.5	.6360	1345.9	644.4	.6932	.001649	.8326	3.474	2.107	942.1
13,000	12.67	-10.74	.9543	1066	726.8	.6113	1293.7	619.4	.6714	.001597	.8194	3.453	2.163	905.6
14,000	9.10	-12.72	.9507	1062	724.0	.5875	1243.2	595.2	.6500	.001546	.8063	3.432	2.220	870.2
15,000	5.54	-14.70	.9470	1058	721.2	.5644	1194.3	571.8	.6292	.001497	.7933	3.411	2.280	836.0
16,000	1.98	-16.68	.9434	1054	718.5	.5420	1147.0	549.1	.6090	.001448	.7804	3.390	2.341	802.9
17,000	-1.59	-18.66	.9397	1050	715.7	.5203	1101.1	527.2	.5892	.001401	.7676	3.369	2.404	770.8
18,000	-5.15	-20.64	.9361	1046	712.9	.4994	1056.9	506.0	.5699	.001355	.7549	3.347	2.470	739.8
19,000	-8.72	-22.62	.9324	1041	710.1	.4792	1014.0	485.5	.5511	.001311	.7424	3.326	2.538	709.8
20,000	-12.28	-24.60	.9287	1037	707.3	.4596	972.6	465.6	.5328	.001267	.7299	3.305	2.608	680.8
21,000	-15.84	-26.58	.9250	1033	704.5	.4406	932.5	446.4	.5150	.001225	.7176	3.283	2.681	652.8
22,000	-19.41	-28.56	.9213	1029	701.6	.4223	893.8	427.9	.4976	.001183	.7054	3.262	2.757	625.7
23,000	-22.97	-30.54	.9175	1025	698.8	.4047	856.4	410.0	.4807	.001143	.6933	3.240	2.834	599.5
24,000	-26.54	-32.52	.9138	1021	695.9	.3876	820.3	392.7	.4642	.001104	.6813	3.218	2.915	574.2
25,000	-30.10	-34.50	.9100	1017	693.1	.3711	785.3	376.0	.4481	.001066	.6694	3.196	2.999	549.7
26,000	-33.66	-36.48	.9062	1012	690.2	.3552	751.7	359.9	.4325	.001029	.6576	3.174	3.087	526.2
27,000	-37.23	-38.46	.9024	1008	687.3	.3399	719.2	344.3	.4173	.000993	.6460	3.153	3.177	503.4
28,000	-40.79	-40.44	.8986	1004	684.4	.3251	687.9	329.3	.4025	.000957	.6345	3.130	3.270	481.5
29,000	-44.36	-42.42	.8948	999	681.5	.3108	657.6	314.9	.3882	.000923	.6230	3.108	3.367	460.3
30,000	-47.92	-44.40	.8909	995	678.5	.2970	628.5	300.9	.3741	.000890	.6116	3.086	3.469	440.0
31,000	-51.48	-46.38	.8871	991	675.6	.2837	600.4	287.5	.3606	.000858	.6005	3.064	3.573	420.3
32,000	-55.05	-48.36	.8832	987	672.6	.2709	573.3	274.5	.3473	.000826	.5894	3.041	3.682	401.3
33,000	-58.61	-50.34	.8793	982	669.7	.2586	547.3	262.0	.3345	.000796	.5784	3.019	3.795	383.1
34,000	-62.18	-52.32	.8754	978	666.7	.2467	522.2	250.0	.3220	.000766	.5675	2.997	3.913	365.5
35,000	-65.74	-54.30	.8714	973	663.7	.2353	498.0	238.4	.3099	.000737	.5567	2.974	4.036	348.6
35,332	-67.6	-55.33	.8693	971	662.1	.2314	489.8	234.5	.3058	.000727	.5530	2.961	4.073	342.9
36,000	-67.6	-56.28	.8693	971	662.1	.2244	474.8	227.3	.2981	.000709	.5460	2.951	4.176	332.4
37,000	-67.6	-55.33	.8693	971	662.1	.2138	452.5	216.7	.2845	.0006766	.5334	2.961	4.376	316.8
38,000	-67.6	-55.33	.8693	971	662.1	.2038	431.2	206.5	.2711	.0006448	.5207	2.961	4.592	301.8
39,000	-67.6	-55.33	.8693	971	662.1	.1942	411.0	196.8	.2584	.0006145	.5083	2.961	4.819	287.7
40,000	-67.6	-55.33	.8693	971	662.1	.1851	391.8	187.6	.2463	.0005857	.4963	2.961	5.055	274.3
41,000	-67.6	-55.33	.8693	971	662.1	.1764	373.4	178.8	.2347	.0005582	.4845	2.961	5.305	261.4
42,000	-67.6	-55.33	.8693	971	662.1	.1681	355.8	170.4	.2237	.0005320	.4730	2.961	5.566	249.1
43,000	-67.6	-55.33	.8693	971	662.1	.1603	339.1	162.4	.2132	.0005071	.4617	2.961	5.839	237.4
44,000	-67.6	-55.33	.8693	971	662.1	.1527	323.2	154.8	.2032	.0004833	.4508	2.961	6.127	226.2
45,000	-67.6	-55.33	.8693	971	662.1	.1456	308.0	147.5	.1936	.0004605	.4400	2.961	6.430	215.6
46,000	-67.6	-55.33	.8693	971	662.1	.1387	293.6	140.6	.1846	.0004390	.4296	2.961	6.745	205.5
47,000	-67.6	-55.33	.8693	971	662.1	.1322	279.8	134.0	.1759	.0004184	.4194	2.961	7.077	195.9
48,000	-67.6	-55.33	.8693	971	662.1	.1260	266.6	127.7	.1676	.0003987	.4094	2.961	7.427	186.6
49,000	-67.6	-55.33	.8693	971	662.1	.1201	254.1	121.7	.1598	.0003800	.3997	2.961	7.792	177.9
50,000	-67.6	-55.33	.8693	971	662.1	.1145	242.2	116.0	.1523	.0003622	.3902	2.961	8.175	169.5
60,000	-67.6	-55.33	.8693	971	662.1	.0713	150.9	72.2	.0942	.0002240	.3069	2.961	13.219	105.6

List of symbols:

- h height
- t temperature
- a velocity of sound
- p pressure
- ρ density
- σ density relative to sea level
- μ coefficient of viscosity
- ν coefficient of kinematic viscosity
- M Mach number

The subscript SL refers to sea level (h = 0)

TABLE 1.II.- CONVERSION OF U.S. CUSTOMARY UNITS TO SI UNITS

Basic quantity	U.S. Customary Unit	Conversion factor[a]	SI Unit
Acceleration	ft/sec^2	0.3048	m/s^2
	g units	9.80665	m/s^2
Area	ft^2	0.09290304	m^2
Density	slugs/ft^3	515.3788	kg/m^3
Force	lb	4.448222	N
Length	ft	0.3048	m
	miles (statute)	1609.344	m
	miles (nautical)	1852	m
Mass	slugs	14.5939	kg
Power	hp	745.6999	W
Pressure	lb/in^2	6894.757	Pa
	lb/ft^2	47.88026	Pa
Velocity	ft/sec	0.3048	m/s
	ft/min	0.00508	m/s
	miles/hr (statute)	0.44704	m/s
	knots	0.5144444	m/s
Viscosity	slugs/ft-sec	47.88026	Pa-s
Weight	lb	4.448222	N

Derived quantity	U.S. Customary Unit	Conversion factor[a]	SI Unit
Power index	$(hp/ft^2)^{1/3}$	20.02217	$(W/m^2)^{1/3}$
Climb parameter	hp/lb	167.64	W/N
Specific fuel consumption	lb/lb/hr (thrust)	0.000277777	N/N/s
	lb/hp/hr (horsepower)	0.000001657	N/W/s
Thrust loading	lb/lb	1	N/N
Power loading	lb/hp	0.005965163	N/W
Wing loading	lb/ft^2	47.88026	Pa

[a]Multiply the value in U.S. Customary Units by the conversion factor to obtain equivalent value in SI Units.

II - DEVELOPMENT AND DESIGN FEATURES OF JET TRANSPORT AIRCRAFT

CONTENTS

		Page
2.0	Introduction	8
2.1	Technology of the Jet Transport	9
2.1.1	Turbojet and Turbofan Propulsion Systems	9
2.1.1.1	Comparative Propulsion-System Efficiency	11
2.1.1.2	Thrust Reverser	16
2.1.1.3	Engine Noise	18
2.1.1.4	Historical Note	22
2.1.2	The Swept Wing	24
2.1.2.1	High-Speed Characteristics	24
2.1.2.2	Low-Speed Characteristics	27
2.1.3	High-Lift Devices	32
2.2	Evolution of the Jet Transport	34
2.2.1	Pioneer Transports	38
2.2.2	First-Generation Transports	42
2.2.2.1	Boeing 707	46
2.2.2.2	McDonnell Douglas DC-8 and Other Four-Engine Transports	50
2.2.2.3	Sud-Aviation Caravelle	52
2.2.3	Second-Generation Transports	55
2.2.3.1	Boeing 727	56
2.2.3.2	McDonnell Douglas DC-9	58
2.2.3.3	Boeing 737	59
2.2.3.4	British Aircraft Corporation VC-10	60
2.2.4	Wide-Body Transports	62
2.2.4.1	Boeing 747	65
2.2.4.2	Lockheed L-1011 and McDonnell Douglas DC-10	68
2.2.5	Dedicated Cargo Transports	70
2.2.6	Business Jets	76
2.2.6.1	Configuration Features	76
2.2.6.2	Representative Aircraft Types	78
2.3	Concluding Remarks	86
SYMBOLS		87
REFERENCES		89
TABLES		92

2.0 Introduction

The development of the propeller-driven aircraft from a curiosity to a highly useful machine is described in chapter 5. By the end of the first 50 years of powered flight, this type of aircraft equipped with a reciprocating engine had about reached the end of what must be ranked as one of the most spectacular engineering achievements in history. Although some further technical refinement was possible, the technology of that class of aircraft was on a plateau with little prospect of major improvement in the future. A revolutionary type of new propulsion system, the jet engine, was introduced in somewhat primitive form in the closing months of World War II. The subsequent development of this entirely new type of propulsion system resulted in advancements in aircraft design that have been almost as spectacular as those which occurred in the first 50 years of powered flight.

The initial applications of jet propulsion were to military aircraft of various types. The first jet-powered transport entered commercial operations in 1952. This event heralded the beginning of a revolution in domestic and international air transportation which has accompanied the development and refinement of the jet-powered transport.

The modern jet transport with its high speed, safety, and economical appeal has altered peoples' concepts of the relative accessibility of various places in the United States and throughout the world. Methods of communication have accordingly changed, as have methods of conducting business operations. Whereas air travel was once regarded as the province of the adventurer and the affluent, all classes of people are now traveling by air both for business reasons and for pleasure. Americans are traveling today by air in unprecedented numbers, on schedules undreamed of 20 or 30 years ago, and are seeing and experiencing cultures in other parts of the country and the world to an extent which would have been incomprehensible to past generations.

Some indication of the size and scope of past, present, and projected future airline transport activity is given by the data presented in table 2.I. The total number of revenue passenger miles flown by scheduled United States carriers is seen to have increased from 8.8 billion in 1949 to 188.5 billion in 1976. The corresponding number in 1986 is forecast to be 346.5 billion. Thus, the number of revenue passenger miles has increased by a factor of more than 20 in the 27-year time period which extends from 1949 to 1976. The introduction of the jet transport marked the beginning of the end of the ocean-going ship as a serious means of overseas travel. The statistics in table 2.I show that overseas travel by air comprised 7.1 billion revenue passenger miles in 1959, 41.5 billion in 1976, and is projected to increase to 79.0 billion by 1986. By way of comparison, in 1939 steamships of all nations are estimated to have operated about 3 billion revenue passenger miles between the United States and other countries of the world. Thus, the airplane has not only surplanted the steamship but has, in fact, generated a new and greatly enlarged market for overseas travel. Air travel today is accepted as a major component of the common-carrier transportation system, and the modern jet transport is largely responsible for the revolution which has made air travel for the masses what it is today.

The technology, development, and design features of the jet transport are briefly described in this chapter. The discussion is divided into the following parts:

2.1 Technology of the Jet Transport
- 2.1.1 Turbojet and Turbofan Propulsion Systems
- 2.1.2 The Swept Wing
- 2.1.3 High-Lift Devices

2.2 Evolution of the Jet Transport
- 2.2.1 Pioneer Transports
- 2.2.2 First-Generation Transports
- 2.2.3 Second-Generation Transports
- 2.2.4 Wide-Body Transports
- 2.2.5 Dedicated Cargo Transports
- 2.2.6 Business Jets

Various issues of Jane's All the World's Aircraft, from which most of the aircraft physical and performance characteristics were obtained, are presented as references 2.1 to 2.6. References 2.7 to 2.42, listed alphabetically are either specifically cited in the text or are offered for additional reading on the subject of jet-transport development.

2.1 Technology of the Jet Transport

The highly developed technology of the propeller-driven aircraft powered with reciprocating engines formed the foundation upon which the development of the jet transport began. The modern jet airliner, however, incorporates many improvements and refinements in such areas as structures, materials, aerodynamics, methods of construction, and onboard systems. A description of these various improvements and innovations is beyond the scope of the present discussion. Two technical innovations which emerged from World War II, however, were to have an enormous influence on future aircraft development and served as cornerstones in the technology of the jet transport. These innovations were the turbine engine and the swept wing.

Because of the importance of these two innovations in the development of the jet transport, they are briefly discussed in the following paragraphs. The powerful high-lift devices developed during and following World War II have also played a very important role in modern transport aircraft because of the necessity for the use of extremely high-wing loadings (see section 3.5.3 of chapter 3); accordingly, a brief description of these devices is given in section 2.1.3. High-lift devices developed before and during World War II are briefly discussed in section 5.4.1.1 of chapter 5.

2.1.1 Turbojet and Turbofan Propulsion Systems

The speed at which a propeller-driven aircraft may fly efficiently is fundamentally limited by the loss in propeller efficiency which occurs as the tip speed of the propeller approaches a Mach number of 1.0. One of the principal

advantages of the turbojet and turbofan types of propulsion system is that they overcome this fundamental limitation of the engine-driven propeller. The air-intake systems for turbojet and turbofan engines are designed in such a way as to limit the velocity of the air at the first stage of compressor blading so that severe adverse Mach number effects are not encountered.

Another advantage found in jet-propulsion systems is the small weight per unit of power and the large amount of power which can be packaged in a single unit. The large amount of air which can be handled by a jet propulsion system and the associated relatively simple rotating parts are responsible for these attributes. An interesting illustration of the power and weight features of jet propulsion can be obtained from a comparison of some of the characteristics of the modern Boeing 747 and the Lockheed 1049G Super Constellation. The Super Constellation is typical of the final generation of high-performance piston-engine transports and is described in section 5.5.1 of chapter 5. Table 2.II compares the total power, the power per engine, and the ratio of power to dry engine weight of the two aircraft. The power in this case is defined as the total amount of power usefully employed in propelling the aircraft at the assumed conditions of weight, speed, and lift-drag ratio L/D given in the table. This power may be thought of as the total number of Btu's supplied to the engine per unit time multiplied by the product of the propulsive efficiency and the cycle efficiency. The power can be quickly calculated with the use of the following simple equation:

$$P = \frac{WV}{(L/D)\,550}$$

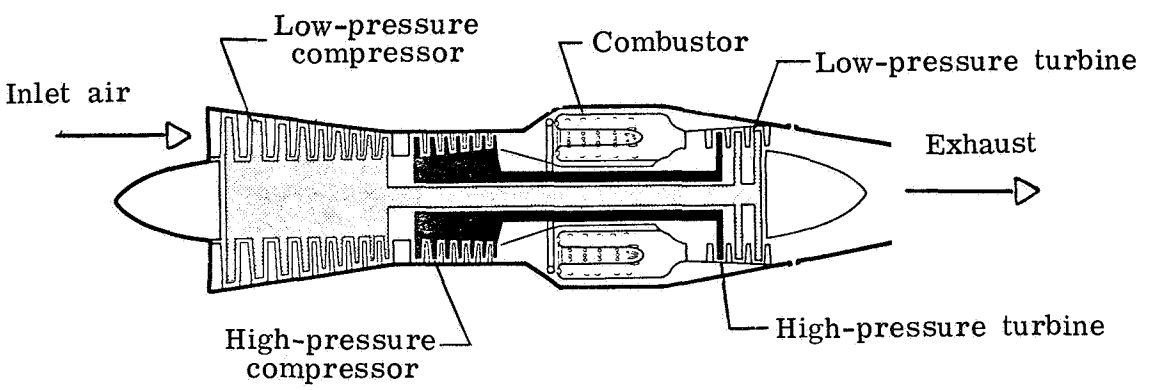
where P is in horsepower and V is in feet per second. The values of W, V, and L/D employed in the equation are given in table 2.II and are only estimates which may not be entirely consistent; they are, however, thought to be sufficiently accurate for the present purpose.

The Boeing 747 cruising at 461 knots at a weight of 700 000 lb is seen to require 59 934 hp; the corresponding values for the Super Constellation are 287 knots, 112 000 lb, and 6585 hp. The power per engine for the two aircraft is seen to be 14 984 hp and 1646 hp for the 747 and Super Constellation, respectively. The Wright 3350 turbocompound engines which powered the Lockheed aircraft are among the most powerful reciprocating engines ever developed for aircraft use. These engines developed a maximum of 3250 hp at take-off; the value given in the table is for a normal cruise power setting. The enormous amount of power generated by the Pratt & Whitney turbofan engines of the 747 as compared to the reciprocating engines which propelled the Super Constellation is obvious. The values of power-to-weight ratio given in table 2.II for the two types of propulsion systems are also of great interest. The weights used in this ratio are the dry, uninstalled engine weights as given in reference 2.41. The turbine engines in the Boeing aircraft develop nearly four times as much power for each pound of engine weight as do the reciprocating engines which power the Lockheed aircraft.

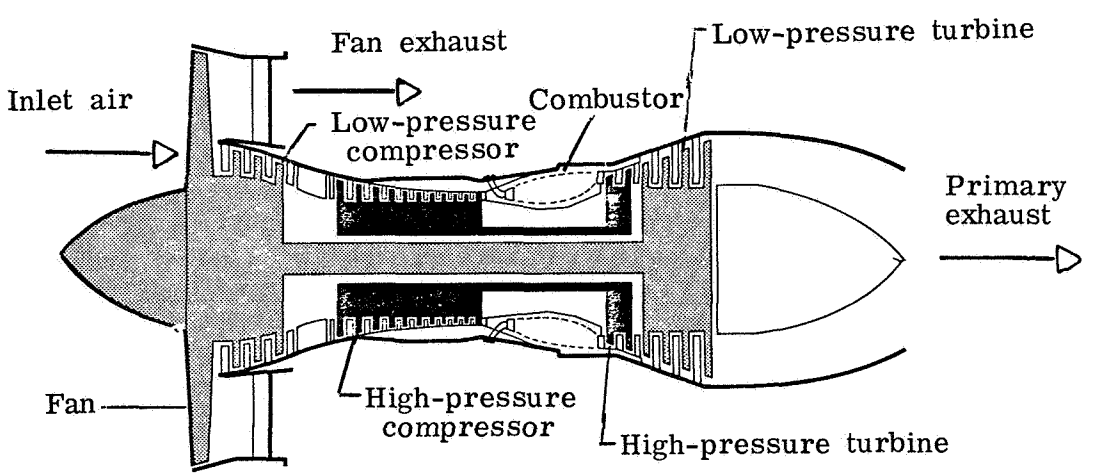
The jet propulsion system avoids the compressibility problem which limits the speed at which the propeller may be efficiently employed, is light in weight for a given amount of power as compared to a reciprocating engine, and can be successfully produced in single units capable of generating very large amounts of power. Jet propulsion systems also require much less maintenance than do reciprocating engines and may be operated for many thousands of hours without major overhaul. Engine failures are also relatively rare with jet propulsion systems. A comparison of the efficiency of various types of propulsion systems is considered in the next paragraph.

2.1.1.1 Comparative Propulsion-System Efficiency

The turbojet and turbofan are the two types of jet propulsion systems which have been employed in subsonic jet transport aircraft. Schematic drawings of these two types of propulsion systems, taken from reference 2.8, are given in figure 2.1. The turbojet shown at the top of the figure consists of high- and



(a) Turbojet.



(b) High bypass ratio turbofan.

Figure 2.1.- Two types of jet propulsion system.

low-pressure compressors, combustors, and high- and low-pressure turbines. In the turbojet, all of the inlet air passes through each element of the engine. The compressors raise the pressure of the inlet air; the pressure ratio varies for different engines but may approach 30 to 1. The high-pressure air enters the combustor where fuel is injected. The fuel-air mixture is ignited and the resulting hot gases pass through the turbines which, in turn, drive the compressors. The exhaust from the turbines provides the thrust that propels the aircraft.

The turbojet shown in figure 2.1(a) is called a twin spool engine. The low-pressure compressor is driven by the low-pressure turbine, and the high-pressure compressor is driven by the high-pressure turbine. These two units rotate at different speeds in order to maintain high efficiency in all stages of compression. The engine shown in figure 2.1(a) has nine stages and seven stages in the low-pressure and high-pressure compressors, respectively, and the low-pressure and high-pressure turbines contain two stages and one stage.

A schematic drawing of a turbofan engine is shown in figure 2.1(b). The turbofan engine contains all of the elements of the turbojet, shown in figure 2.1(a), but in addition, some of the energy in the hot jet exhaust is extracted by a turbine which drives a fan. A portion of the inlet air which enters the fan is bypassed around the engine; the fan then, is somewhat like a propeller being driven by the turbomachinery. Unlike the propeller, however, a single fan stage may contain from 20 to 50 blades, is surrounded by a shroud, and is more like a single stage compressor than a propeller. For example, the pressure ratio across the fan is usually in the range of 1.4 to 2.0; whereas the pressure ratio across the propeller discs of the Lockheed Super Constellation in cruising flight is somewhat less than 1.02.

The bypass ratio of a turbofan engine is defined as the ratio of the mass of air which passes through the fan, but not the gas generator, to that which does pass through the gas generator. Bypass ratios between 1 and 2 are typical of the first turbofan engines which were introduced in the early 1960's. The more modern turbofan engines have bypass ratios which usually fall between 4 and 6, and the engine employed on the Lockheed C-5A has a bypass ratio of 8. The larger the bypass ratio, the greater will be the amount of energy extracted from the hot exhaust of the gas generator; as much as 75 percent of the total thrust of a turbofan engine may be attributed to the fan.

The single-stage front fan shown on the engine in figure 2.1(b) is integral with the low-pressure compressor, and a four-stage turbine drives both the fan and the compressor. Some turbofan engines are of the three spool type. The hot gas generator employs two spools, like the turbojet shown in figure 2.1(a), and a third spool which is independent of the other two contains the fan and its own turbines. Fans of more than one stage have also been used, as have aft mounted fans. The aft-fan design is one in which the fan blades form an extension of an independently mounted turbine situated in the hot exhaust of the gas generator.

The advantages of the turbofan are that, for a given energy addition per unit time (fuel flow rate), the turbofan will produce more thrust and have a higher propulsive efficiency than will a turbojet with a gas generator of the same level of technical sophistication as the turbofan. These advantages can

be explained by the following highly simplified analysis of an idealized turbofan engine. Assume the air which enters the inlet of the engine to have a free-stream velocity of V_i and a uniform exhaust velocity from the fan and gas generator of V_e. The mass flow entering the inlet per unit time is $\dot{m}$. The thrust produced by the engine can then be expressed by the following simple relationship if the static pressure in the exhaust is assumed to have the free-stream static value where the exhaust velocity is measured and the momentum of the fuel itself is neglected:

$$T = \dot{m}(V_e - V_i) = \dot{m}\,\Delta V \tag{2.1}$$

where T is the thrust.

The amount of energy added to the flow by the fuel may be expressed as the difference between the kinetic energy per unit time entering and exhausting from the engine and is given as follows:

$$\dot{E} = \frac{\dot{m}}{2}\left[(V_i + \Delta V)^2 - V_i^2\right] = \dot{m}\,\Delta V V_i\left(1 + \frac{1}{2}\frac{\Delta V}{V_i}\right) \tag{2.2}$$

or with the use of equation (2.1)

$$\dot{E} = TV_i\left(1 + \frac{1}{2}\frac{\Delta V}{V_i}\right) \tag{2.3}$$

The propulsive efficiency is defined as that fraction of the kinetic energy added to the mass flow $\dot{m}$ which is usefully employed in propelling the aircraft. The propulsive efficiency η_p can be expressed in the following form:

$$\eta_p = \frac{TV_i}{\dot{E}} \tag{2.4}$$

Substitution of equations (2.1) and (2.3) for the thrust and kinetic energy gives

$$\eta_p = \frac{2}{2 + \dfrac{\Delta V}{V_i}} \tag{2.5}$$

Equation (2.3) clearly shows that for a given thrust level, the required rate of energy input is reduced as the value of $\Delta V/V_i$ is decreased. For a given thrust level, equation (2.1) shows that as the value of ΔV is decreased the mass-flow rate $\dot{m}$ must increase correspondingly. The most thrust is therefore obtained for a given energy input rate from the addition of a small velocity increment to a large mass-flow rate, and the propulsive efficiency, given by equation (2.5), is increased as the value of ΔV is reduced. The turbofan engine therefore provides higher efficiency and more thrust than a turbojet engine with the same rate of energy input and having the same component (compressor, burner, and turbine) efficiencies. The maximum bypass ratio which can be employed effectively with a given gas generator is dictated by the fan and drive turbine efficiencies and mechanical losses in the transmission system.

The selection of the optimum bypass ratio for a particular aircraft involves trade studies of many factors such as the details of the performance requirements of the aircraft, the efficiencies of the various components of the engine, and the weight and size of the fan and its installation. A detailed analysis of these various factors is beyond the scope of the present discussion. Equations (2.3) and (2.5) do indicate, however, that the desired bypass ratio probably increases as the design cruising speed decreases and, also, as the degree of importance attached to the take-off and climb characteristics is increased. Another important factor in the selection of the bypass ratio, not mentioned so far, is the noise characteristics of the engine. Engine noise is briefly discussed in section 2.1.1.3.

The overall efficiency is shown in figure 2.2 for several types of propulsion systems. The overall efficiency is defined as the product of the propulsive efficiency and the cycle efficiency. The cycle efficiency η_c is the ratio of the time rate of kinetic energy addition in the gas generator to the heating value of the fuel consumed by the engine per unit time; the propulsive efficiency η_p is given by equation (2.5) which has just been discussed. Thus, the overall efficiency is the ratio of the power usefully expended in propelling the aircraft to the heating value of the fuel consumed per unit time. The method of calculating the curves in figure 2.2 is described in appendix A.

The curves in figure 2.2 show the overall propulsion-system efficiency as a function of Mach number for a turbojet and two turbofan engines. The turbojet engine and the turbofan engine of bypass ratio 1.4 have the same gas generator. Both engines show a large increase in efficiency as the Mach number increases. For example, the efficiency of the turbofan with a bypass ratio of 1.4 increases from 8 percent to 27.5 percent as the Mach number is increased from 0.2 to 0.9. The 13-percent improvement in efficiency of the fan engine as compared to the pure jet (at a Mach number of 0.8) results entirely from the addition of the fan. The large increase in efficiency which accompanies an increase in the bypass ratio from 1.4 to 6.0, however, is only partly attributable to the increase in bypass ratio. The overall compressor compression ratio of the engine with bypass ratio of 6.0 is about 25, whereas the corresponding ratio for the other fan engine is about 14. Part of the increase in efficiency shown by the engine of higher bypass ratio is accordingly due to an increase in cycle efficiency.

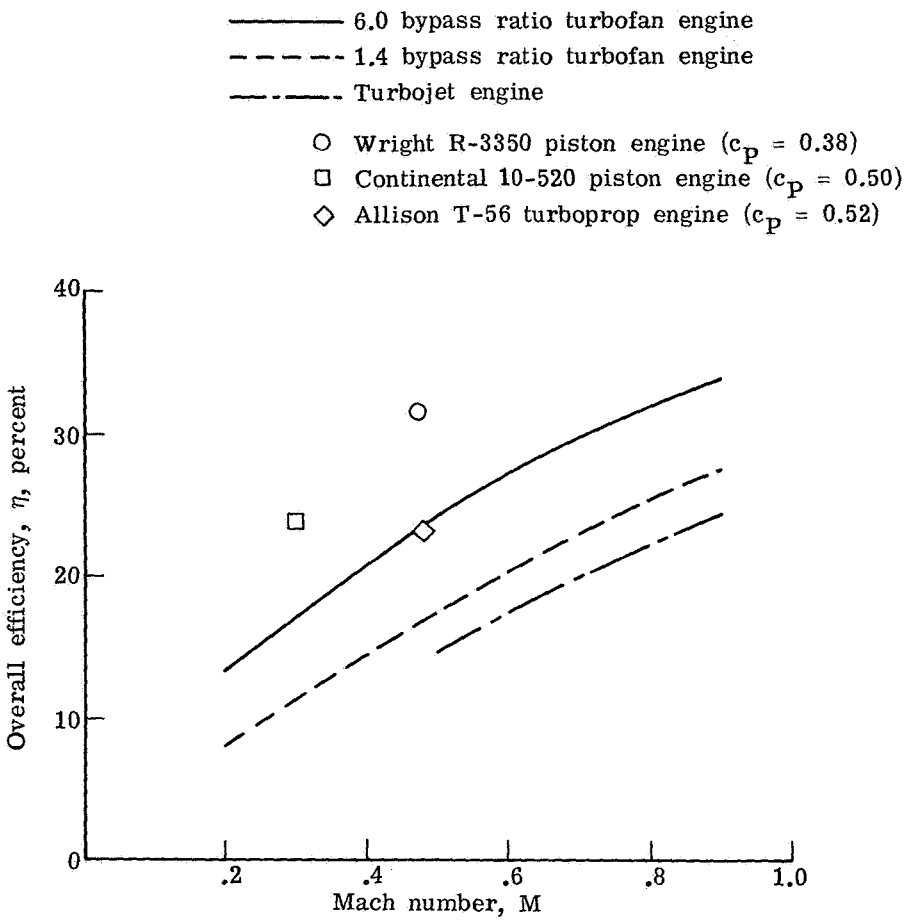


Figure 2.2.- Overall efficiency ($\eta = \eta_c\eta_p$) of several types of aircraft propulsion systems.

Also shown in figure 2.2 are points for two reciprocating engines and a turboprop engine. The Wright R-3350 turbocompound engine employed on the Lockheed Super Constellation was probably the most efficient reciprocating engine ever designed for aircraft use. The overall efficiency of this engine is shown plotted at the cruising speed of the Constellation. Comparison of the point with the curve for the high bypass ratio turbofan engine indicates that the efficiency of the fan engine is as high as that of the Wright engine at a Mach number twice that at which the Constellation cruised. Thus, the overall propulsion efficiency of the 747 flying at its normal cruising speed is about the same as that of the Constellation at its normal cruising speed. The overall efficiency of the engine with a bypass ratio of 1.4, however, is about 20 percent lower than that of the reciprocating engine even at the normal cruise Mach number of the fan engine of about 0.8. The value of the overall efficiency of the 747 is about 32 percent at a Mach number of 0.8. The trends in figure 2.2 clearly show that, with respect to overall propulsion efficiency, the bypass ratio should increase as the cruising speed decreases, and at some speed the propeller or low solidarity fan becomes the most efficient type of propulsion system.

The point indicated by a square symbol in figure 2.2 is for a modern six cylinder, horizontally opposed, reciprocating engine of the type employed in present-day general-aviation aircraft. The value of the efficiency of this engine at a Mach number of 0.3 is about 24 percent as compared to about 17 percent for the turbofan at this same Mach number. The point indicated by a diamond symbol in figure 2.2 is for a contemporary turboprop engine which is employed in a widely used cargo aircraft. The efficiency of this propulsion system is about the same as that of the turbofan at a Mach number of 0.49. The turboprop engine for which the point is shown in figure 2.2 is an old engine which has a compressor compression ratio of only about 10. An engine of more advanced design would be expected to have a higher value of overall propulsion efficiency. The values of the specific fuel consumption c_p for the reciprocating and turboprop engines were obtained from reference 2.41.

The preceding paragraphs have indicated that the turbofan engine, as compared to the reciprocating engine driving a propeller, offers the following advantages:

(1) The turbofan avoids the loss in efficiency, due to compressibility effects which limit the speed at which a propeller-driven aircraft may efficiently cruise.

(2) The weight of the turbofan engine per unit power is significantly less than that of the reciprocating engine.

(3) The turbofan engine is capable of developing a very large amount of power in a single unit without prohibitive mechanical complication.

(4) The overall efficiency of the turbofan propulsion system is about the same as that of the most efficient reciprocating engines ever designed for aircraft use. The turbofan engine attains this efficiency at a higher speed than that which is appropriate for reciprocating engines.

(5) The turbofan engine is more reliable than the reciprocating engine and can be operated many thousands of hours without major maintenance work.

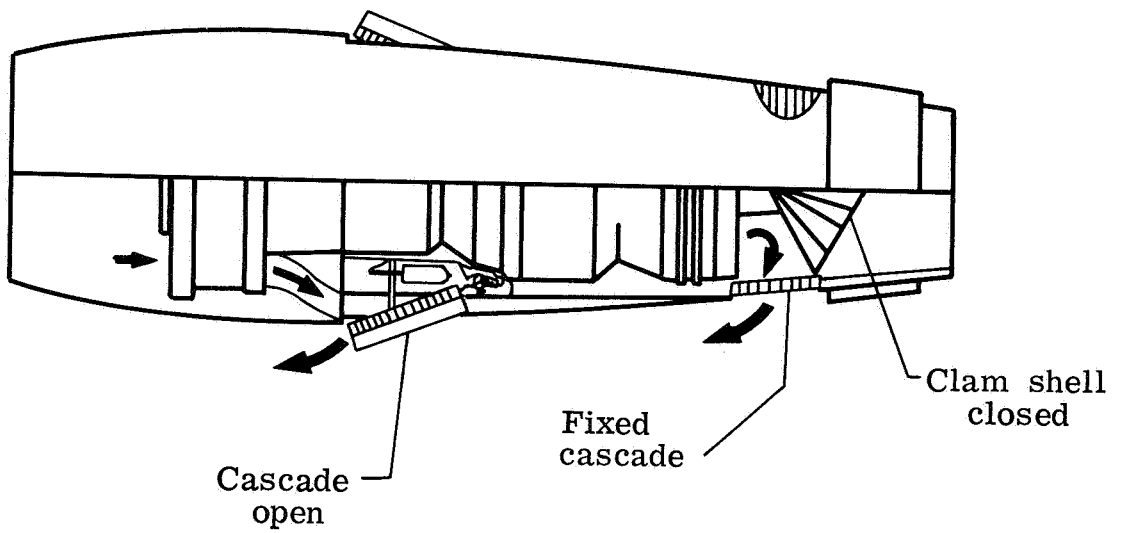
These five basic reasons explain why the turbojet and turbofan propulsion systems have caused a revolution in aircraft design, and in our concepts of the way in which aircraft may be effectively used. The thrust reverser forms an important part of jet propulsion systems as applied to transport aircraft. A brief description of a typical thrust reverser is given in the next section.

2.1.1.2 Thrust Reverser

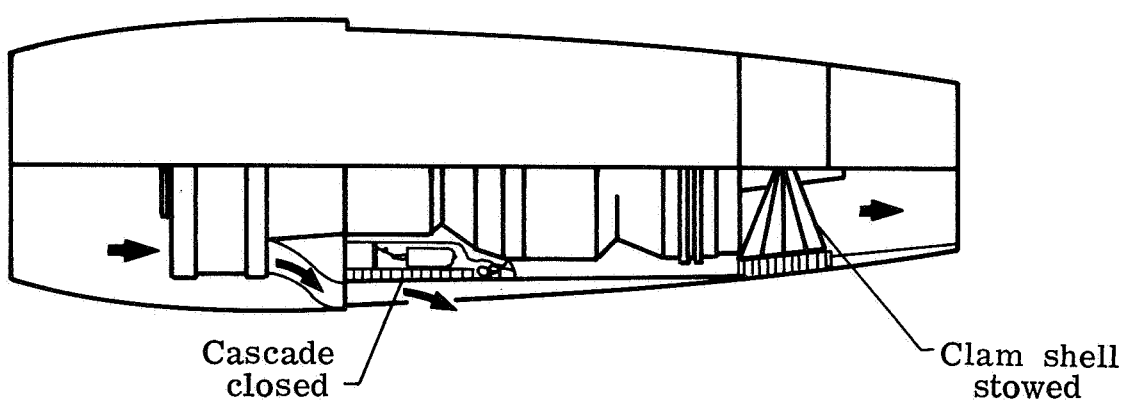
The amount of force required to stop an aircraft in a given distance after touchdown increases with the gross weight of the aircraft and the square of the landing speed. The size of modern transport aircraft and the speed at which they land make the use of wheel brakes alone unsatisfactory for routine operations. Most propeller-driven transports produced since World War II employed reversible pitch propellers to assist in stopping the aircraft on the landing roll-out.

The advent of the turbojet and turbofan types of propulsion system required the development of new concepts for augmenting the stopping power provided by the brakes. Some military aircraft deploy one or more parachutes after touchdown. The aerodyanmic drag of the parachutes provides the additional required stopping force. The parachutes must be detached from the aircraft and repacked following each landing. The use of parachutes as a decelerator is not an attractive alternative for aircraft in commercial transport operations.

The engines of turbojet and turbofan powered transport aircraft are equipped with some form of diverter which, when activated, reverses the thrust and thus provides a stopping force. A schematic drawing of a possible thrust reverser for a high-bypass-ratio turbofan engine is shown in figure 2.3



(a) Reverse thrust configuration.



(b) Forward thrust configuration.

Figure 2.3.- Thrust reverser for turbofan engine.

(ref. 2.8). Both the fan exhaust and the hot exhaust from the gas generator are reversed in the design shown in figure 2.3. The elements of the reverser are cascades and clam shells. A cascade is an array of closely spaced, highly cambered airfoils and is used for changing the direction of airflow; it may also be thought of like the blades of a compressor of constant chord laid out parallel to each other rather than radially about a single axis. The clam shell closes the exhaust nozzle and diverts the gas flow outward and forward.

The engine is shown in the reverse and forward thrust configurations in figures 2.3(a) and 2.3(b), respectively. The fan exhaust is reversed by opening the forward cascade so that the impinging exhaust is turned by the blades in the cascade into the forward direction. In the reverse configuration, the exhaust from the hot gas generator strikes the closed clam shell doors and is diverted forward and outward through circumferential openings in the engine nacelle. Fixed cascades are installed in these openings and aid in turning the exhaust gas forward. In the forward thrust configuration, the stowed clam shell closes the cascade and thus prevents leakage of exhaust gases. The front cascade in the forward thrust configuration is closed on the inside so that the fan exhaust cannot pass through it.

Most thrust reversers employ either or both cascades and clam shells in various configurations depending upon the design of the engine, the bypass ratio, and the type of nacelle in which the engine is mounted. In order to prevent ingestion of hot gases or debris into the engine inlet, the thrust reversers are usually not operated below some minimum speed. This minimum speed depends on the design of the aircraft and engine and their integration; 60 knots is a typical value of the minimum speed for operation of the thrust reverser. Although the primary use of the thrust reverser is to shorten the landing distance, reverse thrust is also employed in flight on some aircraft. In this application, reverse thrust is used when a very rapid, steep descent is required to follow a desired flight profile.

2.1.1.3 Engine Noise

The preceding paragraphs have outlined the many advantages of jet propulsion systems. Noise is a major problem encountered with these types of propulsion systems applied to commercial transport aircraft. The high noise levels of the propulsion system must be considered in relation to the design of the cabin of the aircraft and to the environment external to the aircraft in the vicinity of the airport. The use of light, effective soundproofing material in the cabin has resulted in interior noise levels which are acceptably low without excessive weight penalty.

The primary impact of the high noise levels associated with jet propulsion systems has been felt by people living in communities surrounding the airports from which jet-powered transport aircraft operate. Not only were the early jet transports noisier than contemporary aircraft powered with reciprocating engines, but the increased airline traffic which resulted from the widespread adoption of the jet transport resulted in an increased frequency of aircraft operations at most major airports.

The noise problem became so severe and the associated pressure on the U.S. Congress so great that part 36 of the Federal Air Regulations was formulated and became law on December 1, 1969. These regulations specify certain noise levels which must not be exceeded by new aircraft certified after the date at which the law became effective. The regulation further states that all aircraft operated in the United States must comply with the regulations after January 1, 1985.

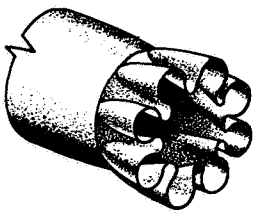
The present certification process for transport aircraft therefore involves experimental measurements of aircraft noise under controlled conditions. The noise level is measured at specified positions under the approach and climb paths of the aircraft and a specified position to the side of the runway. The allowable noise levels vary to some extent with the gross weight of the aircraft and thus reflect what is technically possible and realistic. Lower allowable noise levels will no doubt be specified at some future time to reflect advancements in the state of the art.

Aircraft noise reduction has been the subject of intensive research and development for the past two decades. The aircraft and engine manufacturing companies, as well as various government research and regulatory organizations, have been involved in this work. As a result, much has been learned about methods of noise reduction, and considerable literature exists on the subject.

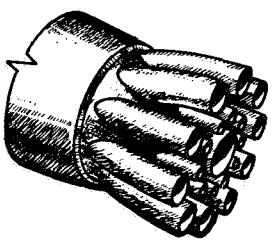
Four lines of approach have been followed in the various studies aimed toward reducing aircraft noise. First, much work has been directed toward obtaining an understanding of the basic noise generation and propagation process. Second, new concepts in engine design have been developed to reduce the amount of noise generated at the source. Third, methods for suppressing and absorbing a portion of the noise emanating from the engine have been found. Fourth, aircraft operational techniques have been devised for minimizing noise impact on communities surrounding the airport.

The early jet transports were powered with turbojet-type engines. The hot, high velocity exhaust is the primary source of noise in this type of propulsion system. The amount of energy in the exhaust which is transformed into noise varies as approximately the eighth power of the exhaust velocity, and the noise-frequency spectrum is related to the circumference of the exhaust jet. The relative amount of noise energy in the lower frequencies increases as the circumference of the jet increases. Many of the early noise suppressors employed on turbojet propulsion systems were based on the concept of effectively breaking the large exhaust jet into a number of small jets so that the relative amount of noise at the lower frequencies is reduced. The amount of attenuation which accompanies transmission of the noise through the atmosphere increases as the noise frequency increases. Thus, by breaking up a large jet into a number of small jets, the amount of energy transmitted as noise over a given distance is reduced. The noise suppressors shown in figures 2.4(a) and 2.4(b) are based on the principle just described.

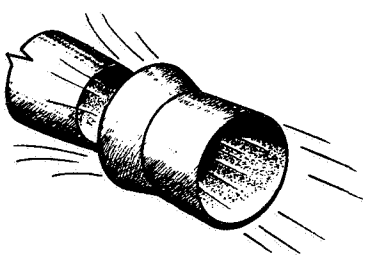
Another type of noise suppressor proposed for the early turbojet powered transports is shown in figure 2.4(c). The ejector-type suppressor entrains free-stream air which is then mixed with the high-velocity exhaust. The



(a) Corrugated-perimeter-type noise suppressor.



(b) Multiple-tube-type noise suppressor.



(c) Ejector-type noise suppressor.

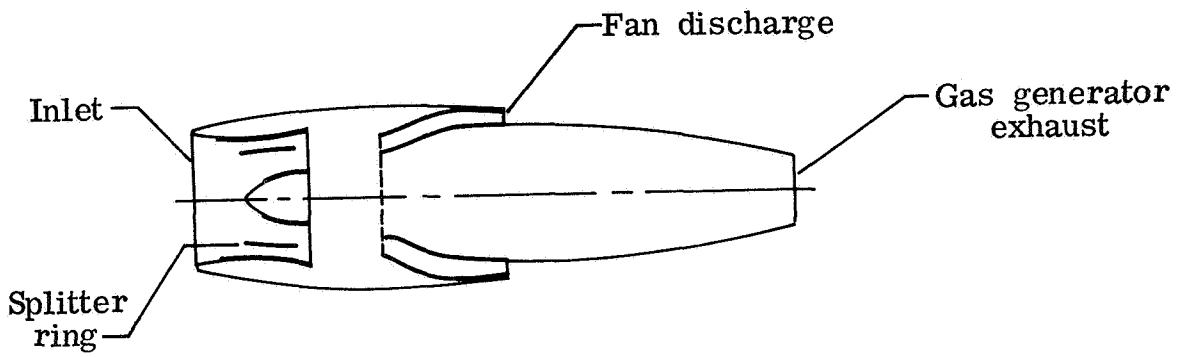
Figure 2.4.- Three types of jet noise suppressor.

velocity of the resulting mixed exhaust is therefore lower than that of the free exhaust of the engine alone, and the noise is accordingly reduced at the source.

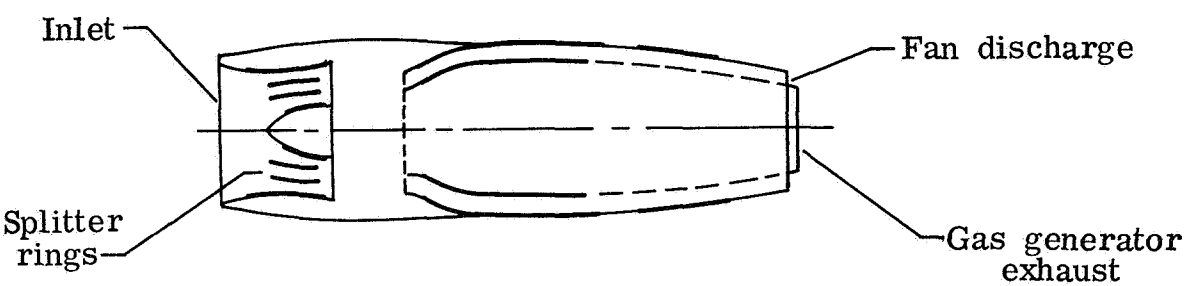
A great deal of information has been accumulated on the manner in which the various components of the engine should be designed so as to reduce the noise generated by the engine. The turbofan engine and the beneficial effects of increasing the bypass ratio on the propulsive efficiency have been discussed in section 2.1.1.1. The advent of the turbofan type of propulsion system had an important effect on the nature of the aircraft noise problem. The extraction of energy from the gas generator for the purpose of driving a fan in a high bypass ratio engine would be expected to reduce the noise of the fan engine, as compared to a turbojet for the same thrust level. The fan itself, however,

was found to constitute a new and highly disturbing source of noise. Studies of the relatively low bypass ratio, first-generation fan engines showed that the noise which was propagated from the inlet and from the fan discharge ducts was greater than that associated with the high-velocity exhaust from the gas generator.

The noise associated with the fan can be greatly reduced by proper detail design of the fan and by the use of acoustic treatment in certain key areas of the inlet and fan discharge ducts. Acoustic treatment consists in the application of sound absorbing material to the interior passages of the nacelle, as shown in figures 2.5(a) and 2.5(b) for short and long fan duct installations.



(a) Short fan duct.



(b) Long fan duct.

Figure 2.5.- Examples of acoustic treatment to short and long fan duct nacelles. (Heavy lines indicate acoustic treatment.)

An experimental application of acoustic treatment to the nacelle of a first generation, low bypass ratio turbofan engine is shown in the photograph given in figure 2.6. The drawings shown in figure 2.5 were taken from reference 2.29 which contains a comprehensive summary of basic information dealing with acoustic treatment for noise suppression. Most modern high bypass ratio engines employ some form of acoustic treatment. The splitter rings shown in figure 2.5 have not been used in any production installations for a number of practical operational reasons, such as possible difficulties in de-icing and the possibil-

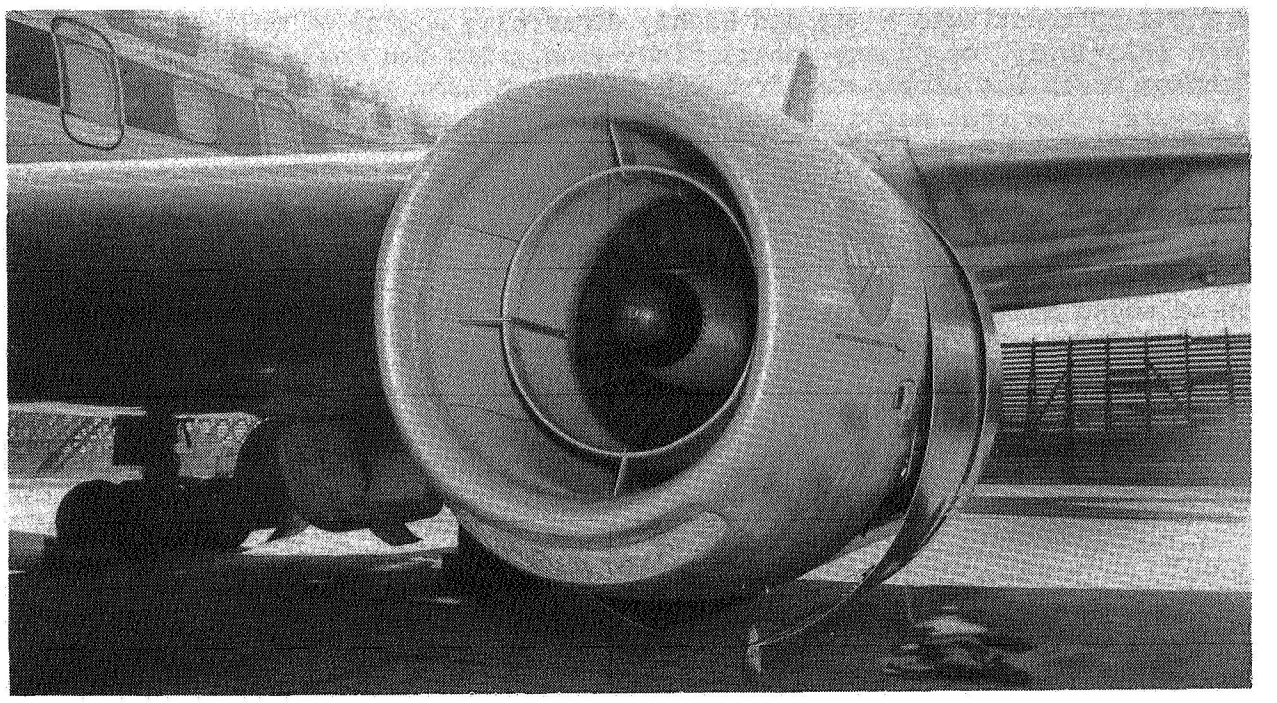


Figure 2.6.- NASA experimental treated nacelle mounted on McDonnell Douglas DC-8 airplane.

ity of the rings being broken by foreign object ingestion with subsequent damage to the rotating parts of the engine.

The development of operational techniques for noise abatement will not be dealt with here other than to indicate that these techniques usually involve (1) selected routing into and out of the airport in order to avoid flight over certain heavily populated areas and (2) the use of power reductions and reduced climb angles on certain segments of the climb following take-off.

2.1.1.4 Historical Note

Before closing this brief discussion of turbojet and turbofan engines, a few comments regarding the origins of these unique types of propulsion systems would seem to be appropriate.

The basic principles of jet propulsion have been known for a long time, and a patent for a sort of jet propulsion system for aircraft was issued in 1917. A young engineer named Sanford Moss ran a small gas-turbine engine in 1907 while an employee of the General Electric Company. The engine had an overall efficiency of only about 5 percent, however, and attracted little interest. Moss later achieved fame for his development of the turbosupercharger.

Air Commodore Sir Frank Whittle (Ret.) is often regarded as the father of modern aircraft jet propulsion systems. As a young officer in Britain's Royal

Air Force, he became interested in advanced forms of aircraft propulsion. He found the 1917 patent on jet propulsion and coupled some of the ideas it contained with gas-turbine principles. He tried without success to obtain official support for research and development of his ideas. He persisted on his own initiative, however, and received his first patent on jet propulsion in January 1930. With private financial support, he began construction of his first engine in 1935. This engine, which had a single-stage centrifugal compressor and a single-stage turbine, was successfully bench tested in April 1937; it was only a laboratory test rig and was never intended for application to a test aircraft.

Although the basic thermodynamic principles of jet propulsion and gas turbines had been known for many years, the application of these principles to the design of a successful aircraft engine presented many difficulties. An aircraft engine must be strong, durable, and above all, light. The major problems in the development of the jet engine were in finding the high-strength, lightweight alloys which could withstand the high temperatures to be expected inside the engine and in developing the proper methods of designing and integrating the various components of the engine. Whittle's successful bench test must be considered a major engineering achievement.

The firm of Power Jets Ltd., with which Whittle was associated, received its first official support in 1938. They received a contract for a Whittle engine, known as the W1, on July 7, 1939. This engine was intended to power a small experimental aircraft. In February 1940, The Gloster Aircraft Company was chosen to develop the aircraft to be powered by the W1 engine. The vehicle, which would be known today as a research aircraft, was covered by specification E28/39, and is frequently referred to by this designation. It was also known as the Pioneer.

The aircraft which emerged from the Gloster factory in 1941 was a small, single-place, low-wing monoplane equipped with a retractable, tricycle landing gear. Air for the engine was supplied by a bifurcated nose inlet which passed the intake air around the pilot in separate ducts to the engine which was located in the rear of the fuselage. The E28/39, which was designed by George Carter of the Gloster Company, weighed 3440 lb, had a wing span of 29 ft, and was capable of a speed of about 340 mph. The W1 engine installed in the aircraft developed 860 lb of thrust.

The historic first flight of the Pioneer took place on May 15, 1941, with Flight Lieutenant P. E. G. Sayer as pilot. The aircraft was used for a number of years in the exploration of the problems of flight with jet propulsion and was finally placed in the Science Museum in London in 1946. A brief but interesting account of the development of the E28/39 and its Whittle W1 engine, together with a detailed discussion of the first British operational fighter, is given in reference 2.31.

Great Britain was not the only European nation to show an interest in jet propulsion prior to 1940. The German aircraft manufacturer, Ernst Heinkel, was searching for new concepts in aircraft propulsion in the mid-1930's. His interest was stimulated when he heard that a young scientist at Goettingen University, Hans Joachim Pabst von Ohain, was investigating a new type of aircraft

engine which did not require a propeller. Ohain joined Heinkel in 1936 and continued with the development of his concepts of jet propulsion. A successful bench test of one of his engines was accomplished in September 1937.

A small aircraft was designed and constructed by Ernst Heinkel to serve as a test bed for the new type of propulsion system. The aircraft, which was designated the He178, was a shoulder wing monoplane in which the pilot's enclosed cockpit was placed ahead of the wing, and the conventional landing gear (tail wheel type) retracted into the side of the fuselage. The air for the 1000-lb thrust engine was supplied by an inlet located in the nose of the fuselage. The fuselage was constructed of metal, and the internally braced wing was made of wood. The wing span of the aircraft was 26 ft, 3 in.; the length was 24 ft, 6 in.; and the area of the wing was 85 ft^2. The aircraft weighed about 4000 lb; and although the maximum speed achieved with the aircraft is not known, the anticipated maximum speed was 527 mph according to reference 2.39.

The Heinkel He178 flew for the first time on August 27, 1939, almost two years before the first flight of the British Gloster E28/39. The pilot, on this historic first flight of a jet-powered airplane, was Flight Captain Erich Warsitz. Little official interest was shown at this time by the German government in the new form of propulsion system demonstrated by the He178, and the aircraft was actually flown only a few times before being retired to the Berlin Air Museum. The aircraft was destroyed during an allied air raid in 1943. Later jet aircraft developments in Germany during World War II are described in references 2.19 and 2.39.

2.1.2 The Swept Wing

The use of wing sweep as a means for increasing the efficiency of aircraft intended for flight at supersonic speeds was first suggested by A. Busemann in 1935 (ref. 2.10). The application of sweep to wings of subsonic aircraft as a means for increasing the critical Mach number was first proposed in the United States by R. T. Jones in 1945 (ref. 2.23). The effectiveness of wing sweep as a means for increasing the critical Mach number, however, had been recognized in Germany at an earlier date. The Messerschmitt Me 163 tailless rocket fighter, for example, employed a sweptback wing, and saw limited operational use toward the end of World War II.

2.1.2.1 High-Speed Characteristics

The critical Mach number of the wing is the flight Mach number of the aircraft at which the local Mach number at some point on the wing reaches the speed of sound. At a Mach number slightly in excess of the critical value, shock waves form on the wing; and further increases in speed cause large changes in the forces, moments, and pressures on the wing. Aircraft do not usually cruise at Mach numbers significantly above the value at which large changes in the wing characteristics begin. The effects on the lift and drag characteristics of increasing the Mach number beyond the critical value are illustrated in figure 5.27 of chapter 5 for a two-dimensional airfoil. A short discussion of the effects of Mach number is contained in section 5.4.1.3 of this same chapter.

The way in which sweepback increases the critical Mach number is illustrated in figure 2.7. If the swept wing is of infinite aspect ratio, the

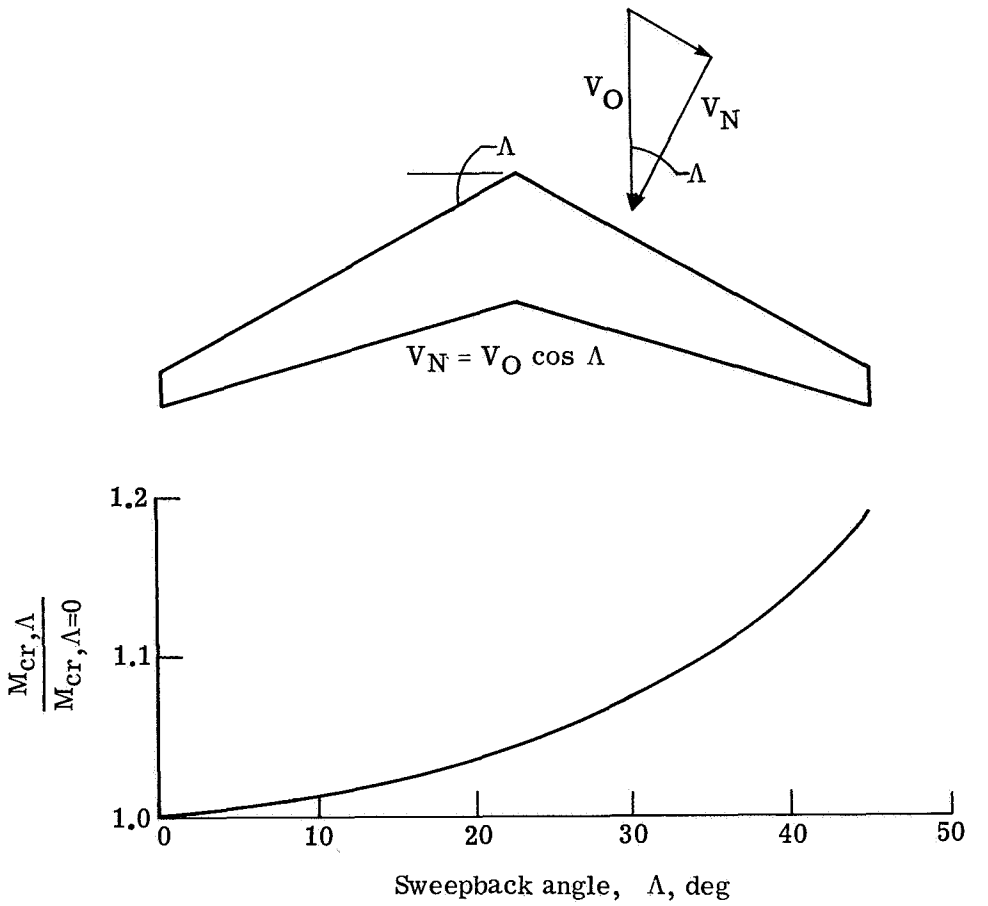


Figure 2.7.- Effect of wing sweepback angle on critical Mach number for wings of constant aspect ratio and streamwise thickness ratio.

critical Mach number of the swept wing is related to that of the corresponding unswept wing as follows:

$$\frac{M_{cr,\Lambda}}{M_{cr,\Lambda=0}} = \frac{1}{\cos \Lambda} \tag{2.6}$$

where Λ is the wing sweep angle, $M_{cr,\Lambda=0}$ is the critical Mach number of the unswept wing, $M_{cr,\Lambda}$ is the critical Mach number of the swept wing, and the airfoil thickness ratio normal to the leading edge, or other appropriate spanwise element, remains constant as the wing is rotated to different angles of sweepback. This relationship is based on the assumption that the critical Mach number of the wing is controlled only by the flow normal to the leading edge

and is independent of the Mach number parallel to the leading edge. Thus, the free-stream Mach number, that is, the flight Mach number of the aircraft, is resolved into components normal and parallel to the leading edge of the wing. The assumption of independence of the two components of the stream Mach number is strictly true only for invisid flow, but the assumption works reasonably well in predicting the effect of sweep on the critical Mach number of wings operating in real flows with viscosity.

The effect of sweepback on the critical Mach number of finite wings is usually analyzed in terms of a wing of given aspect ratio and airfoil thickness ratio in the free-stream direction. The airfoil thickness ratio normal to the leading edge varies, in this case, as the wing sweepback angle is changed. For this reason, and because the flow at the wing root and tip cannot conform to the simple resolution of components normal and parallel to the leading edge, equation (2.6) overestimates the magnitude of the effect of sweepback on the critical Mach number. For a wing with an aspect ratio typical of modern transport aircraft and airfoil sections of constant streamwise thickness ratio, the effect of sweepback on the critical Mach number is given by the following approximate relation for sweep angles up to about 45°:

$$\frac{M_{cr,\Lambda}}{M_{cr,\Lambda=0}} = \frac{1}{\sqrt{\cos \Lambda}} \tag{2.7}$$

The relationship between the critical Mach numbers of the swept and unswept wings, as given by equation (2.7), is shown as a function of sweep angle in the bottom part of figure 2.7.

The effectiveness of sweep in increasing the critical Mach number can be shown by a simple example. Consider an unswept wing of aspect ratio 7.0 which has symmetrical airfoil sections of 12-percent-thickness ratio. The critical Mach number of this wing is about 0.75 according to accepted theoretical methods. A wing of the same aspect ratio and having the same airfoil thickness ratio in the streamwise direction, but having a sweepback angle of 40°, will, according to the curve given in figure 2.7, have a critical Mach number of 0.86. In order to achieve the same increment of 0.11 in critical Mach number on the straight wing of aspect ratio 7.0, a reduction in airfoil thickness ratio from 12 to 4 percent would be required, according to the data given in reference 2.7. Such a reduction in thickness ratio would be structurally incompatible with a wing of aspect ratio 7.0 and, in addition, would greatly reduce the internal wing volume available for fuel storage. The use of swept wings therefore provides significant increases in cruising Mach number and, at the same time, permits the use of aspect ratios sufficiently high to give good values of the maximum lift-drag ratio (see section 3.5.1 of chapter 3), and provides large internal wing volume for fuel.

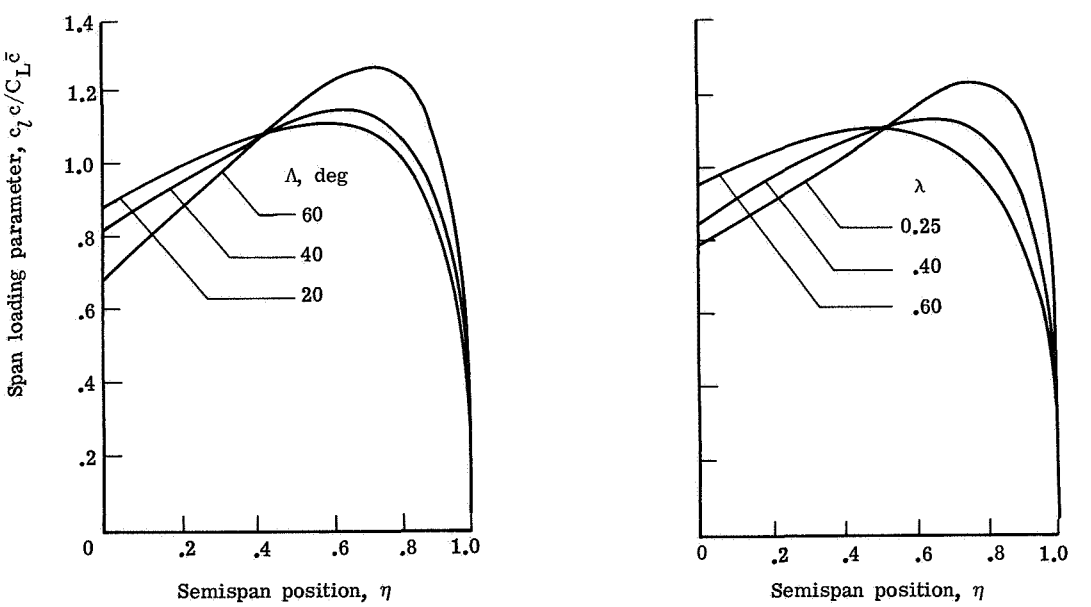
The wing illustrated in figure 2.7 is swept back, as are most of the wings seen on operational aircraft. According to the simple theory in which the streamwise velocity is resolved into components normal and parallel to the leading edge of the wing, the wing however could just as well be swept forward.

The experimental Junkers Ju 287-1, built in Germany during World War II and described in reference 2.39, had sweptforward wings, and one of the business jet transports to be described in a later section of this chapter also incorporates wings with forward sweep.

Sweptforward wings, however, have a fundamental aeroelastic problem which has mitigated against their use. Simply stated, an increase in load on the wing twists the outer portions of the sweptforward wing to higher angles of attack. When the dynamic pressure reaches a critical value, the increment in aerodynamic twisting moment associated with an incremental change in angle of attack is equal to the corresponding incremental change in torsional resisting moment provided by the structure. Any further increase in dynamic pressure will result in the wing twisting off the aircraft. The critical condition at which this catastrophic failure occurs is termed the divergence speed, or divergence dynamic pressure. Structural studies have shown that a sweptforward wing of a given aspect ratio will be heavier than a sweptback wing of the same aspect ratio and sweep angle. The additional weight results from the increased torsional stiffness required to prevent divergence within the flight envelope of the aircraft.

2.1.2.2 Low-Speed Characteristics

The swept wing, along with the advantages just discussed, also introduces some problems which require the most careful consideration in the design of an aircraft having such wings. One of the most serious problems is found in the aerodynamic characteristics at high lift coefficients. The nature of the problem is shown in figure 2.8 in which the variation with spanwise position of the



(a) A = 4.0; λ = 0.4.

(b) A = 4.0; Λ = 40°.

Figure 2.8.- Effect of wing planform shape on span load distribution.

wing aerodynamic load is shown for wings of aspect ratio 4.0 and different sweepback angle and taper ratio. The relative amount of aerodynamic load at each spanwise station is expressed by the span loading parameter C_lc/C_Lc which is the product of the local section lift coefficient at a particular spanwise station and by the wing chord at that position, divided by the product of the wing lift coefficient and the mean aerodynamic chord. The curves in figure 2.8(a) indicate that an increase in sweepback angle from 20° to 60° results in a large increase in the value of the loading parameter near the tip relative to that at the root for wings of aspect ratio 4.0 and taper ratio 0.4. Reducing the taper ratio from 0.6 to 0.25 on wings of aspect ratio 4.0 and 40° of sweepback causes a corresponding increase in the relative amount of load carried near the wing tip, as shown by figure 2.8(b). Variations in the aspect ratio for a given sweepback angle and taper ratio also have an important influence on the shape of the span loading curve.

An increase in the value of the span loading parameter from root to tip indicates that the amount of load carried by each section of the wing increases as the tip is approached. If the wing is tapered, the section lift coefficients increase at a greater rate than the loading parameter. Thus, for untwisted wings equipped with airfoil sections having the same maximum lift coefficients, the initial wing stall would be expected to occur near the wing tip at the spanwise location at which the loading parameter is a maximum. Further increases in angle of attack would cause an inward progression of the stall. A loss in load near the wing tip may, depending on the sweep angle, taper ratio, and aspect ratio, cause a forward shift in the wing aerodynamic center of sufficient magnitude to cause an undesirable increase (reduction in negative value) in the wing pitching-moment coefficient. This type of behavior of the pitching moment is referred to as pitch-up and is in contrast to the desirable pitch-down, or stable pitching-moment break, that is characteristic of most conventional straight wings.

The approximate boundary shown on the left side of figure 2.9 delineates the combinations of wing sweep and aspect ratio which show reduced stability, or pitch-up, at the stall from those combinations which show increased stability at the stall. Combinations of aspect ratio and sweep angle which give reduced stability at the stall are in region II to the right of the boundary. The types of pitching-moment curves which might be expected in region II are indicated at the top right-hand side of figure 2.9. Combinations of sweep and aspect ratio which are characterized by positive stability at the stall are in region I to the left of the boundary, and the corresponding shape of the pitching-moment curves is shown at the lower right-hand side of the figure. If positive stability at the stall is desired, the curve in figure 2.9 indicates that the aspect ratio must decrease as the sweep angle is increased.

The stability boundary given in figure 2.9 was taken from reference 2.28 and is for untwisted wings having a taper ratio of 0.5. The results given in reference 2.32 indicate that increasing the taper ratio from 0.5 to 0 raises the stability boundary; that is, the limiting aspect ratio for stability at the stall is increased for a given sweep angle. Twisting the wing so that the geometric angle of attack of the tip is less than that of the root (termed washout) may be used to reduce the tendency toward tip stall, as can various types of

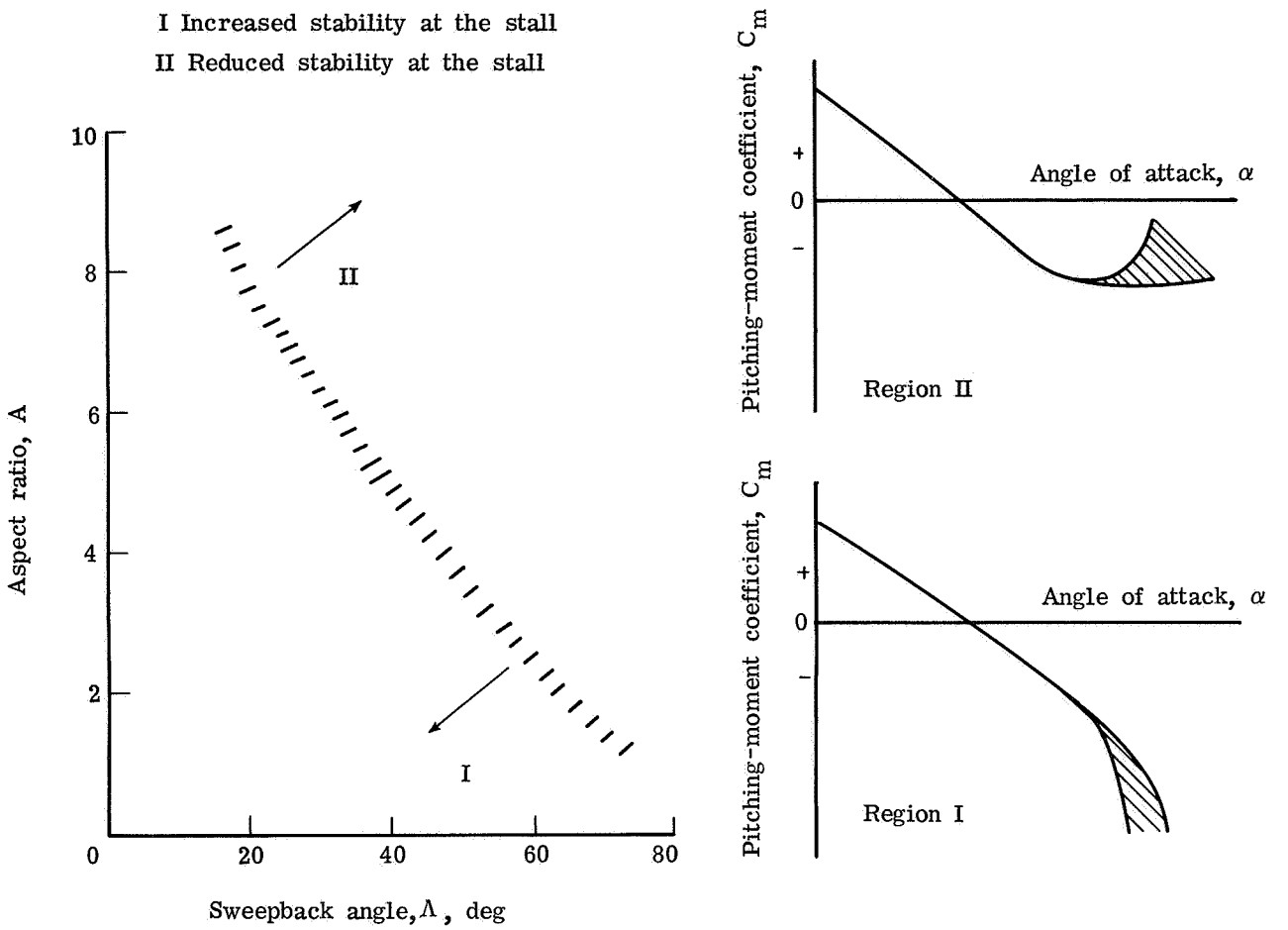
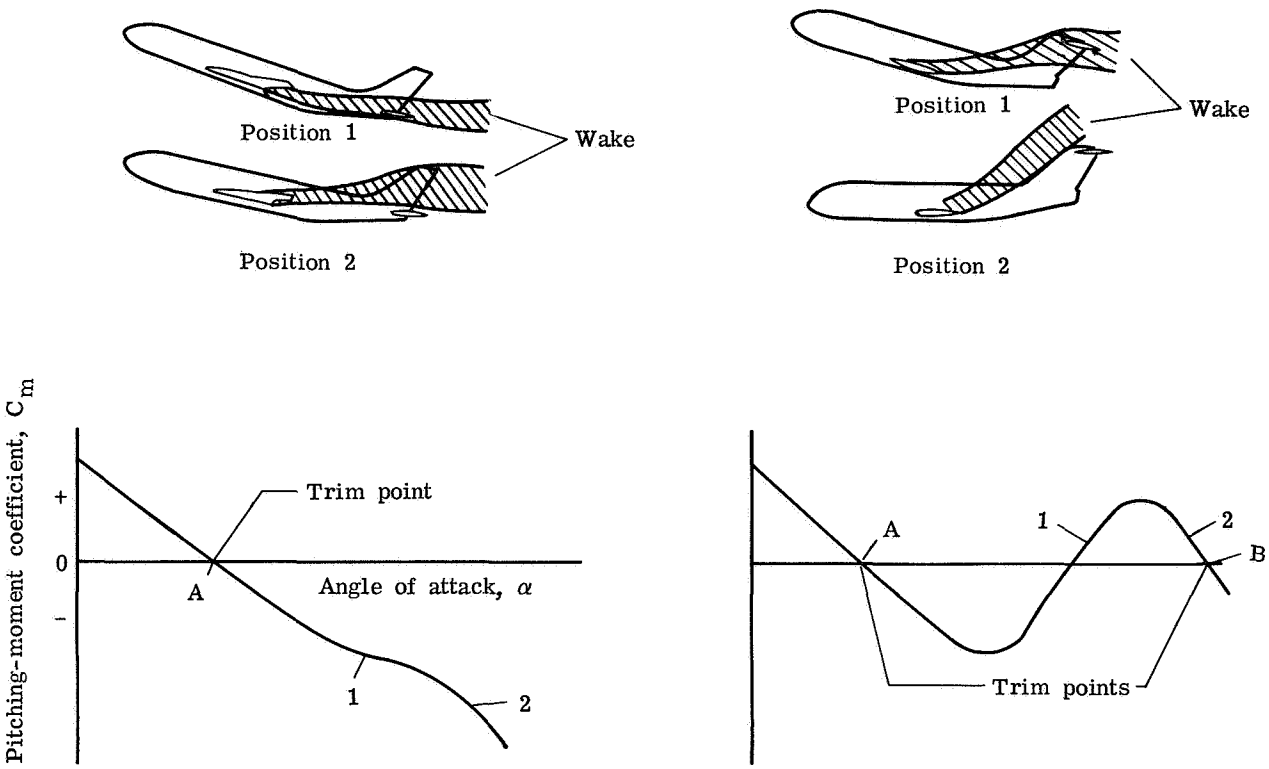


Figure 2.9.- Effect of wing planform shape on static longitudinal stability at stall. Tail off; taper ratio of 0.5.

leading-edge high-lift devices. Some of these devices are briefly discussed in the next section. The spanwise flow along the wing which results from the sweepback causes the boundary layer on the outboard sections of the wing to thicken, as compared to an unswept wing. The thicker boundary layer near the tip of the wing causes the maximum lift capability of these sections to be reduced, as compared to the two-dimensional value. The fences seen on the upper surface of many swept wings are intended to limit the spanwise boundary-layer flow and thus increase the maximum lift capability of the outboard sections.

The discussion so far has dealt only with wing-alone stalling behavior. The stalling and subsequent pitching characteristics of the aircraft, however, are highly dependent upon the details of the aircraft configuration. The longitudinal and vertical position of the horizontal tail with respect to the wing is particularly important. A detailed development of the relationships involved is beyond the scope of the present discussion but may be found in references 2.32 and 2.35.

Some indication of the flow phenomena involved in the wing-tail relationship, however, may be gained from the sketches given in figure 2.10. At the



(a) Low tail. (b) High tail.

Figure 2.10.- Effect of horizontal-tail position on static longitudinal stability.

top left side of the figure is shown an aircraft configuration on which the horizontal tail is slightly above or below the chord plane of the wing. At position 1, the wing is just beginning to stall and the tail is immersed in the wake. The hypothetical pitching-moment curve in the lower portion of figure 2.10 shows that a reduction in stability is beginning at point 1. At position 2, the aircraft is at a higher angle of attack and the wake from the wing passes above the chord plane of the tail. The contribution of the tail to the positive stability of the aircraft is therefore increased at point 2, as compared to point 1, because the tail is operating in a flow field characterized by smaller downwash angles and higher dynamic pressure. The pitching-moment curve shown at the bottom of figure 2.10(a) shows the higher stability of the aircraft at position 2 and indicates that there is no real pitch-up although a small reduction in stability occurs at the stall. The pitching-moment curve for the aircraft configuration with the tail mounted in the low position would be considered acceptable, although not as desirable as that of a design which showed no reduction in stability at the stall.

An aircraft configuration in which the horizontal tail is mounted high above the chord plane of the wing is shown in figure 2.10(b). A greater portion of the wing is stalled on this type of configuration, as compared to the design with the low tail, before the tail encounters the stalled wake. The wake is therefore broader in width and of a lower dynamic pressure for the high tail position. Position 1 in the upper part of figure 2.10(b) shows the high tail immersed in the wide, low-energy wake. The hypothetical pitching-moment curve at the bottom of the figure indicates the large reduction in stability which accompanies an increase in angle of attack, as the tail passes through the wake. Following emergence of the tail from the wake, the aircraft again becomes stable and with further increases in angle of attack reaches a second trim point as indicated by point B on the pitching-moment curve. If the longitudinal control surfaces are in the full nose-down position and the pitching-moment curve appears as depicted in figure 2.10(b), no recovery is possible if the aircraft is allowed to reach the second trim point B.

The preceding discussion is only intended to show the physical nature of the flow interactions which take place between the wing and the tail and should not be construed to mean that a safe aircraft cannot be designed with a high tail. Usually, acceptable pitching-moment characteristics can be obtained with a high tail location by careful tailoring of the wing and tail designs and their relationships to each other. For configurations which employ engines mounted on the aft portion of the fuselage, careful attention must be given to the exact placement of these engines since the wake from the engine nacelles at high angles of attack may combine with that of the wing and contribute to the loss in effectiveness of the horizontal tail. In some cases, acceptable pitching-moment characteristics cannot be achieved by aerodynamic refinements alone. In these cases, mechanical devices such as stick shakers or stick pushers, sometimes both, are employed to prevent the aircraft from entering a potentially dangerous angle-of-attack region. A stick shaker is a mechanical device which causes the control column to vibrate violently as the aircraft approaches a restricted angle-of-attack range. The vibration is intended to alert the pilot to an approaching stall and to make him take corrective action to reduce the angle of attack. A stick pusher causes the control column to be pushed forward mechanically with a considerable force, perhaps 100 lb, as the critical angle-of-attack range is approached. Both devices are sometimes employed together. In this case, the stick shaker is first activated, and if the pilot ignores the warning and permits the aircraft to continue pitching to a higher angle of attack, the stick pusher comes into action. Both the stick pusher and the stick shaker are activated by signals from instruments which sense parameters such as angle of attack, rate of change of angle of attack, attitude and its rate of change, or some combination of these parameters.

The preceding discussion has dealt with the major aerodynamic problem of the swept wing. Other aerodynamic problems of a less fundamental nature are also associated with the use of the swept wing. There are also problems in the areas of structures and aeroelasticity. These problems are, however, beyond the scope of the present discussion. An indication of the nature of the structures and aeroelastic problems, however, is suggested by the drawings of the wings having an aspect ratio of 4 shown in figure 2.8(a), with sweepback angles

of 20°, 40°, and 60°. Increasing the sweepback angle for a given aspect ratio results in an increased length of the wing panel. The length-to-width ratio of the panel, sometimes referred to as the panel aspect ratio, is increased by the factor $1/\cos \Lambda$ for a given aerodynamic aspect ratio. For a given aerodynamic aspect ratio and airfoil thickness ratio, increasing the sweepback angle increases the wing length and causes a reduction in wing bending and torsional stiffness. As a consequence, the problems of aeroelasticity, flutter, and dynamic loads can be intensified by the use of sweepback.

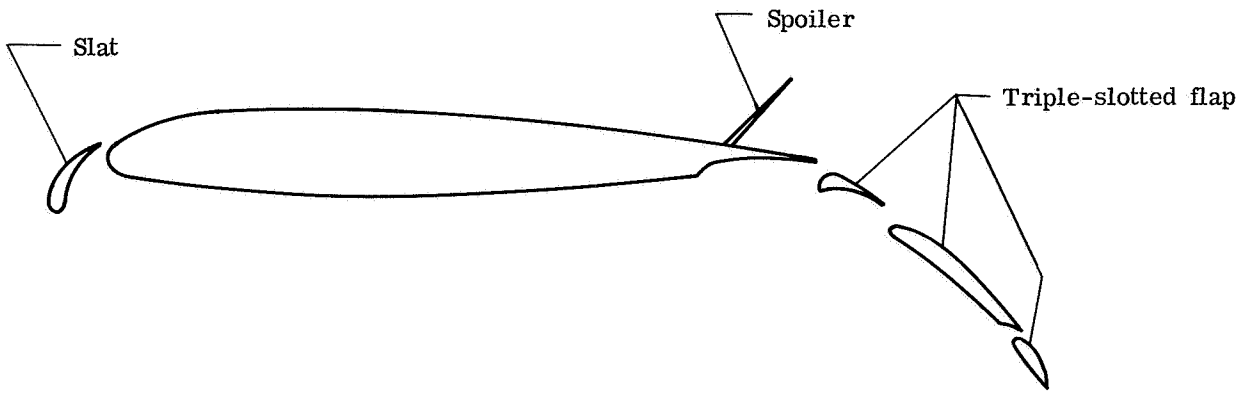
2.1.3 High-Lift Devices

Increases in the capability of high-lift devices have always accompanied the use of higher aircraft wing loadings. This trend has been particularly evident in the evolution of the modern jet transport aircraft. Conversion of the approach lift coefficients given in figure 3.3 of chapter 3 to airplane maximum lift coefficients ($C_{L,max} = C_{L,A} \times 1.69$) shows that lift coefficients of about 3 are being obtained in flight on operational aircraft. The corresponding two-dimensional airfoil maximum section lift coefficients for the flapped sections are probably somewhat in excess of 4. By comparison, the data in figure 5.45 of chapter 5 show that maximum airplane lift coefficients slightly in excess of 2 were being achieved by the end of World War II. The technology for achieving two-dimensional maximum lift coefficients, without boundary-layer control, of about 3.2 existed at the end of World War II, as shown by the comparative data shown in figure 5.25 of chapter 5.

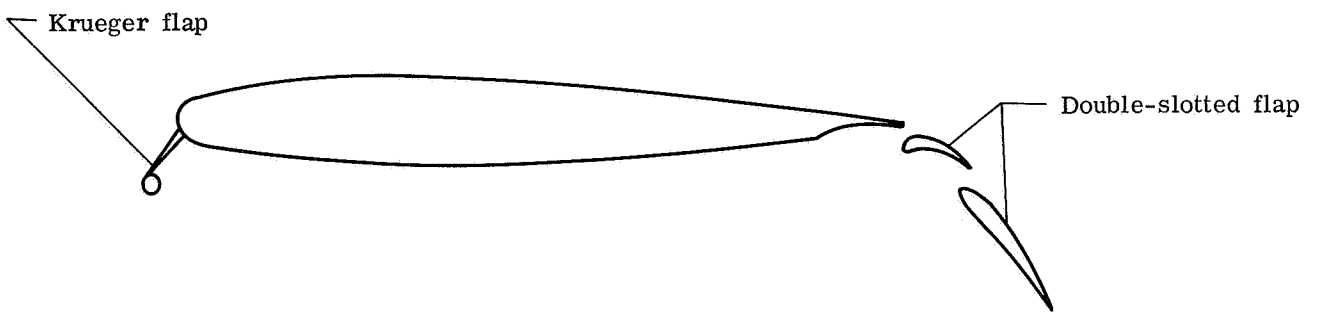
The high-lift system employed on modern jet transport aircraft consists in an assortment of various types of leading- and trailing-edge devices. A number of these devices and the manner in which they are mechanically actuated are described in reference 2.37. Although the detail design and relative effectiveness of the different devices vary, the basic means by which they increase the maximum lift coefficient remain the same. Trailing-edge devices are designed to increase the effective angle through which the flow is turned and thus increase the lifting capability. Leading-edge devices are basically designed to assist the flow in negotiating the sharp turn from the lower surface, around the leading edge, and back for a short distance on the upper surface, without separating.

Two typical high-lift configurations are shown by the sketches in figure 2.11. A wing section equipped with a leading-edge slat and a triple-slotted trailing-edge flap is shown in figure 2.11(a). The trailing-edge flap deploys rearward and downward and separates into three components. The slots in the flap allow flow from the lower surface to the upper surface. The flow through the slots energizes the boundary-layer flow on the top surface, which is negotiating a positive pressure gradient, and prevents separation and subsequent loss of lift. The detail design of the slot contours is very critical and must be carefully worked out in wind-tunnel studies. Both the leading- and trailing-edge devices are completely retracted in cruising flight and are only deployed for landing and take-off.

A wing section equipped with a leading-edge Krueger flap, and a trailing-edge double-slotted flap is shown in figure 2.11(b). The Krueger flap is some-



(a) Airfoil with triple-slotted flap, slat, and spoiler.



(b) Airfoil with double-slotted flap and Krueger flap.

Figure 2.11.- Typical flap systems employed on jet-powered aircraft.

what less effective than the slat, but is probably simpler in mechanical design than the slat. Some aircraft employ slats on the outboard portion of the leading edge, where more powerful flow control is required, and Krueger flaps on the inboard portion of the leading edge. The double-slotted trailing-edge flap is not as powerful as the triple-slotted flap, but is mechanically simpler and easier to implement than the triple-slotted flap. The simple single-slotted flap is often used as a trailing-edge device. This flap consists in a single unsegmented element which is deployed by moving rearward and downward. Although less effective than either of the other two types of trailing-edge devices described, it is by far the most mechanically simple of the three, and the aerodynamic design is the simplest. Many other types and combinations of high-lift devices may be used on jet transport aircraft. The types shown in figure 2.11 are only intended to be representative of typical installations.

Also shown on the upper surface of the wing in figure 2.11(a) is a spoiler in the deployed position. The spoiler is flush with the wing surface when retracted. The action of the spoiler in the deployed position is to "spoil" or separate the flow downstream. The lift of the wing is therefore reduced and the drag increased. These two aerodynamic effects are utilized in several

ways. When deployed on only one wing of an aircraft, they cause that wing to drop and thus serve as a lateral-control device. The wings of many jet transport aircraft employ several spoiler elements on each wing. These elements may act simultaneously or in reduced number, depending on the flight condition and the function which they are intended to fulfill. Some elements of the spoilers are frequently used in combination with conventional ailerons to assist in lateral control. The mix between ailerons and spoilers varies with the flight conditions under which the aircraft is operating. For example, the dynamic pressure corresponding to cruising flight at 35 000 ft and a Mach number of 0.8 is 223 lb/ft^2, whereas that for an approach speed of 135 knots at sea level is 60 lb/ft^2. The need for additional lateral-control devices for flight at low speeds, as compared to cruising flight at high Mach numbers, is clearly shown by the difference in the dynamic pressure for the two flight conditions.

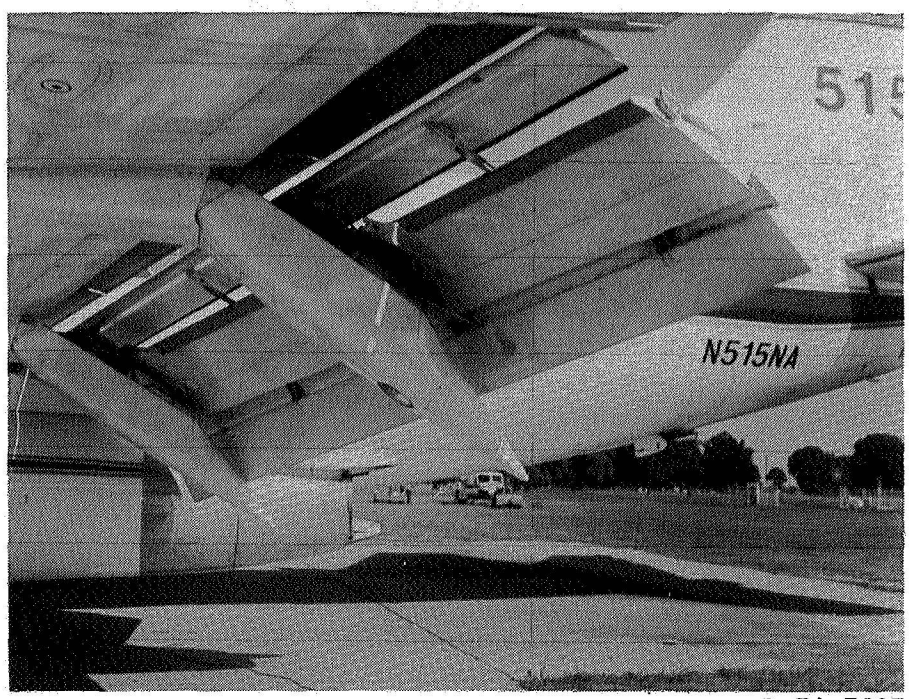
The spoilers are also used to reduce lift and increase drag when deployed symmetrically, that is, in the same manner on each wing. The spoilers are usually deployed in this way immediately after touchdown on landing to assist in stopping the aircraft. The increased aerodynamic drag serves as a braking function for the aircraft, and the reduction in lift increases the percentage of the aircraft weight on the runway and thus increases the effectiveness of the wheel brakes. Many aircraft also utilize symmetrical deployment of the spoilers in flight to increase the rate of descent, for example, to comply with air-traffic-control requirements during the transition from high-altitude cruising flight to flight in the terminal area.

Two views of a triple-slotted flap installed on a Boeing 737 aircraft are shown in figures 2.12 and 2.13. The large fairing shown on the lower side of the wing and flap in figure 2.12 houses the mechanism for deploying the flap. The four segments of the spoiler system employed on each wing are shown in the deflected position in figure 2.13. The leading-edge slat is shown in the deployed position in figure 2.14. A view of the double-slotted flap employed on the McDonnell Douglas DC-10 aircraft is shown in figure 2.15.

2.2 Evolution of the Jet Transport

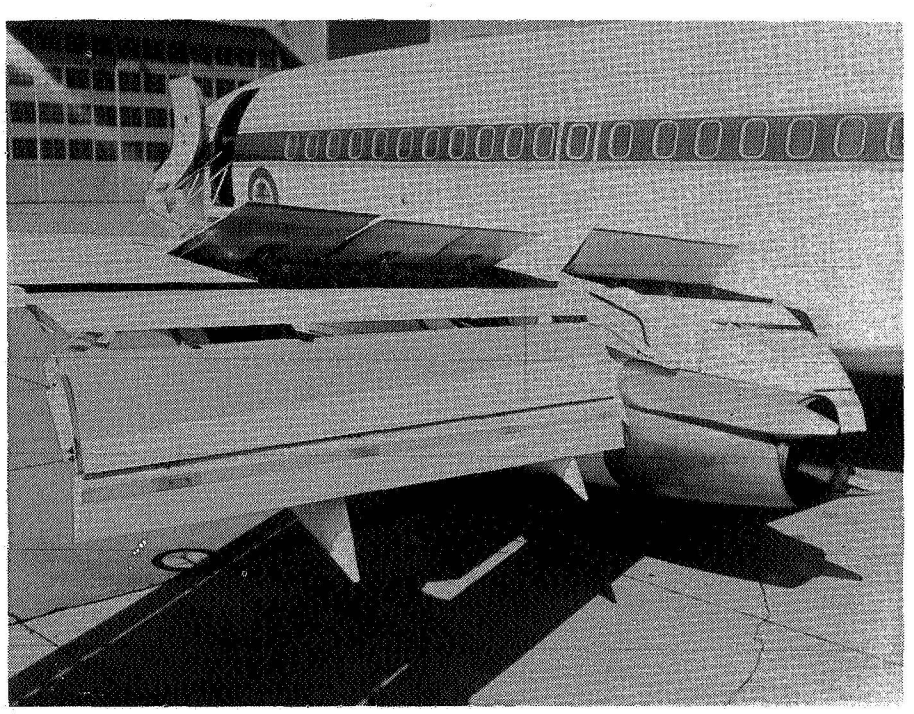
The development and design features of jet transport aircraft from the pioneering DeHavilland Comet of 1949 to the wide-body jets of today are briefly described in this section. The particular aircraft discussed in the following paragraphs were selected because of their significance in the evolution of the modern jet transport, or because they are representative of an important configuration type, or because they are particularly successful. No attempt is made to describe all of the jet transport aircraft which have been developed since the end of World War II.

Successful jet transports tend to have long operational careers and are usually produced in many versions. Engine changes and improvements, changes in wing area and high-lift systems, aerodynamic and structural refinements, and modernization of onboard systems may take place during the production life of a successful aircraft type. "Stretching" is another modification technique frequently employed. In this case, the fuselage is lengthened by the addition of "barrel sections" so that the passenger capacity of the aircraft is accordingly



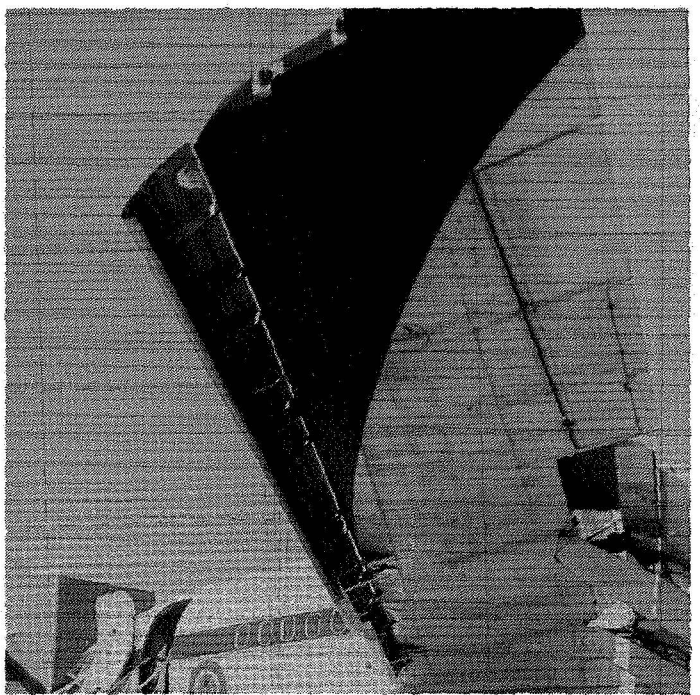
L-74-7627

Figure 2.12.- Lower-surface view of triple-slotted flap on Boeing 737 airplane.



L-74-7628

Figure 2.13.- Upper-surface view showing triple-slotted flap and spoilers on Boeing 737 airplane.



L-74-7621

Figure 2.14.- Lower-surface view of leading-edge slat on Boeing 737 airplane.

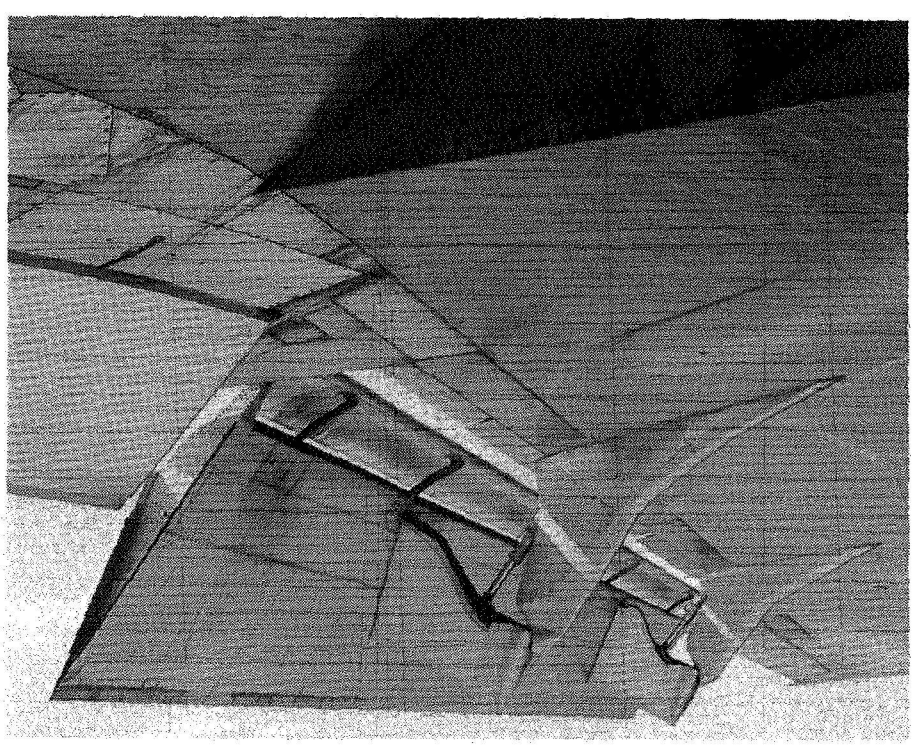


Figure 2.15.- Lower-surface view of double-slotted flap on McDonnell Douglas DC-10 airplane.

increased. A description of the sometimes numerous versions of a particular aircraft is beyond the scope of the present discussion. A representative version of a particular aircraft will be described here. Information on the different versions may be obtained from the references listed at the end of this chapter.

The aircraft to be discussed are listed in tables 2.III and 2.IV, together with some of their important physical and performance characteristics (range and payload defined in fig. 2.16). Also indicated in the tables are the references

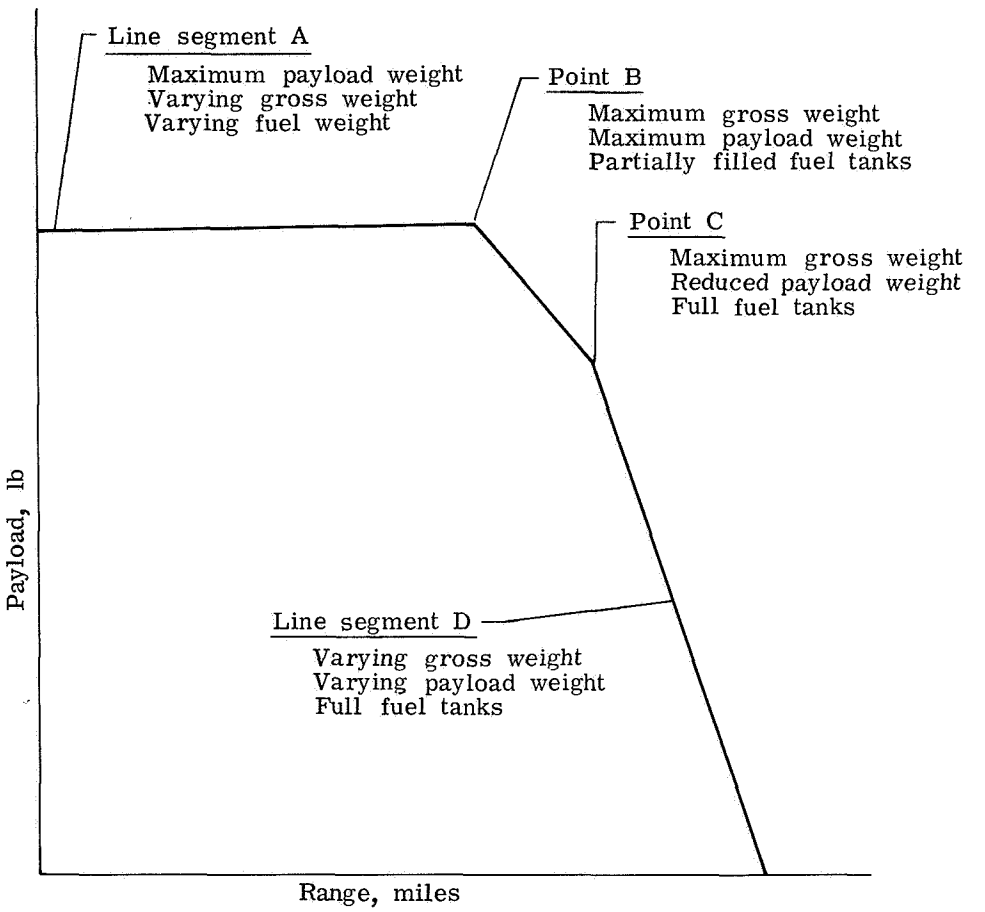


Figure 2.16.- Hypothetical range-payload diagram.

from which the aircraft characteristics were obtained. The various issues of Jane's All The World's Aircraft, which have been published each year since 1909 with the exception of the World War I years, were used as a source for much of the data in the tables. The special summary issues of Flight International Magazine are also a valuable source of aircraft descriptive information and were extensively used in assembling the tables. Photographs of the aircraft described in the following paragraphs and in tables 2.III and 2.IV are contained within figures 2.17 to 2.47. Sources from which these photographs were

obtained are given in table 2.V. References 2.1 to 2.6, 2.13, 2.14, 2.20, 2.22, 2.27, 2.33, and 2.38 were used in compiling the data contained in tables 2.III and 2.IV.

The range-payload diagram is so fundamental to the understanding of transport aircraft performance that a brief description of this diagram is provided at this point. A hypothetical range-payload diagram is given in figure 2.16 in which the range is plotted on the abscissa and the payload, on the ordinate. Point B corresponds to maximum aircraft gross weight and maximum payload weight, with all available seats and cargo space filled but with fuel tanks only partially filled. The gross weight of the aircraft remains the same along the line segment BC; but fuel weight is exchanged for payload weight, that is, payload is off-loaded and the fuel tanks are completely full at point C. Along the line segment D, increases in range are achieved by further reductions in payload although no additional fuel can be carried, and the gross weight is lower than the maximum value. The gross weight of the aircraft along line segment A is less than the maximum value, except at point B, and the fuel load is reduced as the range is reduced. No increase in payload is shown along line segment A because all payload space is filled. The range at maximum payload, point B, and the range and payload for full tanks, point C, are the two combinations of range and payload given in tables 2.III and 2.IV.

2.2.1 Pioneer Tranports

The age of jet transportation began on May 5, 1952, with the inauguration of scheduled service from London to Johannesburg, South Africa. Later in the year, service was established from London to Ceylon and from London to Singapore. Then, in April 1953, scheduled flights were begun from London to Tokyo, a distance of 10 200 miles. The flying time was 36 hr, as compared to 86 hr for the propeller-driven aircraft then in use on the route. The pioneering jet transport which began commercial operations in 1952 was the DeHavilland Comet 1.

The design of the Comet airliner had its origins in the waning days of World War II, and the layout of the aircraft was completed in 1947. The first flight of the prototype took place on July 27, 1949, with John Cunningham as pilot. The performance and physical characteristics of the Comet 1 are given in table 2.III, and a three-view drawing of the aircraft is presented in figure 2.17. A photograph of a Comet 3, similar in appearance to the Comet 1, is given in figure 2.18. The configuration of the Comet was not significantly different from that of contemporary long-range propeller-driven aircraft. A comparison of the characteristics of the Comet, given in table 2.III, with those of the Lockheed Constellation, given in table 5.II of chapter 5, indicates that the Comet was a somewhat lighter aircraft, had a lower wing loading and a wing of lower aspect ratio, but had a cruising speed of 426 knots at 35 000 ft as compared to 288 knots at 23 000 ft for the Constellation. The range with full fuel tanks was 3540 miles with a payload of 12 000 lb. At a reduced range, the maximum number of passengers which could be carried was 48. By present-day standards, the Comet 1 was a small, relatively low performance aircraft. By comparison with other aircraft of the early 1950's, however, it was extremely fast.

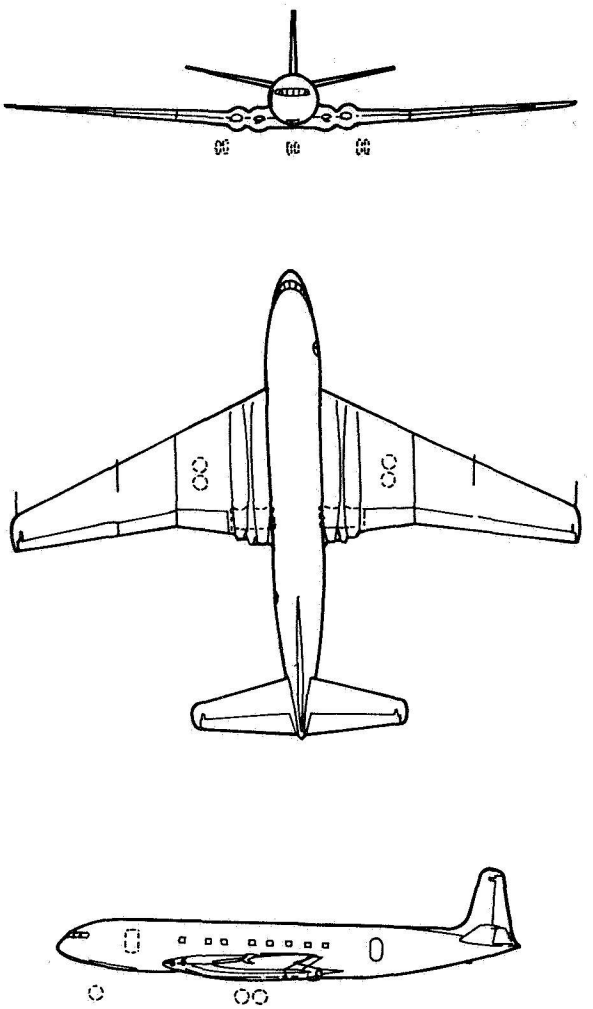


Figure 2.17.- Three-view drawing of prototype of DeHavilland Comet airliner.

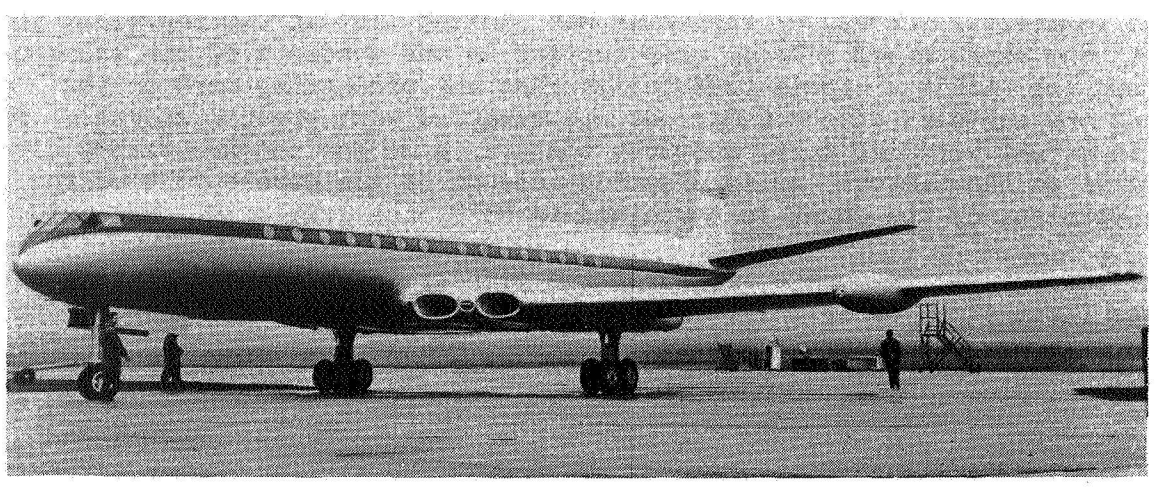


Figure 2.18.- DeHavilland Comet 3 airliner.

The Comet 1 was powered with four DeHavilland Ghost turbojet engines of 4000 lb thrust each. The take-off thrust-to-weight ratio was a very low 0.19. As a consequence of this low thrust-to-weight ratio, very precise control over the aircraft attitude was required during the take-off roll to prevent over-rotation and subsequent high drag and loss of acceleration. At least one aircraft was lost as a result of overrotation during take-off. The four engines were mounted in the wing roots, two on each side of the fuselage. This engine arrangement has the advantages of placing the engines near the longitudinal center-of-gravity position and of minimizing the asymmetrical yawing moment which accompanies loss of an engine during take-off. The proximity of the engines to each other and to the passenger cabin, however, posed a possibly hazardous situation in the event one of the engines disintegrated. Engine disintegration was a very real concern in 1950. Engine maintenance was also complicated by the wing-root mounting arrangement.

The aerodynamic design of the wing was conventional except for the use of 20^{o} of sweepback. The aspect ratio of 6.6 was low, as compared to contemporary long-range propeller-driven aircraft. The high-lift system consisted in a combination of simple plain and split trailing-edge flaps. Some aircraft employed fences on the wings. The aerodynamic controls were hydraulically boosted. The pasenger cabin was pressurized to maintain a cabin altitude of 8000 ft at an aircraft altitude of 40 000 ft.

The Comet 1 was sold to British, French, and Canadian airlines, and it appeared that Great Britain had produced a truly outstanding new aircraft which would be sold in large numbers throughout the world. Prospects for the Comet dimmed, however, when three accidents occurred in which the aircraft disintegrated in flight. All Comet 1 aircraft, over 20 in number, were withdrawn from service in 1954. Extensive laboratory studies were undertaken in an effort to diagnose the problem. Fatigue failure and subsequent rupture of the pressurized fuselage was finally identified as the cause of the accidents. The Comet was completely re-engineered and emerged as a much changed and improved aircraft in 1958. This version, identified as the Comet 4, was not really competitive with the new generation of jet transports coming into use at that time and only 74 were built.

The commercial success of the Comet was limited, but it was the first jet transport and represented a large step forward in our concepts of air transportation and its utility. It is unfortunate that the pioneering work of the designers and builders of the Comet was not rewarded with greater success. The Comet, in highly modified form, survives today as a marine reconnaissance aircraft known as the Nimrod. An interesting account of the development of the various versions of the Comet is contained in reference 2.22.

The Tupolev Tu-104 is the second of the pioneer jet transports. This aircraft was first flown on June 17, 1955, and went into scheduled airline operations in 1956 on the Moscow-Omsk-Irkutsk route. In 1957, an improved version of the aircraft, the Tu-104A, captured a number of records for speed, altitude, distance, and load-carrying capability. The Tu-104 transport was developed from the "Badger" bomber and utilized the same wings, tail surfaces, engines and inlets, landing gear, and fuselage nose section as the earlier bomber aircraft.

The photograph shown in figure 2.19 depicts a Tu-104B, and the data in table 2.III are for this version of the aircraft.



Figure 2.19.- Tupolev Tu-104B airliner.

As can be seen from figure 2.19, the Tu-104B is a low-wing aircraft with a conventional tail arrangement and a wing incorporating pronounced sweepback. The transparent nose adopted from the bomber version of the aircraft is clearly visible in the photograph. The two engines which power the Tu-104 are located in nacelles which are faired into the wing roots. This arrangement is somewhat similar to that employed on the Comet; however, the nacelles are larger and the circular inlets extend forward of the leading edge of the wing, as contrasted with the leading-edge inlets on the Comet. The two main landing-gear struts are fitted with four wheel bogies and retract rearward into pods on the wing. The aircraft has a seating capacity of 100 passengers arranged in a five-abreast configuration. The sweepback angle of the aspect ratio 6.5 wing is 40° from the root to about the midsemispan position and is 37.5° from there to the tip. Each wing has two large fences located in the streamwise position on the top surface of each wing. One of these is located at the position where the sweep angle changes, and the other is located further outboard. As indicated earlier, these fences help control the outward flow of the boundary layer and, hence, improve the stalling characteristics of the wing. Lateral control is provided by conventional ailerons which are operated manually; manual longitudinal control is also used. The rudder is actuated hydraulically. The wings are equipped with trailing-edge Fowler type flaps and have no leading-edge devices. A Fowler flap is similar to the double-slotted flap shown in figure 2.11(b), but without the small segment between the wing and the main portion of the flap.

The Tu-104B is powered by two Mikulin turbojet engines of 21 385 lb thrust each. The engines are equipped with thrust reversers although some of the early models did not have this equipment. These early aircraft employed two braking parachutes to assist in stopping the aircraft on landing. Insofar as can be determined, no other commercial transport aircraft has utilized braking chutes as a routine operational procedure. The gross weight of the aircraft is 167 551 lb, which is somewhat heavier than that of the piston-engine transports at the end of the era in which these aircraft dominated the airlines of the

world. With the large turbojet engines, the thrust-to-weight ratio of the aircraft, 0.26, is nearly as high as any of the large transports whose characteristics are given in table 2.III. The wing loading of 84.8 lb/ft^2 is relatively low compared to more modern designs; however, comparison of the data given in table 2.III for different aircraft indicates that the combination of low-wing loading and relatively simple high-lift devices on the Soviet aircraft give stalling speeds comparable to those of more modern high-performance jet transports.

The range of 1305 miles, given in table 2.III, for the Tu-104 aircraft with maximum payload places it in the short-range category. The cost economical and maximum cruising speeds are 432 and 513 knots, respectively; these speeds correspond to Mach numbers of 0.75 at 35 000 ft and 0.85 at 25 000 ft.

The Tu-104 was built in a number of versions, and some of these are still in use on domestic routes inside the Soviet Union. Production of the aircraft ended after a total of 250 units were constructed. The development history of the Tu-104 series of aircraft is completely described in reference 2.33.

Both the DeHavilland Comet and the Tupolev Tu-104 were pioneers in a new and exciting concept of air transportation and both have a well-deserved place in the history of aeronautical development. In many respects, however, the design of these aircraft reflected the philosophy of contemporary propeller-driven aircraft. For example, the low-wing loadings, unsophisticated high-lift devices, and simple control systems are typical of high-performance propeller-driven transports. The need for high-wing loadings and powerful high-lift devices in order to permit cruising at near maximum values of the lift-drag ratio, but at the same time retaining satisfactory stalling speeds, is discussed in chapter 3. The engine location on the Comet and the Tu-104 are no longer used on modern jet transport aircraft and must be considered obsolete for this type of aircraft. The advantages and disadvantages of mounting the engines in the wing roots were discussed in connection with the description of the Comet. This aircraft, as well as the Tu-104, employed turbojet engines of relatively small diameter. The advent of the high-bypass-ratio turbofan engine with its large diameter fan poses an additional problem with the wing-root engine location because of the difficulty of integrating the large engine into the wing root.

In the next section entitled "First-Generation Transports," three families of transports which were configured and sized so as to exploit more fully the unique capabilities of jet propulsion in commercial aircraft are discussed. These aircraft were responsible for the beginnings of the revolution in air transportation caused by the jet transport, and the configuration concepts of these designs have had a lasting influence on jet-transport aircraft.

2.2.2 First-Generation Transports

This section begins with a brief description of a jet-powered bomber of unique configuration which has had a large influence on transport aircraft design. This aircraft, the Boeing B-47, was powered by six jet engines and

flew for the first time in December 1947. A photograph of the Boeing B-47E is shown in figure 2.20 and the characteristics of the B-47B are given in table 2.III.

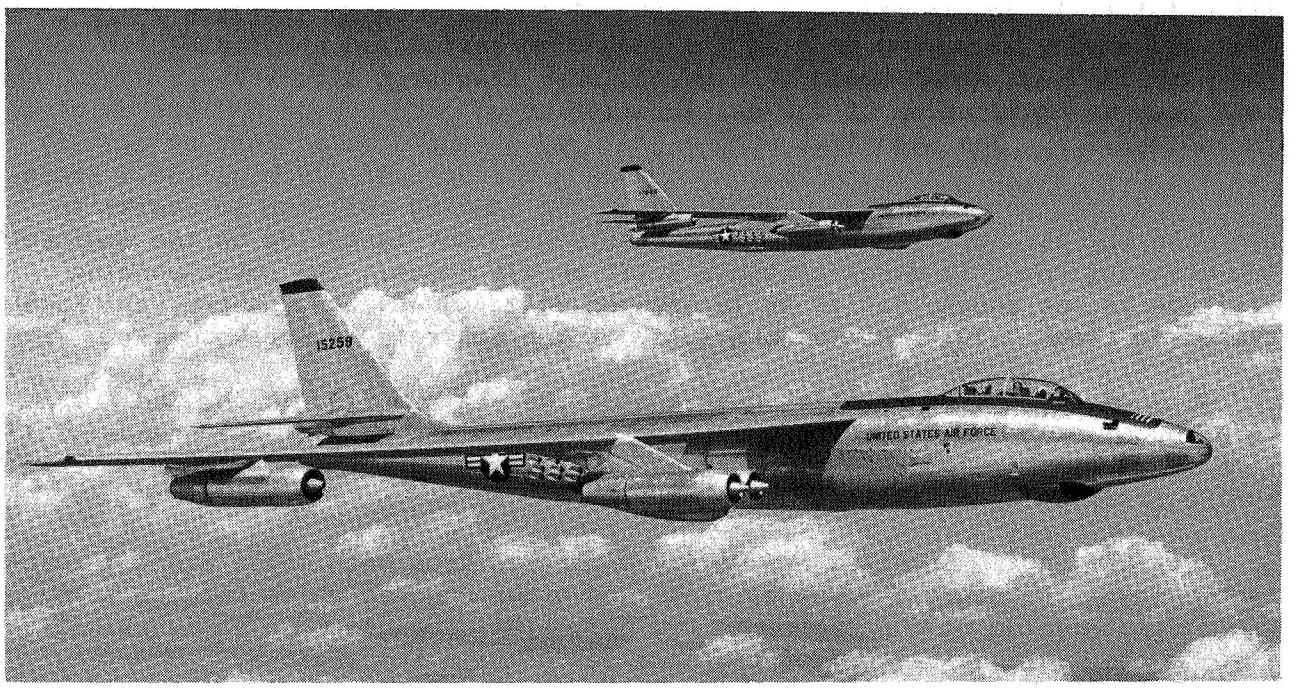


Figure 2.20.- Boeing B-47E bomber.

The aircraft had a high-aspect-ratio swept wing mounted in the "shoulder position" near the top of the fuselage. This wing position allowed the bomb load to be carried in the fuselage, beneath the wing, and near the center of gravity and to be released through doors in the bottom of the fuselage without interference from the structure of the wing center section. The landing gear was an unusual arrangement in which a bogie consisting of two wheels was located along the center line of the fuselage in front and behind the bomb bay. Small, retractable outrigger wheels extended from the inboard engine nacelles to assist in providing lateral balance while the aircraft was on the ground. The arrangement of the engines on this aircraft was entirely new. The nacelles containing the engines were attached to pylons which were mounted to and extended below the wings. Two engines were mounted in each of two nacelles, one of which was attached through a pylon to each wing well outboard of the fuselage. The other two engines were mounted in single nacelles nearly flush with the wing located near the wing tips. The highly efficient wing had an aspect ratio of 9.42 and a sweepback angle of 35° and was equipped with airfoil sections having a thickness ratio of approximately 12 percent in the stream direction.

An indication of the highly refined aerodynamic design of the B-47 is provided by the value of the maximum lift-drag ratio which is estimated to be about 20.6. (The values of the maximum lift-drag ratio given in this chapter

are estimates made by the author and may not agree with those quoted by the aircraft manufacturer. The method employed in making the estimates is described in section 3.5.1 of chapter 3.) By comparison, the famous Boeing B-17 bomber of World War II had a maximum lift-drag ratio of approximately 14 (table 5.II of chapter 5). An examination of the characteristics of the B-47B, given in table 2.III, indicates that the aircraft had a wing loading of 129.6 lb/ft^2. This was a very high wing loading for that time period and was indicative of the wing loadings which would be used on later transport aircraft, as can be seen from an examination of the characteristics of more modern transports given in table 2.III. The high-lift system employed on the aircraft was relatively simple, however, and the stalling speed was a correspondingly high 130.4 knots. Drag producing parachutes were employed in the landing roll-out to assist in stopping the aircraft since thrust reversers were not installed on the engines. The cruising speed is given in table 2.III as 435 knots. The corresponding altitude is not known, but if it is assumed to be 35 000 ft or above, the Mach number is about 0.76. The maximum speed of the aircraft is not known.

One of the most innovative features of the B-47 configuration, and a feature which has had a marked influence on transport designs, is the engine location in nacelles below the wing. A number of advantages may be cited for this engine arrangement as follows:

(1) The engine nacelles are widely separated from each other and the fuselage. Thus, the danger to the aircraft and other engines which results from the disintegration of one engine is reduced. This advantage is somewhat nullified in the B-47 because two of the nacelles contain two engines.

(2) The aircraft is easy to balance because the engines can be located near the aircraft center of gravity.

(3) The weight of the engines mounted outboard on the wing reduces the wing bending moments in flight.

(4) The engines are easy to maintain and can be readily removed because of their proximity to the ground.

(5) Since the engine inlets are usually outboard of the spray pattern from the nose and main landing gear, the outboard wing mounting offers good protection from FOD (foreign object damage) to the engines when the aircraft is operated on the ground.

A number of disadvantages may also be cited for the type of engine arrangement employed on the Boeing B-47 as follows:

(1) Failure of an engine, particularly during take-off or climb, may produce large yawing moments which require immediate correction by the pilot. The magnitude of the corrective yawing moments required to counteract the unsymmetrical thrust in the engine-out condition may determine the necessary size of the rudder.

(2) A small reduction in maximum lift coefficient may result from unfavorable interference effects in the nacelle-wing juncture and from the impingement

of the nacelle wake on the wing at high lift coefficients. The wing-nacelle-pylon relationships must also be carefully tailored, usually in wind-tunnel studies, to eliminate or minimize any interference drag.

(3) The addition of concentrated weights, such as engines or stores, is usually thought to reduce the wing flutter speed. The relationship of the engine center of gravity to the wing elastic axis, as well as the dynamic coupling between the engines and the wing, strongly influence the effect of the engines on the wing flutter speed. These, as well as other relationships, must be carefully tailored by a detailed process involving mathematical analysis and wind-tunnel tests. By this means, a reduction in flutter speed can usually be avoided, or at least minimized.

(4) The dynamic loads imposed on the wing structure during operations on the ground are usually intensified by the concentrated engine masses mounted on the wings.

The unusual configuration of the Boeing B-47 bomber necessitated the development of a new type of wind-tunnel flutter-test technique which has been extensively used in the development of most subsequent multiengine, jet-powered transport aircraft. Flutter tests and analyses had usually been limited to individual components of the aircraft, such as the wing plus aileron and horizontal and vertical tail surfaces. The aircraft as an entity was usually not considered in the determination of the critical flutter speed, nor was such consideration necessary. The concentration of large masses beneath the wings, together with the high degree of flexibility of the wings and other components of the aircraft, required that motions of the complete airplane be considered in determining the critical flutter speeds of the B-47. Both symmetrical and antisymmetrical flutter modes needed to be studied. In a symmetrical mode, each wing deforms in exactly the same way, and the motion of the wings is accompanied by a vertical, up-and-down and pitching motion of the fuselage. In antisymmetrical flutter, the wings on either side of the fuselage deform in exactly opposite directions, and the wing motion is accompanied by a rolling and yawing of the fuselage.

The wind-tunnel technique devised by the Boeing Company to deal with this complex problem is shown schematically in figure 2.21 by the cross-sectional sketch of the wind-tunnel test section. A 3/8-in. rod extended from the floor to the ceiling of the tunnel test section. The model was attached to a gimbal joint located at the center of gravity. The gimbal allowed freedom in pitch and yaw, and was itself attached to the vertical rod by an arrangement of rollers which allowed the model freedom in vertical translation. The snubber lines shown in figure 2.21 were used to arrest the vertical motion of the model if it became too large or uncontrollable. At each tunnel speed, the aircraft model was trimmed so that the lift force balanced the weight of the model. Pitch trim was maintained as the tunnel speed varied by remote adjustment of a tab on the horizontal tail. Limited rolling freedom was provided by looseness in the gimbal joint and flexibility in the mounting rod. The model was constructed in such a way as to simulate the stiffness and mass properties of the aircraft and, accordingly, was quite complex and expensive to design and build.

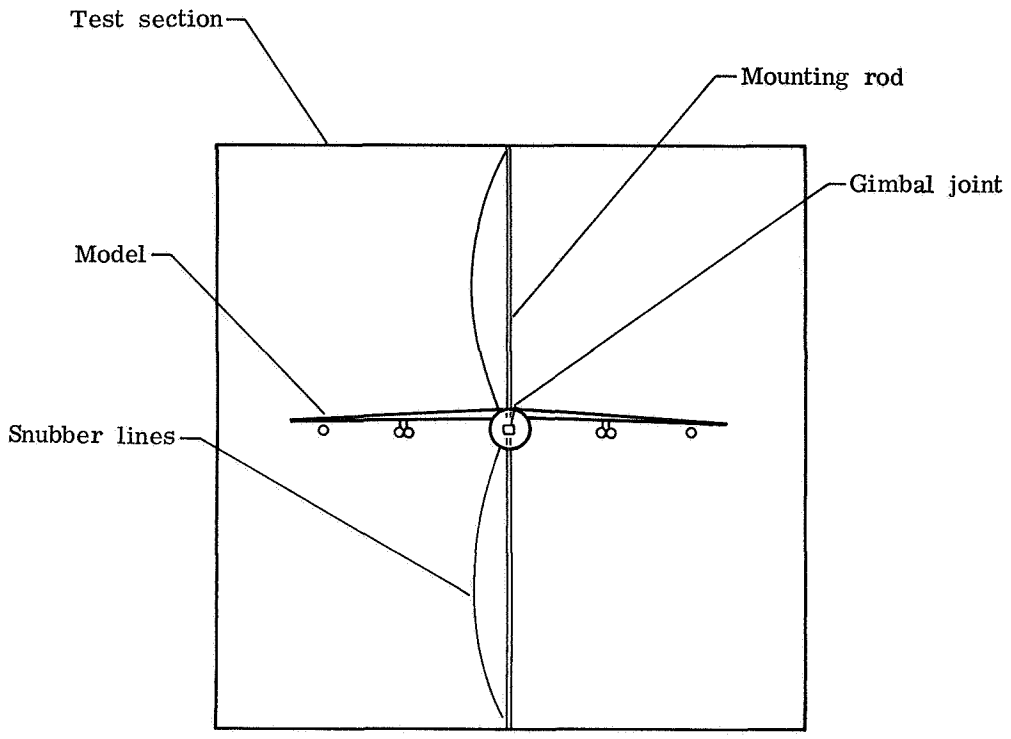


Figure 2.21.- Sketch of flutter model mounted in wind-tunnel test section.

The technique illustrated in figure 2.21 was successfully employed in the development of the B-47 as a means for identifying flutter critical combinations of speed and altitude and development of design fixes for flutter avoidance. A detailed description of the technique is given in reference 2.24. The mounting rod limits the usefulness of the technique to fairly low subsonic speeds because of aerodynamic interference effects associated with the formation of shock waves on the rod at high subsonic Mach numbers. All of the complete model flutter tests made on the B-47 were carried out in a low-speed wind tunnel, and the results were then adjusted for estimated Mach number effects. Later techniques developed by NACA and NASA allow flutter tests of complete airplane models to be made at high subsonic and transonic Mach numbers in a wind tunnel especially designed for high-speed flutter investigations.

The Boeing B-47 was a highly successful bomber of which slightly more than 2000 were built. The aircraft first entered the Strategic Air Command in 1951, and was retired from that service in 1966. As previously indicated, however, the reason for including the B-47 in this discussion does not lie in its importance as a bomber but, rather, in its influence on future transport aircraft design.

2.2.2.1 Boeing 707

The Boeing 707 transport was the first of the long-range and, for its day, high-passenger-capacity aircraft which marked the real beginning of the revolutionary jet age in air transportation. Even today, many people consider the

terms 707 and jet transport to be synonymous. The prototype of this remarkable aircraft first flew in July 1954, and an early production version first entered airline service in the fall of 1958. Over 900 Boeing 707 commercial transports have been built, and the type is still being produced at the rate of 6 to 8 per year. A tanker version of the aircraft, the KC-135, has also been built in large numbers for the U.S. Air Force; and the Airborne Warning and Control System aircraft (AWACS) now being delivered to the Air Force utilizes the basic 707 airplane. It is perhaps worth mentioning that Air Force 1, which is employed to transport the President of the United States, is a Boeing 707.

The prototype of the 707 was known in the Boeing Company as the model 367-80, and within the company it has always been referred to as the Dash-eighty. The aircraft served as a test vehicle for the exploration and development of new ideas for many years. Finally retired in 1972, it was presented to the Smithsonian Institution. A photograph of the aircraft is shown in figure 2.22, and a few of its characteristics are given in table 2.III.

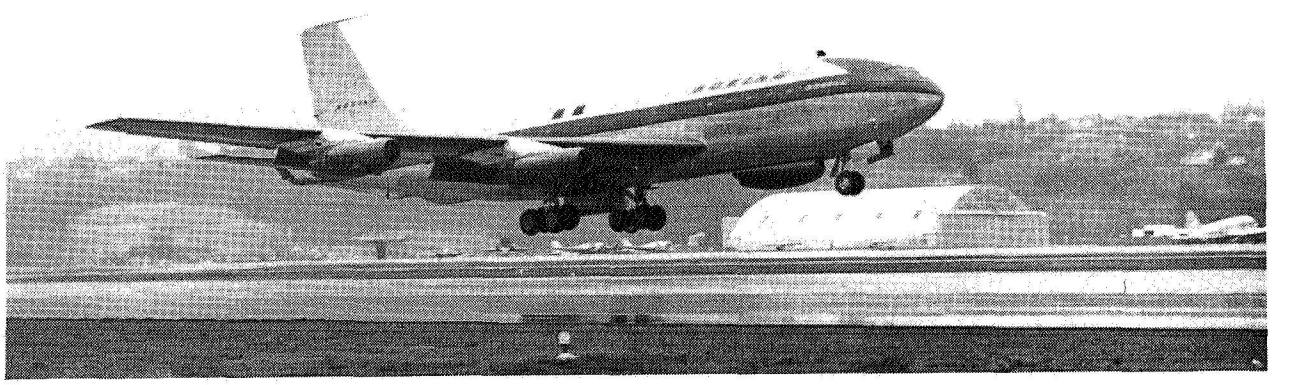


Figure 2.22.- Boeing model 367-80 prototype of Boeing 707 series transports.

A fully developed Boeing 707-320B is shown in figure 2.23, and a three-view drawing of this version is given in figure 2.24. The 707-320B is the last version of the aircraft built solely for passenger use. The variant currently in production is the 707-320C, which is similar in most respects to the 707-320B but is fitted with a cargo door and strengthened floor structure; the aircraft may therefore be used for cargo or mixed cargo and passenger service. Given in table 2.III are data for the 707-320B. Specifications and performance data quoted in the following paragraphs are for this version of the aircraft.

The wing of the Boeing 707 is mounted in the low position, at the bottom of the fuselage; this wing location has been preferred on transports designed for passenger use since the Boeing 247 and Douglas DC-2 of the early 1930's. The wing has an aspect ratio of 7.35; and in order to achieve the desired cruising efficiency at high subsonic Mach numbers, it employs a sweepback angle of 35°. The main landing gear consists of two struts to which are mounted four



Figure 2.23.- Boeing 707-320B airliner.

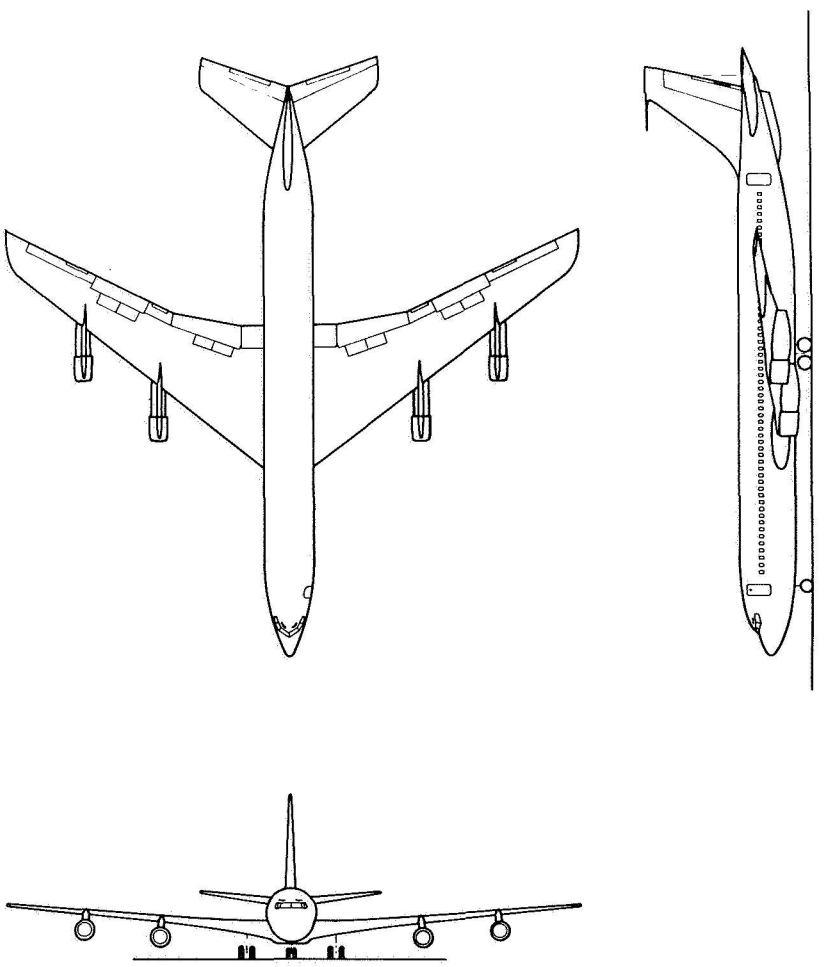


Figure 2.24.- Three-view drawing of Boeing 707-320B airliner.

wheel bogies. The landing gear is attached to the wing and is retracted inboard into the thickened juncture of the wing and fuselage. The nearly straight trailing edge of the wing near the fuselage is dictated by the required storage space for the landing gear in the retracted position. The two-wheel nose gear retracts forward into the fuselage.

The four engines are mounted in a manner similar to that poineered on the B-47 bomber. Each engine is contained in a single nacelle which is attached to the bottom of the wing by a pylon. According to reference 2.27, consideration was given to mounting two engines in each of two nacelles; such an arrangement was employed in mounting the four inboard engines of the B-47. This engine configuration was abandoned on the transport because of the possibility that disintegration of one engine might cause failure of an adjacent engine. This possibility was apparently not acceptable on a passenger-carrying transport. Early versions of the 707 were powered with turbojet engines. Several different engines were used, but most of these early aircraft employed the Pratt & Whitney JT3C engine, which is basically a civil version of the military J-57 turbojet used by such aircraft as the Boeing B-52 bomber and the North American F-100 fighter. Most 707 aircraft manufactured since the early 1960's, however, have been powered with a turbofan version of this engine. The Pratt & Whitney JT3D turbofan engine utilizes the same basic gas generator as the J-57 but has a front-mounted two-stage fan with a pressure ratio of about 1.8. The bypass ratio is 1.43, and the sea-level static thrust is about 19 000 lb. The fan discharges through a short duct which appears somewhat similar to an NACA cowling of the type employed on many radial engines. The short duct can be seen in the photograph in figure 2.23. Thrust reversers are employed to assist in stopping the aircraft on its landing roll-out. Reverse thrust may also be used to increase the rate of descent. The aerodynamic efficiency of the 707-320B may be judged by the value of the maximum lift-drag ratio which is estimated to be in the range from 19 to 19.5. This value of $(L/D)_{max}$ is lower than the value of 20.5 given for the B-47, primarily because of the lower aspect ratio of the wing employed on the 707.

The wing loading of the 707-320B is a relatively high 116 lb/ft^2; however, the landing speed is maintained at a relatively low 105 knots by the use of trailing-edge double-slotted flaps and leading-edge flaps. The lateral control system of the aircraft consists of a combination of spoilers and ailerons which are mixed in their use according to the speed regime in which the aircraft is flying. (See section 2.1.3.) The spoilers are also used for reducing the stopping distance of the aircraft on landing and for rapid descents in flight. Descent rates of as high as 15 000 ft/min can be achieved by deployment of the spoilers and the use of reverse engine thrust.

The elevators and ailerons are aerodynamically balanced and are manually operated by aerodynamic servotabs. In this type of control system, the pilot's primary flight controls deflect tabs on the main control surfaces. The hinge moment of the control surface is altered by deflection of the tab, and, consequently, the floating angle of the surface is altered. This change in angle of the main surface provides the necessary control moments for the aircraft. The spoilers and rudder on the 707 aircraft are operated hydraulically. Small changes in longitudinal trim are made with the use of trim tabs on the eleva-

tors. Large changes in trim, such as are caused by flap deflection, are balanced by adjusting the angle of the horizontal stabilizer. Movement of this surface is power actuated.

The gross weight of the Boeing 707-320B is 336 000 lb, which is more than three times the weight of the Comet 1. The cabin can be configured to carry a mix of first-class and tourist-class passengers or can be configured in an all-tourist arrangement. In the all-tourist configuration, 189 passengers can be accommodated. With a maximum payload of 53 900 lb, the aircraft has a range, without reserves, of 5175 n. mi.; with full fuel tanks and a payload of 33 350 lb, the range is 6500 n. mi. With this range capability, the aircraft is truly capable of connecting many of the important population centers of the world. The aircraft has a maximum cruising speed of 516 knots at 30 000 ft and a cost-economical cruising speed of 478 knots at 35 000 ft; the corresponding cruising Mach numbers are 0.87 and 0.83, respectively. The take-off field length on a standard day is a relatively long 10 000 ft, which can be directly related to the low thrust loading of 0.23 and the high wing loading of 116 lb/ft^2. (See section 3.4.3 of chapter 3.)

By any measure, the 707 series of aircraft must be ranked as one of the most successful transports ever produced. The present fleet of aircraft will no doubt fly on for many years in different parts of the world. Boeing has recently offered a version of the aircraft equipped with modern high-bypass-ratio engines. With these engines, the range of the aircraft will be extended, and it will comply with the noise regulations of part 36 of the Federal Air Regulations. If this version of the 707 is produced in quantity, the longevity of the type will be further extended.

2.2.2.2 McDonnell Douglas DC-8 and Other Four-Engine Transports

The second long-range high-passenger-capacity transport which, along with the Boeing 707, initiated the jet revolution in air transportation was the McDonnell Douglas DC-8 (originally the Douglas DC-8). This aircraft was ordered by Pan American World Airlines in 1955, and the first flight was made in 1958. The aircraft entered airline service in August 1959. The DC-8 was built in many different versions during the years in which it was in production. One of the principal modifications incorporated in the aircraft was a stretched fuselage to provide increased passenger capacity. Over 550 DC-8 aircraft were built before production was terminated in the early 1970's.

In most essential respects, the basic configuration of the McDonnell Douglas DC-8 is the same as that of the Boeing 707. Early versions of the two aircraft were virtually indistinguishable except to a person very familiar with both. There were, of course, many differences in the detailed aerodynamic and structural design and in the systems employed on the aircraft. A photograph of the McDonnell Douglas DC-8 Super 63 is shown in figure 2.25, and some of the characteristics of the aircraft are given in table 2.III. As compared to the early versions of the DC-8, the fuselage of the Super 63 has been stretched by the addition of a 20-ft section ahead of the wing and a 17.8-ft section aft of the wing. Also, the wing span of the aircraft has been increased 6 ft over that of the original DC-8. The wing and engine locations are similar to those used

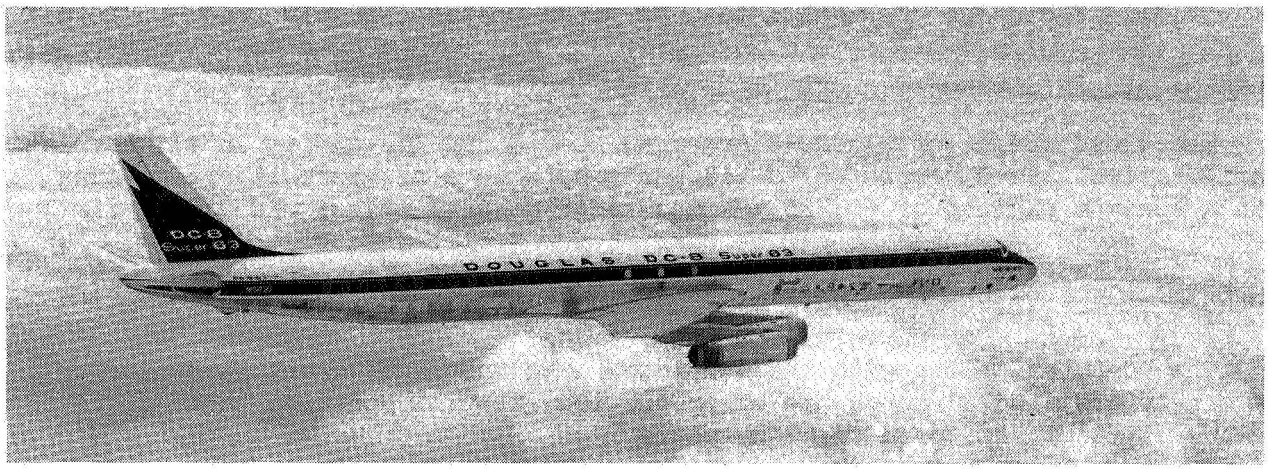


Figure 2.25.- McDonnell Douglas DC-8 Super 63 airliner.

on the 707; however, the aspect ratio and sweepback angle are slightly different. The main landing gear consists of two struts to which are mounted four wheel bogies; the two rear wheels of each bogie can be put in a free swiveling mode to assist in making sharp turns on the ground. The main landing gear is mounted on the wing and retracts inward into the fuselage. The two-wheel nose gear retracts forward into the fuselage.

The aerodynamic efficiency of the DC-8 is indicated by the maximum value of the lift-drag ratio which is estimated to be about 17.9. The value of $(L/D)_{max}$ is lower for the DC-8 than for the 707 because of the DC-8's longer fuselage and corresponding increased ratio of wetted area to wing area. The relationship between wetted area, wing area, and $(L/D)_{max}$ is discussed in section 3.5.1 of chapter 3. The loss in aerodynamic efficiency associated with the long fuselage is more than compensated by increased passenger-carrying capacity and consequent reduction in direct operating costs per seat mile.

The wing is equipped with trailing-edge double-slotted flaps and leading-edge slats over the inboard sections of the wing. These high-lift devices provide a lift coefficient which gives a stalling speed of 107 knots at the maximum landing wing loading. The maximum landing wing loading is somewhat less than the value given in table 2.III which is for maximum take-off gross weight. The lateral control system consists of inboard and outboard ailerons that are connected by a torque tube which acts as a torsion spring. The inboard sections are power operated. The outboard sections only operate at the lower values of the dynamic pressure where they are needed. As the dynamic pressure increases, the aerodynamic resisting moment of the aileron becomes greater in relation to the torque that can be transmitted through the torsion bar; hence, the aileron deflection is reduced. The amount of deflection of the outboard aileron varies smoothly with variation in dynamic pressure and, therefore, provides the desired variation of aerodynamic control moment with speed and altitude. The rudder is also power operated. Both the rudder and the ailerons have a manual reversion mode in the form of aerodynamic servo tabs. Elevator control is manual and consists of an aerodynamic servo system similar to that employed on the 707.

The variable incidence horizontal tail is power operated and is used for longitudinal trim. Wing spoilers are automatically deployed on landing by nosewheel contact with the runway.

The gross weight of the DC-8 Super 63 is 358 000 lb; and in an all-tourist configuration, the aircraft seats 259 passengers in a six-abreast arrangement. With a maximum payload of 67 735 lb, the range is 4245 miles; and with maximum fuel, a payload of 37 101 lb can be carried for a distance of 6084 miles. As can be seen in table 2.III, the cruising speeds of the DC-8 are about the same as those of the 707.

The DC-8 has, along with the 707, been a workhorse of great productivity for many years; and although out of production, it will continue to be operated in many parts of the world for many years.

Two other aircraft of this first generation of large jet transports are nearly the same in configuration as the Boeing 707 and the McDonnell Douglas DC-8. In fact, when seen at the airport, the Convair 880 and 990 are often confused with one or the other of the more familiar 707 or DC-8 aircraft. The Convair 880 first flew in 1959, and the first flight of the more advanced Convair 990 was in 1961. The maximum cruising Mach number of the 990 is 0.89, which is the highest of any of the subsonic jet transports. The high cruising Mach number of the aircraft is due in part to the Whitcomb bumps on the trailing edge of the wing. The two pods mounted on each wing at the trailing edge make the aircraft readily identifiable and are used to increase the critical Mach number.

Both the 880 and the 990 are somewhat smaller and lighter in weight than are the 707 and the DC-8. The gross weight of the 880 is 192 700 lb and that of the 990 is 253 000 lb. The range of neither aircraft is really intercontinental, and the payloads are lower than those of the Boeing and Douglas aircraft. For these reasons, perhaps, and because both aircraft became available to the airlines somewhat later than the 707 and the DC-8, only a relatively small number of Convair jet transports were built. Total production of the 880 was 65, and 37 examples of the 990 were built. At this time, neither type is used in scheduled airline service in the United States.

2.2.2.3 Sud-Aviation Caravelle

The French Sud-Aviation Caravelle was the first really successful short-range jet transport to be developed in the western world. The first flight of the prototype took place in May 1955, and the aircraft entered airline service in Europe in April 1959. As with most successful jet transports, the Caravelle was produced in a number of versions; a total of 280 aircraft of all versions were produced before production was terminated in the early 1970's. Many are still in operation in various parts of the world. A Sud-Aviation Caravelle model V1 is depicted in the photograph of figure 2.26. The aircraft shown carries the markings of United Airlines, which operated a fleet of 20 Caravelles for a number of years. Characteristics of the Caravelle V1-R are given in table 2.III.

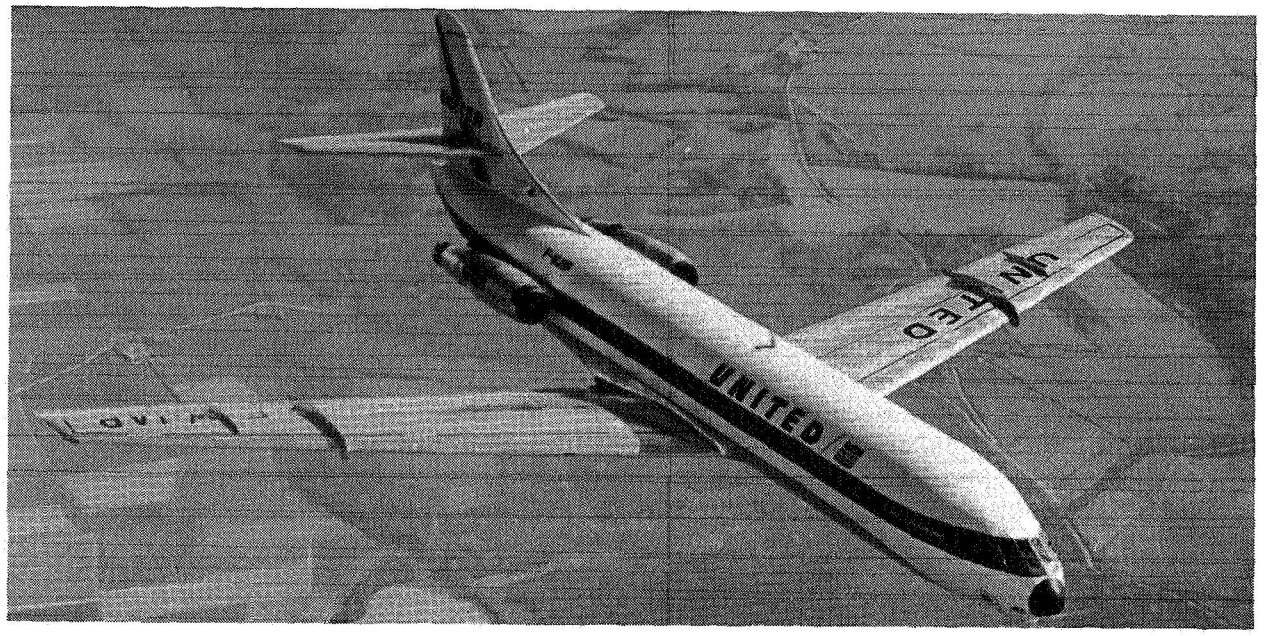


Figure 2.26.- Sud-Aviation Caravelle short-range airliner.

The primary technical significance of the Caravelle was its pioneering use of an entirely new and innovative approach in the integration of the engines and airframe. The photograph of the aircraft, presented in figure 2.26, shows that one of the two engines is mounted on either side at the aft end of the fuselage. This engine arrangement set the pattern for many future jet transport aircraft of two-, three-, and four-engine design. When the engine location proposed for the Caravelle was first made known, many engineers expressed doubts about the practicality of such an arrangement. For example, questions were raised about the operation of the engines in the wake of the wing as the aircraft approached a stalled condition, or the effect on engine operation of large angles of sideslip. The aft-engine location, however, has proved to be highly workable. Some of the advantages and disadvantages of this aft-engine arrangement are as follows:

(1) The short lateral distance between the engines results in relatively small yawing moments following the loss of an engine. The required vertical-tail size is accordingly reduced, as compared to that of an aircraft with wing-mounted engines such as the Boeing 707.

(2) The rear location of the engines results in a relatively low engine-noise level through most of the cabin.

(3) Removal of the engines from the wing results in a small increase in the maximum lift coefficient and elimination of wing-pylon-nacelle interference drag. The integration of the engines at the aft end of the fuselage, however, requires careful design in order to minimize interference drag in this area.

(4) The location of the engines at the aft end of the fuselage, as compared to the underwing position, reduces the problem of interference between the

engines and the ground, a problem which becomes particularly important as the size of the aircraft is reduced.

(5) Mounting the engines on either side of the aft portion of the fuselage prevents location of the horizontal tail in a low position. In the case of the Caravelle and a number of other aircraft, the tail is mounted at some location between the root and tip of the vertical-tail surface. Other aircraft utilize the T-tail position in which the horizontal tail is mounted at the tip of the vertical surface. The use of a high tail position offers several advantages: If the vertical tail is swept back, the horizontal-tail moment arm is increased as the tail is moved toward the tip of the vertical surface. The horizontal-tail size, and hence the weight of the tail, may therefore be reduced for a given level of static longitudinal stability. In the T-tail arrangement, the horizontal tail acts as an end plate and reduces the required size of the vertical surface for a given level of static directional stability. Again, a reduction in tail weight may be realized. Structural and aeroelastic problems may, however, cause some increases in weight of the vertical tail.

(6) The high tail position also has some disadvantages. A brief qualitative discussion of the influence of horizontal-tail position on the static longitudinal stability of swept-wing aircraft is given in section 2.1.2.2. As indicated therein, certain inherent aerodynamic problems are encountered in the design of an aircraft with a high tail location. Careful attention to the detail design of such a configuration is required in order to achieve reasonably acceptable longitudinal aerodynamic characteristics. Lack of proper care in the design process can result in an aircraft with highly undesirable longitudinal aerodynamic characteristics.

(7) The rear engine location results in large concentrated weights at a large distance from the aircraft center of gravity. This arrangement, therefore, causes some problems in aircraft balance for certain loading configurations. These balance problems, however, have been overcome in a large number of highly successful aircraft which employ the aft-engine arrangement.

Other than the engine arrangement, the configuration of the Caravelle is conventional, with the 20° swept wing of aspect ratio 8 mounted in the low position on the fuselage. Two large fences can be seen on each wing in the photograph in figure 2.26. These fences are intended to control the spanwise flow of the boundary layer on the swept wing and thus to improve the stalling characteristics of the aircraft. The wing-pylon-engine arrangement on the 707 type configuration serves this same purpose. The high-lift system consists of trailing-edge Fowler flaps. Large airbrakes are mounted ahead of the flaps on the top and bottom surfaces of the wing. All of the flying controls are hydraulically actuated. The aircraft is powered with two Rolls-Royce Avon turbojet engines of 6750 lb of sea-level static thrust.

A study of the characteristics of the Caravelle, given in table 2.III, indicates that the gross weight of the aircraft is a relatively light 112 500 lb even lighter than the Comet, and that it is capable of a range of 1590 n. mi. with a payload of 16 800 lb. Eighty passengers can be accommodated in a five-abreast configuration. The cost-economical cruising speed of 424 knots at 35 000 ft is somewhat lower than the 478 knots given in the table

for the Boeing 707. The lower cruising speed of the Caravelle would be expected in a short-range airplane and explains the low sweepback angle of the wing. The relatively short landing and take-off field lengths indicate that it was designed to operate from the many small airports appropriate to a short- or medium-range airliner.

The Caravelle has proven to be a highly successful short-range jet transport, and its place in the history of aeronautical development is secure as a result of its pioneering use of the aft-fuselage engine location.

2.2.3 Second-Generation Transports

The second-generation jet transports are considered to be those which first flew in prototype form in the 1960's and were developed in a later time period than the aircraft discussed in section 2.2.2. The following 11 aircraft constitute the second-generation jet transports:

Country	Manufacturer	Model	First flight (a)	Engines	Maximum range, n. mi.
United States	Boeing	727	1963	3	Between 2000 and 3000
United States	McDonnell Douglas	DC-9	1965	2	Between 1000 and 2000
United States	Boeing	737	1967	2	Between 2000 and 3000
United Kingdom	British Aircraft Corporation	1-11	1963	2	Between 1000 and 2000
United Kingdom	Hawker Siddley	Trident	1962	3	Between 2000 and 3000
United Kingdom	British Aircraft Corporation	VC-10	1962	4	Over 3000
Netherlands	Fokker	F-28	1967	2	Under 1000
U.S.S.R.	Tupolev	Tu-134	1964	2	Under 1000
U.S.S.R.	Tupolev	Tu-154	1968	3	Between 2000 and 3000
U.S.S.R.	Ilyushin	Il-62	1963	4	Over 3000
U.S.S.R.	Yakolev	Yak-40	1966	3	Under 1000

[a]First flight dates are for prototype of first version.

All of the aircraft listed are representative of about the same level of technology and have no large state-of-the-art advances over the first-generation jet transports discussed in section 2.2.2. All of the aircraft are equipped with turbofan engines of relatively low bypass ratio which are of about the same level of technical sophistication as the fan engines that powered the first-generation transports. Basically, with a few evolutionary refinements,

the second-generation aircraft represent an application of the technology developed in the first-generation aircraft to transports specifically tailored to various types of airline route structures and payload requirements. All of the aircraft, except the Boeing 737, employ aft-fuselage mounted engines in either two-, three-, or four-engine configurations. Four of these aircraft are briefly described in the following paragraphs; these are the three-engine Boeing 727, the twin-engine McDonnell Douglas DC-9, the twin-engine Boeing 737, and the four-engine BAC VC-10.

2.2.3.1 Boeing 727

By any standard, the three-engine Boeing 727 must be considered the most successful jet transport aircraft yet produced. The prototype first flew in 1963, and the type was first introduced into service by Eastern Airlines in early 1964. Total orders to mid-1978 numbered about 1500, and the aircraft was being produced at the rate of 8 to 11 per month in that year. The 727 is operated all over the world by some 85 airlines; it is rarely possible to visit a domestic airport served by a scheduled airline without seeing a Boeing 727 during the course of a day. The 727 is popular with the airlines primarily because it can be operated profitably over range segments of various lengths and passenger load requirements, and its relatively short field capability permits operation from a large number of airports too small to accommodate 707 class aircraft. Many studies were made over the years in an effort to find a replacement for the ubiquitous Douglas DC-3; though with different range and payload characteristics and with different field length and cruising-speed capabilities, the 727 may be considered as the modern-day counterpart of the DC-3 which first appeared in 1935.

The aircraft was first produced as the 727-100, and a later stretched version designated the 727-200 was introduced. Of the 1500 aircraft so far ordered, over 1000 have been for the 727-200, which is the only version now in production. The aircraft is produced in both passenger and convertible cargo-passenger configurations. A photograph of a 727-200 in American Airlines markings is shown in figure 2.27, and the characteristics of this version of the aircraft are given in table 2.III.

The choice of three engines for the 727 was dictated by a compromise between cost and airport performance. For operation on hot days from airports located at high altitudes, the three-engine arrangement offered significantly better take-off and climb performance with one engine out than was practical for an efficient twin-engine design, but at a great deal lower cost than for a four-engine aircraft. An interesting discussion of this trade-off, as well as other aspects of the design and development of the 727, is contained in reference 2.11.

The most distinguishing recognition feature of the 727 is probably the mounting of the three engines which are located at the aft end of the fuselage. The inlet for the center engine is on top of the fuselage ahead of the vertical tail. The engine itself, however, is located in the fuselage in the same horizontal plane as the two outboard engines and exhausts through the tail end of the fuselage. Placement of the three engines in this way simplifies maintenance

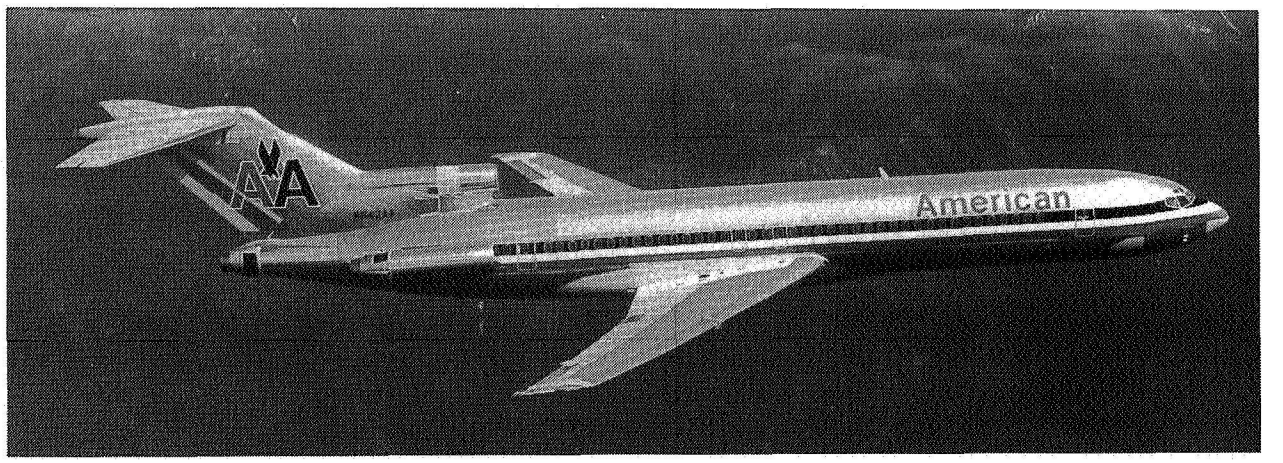


Figure 2.27.- Boeing 727-200 medium-range airliner.

and servicing and allows a high degree of commonality in ground support equipment. This arrangement, however, necessitates the use of an S-shaped duct to deliver air from the upper fuselage mounted inlet to the front face of the center engine. The design of inlet and duct for the center engine requires careful attention if unacceptable internal aerodynamic losses are to be avoided. The advantages and disadvantages of the aft-fuselage engine location have been discussed in section 2.2.2.3 in connection with the twin-engine Caravelle and apply equally well to a three-engine design like the 727.

Power for the 727-200 is supplied by Pratt & Whitney JT8D-17 engines of 16 000 lb thrust each. These engines, which have a bypass ratio of 1.06, have probably been used to power more jet transport aircraft than any other engine.

The 727-200 is seen from figure 2.27 to be a low wing design, and according to the data given in table 2.III, the wing planform geometry is similar to that of the 707. The engine arrangement results in a horizontal tail mounted at the tip of the vertical fin in a T-tail configuration. Some of the advantages and disadvantages of this arrangement are briefly discussed in section 2.1.2. The lateral and longitudinal control surfaces are of the same type, previously described, as those employed on the 707. In contrast to the 707, however, all of the controls on the 727 are hydraulically actuated. In order to allow operation from airports of medium size, the 727 is equipped with very powerful high-lift devices. The trailing edge of the wing has triple-slotted flaps of the type shown schematically in figure 2.11 and illustrated by photographs in figures 2.12 and 2.13. The leading edge has a slat on the outboard two-thirds of the span, and Krueger flaps on the inboard portion of the wing. With these high-lift devices, a stalling speed of 105 knots is obtained at the maximum landing weight of 160 000 lb. The main landing gear employs two wheel bogies instead of the four-wheel type used on the 707. The gear retracts inward into the wing at the root.

The Boeing 727-200 has a gross weight of 210 000 lb and, in full tourist configuration, can accommodate 189 passengers in a six-abreast arrangement. The upper fuselage diameter of the aircraft is the same as that of the 707 and

the shorter range Boeing 737. Thus, to the passenger, all three aircraft appear to have the same cabin size except for length. The 727-200 is capable of a maximum range with full fuel tanks of 3250 n. mi., and with maximum payload it has a range of 2900 n. mi. The cruising speeds of the 727 are comparable with those of the 707 and the DC-8.

2.2.3.2 McDonnell Douglas DC-9

The twin-engine McDonnell Douglas DC-9, in its many versions, generally has a smaller passenger capacity, shorter range, and shorter field length capability than the Boeing 727. It has been produced in five major versions and is now in operation on airlines all over the world. The five versions now in operation vary in (1) passenger capacity from 9 to 139, (2) length from 104 to 133 ft, and (3) gross weight from 80 000 to 122 000 lb. A sixth version, known as the DC-9-80, is now under development. This aircraft will have a gross weight of 141 000 lb, a length of 148 ft, and will be capable of carrying 172 tourist-class passengers. Perhaps more than any other aircraft type, the DC-9 represents an entire family of aircraft. The prototype of the DC-9 first flew in February 1965, and nearly 1000 examples have been produced to date. The type is still in production and seems destined to continue to roll off the production lines for many years to come.

The DC-9-30, one of the most numerous versions of the aircraft, is illustrated in figure 2.28 in the livery of the Royal Dutch Airlines, and some of



Figure 2.28.- McDonnell Douglas DC-9-30 twin-engine short-range airliner.

the characteristics of this aircraft are presented in table 2.III. The basic configuration of the aircraft is seen to be similar to that of the Caravelle in that the two engines are mounted in the aft-fuselage position. The T-tail arrangement employed by the DC-9, however, is different from that of the Caravelle. The engines which power the aircraft are the same basic Pratt & Whitney JT8D turbofans as are employed on the Boeing 727. For this particular version of the DC-9-30, the two engines have 15 500 lb of thrust each.

The sweptback wing of the DC-9 has a somewhat smaller sweep angle than that of the 727, and the cruising speeds given in table 2.III for the aircraft are correspondingly lower than those of the 727. As pointed out in the discussion of the Caravelle, the lower cruising speed of the DC-9 results from tailoring the characteristics of the aircraft to the relatively short-range segments for which it was intended. The high-lift system on all versions of the DC-9 consists in trailing-edge double-slotted flaps and leading-edge slats. The lateral control system utilizes inboard and outboard ailerons, with the outboard ailerons being used only at low speeds as in the DC-8. Speed brakes are mounted on the upper surface of the wing. With the exception of the elevators, all of the control surfaces are hydraulically actuated. Like the DC-8, the elevators are manually controlled through aerodynamic servo tabs.

The gross weight of the DC-9-30 is 109 000 lb, which is about half that of the 727-200, and the 115 tourist-class passengers are seated in a five-abreast configuration. The higher thrust loading and lower wing loading of the DC-9, as compared to the 727, result in a much lower take-off field length for the Douglas aircraft; the landing field lengths for the two aircraft, however, are about the same. The range at maximum payload for the DC-9-30 is 1576 n. mi., which is about one-half that of the Boeing 727. Clearly the DC-9 and 727 are intended for different types of airline-route structures and passenger-load requirements. Both highly successful aircraft complement each other in airline operation, and both seem destined to fly on together for many years.

2.2.3.3 Boeing 737

The twin-engine Boeing 737 was developed as a direct competitor of the McDonnell Douglas DC-9. The 737, however, did not fly until about two years after the DC-9, and although widely used and still in production, the 737 has never enjoyed the great popularity of the DC-9 series. The aircraft has been produced in two versions, the 737-100 and the 737-200. Except for 30 units, all of the aircraft produced have been the 737-200 version, which is a stretched, higher capacity, and heavier aircraft than the 737-100. The total number of orders for the 737 was 530 by mid-1977, and the type will no doubt remain in production for a number of years to come.

A Boeing 737-200 in the markings of United Airlines is shown in figure 2.29, and some of the characteristics of the aircraft are given in table 2.III. The two engines are mounted under the wings in a manner similar to that of the 707. The proximity of the engine nacelles to the under surface of the wing highlights the problem, previously referred to, incurred by the under-wing engine location as the size of the aircraft is reduced. The desire to avoid a high-mounted horizontal tail, and its possible stability problems, apparently was largely responsible for the choice of this engine location instead of the aft-fuselage mounted arrangement. As the photograph shows (fig. 2.29), the horizontal tail is located on the fuselage below the root of the vertical tail. The 737 uses basically the same Pratt & Whitney engines as those employed on the Boeing 727 and the McDonnell Douglas DC-9.

The fuselage of the 737 appears to be quite short and stubby. This appearance is caused by (1) the large upper-fuselage diameter which, as previously



Figure 2.29.- Boeing 737 twin-engine medium-range airliner. (Note under wing location of two engines.)

mentioned, is the same for the 707, 727, and 737 and (2) the shorter length of the 737 as compared to the other two aircraft. The higher fineness ratio fuselage and greater length of the DC-9 results from the use of a five-abreast seating arrangement and consequent smaller fuselage diameter. The short fuselage length of the 737, along with the wide lateral separation of the under-wing-mounted engines, are responsible for the large vertical tail on the aircraft.

The geometry of the wing of the 737 is very similar to that of the DC-9 as is shown by the data in table 2.III. The high-lift and control systems of the 737 are similar to those described for the 727.

An examination of the data in table 2.III for the 737 and the DC-9 shows a close similarity in the size, weight, and performance of the two aircraft. This similarity would be expected since they were designed for similar type operations. The major difference in performance of the two aircraft is the longer range of the 737 with full fuel tanks.

2.2.3.4 British Aircraft Corporation VC-10

Two, heavy, long-range, four-engine jet transports were developed in the 1960's. These were the British VC-10 developed by Vickers Armstrongs, which later was absorbed into the British Aircraft Corporation, and the Soviet Ilyushin Il-62. The two aircraft closely resemble each other in configuration and employ an engine arrangement different from any existing four-engine jet transport. On each aircraft, the four engines are mounted at the aft end of the fuselage, two on either side, in a four-engine adaptation of the twin aft-engine configuration pioneered by the Caravelle. Both aircraft weigh over 300 000 lb, and both were designed for long-range operation. The VC-10 is briefly described in the following paragraphs.

The VC-10 was developed in response to a requirement of the Overseas Division of British Airways, formerly the British Overseas Airways Corporation (BOAC), for use on its long-range routes to Africa, India, and Australia. The first flight took place in June 1962, and the type entered service with BOAC in April 1964. Production of the aircraft was terminated in 1974 after 54 units were manufactured.

A photograph of the VC-10 is presented in figure 2.30, and some of the characteristics of the aircraft are given in table 2.III. The four aft-mounted

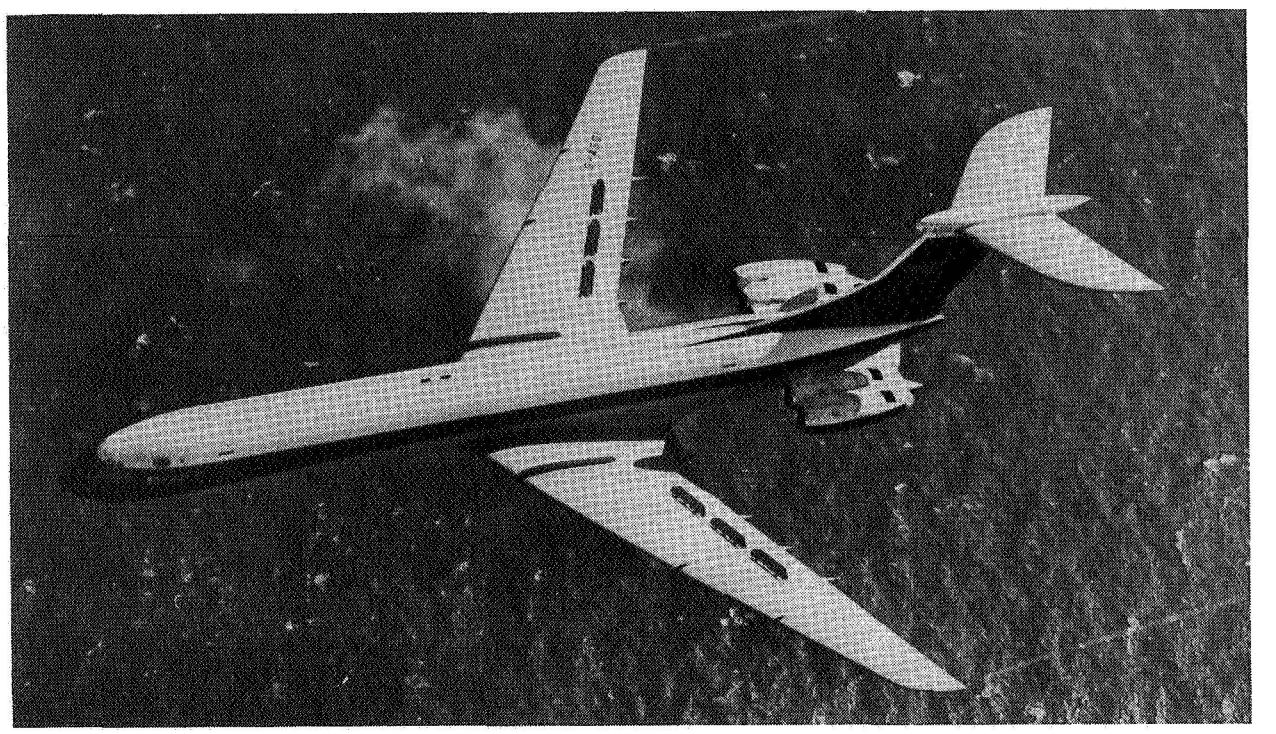


Figure 2.30.- British Aircraft Corporation VC-10 four-engine long-range transport. (Note engine location.)

engines are, of course, the most distinctive feature of the configuration. The power is supplied by Rolls-Royce Conway turbofan engines of 21 000 lb thrust each. These engines have a bypass ratio of 0.6 and employ a four-stage front-mounted fan.

Like all aircraft which employ the aft-engine arrangement, the wing of the VC-10 appears quite clean and uncluttered. The sweepback angle is 33.5°, and the aspect ratio is 7.3. Although the sweep angle is slightly less than that of the Boeing 707, the wing planform geometry employed on the two aircraft is rather similar. The high-lift system consists in trailing-edge Fowler flaps, which are similar to the double-slotted flap shown in figure 2.11 with the small middle element removed, and leading-edge slats. Three leading-edge fences are

employed on each wing; these fences can be seen in the photograph. Lateral control is provided by a combination of ailerons and spoilers. The spoilers are also used as air brakes and can be seen deployed for this purpose in figure 2.30. All control surfaces are hydraulically actuated.

A comparison of the performance of the VC-10 and the Boeing 707-320B, given in table 2.III, indicates that the maximum payload of the two aircraft is about the same, but the maximum range of the 707 is about a thousand miles longer than that of the VC-10 for the maximum payload condition. The cost-economical cruising speeds of the two aircraft are also about the same; however, the maximum cruising speed of the 707 is somewhat higher than that of the VC-10. Many of the airports served by British airways are located in tropical or subtropical areas which are characterized by high temperatures. Such temperatures increase the ground speed required for take-off and reduce the maximum thrust produced by the engines. The VC-10 was accordingly designed to cope with these difficult take-off conditions which, in some cases, were aggravated by airport elevations considerably above sea level. As a consequence, the take-off field length for "standard day" conditions, given in table 2.III is about 2000 ft shorter than that of the 707.

The VC-10 continues in operation on a number of airlines, and several are in use with the Royal Air Force. The economics of the aircraft, however, apparently could not compete successfully with those of the Boeing 707 and the McDonnell Douglas DC-8; hence, the VC-10 enjoyed a relatively limited-production run. The Soviet Il-62, counterpart of the VC-10, is still in production and is widely used on Aeroflot's long-range routes. A total of about 130 of these aircraft is estimated to have been constructed.

2.2.4 Wide-Body Transports

The wide-body jet transports represent the ultimate in subsonic jet transportation in the 1970's. Four families of aircraft make up the fleet of wide-body transports which are in operation on airlines throughout the world. These aircraft are the Boeing 747, the McDonnell Douglas DC-10, and the Lockheed L-1011, which are manufactured in the United States, and the Airbus A-300, which is produced by a consortium of European countries. All these aircraft entered service in the 1970's, all are still in production, and all are expected to continue in service for the foreseeable future. In addition to these aircraft, the Soviet Union has under development a large four-engine wide-body transport. This aircraft, the Ilyushin 86, first flew on December 22, 1976, and airline operations are expected to begin in 1980.

The use of the term "wide body" in describing these aircraft is derived from the interior arrangement of the passenger cabin. Consider first the arrangement of the cabin of a "narrow-body" transport such as the 707 or 727; the interior arrangement of a typical narrow-body aircraft is shown in figure 2.31. The cabin is divided into a small first-class compartment with four-abreast seating and a large tourist-class cabin with six-abreast seating. A single aisle runs the entire length of the cabin with three seats located on either side. For an aircraft of large passenger capacity, the fuselage of the narrow-body type tends to become very long which, in turn, may dictate a long, heavy landing gear

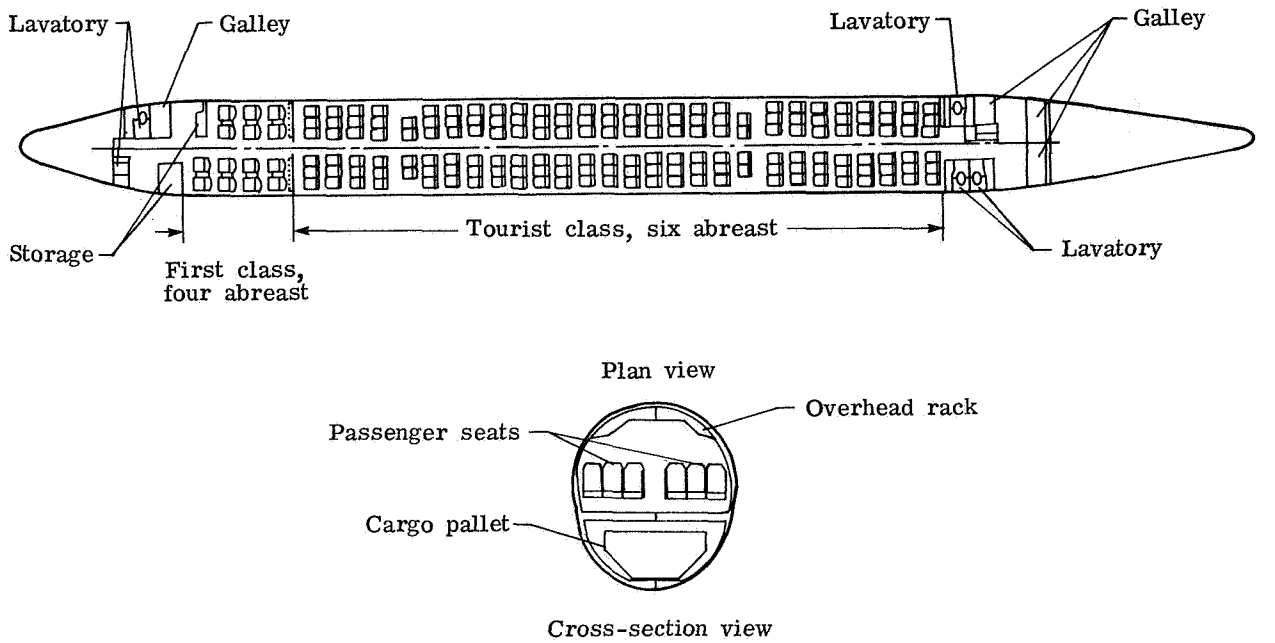


Figure 2.31.- Interior arrangement of narrow-body single-aisle jet transport aircraft.

in order to permit the desired rotation angle at take-off without scraping the rear end of the fuselage on the runway. The long aisle also causes lengthy delays in passenger loading and difficulty for the cabin attendants in serving meals and refreshments. The narrow seats and restricted longitudinal distance between them may also cause passenger discomfort, particularly for large passengers.

A schematic drawing of the interior cabin arrangement of a conceptual wide-body transport is shown in figure 2.32. The first-class cabin consists of a small four-abreast compartment in the forward part of the fuselage and a large seven-abreast tourist cabin. The tourist cabin is divided by two longitudinal aisles which run the length of the cabin. In the particular arrangement shown, two seats are located on either side of the aircraft next to the windows, and three seats are disposed about the center line of the cabin with an aisle on either side. Some wide-body aircraft are designed to accommodate as many as 10-abreast seats. High density versions of the Boeing 747, for example, may seat as many as 516 passengers in a 10-abreast arrangement.

For large capacity aircraft, the double-aisle arrangement offers easy passenger loading and simplifies the serving problem for the cabin attendants. The double-aisle design may also offer the passenger somewhat wider seats and a feeling of greater spaciousness. The landing-gear problem previously referred to is alleviated by the relatively short fuselage offered by the wide-body design for a given passenger capacity.

The large diameter of the fuselage of the wide-body aircraft is often cited as a source of increased skin friction drag. The bulky appearance of these air-

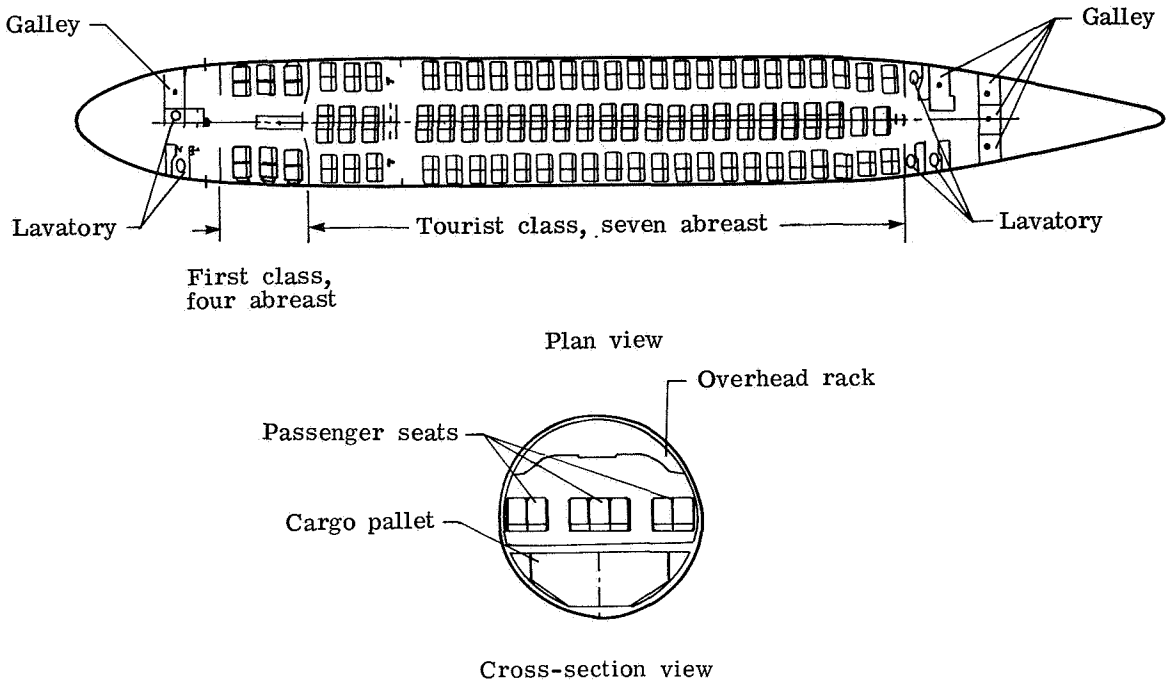


Figure 2.32.- Interior arrangement of wide-body double-aisle jet transport aircraft.

craft is no doubt responsible for this viewpoint. Actually, the ratio of wetted area to wing area for wide- and narrow-body aircraft of the same passenger capacity tends to be nearly the same because of the shorter length of the wide-body aircraft. The trade-offs between fuselage length and diameter can be assessed with the use of figure 3.11 of chapter 3.

The wide-body jet transports are characterized by two other distinguishing features. First, these aircraft are very large as compared with earlier jet transports. For example, one version of the Boeing 747, the largest of the wide-body aircraft, is certified at a maximum take-off gross weight in excess of 800 000 lb. Although the wide-body concept has so far been applied only to very large aircraft, new designs which are now being developed for use in the 1980's utilize the concept in aircraft only slightly larger in size than the 727.

A second distinguishing feature of the wide-body transports is the type of engines used to power them. All of the aircraft are powered by very large engines of high bypass ratio. Because of the high bypass ratio and high compressor compression pressure ratio (see section 2.1.1.1) of these engines, the values of their cruise specific fuel consumption are about 20 percent lower than earlier low bypass ratio engines such as the Pratt & Whitney JT3D. (See figs. 3.13 to 3.16 of chapter 3.) Another outstanding feature of these engines is their relatively low noise levels, as compared to earlier engines, even though the thrust produced by the new engines is significantly higher than values typical of the earlier ones. The low-noise-level characteristic of the high bypass ratio engines results from an improved understanding of the mecha-

nism of noise generation, as influenced by engine design, and through the use of new sound absorbing materials in various parts of the inlets and other flow passages. (See section 2.1.1.3.)

Three families of modern, large, high-bypass-ratio turbofan engines are available. These are the Pratt & Whitney JT9D, the General Electric CF6, and the Rolls-Royce RB.211. Each of these engines is produced in a number of variants with different capabilities. The maximum take-off thrust of the various versions of each family of engines lies in the range from 45 000 to 55 000 lb. The bypass ratios of the engines are 5:1 for the Pratt & Whitney JT9D, 5.9:1 and 4.4:1 for the General Electric CF6, and 4.4:1 for the Rolls-Royce RB.211. As indicated, the CF6 engine is available with two different bypass ratios. The compressor ratios of the different engines fall in the range from 24:1 to 30:1. Detailed information of the various versions of the engines may be found in references 2.5 and 2.21.

In other respects, the wide-body aircraft, as compared to earlier jet transports, have only evolutionally technical refinements. The widespread use of sophisticated, high-speed computational equipment has resulted in more refined aerodynamic and structural design and in improved machine control in manufacturing. As a result of more sophisticated analysis techniques and new developments in transonic aerodynamics, some improvements may be found in wing and airfoil design. Basically, however, the aerodynamic design of the wide-body aircraft is similar to the preceding generation of aircraft. Again, in the area of structural design, no radical innovations are to be found. All of the aircraft use fully powered flight control systems, and all employ sophisticated autopilots and other onboard systems.

The combination of large passenger capacity, more efficient and quieter engines, and more sophisticated detail design has resulted in a series of transport aircraft which are safe, reliable, environmentally acceptable, and, from the airline viewpoint, profitable; from the passenger viewpoint, the aircraft are fast, convenient, and relatively comfortable and offer reasonable fares.

As previously discussed, most jet transport aircraft actually consist of a series of aircraft of varying characteristics which evolve from a single basic design. Each variant of the series has characteristics which are intended to adapt the aircraft to a particular set of operating requirements. The wide-body transports also follow this trend, and the generic aircraft type of each manufacturer actually represents an entire family of aircraft. In the following paragraphs, a brief description of a representative model of the Boeing 747, the McDonnell Douglas DC-10, and the Lockheed L-1011 will be given. Descriptions of the various versions of the different aircraft may be found in references 2.5 and 2.15.

2.2.4.1 Boeing 747

The first of the wide-body turbofan powered transports to enter airline service was the Boeing 747. Design work on this aircraft was initiated in the 1960's, and the first details were announced in April 1966. Simultaneously, Pan American World Airways announced orders for 25 of the new aircraft. The

first flight took place in February 1969, and certification was complete by December of that year. The first passengers were carried on a New York to London flight on January 22, 1970. The 747 aircraft is utilized by 32 airline operators throughout the world. Over 350 units had been produced through 1978, and the type will likely remain in production for the foreseeable future.

A side view of a Boeing 747 in the livery of Pan American World Airways is shown in figure 2.33, and a front view of the aircraft in the landing configuration may be seen in figure 2.34. Some of the characteristics of the Boeing 747-200B are given in table 2.III.

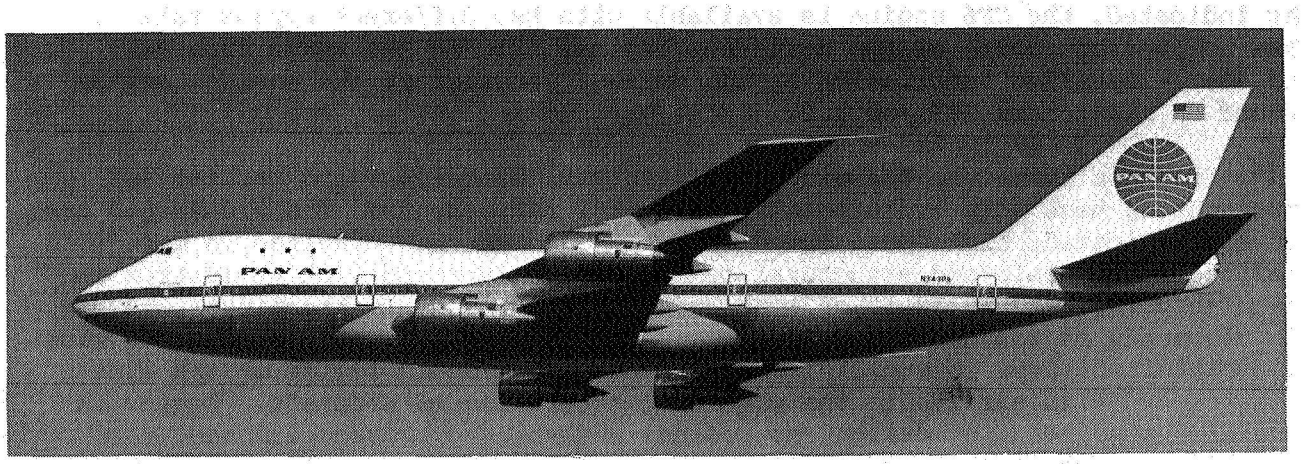


Figure 2.33.- Boeing 747 wide-body transport.



Figure 2.34.- Boeing 747 in landing configuration. (Note four-post main landing gear.)

The appearance of the four-engine 747 is very similar to that of its well-known ancestor, the Boeing 707. In addition to its large size, however, the 747 has two distinguishing features. First, the passenger cabin extends all the way to the forward end of the fuselage. The flight deck, with a small

cabin behind it, is mounted on a second level and is reached by a circular stairway from the main cabin. This interior arrangement results in a distinctive hump in the external appearance of the top, forward end of the fuselage. A second distinguishing feature of the 747 is the main landing gear which is unique for a passenger-carrying aircraft. The main gear consists of four main struts, or posts, to which are attached four wheel bogies. The two rear struts are mounted on the fuselage near the trailing edge of the wing, and retract forward into the fuselage. The other two struts are mounted in the wing, farther forward, and retract inward into the wing. The four post main gear is required in order to distribute properly the large weight of the aircraft on the runway. The photograph of the aircraft in the landing configuration, shown in figure 2.34, clearly shows the extended four strut main gear, as well as the nose gear which retracts forward into the fuselage.

The engines first offered on the 747 were the Pratt & Whitney JT9D turbofans. In addition to these engines, the aircraft is now certified with the General Electric CF6 and the Rolls-Royce RB.211 turbofans. The 747-200B, for which data are given in table 2.III, is powered with four JT9D-7Q engines of 53 000 lb thrust each.

The aerodynamic configuration of the 747 is very similar to that of the 707. The wing of the 747 has slightly more sweepback than that of the 707 and is of somewhat lower aspect ratio. An improved airfoil design is also incorporated in the wing of the 747. The maximum lift-drag ratio of the aircraft, $(L/D)_{max}$, is estimated to be about 17.7, as compared with a value somewhat over 19 for the 707. The lower $(L/D)_{max}$ of the 747, as compared to the 707, results from a larger value of the ratio of wetted area to wing area on the 747.

The high-lift system employed on the 747 is typical of Boeing practice and consists of trailing-edge triple-slotted flaps, similar to those employed on the 727, and leading-edge flaps. The lateral control system utilizes a combination of spoilers together with inboard and outboard ailerons. The spoilers are also used for lift and drag control when deployed symmetrically. The horizontal tail is located in the conventional low position at the rear of the fuselage. Longitudinal control is provided by an elevator and adjustable stabilizer trim system. No trim tabs are employed. All controls are fully powered.

The very large size of the Boeing 747 is the most striking feature of the aircraft. The gross weight of the 747-200B is seen from table 2.III to be 823 000 lb, more than that of any other aircraft ever built. The Lockheed C-5A military cargo transport is the next largest aircraft at a weight of 769 000 lb. The 747-200B can carry a maximum payload of 154 800 lb for a distance of 5190 n. mi., and has a cost-economical cruising speed of 490 knots (Mach number of 0.85) at an altitude of approximately 35 000 ft. With a maximum fuel load and a reduced payload of 100 900 lb, the range is 6640 n. mi. In a maximum capacity configuration, the aircraft can carry 516 passengers with 10-abreast seating. In this arrangement, four seats are placed in the middle of the aircraft between the two aisles, and three seats are located against either side of the cabin. Many other seating arrangements for a smaller passenger load are used in the aircraft. The particular seating arrangement utilized is dictated by the airline using the aircraft and is based on the passenger density anticipated on the various routes served by the aircraft.

The Boeing 747 is available in many versions adapted to various airline needs and must be considered one of the outstanding commercial aircraft in the world today.

2.2.4.2 Lockheed L-1011 and McDonnell Douglas DC-10

The Lockheed L-1011 and the McDonnell Douglas DC-10 are wide-body transports in a weight class which lies between that of the 707 and the very heavy 747. Both aircraft are powered by three high-bypass-ratio turbofan engines located in a new configuration arrangement; one engine is mounted under each wing, and the third engine is mounted at the rear of the aircraft. Each of these aircraft was initially designed to an airline requirement for a high capacity transport with transcontinental range, and growth versions of each are available with intercontinental capability. Initial flights of both aircraft occurred in 1970. An early version of the DC-10 entered airline operation in 1971, and the L-1011 began service in 1972. Both aircraft are in wide use throughout the world and will likely remain in production for many years.

A photograph of the Lockheed L-1011, also known as the TriStar, is shown in figure 2.35, and the McDonnell Douglas DC-10 is depicted in figure 2.36. Some of the characteristics of the two aircraft are given in table 2.III. The three-engine configuration employed on the two aircraft is clearly shown in the photographs. The arrangement employed on these aircraft offers an advantage in aircraft balance, as compared to that in which all three engines are mounted at the rear of the fuselage (Boeing 727, for example) since two of the engines are located near the aircraft center of gravity. Placement of two of the engines under the wing also allows the horizontal tail to be mounted in the highly desirable low position, as contrasted to the T-tail arrangement. The large lateral distance between the wing-mounted engines, however, causes large yawing moments following a power loss of one of these engines, as compared to a power loss of one engine in the arrangement in which all engines are mounted at the rear of the aircraft.



Figure 2.35.- Lockheed L-1011 TriStar three-engine wide-body transport. (Note arrangement of three engines.)

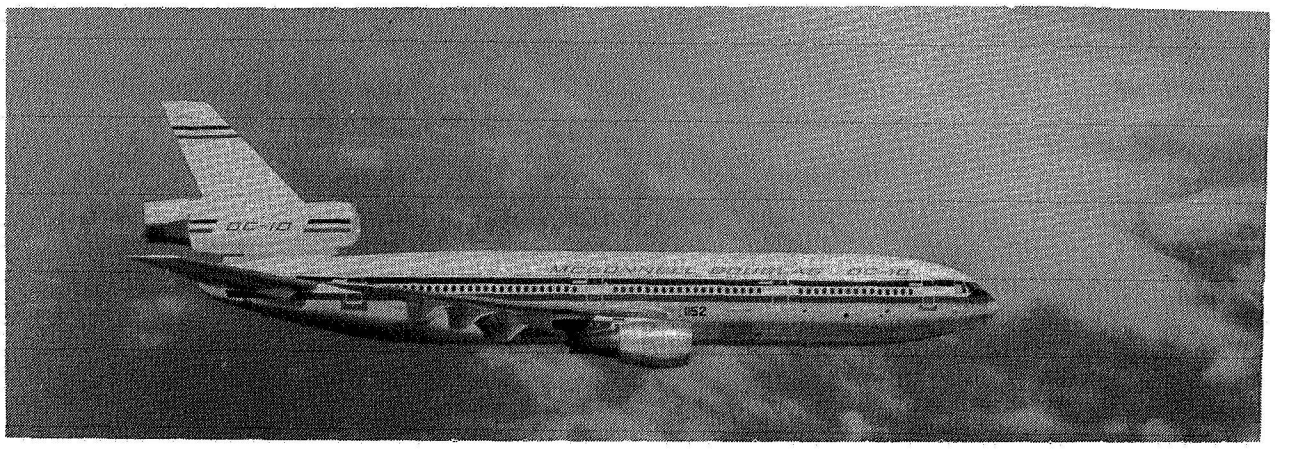


Figure 2.36.- McDonnell Douglas DC-10 three-engine wide-body transport. (Compare mounting of center engine with that of Lockheed L-1011.)

The method of mounting the rear engine is seen to be quite different on the L-1011 and the DC-10. The L-1011 utilizes a mounting arrangement similar to that of the Boeing 727. The center engine is mounted in the aft end of the fuselage and is connected through an S-shaped duct to the large inlet mounted on top of the fuselage. In contrast, the center engine of the DC-10, including inlet and exhaust nozzle, is integrated with the fin above the fuselage. The improved engine efficiency resulting from this straight inlet-engine-nozzle configuration, as compared to the S-shaped duct arrangement, was thought to more than offset the structural complexity (and probable weight increase) of integrating the engine with the fin. The high degree of success enjoyed by the two aircraft, however, suggests that both methods of engine installation can be made to operate successfully.

The Lockheed L-1011-200 is powered with three Rolls-Royce RB.211-524 engines of 48 000 lb thrust each. The McDonnell Douglas DC-10-30 is powered by three General Electric CF6-50C1 engines of 52 500 lb thrust each. This aircraft is also available with a version of the Pratt & Whitney JT9D engines.

The main landing gear of the L-1011 has two struts to which are attached four wheel bogies. Early versions of the DC-10 employed a similar arrangement. The heavier DC-10-30, however, employs a third strut, equipped with a two wheel bogie mounted on the fuselage center line between the other two main landing-gear struts. This arrangement helps to distribute the weight of the aircraft on the runway and thus keeps the runway bearing stress within acceptable limits.

The aerodynamic design of both of the three-engine jet transports is entirely conventional. The wings of both aircraft have about 35° of sweepback with aspect ratios in the range from 7.0 to 7.5 and feature transonic airfoils of advanced design. The wings have double-slotted trailing-edge flaps and leading-edge slats. The trailing-edge flap of the DC-10 is shown in figure 2.15. Lateral control is provided by a combination of ailerons and spoilers. The spoilers are also used to control lift and drag when deployed

symmetrically. Longitudinal control on the L-1011 is provided by a variable incidence stabilizer to which the elevator is mechanically linked. The DC-10 employs separately actuated elevators and stabilizers. Neither aircraft employs longitudinal trim tabs. The maximum lift-drag ratio of the two aircraft is estimated to lie in the range between 17 and 17.5.

The data in table 2.III indicate that the L-1011-200 and the DC-10-30 are very large aircraft. For example, at a gross weight of 468 000 lb and with a maximum payload of 74 200 lb, the L-1011-200 is capable of flying for a distance of 4247 n. mi. With a maximum fuel load and a reduced payload of 42 827 lb, the range is 5395 n. mi. The aircraft is capable of carrying 400 economy-class passengers in a 10-abreast, double-aisle configuration. An interesting feature of the interior design of the L-1011 is the location of the galleys below the passenger deck; food service is provided to the passenger cabin by means of elevators.

The economical cruising speed of the L-1011 is 493 knots at 31 000 ft which corresponds to a Mach number of 0.84. The take-off field length of 8070 ft is relatively short compared to 10 370 ft for the DC-10-30 and 10 200 ft for the 747. According to the data in table 2.III, the values of gross weight, payload weight, and range of the DC-10-30 are significantly larger than the corresponding values for the L-1011-200. A comparison of the values of the wing loading and thrust loading of the two aircraft clearly shows why the take-off distance of the DC-10-30 is greater than that of the L-1011-200. Methods for rapid estimation of the take-off distance are discussed in chapter 3. The cost-economical cruising speeds of the two aircraft are comparable.

The various versions of the DC-10 and the L-1011, along with the 747, form an important part of the world transportation system which may be expected to continue for many years. As airline needs evolve over the years, new and improved versions of these aircraft can be anticipated.

2.2.5 Dedicated Cargo Transports

The jet transport has so far been discussed only in the context of a passenger-carrying aircraft, and those described have indeed been configured with passenger transport as a primary design consideration. Most modern jet airliners, however, have some type of cargo-carrying capability. Even those aircraft which are configured primarily for passengers usually carry a limited amount of cargo, along with baggage, in the hold below the passenger deck. This cargo space is illustrated by the fuselage cross-section views in figures 2.31 and 2.32. Many jet transports are also available in convertible form and may be changed quickly from a passenger to an all-cargo configuration. In this configuration, the passenger seats are removed and cargo is carried in the space usually occupied by the passengers, as well as in the hold. The floor of the passenger cabin on such aircraft is usually strengthened to allow for the higher unit floor loadings likely to be encountered with cargo rather than with passengers. A large cargo door is also provided on these convertible passenger-cargo aircraft. Some jet transports are available in dedicated cargo versions. In addition to special cargo doors and strengthened floors, these aircraft have no

facilities for attending to the needs of passengers, and may even be constructed with no cabin windows. A crew rest compartment is sometimes located immediately behind the flight deck. A Boeing 747 jet freighter is shown in figure 2.37. Note the way in which the nose of the aircraft opens with a visor type door to allow loading large cargo containers.



Figure 2.37.- Cargo being loaded through nose door of Boeing 747 freighter.

Another class of cargo aircraft, designed to meet the special needs of certain types of military operations, has evolved since the end of World War II. These aircraft are required to transport various types of military cargo such as trucks, tanks, jeeps, and artillery pieces, as well as troops. The size and shape of the fuselage is dictated by the number and type of vehicles to be carried, and some important aspects of the overall configuration are strongly influenced by the requirements for cargo handling and loading. One of the best-known military cargo aircraft is the turboprop powered Lockheed C-130 which is shown in figure 5.34 of chapter 5; this aircraft is in use by the military services of over 20 countries throughout the world. The Soviet military services

also operate turboprop powered cargo aircraft of the same configuration concept as the C-130. One of these, the Antonov An-22, is very large with a gross weight of about 550 000 lb.

Two jet-powered cargo aircraft which employ many of the configuration features embodied in the C-130 design have been developed in the United States. These are the Lockheed C-141 StarLifter, and the Lockheed C-5A Galaxy. The C-141 has a gross weight of about 317 000 lb, which places it in the same size class as the Boeing 707-320B, and first flew in December 1963. The very large C-5A has a gross weight of 769 000 lb, in the same weight class as the Boeing 747, and first flew in 1968. The C-141 and the C-5A are similar in appearance, but the difference in size is very obvious when the aircraft are seen side by side. The Soviet Ilyushin Il-76 military transport is similar in appearance to the two Lockheed aircraft and has a gross weight of 350 000 lb. The first flight of the Il-76 took place in 1971. Of these dedicated military cargo transports, the Lockheed C-5A is briefly described in the following paragraphs.

In the early 1960's, several aircraft companies began design studies of a heavy logistic jet transport intended to replace and augment the capabilities of the aging Douglas C-133, and complement the existing fleet of C-141 jet-powered transports. The aircraft was intended to deliver payloads in the range of 100 000 to 200 000 lb over intercontinental distances and be able to operate from semiprepared runways. Following a design competition, Boeing, Douglas, and Lockheed were given contracts for further development of their designs. Concurrently, General Electric and Pratt & Whitney were given design contracts for high bypass ratio, turbofan engines to power the new aircraft. The weight of the aircraft was expected to be in the 700 000-lb class, and the thrust level required of the new engines was about 40 000 lb. The selection of the General Electric Company to develop the engine was announced in August 1965, and in October of that same year, the Lockheed Aircraft Corporation was selected to develop the aircraft. First flight of the C-5A took place on June 30, 1968, and the last of a fleet of 81 aircraft was delivered to the U.S. Air Force in May of 1973. An interesting account of the engineering development of the C-5A is given in reference 2.18. Photographs showing several views of the aircraft are contained in figures 2.38 to 2.41.

The C-5A is a high-wing monoplane with the wing mounted at the top of the fuselage. The aircraft is equipped with four engines mounted in pods which are attached to the lower surface of the wings in much the same fashion as that employed on the 707 and DC-8 aircraft. The General Electric TF-39 engines which power the aircraft develop a take-off thrust of 41 000 lb each and have a bypass ratio of 8.0. The gas generator of this engine serves as the basis of the core of the General Electric CF6 commercial engine which has been previously discussed.

In order to minimize weight and complexity, the landing gear is retracted into blisters located on either side of the fuselage, rather than into the high mounted wing. The aspect ratio 7.8 wing is swept 25^{o} at the quarter chord and is equipped with Fowler type single-slotted flaps and leading-edge slats. Lateral control is provided through a combination of ailerons and spoilers. The ailerons are also used to reduce wing bending moments when the aircraft undergoes normal acceleration as a result of maneuvers or gusts. In this technique,

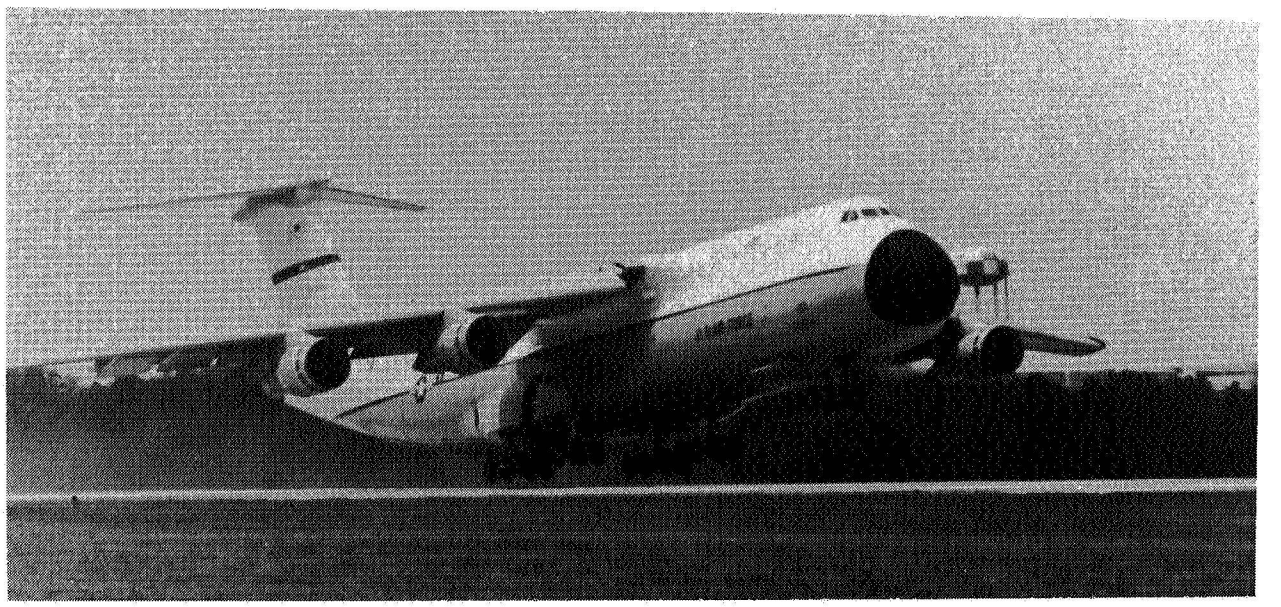


Figure 2.38.- Lockheed C-5A cargo transport.



Figure 2.39.- Lockheed C-5A in approach configuration. (Note 28-wheel landing gear and Fowler flaps.)

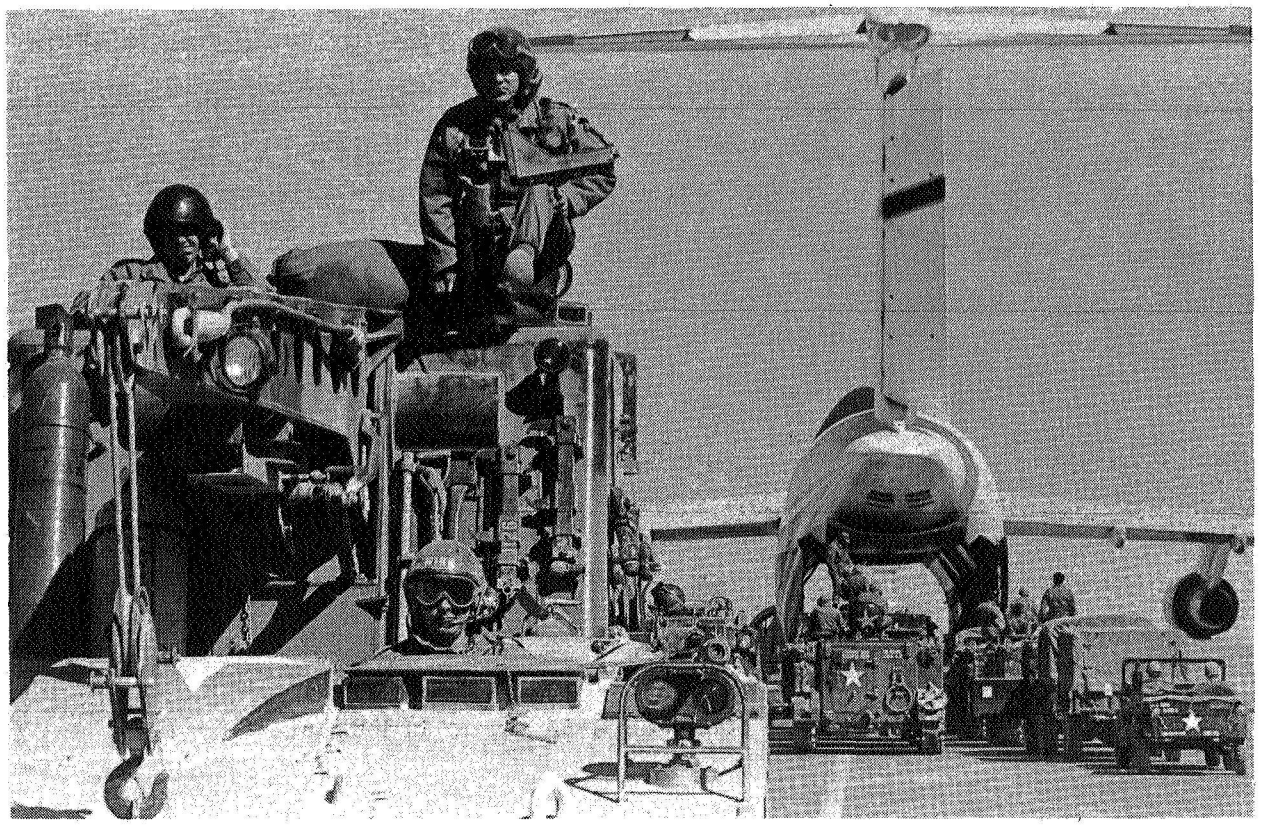


Figure 2.40.- Rear view illustrating fore and aft loading capability of C-5A.

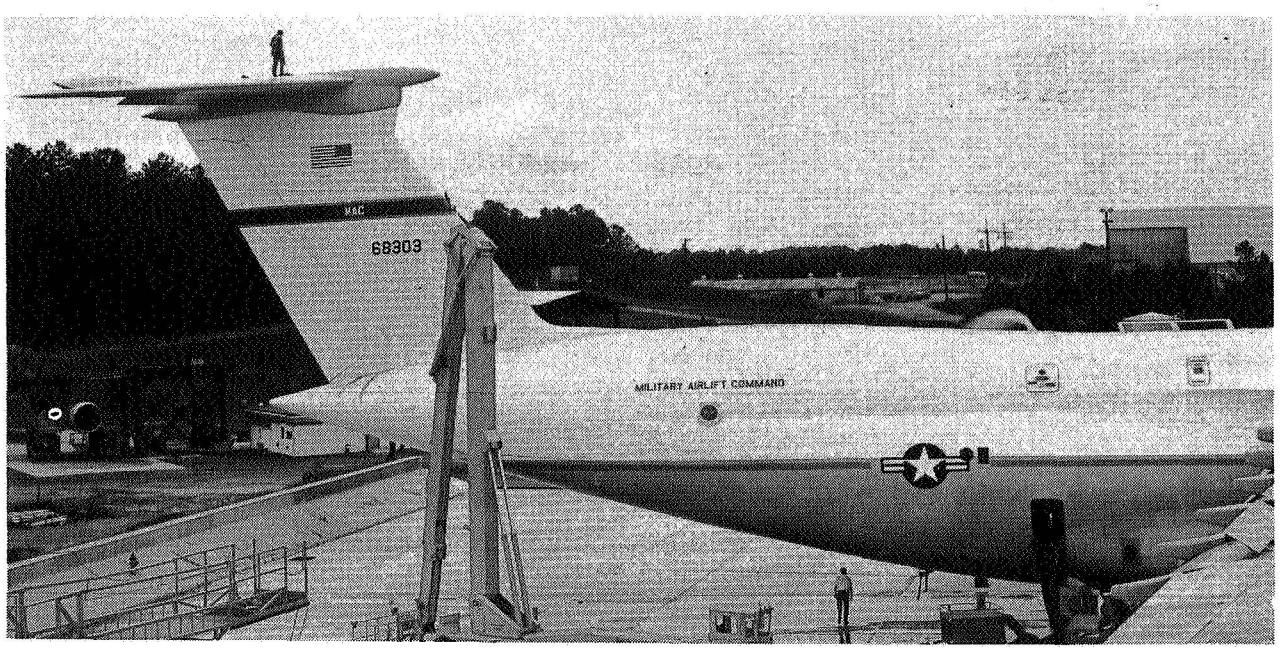


Figure 2.41.- Photograph indicating large size of C-5A by man standing on horizontal tail of aircraft.

called active load distribution control system (ALDCS), the ailerons are symmetrically deflected in response to signals received from accelerometers located in various parts of the aircraft. For a positive acceleration, the ailerons are deflected upward which shifts the load inboard; thus, the wing-root bending moments are reduced. This technique is expected to find application in many new aircraft designs.

The empennage consists in a horizontal tail mounted in the T-position at the top of the swept vertical fin. According to reference 2.18, this arrangement, rather than a low-tail arrangement, results in significant weight savings. (See section 2.1.2.2.) The horizontal tail consists in elevators and an adjustable stabilizer. No trim tabs are provided.

The high-wing position employed on the C-5A is advantageous for a cargo aircraft because it allows trucks and other types of equipment to move beneath the wing, and the bottom of the fuselage can be brought close to the ground for easy cargo loading without causing interference with the engines. A rear door, which serves as a loading ramp when lowered, is deployed from the bottom of the upswept, aft portion of the fuselage. The proximity of the bottom of the fuselage to the ground results in a ramp with only a small inclination to the ground. Vehicles can accordingly be readily driven or pushed into the aircraft. The rear door is also used for aerial deployment of vehicles and equipment by parachute. The fuselage is provided with a forward loading door in the nose of the aircraft. The door is like a visor and lifts up and over the flight deck (somewhat like that shown in figure 2.37 for the Boeing 747 freighter). The entire cross section of the cargo compartment is exposed when the nose visor is raised. Figure 2.40 shows a rear view of the C-5A with both forward and aft doors open and various types of equipment ready for loading.

The length of the C-5A cargo deck, excluding the loading ramps, is about 121 ft, the maximum width is 19 ft, and the height of the cargo compartment is 13.5 ft. In addition to the lower cargo compartment, the fuselage also has an upper deck which is divided into three sections. The forward section contains the flight deck and is followed by a rest area for 15 people. This section is usually occupied by relief crews. The flight crew of five persons consists of the pilot, copilot, flight engineer, navigator and load master. Behind the rest area is a passenger compartment which will accommodate 75 fully equipped troops. The lower cargo compartment may also be utilized for troop transport; for this purpose, the aircraft can carry 270 soldiers. The lower cargo compartment and the upper deck are fully pressurized.

The capability for operation from semiprepared runways was one of the specified design requirements of the C-5A cargo transport. The achievement of a relatively low unit loading on the runway surface was therefore necessary. In order to meet this design requirement, the main landing gear is equipped with 24 wheels and the nose gear, with 4 wheels. The main gear consists of four struts to which are attached six wheel bogies. Each bogie has a two-wheel truck forward of the strut and two two-wheel trucks located side by side behind the strut. In order to provide further flexibility in rapidly adapting the aircraft to various runway bearing capabilities, the pressure in the tires can either be increased or decreased while the aircraft is in flight. The landing-gear bogies may be set at an angle of as much as $\pm 20^{\circ}$ from the center line of the

aircraft to simplify take-off and landing operations in various cross-wind conditions. Ground maneuverability is enhanced by allowing the front two bogies to castor freely while the aircraft is being taxied. The landing gear is also provided with a kneeling capability to lower the floor of the main deck for ease of transferring cargo from a truck to the aircraft. With the landing gear in the kneeling position, the lower deck is just over 4 ft from the ground at the front loading door and just over 5 ft from the ground at the rear door. The highly versatile landing gear may be seen in the photographs in figures 2.38 and 2.39.

With a gross weight of 769 000 lb, the C-5A is a very large aircraft by any standard. The data in table 2.III show that the C-5A, in comparison with the 747-200B, has a larger wing span and area and a greater fuselage length. The 747 is, however, somewhat heavier than the C-5A. An indication of the large size of the aircraft can be obtained from figure 2.41 which shows a man standing on the horizontal tail. The aircraft is capable of performing missions with various combinations of range and payload. Two mission profiles given in table 2.III indicate a range of 3256 n. mi. with a payload of 220 967 lb and 5670 n. mi. with a payload of 112 600 lb. The aircraft has a maximum cruising speed of 470 knots at an altitude of 25 000 ft. This corresponds to a Mach number of 0.78. The stalling speed at maximum landing weight is 104 knots.

2.2.6 Business Jets

The venerable Curtiss Jenny was probably the first aircraft in the United States used for business purposes. In the late 1920's and early 1930's, higher performance aircraft were adapted to business use. These aircraft were of open-cockpit or cabin design and usually had only a single engine, although several Ford trimotor airliners were converted for business use. The long-lived twin-engine Beech model 18, first flown in 1936, was probably the first aircraft designed specifically for business use. Following World War II, the Douglas DC-3 was extensively involved in corporate flying; in the 1950's, a number of smaller aircraft equipped with two reciprocating engines were offered for this use. A large number and variety of such aircraft are still on the market today (See section 5.5.2 of chapter 5.) The first jet-powered aircraft especially designed for corporate use began to appear in the late 1950's and early 1960's. At this point in time, 1980, no fewer than 12 companies are offering about 25 different models of jet-powered business aircraft. Some of the design features and characteristics of business jet aircraft are discussed in the next section, after which six different aircraft are illustrated and described briefly.

2.2.6.1 Configuration Features

Most business jet aircraft are of low wing design and have engines mounted at the aft end of the fuselage. Except for one three-engine and one four-engine design, all of them are powered with two engines. Both pure jets and turbofan engines are used. Most of the modern aircraft produced today have turbofan engines; some of these are repowered versions of aircraft which originally

ppeared with turbojet engines. The wings of most of the aircraft have a modest mount of sweepback although one business jet, to be described later, has a weptforward wing.

Like any aircraft, the size and performance of business jets vary with the unction for which the aircraft has been designed. Aircraft are available which ary in gross weight from about 11 000 to 65 000 lb. Cruising speeds lie in he range from 0.7 to 0.85 Mach number. Ranges vary from intercontinental alues to as low as 1000 n. mi. Most of the new aircraft being produced have t least nonstop transcontinental capability. The number of passengers which an be accommodated, even on aircraft of the same design, varies widely depending on the interior cabin arrangements. Aircraft can be found with the capability of carrying anywhere from 5 to 15 passengers.

Most corporate aircraft are expected to operate from a wide variety of airorts. The landing and take-off field lengths required for these aircraft are ccordingly shorter than those for the larger transport aircraft. The desired anding and take-off field lengths of business jets, as compared with transport ircraft, are usually obtained through a combination of low wing loading and igh thrust-to-weight ratio, together with a relatively simple high-lift system. . simple slotted trailing-edge flap frequently constitutes the entire high-lift ystem.

The small size of many business jets imposes certain design constraints ot encountered in large transport aircraft. One dimension which cannot be caled as the size of an aircraft is reduced is the size of the human body which ccupies the cabin. This essentially invariant dimension is usually a predominant factor in determining the fuselage diameter. A small fuselage diameter is lesirable in order to reduce weight and to maintain as low a value of the ratio f wetted area to wing area as possible. Accordingly, only the very large business jets have a cabin diameter sufficiently large to accommodate a person standng in an upright position. The drawings in figure 2.42 show the cabin size f three business aircraft relative to a 6-ft-high person. Some of the smaller ircraft are essentially sit-down vehicles in much the same sense as an automoile. Some feature a cabin diameter which permits limited mobility in a stooped osture. A cabin floor free of obstructions is a desirable feature intended to educe the possibility of a passenger tripping or falling. Such a floor design equires that the wing carry-through structure be either beneath or behind the abin. There are disadvantages to both arrangements. An increase in fuselage liameter results from passing the wing structure entirely beneath the floor; hereas, placing the wing behind the cabin may result in a center of gravity hich is farther forward than desired. Placement of the wing carry-through tructure behind the cabin combined with the use of a sweptforward wing offers means for overcoming the disadvantages of the other two methods of achieving n unobstructed cabin floor. The German Hansa jet, described later, utilized his design concept.

Two other size-related design factors are worth mentioning. The short disance between the ground and the bottom of the wing precludes the use of the nder-wing-engine mounting and is largely responsible for the aft-engine locaion which is employed on all current business jet aircraft. Two alternative

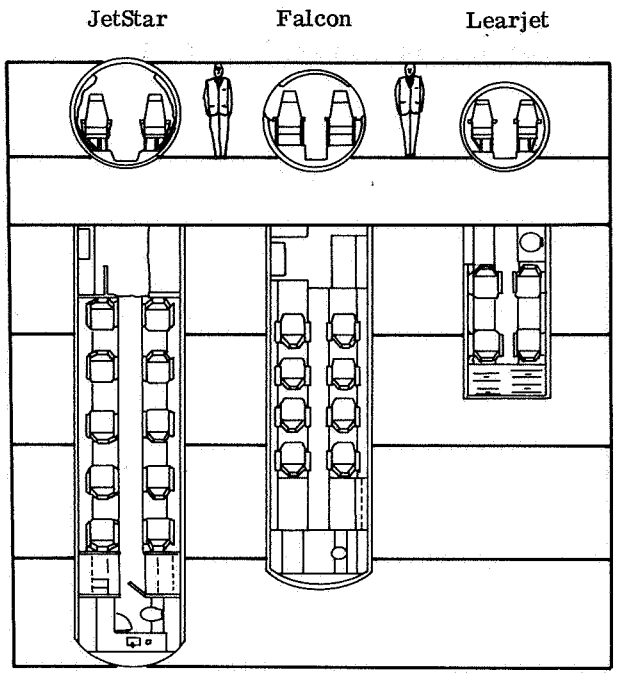


Figure 2.42.- Cabin interiors of three business jet aircraft.

arrangements suggest themselves: (1) a high wing location with engines mounte beneath the wing or (2) a low wing configuration in which the engines are mounted on top of the wing. So far, neither of these arrangements has been utilized on a business jet, although one small transport aircraft (the VFW Fokker 614) has been produced which employs the over-wing-engine arrangement. Finally, the small size of the business jet results in a Reynolds number which is much lower than those characteristic of transport aircraft. That portion of the drag coefficient attributable to skin friction is accordingly higher fo the small aircraft. For example, if all the dimensions of a small business je are assumed to be one-fifth those of a large jumbo jet, the skin-friction drag coefficient of the small aircraft will be about 30 percent higher than that of the jumbo aircraft. The $(L/D)_{max}$ characteristics of the smaller aircraft, therefore, tend to be lower than those of the large transports.

2.2.6.2 Representative Aircraft Types

Six representative business jet aircraft are briefly described in the fol lowing paragraphs. Photographs of the aircraft are presented in figures 2.43 to 2.48, and some of their characteristics are given in table 2.IV. Informati on the many different models of business jet aircraft now available may be found in references such as reference 2.20 and the various issues of Jane's Al the World's Aircraft.

Lockheed JetStar

The first of the dedicated business jets, the Lockheed JetStar, completed its maiden flight in September 1957. Initial development of the aircraft was undertaken as a private venture. The first two prototypes were equipped with two Bristol Siddeley Orpheus turbojet engines. The aircraft was later entered in a U.S. Air Force competition for a small four-engine utility and personal transport. This version was equipped with four Pratt & Whitney JT-12-8 turbojet engines of 3300 lb thrust each. The JetStar won the Air Force competition and in that service is known as the C-140. A photograph of the aircraft is shown in figure 2.43. Production of the original JetStar ended in 1973; however, an improved version, known as the JetStar II, powered with four Garrett TFE 731 turbofan engines of 3700 lb thrust each was offered by Lockheed in 1976, production ending late in 1978. To date, more than 160 JetStar aircraft have been built.



Figure 2.43.- Four-engine Lockheed JetStar.

The JetStar, with a gross weight of 42 500 lb, is one of the heaviest of the business jets. A typical cabin configuration accommodates 8 to 10 passengers. A range of 2100 n. mi. is possible with a payload of 3500 lb. Take-off and landing field lengths are 4700 and 3550 ft, respectively. These field lengths are based on climb and descent over a 50-ft obstacle and are not to be compared with the FAR field lengths given in table 2.III for transport aircraft. Cost-economical cruising speed is 453 knots, which corresponds to a Mach number of about 0.79.

Unlike most business jet aircraft, the high-lift system on the JetStar is relatively complicated and consists in a double-slotted trailing-edge flap and a leading-edge flap. Lateral control is provided by ailerons without the assis-

tance of spoilers, and a speed brake is located on the underside of the fuselage The longitudinal trim system is unusual in that the stabilizer is fixed to the fin which pivots to change the stabilizer angle. An indication of this pivoting action is provided in figure 2.43 by the apparently unpainted portion of the lower part of the fin. All controls are power operated.

Gates Learjet 24B

The prototype Learjet model 23 made its first flight in October of 1963 and may be considered as the progenitor of a whole family of Gates Learjet business aircraft of differing gross weight, passenger capacity, and range. All of the aircraft, however, are of the same basic configuration. The photograph in figure 2.44 and the data in table 2.IV are for the Gates Learjet 24B. Deliver-

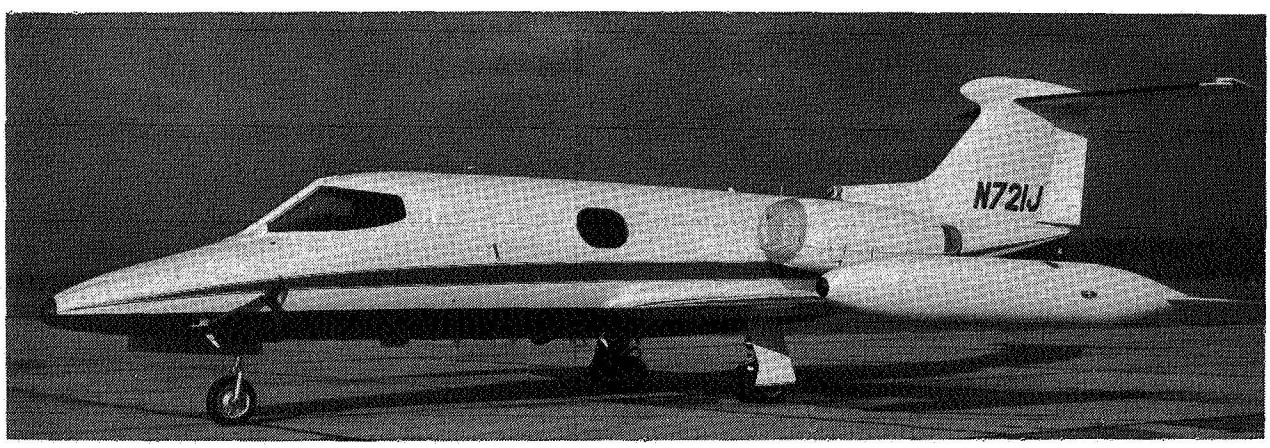


Figure 2.44.- Gates Learjet 24B.

ies of the model 24 began in 1966, and the model 24B was certified in December 1968. Over 700 aircraft of all versions had been built by the end of 1977 and several models were still in production at that time.

The Learjet model 24B is one of the smaller business jets with a gross weight of 13 300 lb. The cabin is often configured to accommodate a maximum of six passengers. The aircraft has a range of 1105 n. mi. with a maximum payload of 1910 lb. With full fuel tanks and a reduced payload, the maximum range achievable is 1775 n. mi. The maximum cruising speed is 464 knots, and the cost-economical speed is 442 knots. Both of these speeds are at 41 000 ft; the corresponding Mach numbers are 0.81 and 0.77. The Learjet 24B is equipped with two General Electric CJ610-4 turbojet engines of 2850 lb thrust each. These engines, together with the low gross weight, give a high take-off thrust-to-weight ratio of 0.43. This value of the thrust-to-weight ratio is much higher than any of those given in table 2.III for transport aircraft and is about the same as that of the well-known North American F-86D fighter of the

1950's. As can be seen from the table, the high thrust-to-weight ratio, coupled with a wing loading of only 57.4 lb/ft^2 gives an outstanding short field capability.

The high-lift system employed is simple and consists only of a single-slotted trailing-edge flap. No leading-edge devices are used. Ailerons, rudder, and elevators are manually actuated. Spoilers for increasing drag and reducing lift are located ahead of the flaps and are power actuated. Longitudinal trim is achieved by varying the incidence of the stabilizer portion of the T-tail. As in the case of the JetStar, part of the fuel load on the Learjet 24B is carried in external tanks.

Dassault-Breguet Falcon 20

The Falcon 20 is one of a series of business jets manufactured by the French firm of Dassault-Breguet. The aircraft, with a gross weight of 28 660 lb, lies in a weight class about midway between the JetStar and the Gates Learjet. Power is supplied by two General Electric CF700 aft fan engines of 4315 lb thrust each. The engines have a bypass ratio of 1.9. The Falcon 20 is used extensively in the United States and is frequently referred to as the Fan-Jet Falcon in this country. The first flight of the aircraft equipped with the General Electric engines took place in July 1964. A photograph of the Falcon 20 is presented in figure 2.45.



Figure 2.45.- Dassault-Breguet Falcon-20 business jet with aft-fan General Electric engines.

The aircraft has a maximum payload capability of 3320 lb and features a cabin which can accommodate 8 to 10 passengers. With a reduced payload of 1600 lb, the aircraft has a range of 1930 n. mi. Maximum cruising speed is 465 knots at 25 000 ft, and cost-economical speed is 405 knots at 40 000 ft. The corresponding Mach numbers are 0.77 and 0.70, respectively. In table 2.IV, the data indicate landing and take-off field lengths about the same for the Falcon 20 as for the JetStar.

The photograph in figure 2.45 shows a large fence on top of the wing part way between the root and the tip. This serves as a flow control device on the 30^{o} sweptback wing. A leading-edge flap, similar to an unslotted slat, is employed inboard of the fence, and a conventional slat is utilized outboard. A single-slotted trailing-edge flap completes the high-lift system. Lateral control is provided by ailerons alone. Spoilers located ahead of the flaps are deployed symmetrically to increase the drag for braking and rapid descent and are not part of the lateral control system. Longitudinal control is provided by elevators, and trim is maintained with an electrically driven stabilizer. With the exception of the stabilizer, all of the movable surfaces are hydraulically actuated.

The Falcon 20 and its derivatives continue in production In addition to use as an executive transport, the aircraft is also available in a cargo version. Over 450 have been produced, with about two-thirds of these being exported to the United States. The lastest in the Falcon series, the Falcon 50, is equipped with three engines located in a manner similar to that of the Boeing 727.

Grumman Gulfstream II

An examination of the data in table 2.IV indicates that the Grumman Gulfstream II, shown in figure 2.46, is heavier in weight, larger in size, faster



Figure 2.46.- Grumman Gulfstream II.

in speed, and longer in range than any of the other business aircraft. For example, the gross weight of the Gulfstream II is 62 500 lb, nearly five times that of the Gates Learjet, and the wing area is about three and a half times that of the Learjet. The Gulfstream II has an intercontinental range capability and a maximum cruising speed of 511 knots, or Mach number of 0.85, at an altitude of 25 000 ft. The aircraft, frequently referred to as the G-II, was developed by Grumman as a jet-powered successor to the highly successful turboprop-power Gulfstream I. (The original Gulfstream II was developed by a division of the Grumman Aerospace Corporation. Recently, however, this division has been sold, and the G-II is now produced by the Gulfstream American Corporation which will also manufacture and market the Gulfstream III.) First flight of the G-II took place in October 1966, and the aircraft has been in continuous production since that time with 200 units having been delivered by the spring of 1977. The end of the line for the G-II is now in sight, however, as the improved Gulfstream III nears flight-test status.

The Gulfstream II is a low-wing configuration incorporating a T-tail and a wing of aspect ratio of 6.0 and 25° sweepback. Power is supplied by two Rolls-Royce Spey MK 511-8 turbofan engines of 11 400 lb thrust each. The engine is equipped with a five-stage fan and has a bypass ratio of 0.64; target type thrust reversers are employed. The high-lift system consists of single-slotted trailing-edge flaps. Lateral control is provided by a combination of ailerons and spoilers. The spoilers may also be deployed symmetrically to increase drag and reduce lift. Elevators are used for longitudinal control, and trim is accomplished with a variable incidence stabilizer. All controls are hydraulically actuated.

The passenger cabin of the aircraft is usually configured for 10 to 14 passengers. The range-payload data given in the references are incomplete but indicate a range of 3375 n. mi. with maximum fuel. Take-off and landing distances are in the same class as the Lockheed JetStar.

Cessna Citation

The Cessna Citation is a small executive jet transport in the same weight class as the Gates Learjet. Low first costs, economy of operation, safety, and viceless handling characteristics were among the objectives of the design. In order to provide wide operational flexibility, the aircraft was designed to take off and land from most fields used by light and medium twin-engine propeller-driven aircraft, and from unpaved runways. The first flight took place in September 1969, and the aircraft was certified in September 1971. That the various versions of the Citation have been widely accepted is clearly demonstrated by the more than 400 aircraft which have been produced; the type is still in production and will likely continue to find a significant share of the business jet market for a number of years. A photograph of a Citation in flight is shown in figure 2.47. The data in table 2.IV are for the Citation model 500.

The Citation has a 7.4 aspect ratio unswept wing mounted near the bottom of the fuselage. The horizontal tail is located near the root of the vertical tail and incorporates a small amount of dihedral to reduce immersion in the jet



Figure 2.47.- Cessna Citation.

exhaust. The vertical tail has a relatively large dorsal fin and a small ventral fin. Power is supplied by two Pratt & Whitney JT15D-1 turbofan engines of 2200 lb thrust each. These engines have a bypass ratio of 3.3.

The high-lift system on the Citation consists of a single-slotted trailing-edge flap; no leading-edge devices are employed. Spoilers located on the upper wing surface ahead of the flap are used as air brakes and are not part of the lateral control system which utilizes only ailerons. Longitudinal control is by elevators, and trim is obtained by an electrically operated trim tab on the elevator. All controls are manually operated.

The Citation 500 has a gross weight of 11 650 lb. The cabin is usually configured to carry five or six passengers. With five passengers, the aircraft has a range of 1140 n. mi. The maximum cruising speed is 420 knots at 26 000 ft the corresponding Mach number is 0.70. The stalling speed of 82 knots is lower than that of any of the other aircraft listed in table 2.IV. This low stalling speed is achieved with the relatively simple high-lift system because the wing loading is only about 45 lb/ft^2. This wing loading together with a thrust-to-weight ratio of 0.38 are responsible for the short take-off and landing field lengths listed in the table.

Two versions of the aircraft, Citation I and Citation II, are now in production. Both of these aircraft are improved versions of the original Citation model 500 to which the above description applies. An entirely new aircraft, the Citation III, is now under development. The first flight of this very advanced design took place in the late spring of 1979.

MBB HFB 320 Hansa

The German MBB HFB 320 Hansa is included in this brief overview of business jet aircraft because of its interesting and unique configuration which features a swept-forward wing. A photograph of the aircraft is shown in figure 2.48. Design of this unusual aircraft was begun in March 1961, and the first flight took place in April 1964. Production of the aircraft began in 1966 and continued until approximately 50 aircraft were manufactured.

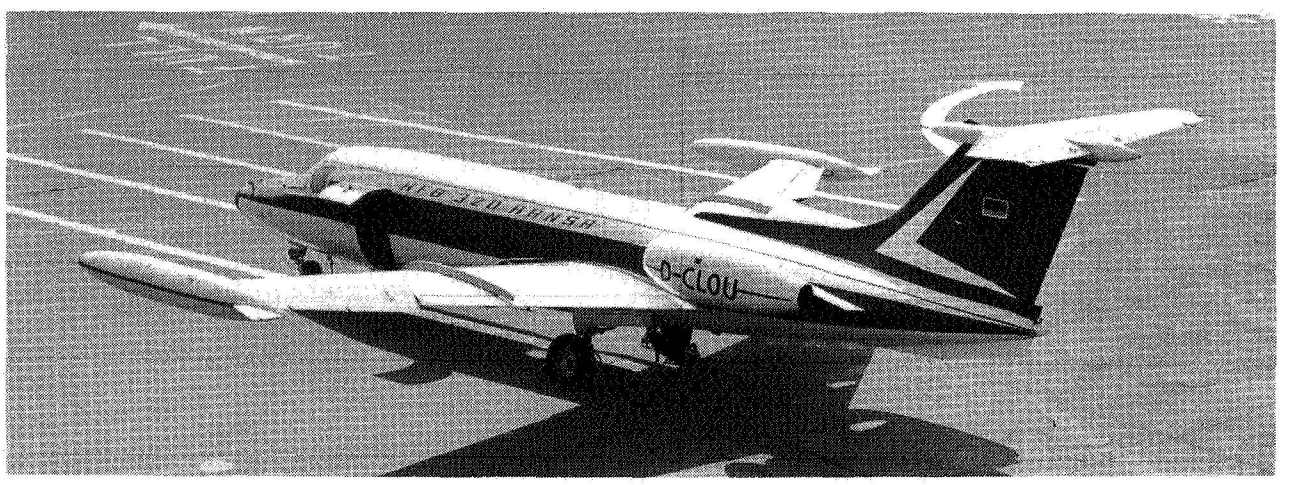


Figure 2.48.- MBB HFB 320 Hansa. (Note unusual swept-forward wings.)

The desirability of an unobstructed cabin floor and some of the means for achieving this objective were discussed in section 2.2.6.1. The wing of the Hansa is mounted near the middle of the fuselage (in the vertical sense), and the wing carry-through structure is located behind the passenger cabin. In order to place the wing aerodynamic center in the desired position relative to the aircraft center of gravity, 15° of forward sweep is incorporated in the wing. Fuel tanks are mounted at each wing tip; the small horizontal surfaces seen at the rear end of the tanks help to stabilize the wing-tank system against divergence. (See section 2.1.2.1.) The landing gear retracts into blisters located on the fuselage at the wing root. The empennage incorporates a horizontal tail mounted at the top of the vertical surface in the T position. Power is supplied by two General Electric CJ610-1 turbojet engines of 2850 lb thrust each.

In contrast to a sweptback wing, which stalls initially at the tip, a wing with forward sweep stalls first at the root. This type of stall can produce pitch-up just as does tip stall on a sweptback wing. An inboard leading-edge

slat and a large upper surface fence located at about mid semispan are used for stall control on the Hansa. The high-lift system utilizes these devices and a trailing-edge double-slotted flap. Upper and lower surface spoilers are deployed symmetrically for the purpose of increasing drag and decreasing lift. Ailerons are used for lateral control. Trim about all three axes is provided by tabs on the ailerons, elevators and rudder; the horizontal stabilizer is not adjustable.

Gross weight of the Hansa is 18 740 lb, and the aircraft can carry a maximum payload of 2650 lb for a distance of 825 n. mi.; with full fuel tanks and a reduced payload of 1760 lb, the range is 1450 n. mi. The cabin is usually configured for 9 passengers. Maximum cruising speed is 443 knots at 26 000 ft; this corresponds to a Mach number of 0.74. Landing and take-off field lengths are comparable with those of the Falcon 20.

A configuration layout incorporating a swept-forward wing would seem to offer interesting possibilities for the business jet aircraft. The reason for the short production life of the Hansa is not known. Perhaps the configuration concepts employed in this aircraft will be examined again at some time in the future. The divergence problem of the swept-forward wing may be alleviated by the use of composite materials which permit a degree of control over wing torsional stiffness not possible with conventional metal structures.

2.3 Concluding Remarks

The introduction of the first jet transport over a quarter of a century ago marked the beginning of the transportation revolution which has taken place since that time. The modern jet transport has altered forever the travel concepts and habits of people all over the world.

The technical foundations which underlie the jet transport are briefly described in chapter 2, along with an account of the technical development of the jet transport from the pioneering DeHavilland Comet of the early 1950's to the highly efficient, safe, reliable, and economical transport aircraft of today. Many of the transport aircraft currently in production will continue to be produced for many years. Improvements, modifications, and adaptations to new routes and markets will be made to current aircraft as time and circumstances change, and as new technologies evolve.

Several entirely new aircraft will probably be developed in the next decade. These new aircraft will no doubt utilize emerging new technologies in aerodynamics, structures, guidance and control, and propulsion. Supercritical aerodynamic design, composite structures, active controls, and engines of improved efficiency and reduced noise are only a few of the new technical developments which suggest themselves. The increased cost of fuel will probably place a new emphasis on energy-efficient aircraft. Accordingly, aerodynamic and propulsion-system efficiency and light structural weight will be of greater importance than ever before in these new aircraft designs.

SYMBOLS

A	aspect ratio, b^2/S
b	span, ft
C_D	wing drag coefficient
C_L	wing lift coefficient
C_m	aircraft pitching-moment coefficient
c	local wing chord, ft
$\bar{c}$	mean aerodynamic chord, ft
c_l	local section lift coefficient
c_p	specific fuel consumption in terms of horsepower (see appendix A)
D	aircraft drag, lb
$\dot{E}$	kinetic energy per unit time, ft-lb/sec
L	aircraft lift, lb
L/D	lift-drag ratio
l	fuselage length, ft
l_T	take-off field length, ft
l_L	landing field length, ft
M	Mach number
$M_{cr,\Lambda}$	critical Mach number of wing with sweepback angle Λ
$M_{cr,\Lambda=0}$	critical Mach number of wing with zero sweepback
$\dot{m}$	mass-flow rate, slug/sec
P	engine power, hp
R	range, n. mi.
S	wing area, ft^2
T	thrust, lb

V	velocity, ft/sec
V_c	maximum cruising speed, knots
V_{ce}	cost-economical cruising speed, knots
V_e	exhaust velocity, ft/sec
V_i	inlet velocity, ft/sec
V_N	velocity normal to wing leading edge, ft/sec
V_0	free-stream velocity, ft/sec
V_s	stalling speed, knots
W	weight, lb
W_e	empty weight, lb
W_g	maximum gross weight, lb
W_L	maximum landing weight, lb
W_p	payload weight, lb
y	distance along wing span measured from wing center line, ft
α	angle of attack, deg
η	overall propulsion-system efficiency, $\eta_p\eta_c$, percent (see fig. 2.2), semispan wing position, $2y/b$ (see fig. 2.8)
η_c	engine cycle efficiency, percent
η_p	propulsive efficiency, percent
Λ	sweepback angle measured at quarter-chord line, deg
λ	wing taper ratio, $\frac{\text{Tip chord}}{\text{Root chord}}$

Abbreviations:

FAR	Federal Air Regulation
max	maximum

REFERENCES

2.1 Bridgman, Leonard, ed.: Jane's All the World's Aircraft, 1952-53. McGraw-Hill Book Co., Inc.

2.2 Bridgman, Leonard, ed.: Jane's All the World's Aircraft, 1954-55. McGraw-Hill Book Co., Inc.

2.3 Taylor, John W. R., ed.: Jane's All the World's Aircraft, 1966-67. McGraw-Hill Book Co., c.1966.

2.4 Taylor, John W. R., ed.: Jane's All the World's Aircraft, 1970-71. McGraw-Hill Book Co., c.1970.

2.5 Taylor, John W. R., ed.: Jane's All the World's Aircraft, 1974-75. Franklin Watts, Inc., c.1974.

2.6 Taylor, John W. R., ed.: Jane's Pocketbook of Commercial Transport Aircraft. Macmillan Pub. Co., Inc., c.1973.

2.7 Abbott, Ira H.; Von Doenhoff, Albert E.; and Stivers, Louis S., Jr.: Summary of Airfoil Data. NACA Rep. 824, 1945. (Supersedes NACA WR L-560.)

2.8 The Aircraft Gas Turbine Engine and Its Operation. Part No. PWA 182408, PWA Oper. Instr. 200, Pratt & Whitney Aircraft, June 1952. Reprinted with revisions May 1974.

2.9 Andrews, C. F.: Vickers Aircraft Since 1908. Funk & Wagnalls, 1969.

2.10 Busemann, A.: Aerodynamic Lift at Supersonic Speeds. Ae. Techl. 1201, Rep. No. 2844, British A.R.C., Feb. 3, 1937. (From Luftfahrtforschung, Bd. 12, Nr. 6, Oct. 3, 1935, pp. 210-220.)

2.11 Case Study in Aircraft Design - The Boeing 727. Professional Study Series, American Inst. Aeronaut. & Astronaut., Sept. 14, 1978.

2.12 The Commercial Air Transport Market - 1976-1991. Rep. C1-804-4022A, Douglas Aircraft Co., Oct. 1976.

2.13 Commercial Aircraft of the World. Flight Int., vol. 104, no. 3370, Oct. 18, 1973.

2.14 Commercial Aircraft of the World. Flight Int., vol. 112, no. 3578, Oct. 8, 1977.

2.15 Commercial Aircraft of the World. Flight Int., vol. 114, no. 3634, Nov. 11, 1978.

2.16 Davies, R. E. G.: Airlines of the United States - Since 1914. Putnam & Co., Ltd. (London), c.1972.

2.17 FAA Statistical Handbook of Aviation. U.S. Dep. Trans., 1968.

2.18 Garrard, Wilfred C.: The Lockheed C-5 Case Study in Aircraft Design. Professional Study Series, American Inst. Aeronaut. & Astronaut.

2.19 Green, William: War Planes of the Second World War - Fighters. Volume One, Hanover House, 1960.

2.20 International Business Jet and Turboprop Directory. Flight Int., vol. 113, no. 3591, Jan. 14, 1978.

2.21 International Turbine Engine Directory. Flight Int., vol. 113, no. 3590 Jan. 7, 1978.

2.22 Jackson, A. J.: De Havilland Aircraft - Since 1915. Putnam & Co., Ltd. (London), c.1962.

2.23 Jones, Robert T.: Wing Plan Forms for High-Speed Flight. NACA Rep. 863 1947. (Supersedes NACA TN 1033.)

2.24 Kinnaman, E. Berkeley: Flutter Analysis of Complex Airplanes by Experimental Methods. J. Aeronaut. Sci., vol. 19, no. 9, Sept. 1952, pp. 577-584.

2.25 Miller, Ronald; and Sawers, David: The Technical Development of Modern Aviation. Praeger Pub., c.1968.

2.26 1973/74 Aerospace Facts and Figures. Aero-Space Industries Assoc. of America, Inc., c.1973.

2.27 Pedigree of Champions - Boeing Since 1916. Doc. No. D4889, Fourth ed. Boeing Co., 1977.

2.28 Polhamus, Edward C.; and Hallissy, Joseph M., Jr.: Effect of Airplane Configuration on Static Stability at Subsonic and Transonic Speeds. NACA RM L56A09a, 1956.

2.29 Progress of NASA Research Relating to Noise Alleviation of Large Subsoni Jet Aircraft. NASA SP-189, 1968.

2.30 Research and Development Contributions to Aviation Progress (RADCAP) - Executive Summary. U.S. Air Force, Aug. 1972. (Available as NASA CR-129574.)

2.31 Shacklady, Edward: The Gloster Meteor. MacDonald Aircraft Monographs, Doubleday & Co., Inc., 1963.

2.32 Spreeman, Kenneth P.: Design Guide for Pitch-Up Evaluation and Investigation at High Subsonic Speeds of Possible Limitations Due to Wing-Aspect-Ratio Variations. NASA TM X-26, 1959.

2.33 Stroud, John: Soviet Transport Aircraft Since 1945. Funk & Wagnalls, 1968.

2.34 Taylor, John W. R., ed.: Jane's 100 Significant Aircraft - 1909-1969. McGraw-Hill Book Co., c.1969.

2.35 Taylor, Robert T.; and Ray, Edward J.: Factors Affecting the Stability of T-Tail Transports. J. Aircr., vol. 3, no. 4, July-Aug. 1966, pp. 359-364.

2.36 Thoren, R. L.: Recent Engineering Advances on the Lockheed L-1011. AIAA Paper No. 69-828, July 1969.

2.37 Torenbeek, Egbert: Synthesis of Subsonic Airplane Design. Delft Univ. Press, The Netherlands, c.1976.

2.38 Wagner, Ray: American Combat Planes. Hanover House, 1960.

2.39 Wagner, Ray; and Nowarra, Heinz: German Combat Planes. Doubleday & Co., Inc., 1971.

2.40 Wigton, Don, Compiler: From Jenny to Jet - Pictorial Histories of the World's Great Airlines. Bonanza Books, c.1963.

2.41 Wilkinson, Paul H.: Aircraft Engines of the World - 1966/67. Rev. ed. Publ. by author (5900 Kingswood Road, N.W., Washington, DC 20014), c.1967.

2.42 World Airline Directory. Flight Int., vol. 113, no. 3605, Apr. 22, 1978.

TABLE 2.I.- REVENUE PASSENGER MILES FLOWN BY SCHEDULED U.S. AIR CARRIERS

[Compiled from statistics given in refs. 2.12, 2.17, and 2.26]

Year	Domestic flights, billions of miles	International flights, billions of miles	Total
1949	-----	----	8.8
1959	25.4	7.1	32.5
1969	106.0	30.1	136.1
1976	147.0	41.5	188.5
[a]1986	267.5	79.0	346.5

[a]Projected activity.

TABLE 2.II.- PERTINENT CHARACTERISTICS OF BOEING 747 AND LOCKHEED 1049G SUPER CONSTELLATION

Measurement	Lockheed 1049G	Boeing 747
Weight, W, lb	112 000	700 000
Speed, V, knots	287	461
Altitude, ft	23 000	35 000
Lift-drag ratio, L/D . .	15	16
Number of engines	4	4
Total cruise power, hp . .	6 585	59 934
Power per engine, hp . . .	1 646	14 984
Dry engine weight, lb . .	3 675	8 600
Power-to-weight ratio . .	0.45	1.74

TABLE 2.III.- CHARACTERISTICS OF JET TRANSPORT AIRCRAFT

b, ft	ℓ, ft	S, ft^2	A	Λ, deg	W_g, lb	W_L, lb	W_e, lb	T/W_g	W_g/S	V_c, knots	V_{ce}, knots	V_s, knots	Range, n. mi. (a)		ℓ_T, ft	ℓ_L, ft	Number of passengers	First flight	Number built or on order
													Maximum payload	Full fuel tanks	(b)	(b)	(c)		
DeHavilland Comet 1 airplane (refs. 2.1, 2.2., and 2.22) powered by four DH Ghost turbojet engines of 5000 lb thrust each																			
115	93	2015	6.6	20	105 000	-------	-------	0.19	52.1	426 (h = 35 000)	---	-----	----	3540 (W_p = 12 000)	-------	----	48	7/27/49	----
Tupolev Tu-104B airplane (refs. 2.3, 2.6, and 2.33) powered by two Mikulin turbojet engines of 21 385 lb thrust each																			
113.3	131.5	1975	6.5	40 and 37.5	167 551	141 096	93 696	0.26	84.8	513	432	110	[d]1305 (W_p = 26 455)	1925 (W_p = 13 225)	[e]7 220	[e]6070	100 (5 abreast)	6/17/55	250
Boeing B-47B airplane (refs. 2.27 and 2.38) powered by six General Electric J-47 turbojet engines of 5800 lb thrust each																			
116	107.1	1428	9.42	35	185 000	78 000	-------	0.19	129.6	435	---	130.4	----	----	-------	----	---	12/17/47 [f]4/26/52	2031
Boeing 367-80 airplane (ref. 2.2) powered by four Pratt & Whitney JT3C turbojet engines of 10 000 lb thrust each																			
129.7	127.8	2400	7.0	35	190 000	92 120	-------	0.21	79.2	478	---	-----	3870 (W_p = 10 000)	----	-------	----	---	7/15/54	1
Boeing 707-320B airplane (refs. 2.5, 2.6, and 2.13) powered by four Pratt & Whitney JT3D-7 turbofan engines of 19 000 lb thrust each																			
145.8	152.8	2892	7.4	35	336 000	247 000	147 000	0.23	116.2	516 (h = 30 000)	478 (h = 35 000)	105	5175 (W_p = 53 900)	6500 (W_p = 33 350)	10 000	6250	189 (6 abreast)	1959	[g]943
McDonnell Douglas DC-8 Super 63 airplane (refs. 2.4, 2.6, and 2.13) powered by four Pratt & Whitney JT3D-7 turbofan engines of 19 000 lb thrust each																			
148.4	187.5	2926.8	7.5	30.6	358 000	245 000	158 300	0.21	122.3	518 (h = 29 000)	473 (h = 35 000)	107	4245 (W_p = 67 735)	6084 (W_p = 37 101)	10 440	5900	259 (6 abreast)	1958 [f]1966	556
Sud-Aviation Caravelle VI-R airplane (refs. 2.3 and 2.6) powered by two Rolls-Royce Avon turbojet engines of 12 000 lb thrust each																			
112.5	105	1579	8	20	114 640	104 990	59 985	0.21	72.6	457 (h = 25 000)	424 (h = 35 000)	-----	1590 (W_p = 16 800)	----	6 750	5650	80 (5 abreast)	5/27/55 [f]2/6/61	280
Boeing 727-200 airplane (refs. 2.5., 2.6, and 2.14) powered by three Pratt & Whitney JT8D-17 turbofan engines of 16 000 lb thrust each																			
108	153.2	1650	7.1	32	210 000	160 000	103 000	0.23	127.3	530 (h = 25 000)	477 (h = 33 000)	105.4	2900 (W_p = 41 000)	3250 (W_p = 36 000)	9 950	4900	189 (6 abreast)	1963 [f]1967	[g]1500

[a]With no allowance for reserve fuel.
[b]FAR field lengths.
[c]All-tourist seating arrangement.
[d]With allowance for reserve fuel.
[e]Not FAR field lengths.
[f]First flight of particular version for which data are given.
[g]Still in production.

TABLE 2.III.- Concluded

b, ft	ℓ, ft	S, ft^2	A	Λ, deg	W_g, lb	W_L, lb	W_e, lb	T/W_g	W_g/S	V_c, knots	V_{ce}, knots	V_s, knots	Range, n. mi. (a) Maximum payload	Range, n. mi. (a) Full fuel tanks	ℓ_T, ft (b)	ℓ_L, ft (b)	Number of passengers (c)	First flight	Number built or on order
McDonnell Douglas DC-9-30 airplane (refs. 2.5, 2.6, and 2.14) powered by two Pratt & Whitney JT8D-15 turbofan engines of 15 500 lb thrust each																			
93.3	119.3	1001	8.7	24.5	109 000	99 000	56 000	0.28	108.9	503 (h = 26 000)	454 (h = 33 000)	104	1576 (W_p = 31 000)	1922 (W_p = 27 527)	6 200	4700	115 (5 abreast)	1965 [f]1966	[g]900
Boeing 737-200 airplane (refs. 2.5, 2.6, and 2.14) powered by two Pratt & Whitney JT8D-17 turbofan engines of 16 000 lb thrust each																			
93	100	980	8.8	25	117 500	105 000	60 980	0.27	119.9	490 (h = 25 000)	436 (h = 33 000)	101	1520 (W_p = 34 000)	2680 (W_p = 21 750)	6 475	4430	130 (6 abreast)	1967	[g]530
British Aircraft Corporation VC-10 airplane (refs. 2.3 and 2.6) powered by four Rolls-Royce Conway RC042 turbofan engines of 21 000 lb thrust each																			
142.2	158.8	2932	7.3	32.5	314 000	216 000	146 979	0.27	107.1	494	478 (h = 38 000)	120	5040 (W_p = 39 769)	----	8 280	6380	151 (6 abreast)	6/29/62	54
Boeing 747-200B airplane (refs. 2.5, 2.6, and 2.14) powered by four Pratt & Whitney JT9D-7Q turbofan engines of 53 000 lb thrust each																			
195	231	5500	6.9	37.5	823 000	564 000	371 700	0.26	150	516	490	109	5190 (W_p = 154 800)	6640 (W_p = 100 900)	10 200	6150	516 (10 abreast)	2/9/69	[g]345
Lockheed L-1011-200 airplane (refs. 2.5 and 2.14) powered by three Rolls-Royce RB.211-524 turbofan engines of 48 000 lb thrust each																			
155.3	177.7	3456	7.0	35	468 000	368 000	245 800	0.31	135.4	528 (h = 31 000)	493 (h = 31 000)	109	4247 (W_p = 74 200)	5395 (W_p = 42 827)	8 070	5820	400 (10 abreast)	11/16/70	167
McDonnell Douglas DC-10-30 airplane (refs. 2.5 and 2.14) powered by three General Electric CF6-50C1 turbofan engines of 52 500 lb thrust each																			
165.3	181.6	3647	7.5	35	575 000	403 000	368 000	0.27	158	516 (h = 31 000)	499 (h = 31 000)	---	5380 (W_p = 106 541)	6425 (W_p = 65 975)	10 370	5830	380 (10 abreast)	8/70	[g]258
Lockheed C-5A airplane (ref. 2.5) powered by four General Electric TF-39 turbofan engines of 41 000 lb thrust each																			
222.8	247.8	6200	7.8	25	769 000	635 850	--------	0.21	124	470 (h = 25 000)	---	104	3256 (W_p = 220 967)	5670 (W_p = 112 600)	[e]8 400	[e]3600	---	6/30/68	81

[a]With no allowance for reserve fuel.
[b]FAR field lengths.
[c]All-tourist seating arrangement.
[d]With allowance for reserve fuel.
[e]Not FAR field lengths.
[f]First flight of particular version for which data are given.
[g]Still in production.

TABLE 2.IV.- CHARACTERISTICS OF BUSINESS JET AIRCRAFT

b, ft	l, ft	S, ft^2	A	Λ, deg	W_g, lb	W_L, lb	W_e, lb	T/W_g	W_g/S	V_c, knots	V_{ce}, knots	V_s, knots	Range, n. mi. (a)		ℓ_T, ft (b)	ℓ_L, ft (b)	Number of passengers	First flight	Number built or on order
													Maximum payload	Full fuel tanks					
Lockheed JetStar airplane (refs. 2.3, 2.5, and 2.20) powered by four Pratt & Whitney turbojet engines of 3300 lb thrust each																			
54.5	60.5	542.5	5.3	30	42 500	35 000	21 676	0.31	78.3	493 (h = 21 000)	453	106	2100 (W_p = 3500)	-----	[c]4700	[c]3550	8 to 10	9/4/57	[d]Over 160
Gates Learjet 24B airplane (ref. 2.3) powered by two General Electric CJ610-4 turbojet engines of 2850 lb thrust each																			
35.5	43.3	231.8	5.4	13	13 300	11 880	6 700	0.43	57.4	464 (h = 41 000)	442 (h = 41 000)	90	1105 (W_p = 1910)	1775	3100	3350	6	10/7/63 (Model 23)	[d]Over 700
Dassault-Breguet Falcon 20 airplane (refs. 2.5 and 2.20) powered by two General Electric CF700 turbofan engines of 4315 lb thrust each																			
53.5	56.3	440	6.5	30	28 660	15 970	------	0.30	65.1	465 (h = 25 000)	405 (h = 40 000)	82	----- (W_p = 3320)	1930 (W_p = 1600)	4750 (W_g = 27 130)	3220	8 to 10	7/10/64	[d]450
Grumman Gulfstream II airplane (refs. 2.5 and 2.20) powered by two Rolls-Royce Spey MK 511-8 turbofan engines of 11 400 lb thrust each																			
68.8	79.9	793.5	6.0	25	62 500	58 500	37 186	0.36	79	511 (h = 25 000)	111	---	-----	3375	5000	3190	10 to 14	10/2/66	[d]Over 200
Cessna Citation 500 airplane (ref. 2.5) powered by two Pratt & Whitney JT15D-1 turbofan engines of 2200 lb thrust each																			
43.8	43.5	260	7.4	0	11 650	11 000	6 390	0.38	44.8	420 (h = 26 000)	---	82	1140 (5 passengers)	-----	3275	2780	5 or 6	9/16/69	[d]Over 400
MBB HFB 320 Hansa airplane (refs. 2.3 and 2.6) powered by two General Electric CJ610-1 turbojet engines of 2850 lb thrust each																			
47.5	54.5	324.4	7.0	-15	18 740	17 860	10 670	0.31	57.8	443 (h = 26 000)	390 (h = 39 000)	88	825 (W_p = 2650)	1450 (W_p = 1760)	4650	2900	9 or 10	4/64	~50

[a]With 45 min reserve fuel.
[b]FAR field lengths.
[c]Not FAR field lengths.
[d]Still in production.

TABLE 2.V.- PHOTOGRAPH CREDITS

Figure	Photograph	Source
2.6	Nacelle with acoustic treatment	McDonnell Douglas Corporation
2.12	Boeing 737 with triple-slotted flap	NASA Langley Research Center
2.13	Boeing 737 with triple-slotted flap and spoilers	NASA Langley Research Center
2.14	Boeing 737 with leading-edge slat	NASA Langley Research Center
2.18	DeHavilland Comet 3	David A. Anderton
2.19	Tupolev Tu-104B	Flight International, London
2.20	Boeing B-47E	The Boeing Company
2.22	Boeing 367-80	The Boeing Company
2.23	Boeing 707-320B	The Boeing Company
2.25	McDonnell Douglas DC-8 Super 63	McDonnell Douglas Corporation
2.26	Sud-Aviation Caravelle V1-R	United Airlines
2.27	Boeing 727-200	The Boeing Company
2.28	McDonnell Douglas DC-9-30	McDonnell Douglas Corporation
2.29	Boeing 737	The Boeing Company
2.30	British Aircraft Corporation VC-10	Flight International, London

TABLE 2.V.- Concluded

Figure	Photograph	Source
2.33	Boeing 747	The Boeing Company
2.34	Boeing 747 in landing configuration	The Boeing Company
2.35	Lockheed L-1011, TriStar	Lockheed Aircraft Corporation
2.36	McDonnell Douglas DC-10	McDonnell Douglas Corporation
2.37	Boeing 747 Freighter	The Boeing Company
2.38	Lockheed C-5A	Lockheed Aircraft Corporation
2.39	Lockheed C-5A	Lockheed Aircraft Corporation
2.40	Lockheed C-5A being loaded	Lockheed Aircraft Corporation
2.41	Tail assembly of Lockheed C-5A	Lockheed Aircraft Corporation
2.43	Lockheed JetStar	Peter C. Boisseau
2.44	Gates Learjet 24B	Peter C. Boisseau
2.45	Dassault-Breguet Falcon 20	Peter C. Boisseau
2.46	Grumman Gulfstream II	Peter C. Boisseau
2.47	Cessna Citation	Cessna Aircraft Company
2.48	MBB HFB 320 Hansa	Flight International, London

III - SIZING OF JET-POWERED CRUISING AIRCRAFT

CONTENTS

		Page
3.0	Introduction	101
3.1	Scope of Data	101
3.2	Performance Objectives	101
3.3	Sizing Procedure	103
3.4	Airport Performance	104
	3.4.1 Landing Field Length	105
	3.4.2 Missed Approach	108
	3.4.3 Take-Off Field Length	111
	3.4.4 Second-Segment Climb Gradient	117
	3.4.5 Take-Off and Landing Weight Relationships	118
3.5	Cruising Performance	119
	3.5.1 Aircraft Lift-Drag Characteristics	121
	3.5.1.1 Airplane Efficiency Factor	123
	3.5.1.2 Estimation of Maximum Lift-Drag Ratio	125
	3.5.1.3 Variation of Lift-Drag Ratio With Lift Coefficient	129
	3.5.2 Engine Characteristics	131
	3.5.3 Cruise Matching	137
	3.5.4 Off-Design Cruise Operation	141
3.6	Aircraft Matching	143
	3.6.1 Take-Off and Climb Calculation	146
	3.6.2 Landing and Missed Approach Calculation	147
3.7	Aircraft Weight Relationships	148
	3.7.1 Useful Load Fraction	148
	3.7.2 Aircraft Gross Weight Estimation	150
3.8	Aircraft Range and Fuel Fraction	151
3.9	Aircraft Sizing	154
3.10	Cruise Performance Map	156
	3.10.1 Method of Analysis	156
	3.10.2 Sample Cruise Performance Map	161

Page

SYMBOLS 164

REFERENCES 168

TABLES 170

3.0 Introduction

Rapid methods for estimating the size, weight, and thrust of jet-powered aircraft intended to meet specified performance objectives are developed and discussed in chapter 3. The methods developed are for jet-powered aircraft intended for steady cruising flight and do not encompass modern, highly maneuvering fighter aircraft. The approach employed in the sizing procedure makes extensive use of correlations of the characteristics of existing aircraft in terms of well-known aircraft design parameters. The resulting methods are simple and require only the use of a pocket scientific computer, or slide rule, for rapid application to a specific sizing problem. The physical interrelationships between the various design parameters and their influence on aircraft characteristics are also easily understood. The procedures and methods described are only approximate but will yield results of acceptable accuracy for many purposes.

3.1 Scope of Data

Many of the quantitative relationships employed in the present chapter are based on correlations of the characteristics of present-day turbojet-turbofan powered aircraft. The characteristics of the aircraft listed in table 3.I were utilized in developing the various correlations. The list consists of approximately 35 aircraft, including various versions of a given design and encompasses long-, medium-, and short-range commercial transport aircraft as well as the smaller executive jet transports. The gross weights of the aircraft analyzed extended from 10 500 lb to approximately 800 000 lb. Aircraft which entered service in the time period from 1958 to the present were considered. All jet-powered cruising aircraft developed in this time period were not analyzed; however, a sufficient number were considered to yield meaningful trends. The information for the different aircraft were obtained primarily from references 3.1, 3.2, and 3.3. Information on a given aircraft was not always consistent among different references. In all cases, data for a given aircraft were taken from a single source. All of the performance parameters for a particular aircraft were not necessarily employed in developing the various correlations because of incompleteness in the data for a particular aircraft or because of inexplicable inconsistencies with well-defined trends. Certain of the characteristics of some of the Soviet aircraft, for example, did not appear reasonable, perhaps because of unknown differences in definition of quantities, and were not used. Only those data were used which appeared credible when considered in relation to the particular aircraft being examined and the trends shown by similar aircraft.

3.2 Performance Objectives

Civil aircraft in the United States are certified under either part 23 or part 25 of the Federal Air Regulations (FAR). Aircraft of less than 12 500 lb gross weight may be certified under FAR part 23, whereas aircraft with a higher gross weight must be certified under the rules of FAR part 25. The rules governing the certification of transport-category aircraft, part 25, are different and more stringent, in many respects, than those for aircraft designed to the

criteria of part 23. All commercial jet-powered transport aircraft and most, if not all, executive jet aircraft are designed to the criteria of FAR part 25. The definitions of airport field lengths and required climb gradients utilized in chapter 3 are therefore those of FAR part 25 (ref. 3.4) and FAR part 121 (ref. 3.5) which govern certain operational aspects of transport aircraft. The airport field lengths presented and discussed in chapter 3 should not be compared with those given in chapter 6 for propeller-driven aircraft. The field lengths used in chapter 6 are for aircraft designed in accordance with the criteria of FAR part 23.

Modern jet-powered cruising aircraft are usually designed to meet, as a minimum, the following performance criteria:

- Airport Performance
  - FAR landing field length; missed approach requirement
  - FAR balanced take-off field length; second-segment climb gradient requirement
- Cruise Performance
  - Cruising speed usually expressed in terms of Mach number
  - Range
  - Payload

The specification of these performance objectives together with appropriate engine and aerodynamic data (contained herein) permit the rapid estimation of the following important aircraft parameters:

Gross weight

Fuel weight

Empty weight

Wing area and wing loading

Engine thrust and thrust loading

The cruising altitude is also given by the analysis. Compliance with FAR noise regulations in the vicinity of airports imposes additional constraints in the aircraft sizing process. The characteristics of the engine, as well as the aerodynamic characteristics of the aircraft in the landing and take-off configurations, influence the noise of the aircraft as experienced by observers on the ground. For simplicity, noise constraints are not considered in the present analysis although such constraints could be included without altering the other elements of the sizing process.

3.3 Sizing Procedure

The procedure by which an aircraft is sized to meet a given set of performance objectives is illustrated in approximate form by the flow diagram shown in figure 3.1. The process will now be briefly described.

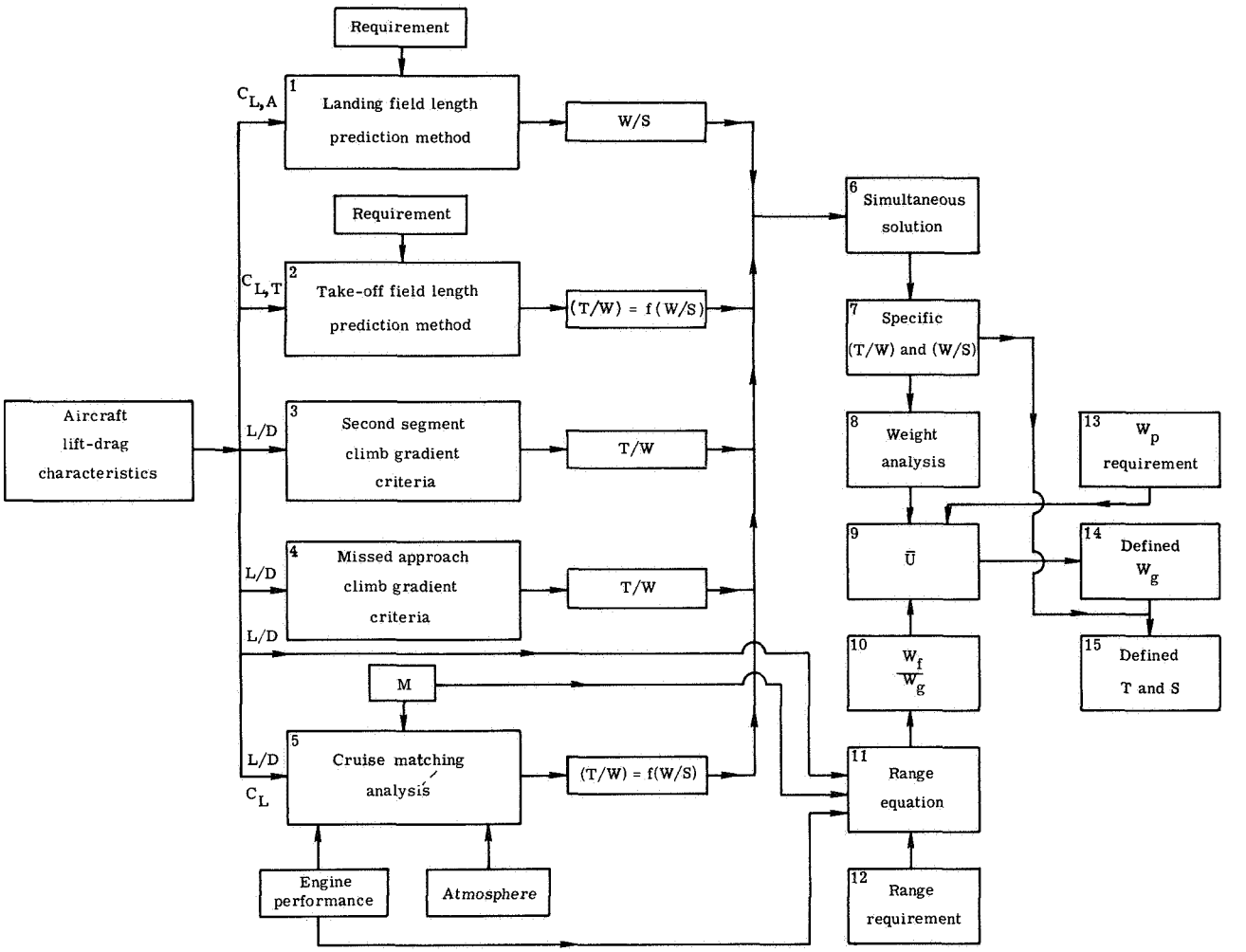


Figure 3.1.- Aircraft-sizing flow diagram for jet-powered aircraft.

The blocks in the first column represent analysis methods for different flight conditions or performance objectives, developed herein, which are utilized in the first steps toward sizing the aircraft. The landing-field-length block in the first column yields the output wing loading necessary to meet the input required landing field length and for the input approach lift coefficient. The approach lift coefficient depends upon the type of high-lift system and is chosen on the basis of statistical data for current aircraft. Block 2, take-off field length, yields an output curve of airplane thrust-to-weight ratio as a function of wing loading for a given input lift-off lift coefficient and for a required take-off field length. The lift-off lift coefficient is again determined on the basis of statistical data for current aircraft. Blocks 3 and 4

pertain to criteria for emergency situations which follow loss of an engine in critical flight regimes and yield required values of the airplane thrust-to-weight ratio. The input aircraft lift-drag ratio for these two flight conditions is obtained from rapid approximation methods. Block 5 represents the cruise matching analysis which yields a curve of take-off thrust-to-weight ratio as a function of wing loading. The defined thrust loading is sufficient for each wing loading to permit steady flight at the specified cruise Mach number and at the design lift coefficient which is usually near that for maximum lift-drag ratio. The altitude for cruise also comes from this analysis. The inputs to the cruise matching analysis are aircraft lift-drag ratio L/D, engine performance, cruise Mach number M, and characteristics of the atmosphere.

Rapid methods are presented for estimating the lift-drag ratio in terms of certain geometric characteristics of the aircraft. The characteristics of four representative turbofan engines are presented in a convenient nondimensional form that permits easy scaling of pertinent parameters to different engine thrust levels. The appropriate characteristics of the atmosphere are presented in a form which relates wing loading and altitude to Mach number and lift coefficient.

The outputs of the analyses represented by the first column in figure 3.1 constitute a set of relationships which, when considered simultaneously, yield unique values of wing loading and thrust loading that are required to meet the desired performance objectives. The output values of wing loading and thrust loading are utilized in the weight analysis, block 8 of figure 3.1, to yield a specific value of the ratio of payload weight W_p plus fuel weight W_f to aircraft gross weight W_g; that is $(W_p + W_f)/W_g$ or $1 - (W_e/W_g) = \bar{U}$. The fuel fraction W_f/W_g is determined from the Breguet range equation for the specified range and cruise Mach number. (See section 3.5.) The process is shown in blocks 12, 11, and 10 of figure 3.1. The payload weight W_p is, of course, specified. Since $1 - (W_e/W_g)$ and W_f/W_g are now known and W_p is a specified quantity, the gross weight may be immediately determined. Such quantities as wing area, total thrust, fuel load, and operating weight empty may then be calculated. Thus, the aircraft has been grossly sized to meet the desired performance objectives.

The analyses represented by the various blocks in figure 3.1 are described in some detail in the next sections of this chapter. The process of sizing an aircraft with the use of these analyses is illustrated quantitatively by an example in chapter 4.

3.4 Airport Performance

Methods for estimating the FAR landing and take-off field lengths are developed and discussed in this section. As will be seen, these field lengths contain certain safety margins to allow for emergency situations. The one-engine inoperative climb characteristics are also considered in relation to the FAR requirements for the missed approach situation in the landing phase of flight and the second-segment climb gradient following take-off. As previously noted, the field lengths discussed in chapter 3 should not be compared with those of chapter 6 for aircraft designed to FAR part 23.

3.4.1 Landing Field Length

The landing field length utilized herein is that defined by the Federal Air Regulations for transport-category aircraft. Briefly, the landing distance is measured, horizontally, from the point at which the aircraft is 50 ft above the surface, in steady gliding flight at an approach speed not less than 1.3 times the stalling speed (in knots), to the point at which the aircraft is brought to a complete stop on a hard, dry, smooth runway surface (ref. 3.4). The FAR landing field length is obtained by dividing the measured landing distance by 0.6 in order to account for the possibility of variations in approach speed, touchdown point, and other deviations from standard procedures. (See ref. 3.5.) A sketch depicting the FAR landing field length is shown in figure 3.2. The FAR landing field length as defined in figure 3.2 usually appears in specifications for transport aircraft designed to the criteria of FAR part 25 and is the distance employed in chapter 3.

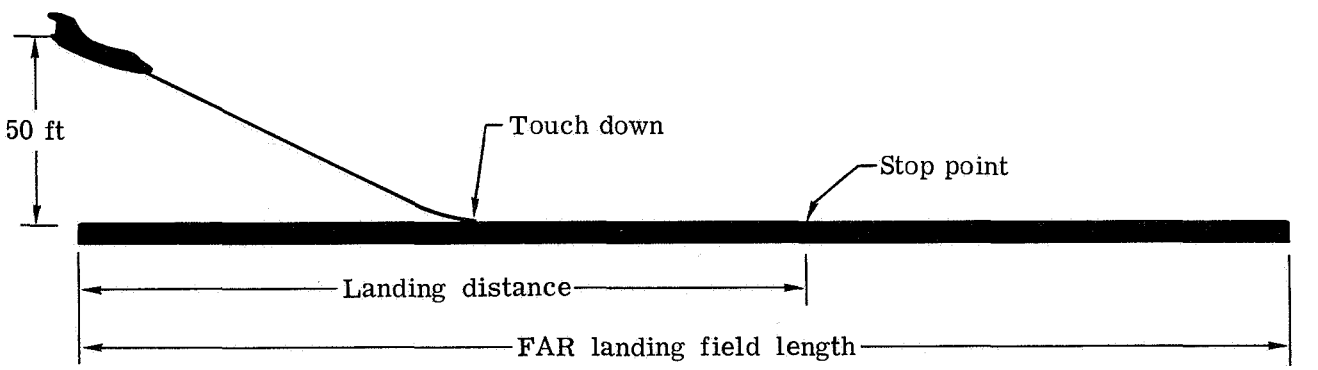


Figure 3.2.- Landing field length.

The procedure for estimating the FAR landing field length is divided into two steps. The first step relates the approach speed to the wing loading and the lifting capability of the wing and flap system; the second step expresses the actual FAR landing field length as a function of the approach speed.

In figure 3.3 the approach speed (in knots) is plotted on the ordinate as a function of the square root of the wing loading. The wing loading is divided by the density ratio σ to provide a means of correcting for nonstandard atmospheric conditions. In all calculations the value of σ was taken as 1.0. Straight lines were calculated for values of the approach lift coefficient from 1.2 to 2.0 with the use of the relation

$$V_A = 17.15\sqrt{\frac{W}{S}\frac{1}{\sigma}\frac{1}{C_{L,A}}} \tag{3.1}$$

where

V_A approach speed, knots

W/S wing loading, lb/ft^2

σ density ratio

$C_{L,A}$ approach lift coefficient

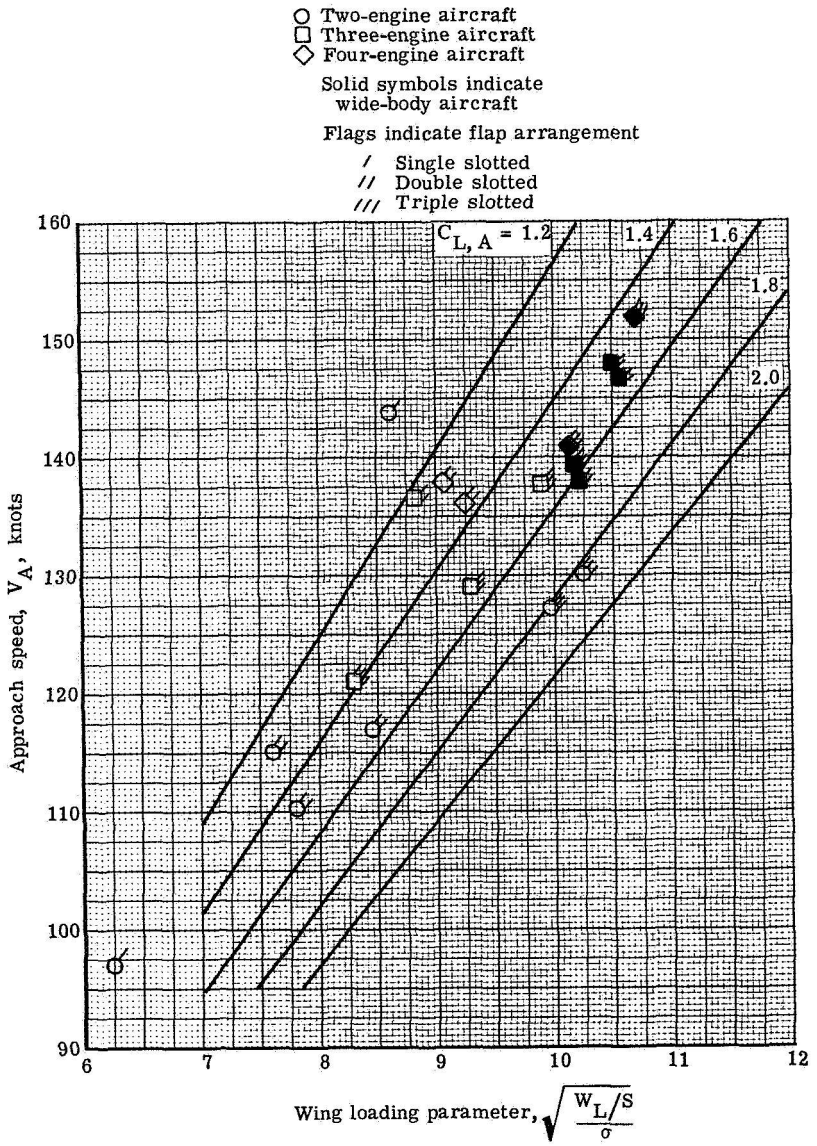


Figure 3.3.- Approach speed as function of wing loading parameter for a number of jet-powered aircraft.

Since the approach speed is defined as 1.3 times the stalling speed, the approach lift coefficient is the maximum lift coefficient divided by 1.69. The points express the relationship between wing loading and approach speed for 18 different aircraft equipped with single-, double-, and triple-slotted flaps. The wing loadings for the different aircraft are all for the maximum landing weight condition. From figure 3.3, the data indicate that an average value of approach lift coefficient of about 1.5 is used for a wing with double- or triple-slotted flaps and leading-edge devices.

The FAR landing field length is shown in figure 3.4 for a number of aircraft as a function of the square of the approach speed. The data for the different aircraft are seen to form a good linear correlation. Thus, the information presented in figures 3.3 and 3.4 provides an easy method for estimating the approach speed and landing distance in terms of the wing loading and type of high-lift system.

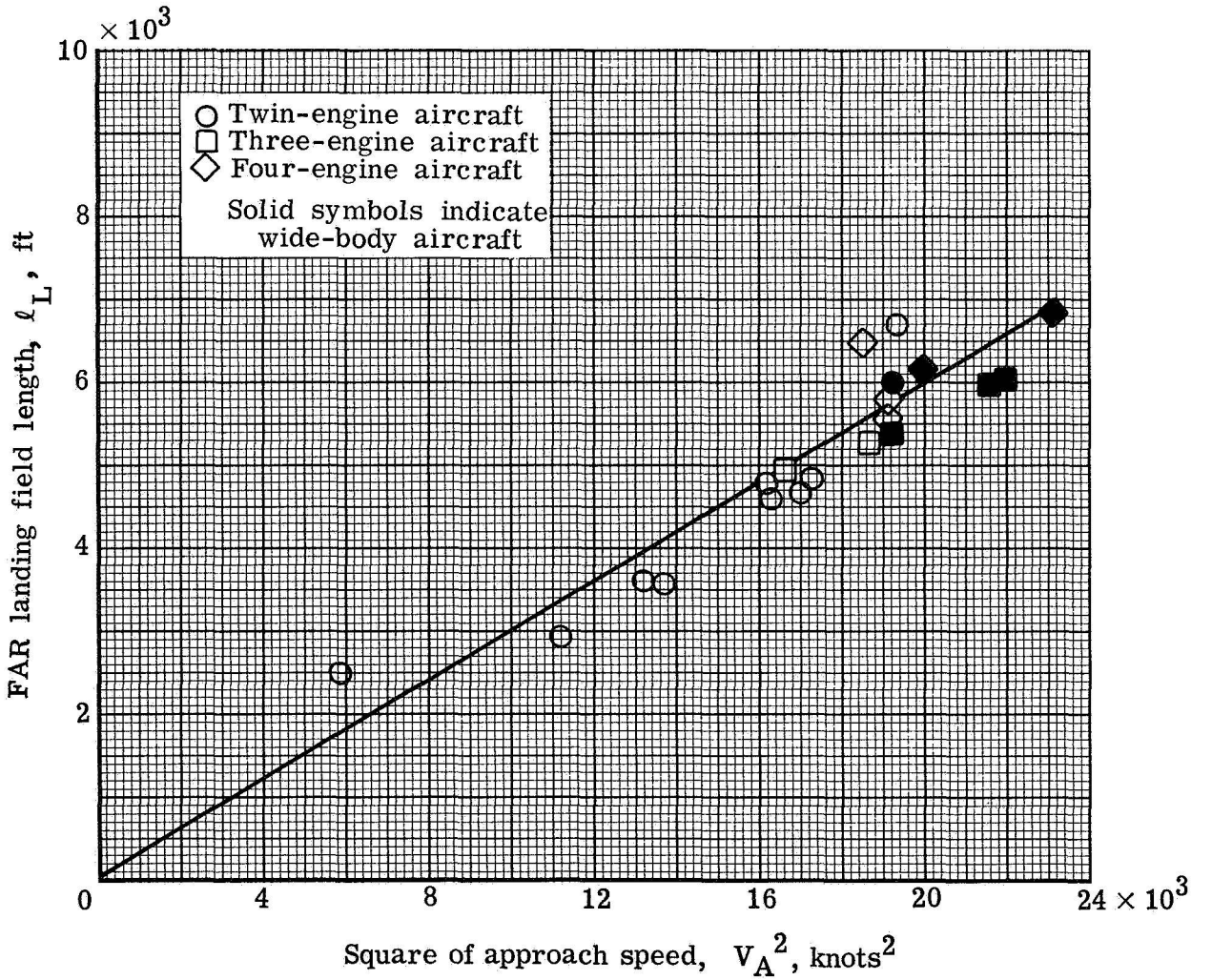


Figure 3.4.- FAR landing field length as a function of square of approach speed for a number of jet-powered aircraft.

3.4.2 Missed Approach

The missed approach must also be considered in relation to the landing maneuver. The missed approach is a situation in which the aircraft is on final approach to a landing but does not land for one of several reasons; instead, power is applied and the aircraft climbs, usually to circle the airport and initiate another landing approach. Federal Air Regulations (ref. 3.4) for transport-category aircraft require the installation of sufficient thrust so that the aircraft can climb from a missed approach, in the approach configuration, at a specified gradient with one engine inoperative and at maximum landing weight. The specified climb gradients are 2.7 percent for four-engine aircraft, 2.4 percent for three-engine aircraft, and 2.1 percent for two-engine aircraft.

A simple relationship for estimating the thrust required to meet the wave-off climb gradient requirement may be derived by balancing the forces along the flight path as follows:

$$T = D + W \sin \gamma \tag{3.2}$$

where

T engine thrust, lb

D aircraft drag, lb

W aircraft weight, lb

γ flight-path angle

For small values of the flight-path angle, $\sin \gamma$ is approximately equal to the angle γ, expressed in radians, which in turn represents the climb gradient, in percent, divided by 100. With this simplification and dividing by the aircraft weight, equation (3.2) takes the form

$$\frac{T}{W} = \frac{1}{L/D} + \gamma \tag{3.3}$$

where L/D is the lift-drag ratio of the aircraft in the approach configuration. In order for the climb gradient criteria to be satisfied with one engine inoperative, the thrust-to-weight ratio with all engines operating may be determined from a modification of equation (3.3). If N is the number of engines, the required thrust-to-weight ratio with all engines operating is given by the expression

$$\frac{T}{W} = \left(\frac{N}{N - 1}\right)\left(\frac{1}{L/D} + \gamma\right) \tag{3.4}$$

where, for wave-off, the weight W should be the maximum landing weight.

The lift-drag ratio of an aircraft in the approach configuration is difficult to estimate accurately and is dependent upon the detail design of the high-lift system and the extent to which it is deployed in any given situation. Hence, the determination of the thrust-to-weight ratio required to meet the wave-off climb requirement should, whenever possible, be accomplished with a knowledge of the lift and drag characteristics of the particular configuration under consideration. In order to provide some illustrative information on the thrust-to-weight ratio requirements, however, the lift-drag ratios have been computed for several aircraft having wings equipped with double-slotted flaps and leading-edge slats. The wings were swept back 33° along the quarter chord line, had taper ratios of 0.5, and had aspect ratios of 6, 8, and 10. The 25-percent-chord double-slotted flaps were assumed to influence 65 percent of the exposed wing area, and the leading-edge slats were assumed to extend over essentially the entire semispan of the wing.

The lift and drag characteristics of the sample wings were estimated with the aid of the methods and data of references 3.6 and 3.7. Approach lift coefficients of 1.3, 1.5, and 1.7 were estimated to require trailing-edge flap deflections of 15°, 25°, and 35°, along with appropriate deployment of the leading-edge slats. The maximum lift coefficients corresponding to the approach lift coefficients of 1.3, 1.5, and 1.7 can be determined through multiplication by the factor 1.69 and are 2.2, 2.54, and 2.87, respectively. Flap deflections required for other approach lift coefficients were determined from a faired line through the three estimated points. A knowledge of the flap deflections is necessary in order to estimate the drag associated with the high-lift system.

The drag coefficient of the aircraft with flaps deployed is given by the expression

$$C_D = C_{D,0} + \Delta C_{D,f} + \Delta C_{D,s} + \Delta C_{D,g} + (C_{D,i})_{clean} + \Delta C_{D,i} \tag{3.5}$$

where

C_D total drag coefficient

$C_{D,0}$ zero-lift drag coefficient of aircraft in the clean condition

$\Delta C_{D,f}$ increment in profile drag coefficient due to trailing-edge flap deflection (For a given flap design, $\Delta C_{D,f}$ depends on flap deflection.)

$\Delta C_{D,s}$ increment in profile drag coefficient due to slat deflection (For a given slat design, $\Delta C_{D,s}$ depends on slat deflection.)

$\Delta C_{D,g}$ increment in profile drag coefficient due to landing-gear extension

$(C_{D,i})_{clean}$ induced drag coefficient of aircraft at the desired lift coefficient but calculated with an efficiency factor appropriate to clean aircraft

$\Delta C_{D,i}$ increment in induced drag coefficient caused by reduction in airplane efficiency factor which accompanies flap deflection

The zero-lift drag coefficient for the aircraft in the clean condition was assumed to be 0.02 in the present calculations.

The increments in profile drag coefficient associated with trailing-edge flap deflection were estimated (ref. 3.6) to be 0.01, 0.02, and 0.03 for flap deflections of 15°, 25°, and 35°. The increments in profile drag for other flap deflections were taken from a faired line through these three points. The increment in profile drag coefficient associated with slat deflection $\Delta C_{D,s}$ was assumed to be zero because of the scarcity of data on which to base a meaningful estimate. The landing gear drag was taken to be 0.015 on the basis of data given in the paper by J. G. Callaghan of reference 3.8. The total induced drag coefficient

$$C_{D,i} = (C_{D,i})_{clean} + \Delta C_{D,i}$$

was evaluated for a single aspect ratio and several flap deflections according to the detailed methods described in reference 3.7. The results indicated that the total induced drag coefficient could be approximated with good accuracy by the following simple expression:

$$C_{D,i} = \frac{C_L^2}{\pi A \varepsilon} \tag{3.6}$$

where

C_L lift coefficient

A wing aspect ratio

ε Oswald's airplane efficiency factor

In this case the value of the airplane efficiency factor ε was taken to be 0.7 rather than 0.85 which is a more appropriate value for an aircraft in the clean condition. A more detailed discussion of the airplane efficiency factor ε is given in section 3.5.1. The lift-drag ratios were accordingly calculated with the use of the following equation:

$$\frac{L}{D} = \frac{C_L}{C_{D,p} + \frac{C_L^2}{\pi A(0.7)}} \tag{3.7}$$

where

$$C_{D,p} = C_{D,0} + \Delta C_{D,f} + \Delta C_{D,g}$$

The results of these calculations for aspect ratios of 6, 8, and 10 and lift coefficients from 1.2 to 1.8 are given in table 3.II.

With the use of the data given in table 3.II and equation (3.4), the values of thrust-to-weight ratio required to meet the missed approach criteria were determined for the different aspect ratios and approach lift coefficients. The calculated results are shown by the curves in figure 3.5 which represent the required thrust-to-weight ratio as a function of approach lift coefficient for two-, three-, and four-engine aircraft having aspect ratios of 6, 8, and 10. If information on the lift-drag characteristics of the specific aircraft under consideration is not available, the curves of figure 3.5 may be used to obtain a first estimate of the thrust-to-weight ratio required to meet the appropriate missed approach climb gradient criterion if the high-lift system is generally similar to that considered in calculating the lift-drag ratios in table 3.II.

3.4.3 Take-Off Field Length

The FAR take-off field length, often called the FAR balanced field length, contains certain inherent safety features to account for engine failure situations. This take-off field length is defined in several slightly different ways and is described fully in reference 3.4. Briefly, if an engine should fail during the take-off roll at a critical speed, called the decision speed V_1, the pilot is offered the option of two safe courses of action. He may elect to continue the take-off on the remaining engines, in which case, the take-off distance is defined as the distance from the point where the take-off run is initiated to the point where the aircraft has reached an altitude of 35 ft. In the second alternative, the pilot may elect to shut down all engines and apply full braking. The decision speed V_1 is chosen in such a way that the sum of the distance required to accelerate to V_1 and then decelerate to a stop is the same as the total distance for the case in which the take-off is continued following engine failure. If an engine should fail before V_1 is reached, the aircraft is usually brought to a stop on the runway; whereas, if an engine fails at a speed greater than V_1, the take-off is continued. The distances are based on smooth, hard, dry runway surfaces. A somewhat idealized sketch of the FAR take-off field length is shown in figure 3.6.

A relationship between the FAR take-off field length and the aircraft wing loading, thrust loading, and maximum lift coefficient will now be developed.

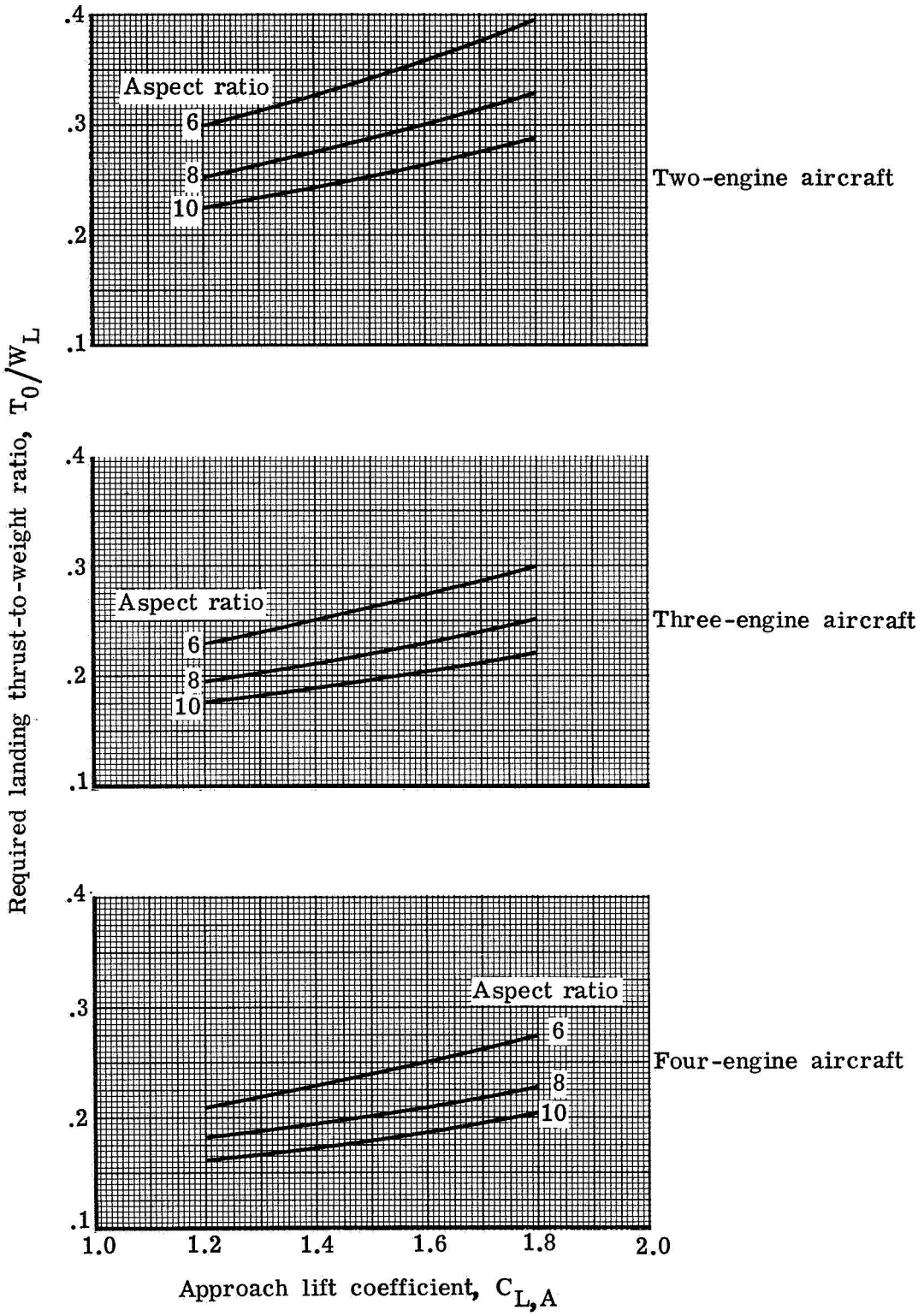


Figure 3.5.- Landing thrust-to-weight ratio, all engines operating, required to meet missed approach criterion for jet-powered transport aircraft.

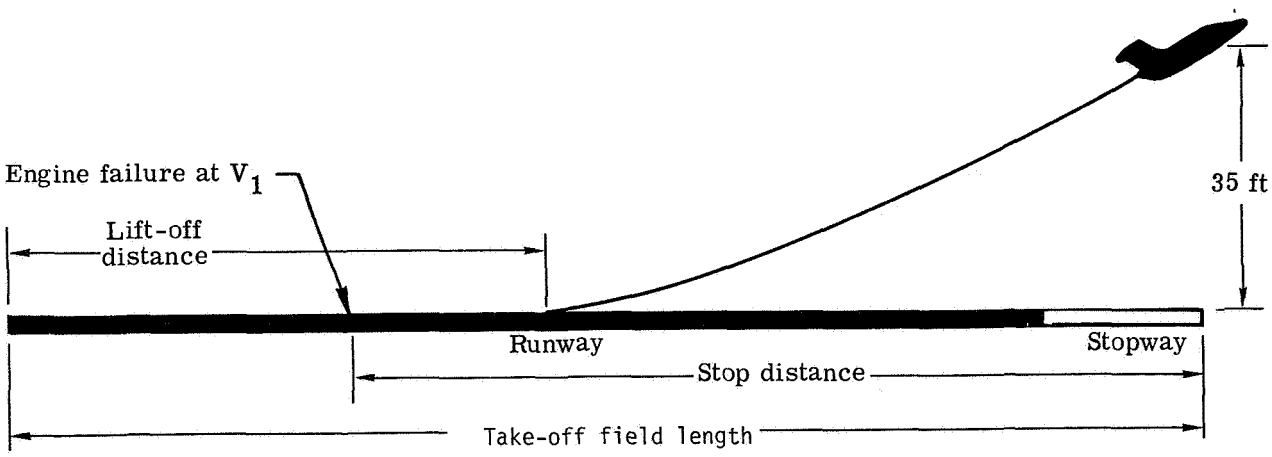


Figure 3.6.- FAR balanced take-off field length.

In order to isolate the significant parameters controlling the take-off distance, assume that the aerodynamic drag during take-off roll and the rolling friction resulting from contact between the aircraft wheels and the ground are zero. The following basic physical relations may be employed to derive an expression for the distance $\ell_{T,g}$ required to accelerate to the lift-off speed corresponding to the lift coefficient $C_{L,lo}$ at lift-off:

$$\ell_{T,g} = \frac{V_{lo}^2}{2a} \tag{3.8}$$

$$\frac{T_0}{W_g} = \frac{a}{g} \tag{3.9}$$

$$V_{lo} = \sqrt{\frac{W_g}{SC_{L,lo}\left(\frac{\rho}{2}\right)}} \tag{3.10}$$

where

a average acceleration of aircraft along ground, ft/sec^2

ρ atmospheric density

g acceleration due to gravity

V_{lo} lift-off speed corresponding to $C_{L,lo}$

$\frac{T_0}{W_g}$ aircraft thrust-to-weight ratio with all engines operating, expressed in terms of maximum take-off gross weight and maximum sea-level static thrust

Equations (3.8), (3.9), and (3.10) may be combined in such a way as to give the following expression:

$$\ell_{T,g} = \frac{K}{\sigma C_{L,lo}} \frac{(W_g/S)}{(T_0/W_g)} \tag{3.11}$$

where

$$K = \frac{1}{\rho_0 g}$$

$$\sigma = \frac{\rho}{\rho_0}$$

and ρ_0 is the atmospheric density for standard sea-level conditions. The length $\ell_{T,g}$ defined by equation (3.11) is the ground run to lift-off on the assumption of zero aerodynamic drag and rolling friction. The actual ground-run distance would be expected to be somewhat larger than that given by equation (3.11). The assumption is now made that, for the class of aircraft considered, the FAR take-off field length should bear a nearly constant relationship to the ground run with all engines operating. On the basis of this assumption, a close correlation might be expected between the FAR take-off field length ℓ_T and the parameter $\frac{W_g/S}{\sigma C_{L,lo}(T_0/W_g)}$.

The lift coefficient $C_{L,lo}$ which appears in the parameter $\frac{W_g/S}{\sigma C_{L,lo}(T_0/W_g)}$ is not readily derivable from data given in tables of aircraft specifications. The maximum lift coefficient for the aircraft in the take-off configuration $C_{L,T}$, however, may be utilized in the take-off parameter. The FAR field length is shown in figure 3.7 as a function of $\frac{W_g/S}{\sigma C_{L,T}(T_0/W_g)}$ for 19 different aircraft. The value of $C_{L,T}$ was taken to be 1.44 times the lift coefficient corresponding to the steady-state second-segment climb speed V_2 since the value of V_2 is defined as 1.2 times the stalling speed for the aircraft in the take-off configuration (ref. 3.4). Values of V_2 are given in the tables of specifications presented in reference 3.3 and the corresponding values of

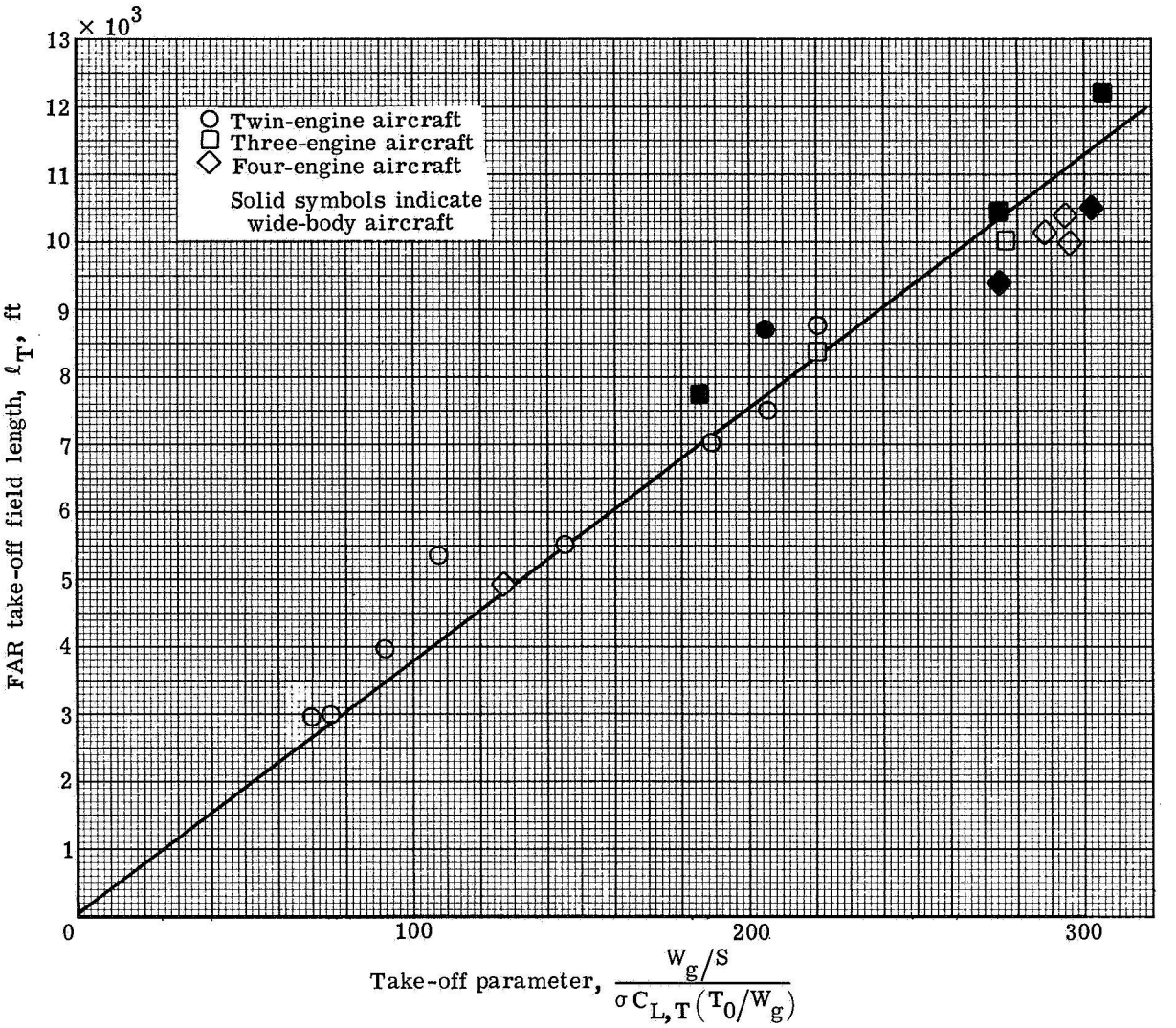


Figure 3.7.- FAR take-off field length as function of take-off parameter for a number of jet-powered aircraft.

lift coefficient were computed from the given speed and wing loading. The correlation shown by the data in figure 3.7 appears to provide an adequate means for estimating the FAR take-off field length.

A means for estimating $C_{L,T}$ (on the basis of contemporary practice) is provided in figure 3.8 which shows the second-segment climb speed V_2 as a function of the square root of the wing loading $\sqrt{\frac{W_g/S}{\sigma}}$ for a number of aircraft.

The flags on the symbols in figure 3.8 indicate that the type of trailing-edge high-lift system employed has little effect on the lift coefficient used in the second-segment climb. A good average value of the lift coefficient for the second-segment climb $C_{L,2}$ might be about 1.4. Consequently, the corresponding average maximum lift coefficient for the aircraft in the take-off configu-

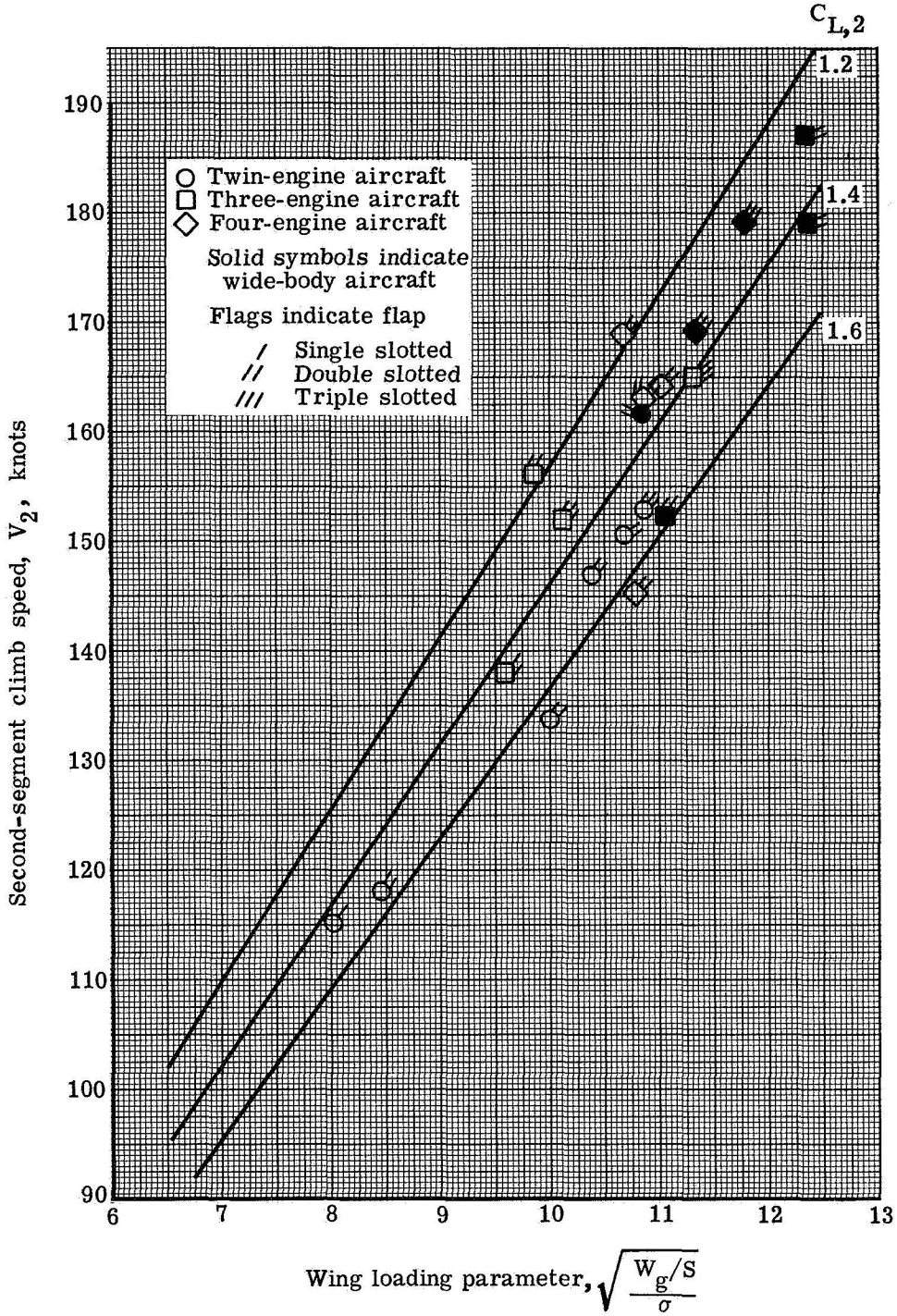


Figure 3.8.- Second-segment climb speed as function of wing loading parameter for a number of jet-powered aircraft.

ration is about 2.0. Methods for determining more exact values of the maximum lift coefficient in the take-off configuration and the second-segment climb lif

coefficient to be employed in a particular case are described in section 3.6 on aircraft matching procedure. Figures 3.7 and 3.8 provide the necessary information for estimating the FAR take-off field length in terms of significant aircraft design parameters.

3.4.4 Second-Segment Climb Gradient

Another factor which must be considered in relation to the take-off maneuver is the FAR second-segment climb gradient requirement. The second-segment climb is that portion of the flight path, following take-off, conducted at V_2, which extends from an altitude of 35 to 400 ft. The Federal Air Regulations require that sufficient thrust be installed in the aircraft so that in the event of an engine failure, the following second-segment climb gradients may be sustained, that is, 3 percent for four-engine aircraft, 2.7 percent for three-engine aircraft, and 2.4 percent for two-engine aircraft. The aircraft must satisfy these requirements with flaps in the take-off position but with the landing gear retracted. The required thrust-to-weight (maximum take-off weight) ratio was estimated with the use of equation (3.4) for a range of lift coefficients extending from 1.2 to 1.8 and for aspect ratios of 6, 8, and 10. The aircraft lift-drag ratios were estimated in the same fashion as described for the missed approach case, given in section 3.4.2, except that no drag increment was added for the landing gear. The resulting lift-drag ratios are given in table 3.III.

With the use of equation (3.4) and the data given in table 3.III, the values of thrust-to-weight ratio required to meet the second-segment climb gradient criteria were determined for the different aspect ratios and climb lift coefficients. The calculated results are shown by the curves in figure 3.9 which represent the required thrust-to-weight ratio as a function of lift coefficient for two-, three-, and four-engine aircraft having aspect ratios of 6, 8, and 10. If information on the lift and drag characteristics of the specific aircraft under consideration is not available, the curves of figure 3.9 may be used to obtain a first estimate of the thrust-to-weight ratio required to meet the appropriate second-segment climb gradient criterion if the high-lift system is generally similar to that considered in calculating the lift-drag ratios given in table 3.III.

Comparison of the curves of figures 3.5 and 3.9 indicates that, for a given lift coefficient and aspect ratio, the required thrust-to-weight ratio is greater for the missed approach case than for the second-segment climb gradient. The drag of the extended landing gear in the missed approach condition is responsible for this result, however, the maximum take-off weight is greater than the maximum landing weight in most cases. Accordingly, the required thrust-to-weight ratio, in terms of maximum take-off weight, is frequently higher for the second-segment climb gradient than for the missed approach. The relationship between maximum take-off weight and maximum landing weight is discussed in the next section.

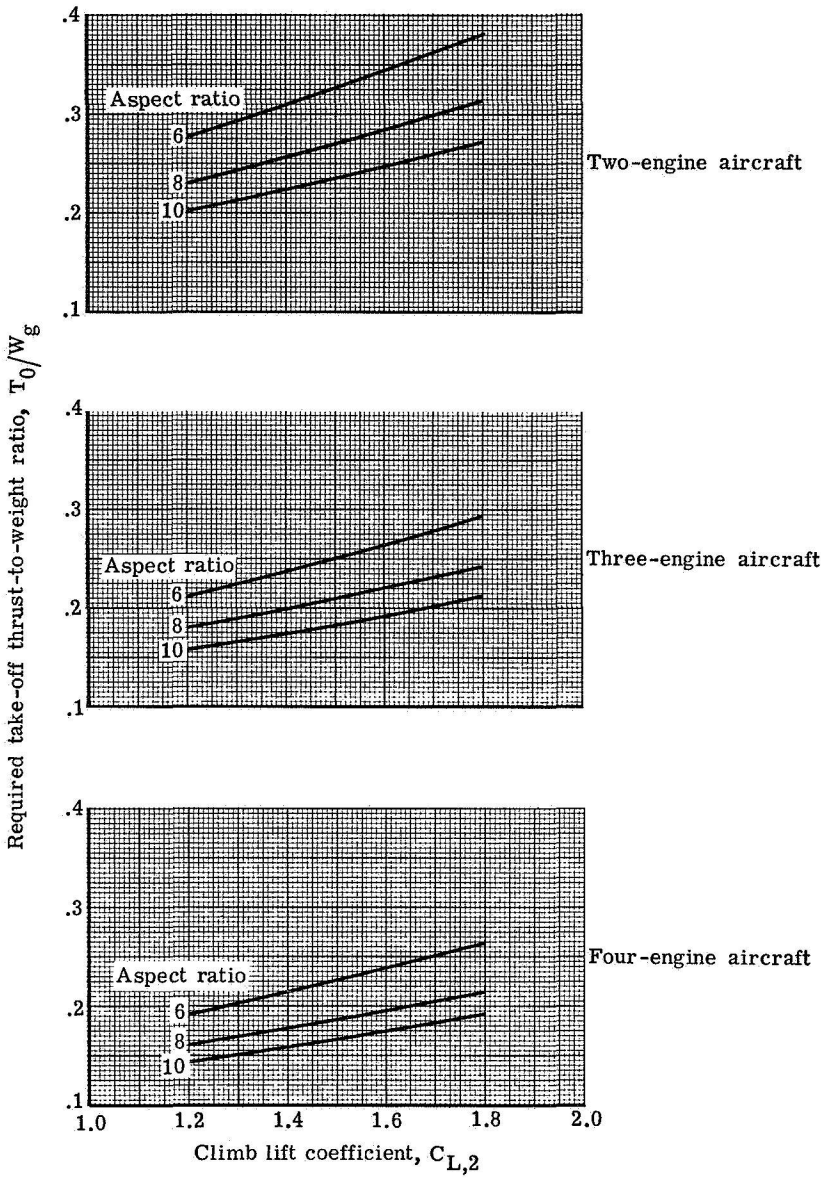


Figure 3.9.- Take-off thrust-to-weight ratio, all engines operating, required to meet second-segment climb gradient criterion for jet-powered transport aircraft.

3.4.5 Take-Off and Landing Weight Relationships

The wing loading W/S and thrust loading T/W have been used repeatedly in the preceding discussion of the landing and take-off maneuvers. In order to relate the thrust requirements for these two maneuvers, the maximum landing weight must be known in terms of the maximum take-off weight. The relationship between these two weights varies in accordance with the mission for which the aircraft is intended. The ratio of maximum landing weight to maximum take-off gross weight W_L/W_g is shown in figure 3.10 for 24 different aircraft in three

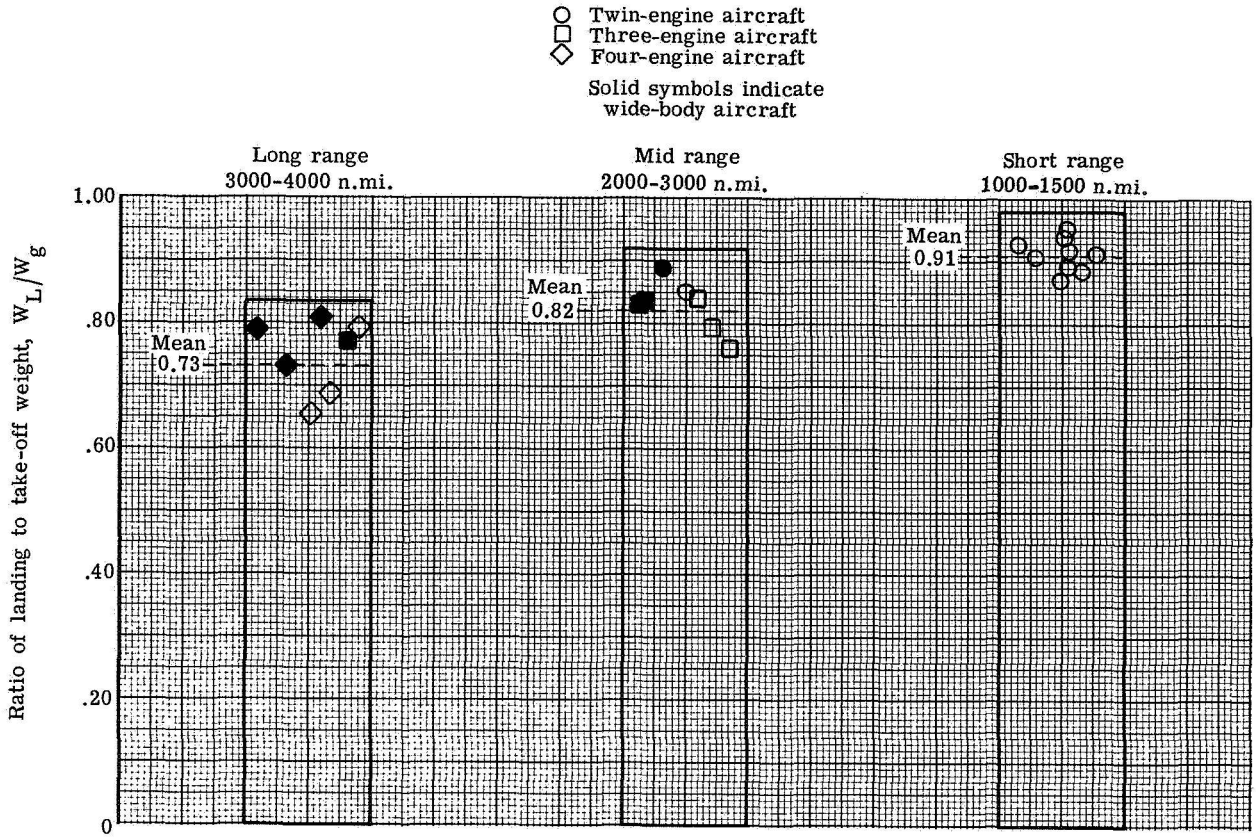


Figure 3.10.- Ratio of maximum landing weight to maximum take-off weight for a number of jet-powered aircraft.

groups categorized as long-range, mid-range, and short-range aircraft. Typically, the ranges at maximum payload for the three categories are 3000 to 4000, 2000 to 3000, and 1000 to 1500 n. mi.; the mean values of the weight ratios are 0.73, 0.82, and 0.91 for long-, mid-, and short-range aircraft. The higher weight ratios for the shorter range aircraft reflect the use of these aircraft on short route segments without refueling at each stop. Some of the small business jets have the same maximum landing and take-off weight. In this case, the thrust-to-weight ratio required to meet the wave-off criterion is higher than that for the second-segment climb gradient. The information in figure 3.10 may be used as a guide for estimating the maximum landing weight in terms of maximum take-off gross weight in the absence of more specific information.

3.5 Cruising Performance

A cruise matching analysis is indicated in block 5 of figure 3.1. This analysis which will now be discussed provides a method for matching the engine to the airframe in such a way as to permit cruising in a specified manner. The cruising criterion to be used herein is that the pertinent engine and airframe characteristics will be matched in such a way as to permit achievement of a specified design range at a given cruising Mach number for a minimum amount of

fuel. The quantitative relationship between the range, the significant aircraft and engine characteristics, and the fuel used during cruising flight is given by the well-known Breguet range equation:

$$R = \frac{V(L/D)}{c} \log_e \frac{1}{1 - \frac{W_f}{W_g}} \tag{3.12}$$

where

R range, n. mi.

V speed, knots

L/D aircraft lift-drag ratio

c engine specific fuel consumption, pounds of fuel per pound of thrust per hour

W_g aircraft gross weight, lb

W_f aircraft fuel weight, lb

The parameter $\frac{V(L/D)}{c}$ is often called the Breguet factor which is designated by the symbol B. Equation (3.12) may also be written in the useful form

$$\frac{W_f}{W_g} = 1 - \frac{1}{e^{R/B}} \tag{3.13}$$

which explicitly gives the fuel fraction necessary for a specified range. The Breguet range equation as given by equations (3.12) and (3.13) is applicable to jet-powered aircraft and takes a somewhat different form when applied to propeller-driven aircraft. The range of propeller-driven aircraft is discussed in section 6.9 of chapter 6.

According to equation (3.13), the desired range is achieved with the minimum fuel fraction when the aircraft is flown at the maximum value of the Breguet factor B. The Breguet factor may also be written in the form

$$B = \frac{V(L/D)}{c} = \frac{aM(L/D)}{c} \tag{3.14}$$

where

a speed of sound, knots

M cruising Mach number

The speed of sound decreases with altitude until the tropopause (about 35 000 ft) is reached after which it remains constant with further increases in altitude up to about 105 000 ft. Regardless of the altitude at which the aircraft is matched, equation (3.14) shows, however, that the minimum fuel fraction for a given range is obtained when the Breguet factor is a maximum. The cruising Mach number is considered as a specified quantity and, for the altitude for which the aircraft is matched, is usually chosen to be somewhat less than the force divergence Mach number, that is, the Mach number at which large changes in aerodynamic characteristics occur as a result of the formation of shock waves on the aircraft. The Breguet factor at this Mach number will be a maximum when the aircraft is operated at the maximum value of the lift-drag ratio. The aircraft will therefore be matched in such a way that sufficient thrust is available to balance the drag in level, unaccelerated flight at the maximum lift-drag ratio and the specified design Mach number. The aircraft, however, will usually be operated under a variety of conditions. A discussion of the manner in which the range for a given fuel fraction varies with altitude and Mach number is contained in section 3.10.

3.5.1 Aircraft Lift-Drag Characteristics

Highly sophisticated and accurate methods are available for estimating the lift and drag characteristics of aircraft. For example, detailed methods for calculating drag polars are given in references 3.6, 3.7, and 3.9. The scope of current development work on drag prediction methods can be judged from the collections of papers contained in references 3.8 and 3.10. Described herein is a method which permits a rapid estimation of the aircraft lift-drag characteristics. The method, although approximate, may be used with reasonable accuracy in those cases where time does not permit more lengthy calculations or where the nature of the desired results does not justify such calculations.

If the drag polar is assumed to be symmetrical about zero lift, the drag coefficient at any lift coefficient below the stall may be expressed as follows:

$$C_D = C_{D,0} + \frac{C_L^2}{\pi A \epsilon} \tag{3.15}$$

where

$C_L^2/\pi A\epsilon$ induced drag coefficient, $C_{D,i}$

C_D total drag coefficient

$C_{D,0}$ zero-lift drag coefficient

C_L lift coefficient

A wing aspect ratio

ε Oswald's airplane efficiency factor (to be discussed in section 3.5.1.1)

The value of the lift-drag ratio is given by the expression

$$\frac{L}{D} = \frac{C_L}{C_{D,0} + \frac{C_L^2}{\pi A \varepsilon}} \tag{3.16}$$

The value of the lift coefficient for the maximum value of L/D, and the value of $(L/D)_{max}$ may be deduced by taking the derivative of equation (3.16) with respect to C_L and equating this derivative to zero. Thus,

$$\frac{d(L/D)}{dC_L} = \frac{\left(C_{D,0} + \frac{C_L^2}{\pi A \varepsilon}\right) - \frac{2C_L^2}{\pi A \varepsilon}}{\left(C_{D,0} + \frac{C_L^2}{\pi A \varepsilon}\right)^2} \tag{3.17}$$

Equating equation (3.17) to zero gives

$$\frac{C_L^2}{\pi A \varepsilon} = C_{D,0} \tag{3.18}$$

Equation (3.18) indicates the very important result that the induced drag coefficient is equal to the zero-lift drag coefficient at the maximum value of the lift-drag ratio. The total drag coefficient at $(L/D)_{max}$ is then equal to twice the zero-lift drag coefficient or twice the induced drag coefficient. From equation (3.18), the lift coefficient $C_{L,m}$ corresponding to $(L/D)_{max}$ is given by

$$C_{L,m} = \sqrt{C_{D,0} \pi A \varepsilon} \tag{3.19}$$

Since the total drag coefficient at $(L/D)_{max}$ is twice the zero-lift drag coefficient,

$$(L/D)_{max} = \frac{\sqrt{C_{D,0}\pi A\epsilon}}{2C_{D,0}}$$

or, more conveniently,

$$(L/D)_{max} = \frac{1}{2}\sqrt{\frac{\pi A\epsilon}{C_{D,0}}} \tag{3.20}$$

Equations (3.19) and (3.20) are simple expressions which are extremely useful and will be employed in subsequent analysis.

3.5.1.1 Airplane Efficiency Factor

The expression, equation (3.15), for the variation of drag coefficient with lift coefficient contains an efficiency factor ϵ in the denominator. The efficiency factor may be defined in several ways depending upon the manner in which the equation for the drag polar is written and depending upon whether the equation is for the entire airplane or for the wing alone. A short explanation of the meaning of the efficiency factor ϵ, as used in equation (3.15), would therefore appear to be appropriate.

The efficiency factor used in equation (3.15) is applicable to the entire aircraft and accounts for the influence of two important factors on the drag due to lift. A wing operating in an inviscid flow generates a drag due to lift, or induced drag, which can be expressed in coefficient form by the following equation:

$$C_{D,i} = \frac{C_L^2}{\pi Au} \tag{3.21}$$

where u is a number whose value depends upon the shape of the span loading. Equation (3.21) was first developed by Prandtl and his associates during, or just after, World War I. The factor u was shown to be 1.0 for a wing with elliptical span loading and to be less than 1.0 for all other span loadings. The planform shape necessary in order to achieve an elliptical span loading on an untwisted wing was also found to be elliptical. Thus, this shape wing provides the minimum induced drag coefficient for a given aspect ratio and lift

coefficient. Most wings, however, are not elliptical in shape but employ either straight leading and trailing edges or such edges made up of straight elements. The value of u is given in reference 3.11 for unswept wings of different aspect ratio and taper ratio. For example, a wing of aspect ratio 8 and taper ratio of 0.5 is shown in reference 3.11 to have a value of u of about 0.97 to 0.98. Thus, the departure from an elliptical span loading does not have a large effect on the induced drag coefficient for wings of conventional aspect ratio and taper ratio. The influence of the span loading on the induced drag coefficient becomes more pronounced for higher aspect ratios and, in particular, for more highly tapered wings.

The second effect which the efficiency factor ε accounts for is the variation of the viscous drag coefficient with lift coefficient. Oswald showed in reference 3.12 that the viscous drag coefficient, as well as the inviscid induced drag coefficient, varies linearly as the square of the lift coefficient. The variation of the total drag coefficient with lift coefficient was thus indicated to be given by an expression like equation (3.21) but in which the parameter u is replaced by the efficiency factor ε which accounts for the effects of departure from an elliptic span loading as well as the variation of viscous drag coefficient with lift coefficient. Thus,

$$C_{D,i} = \frac{C_L^2}{\pi A \varepsilon} \tag{3.22}$$

The factor ε is sometimes applied to the variation of the drag coefficient of the wing alone and, in this case, is referred to as the span efficiency factor. As defined by Oswald, ε accounts for the variation of drag coefficient with lift coefficient for the entire airplane and is called the airplane efficiency factor. The parameter ε as used herein applies in all cases to the entire aircraft.

In order to provide some further insight into the meaning of the parameter ε, a derivation will now be given which follows the approach employed by Perkins and Hage in reference 3.13. If the variation of viscous drag coefficient with lift coefficient is represented by an expression of the form

$$\Delta C_D = K C_L^2$$

where K is a constant of proportionality, the equation for the drag polar takes the form

$$C_D = C_{D,0} + K C_L^2 + \frac{C_L^2}{\pi A u}$$

or

$$C_D = C_{D,0} + \left(K + \frac{1}{\pi A u}\right) C_L^2 = C_{D,0} + \left(K\pi A + \frac{1}{u}\right)\frac{C_L^2}{\pi A}$$

and finally

$$C_D = C_{D,0} + \frac{C_L^2}{\pi A \epsilon}$$

from which the airplane efficiency factor is given as

$$\epsilon = \frac{1}{\pi K A + \frac{1}{u}} \tag{3.23}$$

Equation (3.23) indicates the very important result that the airplane efficiency factor decreases with increasing aspect ratio for a given value of K. The variation in viscous drag coefficient with lift coefficient becomes a larger proportion of the total drag coefficient increment due to lift as the aspect ratio increases, and, hence, is responsible for the effect of aspect ratio on the airplane efficiency factor indicated by equation (3.23).

The value of the airplane efficiency factor for clean aircraft (flaps and landing gear retracted) is usually between 0.70 and 0.85 according to reference 3.13. Flight and wind-tunnel data presented in the paper by J. G. Callaghan of reference 3.8 indicate that values of ϵ from 0.74 to 0.80 were obtained for a number of aircraft. The value of the airplane efficiency factor was taken to be 0.85 for all clean, jet-powered aircraft considered in chapter 3.

3.5.1.2 Estimation of Maximum Lift-Drag Ratio

Presented now is a method which permits a rapid estimation of the aircraft maximum lift-drag ratio. The method makes use of equation (3.20) which is repeated here for convenience

$$(L/D)_{max} = \frac{1}{2}\sqrt{\frac{\pi A \epsilon}{C_{D,0}}} \tag{3.20}$$

The value of the zero-lift drag coefficient in equation (3.20) is estimated by extrapolating a known value for a current, reference aircraft to other configurations in accordance with the relation

$$\frac{C_{D,0}}{(C_{D,0})_{ref}} = \frac{A_t/S}{(A_t/S)_{ref}} \tag{3.24}$$

where

A_t total aircraft wetted area

S wing area

and the subscript ref refers to the reference aircraft which is a modern, four-engine, long-range transport. This extrapolation implies that all of the aircraft are of the same general configuration, operate at the same Reynolds number, and are designed with the same degree of excellence as the reference aircraft and that the interference drag, drag due to roughness, etc., vary directly with the wetted area. These assumptions are probably reasonable for well-designed aircraft. The accuracy of the extrapolation, however, would be expected to deteriorate if the configuration considered departs too radically from typical present-day jet transports and executive jet aircraft.

The wetted area of all aircraft, including the reference aircraft, is represented by an analytical expression in which the fuselage is simulated by a circular cylinder of constant diameter that is closed at the aft end by a cone with height of approximately twice the fuselage diameter and at the front end by a hemisphere. The expression developed for the ratio of the wetted area to wing area is as follows:

$$\frac{A_t}{S} = \frac{\pi d^2}{S}\left(\frac{l}{d} - 1.0\right) + 2\left(1 + \frac{S_t}{S}\right) + \frac{A_n}{S} \tag{3.25}$$

where

A_t total wetted area

S wing area

l/d fuselage length-to-diameter ratio

S_t sum of vertical and horizontal tail area

A_n nacelle wetted area

Calculations were made of the maximum lift-drag ratio with the use of equations (3.20) and (3.25) for aircraft with a variety of aspect ratios, fuselage length-to-diameter ratios, and ratios of fuselage cross-sectional area to wing area. The value of A_t/S for the reference aircraft was 5.0, and the corresponding value of $C_{D,0}$ for this aircraft, derived from a known value of $(L/D)_{max}$ with the use of equation 3.20, was 0.0131. An examination of the characteristics of 10 current aircraft yielded average values of 0.44 and 0.47 for A_n/S and S_t/S, respectively. These values were used in all calculations of the maximum lift-drag ratio. The results are expressed in the form of a design chart which is presented in figure 3.11. The chart, which is thought to be

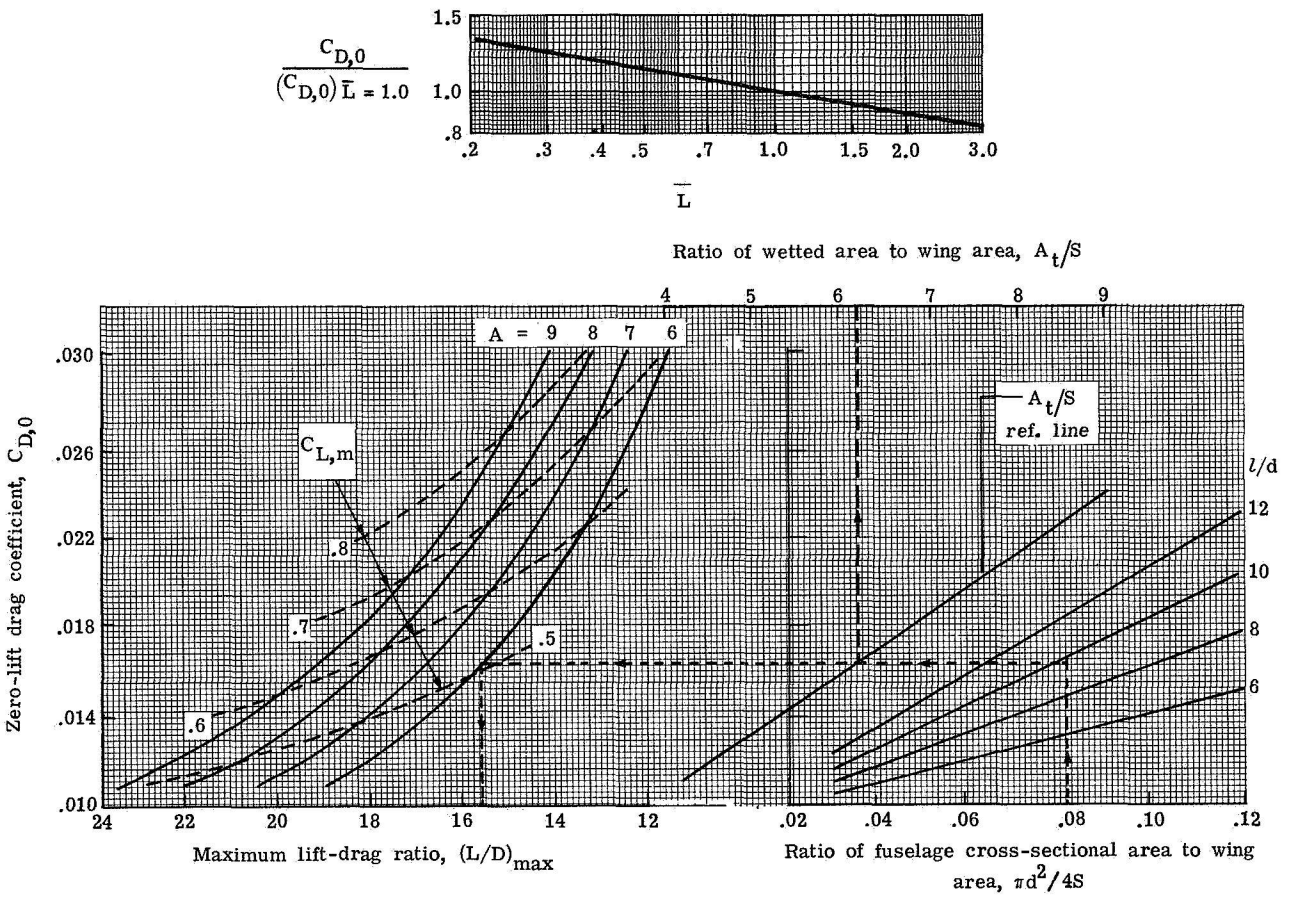


Figure 3.11.- Chart for estimating maximum lift-drag ratio.

self-explanatory, permits the estimation of $C_{D,0}$, profile drag coefficient, A_t/S, ratio of wetted area to wing area, $(L/D)_{max}$, maximum lift-drag ratio, and $C_{L,m}$, lift coefficient for $(L/D)_{max}$, for given input values of the ratios of fuselage cross-sectional area to wing area and fuselage length to diameter.

The effect on $C_{D,0}$ of a difference in the Reynolds number of the aircraft under consideration and that of the reference aircraft may be estimated with the use of the following approximate formula, given by Hoerner in reference 3.14,

for the variation of the turbulent skin friction coefficient with Reynolds number:

$$c_f = k(1/R)^m \tag{3.26}$$

where

c_f skin friction coefficient for single surface

R Reynolds number based on surface length

and k and m are constants which vary with the Reynolds number range of interest. For Reynolds numbers in the range from 1×10^6 to 1×10^8, values of k and m of 0.044 and 1/6 should be used. Most transport and business jet aircraft operate in this Reynolds number range. The drag coefficient of the reference aircraft $(C_{D,0})_{ref}$ may be related the drag coefficient $C_{D,0}$ of any geometrically similar aircraft operating at a different Reynolds number by the use of equation (3.26). The relationship takes the form

$$\frac{C_{D,0}}{(C_{D,0})_{ref}} = \left(\frac{R_{ref}}{R}\right)^{1/6} \tag{3.27}$$

Any convenient length may be used in forming the Reynolds number. The root chord of the wing is usually given in aircraft specification tables and will be used herein as the reference length in calculating the Reynolds number. Although the aircraft for which the value of $C_{D,0}$ is desired will usually not be geometrically similar to the reference aircraft, equation (3.27) provides a reasonable means for approximating the effect of Reynolds number on the value of $C_{D,0}$ determined from equations (3.24) and (3.25).

Estimation of the approximate effect of Reynolds number on the value of the zero-lift drag coefficient may be further simplified if the aircraft of interest is assumed to cruise at about the same altitude as the reference aircraft. Such an assumption is frequently reasonable since the optimum cruise altitude for many jet transports lies in the range from 34 000 to 38 000 ft, and the effects on Reynolds number of differences in altitude within this range are relatively small. On the assumption that changes in the ratio of density to viscosity may be neglected, equation (3.27) takes the form

$$\frac{C_{D,0}}{(C_{D,0})_{ref}} = \left[\frac{(V_c c_r)_{ref}}{V_c c_r}\right]^{1/6} \tag{3.28}$$

where

V_c cruising speed, knots

c_r root chord, ft

The use of speed in knots and chord in feet is convenient and is permissable since the conversion factor necessary for dimensional consistancy appears in both the numerator and denominator. The value of $(V_c c_r)_{ref}$ is 1.63×10^4 for an altitude of 35 000 ft. With the use of this quantity, equation (3.28) may be written as

$$\frac{C_{D,0}}{(C_{D,0})_{ref}} = \left(\frac{1.63 \times 10^4}{V_c c_r}\right)^{1/6} = \left(\frac{1}{\bar{L}}\right)^{1/6} \tag{3.29}$$

where

$$\bar{L} = \frac{V_c c_r}{1.63 \times 10^4}$$

The ratio $\dfrac{C_{D,0}}{(C_{D,0})_{\bar{L}=1.0}}$ is plotted against $\bar{L}$ in the upper portion of figure 3.11.

The procedures just outlined have been found to yield values of $(L/D)_{max}$ which are accurate to within about 5 percent for those cases in which $(L/D)_{max}$ is known with reasonable certainty. Values of $(L/D)_{max}$, $C_{L,m}$ and $C_{D,0}$ calculated by the methods described herein are given in table 3.IV, together with appropriate geometric parameters, for a number of wide- and narrow-body transport aircraft and two small business jets. The information in table 3.IV may be of some use as a guide to the geometric characteristics typical of different classes of aircraft, as well as showing the range of values of several pertinent aerodynamic parameters characteristic of modern jet transport aircraft.

3.5.1.3 Variation of Lift-Drag Ratio With Lift Coefficient

The value of the lift-drag ratio at lift coefficients different from that for $(L/D)_{max}$ is frequently needed. A generalized relationship which permits the determination of the lift-drag ratio at any lift coefficient in terms of $(L/D)_{max}$ and the value of the lift coefficient at $(L/D)_{max}$ is easily derived. As was shown in section 3.5.1, the induced drag coefficient is equal to the

zero-lift drag coefficient at $(L/D)_{max}$ for drag polars which are symmetrical around the zero-lift axis. Thus, at $(L/D)_{max}$

$$C_{D,i} = C_{D,0} = \frac{C_{D,m}}{2}$$

or

$$C_{D,0} + \frac{C_{L,m}^2}{\pi A \varepsilon} = 2C_{D,0} = 2C_{D,i}$$

where

$C_{D,i}$ induced drag coefficient

$C_{D,0}$ zero-lift drag coefficient

$C_{D,m}$ total drag coefficient at $(L/D)_{max}$

The ratio of the drag coefficient at any lift coefficient to that at the lift coefficient for $(L/D)_{max}$ can then be written in the form

$$\frac{C_D}{C_{D,m}} = \frac{C_{D,0} + \frac{C_L^2}{\pi A \varepsilon}}{C_{D,0} + \frac{C_{L,m}^2}{\pi A \varepsilon}} = \frac{1}{2}\left(1 + \bar{C}_L^2\right) \tag{3.30}$$

where

C_D total drag coefficient at any lift coefficient C_L

$\bar{C}_L$ $= C_L/C_{L,m}$

Multiplying equation (3.30) by $C_{L,m}/C_L$ and rearranging terms results in the following generalized expression:

$$\frac{L/D}{(L/D)_{max}} = \frac{2}{\frac{1}{\bar{C}_L} + \bar{C}_L} \tag{3.31}$$

The ratio $(L/D)/(L/D)_{max}$, as determined from equation (3.31), is plotted in figure 3.12 as a function of $\bar{C}_L$. The curve given in figure 3.12 is applicable

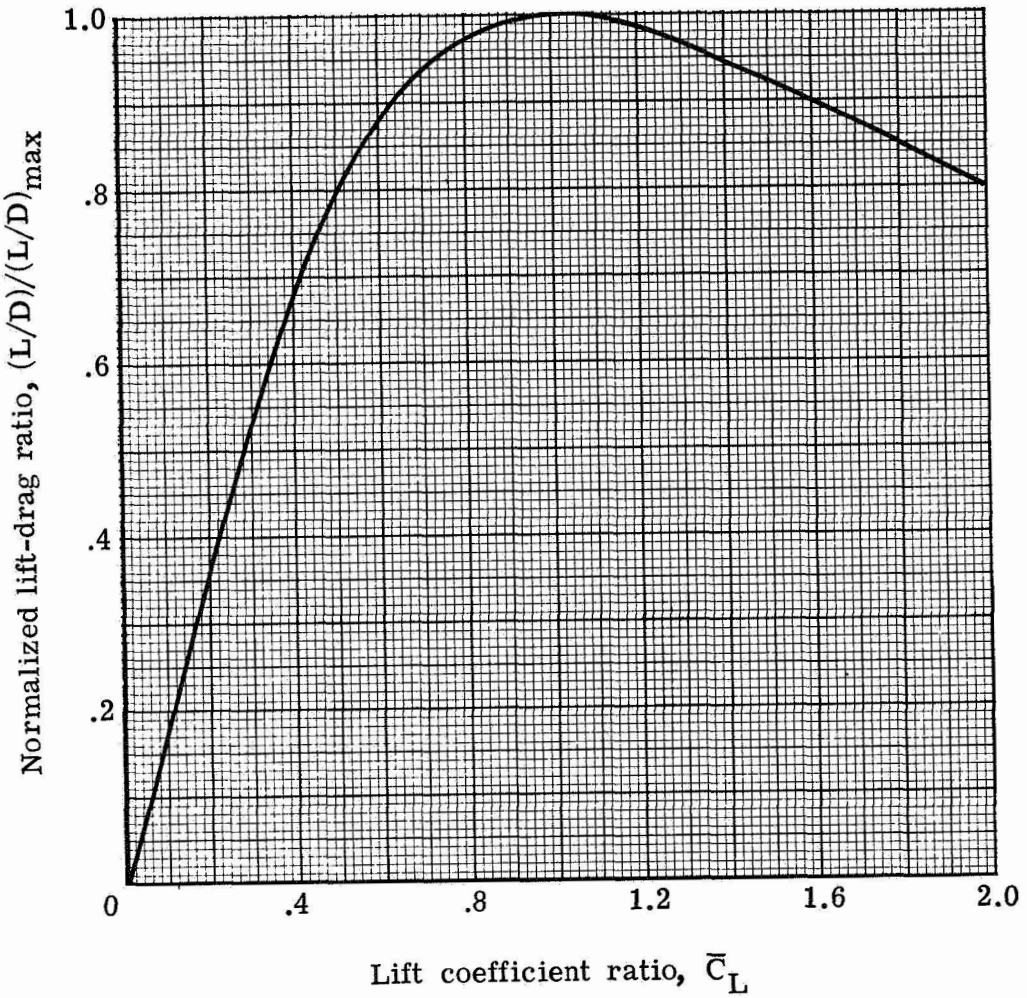


Figure 3.12.- Normalized lift-drag ratio as function of lift coefficient ratio.

to all aircraft below the stall as long as the airplane efficiency factor ε is essentially invariant with lift coefficient and as long as the departure from the assumed symmetrical drag polar is not too large.

3.5.2 Engine Characteristics

The engines must provide sufficient thrust to balance the aircraft drag in cruising flight at the desired combination of altitude and Mach number at which the aircraft is to be operated. The thrust which the engine is capable of producing is primarily a function of the altitude and Mach number, with the amount of the variation depending upon the detailed design of the engine. The

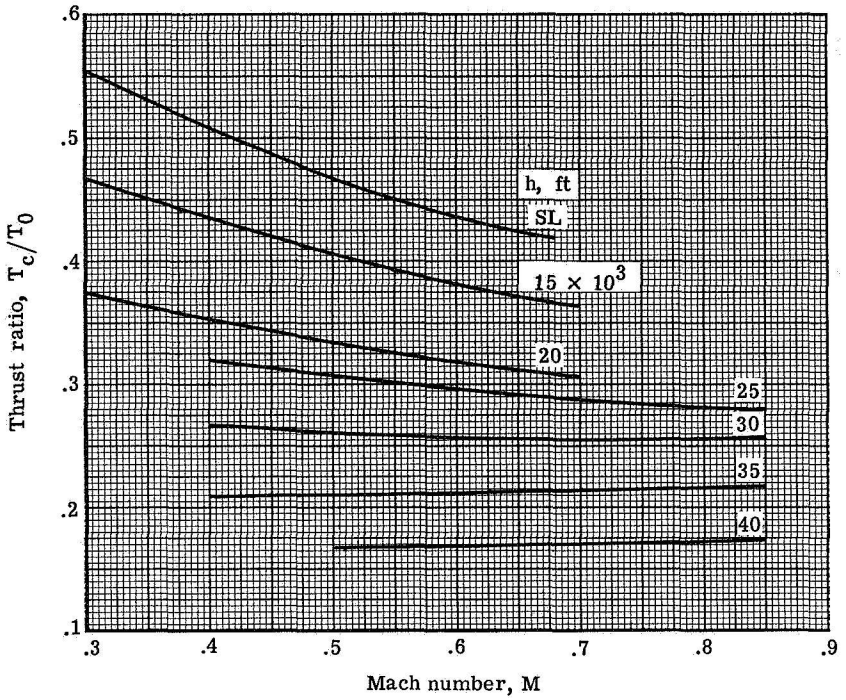
thrust capabilities of the engine also depend upon the ambient temperature at a given altitude and Mach number. For the sake of simplicity, however, the temperatures corresponding to a standard day are assumed in the present discussion; hence, independent effects of temperature are not considered. "Hot day" effects on thrust are important, however, and must be considered in the detailed sizing of real aircraft.

Two different thrust ratings are given on the FAA type certificate data sheet for a particular engine. (See ref. 3.15.) These ratings are defined as the maximum take-off thrust, which can be used for only short periods of time, and the maximum continuous thrust. The maximum continuous thrust is almost always less than the maximum take-off thrust. The manufacturer may define additional ratings such as maximum cruise thrust and maximum climb thrust. The thrust levels defined by these ratings are less than maximum continuous thrust and are dictated by considerations of engine life, maintenance, etc. The maximum take-off thrust and maximum continuous thrust ratings will be used in the engine data to be presented herein.

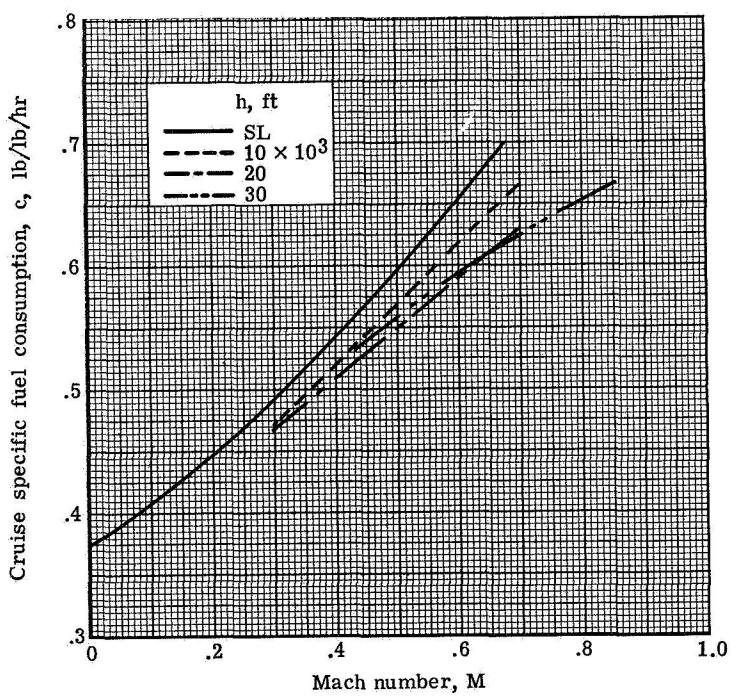
A relationship between the maximum continuous thrust T_c and maximum take-off thrust T_0 is needed for use in matching the engine to the aircraft so that sufficient thrust is available for cruising flight at the desired conditions. The ratio of maximum continuous thrust to maximum sea-level thrust T_c/T_0 is presented as a function of Mach number for different altitudes for four different turbofan engines in figures 3.13(a), 3.14(a), 3.15(a), and 3.16(a). Engines A and B (figs. 3.13 and 3.14) are modern high compression ratio engines with bypass ratios of 4.5 and 6.0, respectively, whereas engines C and D (figs. 3.15 and 3.16) are older engines with bypass ratios of 1.4 and 1.1, respectively. No absolute values of thrust are given for the engines. The data presented should be considered as representative of generic classes of engines which can be scaled to different thrust levels. The availability of actual engines of different thrust levels can be determined from documents such as reference 3.2 or from manufacturers' brochures.

The amount of fuel that the engine consumes in order to produce a given amount of thrust is another important performance parameter which is used in determining the fuel load required to give a desired range. (See eq. (3.13).) The specific fuel consumption c, expressed in pounds of fuel per pound of thrust per hour (lb/lb/hr) is presented as a function of Mach number for different altitudes in figures 3.13(b), 3.14(b), 3.15(b), and 3.16(b). These data correspond to the maximum continuous thrust rating used in parts (a) of figures 3.13 to 3.16. The minimum specific fuel consumption usually occurs at a thrust level somewhat below the maximum continuous value; however, the values given in parts (b) of the figures will be used in the illustrative example described in chapter 4.

The values of thrust-to-weight ratio utilized in section 3.4 on airport performance, as well as those to be employed in the next section on cruise matching (section 3.5.3), are based on installed thrust, that is, the thrust of the engines as installed in the aircraft. The installed engine thrust is somewhat less than the uninstalled value quoted for the engine by the manufacturer. The differences between the two values are attributed to such factors as inlet losses, nozzle losses, drag increments associated with discharge of

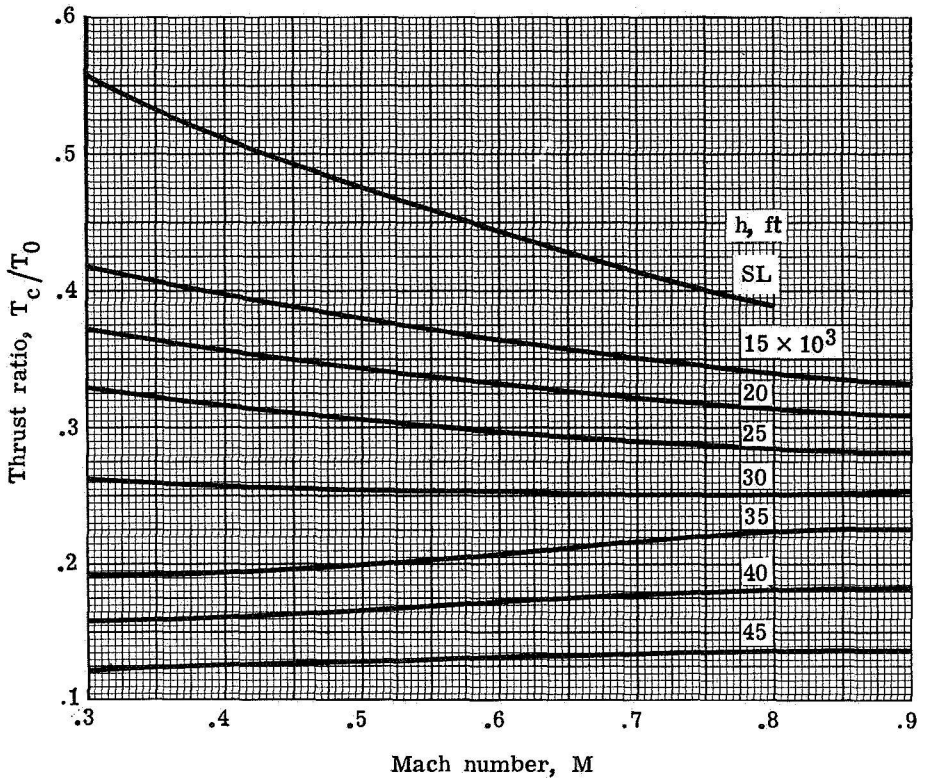


(a) Thrust relationships.

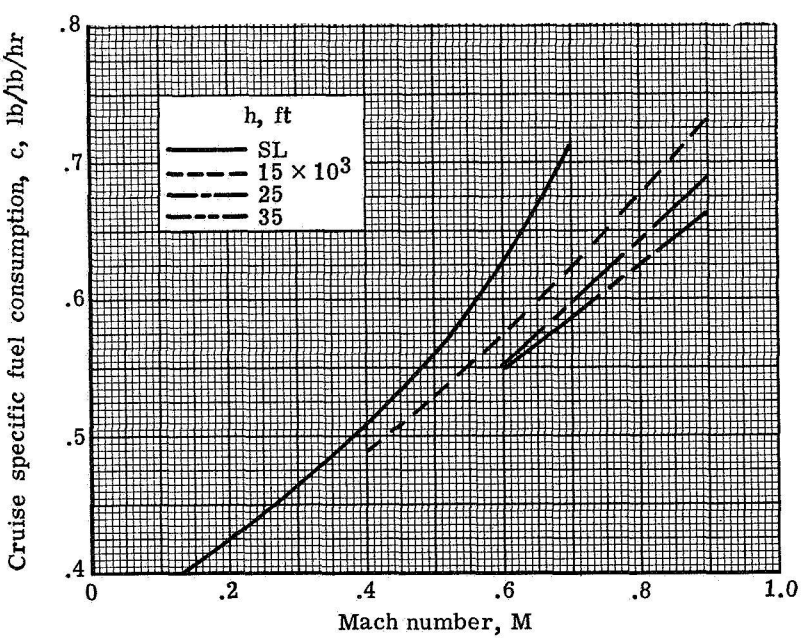


(b) Cruise specific fuel consumption.

Figure 3.13.- Characteristics of turbofan engine A as function of Mach number and altitude.

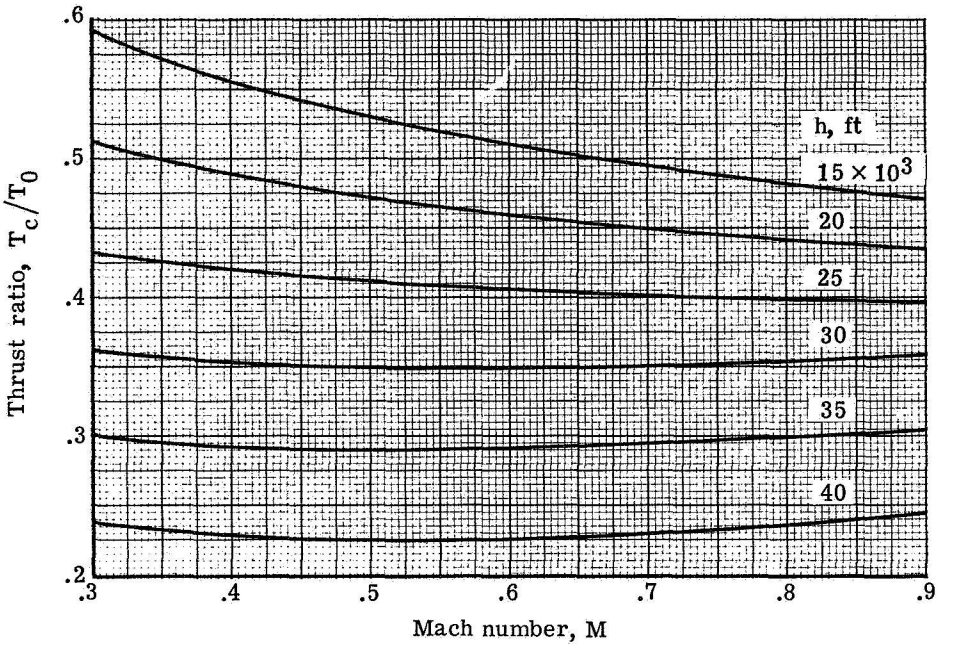


(a) Thrust relationships.

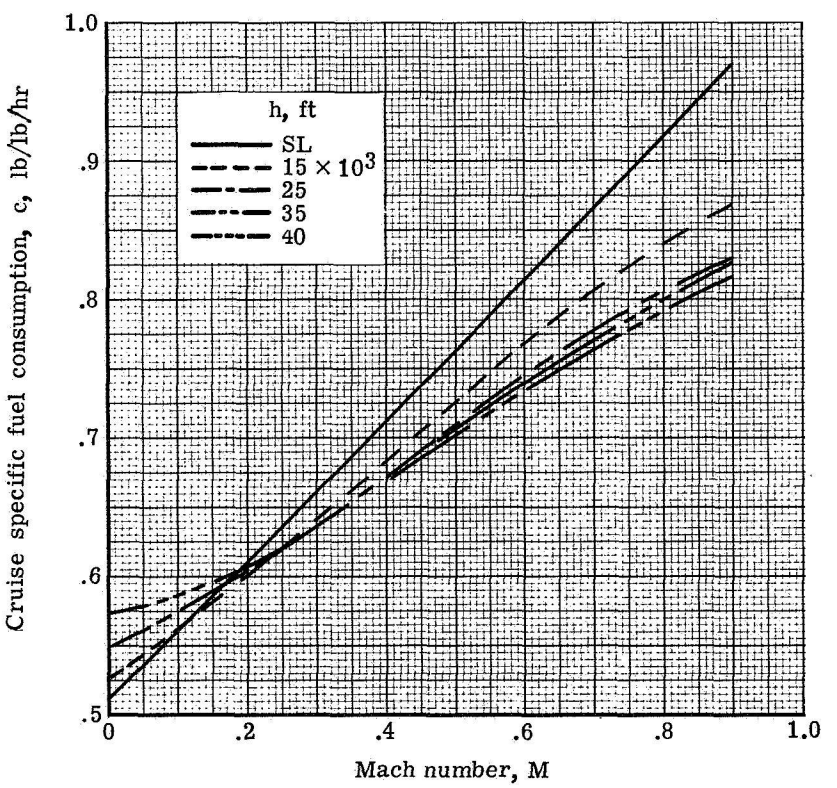


(b) Cruise specific fuel consumption.

Figure 3.14.- Characteristics of turbofan engine B as function of Mach number and altitude.

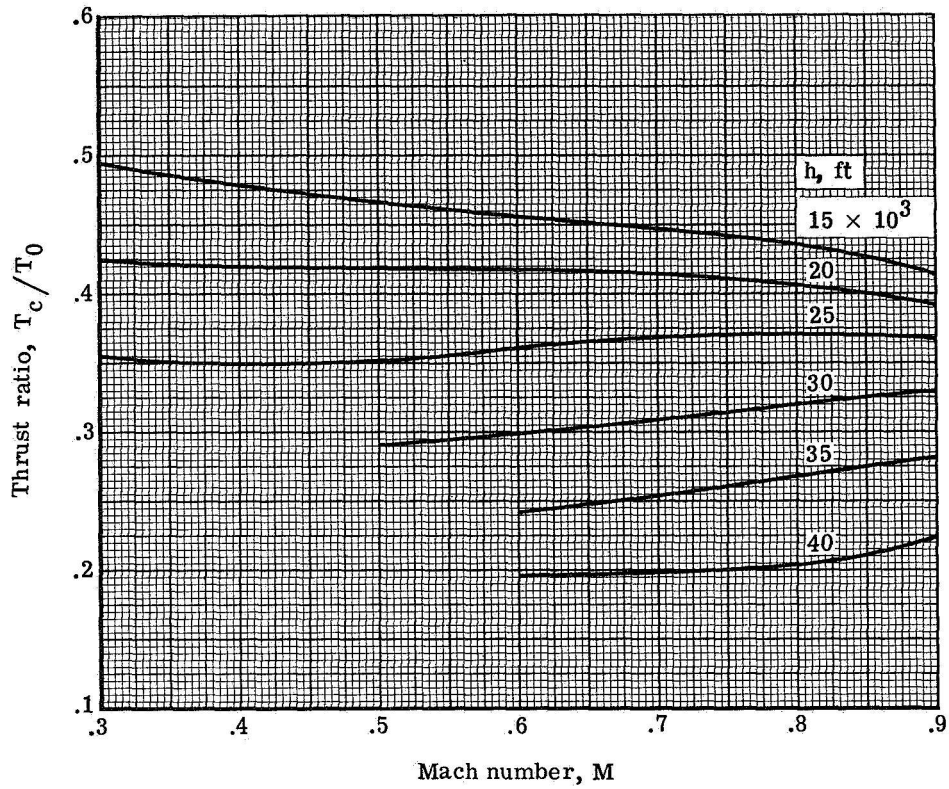


(a) Thrust relationships.

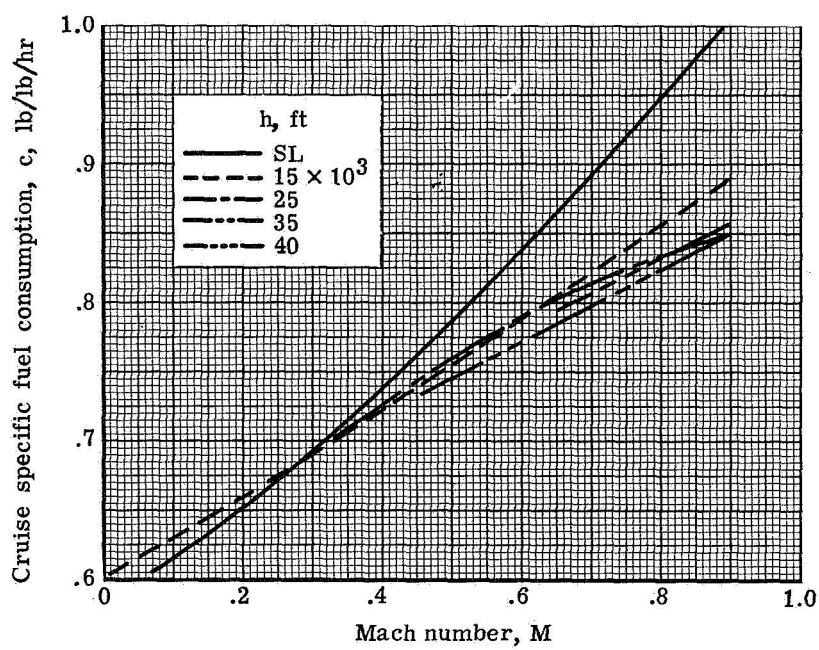


(b) Cruise specific fuel consumption.

Figure 3.15.- Characteristics of turbofan engine C as function of Mach number and altitude.



(a) Thrust relationships.



(b) Cruise specific fuel consumption.

Figure 3.16.- Characteristics of turbofan engine D as function of Mach number and altitude.

the fan air on the surfaces of nacelles, etc. A good discussion of these effects is given in reference 3.16 which indicates that the installation thrust loss in cruising flight is about 5 percent. Required thrust levels determined by the methods described in chapter 3 should therefore be increased a small amount for comparison with uninstalled values given in tables of specifications for different engines. The installation losses are somewhat larger than 5 percent for the aircraft at the low speeds corresponding to the early stages of the take-off run. No allowance is made for this small effect in the present analysis. According to reference 3.16, the specific fuel consumption in cruising flight should be increased by about 2 percent because of installation losses. Again, this small effect has been neglected herein.

3.5.3 Cruise Matching

The relationship between the wing loading and thrust loading for the cruise condition must be chosen in such a way that the aircraft can fly with sufficient thrust to balance the drag at the desired Mach number and at an altitude which permits operation at some specified design lift coefficient. Typically, for the purpose of matching the engine to airframe, the specified lift coefficient is chosen to be that for maximum lift-drag ratio, and the wing loading and thrust loading are based on maximum take-off gross weight. The use of the maximum take-off gross weight allows some thrust margin at match condition because of the reduction in weight resulting from fuel consumed in the take-off and subsequent climb to altitude. Thus, if T_c is the cruise thrust and D is the cruise drag

$$T_c = D = \frac{W_g}{(L/D)_{max}}$$

where W_g is the maximum take-off gross weight and $(L/D)_{max}$ is the maximum lift-drag ratio. If T_c/T_0 is the ratio of cruise thrust to maximum take-off thrust, then

$$\frac{T_c}{T_0} = \frac{W_g}{T_0 (L/D)_{max}}$$

or

$$\frac{T_0}{W_g} = \frac{1}{(T_c/T_0)\,(L/D)_{max}} \qquad (3.32)$$

The required maximum take-off thrust-to-weight ratio which must be installed in the aircraft, therefore, varies inversely as the product of the maximum lift-drag ratio and the ratio of cruise thrust to maximum take-off thrust. (The effect of aircraft gross weight of matching at a value of the lift-drag ratio less than the maximum is considered in chapter 4.) The thrust ratio T_C/T_0 has been discussed in section 3.5.2 and the variation of the thrust ratio with Mach number and altitude is given in figures 3.13 to 3.16. A connecting link between the thrust ratio T_C/T_0 and the wing loading is needed in order to provide a relationship between the take-off thrust-to-weight ratio and the take-off wing loading as shown by the output of block 5 in figure 3.1. Such a connecting link will now be developed.

Consider the relationship between lift coefficient, Mach number, dynamic pressure, and wing loading given by the following expression:

$$\frac{W}{S} = C_L q = C_L M^2 \frac{q}{M^2} \tag{3.33}$$

where q is the dynamic pressure in pounds per square foot. The ratio q/M^2 can be rewritten in other terms as follows:

$$\frac{q}{M^2} = \frac{\frac{1}{2}\rho V^2}{V^2/a^2} = \frac{1}{2}\rho a^2$$

where a is the speed of sound given by

$$a^2 = \gamma \frac{p}{\rho}$$

where p is the static pressure and γ is the ratio of specific heats, which for air is approximately 1.4. Consequently, the ratio q/M^2 can be expressed as

$$\frac{q}{M^2} = \frac{\gamma}{2} p \tag{3.34}$$

The quantity q/M^2 is, therefore, solely a function of atmospheric pressure and is shown in figure 3.17 as a function of altitude for a standard atmosphere. The data in figure 3.17 were taken from reference 3.17. (See table 1.I of chapter 1.)

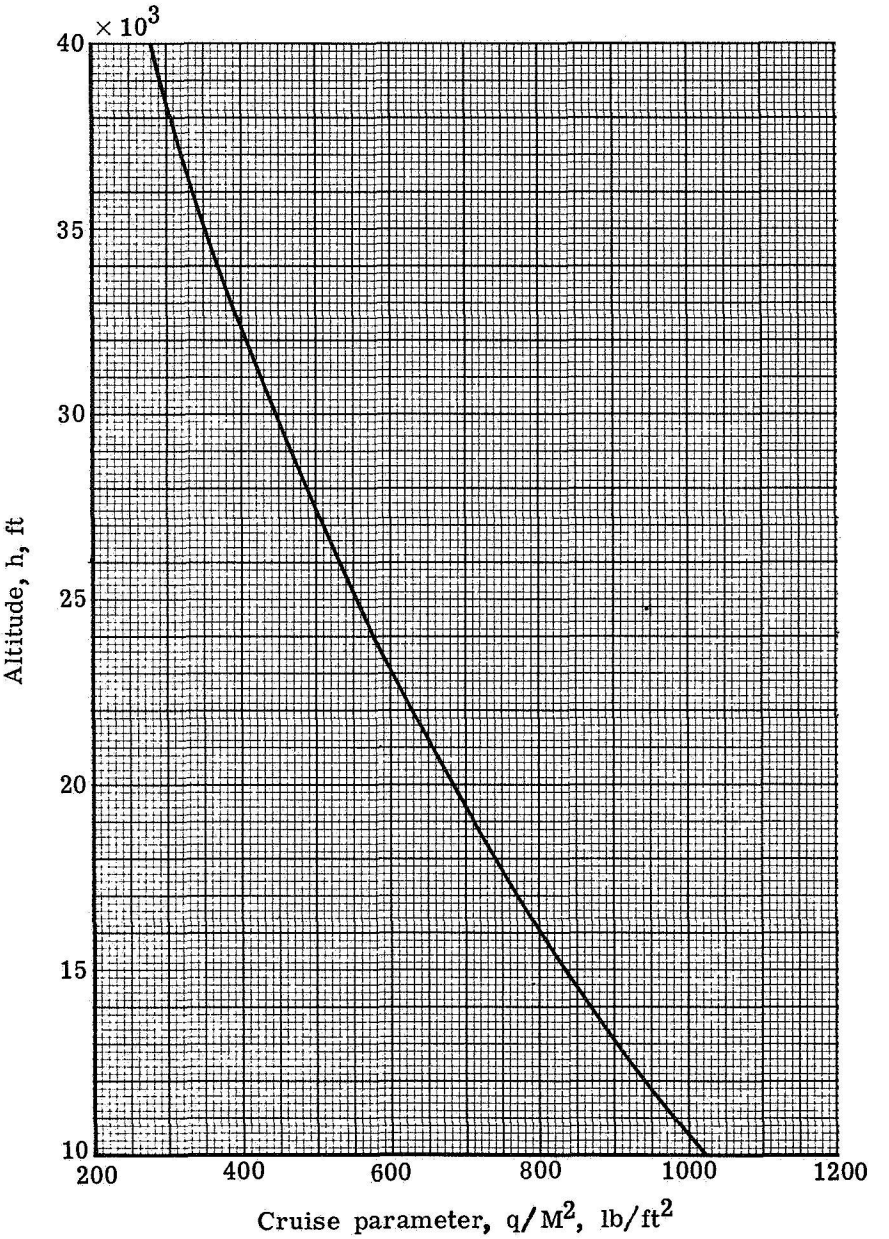


Figure 3.17.- Variation of cruise parameter with altitude for standard atmosphere.

Equations (3.33) and (3.34) show that a unique relationship exists between the wing loading and altitude for a given value of the cruise parameter $C_L M^2$. Thus, for specified values of cruise Mach number and lift coefficient, the necessary cruise altitude is known as a function of wing loading. With the use of equation (3.33) and the data of figure 3.17, a generalized matching chart may be constructed which relates wing loading, the cruise parameter $C_L M^2$, and the altitude. Such a chart is presented in figure 3.18 in which altitude is plotted as a function of the cruise parameter for a number of different values of the wing loading. The use of the chart in figure 3.18 is illustrated by the

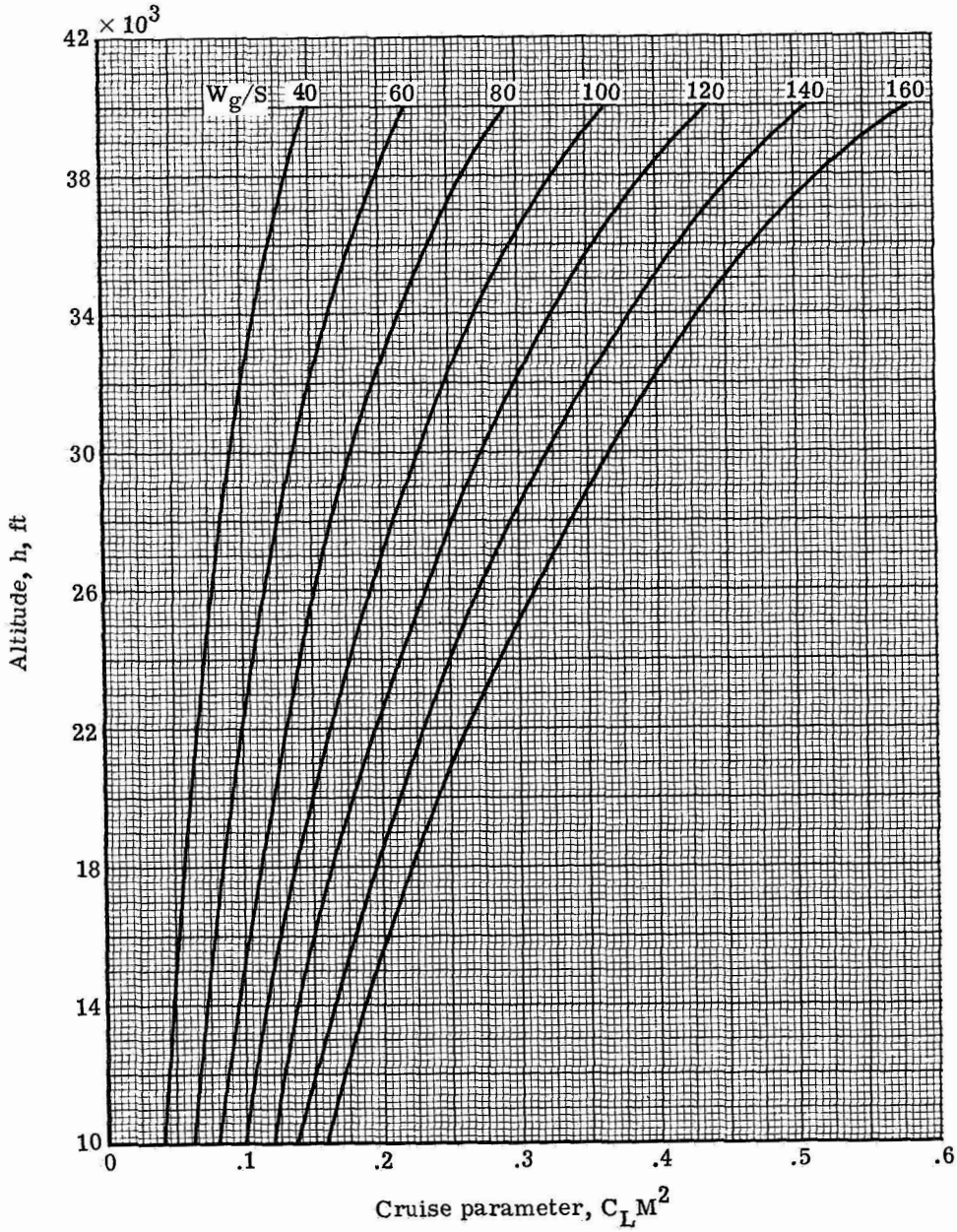


Figure 3.18.- Cruise matching chart.

following simple example. A cruise Mach number of 0.80 and a design cruise lift coefficient of 0.47 are assumed. The cruise parameter for this case is, therefore, 0.30. The altitudes corresponding to steady cruising flight at wing loadings of 80, 100, 120, and 140 lb/ft^2 are desired. The wing loadings and corresponding altitudes obtained from the matching chart of figure 3.18 are given in table 3.V in which h is the altitude in feet. Also given in table 3.V are values of the thrust ratio T_c/T_0 obtained from figure 3.13(a) for the altitudes derived from figure 3.18 and the different assumed wing loadings. The data in table 3.V illustrate the method for determining the desired relationship between the wing loading and the thrust ratio. Data of the type derived in table 3.V together with equation (3.32) provide the means for constructing a curve of take-off thrust-to-weight ratio against take-off wing loading. Any combination of wing loading and thrust loading given by this curve corresponds to an aircraft with the engine matched to the airframe in such a way that flight is possible at the design lift coefficient and Mach number and at maximum gross weight.

3.5.4 Off-Design Cruise Operation

The procedure just described suggests the use of maximum take-off gross weight and a lift coefficient corresponding to the maximum lift-drag ratio in determining the functional relationship between thrust loading and wing loading for cruise matching. With this method of cruise matching, sufficient thrust is usually available for operation at lower weights and other altitudes if the aircraft flies at or near $(L/D)_{max}$. Other flight conditions for which the adequacy of the available thrust should be investigated may suggest themselves.

Consider, for example, that an aircraft is operated at constant gross weight and at the design Mach number but at altitudes lower than that altitude for which the cruise matching was made. The following procedure is suggested as a means for checking the adequacy of the engine thrust at lower altitudes. Assume that the aircraft is matched at $(L/D)_{max}$ with a wing loading of 105 lb/ft^2 and has values of design lift coefficient $C_{L,m}$ and cruise Mach number M of 0.6 and 0.8, respectively. The cruise parameter C_LM^2 is therefore 0.38, and the corresponding altitude for the matched condition is found from figure 3.18 to be 40 000 ft. A check of the adequacy of the thrust in balancing the drag is desired at altitudes from 40 000 to 25 000 ft with the cruise Mach number held constant at 0.8 and constant maximum gross weight.

Table 3.VI illustrates the method for checking the adequacy of the available thrust. The manner in which table 3.VI is constructed and interpreted is best understood by describing each of the columns as follows:

① h, altitude given in feet

② $C_L/C_{L,m}$, lift coefficient at any altitude divided by the lift coefficient for $(L/D)_{max}$, obtained by taking the cruise parameter C_LM^2 at each altitude as defined by the 105 lb/ft^2 wing loading line and dividing these values of C_LM^2 by the value (from fig. 3.18) for the match condition at 40 000 ft; the ratio $C_L/C_{L,m}$ is given directly since the Mach number is constant

③ $(L/D)/(L/D)_{max}$, lift-drag ratio at any altitude divided by the maximum value of lift-drag ratio, obtained from figure 3.12 with the use of the values of $C_L/C_{L,m}$ given in ②

④ D/D_{match}, ratio of the drag at any altitude to the drag at the match condition, obtained by taking the reciprocal of the values in ③ since the weight is constant

⑤ T_c/T_0, ratio of the thrust at any altitude to the maximum take-off thrust, obtained from figure 3.13(a) for engine A; the value of 0.175 is for the match condition at 40 000 ft

⑥ T_c/T_{match}, ratio of the thrust at any altitude to the thrust at the match condition, obtained by dividing the values in ⑤ by the thrust ratio T_c/T_0 for the match condition which, in this case, is 0.175

Comparison of column ⑥ with column ④ in table 3.VI indicates that the thrust ratio T_c/T_{match} increases faster than the drag ratio D/D_{match} as the altitude is decreased from 40 000 ft to 25 000 ft. Thus, since $D_{match} = T_{match}$ at 40 000 ft, sufficient thrust is available to operate the aircraft at the different altitudes investigated. The procedure just described can easily be expanded to handle other situations such as those in which different values of Mach number and gross weight are assumed for different altitudes. For example, if the Mach number is varied as the altitude is decreased, the value of $C_L/C_{L,m}$ in column ② of table 3.VI can easily be determined. If the ratio of the cruise parameter at some altitude to that at the matching altitude is denoted by C, then

$$\frac{C_L M^2}{C_{L,m} M^2_{match}} = C$$

or

$$\frac{C_L}{C_{L,m}} = C \frac{M^2_{match}}{M^2} \tag{3.35}$$

and the relation (3.35) may be used for determining the lift coefficient ratio. A somewhat similar relationship may be developed for determining the drag ratio given in column ④ of table 3.VI if the aircraft weight is varied as the altitude is decreased. Thus, for a given value of $C_L/C_{L,m}$,

$$\frac{L/D}{(L/D)_{match}} = C_1$$

or

$$\frac{L}{L_{match}} \frac{D_{match}}{D} = C_1$$

Since

$$\frac{L}{L_{match}} = \frac{W}{W_{match}}$$

then

$$\frac{D_{match}}{D} = C_1 \frac{W_{match}}{W}$$

or

$$\frac{D}{D_{match}} = \frac{1}{C_1} \frac{W}{W_{match}} \tag{3.36}$$

and equation (3.36) may be used for calculating the drag ratio given in column ④ of table 3.VI. The thrust ratio T_c/T_0 can, of course, be corrected for Mach number effects with the use of the engine data given in figures 3.13 to 3.16.

3.6 Aircraft Matching

The procedure by which an aircraft is sized to meet a given set of performance objectives is described in section 3.3 and the process is illustrated by the flow diagram presented in figure 3.1. The analyses and procedures necessary to generate the outputs of blocks 1 to 5 of figure 3.1 have been described and discussed in sections 3.4 and 3.5; a simultaneous solution of these outputs is shown in blocks 6 and 7 of figure 3.1. The indicated simultaneous solution provides the specific values of wing loading and thrust loading necessary for the aircraft to achieve the desired performance objectives. Graphical methods for obtaining the desired specific values of the wing loading and thrust loading will now be described.

The process for obtaining specific values of wing loading and thrust loading is illustrated by the hypothetical matching chart presented in figure 3.19.

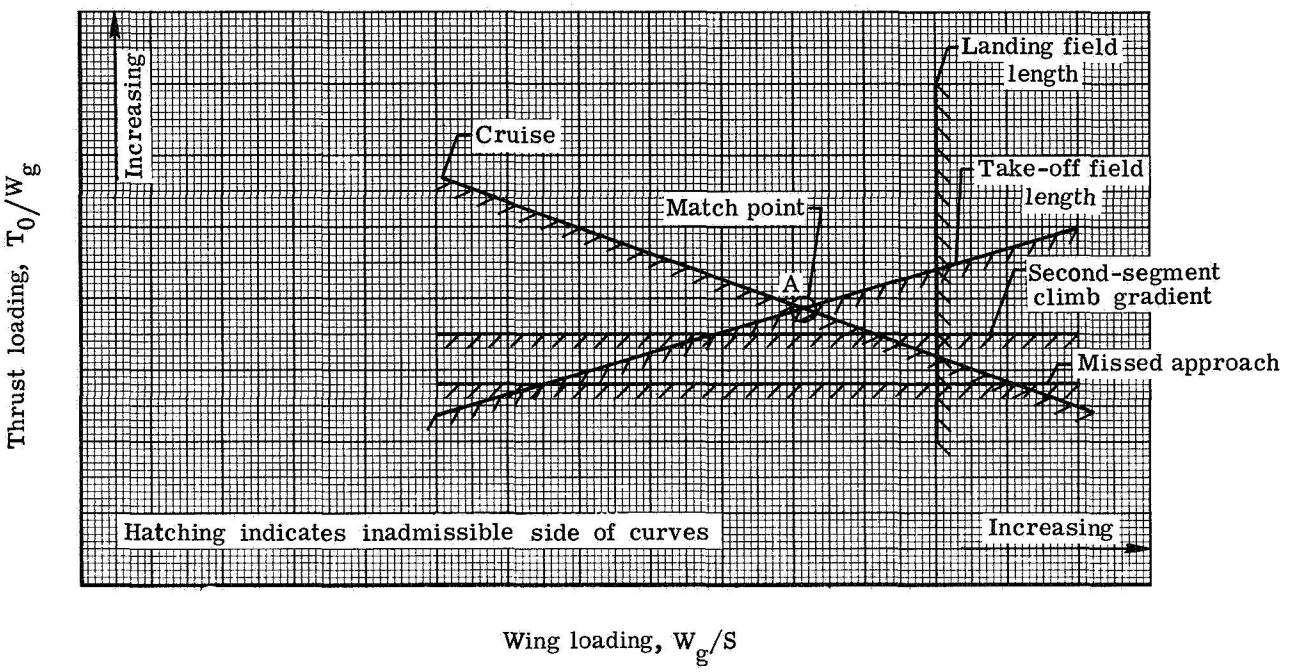


Figure 3.19.- Hypothetical aircraft matching chart, first method.

The take-off thrust loading is plotted on the ordinate as a function of the take-off wing loading on the abscissa. The curve labeled "take-off field length" represents the variation of thrust loading with wing loading corresponding to a specified field length and for an assumed value of the maximum lift coefficient $C_{L,T}$ determined from the statistical data discussed in section 3.4.3. The second-segment climb gradient constraint line is determined by the methods described in section 3.4.4 for the aircraft with known aspect ratio and employing a given number of engines. The value of the second-segment climb gradient lift coefficient $C_{L,2}$ used in determining the constraint line is related to the maximum lift coefficient $C_{L,T}$ by the factor 1.44; that is,

$$C_{L,T} = 1.44C_{L,2}$$

The cruise constraint line shown in figure 3.19 is constructed with the use of the cruise matching procedure described in section 3.5.3 and for known values of the maximum lift-drag ratio $(L/D)_{max}$ and corresponding lift coefficient $C_{L,m}$ and for a specified cruise Mach number and engine performance.

The landing-field-length constraint line in figure 3.19 is determined by the methods described in section 3.4.1 and makes use of an assumed value of the approach lift coefficient $C_{L,A}$. The missed approach constraint line is determined by the methods of section 3.4.2 and is also based on the assumed value of the approach lift coefficient $C_{L,A}$. The wing loadings and thrust loadings determined from the landing field length and missed approach calculations are based on maximum landing weight and must be adjusted to the take-off gross weight condition so that all of the constraint curves shown in figure 3.19 will be based on the same weight. Thus, if W_L/W_g is the ratio of maximum landing weight to maximum take-off weight as discussed in section 3.4.5, the landing wing loading and missed approach thrust loading may be expressed in terms of take-off gross weight by the following relations:

$$\frac{W_g}{S} = \frac{W_L/S}{W_L/W_g} \tag{3.37}$$

$$\frac{T_0}{W_g} = \frac{T_0/W_L}{W_L/W_g} \tag{3.38}$$

The intersection of the cruise line and the take-off field length line, denoted by point A in figure 3.19, gives values of the wing loading and thrust loading which satisfy the airport and cruise performance specifications of the aircraft. The landing field length and missed approach constraints are not critical in the illustrative example. The use of lower values of the approach lift coefficient and perhaps a simpler flap system should accordingly be possible. The lift-drag ratio in the approach condition is lower than in the climb configuration because of the extended landing gear. However, the thrust-to-weight ratio required to meet the missed approach criterion is, in this case, lower than that needed for the second-segment climb gradient criterion. The difference in maximum gross weight of the aircraft in the take-off and landing configurations more than offsets the effect of the lower value of L/D of the aircraft in the approach condition, and is responsible for the lower value of T/W needed to meet the missed approach requirement.

Point A in figure 3.19 defines an engine size which is slightly larger than that required to meet the second-segment climb gradient requirement. The use of maximum lift coefficients $C_{L,T}$ and second-segment climb gradient lift coefficients $C_{L,2}$ somewhat higher than those assumed would lower the slope of the take-off field length line and raise the second-segment climb gradient line. The intersection of the cruise line, take-off field length line, and second-segment climb gradient line at a single point gives the minimum thrust loading, and corresponding wing loading, needed to satisfy the three constraints. A minimum thrust loading means a minimum size engine for a given aircraft weight and is usually desirable.

3.6.1 Take-Off and Climb Calculation

A systematic procedure for determining the values of $C_{L,T}$ and $C_{L,2}$ necessary for the simultaneous intersection of the cruise, take-off field length, and second-segment climb gradient lines is described with the use of the following form:

①	②	③	④	⑤
$C_{L,2}$	T_m/W_g	$C_{L,T}$	$\frac{W_g/S}{\sigma C_{L,T}(T_0/W_g)}$	W_g/S

where

① Several values of $C_{L,2}$, the lift coefficient for second-segment climb gradient, are selected. The value of the lift coefficient corresponding to the matching point is assumed to be within the chosen range.

② The value of T_m/W_g, the thrust-to-weight ratio, needed to satisfy the second-segment climb gradient criterion is found from figure 3.9 for the values of $C_{L,2}$ given in ① .

③ $C_{L,T}$, maximum lift coefficient, is obtained by multiplying the values of $C_{L,2}$ given in ① by 1.44.

④ $\frac{W_g/S}{\sigma C_{L,T}(T_0/W_g)}$, take-off parameter, is obtained from figure 3.7 for the specified take-off field length.

⑤ W_g/S, wing loading, is obtained by multiplying ④ by ② and ③ .

Columns ② and ⑤ represent a set of values of T_0/W_g and W_g/S which uniquely satisfy both the take-off field length and the second-segment climb gradient. A form of the matching chart which utilizes values of T_0/W_g and W_g/S determined in the manner just described is shown in figure 3.20. All points along the line labeled "take-off field length" represent combinations of values of wing loading and thrust loading which satisfy both field length and climb requirements. The lift coefficients $C_{L,T}$ and $C_{L,2}$ are different for each combination of thrust loading and wing loading along the line which implies the use of different flap deflections, or perhaps, for large differences in lift coefficient, different flap designs. The point A on figure 3.20 represents the combination of wing loading and thrust loading which satisfies the cruise constraint as well as the take-off and second-segment climb constraints.

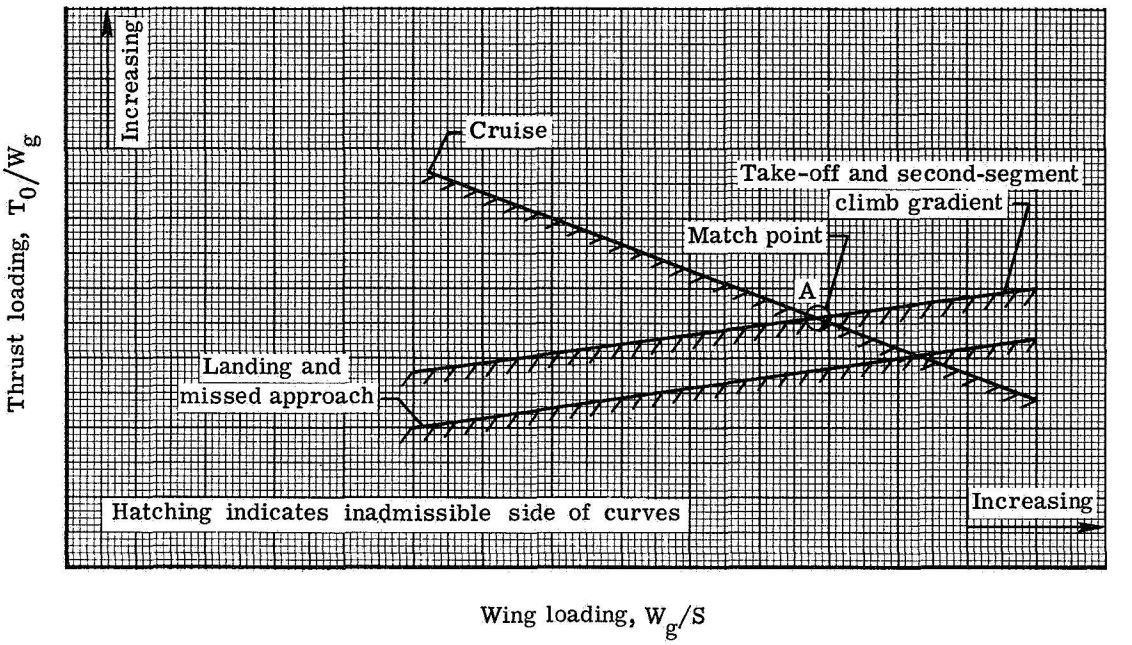


Figure 3.20.- Hypothetical aircraft matching chart, second method.

3.6.2 Landing and Missed Approach Calculation

The line labeled "landing and missed approach" in figure 3.20 represents sets of values of wing loading and thrust loading which satisfy both the landing field length and missed approach requirements. The method of determining the landing line is essentially similar to that used for calculating the take-off line and is outlined as follows:

①	②	③
$C_{L,A}$	W_L/S	T_0/W_L

where

① Several values of $C_{L,A}$, the approach lift coefficient, are selected.

② W_L/S, landing wing loading, is determined from figures 3.3 and 3.4 for each assumed value of $C_{L,A}$ and for the specified landing field length.

③ T_0/W_L, thrust-to-weight ratio, is determined for each value of $C_{L,A}$ from figure 3.5.

Columns ② and ③ constitute a set of values of W_L/S and T_0/W_L which satisfies both the landing field length and the missed approach criterion. The values of W_L/S and T_0/W_L must be adjusted with the use of equations (3.37) and (3.38) in order that all curves on the matching chart will be based on the same aircraft weight.

The form of the matching chart shown in figure 3.19 is useful in illustrating how the different constraints influence the selection of the design values of wing loading and thrust loading. The matching chart shown in figure 3.20, however, represents a systematic method for determining a more precise matching point and should be used in most actual matching studies.

The curves in figures 3.19 and 3.20 are only illustrative in nature and do not represent an actual sizing calculation. The relative position of the constraint curves depends upon the performance requirements and upon the aircraft and engine characteristics. Hence, the position of these curves will vary from case to case. A better understanding of the aircraft matching procedure can probably be achieved through study of the illustrative example given in chapter 4.

3.7 Aircraft Weight Relationships

Block 8 of the flow diagram presented in figure 3.1 indicates that the output of the matching process is used in an aircraft weight analysis to yield a specific value of the useful load fraction. The fuel fraction shown by block 1(and the payload shown by block 13 are then used with the useful load fraction t(define the aircraft gross weight. Other important weight elements such as the empty weight and the fuel weight can be determined once the gross weight is known. Sophisticated methods are available for estimating aircraft weights witl a high degree of precision. These methods, however, are complicated, very detailed, and do not lend themselves to the type of aircraft sizing analysis being developed herein. A number of other weight estimation methods of varying degrees of sophistication and accuracy are available. The method adopted for u: here is quite simple. The estimation of the useful load fraction is considered first, after which a method of determining aircraft gross weight is described.

3.7.1 Useful Load Fraction

In reference 3.18, Wilson describes a method of weight estimation which su(gests a relationship between the thrust loading T_0/W_g and the physical charac teristics of the aircraft. From an analysis of a large number of aircraft, the gross weight is shown in reference 3.18 to be related to the fuel weight, propu sion system weight, and payload weight in the following way:

$$W_f + W_t + W_p = 0.6W_g \tag{3.39}$$

where

W_g gross weight, lb

W_f fuel weight, lb

W_t propulsion system weight, lb

W_p payload weight, lb

The data used in formulating this relationship were based on propeller-driven aircraft of pre-1940 vintage. A recent examination of the weights of a large number of modern aircraft, including jet-powered aircraft, indicates that equation (3.39) still provides a close approximation to current weight relationships, although some questions exist in connection with the definition of propulsion system weight. Fortunately, for purposes of the present analysis, the value of the constant 0.6 is unimportant and will be replaced by an undefined constant C. Equation (3.39) may then be rewritten in the following useful form:

$$\frac{W_p + W_f}{W_g} - C = -\frac{W_t}{W_g}$$

or

$$\frac{W_p + W_f}{W_g} - C = -\frac{W_t/T_0}{T_0/W_g} \tag{3.40}$$

where W_t/T_0 is the weight per pound of thrust of the propulsion system and T_0/W_g is the thrust-to-weight ratio of the aircraft. If the assumption is made that the weight per unit of thrust of the propulsion system is relatively constant for different engines, a correlation should exist between the useful load fraction

$$\frac{W_p + W_f}{W_g} = 1 - \frac{W_e}{W_g}$$

and the aircraft thrust-to-weight ratio T_0/W_g.

The useful load fraction expressed in the form $1 - (W_e/W_g)$ is presented in figure 3.21 as a function of T_0/W_g for 41 different jet-powered aircraft

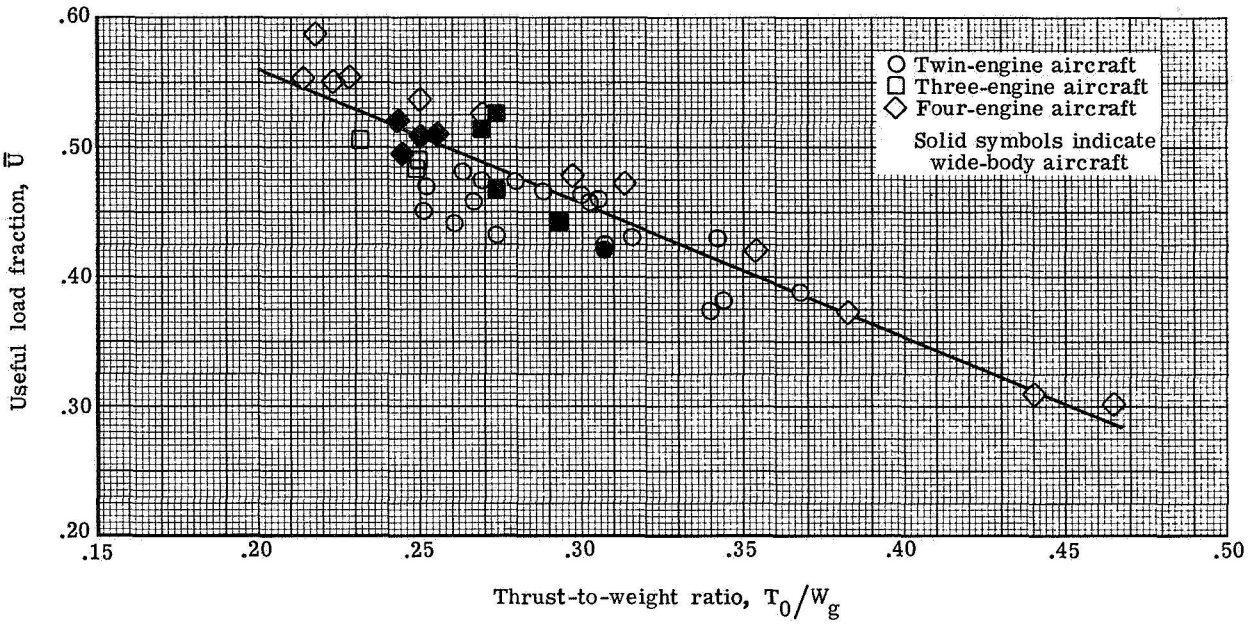


Figure 3.21.- Useful load fraction as function of take-off thrust-to-weight ratio for a number of jet-powered aircraft.

which vary in gross weight from under 10 000 lb to over 800 000 lb and have thrust-to-weight ratios extending from about 0.23 to 0.46. In addition to the aircraft listed in table 3.I, data obtained from three jet-powered STOL (short take-off and landing) aircraft studies are included in figure 3.21. The thrust used in forming the aircraft thrust-to-weight ratio is the uninstalled value for the engines alone. Although considerable scatter is present, the data in figure 3.21 show a reasonable correlation between the useful load fraction and the aircraft thrust-to-weight ratio. A suggested fairing of the data points is shown by the line in figure 3.21. Most of the points fall within a scatter band of ±10 percent of the faired line. This fairing is suggested as a means for finding the useful load fraction in terms of the aircraft thrust-to-weight ratio. The data of figure 3.21, however, should only be used for estimating the useful load fraction of aircraft of the same general configuration class and weight range as those for which the correlation was developed.

3.7.2 Aircraft Gross Weight Estimation

If the useful load fraction, $1 - (W_e/W_g)$, corresponding to a given value of thrust loading is denoted by U, then

$$1 - \frac{W_e}{W_g} = \bar{U} = \frac{W_p + W_f}{W_g}$$

or

$$\frac{W_p}{W_g} = \bar{U} - \frac{W_f}{W_g}$$

and

$$W_g = \frac{W_p}{\bar{U} - (W_f/W_g)} \tag{3.41}$$

Equation (3.41) indicates that the gross weight of the aircraft can be determined if the payload weight and the fuel fraction are known along with the useful load fraction $\bar{U}$. The value of the aircraft thrust loading T_0/W_g and hence the useful load fraction $\bar{U}$ are known from the matching process described in section 3.6. The payload weight is usually a specified quantity. The fuel fraction may be determined in terms of the specified range and the Breguet factor at which the aircraft is to operate. The determination of the fuel fraction is considered in the next section.

3.8 Aircraft Range and Fuel Fraction

The Breguet range equation was discussed in section 3.5 and was given in a form convenient for calculating the fuel fraction necessary for a given range by equation (3.13) which is repeated here for convenience

$$\frac{W_f}{W_g} = 1 - \frac{1}{e^{R/B}} \tag{3.13}$$

where

W_f fuel weight, lb

W_g aircraft gross weight, lb

R range, n. mi.

B Breguet factor, $\frac{V(L/D)}{c}$

and

V velocity, knots

L/D lift-drag ratio

c specific fuel consumption, pounds of fuel per pound of thrust per hour

In the application of equation (3.13) for the determination of fuel fraction consideration must be given to the lift-drag ratio L/D at which the aircraft will operate during different portions of its cruising flight. According to the discussions of section 3.5, the aircraft is matched in such a way that sufficient thrust is available to fly at the desired cruise Mach number and at the maximum value of the lift-drag ratio. Flight at a constant value of the lift-drag ratio requires a continuous climb because of the reduction in weight resulting from the fuel consumed. A continuous climb is seldom possible because of air traffic control limitations. A continuous climb can sometimes be approximated by a series of constant altitude segments in which each segment is flown at an altitude higher than the preceding one. Critical mission constraints as imposed by air traffic control or stage length, for example, may be imposed which prevents any portion of the flight from being conducted at the maximum value of the lift-drag ratio. A simplified approach which will be used here is to consider the entire flight to be made at a constant altitude with the lift coefficient at the beginning of cruise taken to be that for maximum L/D. The lift coefficient at the end of cruise is determined on the basis of the landing weight. The lift-drag ratio for this condition can be found from the generalized L/D curve of figure 3.12. The fuel fraction is then estimated with the use of equation (3.13) and a lift-drag ratio which is the average of the initial and final cruise values. A first estimate of the ratio of landing weight to take-off weight can be made with the data given in figure 3.10. A more accurate estimate of the landing weight is possible after a first estimate of the cruise fuel is obtained. A second iteration may then be desirable using the new landing weight. No specific allowance is made for off design operation such as climb fuel; however, this unconservative assumption is, to some extent, offset by fuel savings in the descent portion of flight. Further, no allowance is made for "start-up" and taxi fuel which is usually small.

Another important factor which must be considered in estimating the fuel fraction is the amount of reserve fuel which is carried to allow for unplanned situations. Reserve fuel requirements are discussed at some length in part 121 of the Federal Air Regulations, reference 3.5. Specific rules for calculating the amount of reserve fuel are given by the Air Transport Association in reference 3.19. The amount of reserve fuel given by these rules is in excess of minimum FAR requirements but is representative of current airline operational practices. The amount of reserve fuel specified by reference 3.19 depends upon the type of aircraft and the nature of its operation. For example, aircraft in domestic and international operations carry different amounts of reserve fuel, as do supersonic and subsonic transport aircraft. The reserve fuel rules are also different for propeller-driven aircraft equipped with reciprocating engines and for turbine-powered aircraft.

The reserve fuel requirements specified by reference 3.19 for subsonic, turbine-powered aircraft employed in domestic and international operations are given as follows:

Domestic operations

(1) Fly for 1 hr at normal cruise altitude at a fuel flow for end of cruise weight at the speed for 99 percent maximum range.

(2) Exercise a missed approach and climbout at the destination airport; fly to and land at an alternate airport 200 n. mi. distant.

International operations

(1) Fly for 10 percent of trip air time at normal cruise altitude at a fuel flow for end of cruise weight at the speed for 99 percent maximum range.

(2) Exercise a missed approach and climbout at the destination airport; fly to an alternate airport 200 n. mi. distant.

(3) Hold for 30 min at alternate airport at 1500 ft altitude.

(4) Descend and land at alternate airport.

Flight to alternate airport (all airplanes)

(1) Power or thrust setting shall be 99 percent of maximum subsonic range.

(2) Power setting for holding shall be for maximum endurance or the minimum speed for comfortable handling, whichever is greater.

(3) Cruise altitude shall be the optimum for best range except that it shall not exceed the altitude where cruise distance equals climb plus descent distance.

The determination of the exact amount of reserve fuel needed for any given aircraft requires a fairly detailed calculation. The addition of an increment of 400 to 600 miles to the design range is suggested as a means for quickly obtaining a rough approximation to average reserve fuel requirements.

With the above qualification on the value of the range to be used in equation (3.13), the fuel fraction may now be calculated. The variation of the speed of sound with altitude is given in figure 3.22 as an aid in calculating the Breguet factor. One of the small pocket electronic computers which have the capability for evaluating exponential functions is ideal for evaluating

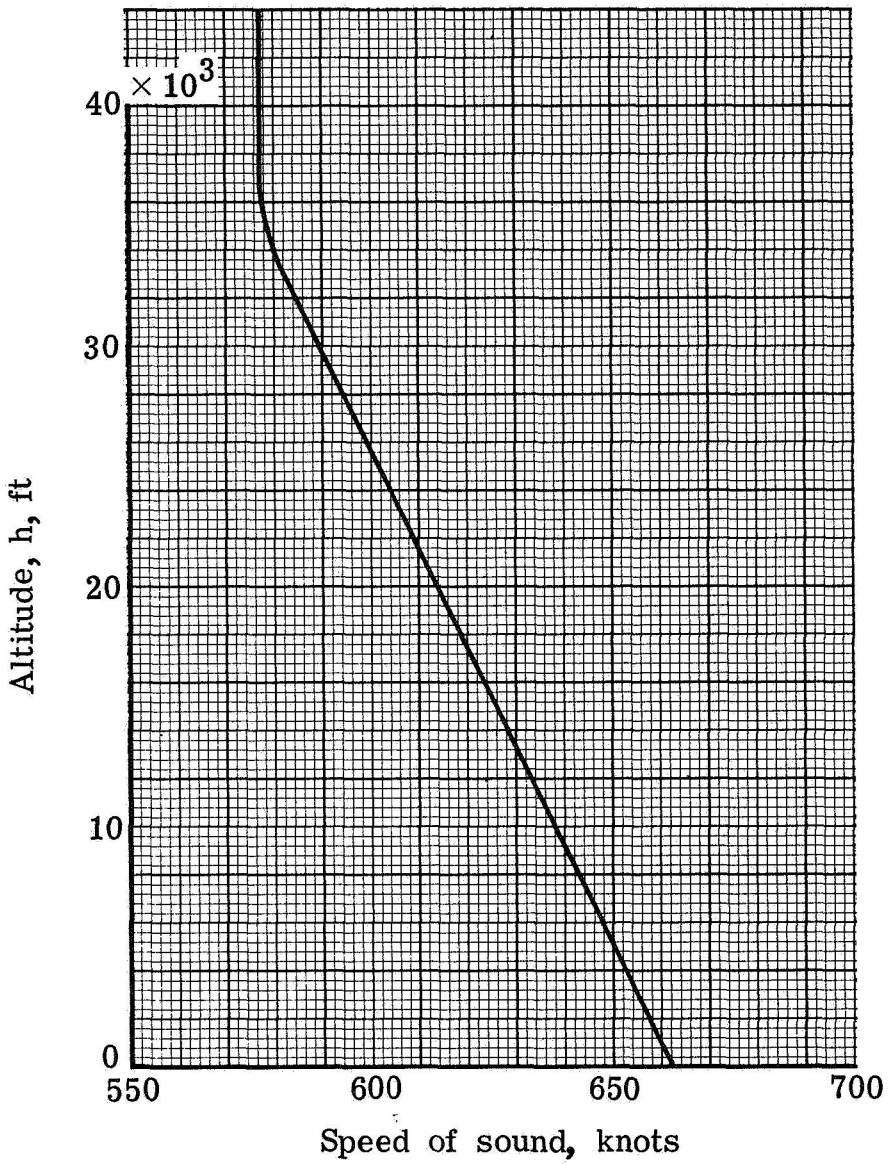


Figure 3.22.- Variation of speed of sound with altitude for standard atmosphere.

equation (3.13) in a rapid and highly accurate manner. The fuel fraction may also be determined from figure 3.23 which gives the desired quantity as a function of range for different values of the Brequet factor.

3.9 Aircraft Sizing

All the procedures have now been developed which permit the sizing, as outlined in the flow diagram of figure 3.1, of a jet-powered cruising aircraft to meet a prescribed set of performance objectives.

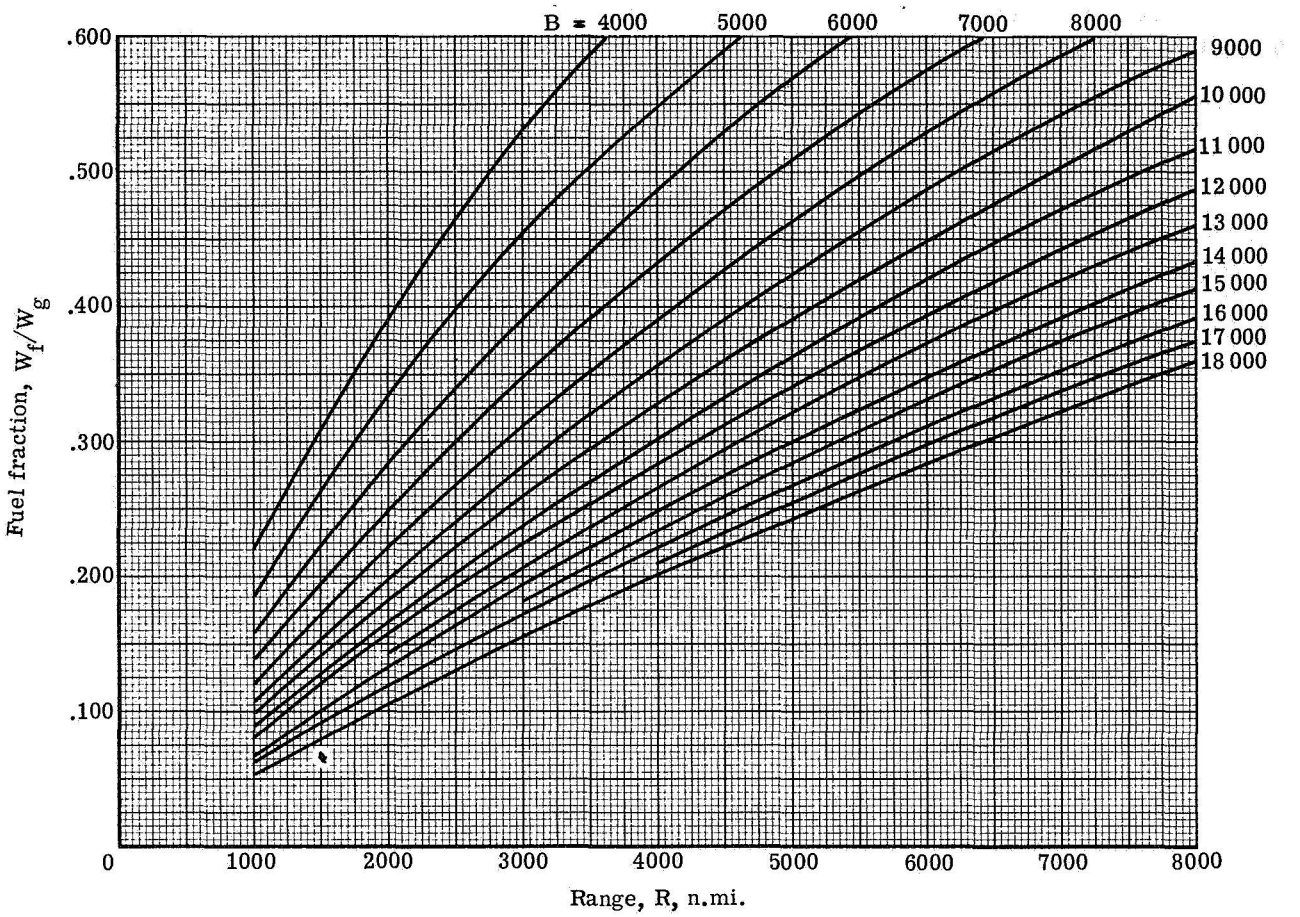


Figure 3.23.- Fuel fraction as function of range and Breguet factor.

The matching procedure described in section 3.6 gives values of the wing loading and thrust loading needed to meet cruise and airport performance objectives. The useful load fraction is determined according to the method described in section 3.7, and determination of the fuel fraction necessary to meet the desired range is described in section 3.8. The gross weight can then be calculated by the expression given by equation (3.41) which is repeated here for convenience:

$$W_g = \frac{W_p}{\bar{U} - (W_f/W_g)} \tag{3.41}$$

With the gross weight and payload weight known, the fuel weight and empty weight can be calculated since the fuel fraction and useful load fractions are known. The wing loading, power loading, and gross weight are known; hence, the wing area and engine thrust can be calculated. The basic physical characteristics of size, weight, and thrust of the aircraft have now been completely determined.

In the next chapter (chapter 4) an illustrative example of the sizing of a jet-driven aircraft according to the methods described will be considered in detail.

3.10 Cruise Performance Map

In the preceding sections, the range at a given Mach number was specified, and the fuel fraction was determined for a flight profile of constant altitude at which the aircraft was operating at the maximum value of the lift-drag ratio at the beginning of cruising flight. This procedure provides a reasonable basis for determining a conservative value of the fuel fraction for a given speed and range, but provides no indication of the manner in which the range varies with speed and altitude for a given fuel fraction. Methods will now be presented for constructing a cruise performance map from which, for a given fuel fraction and matching point parameters, the range may be determined at any combination of Mach number and altitude consistent with the capabilities of the engine and the aerodynamic constraints within which the aircraft must operate. The methods to be described assume that the aircraft is matched at the maximum value of the lift-drag ratio and utilizes matching point values of wing loading and thrust loading based on maximum gross weight. The methods may easily be extended, however, to aircraft matched at other values of L/D and other weight conditions.

3.10.1 Method of Analysis

For a given altitude, wing loading, and fuel fraction the ratio of the range at any Mach number to that for the Mach number corresponding to the maximum lift-drag ratio $(L/D)_{max}$ can be expressed in the following form:

$$\frac{R}{R_m} = \frac{B}{B_m} = \frac{c_m V (L/D)}{c V_m (L/D)_{max}} \tag{3.42}$$

where the subscript m refers to conditions at $(L/D)_{max}$. The relationship between the speed ratio V/V_m and the corresponding ratio of values of L/D can be obtained from equation (3.31) which is repeated here for convenience

$$\frac{L/D}{(L/D)_{max}} = \frac{2}{\frac{1}{\bar{C}_L} + \bar{C}_L} \tag{3.31}$$

This equation can be put in the following form:

$$\frac{L/D}{(L/D)_{max}} = \frac{2}{\bar{V}^2 + (1/\bar{V}^2)} \tag{3.43}$$

where $\bar{V} = V/V_m = 1/\sqrt{\bar{C}_L}$. Equation (3.42) can then be written as

$$\frac{B}{B_m} = \frac{c_m}{c}\left[\frac{2}{\bar{V} + (1/\bar{V}^3)}\right] \tag{3.44}$$

For constant altitude,

$$\frac{V}{V_m} = \frac{M}{M_m} = \bar{M}$$

and equation (3.44) can then be written in the form

$$\frac{B}{B_m} = \frac{c_m}{c}\left[\frac{2}{\bar{M} + (1/\bar{M}^3)}\right] \tag{3.45}$$

The ratio c_m/c can be approximated with the use of the curves of specific fuel consumption given in figures 3.13 to 3.16 for several engines. (For simplicity, the variation in specific fuel consumption which accompanies a reduction in thrust below the maximum continuous value has been neglected in the present analysis.) The variation of the specific fuel consumption c with Mach number M can usually be approximated with sufficient accuracy by a straight line equation of the form

$$c = c_0 + KM$$

or

$$\frac{c}{c_0} = 1 + \left(\frac{KM_m}{c_0}\right)\bar{M} \tag{3.46}$$

where c_0 is the value of c for a Mach number of zero, and K is the measured slope of the curve. The ratio c_m/c may then be written in the following form:

$$\frac{c_m}{c} = \frac{1 + \dfrac{KM_m}{c_0}}{1 + \left(\dfrac{KM_m}{c_0}\right)\bar{M}}$$

or

$$\frac{c_m}{c} = \frac{1 + \bar{K}}{1 + \bar{K}\bar{M}} \tag{3.47}$$

where

$$\bar{K} = \frac{KM_m}{c_0}$$

Substitution of equation (3.47) into equation (3.45) gives the following equation for the Breguet range factor ratio:

$$\frac{B}{B_m} = \left(\frac{1 + \bar{K}}{1 + \bar{K}\bar{M}}\right)\left[\frac{2}{\bar{M} + (1/\bar{M}^3)}\right] \tag{3.48}$$

Equation (3.48) is applicable at any constant altitude and may be used as a basis for constructing a cruise performance map. The values of B_m and M_m are, however, a function of altitude, and this must be considered in order to give a true comparative picture of the manner in which range, or range ratio, varies with Mach number for different altitudes. For simplicity, the effects of variations in the Mach number and Reynolds number are ignored, hence, the value of $(L/D)_{max}$ is independent of speed and altitude. The first step in constructing a cruise performance map is to calculate, with the use of equation (3.48), the range ratio as a function of Mach number for the altitude corresponding to the matching point of the aircraft. The curve determined by equation (3.48) for the matching point Mach number and altitude is then adjuste in such a way as to show the effects of the variation with altitude of B_m and M_m on the comparative cruise performance at different altitudes. Methods for making these adjustments will now be discussed.

The Mach number for $(L/D)_{max}$ at any altitude, M_m, expressed in terms of that at the matching point altitude, M_m', is given by the expression

$$\frac{M_m}{M_m'} = \frac{a_m'}{a_m}\sqrt{\frac{\sigma_m'}{\sigma_m}} \tag{3.49}$$

since the lift coefficient and dynamic pressure for constant $(L/D)_{max}$ and win loading are the same at all altitudes.

The range factor at $(L/D)_{max}$ at any altitude is related to that at the matching point altitude by the following expression:

$$\frac{B_m}{B'_m} = \left(\frac{V_m}{V'_m}\right)\left(\frac{c'_m}{c_m}\right) = \sqrt{\frac{\sigma'_m}{\sigma_m}}\left(\frac{c'_m}{c_m}\right) \tag{3.50}$$

where the values of the specific fuel consumption may be obtained from the engine performance data. The range ratio at any speed and altitude is then given by

$$\frac{B}{B'_m} = \left(\frac{B}{B_m}\right)\left(\frac{B_m}{B'_m}\right) \tag{3.51}$$

The ratio B/B_m is obtained from equation (3.48) for different values of M/M_m and B_m/B'_m is given by equation (3.50). The actual Mach numbers are obtained by multiplying various assumed values of the Mach number ratio M/M_m by the value of the Mach number M_m corresponding to the altitude for which the range and Mach number curve is being constructed. Although the range ratio B/B_m given by equation (3.48) is dependent upon the value of M_m and the slope K of the specific fuel consumption curve, the magnitude of the effects of variations of these quantities with altitude in any given case is usually relatively small. Consequently, sufficient accuracy can often be achieved by using the values of B/B_m for the matching point Mach number and altitude, together with values of B_m/B'_m and M_m obtained from equations (3.50) and (3.49), respectively, for each altitude for which the curve of range against Mach number is desired.

Portions of the cruise performance map, constructed according to the methods just discussed, may involve combinations of Mach number and altitude which are not consistent with the capabilities of the engine and the aerodynamic constraints imposed by the design of the aircraft. Methods for estimating the limits imposed by the thrust capabilities of the engine, at both high and low Mach numbers, will now be discussed. Also considered briefly will be the limits imposed by the maximum lift coefficient at low speeds and the onset of adverse Mach number effects at high speeds.

The thrust limit Mach numbers are defined as the maximum and minimum Mach numbers, at a given altitude, for which sufficient thrust is available to balance the drag in unaccelerated, level flight. As in the preceding development of cruise performance curves, the following method for determining the thrust limits assumes that the aircraft was matched to cruise at $(L/D)_{max}$ and employs matching point values of the wing loading W_g/S and thrust loading T_0/W_g. The method, however, can be used for any value of matching point L/D and for aircraft weights less than maximum take-off gross weight. Maximum cruise thrust is also assumed, but other values of the thrust could be employed.

The lift-drag ratio at which the thrust exactly balances the drag at some altitude other than that corresponding to the matching point, expressed as a fraction of $(L/D)_{max}$, is given by the following relationship which is based on equation (3.32):

$$\frac{(L/D)_h}{(L/D)_{max}} = \frac{1}{(T_c/T_0)_h (T_0/W_g)(L/D)_{max}} \tag{3.52}$$

where $(L/D)_h$ is the lift-drag ratio at altitude h and thrust limit Mach number M_h and where the thrust ratio T_c/T_0 is the ratio of maximum cruising thrust at the same altitude and Mach number to the maximum take-off thrust. The ratio $(L/D)_h/(L/D)_{max}$ can be determined with the use of values of T_c/T_0 chosen from the data given in figures 3.13 to 3.16 for the specified altitude and engine type.

An expression for the thrust limit Mach number M_h corresponding to the altitude h and $(L/D)_h$ can be derived from equations (3.33) and (3.34) as follows:

$$M_h = 0.0261 \sqrt{\frac{W_g/S}{C_{L,h}(p_h/p_0)}} \tag{3.53}$$

where p_h/p_0 is the ratio of the atmospheric pressure at altitude h to that at sea level. This ratio can be found in table 1.I of chapter 1. The constant 0.0261 is obtained from the numerical value of the atmospheric pressure at sea level, expressed in pounds per square foot, and the value of γ which is 1.4. The lift coefficient $C_{L,h}$ can be obtained from the ratio $(L/D)_h/(L/D)_{max}$ given by equation (3.52) with the use of the generalized curve of $(L/D)/(L/D)_{ma}$ against $\bar{C}_L$ in figure 3.12 and the lift coefficient $C_{L,m}$ for $(L/D)_{max}$.

The curve given in figure 3.12 shows the two values of $\bar{C}_L$ can be obtained for each value of the ratio $(L/D)/(L/D)_{max}$. The high and low values of $C_{L,h}$ give low and high Mach number thrust limits, respectively, when used in equation (3.53). The values of the thrust ratio T_c/T_0 at the high and low thrust limit Mach numbers will usually be significantly different. Two separate calculations will then be required for the two limits since the value of the ratios $(L/D)_h/(L/d)_{max}$, obtained from equation (3.52), will be different for the two cases. For the high Mach number limit case, however, the thrust ratio for some altitudes is relatively constant over a broad range of Mach numbers; and, in these cases, no assumption of the thrust limit Mach number need be made in choos ing the value of T_c/T_0 to be used in equation (3.52). In those cases in which the thrust ratio T_c/T_0 varies significantly with Mach number, a value of thrus limit Mach number must be assumed in choosing T_c/T_0. If the value of M_h determined from equation (3.53) differs from that assumed in choosing T_c/T_0, the desired accuracy of the thrust limit Mach number may dictate that another iteration is required.

The limits imposed on the cruise performance by the low-speed maximum lift cofficient $C_{L,max}$ may be estimated with the use of the lift coefficient at $(L/D)_{max}$, $C_{L,m}$, and an assumed value of the low-speed maximum lift coefficient. For a given altitude, the Mach number corresponding to the maximum lift coefficient $M_{C_{L,max}}$, may be estimated with the use of the following relation:

$$M_{C_{L,max}} = M_m \sqrt{\frac{C_{L,m}}{C_{L,max}}} \tag{3.54}$$

Contemporary swept-wing transport aircraft may be expected to have values of low-speed maximum lift coefficient of about 1.2. Although the value of the maximum lift coefficient varies somewhat with Mach number, these variations are neglected in the present analysis.

The limits imposed by the onset of adverse compressibility effects, such as drag divergence or buffet, at the higher cruise Mach numbers depend upon the aerodynamic design of the aircraft. The sweepback and thickness ratio of the wing, the fineness ratio of the fuselage, the detailed shape of the various parts of the aircraft, and the lift coefficient at which the aircraft is operating all play an important part in defining the high Mach number limits. Methods for estimating the drag divergence Mach number are beyond the scope of the present discussion but may be found in various textbooks and design manuals such as references 3.6, 3.7, and 3.9. Actual wind-tunnel or flight data on a configuration similar to the one of interest will probably provide the best basis for estimating the high Mach number limits.

3.10.2 Sample Cruise Performance Map

A sample cruise performance map, constructed by the methods described in section 3.10.1, is presented in figure 3.24. The sample aircraft was matched at a Mach number M_m' of 0.75 and an altitude of 40 000 ft. The matching point parameters were $(L/D)_{max} = 18$ (for simplicity, assumed to be constant until the drag divergence Mach number is exceeded), $C_{L,m} = 0.6$, $W_g/S = 93.3$ lb/ft^2, and $T_0/W_g = 0.31$. The aircraft was assumed to be powered by type B turbofan engines (fig. 3.14) and to have a low-speed maximum lift coefficient of 1.2.

The range data in figure 3.24 are in the form of the ratio of the Breguet factor at any combination of altitude and Mach number to that at the match point altitude and Mach number. The range factor ratio B/B_m', is given as a function of flight Mach number for six different altitudes. Also shown in figure 3.24 are the calculated thrust and $C_{L,max}$ limits and an assumed drag divergence limit based on wind-tunnel data. The thrust limit for Mach numbers below those for $(L/D)_{max}$ is not shown since the aircraft has negative speed stability under these flight conditions and, consequently, is seldom operated in this regime.

In figure 3.24, the curves of B/B_m' against Mach number are relatively insensitive to changes in Mach number from that for $(L/D)_{max}$ to values about

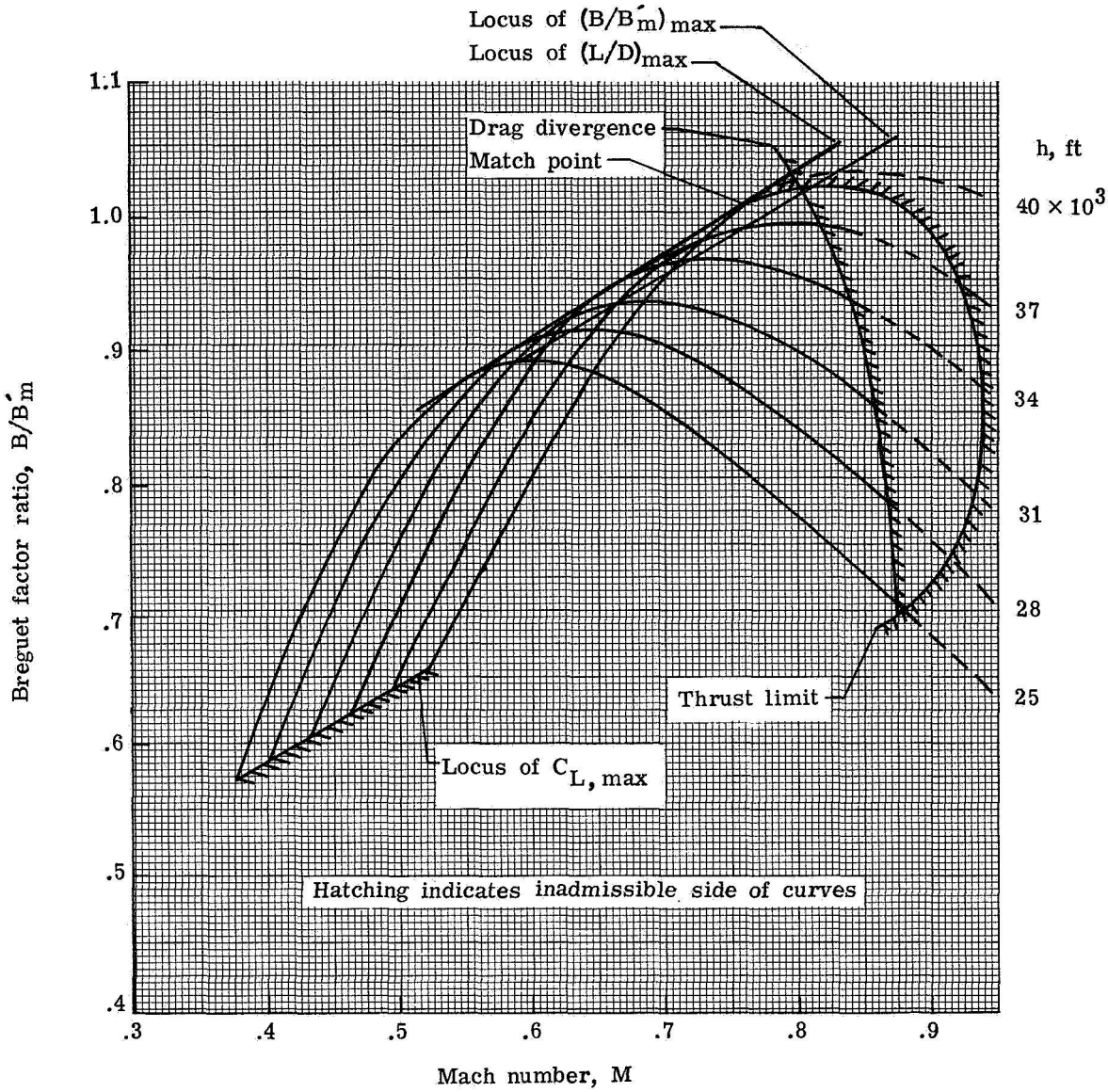


Figure 3.24.- Cruise performance map of hypothetical transport aircraft equipped with high-bypass-ratio turbofan engine. (All performance curves are for constant wing loading.)

20 percent higher than this Mach number. Thus, a good deal of flexibility in choice of cruise Mach number is available without an attendant large effect on range for a given fuel fraction. For a given altitude, the longest range is obtained for a Mach number which is about 10 percent higher than that for $(L/D)_{max}$; the range at this speed is about 3 percent higher than that at $(L/D)_{max}$. The curves show that the fuel fraction calculated for the match point Mach number will give the desired range not only at this Mach number, but also at a higher Mach number and altitude slightly lower than that at which the aircraft is matched. Approximate locii of $(B/B'_m)_{max}$ and B_m/B'_m are shown.

The relationship between the Mach number for $(L/D)_{max}$ and that for maximum range is dependent upon the nature of the curve of engine specific fuel consumption versus Mach number and, hence, is dependent on the particular type of engine with which the aircraft is equipped.

The curves of range ratio are shown in figure 3.24 as dashed lines for Mach numbers beyond the drag divergence limit line to indicate that the large increases in drag coefficient which accompany increases in Mach number beyond that for drag divergence have not been incorporated in the procedure employed in calculating the curves. The range ratio decreases much more rapidly with Mach number beyond drag divergence than is indicated by the dashed lines. The shape of the curves in this Mach number range is of little interest, however, since cruising flight is usually not undertaken for Mach numbers much beyond drag divergence.

A qualitative indication of the climbing capability of the aircraft at different altitudes can be obtained by comparing the thrust limit Mach number with the cruising Mach number. (See fig. 3.24.) For example, the maximum angle of climb is achieved at $(L/D)_{max}$, and the magnitude of this angle increases as the difference between the Mach number for $(L/D)_{max}$ and that for the thrust limit increases. The maximum cruising Mach number occurs at the intersection of the thrust limit and drag divergence lines and, for the hypothetical aircraft of figure 3.24, is 0.875 at an altitude slightly less than 25 000 ft. The range at this maximum speed point is only about 65 percent of that achievable at the matching point. For this condition, as well as for the matching point at Mach number 0.75 and 40 000 ft altitude, there is no excess thrust available for climbing at the gross weight condition for which the cruise performance map was constructed. The low-speed maximum lift coefficient imposes no significant limitation to cruising performance for the aircraft whose characteristics are depicted in figure 3.24.

The methods described and discussed in this section provide a good indication of the nature of the cruise performance characteristics of a jet transport aircraft. The performance map shown in figure 3.24 is for the maximum gross weight condition. Maps may also be constructed for lighter weight conditions in order to obtain a complete picture of the cruise performance characteristics of a particular aircraft.

SYMBOLS

A	aspect ratio, b^2/S
A_n	nacelle wetted area, ft^2
A_t	total aircraft wetted area, ft^2
a	*speed of sound, ft/sec (see eq. (3.14)) or acceleration of aircraft,* ft/sec^2 (see eq. (3.8))
a_m	speed of sound for aircraft operating at $(L/D)_{max}$ and altitude h
a_m'	speed of sound for aircraft operating at $(L/D)_{max}$ and matching point altitude
B	Breguet factor, $\frac{V(L/D)}{c}$ where V *is in knots*
B_m	Breguet factor for aircraft operating at $(L/D)_{max}$ and altitude h
B_m'	Breguet factor for aircraft operating at $(L/D)_{max}$ and matching point altitude
b	wing span, ft
C, K, k	constants
C_D	total drag coefficient
$C_{D,i}$	induced drag coefficient, $C_L^2/\pi A\epsilon$
$C_{D,m}$	drag coefficient at $(L/D)_{max}$
$C_{D,p}$	total profile drag coefficient, $C_{D,0} + \Delta C_{D,f} + \Delta C_{D,g} + \Delta C_{D,s}$
$C_{D,0}$	drag coefficient at zero lift
$\Delta C_{D,f}$	increment in profile drag coefficient due to trailing-edge flap deflection
$\Delta C_{D,g}$	increment in profile drag coefficient due to landing-gear extension
$\Delta C_{D,s}$	increment in profile drag coefficient due to slat deflection
C_L	lift coefficient
$\bar{C}_L$	lift coefficient ratio, $C_L/C_{L,m}$
$C_{L,A}$	approach lift coefficient, $C_{L,max}/1.69$

$C_{L,h}$ lift coefficient for altitude h and thrust limit Mach number

$C_{L,lo}$ lift-off lift coefficient

$C_{L,m}$ lift coefficient for $(L/D)_{max}$

$C_{L,max}$ maximum lift coefficient for aircraft configuration defined in text

$C_{L,T}$ maximum lift coefficient for aircraft in take-off configuration

$C_{L,2}$ second-segment climb gradient lift coefficient, $C_{L,T}/1.44$

c specific fuel consumption, pounds of fuel per pound of thrust per hour

c_r root chord, ft

c_m specific fuel consumption for aircraft operating at $(L/D)_{max}$ and altitude h

c_m' specific fuel consumption for aircraft operating at $(L/D)_{max}$ and matching point altitude

c_0 specific fuel consumption for sea-level static thrust conditions

D drag, lb

D_{match} drag at W_g and $(L/D)_{max}$, lb

d fuselage diameter, ft

g acceleration due to gravity, ft/sec^2

h altitude, ft

L lift, lb

$\bar{L}$ scale parameter, $\frac{V_c c_r}{1.63 \times 10^4}$ where V is in knots and c_r is in ft

L/D lift-drag ratio

$(L/D)_{max}$ maximum lift-drag ratio

l fuselage length, ft

ℓ_L FAR landing field length, ft

ℓ_T FAR balanced take-off field length, ft

$\ell_{T,g}$ take-off ground run, ft

M	Mach number
$\bar{M}$	Mach number ratio, M/M_m
M_m	Mach number for aircraft operating at $(L/D)_{max}$ and altitude h
M_m'	Mach number for aircraft operating at $(L/D)_{max}$ and matching point altitude
$M_{C_{L,max}}$	Mach number for maximum lift coefficient for aircraft in clean condition operating at altitude h
p	atmospheric pressure, lb/ft^2
p_h	atmospheric pressure at altitude h
p_0	atmospheric pressure at sea level
q	dynamic pressure, lb/ft^2
R	range, n. mi.
R_m	range for aircraft operating at $(L/D)_{max}$ and altitude h
S	wing area, ft^2
S_t	sum of horizontal and vertical tail areas, ft^2
T	engine thrust, lb
T_c	maximum continuous thrust (used in cruise flight), lb
T_{match}	thrust at $(L/D)_{max}$ and W_g, lb
T_0	maximum sea-level static thrust, lb
$\bar{U}$	useful load fraction, $1 - \frac{W_e}{W_g} = \frac{W_p + W_f}{W_g}$
u	span loading parameter
V	speed, knots or ft/sec
$\bar{V}$	speed ratio, V/V_m
V_A	appraoch speed, knots
V_c	cruising speed, knots
V_{lo}	lift-off speed, knots

V_m	speed for aircraft operating at $(L/D)_{max}$ and altitude h
V_m'	speed for aircraft operating at $(L/D)_{max}$ and matching point altitude
V_1	decision speed, knots
V_2	second-segment climb gradient speed, knots
W	weight, lb
W_e	empty weight, lb
W_f	fuel weight, lb
W_g	maximum take-off gross weight, lb
W_L	maximum landing weight, lb
W_p	payload weight, lb
W_t	propulsion system weight, lb
γ	ratio of specific heats or flight-path angle
ϵ	Oswald's airplane efficiency factor (e in ref. 3.12)
ρ	atmospheric density, slugs/ft^3
ρ_0	atmospheric density at sea level
σ	density ratio, ρ/ρ_0
σ_m	atmospheric density for aircraft operating at $(L/D)_{max}$ and altitude h
σ_m'	atmospheric density for aircraft operating at $(L/D)_{max}$ and matching point altitude

REFERENCES

3.1 Taylor, John W. R., ed.: Jane's All the World's Aircraft, 1967-68. McGraw-Hill Book Co., c.1967.

3.2 Taylor, John W. R., ed.: Jane's All the World's Aircraft, 1972-73. McGraw-Hill Book Co., c.1972.

3.3 Flight International Magazine, vol. 104, no. 3370, Oct. 18, 1973, pp. 644-648.

3.4 Airworthiness Standards: Transport Category Airplanes. FAR Pt. 25, FAA, Feb. 1, 1965.

3.5 Certification and Operations: Domestic, Flag, and Supplemental Air Carriers and Commercial Operators of Large Aircraft. FAR Pt. 121, FAA, June 1974, paragraph 121.195.

3.6 Roskam, Jan: Methods for Estimating Drag Polars of Subsonic Airplanes. Pub. by author (519 Boulder, Lawrence, Kansas 66044), c.1971.

3.7 Smith, C. W., ed.: Aerospace Handbook. Second ed. FZA-381-II, Convair Aerosp. Div., General Dynamics Corp., Oct. 1972; Rev. A, Nov. 1973.

3.8 Prediction Methods for Aircraft Aerodynamic Characteristics. AGARD-LS-67, May 1974.

3.9 Hoak, D. E.; Finck, R. D..; et al.: USAF Stability and Control Datcom. U.S. Air Force, Oct. 1960. (Revised Feb. 1972.)

3.10 Aerodynamic Drag. AGARD-CP-124, Oct. 1973.

3.11 Abbott, Ira H.; and Von Doenhoff, Albert E.: Theory of Wing Sections. Dover Publ., Inc., c.1959.

3.12 Oswald, W. Bailey: General Formulas and Charts for the Calculation of Airplane Performance. NACA Rep. 408, 1932.

3.13 Perkins, Courtland D.; and Hage, Robert E.: Airplane Performance Stability and Control. John Wiley & Sons, Inc., c.1949.

3.14 Hoerner, Sighard F.: Fluid-Dynamic Drag. Hoerner Fluid Dynamics (Brick Town, N.J.), c.1965.

3.15 The Aircraft Gas Turbine Engine and Its Operation. Part No. PWA 182408, PWA Oper. Instr. 200, Pratt & Whitney Aircraft, June 1952. Reprinted with revisions May 1974, p. 144.

3.16 Swan, Walter C.; and Schott, Gerardus J.: New Engine Cycles - Opportunity for Creativity. Astronaut. & Aeronaut., vol. 13, no. 1, Jan. 1975, pp. 24-35.

3.17 The Staff of Ames 1- by 3-Foot Supersonic Wind-Tunnel Section: Notes and Tables for Use in the Analysis of Supersonic Flow. NACA TN 1428, 1947.

3.18 Wilson, R. C.: Preliminary Airplane Design. Pitman Pub. Co., c.1941.

3.19 Standard Method of Estimating Comparative Direct Operating Costs of Turbine Powered Transport Airplanes. Air Transp. Assoc. America, Dec. 1967.

TABLE 3.I.- AIRCRAFT ANALYZED

Boeing 707*
Boeing 727*
Boeing 737
Boeing 747*
McDonnell Douglas DC-8*
McDonnell Douglas DC-9*
McDonnell Douglas DC-10*
Lockheed L-1011
Lockheed C-5A
Lockheed JetStar
Airbus A-300
British Aircraft Corporation VC-10*
British Aircraft Corporation BAC 1-11
Dassault Mercure
Illushyn Ill-62
Tupelov Tu-134
Tupelov Tu-154
Yakovlev Yak-40
Hawker Siddeley HS-125
Hawker Siddeley HS-146
Hawker Siddeley Trident
Fokker-VFW F28
VFW-Fokker VFW 614
Grumman Gulfstream II
MBB HFB 320 Hansa
Dassault-Breguet Falcon
Rockwell International Sabreliner
IAI Commodore Jet
Cessna Citation
Gates Learjet

*More than one version considered.

TABLE 3.II.- LIFT-DRAG RATIO FOR AIRCRAFT

IN APPROACH CONFIGURATION

C_L	L/D for A of -		
	6	8	10
1.2	7.9	9.7	11.2
1.4	7.1	8.7	10.1
1.6	6.3	7.8	9.1
1.8	5.7	7.0	8.2

TABLE 3.III.- LIFT-DRAG RATIO FOR AIRCRAFT

IN CLIMB CONFIGURATION

C_L	L/D for A of -		
	6	8	10
1.2	8.8	11.0	13.0
1.4	7.6	9.6	11.3
1.6	6.7	8.4	9.9
1.8	6.0	7.5	8.8

TABLE 3.IV.- ESTIMATED GEOMETRIC AND AERODYNAMIC CHARACTERISTICS OF REPRESENTATIVE AIRCRAFT

A	ℓ/d	$\pi d^2/4S$	A_t/S	$\bar{L}$	$C_{D,0}$	$C_{L,m}$	$(L/D)_{max}$
Narrow-body transport							
7.4	11.8	0.039	5.00	1.0	0.0131	0.51	19.4
7.5	13.59	.051	5.95	1.0	.0156	.56	17.92
7.0	9.4	.072	5.80	.74	.0160	.55	17.10
7.0	11.1	.072	6.29	.74	.0173	.57	16.42
8.8	7.9	.121	6.72	.64	.0190	.67	17.59
8.7	9	.111	6.93	.64	.0196	.67	17.23
8.5	7.5	.096	5.88	.64	.0166	.61	18.49
Wide-body transport							
7.0	10.3	0.069	5.95	1.34	0.0148	0.53	17.74
7.6	8.7	.095	6.31	1.13	.0162	.57	17.70
7.0	9.1	.088	6.23	1.07	.0161	.55	17.02
7.7	9.2	.096	6.53	1.0	.0171	.59	17.33
Business jet							
5.0	8.7	0.085	6.00	0.24	0.0199	0.52	12.94
6.0	9.4	.072	5.80	.47	.0172	.52	15.25

TABLE 3.V.- SAMPLE CRUISE MATCHING

W/S	h	T_c/T_0
80	40 000	0.174
100	36 200	.205
120	32 000	.235
140	28 300	.265

TABLE 3.VI.- ALTITUDE EFFECTS ON THRUST AND DRAG

①	②	③	④	⑤	⑥
h	$C_L/C_{L,m}$	$(L/D)/(L/D)_{max}$	D/D_{match}	T_c/T_0	T_c/T_{match}
40 000	1.00	1.00	1.00	0.175	1.0
35 000	.76	.96	1.04	.215	1.23
30 000	.62	.89	1.12	.255	1.46
25 000	.50	.80	1.25	.280	1.60

IV - APPLICATION OF SIZING METHOD FOR JET-POWERED CRUISING AIRCRAFT

CONTENTS

		Page
4.0	Introduction	176
4.1	Performance Objectives	176
4.2	Aircraft Description	177
4.3	Scope of Studies	179
4.4	Airfield Performance	180
	4.4.1 Landing Performance	180
	4.4.2 Take-Off Performance	181
4.5	Cruise Matching	182
4.6	Aircraft Matching	183
	4.6.1 Match Point Parameters	186
	4.6.2 Take-Off Lift Coefficients	191
4.7	Aircraft Sizing	192
	4.7.1 Aircraft Fuel Fraction	192
	4.7.2 Aircraft Weights and Sizes	196
4.8	Design Trends	197
4.9	Resized Aircraft	207
SYMBOLS		213
TABLES		216

4.0 Introduction

The procedures for sizing jet-powered cruising aircraft described in chapter 3 are illustrated in chapter 4 through application to a specific design problem. An executive jet transport capable of carrying 10 passengers on a nonstop flight from the East Coast to the West Coast of the United States has been chosen for study. Three variants of the aircraft are analyzed: one aircraft cruises at a Mach number of 0.8 and utilizes two low-bypass-ratio turbofan engines; another aircraft cruises at a Mach number of 0.7 and employs low-bypass-ratio turbofan engines; and the third cruises at a Mach number of 0.7 and employs high-bypass-ratio turbofan engines. Each aircraft is to be sized for three different take-off field lengths and for two different values of cruise lift-drag ratio. The following sections outline the performance objectives, describe the aircraft and the computational procedures used in the sizing process, show the matching charts for the different aircraft, and illustrate the effect of variations in several design parameters on the physical characteristics of the aircraft.

4.1 Performance Objectives

A nonstop, transcontinental range is required in the example aircraft. A New York to Los Angeles trip will be used to estimate the range required in the aircraft. The distance between these two cities is approximately 2174 n. mi. If 500 n. mi. is added to cover necessary fuel reserves, the total design range becomes 2674 n. mi.

The payload is intended to consist of 10 passengers with their baggage, a crew of two pilots and one cabin attendant, and a capacity for 500 lb of cargo or additional baggage. The typical passenger or crew member is assumed to weigh 175 lb and to carry 30 lb of baggage. The total payload weight is summarized as follows:

Ten passengers at 205 lb each, lb	2050
Three crew members at 205 lb each, lb	615
Cargo, lb	500
Total payload weight, lb	3165

As indicated in section 4.0, aircraft intended for cruise flight at Mach numbers of 0.8 and 0.7 will be studied. A FAR landing field length of 5000 ft is desired in all cases. Each of the aircraft variants is to be sized for FAR balanced take-off field lengths of 6000, 7000, and 8000 ft. The landing and take-off field lengths are to be based on sea-level standard-day atmospheric characteristics.

4.2 Aircraft Description

The aircraft intended to cruise at a Mach number of 0.8 is to have a wing of aspect ratio 7 and sweepback angle of 34° at the quarter-chord line. This aircraft is to utilize the low-bypass-ratio engine, designated engine D in chapter 3, for which characteristics are given in figures 3.16(a) and 3.16(b). The aircraft intended to cruise at a Mach number of 0.7 is to employ a wing of aspect ratio 8 and sweepback angle of about 24° at the quarter-chord line. This aircraft is to be sized with both low- and high-bypass-ratio engines. The low-bypass-ratio engine is the same engine D used for the aircraft intended to cruise at a Mach number of 0.8; whereas, the high-bypass-ratio engine is engine A of chapter 3. The characteristics of engine A were given in figures 3.13(a) and 3.13(b). The basic characteristics of the three aircraft variants to be studied, designated aircraft variants 1, 2, and 3, are as follows:

Aircraft variant	Mach number	Aspect ratio	Sweepback angle, deg	Engine
1	0.8	7	34	D
2	.7	8	24	D
3	.7	8	24	A

The maximum lift-drag ratios of the aircraft to be sized are estimated according to the methods of section 3.5.1 of chapter 3. The fuselage of each of the aircraft is assumed to have a fineness ratio of 8.5 and to have a ratio of fuselage cross-sectional area to wing area of 0.120. The zero-lift drag coefficient corresponding to these design parameters is found from figure 3.11 to be 0.0183 for aircraft of the same size as the reference aircraft used in constructing figure 3.11. The reference aircraft was a large narrow-body four-engine transport. The executive aircraft to be studied herein is assumed to be 0.34 the size of the reference transport aircraft; that is, the value of $\bar{L}$ used in figure 3.11 for correcting the zero-lift drag coefficient for the effect of size is 0.34. With the use of the value of $\bar{L}$ and the curve from figure 3.11, the correction factor for the zero-lift drag coefficient is found to be 1.2. Hence, the zero-lift drag coefficient $C_{D,0}$ for the executive jet aircraft is

$$C_{D,0} = 1.2\ (0.0183) = 0.0220$$

The values of maximum lift-drag ratio $(L/D)_{max}$ and the corresponding value of lift coefficient $C_{L,m}$ may now be read from figure 3.11 or calculated from equations (3.19) and (3.20) which, for convenience, are repeated here as follows:

$$C_{L,m} = \sqrt{\pi A \epsilon C_{D,0}} \tag{4.1}$$

$$(L/D)_{max} = \frac{1}{2}\sqrt{\frac{\pi A \epsilon}{C_{D,0}}} \tag{4.2}$$

The values of $(L/D)_{max}$ and $C_{L,m}$, as well as the values of $0.97(L/D)_{max}$ and the corresponding values of lift coefficient $C_{L,0.97}$, are given in the following table:

Aircraft variant	$C_{D,0}$	$(L/D)_{max}$	$C_{L,m}$	$0.97(L/D)_{max}$	$C_{L,0.97}$
1	0.0220	14.6	0.64	14.2	0.49
2	.0220	15.6	.69	15.1	.53
3	.0220	15.6	.69	15.1	.53

The values of lift coefficient corresponding to $0.97(L/D)_{max}$ were obtained with the use of the value of $C_{L,m}$ and the generalized curve given in figure 3.12. Cruise matching (see section 3.5.3 of chapter 3) is to be studied for $(L/D)_{max}$ and $0.97(L/D)_{max}$ at the beginning of cruising flight for all cases. The lower lift-drag case is of interest because of the correspondingly lower values of lift coefficient and altitude at the matched condition. A reduced engine size and weight might accordingly be expected for these cases.

The ranges of lift coefficients to be used in the determination of the landing and take-off performance were chosen to be representative of current state of the art and are as follows:

$$C_{L,A} = 1.2 \text{ to } 1.8$$

$$C_{L,max} = 2.03 \text{ to } 3.04$$

$$C_{L,2} = 1.2 \text{ to } 1.8$$

$$C_{L,T} = 1.7 \text{ to } 2.6$$

where

$C_{L,A}$ approach lift coefficient

$C_{L,max}$ maximum lift coefficient for aircraft in landing configuration

$C_{L,2}$ second-segment climb gradient lift coefficient

$C_{L,T}$ maximum lift coefficient for aircraft in take-off configuration

The relationships between $C_{L,A}$ and $C_{L,max}$ and between $C_{L,2}$ and $C_{L,T}$ were given in chapter 3 and are repeated here for convenience as

$$C_{L,max} = 1.69C_{L,A}$$

$$C_{L,T} = 1.44C_{L,2}$$

4.3 Scope of Studies

Three different aircraft variants are to be analyzed. Each aircraft is to be sized for three different take-off field lengths and two different values of lift-drag ratio L/D corresponding to the beginning of cruising flight. One landing field length is to be used in all cases. Six matching points, discussed in section 3.6 of chapter 3, might be anticipated for each of the three aircraft variants. The following quantities are to be calculated for each matching point:

(1) Gross weight

(2) Empty weight

(3) Fuel weight

(4) Wing area

(5) Total thrust

(6) Fuselage diameter

These parameters are to be shown as a function of take-off field length for the three aircraft variants and for each of the two initial values of cruising lift-drag ratio. All aircraft have the same ratio of fuselage cross-sectional area to wing area. Hence, the diameter of the fuselage varies as the square root of the wing area for the different aircraft. If some particular value of fuselage diameter is desired, the initial sizing of the aircraft may yield values of wing area which, when taken with the desired fuselage diameter, give values of the ratio of fuselage cross-sectional area to wing area different from the assumed value of 0.12. A second sizing iteration using values of L/D appropriate to a revised ratio of cross-sectional area to wing area may then be required, depending upon the nature of the desired results.

4.4 Airfield Performance

Airfield performance embraces the following four elements:

(1) Landing field length requirement

(2) Satisfaction of climb gradient criterion following a missed approach

(3) Take-off field length requirement

(4) Satisfaction of second-segment climb gradient criterion following take-off

The second method of airfield performance calculation, described in sections 3.6.1 and 3.6.2 of chapter 3, is to be utilized in the sizing studies contained herein. This method yields a single line of thrust loading against wing loading for the landing maneuver, and another single line for the take-off maneuver. All points along these lines define combinations of thrust loading and wing loading which satisfy both the field length requirement and the appropriate climb gradient criterion.

4.4.1 Landing Performance

The specifications for all of the aircraft require a landing field length of 5000 ft on a standard day at sea level. An examination of figure 3.4 of chapter 3 indicates that the maximum approach speed for the specified field length is 129 knots. This approach speed is employed with figure 3.3 to obtain the wing loading corresponding to various assumed approach lift coefficients. The thrust-to-weight ratio needed to satisfy the missed approach climb gradient criterion is then obtained from figure 3.5 for the different assumed approach lift coefficients. Detailed calculations are contained in the two parts of table 4.I for aircraft variant 1 and aircraft variants 2 and 3. The calculations are perhaps best understood by identifying each of the columns in table 4.I as follows:

① V_A, approach speed, in knots, determined from figure 3.4 for the specified field length of 5000 ft

② $C_{L,A}$, approach lift coefficient for the range of values given in section 4.2

③ $\sqrt{W_L/S}$, wing loading parameter, obtained from figure 3.3 for the values of approach speed V_A and lift coefficient $C_{L,A}$ given in ① and ②, respectively, or by the expression

$\sqrt{W_L/S} = 1.69V_A\sqrt{C_{L,A}(\rho_0/2)}$; the weight W_L is the maximum landing weight

④ W_L/S, the square of ③

⑤ T_0/W_L, value of the thrust loading required to meet the climb gradient criterion following a missed approach; values of T_0/W_L are determined from figure 3.5 for the values of $C_{L,A}$ given in ②

⑥ W_L/W_g, ratio of maximum landing weight to maximum take-off gross weight; determined on the basis of information given in figure 3.10

⑦ W_g/S, value of the landing wing loading W_L/S expressed in terms of the maximum take-off gross weight condition; obtained by dividing ④ by ⑥ (see eq. (3.37))

⑧ T_0/W_g, landing thrust loading, expressed in terms of the maximum take-off gross weight condition; obtained by multiplying ⑤ by ⑥

Columns ⑦ and ⑧ represent pairs of values of wing loading and thrust loading, expressed in terms of maximum take-off gross weight, which simultaneously satisfy the 5000-ft landing field length and the climb gradient criterion. A single line of thrust loading against wing loading therefore may be used to express the required relationships between these parameters for the specified landing maneuver. The lift coefficient $C_{L,A}$ increases along this line as the wing loading and thrust loading increase.

4.4.2 Take-Off Performance

The specifications require that each aircraft variant be sized for FAR take-off field lengths of 6000, 7000, and 8000 ft. The data contained in figure 3.7 indicates required values of the take-off parameter $\frac{W_g/S}{\sigma C_{L,T}(T_0/W_g)}$ of 159, 185, and 212 corresponding to the specified field lengths of 6000, 7000, and 8000 feet, respectively. The thrust-to-weight ratios needed to satisfy the second-segment climb gradient criterion are obtained from figure 3.9 for a range of assumed values of climb lift coefficient $C_{L,2}$. The maximum lift coefficient in the take-off configuration $C_{L,T}$ is related to the climb lift coefficient $C_{L,2}$ by the following relation:

$$C_{L,T} = 1.44C_{L,2}$$

since the climb speed V_2 is 1.2 times the stall speed in the take-off configuration. Thus, for each value of the climb lift coefficient and for a given value of the take-off parameter $\frac{W_g/S}{\sigma C_{L,T}(T_0/W_g)}$, all the needed information is available for determining the relationship between W_g/S and T_0/W_g required to satisfy the field length requirement and climb criterion.

The detailed calculations for the three different take-off field lengths are contained in tables 4.II(a) and 4.II(b) for aircraft variant 1 and aircraft variants 2 and 3, respectively. The calculations are perhaps best understood by identifying each of the columns in table 4.II as follows:

① ℓ_T, specified field length

② $C_{L,2}$, second-segment climb lift coefficient for range of values given in section 4.2

③ $C_{L,T}$, maximum lift coefficient in the take-off configuration for $C_{L,T} = 1.44C_{L,2}$

④ T_0/W_g, value of the thrust loading required to meet the second-segment climb gradient criterion; values of T_0/W_g are obtained from figure 3.9 for the values of $C_{L,2}$ given in ②

⑤ $\dfrac{W_g/S}{\sigma C_{L,T}(T_0/W_g)}$, aircraft take-off parameter; obtained from figure 3.7 for the three different field lengths

⑥ W_g/S, wing loading; obtained by multiplication of ⑤ by ③ and ④

Columns ④ and ⑥ represent pairs of values of thrust loading and wing loading expressed in terms of maximum take-off gross weight which simultaneously satisfy the take-off field length requirement and the second-segment climb gradient criterion. A single line of thrust loading against wing loading may therefore be used to represent the required relationship between these parameters for each of the three specified field lengths. The values of $C_{L,2}$ and $C_{L,T}$ increase along this line as the wing loading and thrust loading increase.

4.5 Cruise Matching

The cruise matching procedure defines a relationship between the wing loading and the thrust loading such that, for a given value of wing loading, sufficient thrust is available to permit cruising flight at the design Mach number, at a specified lift coefficient, and for the maximum gross weight condition. The process is described in section 3.5.3 of chapter 3. The values of L/D and corresponding lift coefficients to be used in the matching process for the three aircraft variants are given in section 4.2, as are the engines to be used in each case. Aircraft variants 1 and 2 employ the same engines but different wings; whereas, aircraft variants 2 and 3 use the same wing but different engines. Hence, a separate matching calculation is required for each aircraft; and according to section 4.2, each aircraft must be matched for two different values of cruise lift-drag ratio. The detailed calculations for the three different aircraft variants are contained in table 4.III. The calculations are perhaps best understood by identifying each of the columns in table 4.III as follows:

① Engine type specified in section 4.2

② M, cruising Mach number; given in section 4.2

③ L/D, lift-drag ratio at the beginning of cruising flight; given in section 4.2

④ C_L, lift coefficient corresponding to value of L/D given in ③ (see section 4.2)

⑤ $C_L M^2$, cruise parameter; obtained from multiplication of ④ by the square of ②

⑥ W_g/S, assumed variation of wing loading to be used in cruise matching

⑦ h, altitude at the beginning of cruising flight; obtained with the use of the data given in ⑤ and ⑥ and the cruise matching chart given in figure 3.18

⑧ T_c/T_0, thrust ratio; obtained from figure 3.13 for engine A and figure 3.16 for engine D with the use of the data given in ② and ⑦

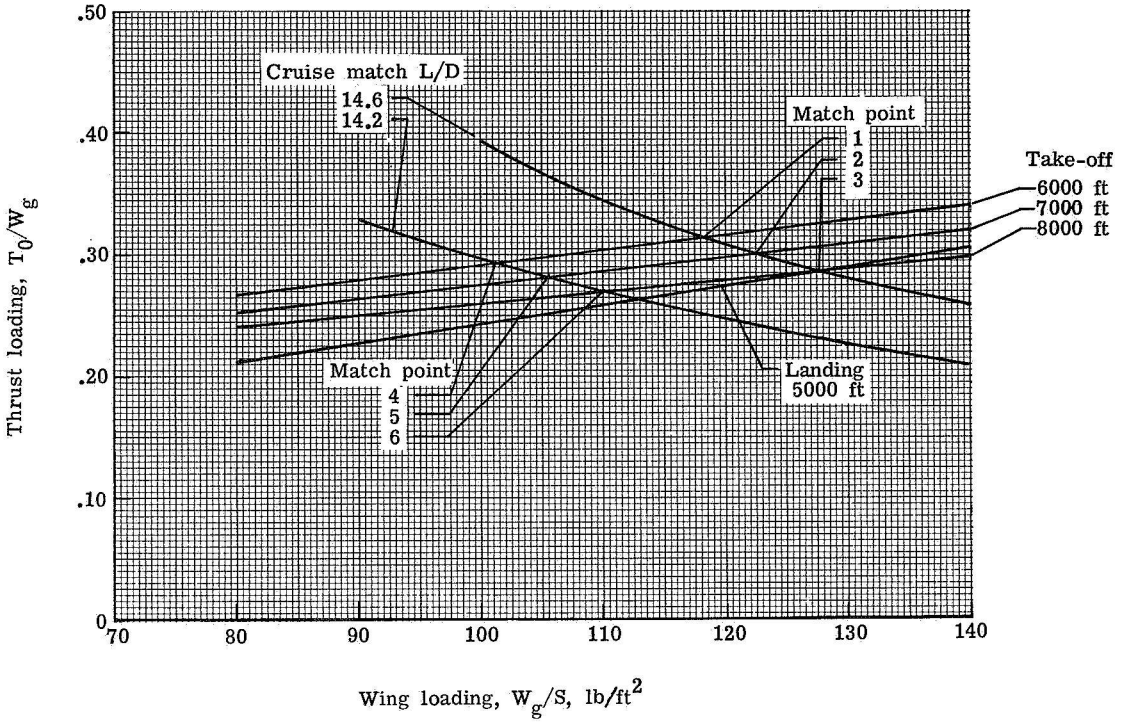
⑨ T_0/W_g, thrust loading; expressed as the ratio of maximum take-off thrust to maximum take-off gross weight; values of T_0/W_g are obtained by taking the reciprocal of the product of ③ and ⑧ :

$$\frac{T_0}{W_g} = \frac{1}{(L/D)(T_c/T_0)}$$

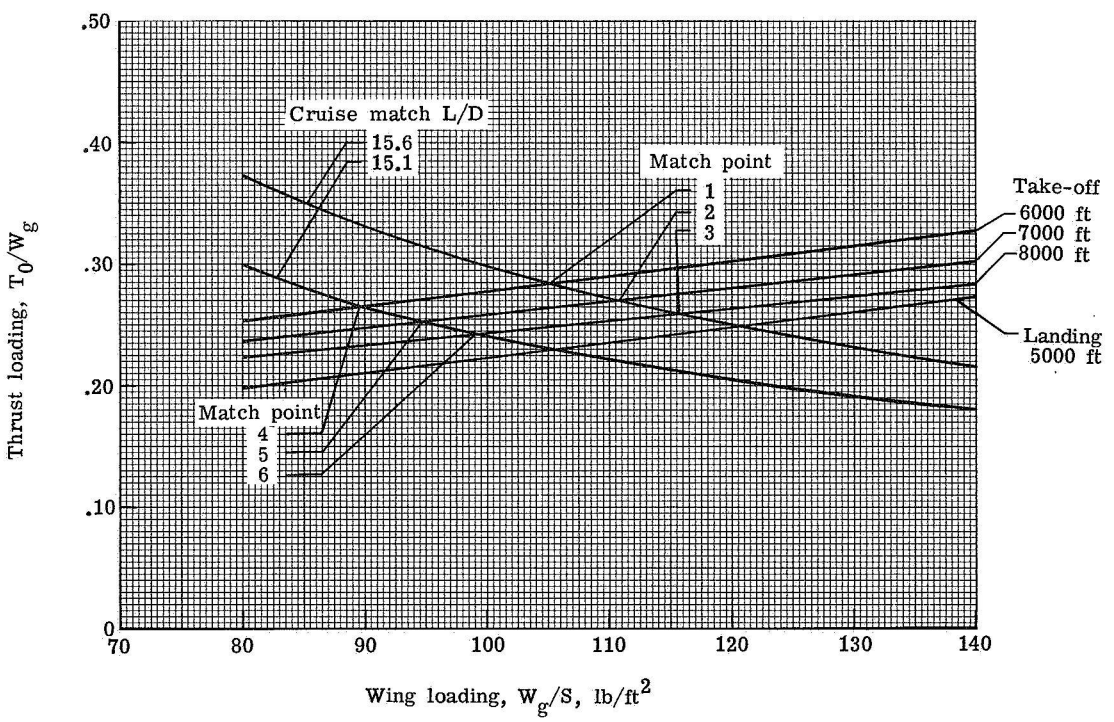
The wing loading W_g/S and thrust loading T_0/W_g given by columns ⑥ and ⑨ represent pairs of these parameters which permit cruising flight to begin at the desired values of Mach number and lift-drag ratio given by columns ② and ③. A single line of thrust loading against wing loading may therefore be used to represent the necessary relationship between these parameters for cruising flight under the specified design constraints.

4.6 Aircraft Matching

From the data of table 4.III, aircraft matching charts similar in form to the chart shown conceptionally in figure 3.20 of chapter 3 have been constructed and are presented in figures 4.1(a), (b), and (c) for aircraft variants 1, 2, and 3. The landing and take-off constraint lines indicate an increase in required thrust loading with increasing wing loading; whereas, the cruise constraint lines show a reduction in required thrust loading with increasing wing loading. The cruise match lines indicate that, for a given wing loading, a reduction in the required thrust loading accompanies a reduction in the initial value of cruising lift-drag ratio. This reduction results from the lower lift

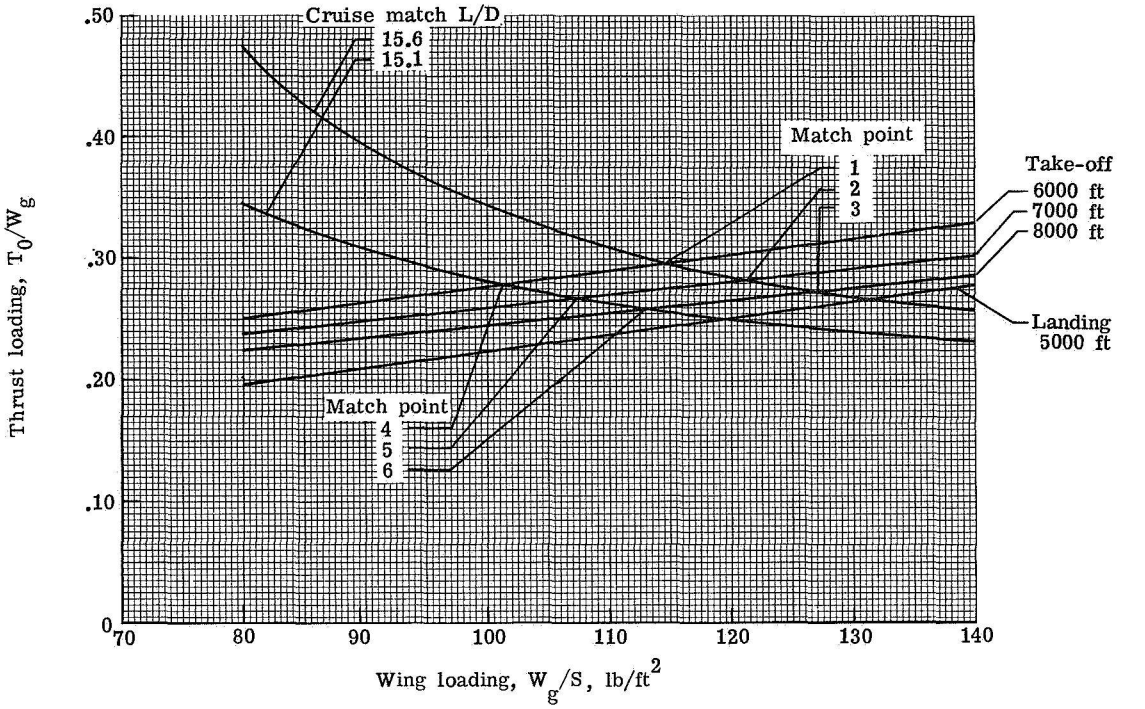


(a) Aircraft variant 1.



(b) Aircraft variant 2.

Figure 4.1.- Aircraft matching chart for aircraft variants 1, 2, and 3.



(c) Aircraft variant 3.

Figure 4.1. - Concluded.

coefficient corresponding to the reduced lift-drag ratio. The cruising altitude is thus lowered; hence, the thrust ratio T_c/T_0 for the engine is increased. The thrust-to-weight ratio T_0/W_g is given by the relation

$$\frac{T_0}{W_g} = \frac{1}{(L/D)\,(T_c/T_0)} \tag{4.3}$$

For the two values of L/D investigated, the increase of the thrust ratio T_c/T_0 corresponding to the lower value of L/D is greater than the reduction in L/D. Accordingly, reducing the initial cruising lift-drag ratio from $(L/D)_{max}$ to $0.97(L/D)_{max}$ results in a reduction in required thrust-to-weight ratio T_0/W_g corresponding to a given wing loading. The reduction in required thrust loading as the wing loading is increased, shown by the cruise match lines for a given cruise L/D, also results from a reduction in altitude and consequent increase in the value of the thrust ratio T_c/T_0.

The aircraft matching points, numbered 1 to 6 in figures 4.1(a) to (c) are determined by the intersection of the cruise match lines with the critical field length constraint line. The take-off constraint is seen to be critical in all cases except for match point 3 in figure 4.1(a), in which case the landing and take-off constraint lines have an almost identical intersection with the cruise

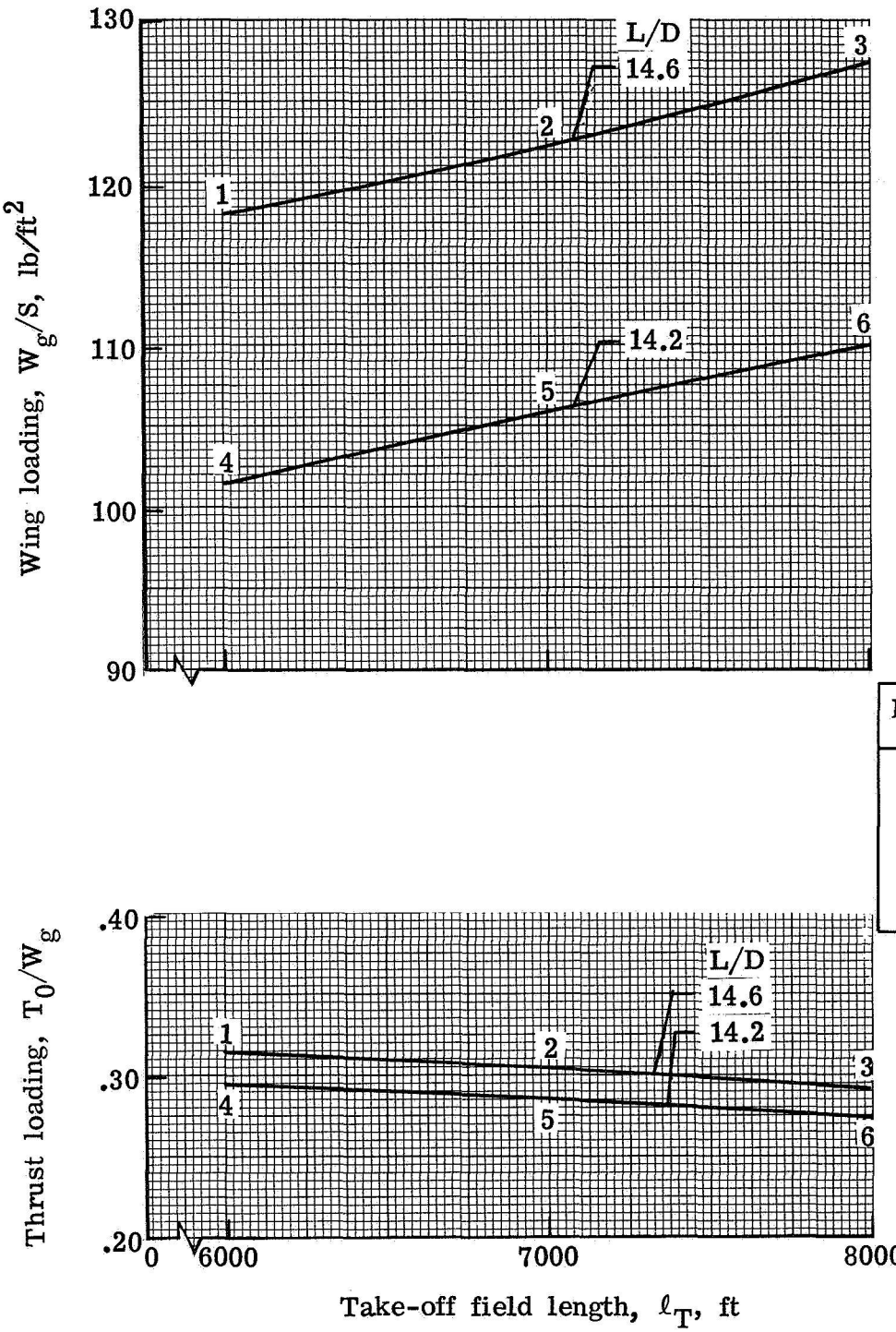
line. An increase in the value of the ratio of maximum landing weight to maximum take-off weight could cause the landing constraint to become critical, as could an increase in take-off field length or a reduction in landing field length.

4.6.1 Match Point Parameters

The match points represent the combination of wing loading and thrust loading which yields the smallest engine necessary to meet the design constraints. The wing loading and thrust loading corresponding to each of the match points are shown as a function of the take-off field length in figures 4.2(a), (b), and (c) for aircraft variants 1, 2, and 3, respectively. The match points are identified in figures 4.2(a) to (c) by the same numbers used previously in figures 4.1(a) to (c). Also shown in each figure is a tabulation of the maximum lift coefficient in the take-off configuration $C_{L,T}$ corresponding to each match point. The values of $C_{L,T}$ were obtained for the wing loading at each match point by interpolation of the take-off data of table 4.II. The wing loading and thrust loading show a consistent variation with take-off field length for the three different aircraft.

Comparisons of the different aircraft are of particular interest. For example, the values of wing loading and thrust loading corresponding to each match point for aircraft variant 2 are significantly lower than those for aircraft variant 1 for the same take-off field length. Aircraft variants 1 and 2 employ the same engine but differ in wing aspect ratio and cruising speed. The aspect-ratio-8 wing of aircraft variant 2 gives $(L/D)_{max} = 15.6$ for this variant as compared to $(L/D)_{max} = 14.6$ for aircraft variant 1 which has a wing of aspect ratio 7. The value of the cruise parameter $C_L M^2$ decreases from 0.410 (at $(L/D)_{max}$) for aircraft variant 1 to 0.338 for aircraft variant 2. (See table 4.III.) This reduction in value of the cruise parameter is caused primarily by the lowering of the cruise Mach number from 0.8 to 0.7. The reduction in value of the cruise parameter, however, is not quite proportional to the square of the Mach number since the lift coefficient corresponding to $(L/D)_{max}$ is about 7 percent higher for aircraft variant 2 than for aircraft variant 1. Both the higher value of cruise lift-drag ratio and the lower value of cruise parameter of aircraft variant 2 as compared to aircraft variant 1 result in a reduction in required thrust loading for a given wing loading. Thus, the cruise constraint line of aircraft variant 2 (fig. 4.1(b)) is lower than that of aircraft variant 1 (fig. 4.1(a)) for a given wing loading; hence, the cruise line intersects the take-off field length lines at lower values of the wing loading. The take-off field length constraint lines of aircraft variant 2 give a somewhat lower value of required thrust loading for a given wing loading because of the higher lift-drag ratio in the take-off configuration of aircraft variant 2 with the aspect-ratio-8 wing. The net effect of these various influences is to cause the observed reductions (figs. 4.2(a) and 4.2(b)) in wing loading and thrust loading at corresponding match points of aircraft variant 2 as compared to aircraft variant 1.

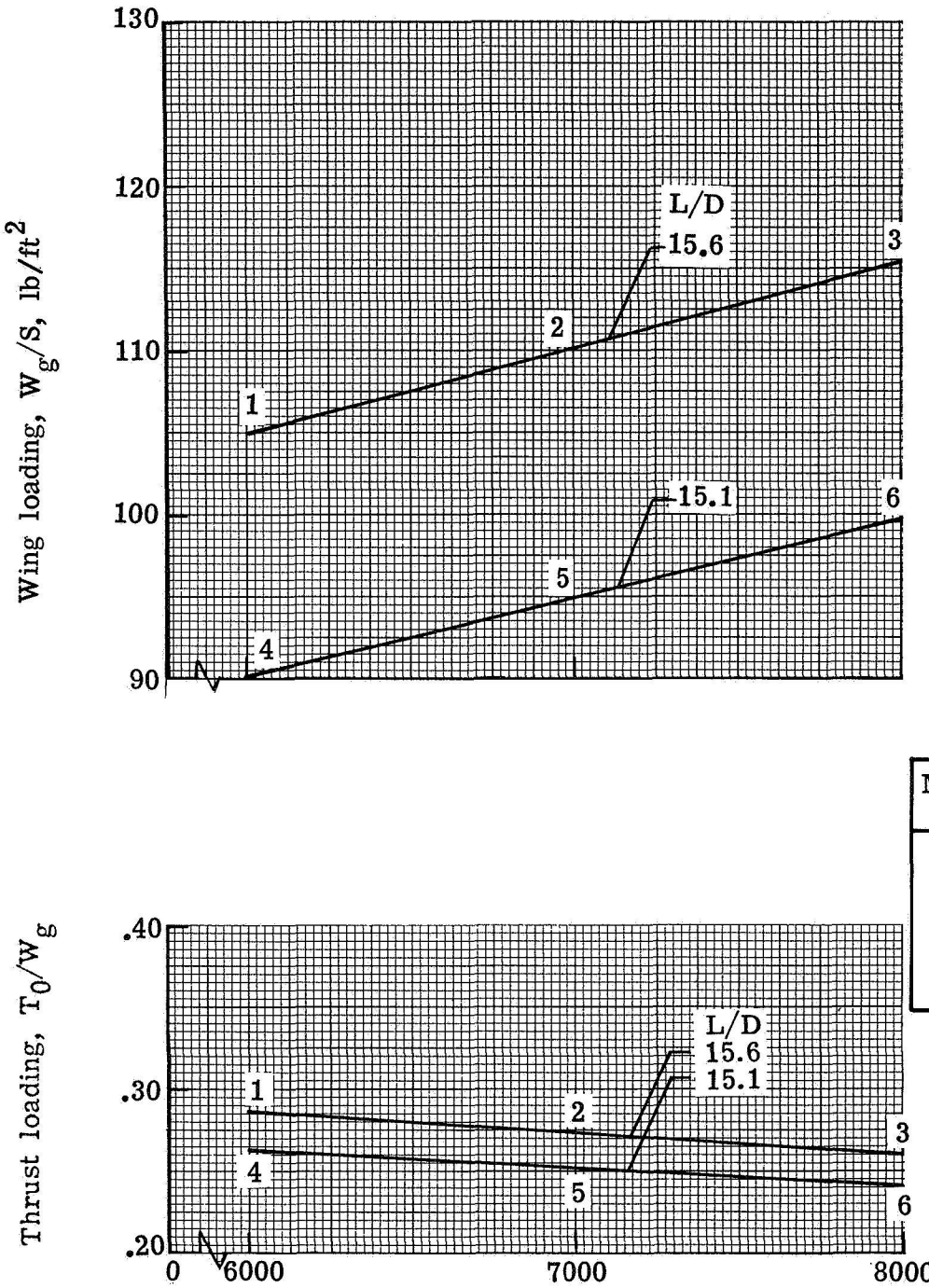
Aircraft variants 2 and 3 differ only in the type of engine. Aircraft variant 2 employs a low-bypass-ratio engine (engine D) which typifies the first generation of relatively inefficient fan engines; aircraft variant 3 employs a



Match point	$C_{L,T}$
1	2.33
2	2.20
3	2.08
4	2.16
5	2.02
6	1.95

(a) Aircraft variant 1.

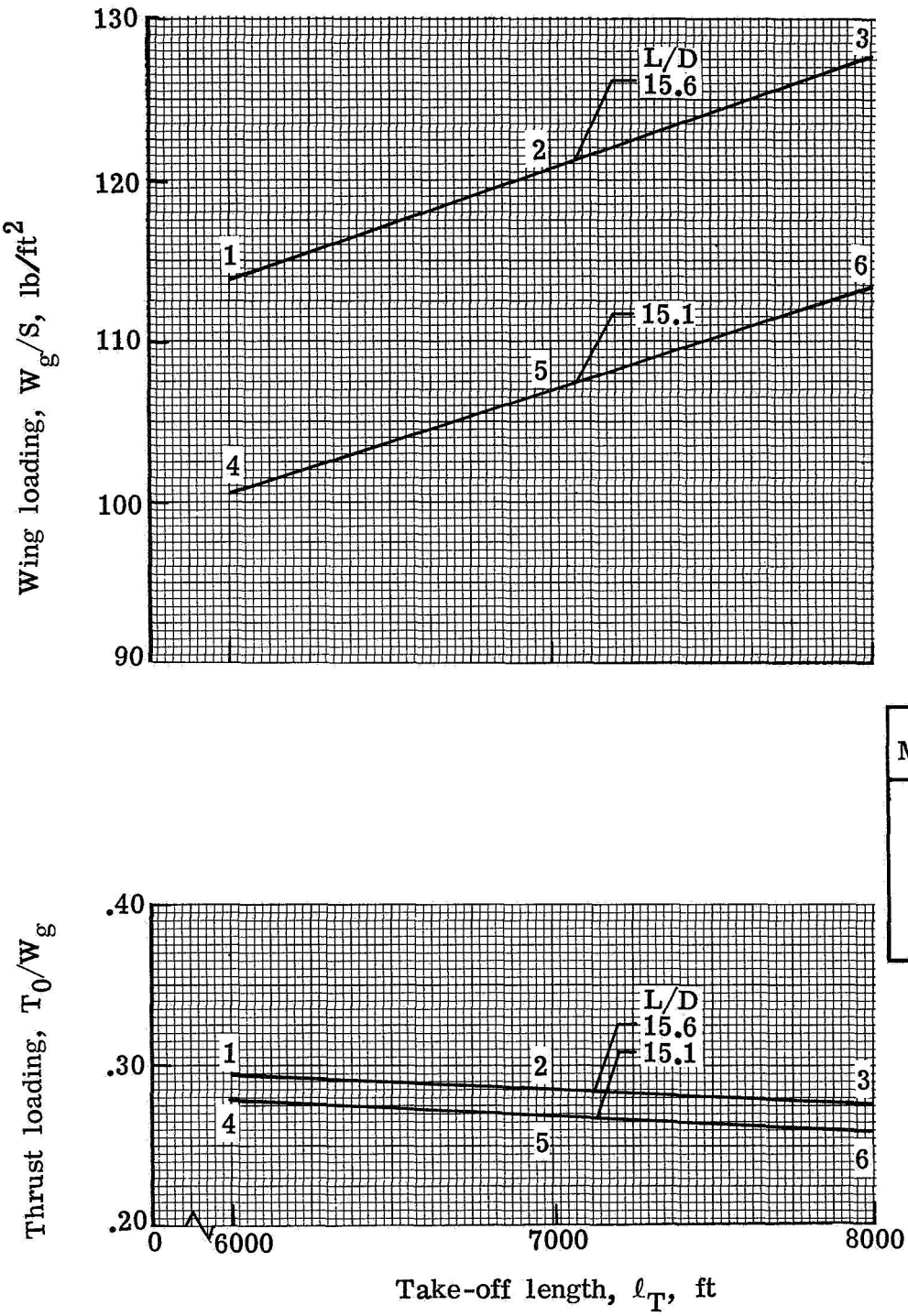
Figure 4.2.- Characteristics at matching points of aircraft variants 1, 2, and 3 as function of take-off field length.



Match point	$C_{L,T}$
1	2.30
2	2.18
3	2.08
4	2.26
5	2.02
6	1.91

(b) Aircraft variant 2.

Figure 4.2.- Continued.



Match point	$C_{L,T}$
1	2.42
2	2.30
3	2.20
4	2.26
5	2.16
6	2.06

(c) Aircraft variant 3.

Figure 4.2.- Concluded.

modern high-bypass-ratio turbofan engine (engine A) which has a specific fuel consumption about 23 percent lower than that of engine D at a Mach number of 0.7. (See figs. 3.13 and 3.16 of chapter 3.) A comparison of wing loadings and thrust loadings for aircraft variants 2 and 3 at corresponding match points (figs. 4.2(b) and 4.2(c)) indicates that aircraft variant 3 has significantly higher wing loadings and somewhat higher thrust loadings. For example, at match point 2, aircraft variant 3 has a wing loading of about 121 lb/ft^2 as compared to 110 lb/ft^2 for aircraft variant 2. The comparative thrust loadings for aircraft variant 3 and aircraft variant 2 are 0.285 and 0.273, respectively. The differences between thrust loading and wing loading at corresponding match

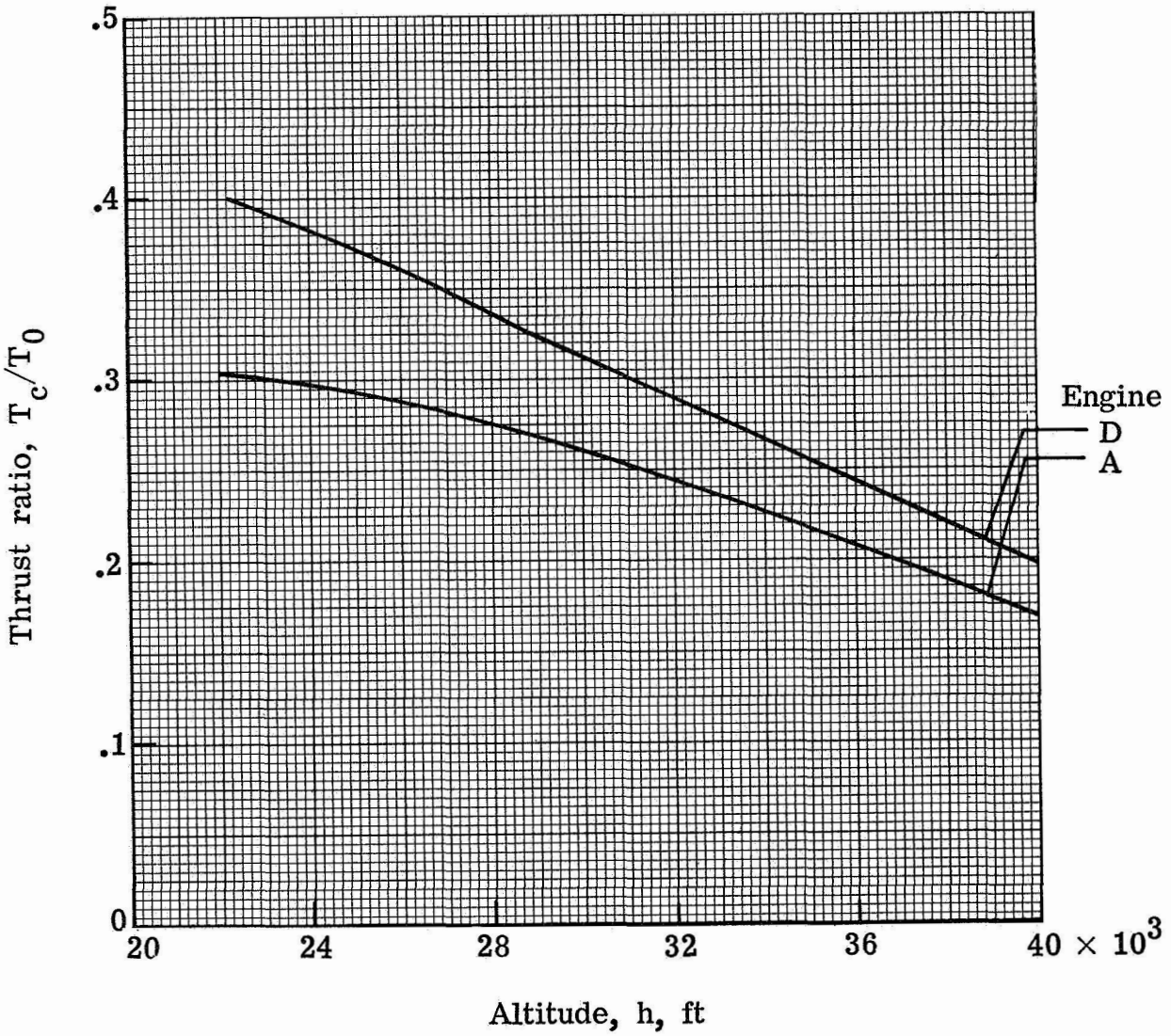


Figure 4.3.- Variation of thrust ratio with altitude for engines A and D at Mach number of 0.7.

points are explained by the difference in thrust ratio T_c/T_0 exhibited by engine A as compared to engine D for a given altitude. The difference in thrust ratio for the two engines is highlighted by the curves in figure 4.3 which were constructed by cross-plotting the engine data given in figures 3.13 and 3.16 of chapter 3. Shown in figure 4.3 is the thrust ratio T_c/T_0 as a function of altitude for engines A and D at a Mach number of 0.7. The value of the thrust ratio of engine A is about 25 to 15 percent lower than that of engine D as the altitude is increased from 22 000 ft to 40 000 ft. The matching thrust loading corresponding to given values of lift-drag ratio, wing loading, and cruise parameter is accordingly higher for the lower value of thrust ratio as shown by equation (4.3). The large magnitude of the effect of the lower values of T_c/T_0 for engine A is evident for a given value of wing loading by comparing the matching charts for aircraft variants 2 and 3 given in figures 4.1(b) and 4.1(c). The effect of a large vertical displacement of the cruise match lines, however, causes a large increase in wing loading but a relatively small increase in thrust loading for a given match point because of the nature of the slopes of the cruise match and take-off lines in figures 4.1(b) and 4.1(c). Thus, for corresponding matching points, the data of figures 4.2(b) and 4.2(c) show large increases in the wing loading for the aircraft with engine A as compared to that with engine D, but only a relatively small increase in required thrust loading.

4.6.2 Take-Off Lift Coefficients

An examination of the maximum lift coefficient data in figures 4.2(a), 4.2(b), and 4.2(c) indicates values of $C_{L,T}$ which vary from a high of 2.42 for aircraft variant 3-1 to a low of 1.91 for aircraft variant 2-6. The designations 3-1 and 2-6 are used to identify the aircraft variant and the particular match point. For example, the number 3-1 indicates aircraft variant 3 and match point 1. This system of aircraft designation is used in subsequent sections of this chapter. The indicated range of $C_{L,T}$ corresponds to a range in second-segment climb gradient lift coefficient $C_{L,2}$ from 1.71 to 1.33. An examination of the data given in figure 3.8 indicates that present-day aircraft do not use values of $C_{L,2}$ in excess of 1.6. The corresponding value of $C_{L,T}$ is 2.3; however, a value of 2.46 does not seem unreasonable. Should the aircraft matching process yield a value of $C_{L,T}$ which is clearly beyond the state of the art, however, the values of wing loading and thrust loading must be adjusted to obtain the desired field length with the available values of $C_{L,T}$. One method of handling this case is to increase by a constant percentage the values of T_0/W_g obtained from figure 3.9, and tabulated in column 4 of table 4.II, for each value of assumed achievable lift coefficient $C_{L,2}$. A new take-off line is then obtained which intersects the cruise constraint line at a lower value of wing loading, higher value of thrust loading, and reduced value of required $C_{L,T}$. The percentage by which the values of T_0/W_g obtained from figure 3.9 for a given lift coefficient are increased must be assumed, and more than one iteration may be necessary. Other approaches for obtaining a match point for different lift coefficients are possible and may be investigated by the reader.

4.7 Aircraft Sizing

Estimation of the various aircraft weights and sizes with the use of relationships which utilize match point parameters, payload, and design range was discussed in section 3.7 of chapter 3. The method requires the determination of the fuel fraction corresponding to the design range. Calculation of the fuel fraction was discussed in section 3.8 of chapter 3; the procedure described therein will now be applied to the determination of the fuel fraction corresponding to the six match points of each of the three aircraft variants and for the design range of 2674 n. mi.

4.7.1 Aircraft Fuel Fraction

The fuel fraction necessary for a specified range is given by equation (3.13) of chapter 3 and is repeated here for convenience

$$\frac{W_f}{W_g} = 1 - \frac{1}{e^{R/B}} \tag{4.4}$$

where

W_f fuel weight, lb

W_g aircraft gross weight, lb

R range, n. mi.

B Breguet factor, $\frac{V(L/D)}{c}$

and where

V speed, knots

L/D lift-drag ratio

c specific fuel consumption, pounds of fuel per pound of thrust per hour

Each aircraft is assumed to fly the entire design range at a constant altitude. The value of the lift-drag ratio employed in the Breguet factor must, therefore, be an average of the initial and final values. Thus,

$$(L/D)_{av} = \frac{(L/D)_o + (L/D)_{final}}{2} \tag{4.5}$$

The average value of the lift-drag ratio can also be written in the following useful form:

$$(L/D)_{av} = (L/D)_{max} \frac{K_o + K_{final}}{2} \tag{4.6}$$

where

$$K_o = \frac{(L/D)_o}{(L/D)_{max}}$$

$$K_{final} = \frac{(L/D)_{final}}{(L/D)_{max}}$$

The value of K_o is assumed, and K_{final} is easily found with the use of the generalized relationship in which the ratio $(L/D)/(L/D)_{max}$ is expressed as a function of $C_L/C_{L,m}$ where $C_{L,m}$ is the lift coefficient for $(L/D)_{max}$ and C_L is the lift coefficient corresponding to L/D. This generalized relationship is given graphically in figure 3.12 where the lift coefficient ratio $C_L/C_{L,m}$ is defined by $\bar{C}_L$. If the ratio of maximum landing weight to take-off gross weight is defined by W_L/W_g, the lift coefficient ratio at the end of the flight $\bar{C}_{L,final}$ is given by

$$\bar{C}_{L,final} = \bar{C}_{L,o}(W_L/W_g)$$

where $\bar{C}_{L,o}$ is the initial value of lift coefficient at the beginning of the flight. The value of K_{final} in equation (4.6) may then be found directly from figure 3.12 with the value of $\bar{C}_{L,final}$ obtained from $\bar{C}_{L,final} = \bar{C}_{L,o}(W_L/W_g)$. Two values of initial cruise lift-drag ratio are specified in the present analysis: $(L/D)_{max}$ and $0.97(L/D)_{max}$; the value of the weight ratio W_L/W_g is assumed to be 0.8 in all cases. The average values of the cruise lift-drag ratio for the two cases are calculated as follows:

For the case of $K_o = 1.0$ (i.e., the initial cruise lift-drag ratio is $(L/D)_{max}$),

$$\bar{C}_{L,o} = 1.0$$

$$\bar{C}_{L,final} = 0.8$$

$$K_{final} = 0.975$$

and, with the use of equation (4.6),

$$(L/D)_{av} = (L/D)_{max} \frac{1 + 0.975}{2} = 0.99(L/D)_{max} \tag{4.7}$$

For the case of $K_o = 0.97$ (i.e., the initial cruise lift-drag ratio is $0.97(L/D)_{max}$),

$$\bar{C}_{L,o} = 0.78$$

$$\bar{C}_{L,final} = 0.8(0.78) = 0.62$$

$$K_{final} = 0.89$$

and

$$(L/D)_{av} = (L/D)_{max} \frac{0.97 + 0.89}{2} = 0.93(L/D)_{max} \tag{4.8}$$

Relations (4.7) and (4.8) give the average cruise lift-drag ratio for the cases in which the initial cruise lift-drag ratio is $(L/D)_{max}$ and $0.97(L/D)_{max}$, respectively.

The detailed calculations of the fuel fraction corresponding to the six match points are given in table 4.IV. The calculations are perhaps best understood by identifying each of the columns in table 4.IV as follows:

① $(L/D)_o$, lift-drag ratio at the beginning of cruising flight; given in section 4.2

② $(L/D)_{av}$, average value of the lift-drag ratio; obtained from the values of $(L/D)_{max}$ given on page 178 and the constants contained in relations (4.7) and (4.8)

③ Engine type specified in section 4.2

④ Match point number corresponding to the match point numbers given in figure 4.1

⑤ W_g/S, wing loading corresponding to the match points of ④; values are read from figure 4.1

⑥ T_0/W_g, thrust loading corresponding to the match points of ④; values are read from figure 4.1

⑦ h, altitude, corresponding to the wing loadings given in ⑤; values are interpolated from ⑥ and ⑦ of table 4.III

⑧ a, speed of sound, in knots, for the altitude given in ⑦; values are determined from figure 3.22 of chapter 3

⑨ M, design cruise Mach number, given in section 4.2

⑩ V, cruise speed, in knots; obtained by multiplication of ⑨ by ⑧

⑪ c, specific fuel consumption for Mach number and altitude given in ⑨ and ⑦, respectively; values are obtained from figure 3.13(b) for engine A and figure 3.16(b) for engine D

⑫ B, Breguet factor; obtained by the expression $\frac{② \times ⑩}{⑪}$

⑬ R, design range, in n. mi

⑭ W_f/W_g, fuel fraction; obtained with the use of equation (4.4) and the values from ⑫ and ⑬

An examination of the fuel fraction data given in column ⑭ of table 4.IV indicates that the fuel fraction is dependent upon the aircraft variants 1, 2, and 3 and upon the initial value of the cruising lift-drag ratio, but is insensitive to the take-off field length. The take-off field length influences the Breguet factor for a given aircraft variant and $(L/D)_o$ only to the extent that the cruising altitude may be somewhat different for the different field lengths because of variations in wing loading for the different match points. The different altitudes influence the speed of sound below the tropopause and the

specific fuel consumption. The effects shown by the data of table 4.IV are, however, relatively insignificant for aircraft of the same variant and initial value of cruise lift-drag ratio.

4.7.2 Aircraft Weights and Sizes

The aircraft gross weight may be determined with the use of equation (3.41) of chapter 3 and the known values of fuel fraction, thrust loading, and design payload. Equation (3.41) is repeated here for convenience as

$$W_g = \frac{W_p}{\bar{U} - (W_f/W_g)} \tag{4.9}$$

where

W_g gross weight, lb

W_p payload weight, lb

W_f/W_g fuel fraction corresponding to particular match points

and where $\bar{U}$ is the useful load fraction obtained from figure 3.21 of chapter 3 together with the value of the thrust loading at a particular match point. Sufficient information is now available to calculate the desired gross physical characteristics of the aircraft.

The detailed calculations of the gross physical characteristics of the aircraft corresponding to each of the six match points are given in table 4.V. The calculations are perhaps best understood by identifying each of the columns in table 4.V as follows:

① $(L/D)_o$, lift-drag ratio at the beginning of cruising flight; given in section 4.2

② Match point number corresponding to the match point numbers given in figure 4.1

③ W_g/S, wing loading, corresponding to the match points of ②; values are read from figure 4.1

④ T_0/W_g, thrust loading, corresponding to the match points of ②; values are read from figure 4.1

⑤ W_f/W_g, fuel fraction; taken from ⑭ of table 4.IV for the appropriate match point

⑥ W_p, design payload of 3165 lb

⑦ $\bar{U}$, useful load fraction; taken from figure 3.21 of chapter 3 for the thrust loading in ④

⑧ W_g, gross weight; obtained by the expression $\frac{⑥}{⑦ - ⑤}$ (see eq. (4.9))

⑨ W_e, empty weight; obtained by the expression ⑧ (1 - ⑤) - ⑥; that is, $W_e = W_g\left(1 - \frac{W_f}{W_g}\right) - W_p$

⑩ W_f, fuel weight; obtained by multiplication of ⑧ by ⑤

⑪ S, wing area; obtained by dividing ⑧ by ③

⑫ T_0, maximum engine thrust; obtained by multiplication of ⑧ by ④

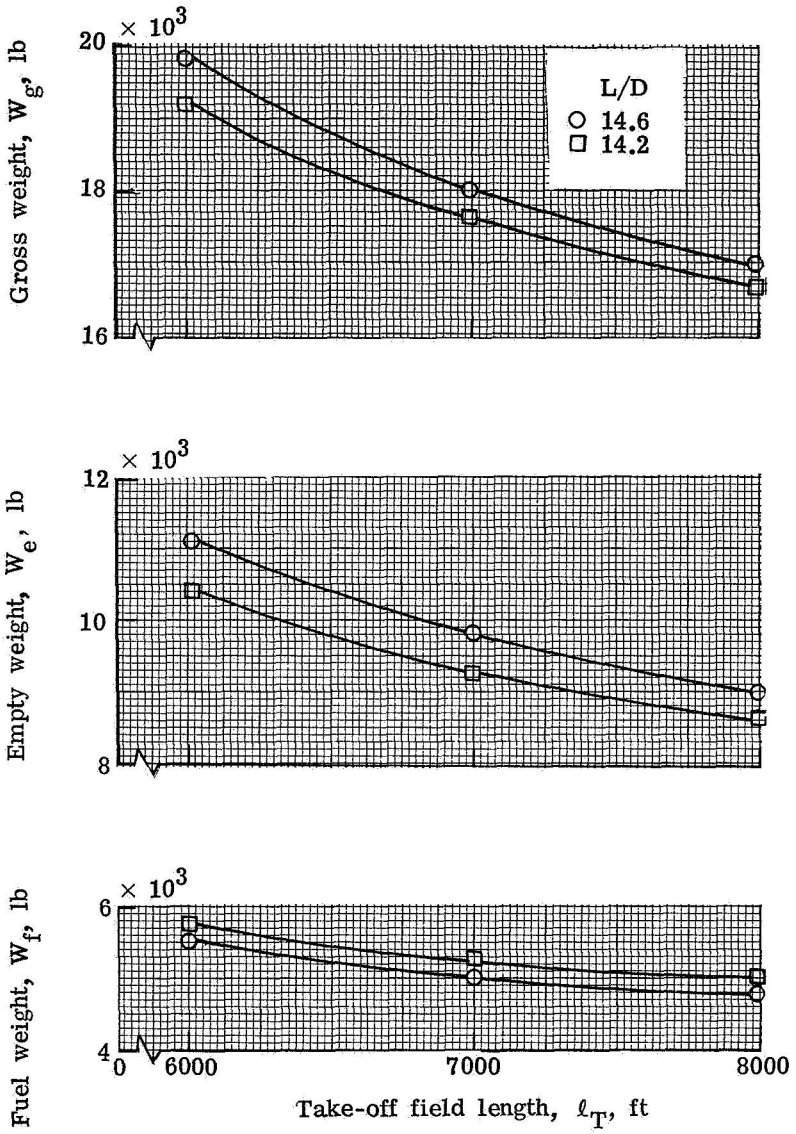
⑬ A_f/S, ratio of fuselage cross-sectional area to wing area for design value of 0.120

⑭ d, fuselage diameter; obtained from $\sqrt{\frac{4}{\pi}(⑬ \times ⑪)}$.

4.8 Design Trends

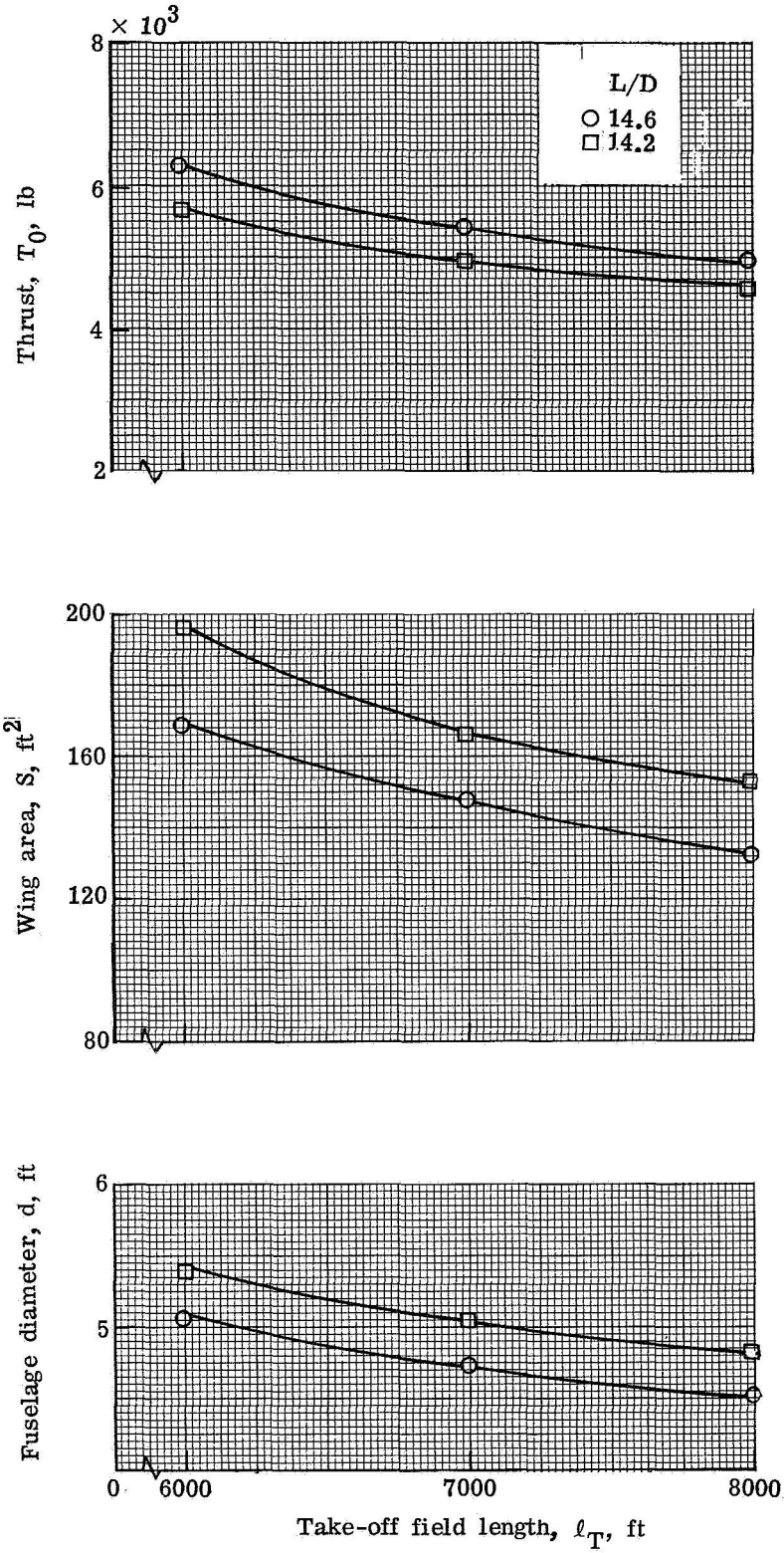
The significant physical characteristics found for the different aircraft by the calculations contained in table 4.V are plotted against the design take-off field length in figures 4.4, 4.5, and 4.6. Gross weight, empty weight, and fuel weight are given in figures 4.4(a), 4.5(a), and 4.6(a), and the total thrust, wing area, and fuselage diameter are given in figures 4.4(b), 4.5(b), and 4.6(b). The variation of the physical characteristics of the different aircraft with field length are given for each of the two initial values of cruising lift-drag ratio.

Two significant trends are evident in the data for each aircraft. Reductions in the physical parameters of the aircraft are seen to accompany an increase in design take-off field lengths. For example, the gross weight of aircraft variant 1 for an initial cruising lift-drag ratio L/D of 14.6 is seen in figure 4.4(a) to decrease from about 20 000 lb to 17 000 lb as the take-off field length is increased from 6000 to 8000 ft. This trend results from the lower required thrust-to-weight ratio and, hence, smaller engine size for the longer take-off field lengths. A reduced engine thrust-to-weight ratio gives an increased value of useful load fraction, as shown by the weight correlation data given in figure 3.21 of chapter 3; hence, for a given fuel fraction and payload, it yields a lower gross weight. (See eq. (4.9).)



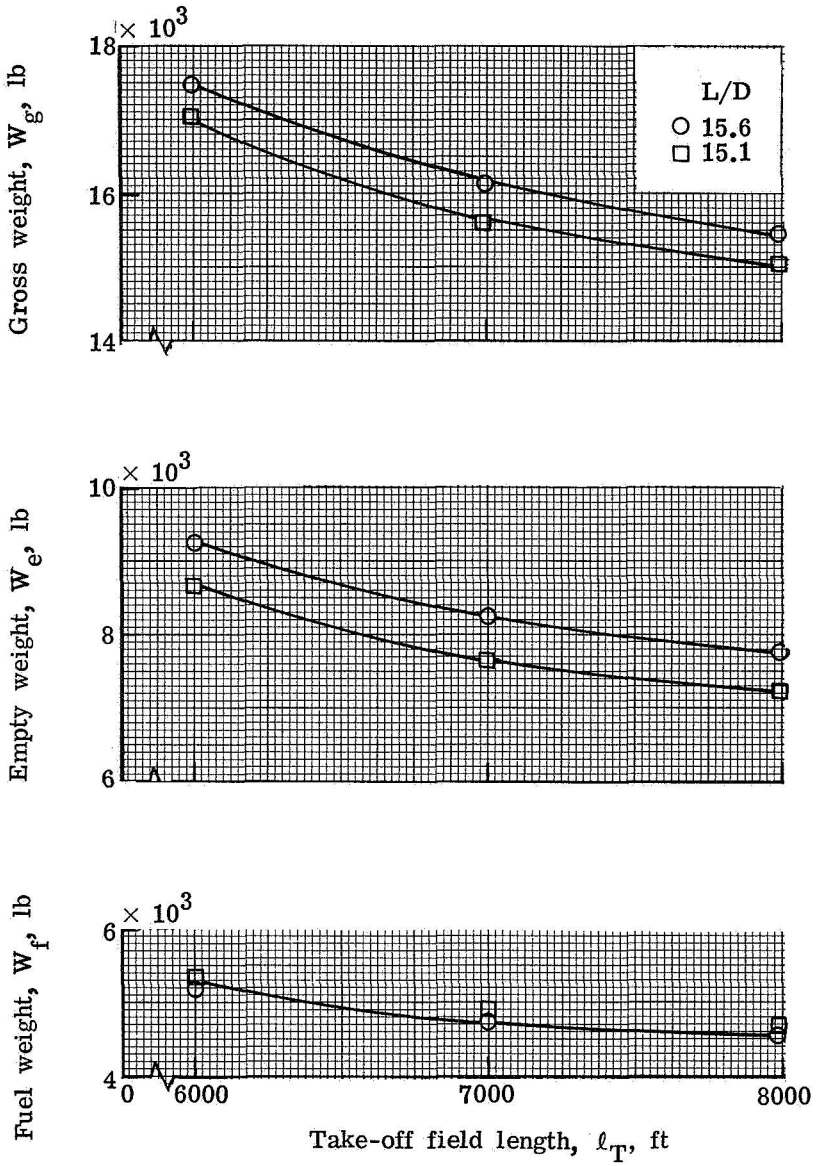
(a) Weight data.

Figure 4.4.- Physical characteristics of aircraft variant 1 as function of take-off field length.



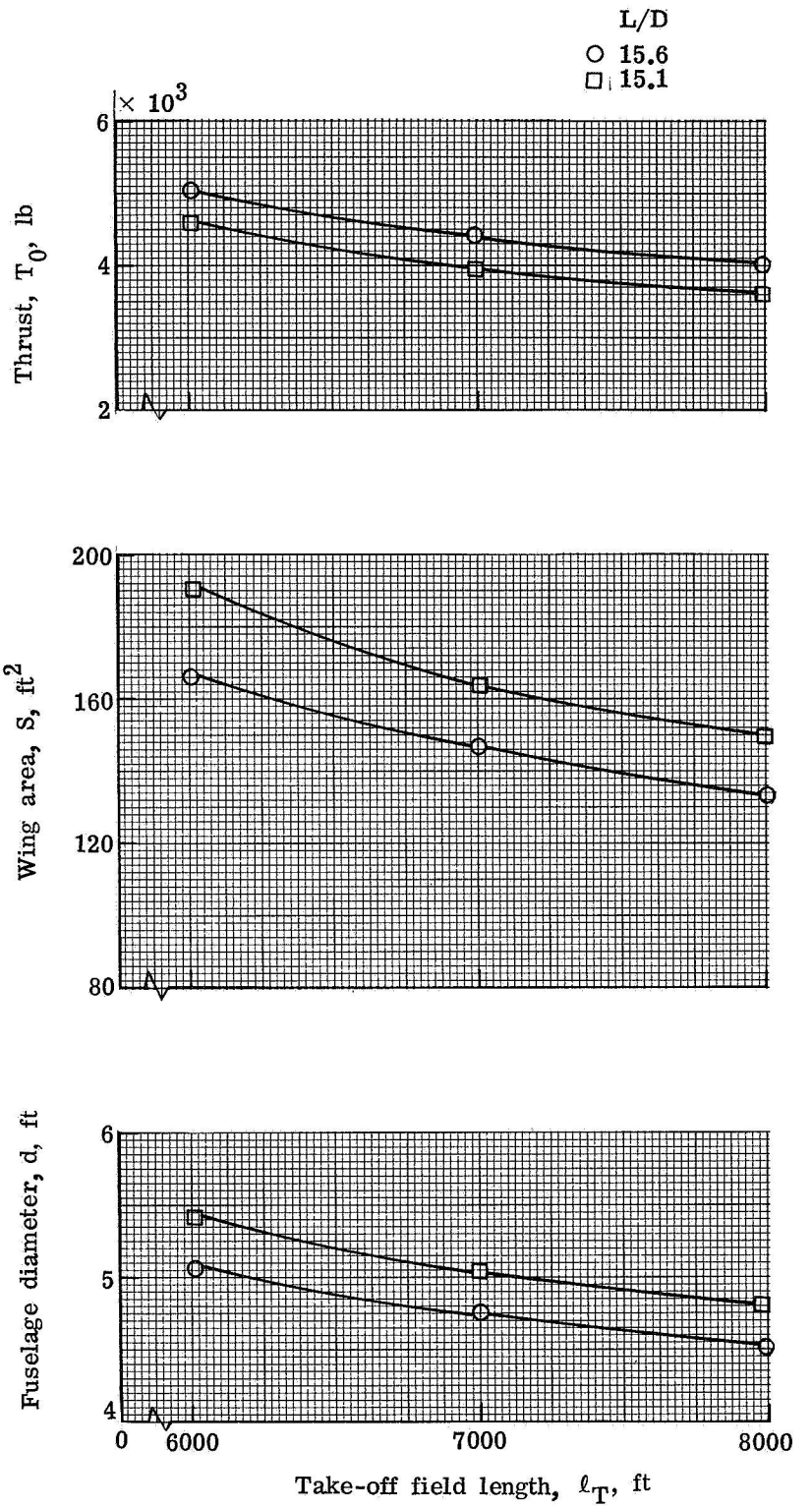
(b) Thrust, wing area, and fuselage diameter.

Figure 4.4.- Concluded.



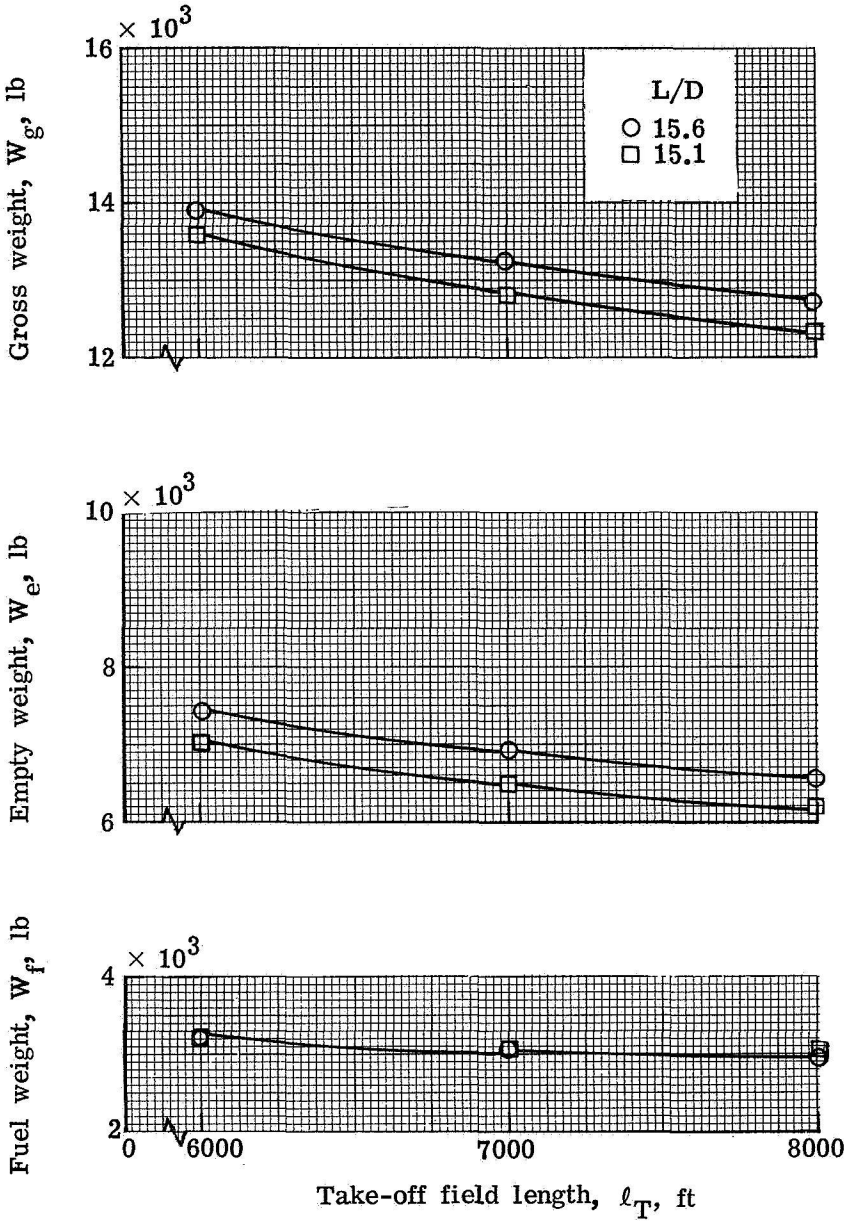
(a) Weight data.

Figure 4.5.- Physical characteristics of aircraft variant 2 as function of take-off field length.



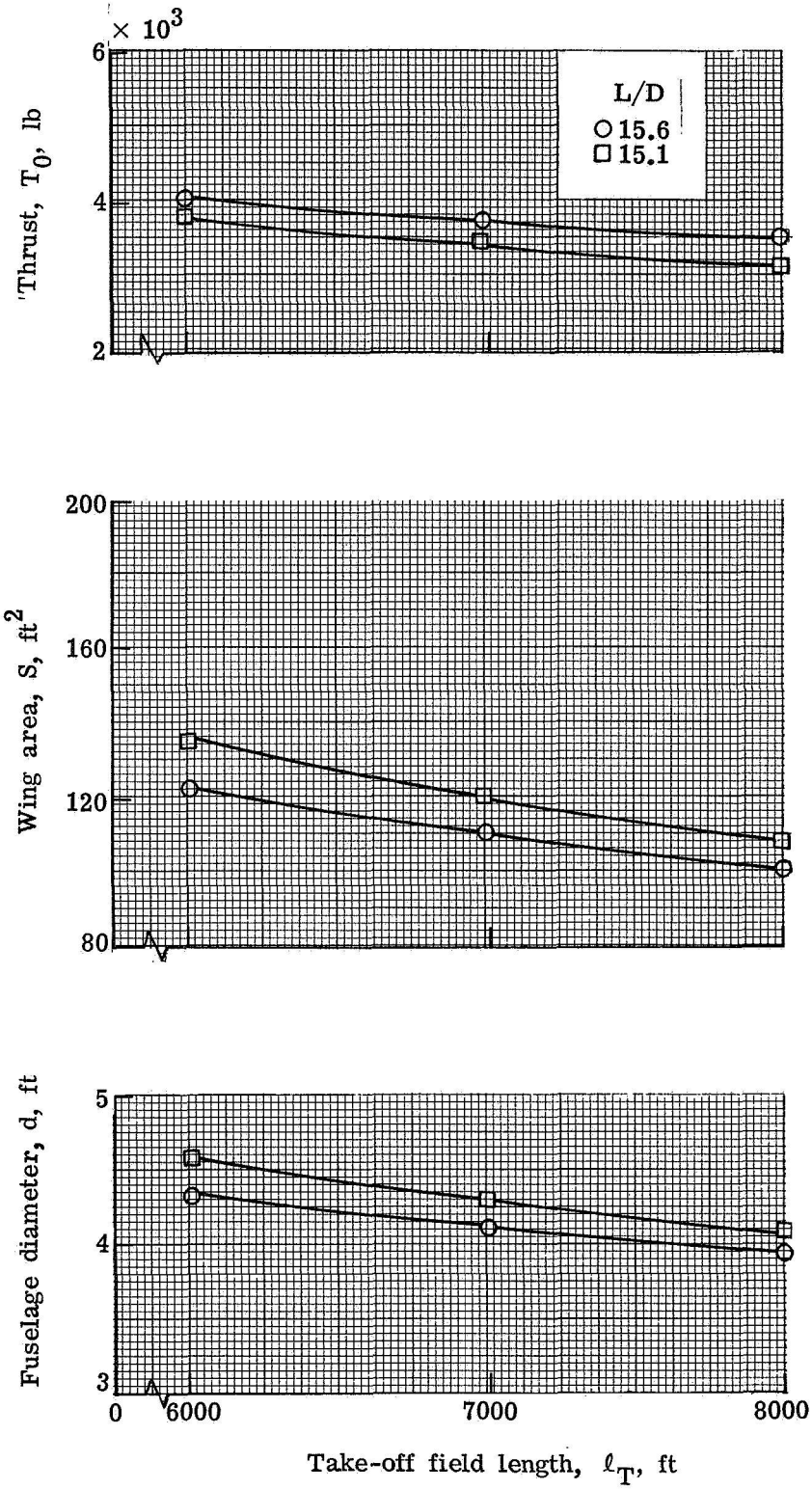
(b) Thrust, wing area, and fuselage diameter.

Figure 4.5.- Concluded.



(a) Weight data.

Figure 4.6.- Physical characteristics of aircraft variant 3 as function of take-off field length.



(b) Thrust, wing area, and fuselage diameter.

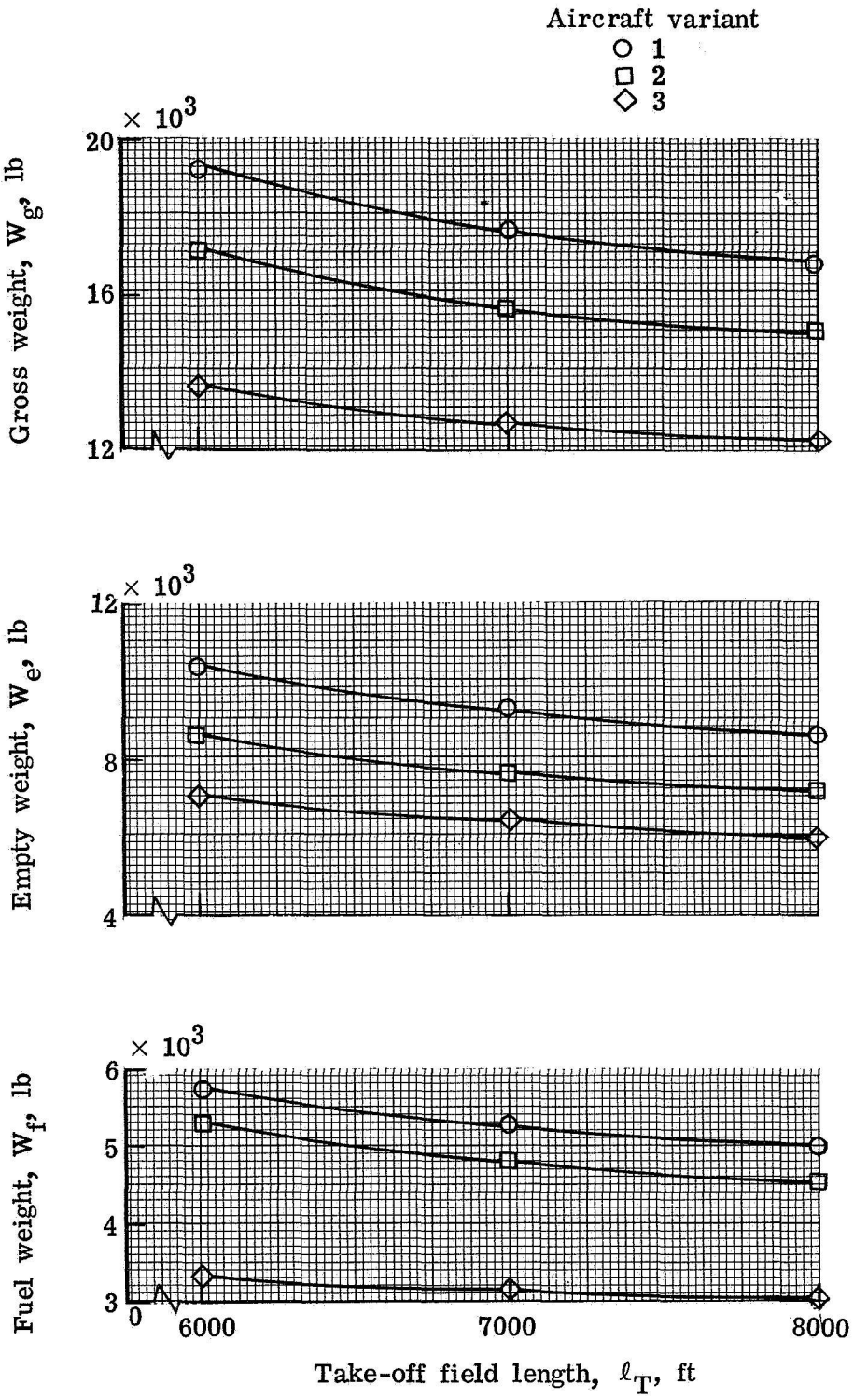
Figure 4.6.- Concluded.

The choice of the design initial value of cruising lift-drag ratio has an interesting effect on the aircraft characteristics. An examination of the data in figures 4.4(a), 4.5(a), and 4.6(a) shows that the gross weight and empty weight for each of the aircraft are somewhat lower for the smaller of the two values of initial cruising lift-drag ratio. This trend results from the lower lift coefficient associated with an initial value of L/D of $0.97(L/D)_{max}$ as compared to $(L/D)_{max}$. An examination of figure 3.12 of chapter 3 shows that the lift coefficient corresponding to $0.97(L/D)_{max}$ is only 80 percent of that for $(L/D)_{max}$. The cruising altitude is therefore reduced for the lower value of L/D. Hence, the thrust ratio T_c/T_0 is increased; and according to equation (4.3), the required take-off thrust-to-weight ratio is reduced. This trend is clearly shown and was discussed in connection with figures 4.2(a), (b), and (c). The lower values of required take-off thrust-to-weight ratio yield higher values of useful load fraction and consequent reductions in gross weight. The choice of $0.97(L/D)_{max}$ or $(L/D)_{max}$ for the initial value of the cruising lift-drag ratio L/D is shown in figures 4.4(a), 4.5(a), and 4.6(a) to have little effect on the fuel weight. The fuel fraction is somewhat higher for the lower value of initial cruising lift-drag ratio (shown by the data in table 4.IV) but the lower gross weight for $0.97(L/D)_{max}$ results in an actual fuel weight which is about the same for the two values of initial cruising lift-drag ratio.

The actual differences in the weights for the two cases are relatively small and probably not particularly important. The significance of these differences would seem to be that the aircraft weights, at least for the cases considered, are relatively insensitive to a reduction in initial cruising value of lift-drag ratio from $(L/D)_{max}$ to $0.97(L/D)_{max}$. The extent to which $(L/D)_o$ may be reduced without causing increases in aircraft weight is beyond the scope of the present study but may be determined by additional analyses of the type contained herein. The aircraft weights might be expected to increase significantly if the chosen value of the cruising lift-drag ratio lies on the linear portion of the generalized lift-drag ratio curve of figure 3.12. Along this portion of the curve, large reductions in lift-drag ratio accompany relatively small reductions in the lift coefficient.

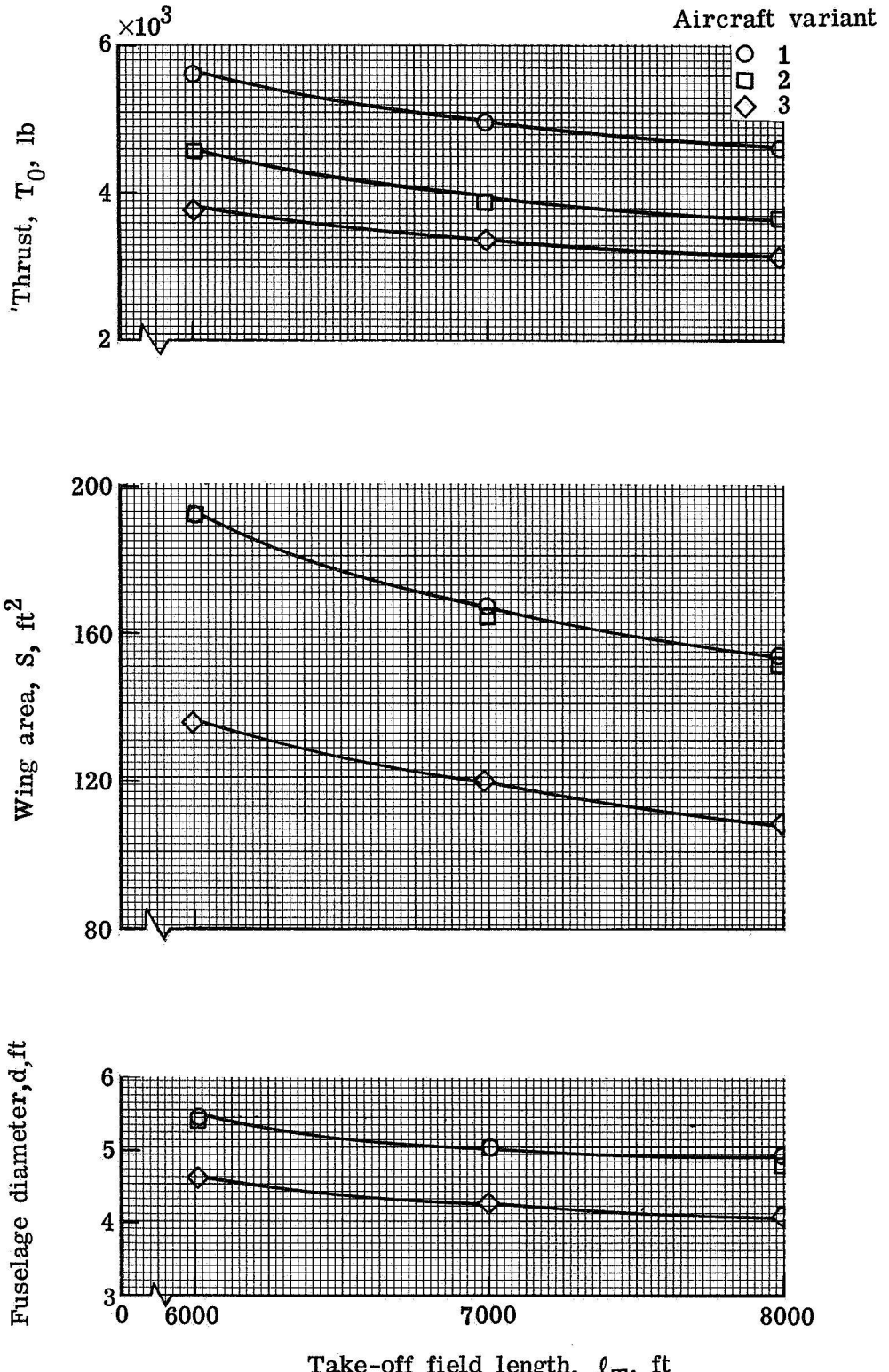
A comparison of the physical characteristics of aircraft variants 1, 2, and 3 for an initial value of the lift-drag ratio of 97 percent of the maximum value is shown in figures 4.7(a) and (b). The effect of the higher aspect ratio wing and slightly lower specific fuel consumption of aircraft variant 2, as compared to aircraft variant 1, causes some reductions in the aircraft weights. The use of the high-bypass-ratio turbofan engine, however, causes a dramatic reduction in the gross weight and fuel weight of aircraft variant 3, as compared to aircraft variant 2. The low specific fuel consumption of the high-bypass-ratio engine employed in aircraft variant 3 is responsible for this trend. A comparison of the data in column (11) of table 4.IV indicates that the specific fuel consumption of engine A is about 78 percent of that for engine D at a Mach number of 0.7.

The wing areas of aircraft variants 1 and 2, given in figure 4.7(b), are seen to be about the same for each of the take-off field lengths. The wing area of aircraft variant 3, however, is about 30 percent lower than that of the other two aircraft for the three different field lengths. The lower gross



(a) Weight data.

Figure 4.7 - Comparison of the characteristics of aircraft variants 1, 2, and 3 for a lift-drag ratio of 97 percent of the maximum value.



(b) Thrust, wing area, and fuselage diameter.

Figure 4.7.- Concluded.

weights (fig. 4.7(a)) and higher wing loadings (fig. 4.2) of aircraft variant 3, as compared to the other aircraft variants, are responsible for this result.

All of the physical characteristics which have been discussed and compared in figures 4.4 to 4.7 are for aircraft which are geometrically similar. Thus, all dimensions of the aircraft vary in the same proportion as the size of the aircraft varies. The effect of this geometric scaling becomes apparent in a comparison of the fuselage diameters of the three aircraft variants shown in figure 4.7(b). The fuselage diameters of aircraft variants 1 and 2 are essentially the same at each field length, and some small reduction in fuselage diameter accompanies an increase in field length for these two aircraft. The fuselage diameter of aircraft variant 3 is significantly smaller than those of aircraft variants 1 and 2 for each field length. These results follow from the wing-area trends shown in figure 4.7(b) and the geometric similarity expressed by the constant ratio of fuselage area to wing area of 0.12 which was used in all cases. The fuselage diameters of all of the aircraft are probably too small for consideration in a long-range executive aircraft of the type analyzed. If all of the aircraft were resized for a constant, somewhat larger fuselage diameter, the comparative physical characteristics of aircraft variants 1 and 2 would probably not change to any large extent. The characteristics of aircraft variant 3 relative to those of aircraft variants 1 and 2, however, might be expected to show a significant change because of the large difference in fuselage diameter of aircraft variant 3 as compared to aircraft variants 1 and 2. (See fig. 4.7(b).) Considered in the next section is the effect of resizing aircraft variants 2 and 3 for increased fuselage diameter and for a single take-off field length and initial value of cruising lift-drag ratio.

4.9 Resized Aircraft

The versions of aircraft variants 2 and 3 chosen for resizing were those having a design take-off field length of 7000 ft and an initial value of cruising lift-drag ratio of $0.97(L/D)_{max}$. As previously described, these aircraft variants are identified by the designations 2-5 and 3-5; the resized aircraft variants are referred to by the designations 2-5a and 3-5a. Aircraft variants 2-5a and 3-5a are both to be sized with a fuselage diameter of 5.5 ft. The fuselage diameter of aircraft variant 2-5 and aircraft variant 3-5 were 5.01 ft and 4.29 ft, respectively, as shown by the data in column (14) of table 4.V. The fuselage diameter of aircraft variant 2-5a is only increased by about 6 in. (or 10 percent), whereas the fuselage diameter of aircraft variant 3-5a is increased by nearly 15 in. (or about 29 percent). The effect on the maximum lift-drag ratio of the increased fuselage size would therefore be expected to be relatively small for aircraft variant 2-5a, as compared to that for aircraft variant 3-5a.

The values of the ratios of fuselage cross-sectional area to wing area needed for estimating the maximum lift-drag ratio of aircraft variants 2-5a and 3-5a are developed by the data contained in the following table:

	Aircraft variant	A_f/S
①	2-5	0.120
②	2-5.1	.145
③	2-5a	.139
④	3-5	.120
⑤	3-5.1	.199
⑥	3-5a	.171

The data in the table are explained as follows:

① and ④ ratios of fuselage cross-sectional area to wing area assumed in the sizing of aircraft variants 2-5 and 3-5

② and ⑤ ratios of fuselage cross-sectional area to wing area of fictitious aircraft which have the desired fuselage diameter of 5.5 ft and wing areas given by the data in column (11) of table 4.V

③ and ⑥ ratios of fuselage cross-sectional area to wing area for aircraft variants 2-5a and 3-5a, respectively; these values of A_f/S were obtained by a trial and error process involving two approximations: (1) aircraft variants were sized for values of A_f/S midway between the high and low values for each aircraft variant given in the table and (2) aircraft were sized for values of A_f/S which were adjusted from the midpoint values to give fuselage diameters which were a closer approximation to the desired 5.5 ft; these are the values given in the table for aircraft variants 2-5a and 3-5a

The nomograph given in figure 3.11 of chapter 3 was used for estimating the value of $(L/D)_{max}$ for aircraft variants 1, 2, and 3 in the original sizing process. The values of A_f/S assumed for aircraft variants 2-5a and 3-5a, however, extend beyond those given in figure 3.11. The methods of section 3.5.1.2 of chapter 3, which were used in the construction of figure 3.11, are therefore employed for estimating the maximum lift-drag ratios of aircraft variants 2-5a and 3-5a. This method involves the calculation of the ratio of total aircraft wetted area to wing area A_t/S and comparison of this value to that of a known reference aircraft for which the zero-lift drag coefficient $C_{D,0}$ is known. The ratio A_t/S is given by equation (3.25) of chapter 3 and is repeated here in slightly different form as follows:

$$\frac{A_t}{S} = 4\,\frac{A_f}{S}\left(\frac{l}{d} - 1\right) + 2\left(1 + \frac{S_t}{S}\right) + \frac{A_n}{S} \tag{4.10}$$

where

l/d fuselage fineness ratio

S_t/S ratio of tail area to wing area

A_n/S ratio of nacelle total wetted area to wing area

Average values of S_t/S and A_n/S were given in chapter 3 as 0.47 and 0.44, respectively. With the use of these values and a fuselage fineness ratio of 8.5, equation (4.10) takes the form

$$\frac{A_t}{S} = 30\,\frac{A_f}{S} + 3.38 \tag{4.11}$$

Values of A_t/S and $C_{D,0}$ of 5.0 and 0.0131 were given in chapter 3 for the reference aircraft.

Calculations of the aerodynamic data for aircraft variants 2-5a and 3-5a are contained in table 4.VI. These calculations are explained as follows:

① Aircraft designation

② A_f/S, assumed value of ratio of fuselage cross-sectional area to wing area

③ A_t/S, ratio of total aircraft wetted area to wing area; calculated from equation (4.11) using the data of ②

④ $C_{D,0}$, zero-lift drag coefficient; obtained from the expression $\frac{③}{5.0} \times 0.0131$

⑤ $C_{D,0}$, zero-lift drag coefficient corrected for the difference in size of the reference aircraft compared to the aircraft being analyzed (see section 4.2)

⑥ $(L/D)_{max}$, maximum value of the lift-drag ratio; obtained with the use of ⑤ and equation (4.2)

⑦ $0.97(L/D)_{max}$, design initial cruising value of lift-drag ratio

⑧ $(L/D)_{av}$, average value of lift-drag ratio; obtained from the values in ⑥ and equation (4.8)

⑨ $C_{L,m}$, lift coefficient at $(L/D)_{max}$; obtained from equation (4.1) with the use of the values in ⑤

⑩ $C_{L,0.97}$, lift coefficient for $0.97(L/D)_{max}$; obtained from the values in ⑨ and figure 3.12 of chapter 3.

The maximum values of the lift-drag ratio of aircraft variants 2-5a and 3-5a (column ⑥ of table 4.VI) are 15.03 and 14.14, respectively, as compared to a value of 15.6 (section 4.2) for aircraft variants 2-5 and 3-5. These reductions in the value of the maximum lift-drag ratio correspond to a decrease of about 4 percent for aircraft variant 2-5a and about 9 percent for aircraft variant 3-5a. In addition, the value of $C_{L,m}$ is increased from 0.69 (section 4.2) for aircraft variant 3-5 to 0.76 (table 4.VI) for aircraft variant 3-5a. This increase in lift coefficient indicates that for a given wing loading and Mach number, aircraft variant 3-5a must cruise at a higher altitude than aircraft variant 3-5. Both the higher altitude and lower value of lift-drag ratio imply a higher maximum thrust-to-weight ratio at a given wing loading for aircraft variant 3-5a, as compared to aircraft variant 3-5. (See eq. (4.3).) The lift coefficient $C_{L,m}$ of aircraft variant 2-5a is 0.71 which is not greatly different from the value of 0.69 (section 4.2) for aircraft variant 2-5.

The aerodynamic data in table 4.VI were used in a cruise matching analysis for aircraft variants 2-5a and 3-5a; the calculations are contained in table 4.VII. These data and the take-off data in table 4.III for a 7000 ft field length were used to construct the aircraft matching chart presented in figure 4.8 for aircraft variants 2-5a and 3-5a. The higher required thrust loading at a given wing loading is evident for aircraft variant 3-5a, as compared to aircraft variant 2-5a. Calculations of the fuel fraction and physical characteristics of the two resized aircraft are contained in tables 4.VIII and 4.IX. The calculation procedure and format of presentation in these tables and in table 4.VII are the same as those employed and fully described in sections 4.5 and 4.7. Accordingly, no further discussion of the methods employed in obtaining the data in these tables is offered.

A number of important characteristics of aircraft variants 2-5, 3-5, 2-5a, and 3-5a have been taken from tables 4.V and 4.IX and are listed in table 4.X. An examination of the comparative data in table 4.X indicates that the gross weights of aircraft variant 2-5 and aircraft variant 3-5 were increased by about 1900 and 2300 lb, respectively, as a result of increasing the fuselage diameter. This weight increase results primarily from a reduction in the cruising lift-drag ratio of both aircraft, but the weight is also influenced by the increase in required thrust loading which accompanied an increase in fuselage diameter in both cases. Aircraft variant 3-5a shows a gross weight of 2270 lb less than that of aircraft variant 2-5a. As would be expected, a slightly larger increment in gross weight exists between aircraft variant 3-5 and aircraft variant 2-5. The empty weight and fuel weight of aircraft variant 3-5a are also less than those weights for aircraft variant 2-5a, as was the case for aircraft variants 3-5 and 2-5. An examination of the values of fuselage diam-

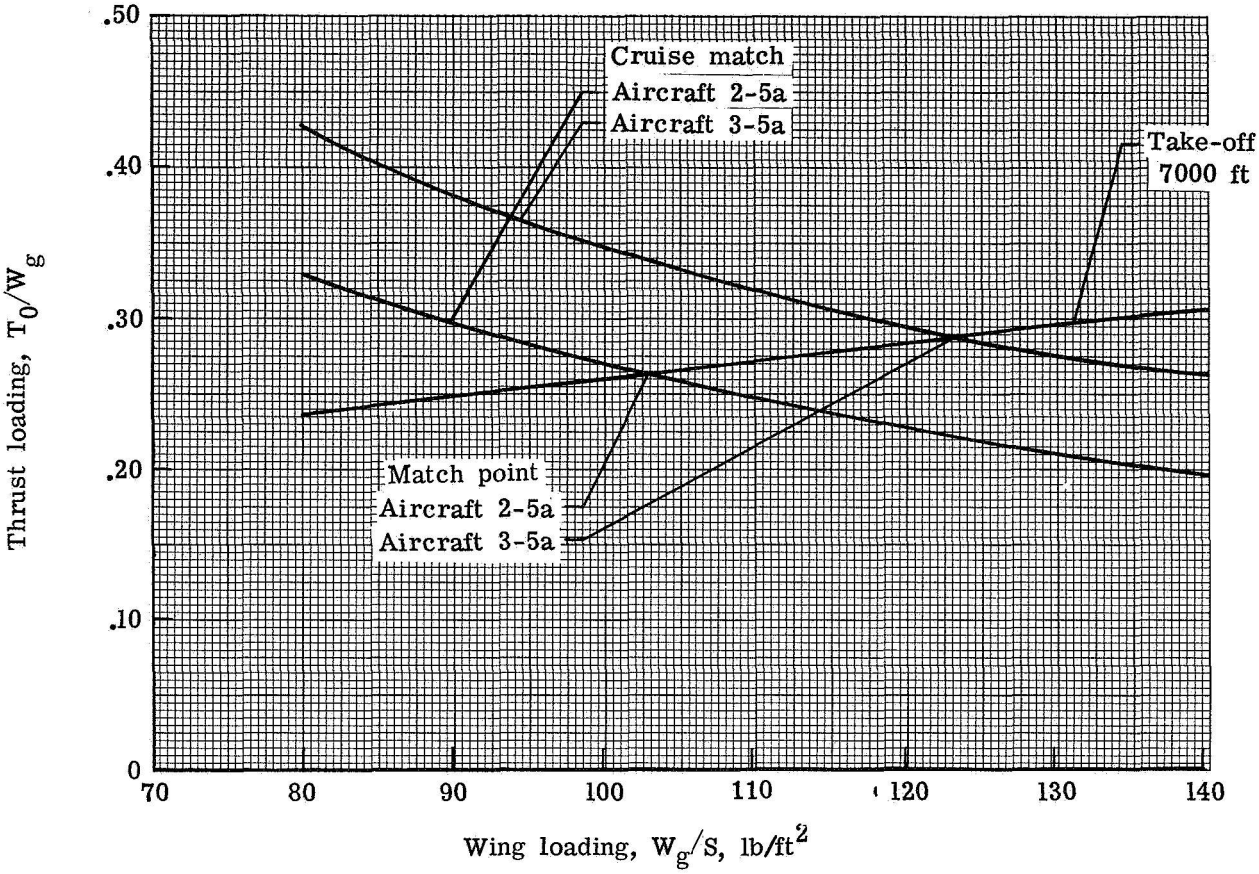


Figure 4.8.- Aircraft matching chart for resized aircraft variants 2-5a and 3-5a.

eter shows that aircraft variant 2-5a has the desired fuselage diameter of 5.5 ft, and aircraft variant 3-5a has a fuselage diameter of only 0.3 of a foot less than the desired value. Another resizing of aircraft variant 3-5a would be necessary if a fuselage diameter of exactly 5.5 ft were required. Since the fuselage diameter of aircraft variant 3-5a is slightly undersized, a resizing would be expected to reduce by a small amount the weight advantage of aircraft variant 3-5a, as compared to aircraft variant 2-5a.

The wing loading and power loading data shown in table 4.X show little difference in value for aircraft variants 2-5 and 2-5a; however, both loadings are increased noticeably for aircraft variant 3-5a, as compared to aircraft variant 3.5. The maximum lift coefficient in the take-off configuration $C_{L,T}$ is increased somewhat for aircraft variant 3 as a result of the increased fuselage diameter; the value of 2.40 for aircraft variant 3-5a, however, is probably within the state of the art.

The data in table 4.X suggest that the trends shown by the characteristics of the geometrically similar aircraft are not influenced to any large degree by changes in fuselage diameter of the magnitude considered. The actual values of the aircraft physical characteristics, however, are altered significantly

by the change in fuselage diameter. Thus, if an actual aircraft dimension is important, the sizing process should be carried out in such a way that the final iteration yields an aircraft which has the critical dimension reasonably close to the desired value.

SYMBOLS

A	aspect ratio, b^2/S
a	speed of sound, knots
A_f	maximum fuselage cross-sectional area, ft^2
A_n	nacelle wetted area, ft^2
A_t	total aircraft wetted area, ft^2
B	Breguet factor, $\frac{V(L/D)}{c}$, where V is in knots
b	wing span, ft
$C_{D,0}$	drag coefficient at zero lift
C_L	lift coefficient
$\bar{C}_L$	lift coefficient ratio, $C_L/C_{L,m}$
$C_{L,A}$	approach lift coefficient, $C_{L,max}/1.69$
$C_{L,m}$	lift coefficient for $(L/D)_{max}$
$C_{L,max}$	maximum lift coefficient for aircraft in landing configuration
$C_{L,T}$	maximum lift coefficient for aircraft in take-off configuration
$C_{L,2}$	second-segment climb gradient lift coefficient, $C_{L,T}/1.44$
$\bar{C}_{L,final}$	lift coefficient ratio at end of flight
$\bar{C}_{L,o}$	lift coefficient ratio at beginning of flight
$\bar{C}_{L,0.97}$	lift coefficient for a lift-drag ratio of 97 percent of maximum value
c	specific fuel consumption, pounds of fuel per pound of thrust per hour
d	fuselage diameter, ft
h	altitude, ft
K	constant
$\bar{L}$	scale parameter, $\frac{V_c c_r \times 10^{-4}}{1.63}$ where cruising speed V_c is in knots and root chord c_r is in feet

l fuselage length, ft

ℓ_L FAR landing field length, ft

ℓ_T FAR balanced take-off field length, ft

L/D lift-drag ratio

$(L/D)_{av}$ average lift-drag ratio for design range

$(L/D)_{final}$ lift-drag ratio at end of flight

$(L/D)_{max}$ maximum lift-drag ratio

$(L/D)_o$ lift-drag ratio at beginning of flight

M Mach number

R range, n. mi.

S wing area, ft^2

S_t sum of horizontal and vertical tail areas, ft^2

T engine thrust, lb

T_c maximum continuous thrust (used in cruise flight), lb

T_0 maximum sea-level static thrust, lb

$\bar{U}$ useful load fraction, $1 - \frac{W_e}{W_g}$

V speed, knots

V_A approach speed, knots

V_2 second-segment climb gradient speed, knots

W_e empty weight, lb

W_f fuel weight, lb

W_g maximum take-off gross weight, lb

W_L maximum landing weight, lb

W_p payload weight, lb

ε Oswald's airplane efficiency factor

ρ	atmospheric density, slugs/ft^3
ρ_0	atmospheric density at sea level
σ	density ratio, ρ/ρ_0

TABLE 4.I.- LANDING PERFORMANCE FOR THREE DIFFERENT AIRCRAFT VARIANTS

①	②	③	④	⑤	⑥	⑦	⑧
V_A	$C_{L,A}$	$\sqrt{W_L/S}$	W_L/S	T_0/W_L	W_L/W_g	W_g/S	T_0/W_g
Aircraft variant 1[a]							
129	1.2	8.24	67.85	0.277	0.8	84.81	0.222
↓	1.3	8.57	73.51	.287	↓	91.89	.230
	1.4	8.90	79.16	.300		98.95	.240
	1.5	9.21	84.82	.315		106.03	.252
	1.6	9.51	90.47	.328		113.09	.262
	1.7	9.81	96.13	.345		120.16	.276
	1.8	10.10	101.78	.363		127.23	.290
Aircraft variants 2 and 3[a]							
129	1.2	8.24	67.85	0.252	0.8	84.81	0.202
↓	1.3	8.57	73.51	.266	↓	91.89	.213
	1.4	8.90	79.16	.275		98.95	.220
	1.5	9.21	84.82	.287		106.03	.230
	1.6	9.51	90.47	.300		113.09	.240
	1.7	9.81	96.13	.313		120.16	.250
	1.8	10.10	101.78	.330		127.23	.264

[a]Designation described in section 4.2.

TABLE 4.II.- TAKE-OFF PERFORMANCE FOR THREE DIFFERENT AIRCRAFT VARIANTS

(a) Aircraft variant 1[a]

①	②	③	④	⑤	⑥
ℓ_T	$C_{L,2}$	$C_{L,T}$	T_0/W_g	$\frac{W_g/S}{\sigma C_{L,T}(T_0/W_g)}$	W_g/S
6000	1.2	1.73	0.255	159	70.14
↓	1.3	1.87	.267	↓	79.39
↓	1.4	2.02	.283	↓	90.89
↓	1.5	2.16	.295	↓	101.31
↓	1.6	2.30	.315	↓	115.20
↓	1.7	2.45	.330	↓	128.55
↓	1.8	2.59	.345	↓	142.07
7000	1.2	1.73	.255	185	81.61
↓	1.3	1.87	.267	↓	92.37
↓	1.4	2.02	.283	↓	105.76
↓	1.5	2.16	.295	↓	117.88
↓	1.6	2.30	.315	↓	134.03
↓	1.7	2.45	.330	↓	149.57
↓	1.8	2.59	.345	↓	165.31
8000	1.2	1.73	.255	212	93.52
↓	1.3	1.87	.267	↓	105.85
↓	1.4	2.02	.283	↓	121.19
↓	1.5	2.16	.295	↓	135.09
↓	1.6	2.30	.315	↓	153.59
↓	1.7	2.45	.330	↓	171.40
↓	1.8	2.59	.345	↓	189.43

[a]Designation described in section 4.2.

TABLE 4.II.- Concluded

(b) Aircraft variants 2 and 3[a]

①	②	③	④	⑤	⑥
ℓ_T	$C_{L,2}$	$C_{L,T}$	T_0/W_g	$\frac{W_g/S}{\sigma C_{L,T}(T_0/W_g)}$	W_g/S
6000	1.2	1.73	0.230	159	63.27
↓	1.3	1.87	.243	↓	72.25
↓	1.4	2.02	.256	↓	82.22
↓	1.5	2.16	.270	↓	92.73
↓	1.6	2.30	.285	↓	104.22
↓	1.7	2.45	.300	↓	116.87
↓	1.8	2.59	.315	↓	129.72
7000	1.2	1.73	.230	185	73.61
↓	1.3	1.87	.243	↓	84.07
↓	1.4	2.02	.256	↓	95.67
↓	1.5	2.16	.270	↓	107.89
↓	1.6	2.30	.285	↓	121.27
↓	1.7	2.45	.300	↓	135.98
↓	1.8	2.59	.315	↓	150.93
8000	1.2	1.73	.230	212	84.35
↓	1.3	1.87	.243	↓	96.33
↓	1.4	2.02	.256	↓	109.63
↓	1.5	2.16	.270	↓	123.64
↓	1.6	2.30	.285	↓	138.97
↓	1.7	2.45	.300	↓	155.82
↓	1.8	2.59	.315	↓	172.96

[a]Designation described in section 4.2.

TABLE 4.III.- CRUISE MATCHING FOR THREE DIFFERENT AIRCRAFT VARIANTS

①	②	③	④	⑤	⑥	⑦	⑧	⑨
Engine	M	L/D	C_L	C_LM^2	W_g/S	h	T_c/T_0	T_0/W_g
Aircraft variant 1[a]								
D	0.8	14.6	0.64	0.410	80			
					90			
					100	42 000	0.174	0.394
					110	40 500	.196	.349
					120	38 900	.221	.310
					130	37 500	.241	.284
					140	35 800	.262	.261
		14.2	.49	.314	80	41 200	.190	.371
					90	39 500	.213	.331
					100	37 500	.240	.293
					110	35 700	.263	.268
					120	33 500	.289	.244
					130	31 600	.310	.227
					140	29 700	.331	.213
Aircraft variant 2[a]								
D	0.7	15.6	0.69	0.338	80	42 400	0.175	0.366
					90	40 500	.195	.329
					100	38 600	.216	.297
					110	36 600	.237	.270
					120	34 700	.259	.248
					130	33 200	.276	.232
					140	31 100	.297	.216
		15.1	.53	.260	80	38 000	.223	.297
					90	35 800	.246	.269
					100	33 300	.274	.242
					110	31 000	.298	.222
					120	28 900	.322	.206
					130	27 100	.343	.193
					140	25 100	.370	.179
Aircraft variant 3[a]								
A	0.7	15.6	0.69	0.338	80	42 400	0.135	0.475
					90	40 500	.163	.393
					100	38 600	.186	.345
					110	36 600	.207	.310
					120	34 700	.224	.286
					130	33 000	.237	.270
					140	31 100	.251	.255
		15.1	.53	.260	80	38 000	.193	.343
					90	35 800	.215	.308
					100	33 300	.235	.282
					110	31 000	.251	.264
					120	28 900	.265	.250
					130	27 100	.274	.242
					140	25 100	.285	.232

[a]Designation described in section 4.2.

TABLE 4.IV.- FUEL FRACTION FOR THREE DIFFERENT AIRCRAFT VARIANTS

①	②	③	④	⑤	⑥	⑦	⑧	⑨	⑩	⑪	⑫	⑬	⑭
$(L/D)_o$	$(L/D)_{av}$	Engine	Match point	W_g/S	T_0/W_g	h	a	M	V	c	B	R	W_f/W_g
Aircraft variant 1[a]													
14.6	14.45	D	1	118.0	0.315	39 200	576	0.8	460.8	0.823	8 090.6	2674	0.281
↓	↓	↓	2	122.5	.300	38 500	↓	↓	↓	↓	↓	↓	↓
↓	↓	↓	3	127.5	.290	37 900	↓	↓	↓	↓	↓	↓	↓
14.2	13.58	↓	4	101.5	.295	37 300	↓	↓	↓	↓	7 603.5	↓	.296
↓	↓	↓	5	106.0	.283	36 400	↓	↓	↓	↓	↓	↓	↓
↓	↓	↓	6	110.0	.273	35 700	↓	↓	↓	↓	↓	↓	↓
Aircraft variant 2[a]													
15.6	15.44	D	1	105.0	0.285	37 600	576	0.7	403.2	0.804	7 743.1	2674	0.292
↓	↓	↓	2	110.0	.270	36 600	↓	↓	↓	↓	↓	↓	↓
↓	↓	↓	3	115.5	.260	36 000	↓	↓	↓	↓	↓	↓	↓
15.1	14.51	↓	4	90.0	.265	35 600	↓	↓	↓	↓	7 276.7	↓	.308
↓	↓	↓	5	95.1	.251	34 600	578	↓	404.6	↓	7 302.0	↓	.307
↓	↓	↓	6	99.7	.245	33 300	581	↓	406.7	↓	7 339.9	↓	.305
Aircraft variant 3[a]													
15.6	15.44	A	1	114.0	0.294	36 200	576	0.7	403.9	0.625	9 978.0	2674	0.235
↓	↓	↓	2	121.0	.285	35 000	577	↓	404.0	↓	9 980.1	↓	.235
↓	↓	↓	3	127.5	.275	34 100	580	↓	406.7	↓	10 047.1	↓	.234
15.1	14.51	↓	4	101.0	.280	33 000	583	↓	408.1	↓	9 474.5	↓	.246
↓	↓	↓	5	107.0	.267	31 800	585	↓	409.5	↓	9 507.0	↓	.245
↓	↓	↓	6	113.5	.257	30 800	588	↓	411.6	.630	9 479.9	↓	.246

[a]Designation described in section 4.2.

TABLE 4.V.- AIRCRAFT CHARACTERISTICS FOR THREE DIFFERENT AIRCRAFT VARIANTS

①	②	③	④	⑤	⑥	⑦	⑧	⑨	⑩	⑪	⑫	⑬	⑭
$(L/D)_o$	Match point	W_g/S	T_0/W_g	W_f/W_g	W_p	$\bar{U}$	W_g	W_e	W_f	S	T_0	A_f/S	d
Aircraft variant 1[a]													
14.6	1	118.0	0.315	0.281	3165	0.440	19 906	11 147	5594	168.7	6270	0.120	5.08
↓	2	122.5	.300	↓	↓	.456	18 086	9 839	5082	147.6	5426	↓	4.75
↓	3	127.5	.290	↓	↓	.467	17 016	9 070	4782	133.5	4935	↓	4.52
14.2	4	101.5	.295	.296	↓	.460	19 299	10 421	5712	190.1	5693	↓	5.39
↓	5	106.0	.283	↓	↓	.475	17 682	9 283	5234	166.8	5004	↓	5.05
↓	6	110.0	.273	↓	↓	.484	16 835	8 687	4983	153.1	4596	↓	4.84
Aircraft variant 2[a]													
15.6	1	105.0	0.285	0.292	3165	0.473	17 486	9 215	5106	166.5	4984	0.120	5.04
↓	2	110.0	.270	↓	↓	.488	16 148	8 268	4715	146.8	4360	↓	4.74
↓	3	115.5	.260	↓	↓	.497	15 439	7 766	4508	133.7	4014	↓	4.52
15.1	4	90.0	.265	.308	↓	.493	17 108	8 674	5269	190.1	4534	↓	5.39
↓	5	95.1	.251	.307	↓	.510	15 591	7 640	4787	164.0	3913	↓	5.01
↓	6	99.7	.245	.305	↓	.516	15 000	7 260	4575	150.5	3675	↓	4.79
Aircraft variant 3[a]													
15.6	1	114.0	0.294	0.235	3165	0.463	13 882	7 454	3262	121.8	4081	0.120	4.31
↓	2	121.0	.285	.235	↓	.473	13 298	7 008	3125	109.9	3790	↓	4.10
↓	3	127.5	.275	.234	↓	.482	12 762	6 611	2986	100.1	3510	↓	3.91
15.1	4	101.0	.280	.246	↓	.479	13 584	7 077	3342	134.5	3803	↓	4.53
↓	5	107.0	.267	.245	↓	.491	12 866	6 549	3152	120.6	3435	↓	4.29
↓	6	113.5	.257	.246	↓	.502	12 363	6 157	3041	108.9	3177	↓	4.08

[a]Designation described in section 4.2.

TABLE 4.VI.- AERODYNAMIC DATA FOR RESIZED AIRCRAFT VARIANTS

①	②	③	④	⑤	⑥	⑦	⑧	⑨	⑩
Aircraft variant (a)	A_f/S	A_t/S	$C_{D,0}$ for $\bar{L} = 1.0$	$C_{D,0}$ for $\bar{L} = 0.34$	$(L/D)_{max}$	$0.97(L/D)_{max}$	$(L/D)_{av}$	$C_{L,m}$	$C_{L,0.97}$
2-5a	0.139	7.55	0.0197	0.0237	15.03	14.58	13.98	0.71	0.56
3-5a	.171	8.51	.0223	.0267	14.14	13.71	13.15	.76	.59

[a]Designation described in section 4.9.

TABLE 4.VII.- CRUISE MATCHING FOR RESIZED AIRCRAFT VARIANTS

①	②	③	④	⑤	⑥	⑦	⑧	⑨
Engine	M	$(L/D)_{0.97}$	$C_{L,0.97}$	$C_L M^2$	W_g/S	h	T_c/T_0	T_0/W_g
Aircraft variant 2-5a[a]								
D	0.7	14.58	0.56	0.274	80	39 000	0.210	0.327
					90	37 200	.230	.298
					100	34 700	.256	.268
					110	32 900	.277	.248
					120	30 400	.307	.223
					130	28 600	.326	.210
					140	26 700	.350	.196
Aircraft variant 3-5a[a]								
A	0.7	13.71	0.59	0.290	80	39 900	0.170	0.429
					90	37 800	.195	.374
					100	35 700	.210	.347
					110	33 600	.227	.321
					120	31 500	.246	.297
					130	29 500	.266	.274
					140	27 700	.275	.265

[a]Designation described in section 4.9.

TABLE 4.VIII.- FUEL FRACTION FOR RESIZED AIRCRAFT VARIANTS

①	②	③	④	⑤	⑥	⑦	⑧	⑨	⑩	⑪	⑫	⑬	⑭	⑮
Aircraft variant (a)	$(L/D)_o$	$(L/D)_{av}$	Engine	Match point (b)	W_g/S	T_0/W_g	h	a	M	V	c	B	R	W_f/W_g
2-5a	14.58	13.98	D		103	0.260	34 200	579	0.7	405	0.804	7042	2674	0.316
3-5a	13.71	13.15	A		125	.285	30 500	587	.7	412	.625	8669	2674	.265

[a]Designation described in section 4.9.
[b]See figure 4.8.

TABLE 4.IX.- PHYSICAL CHARACTERISTICS FOR RESIZED AIRCRAFT VARIANTS

①	②	③	④	⑤	⑥	⑦	⑧	⑨	⑩	⑪	⑫	⑬	⑭	⑮
Aircraft variant (a)	$(L/D)_o$	Match point (b)	W_g/S	T_0/W_g	W_f/W_g	W_p	$\bar{U}$	W_g	W_e	W_f	S	T_0	A_f/S	d
2-5a	14.58		103	0.260	0.316	3165	0.497	17 486	8796	5526	170	4546	0.139	5.5
3-5a	13.71		125	.285	.265	3165	.473	15 216	8019	4032	122	4337	.171	5.2

[a]Designation described in section 4.9.
[b]See figure 4.8.

TABLE 4.X.- COMPARISON OF CHARACTERISTICS FOR SEVERAL AIRCRAFT VARIANTS

Characteristic	Aircraft variant 2-5	Aircraft variant 2-5a	Aircraft variant 3-5	Aircraft variant 3-5a
W_g	15 591	17 486	12 866	15 216
W_e	7 640	8 796	6 549	8 019
W_f	4 787	5 526	3 152	4 032
S	164	170	120	122
T_0	3 913	4 546	3 435	4 337
d	5.0	5.5	4.3	5.2
l	42.5	46.8	36.6	44.2
b	36.2	36.9	31.0	31.2
W_g/S	95	103	107	125
T_0/W_g	0.251	0.260	0.267	0.285
$(L/D)_{av}$ . . .	14.51	13.98	14.51	13.51

V - DEVELOPMENT AND DESIGN FEATURES OF PROPELLER-DRIVEN AIRCRAFT

CONTENTS

		Page
5.0	Introduction	229
5.1	The Heritage of World War I	230
5.2	Time of Little Change, 1918-1926	234
	5.2.1 Monoplane Developments	236
	5.2.2 High-Speed Racing Aircraft	237
5.3	Time of Revolution, 1926-1939	241
	5.3.1 Monoplanes and Biplanes	244
	5.3.2 Synergistic Developments	250
	5.3.3 General Aviation at End of Decade	257
5.4	Time of World War II, 1939-1945	261
	5.4.1 Aerodynamic Problems and Refinements	262
	5.4.1.1 Airfoils and High-Lift Devices	262
	5.4.1.2 Drag Cleanup	265
	5.4.1.3 Compressibility Effects	268
	5.4.1.4 Flying and Handling Qualities	271
	5.4.1.5 Summary Comments	273
	5.4.2 Examples of World War II Aircraft	274
	5.4.2.1 Bomber Aircraft	275
	5.4.2.2 Fighter Aircraft	277
	5.4.3 Summary Comments	281
5.5	Time of Maturity, 1945-1977	281
	5.5.1 Transport Aircraft	281
	5.5.2 General Aviation Aircraft	285
	5.5.2.1 Contemporary Types	286
	5.5.2.2 Other Types of General Aviation Aircraft	291
5.6	Design Trends	291
	5.6.1 Maximum Speed	292
	5.6.2 Stalling Speed, Wing Loading, and Maximum Lift Coefficient	294
	5.6.3 Power Loading	296
	5.6.4 Zero-Lift Drag Coefficient and Skin Friction Parameter	297
	5.6.5 Maximum Lift-Drag Ratio	299

Page

SYMBOLS 301

REFERENCES 303

TABLES 308

5.0 Introduction

The development of the aircraft from the Wright "Flyer" of 1903 to the magnificent machines of today must be ranked as one of the great engineering achievements of all time. In no other type of vehicle is there less margin for error. Each curve, each shape, and each detailed part must be meticulously designed on the basis of quantitative, scientific data, and with deep insight into the complex process of design trade-off if the aircraft is to achieve its desired characteristics.

The tremendous advancements in airplane design since 1903 result from major technological advances in such fields as aerodynamics, stability and control, propulsion systems, structures, materials, internal systems, and manufacturing techniques. Private individuals, research laboratories operated by civil and military elements of the govenment, universities and other organizations, as well as industrial research, design, engineering, and manufacturing teams have all been involved in the evolution of the airplane to its present state of perfection.

Advancements in aircraft design have usually come by slow and painstaking work, stimulated occasionally by a brilliant insight or development. The evolution of the modern airplane has been characterized by a series of technological levels which extend over a period of years. Each level of technology has tended to be exemplified by an aircraft configuration type which is gradually improved by a number of relatively small technological advancements without any major conceptual change. Occasionally, new technology in a number of disciplines has been combined synergistically in a new design to produce an aircraft of a new and higher level of technology. The Douglas DC-3 transport, to be described in this chapter, is a good example of this type of advancement in aircraft design.

The development of practical means for jet propulsion caused a revolution in aircraft design. A brief review of the development of the jet-powered transport is contained in chapter 2. Chapter 5 attempts to show some of the highlights of the development of the propeller-driven aircraft from 1918 to the present. The year 1918 was chosen for the beginning of the discussion because the airplane had by that time, at the conclusion of World War I, evolved into a few fairly definitive configuration types, as compared to the bewildering profusion of types which marked the early years of aircraft experimentation.

A brief summary of the state of aeronautical technology at the end of World War I will be given, after which the development of the propeller-driven aircraft will be discussed within the framework of the following four time periods:

(1) Time of little change, 1918-1926

(2) Time of revolution, 1926-1939

(3) Time of refinement, 1939-1946

(4) Time of maturity, 1946-1976

Some of the significant milestones in aircraft development, including photographs and descriptions of aircraft typical of a particular technological level, will be discussed for each time period. The discussion is related primarily to aircraft configuration evolution and, to a lesser extent, to developments in aircraft construction and propulsion. No attempt will be made to describe all of the many significant aircraft produced in the four time periods. The discussion is restricted primarily to aircraft developed in the United States in order to reduce the scope of material to be considered. No adverse reflection on the quality of the many fine foreign designs developed over the years is intended by their exclusion.

Both civil and military aircraft are discussed in the ensuing paragraphs. The seaplane, once an important class of aircraft, but now almost extinct, is omitted from the discussion. An account of the development of British flying boats and amphibians is given in reference 5.27; data on seaplanes are, of course, presented in the various issues of Jane's All the World's Aircraft (for example, refs. 5.1 to 5.12). Jane's All the World's Aircraft has been published each year since 1909, with the exception of the World War I years, and forms an invaluable reference source for anyone interested in aircraft development.

The aircraft to be discussed in the following paragraphs are listed in table 5.I, together with some of their performance and physical characteristics. The methods employed for estimating the aerodynamic parameters given in table 5.I are contained in appendix B. Credits for the photographs are given in table 5.II.

The references used in obtaining the characteristics of the aircraft are listed in the tables or are specifically cited in the text. A few references which provide useful background material, but are not specifically cited, are offered for additional reading on the subject of aircraft development. For convenience, references 5.13 to 5.78 are listed alphabetically.

5.1 The Heritage of World War I

The development of aircraft in the time period between the Wright Brothers' first flight in 1903 and the outbreak of World War I in 1914 was characterized by a proliferation of aircraft configuration types. A few of these aircraft flew moderately well, some poorly, and some not at all. There was little scientific and engineering foundation for the design of aircraft, and many of the aircraft built during this time period were constructed by nontechnical people as backyard-type projects. As a consequence, no definitive configuration types had crystallized by the beginning of World War I, and no aircraft had been designed to accomplish a specific mission.

The demands of combat aviation, together with the constant vying for air superiority by the opposing powers, resulted in the development of the airplane from a curiosity in 1914 to a highly useful and versatile vehicle by the end of the war in November of 1918. A multitude of aircraft types were tested in combat, and literally hundreds of prototypes were built and flown. These numbers become believable when one considers that the prototype of a fighter air-

craft could be designed, constructed, and flown within a period of a few weeks. In contrast to the essentially job shop approach to aircraft construction which prevailed prior to 1914, an aircraft industry was developing and was being nurtured by large expenditures of money by the belligerent governments. The engineering principles of aircraft design were also beginning to take shape. Government laboratories, such as the Royal Aeronautical Establishment in England, contributed greatly to the foundations of aeronautical engineering. Scientific and engineering laboratories also existed in France and Germany, and the National Advisory Committee for Aeronautics (NACA) was established in the United States by act of Congress in 1915. The results of NACA research on aircraft design, however, did not begin to have a significant impact until the mid to late 1920's. In contrast to the European powers, the United States had essentially no air force and no real aircraft industry when war was declared on Germany in April of 1917. Accordingly, the United States relied almost entirely on tried and proven European aircraft designs. Some of these aircraft were produced by European companies, while others were manufactured under license in the United States.

An amazing variety of aircraft types were built and tested in the continual quest for better fighting machines. Monoplanes, biplanes, and triplanes were employed in military operations at various stages of the war, and at least two quadraplanes were tested in prototype form. The wings of most of these aircraft were supported externally by a combination of wires and struts, although the Dutch designer Anthony H. G. Fokker, who supplied aircraft for the Germans, developed a number of machines with internally braced cantilever wings of wood construction. Both tractor and pusher type engine installations were employed. Multiengine bombers frequently utilized a combination of pusher and tractor powerplant installations. The pusher type configuration was used extensively as a fighter, particularly by the British, in the early stages of the war because a machine gun could be fired in the forward direction without hitting the propeller. The development of a successful interrupter gear which permitted the machine guns to fire between the blades of the propeller, however, spelled the end of the pusher as a fighter. The internal structure of most of the aircraft consisted of a wood framework braced with wire and covered externally with cloth. Some aircraft employed a mixture of metal and wood in their construction, and experiments were conducted with all-metal aircraft employing internal bracing of the wings. Dornier and Junkers in Germany were among the pioneers in all-metal aircraft construction. The types of alloys available at that time, however, did not lend themselves to the lightweight required in aircraft design, and the concepts of light, stressed skin metal construction lay in the future. All-metal aircraft did not play an important role in World War I. The use of plywood as an external covering, together with a minimum of internal structure, was also employed, particularly in fuselage design, by several manufacturers. This type of construction, called monocoque, is described in more detail in section 5.2.2 of this chapter.

Two vastly different types of engines were employed in World War I aircraft. Water-cooled engines of 4, 6, 8, and 12 cylinders were extensively utilized. In concept, these engines were not unlike the present-day automobile engine. The rotary was another type of engine which was extensively employed. This engine had cylinders arranged radially around a crankshaft; but unlike the modern radial engine, the crankshaft was fixed to the aircraft, and the cylin-

ders and crankcase rotated around it. This engine type was relatively light and was air cooled, advantages which accounted for its use. The rotary engine, conceived in France, had a primitive control system and introduced undesirable gyroscopic moments in the aircraft which adversely affected flying characteristics. The rotary engine is a curiosity which rapidly vanished from the scene following the close of World War I.

Out of the profusion of aircraft types explored in the hectic days of World War I, the externally braced biplane emerged as the most practical aircraft consistent with military requirements and the state of technology as it existed at that time. The biplane concept was applied to fighters, observation and reconnaissance aircraft, multiengine bombers, as well as to flying boats and various patrol craft, and may be considered the standard aircraft concept to emerge from World War I. Typical of this class of aircraft is the DeHavilland DH-4, illustrated in figure 5.1. The DeHavilland 4, or DH-4 as

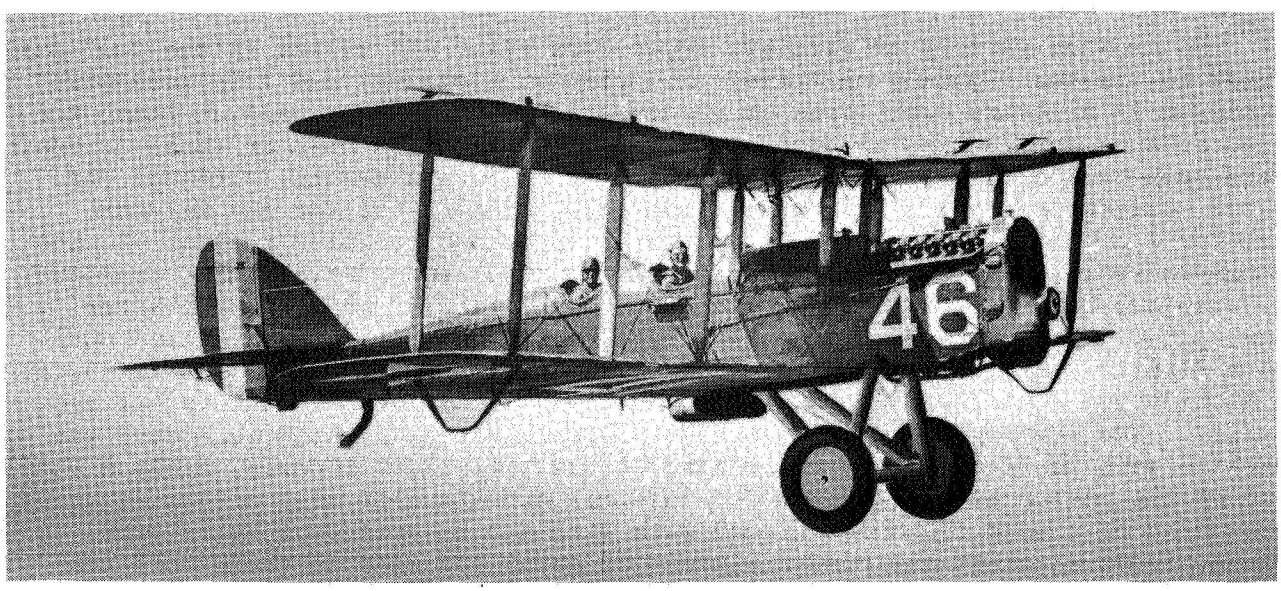


Figure 5.1.- DeHavilland DH-4B observation plane; circa 1920.

it was commonly referred to, was originally designed and produced in England; however, several thousand were manufactured under license in the United States. It was the only aircraft produced in the United States which saw combat service during World War I. An examination of figure 5.1 shows the aircraft to be a strut and wire braced biplane equipped with a fixed landing gear. The powerplant was a 12-cylinder V-type engine which developed about 400 hp. As can be seen from the photograph of figure 5.1, the radiator was positioned in the nose of the aircraft and provided the necessary heat exchanger for cooling the water which circulated through the engine. The engine was a wartime development in the United States and was referred to as the Liberty engine. Although the propeller is not visible in the photograph, it was of fixed pitch design and wooden construction. The speed and altitude ranges through which the aircraft operated were not sufficiently large to warrant the use of any

type of variable pitch propeller. The internal structure of the aircraft consisted of a wood framework braced with wire, and the covering was a fabric such as linen which was "doped" to provide a tight and weather-proof skin.

No brakes were employed on the landing gear, and there was no means of steering the aircraft on the ground other than with the rudder acting under the slipstream from the propeller. The tail of the aircraft was supported by a skid which, on landing, served as a sort of brake as the aircraft moved across the unpaved fields typical of the time period. The tail skid also served as a means for keeping the aircraft headed in a given direction. Crosswind operations were rarely undertaken in that time period. Most airports were roughly rectangular or circular in shape so that the pilot was always able to take off or land directly into the wind.

The control surfaces of the aircraft were directly connected by cables to the control stick and rudder pedals. The relationships between the size of the control surfaces, the desired response characteristics of the aircraft, and the control forces required by the pilot were little understood in 1918. As a consequence, the flying and handling characteristics of aircraft of that day generally varied from poor to terrible as judged by modern-day standards. A fine-handling aircraft, of which there were a few, was more a matter of luck than anything else. A quantitative indication of the flying and handling characteristics of an aircraft which was a contemporary of the DH-4 is given by Perkins in reference 5.60, and interesting qualitative comments on the flying characteristics of World War I aircraft are contained in references 5.24 and 5.69.

Typically, the crew rode in an open cockpit exposed to the elements. In fact, pilots of that day, and for many years thereafter, felt that "feeling the wind in their face" was necessary in order to fly the aircraft with skill and safety. The well-equipped pilot's instrument panel usually consisted of oil temperature and pressure gages, water temperature gage, and tachometer. These instruments, together with some sort of fuel indicating gage, served to indicate the health of the propulsion system. In the way of flight instruments, an altimeter, airspeed indicator, and compass usually completed the instrument panel. Radios for navigational purposes were largely unknown. The aircraft was usually not equipped with an electrical system, except for the engine driven magneto to operate the spark plugs, nor was there any type of self-starter. The traditional method of swinging the propeller by hand was the usual procedure for bringing the engine to life.

Some of the physical and performance characteristics of the DH-4 are given in table 5.I. The aircraft had a gross weight of 4595 lb and a maximum speed of 124 mph which was above average for 1918. The wing loading was a low 10.4 lb/ft^2 and was dictated by the small available landing field lengths and consequent need for low stalling speeds. By comparison, a modern jet transport may have a wing loading as high as 150 lb/ft^2. The zero-lift drag coefficient $C_{D,0}$ and the maximum lift-drag ratio $(L/D)_{max}$ are given in table 5.I(b) and are 0.0496 and 7.7, respectively. To provide some perspective to these numbers, the corresponding values for the modern jet transport might be 0.0160 and 18.0.

The biplane concept, as typified by the DH-4 shown in figure 5.1, represents the level of aeronautical technology which existed at the end of World

War I. The basic biplane formula was refined and improved for many years, as will be seen in subsequent sections of this chapter. In fact, biplanes were in series production right up to the beginning of World War II. Even today, biplanes are flown for sport, aerobatics, and just plain fun.

Before leaving World War I, mention should be made of the extensive literature which exists on the subject of aviation and aircraft developments during this period. A few sample works which may be of interest are given in the list of references at the end of this chapter. A broad view of combat aircraft from 1909 to the present is given in reference 5.70. Fighter aircraft of World War I are described in reference 5.53, and attention is focused on the triplane in reference 5.43. An interesting account of the development of very large German bombers is given in reference 5.42, and reference 5.76 describes all types of German combat aircraft. British aviation developments during the war are discussed fully in reference 5.59. A complete description of the many types of aircraft engines developed in World War I is given reference 5.18.

5.2 Time of Little Change, 1918-1926

The pace of aircraft development and production was extremely slow during the time period from the armistice of November 1918 until about 1926. World War I was thought to be the war "to end all wars," the war "to make the World safe for democracy." Military appropriations, including funds for new aircraft, were accordingly small. The primary financial base underlying the development and production of new aircraft and advanced technology had accordingly dried up. The military made use of leftover and modified aircraft from World War I, of which the DeHavilland 4, previously described, was a prime example. In fact, the DH-4 continued to serve in various capacities in the Army Air Corps of the United States until the early 1930's. There was, of course, some development activity sponsored by both the Army and the Navy, and a number of prototypes of new aircraft were produced. These prototypes, however, usually followed the familiar biplane formula which emerged from World War I. Some small production contracts, generally no more than 15 or 20 aircraft, were placed with the existing manufacturers for some of these prototypes. Hence, the industry did not entirely collapse.

The requirements of civil aviation during this time period presented little incentive for advanced aircraft developments. No airlines devoted to the transportation of passengers existed in the United States; however, the government operated a primitive airmail service which linked various cities in the United States, and the first coast-to-coast airmail service was established in 1921. The aircraft employed for carrying the mails consisted mostly of surplus World War I aircraft, with the ubiquitous DH-4 being the mainstay of the operation. Many modifications were made to the DH to make it more suitable for airmail service, and the aircraft was utilized in the carrying of the mails up until at least 1927 or 1928.

General aviation as we know it today existed only in the form of the barnstormers. These gypsy pilots roamed the country from town to town offering 5- to 10-min rides for sums of around $5.00. The aircraft which served as the workhorse for the gypsy pilot was the Curtiss JN-4D or Jenny. This aircraft

was a trainer which served during World War I to introduce thousands of neophytes to the mysteries of flying. The Jenny was similar in configuration to the DH-4 pictured in figure 5.1 but, instead of having an engine of more than 400 hp, was equipped with the Curtiss OX-5 engine of 90 hp. The aircraft was accordingly quite slow and had a cruising speed which differed by not a very large amount from the stalling speed. These Curtiss Jennys were available in large numbers following the end of World War I and could be purchased for as little as a few hundred dollars. Obviously, no new aircraft suited to the demands of the barnstormers could be developed and produced for any such ridiculously low price. Thus, the private sector provided no market for the development and production of new aircraft.

In contrast to the slow development of airline aviation in the United States, European air transport began almost immediately after the cessation of hostilities in 1918. The major capitals of Europe were soon connected by primitive passenger-carrying airlines. The aircraft types utilized for carrying passengers were at first hastily converted military bomber and observation types. Later, new aircraft were constructed for the infant airlines; however, these aircraft usually followed the standard biplane formula developed during World War I. Typical of these transport aircraft is the Handley Page trimotor shown in figure 5.2. The aircraft was a multibay biplane, similar in configu-

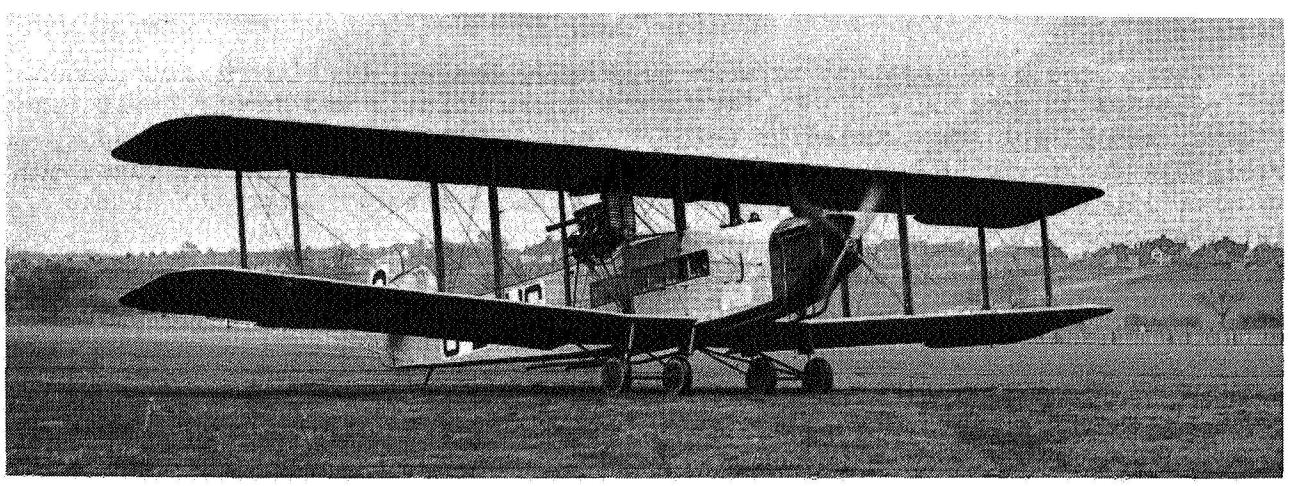


Figure 5.2.- Handley Page model W8F 12-passenger trimotor transport; 1924.

ration to the bomber types of the war, but employed an enclosed cabin capable of carrying 10 passengers. The two pilots were accommodated in an open cockpit just forward of the leading edge of the upper wing as can be seen in figure 5.2. Note the four-blade propellers and the multiple wheels of the landing gear. The use of the four-wheel gear was no doubt a concession to the relatively soft sod or mud landing fields of the period. A glance at the characteristics of the aircraft, given in table 5.I, indicates a relatively heavy machine of 13 000 lb gross weight, but with only 850 hp as the combined output of the three engines. The wing loading was a very low 5.9 lb/ft^2 in order that the

aircraft could operate out of the small fields which existed at that time. The cruising speed was a modest 85 mph; the drag coefficient at zero lift was 0.0549, which was larger than that of the DH-4. Although the use of multiple engines is usually thought to increase safety and reliability, that was not the case with the Handley Page trimotor. The aircraft could not maintain level flight following the loss of one engine according to the information given in reference 5.49. The Handley Page trimotor was put into operation by the British Imperial Airways and the Belgium Sabena Airway Systems in about 1924 and continued in operation, at least to some limited extent, until about 1931. In fact, very large multiengine biplanes were utilized on some European airlines right up until the beginning of World War II.

5.2.1 Monoplane Developments

Aircraft employing the monoplane configuration had been built since the early days of aviation. The first nonstop flight across the English Channel was made in 1909 by Bleriot, flying a wire-braced monoplane, and many early World War I fighters were also monoplanes (ref. 5.53). Most early monoplanes employed a multitude of wires and struts in order to provide strength and rigidity to the wings. As a consequence, the drag characteristics of these aircraft showed little if any improvement as compared to contemporary biplane drag characteristics. Furthermore, there seemed to be a lack of confidence in the structural integrity of the monoplane configuration.

There were also experiments with internally braced, cantilever monoplanes. As indicated in section 5.1, the German designers Dornier and Junker built cantilever monoplanes constructed of metal. The materials and design methods available during World War I, however, did not lend themselves to the construction of light, all-metal cantilever designs. Another early proponent of the cantilever monoplane was the Dutch designer, Anthony H. G. Fokker. Fokker designed and built fighter aircraft for the German Air Force during World War I. His first cantilever monoplane fighter was the model D-8 which featured an internally braced wing mounted on struts above the fuselage. In contrast to accepted practice of the day, the wing employed an airfoil section with a thickness-to-chord ratio of about 16 percent. Contemporary designers mistakenly thought that thin wings of 6 to 8 percent in thickness ratio were necessary to obtain efficient aerodynamic characteristics. The DH-4, for example, had wings of 6 percent thickness. Today, most subsonic aircraft, except those for which compressibility effects are important, have thickness ratios in the range from 12 to 18 percent. The thick section of the Fokker wing allowed the use of two deep, built-up, wooden box spars. The ribs were of plywood, and the entire wing surface, including the ailerons, was covered with plywood. The resulting structure was extremely strong and stiff. Some of the early production models of this 1918 fighter suffered structural failure of the wings in flight. The problem and subsequent solution are described by Fokker in his autobiography (ref. 5.30). From the description which he provides, the problem would be termed today as aeroelastic divergence. Problems of divergence and flutter on cantilever wings were not understood during this time period and contributed to the suspicion and delayed general acceptance of this type of wing design.

Fokker, however, had faith in his approach to cantilever wing construction and developed in 1920 and 1921 a single-engine transport employing an internally braced wing similar in concept to that of the D-8 fighter. This aircraft, known as the Fokker F-2, is depicted in figure 5.3. The aircraft seated three or four



Figure 5.3.- Fokker F-2 four-passenger transport; 1920.

passengers in an enclosed cabin, and a single pilot was located in an open cockpit just under the leading edge of the wing. The absence of external struts and wires to support the wing is obvious from the photograph. The relative aerodynamic cleanliness of the design would be expected to produce a correspondingly low value of the zero-lift drag coefficient. The data in table 5.I, however, suggest that the value of $C_{D,0}$ is not much better for the Fokker than for the DH-4. The open cockpit together with a poor engine installation and consequent high cooling drag suggest themselves as possible reasons for the relatively high zero-lift drag coefficient. The wooden cantilever wing and steel tube, fabric covered fuselage formed the basis for a long line of Fokker aircraft which were built right up to World War II. An improved and larger version of the Fokker F-2, known as the T-2, was the first aircraft to fly nonstop across the United States. This flight was made by the U.S. Army Air Service in 1923. The famous Fokker trimotor was very similar in configuration to the F-2 but employed three modern engines, had a fully enclosed cabin and cockpit, and was much larger than the F-2. The first of these Fokker trimotors was employed by Richard E. Byrd and Floyd Bennett in their historic first flight over the North Pole in 1926.

5.2.2 High-Speed Racing Aircraft

The national and international air races helped stimulate and maintain public interest and support for aviation during the years immediately following World War I. The races also provided a focus for the development of new, high-performance aircraft. Many of these special aircraft were government sponsored. The Army and the Navy sponsored such developments in the United States, as did

the Air Forces of France, Great Britain, and Italy in Europe. The most successful of these aircraft were highly developed forms of the biplane configuration. Typical of such aircraft is the 1923 Curtiss R2C-1 racer shown in figure 5.4.



Figure 5.4.- Curtiss R2C-1 racer; 1923.

The aircraft is seen to be extremely clean aerodynamically and had a phenomenally low zero-lift drag coefficient of 0.0206 (table 5.I). The aircraft achieved a maximum speed of 267 mph with a liquid-cooled engine of about 500 hp. Some of the features which accounted for the low drag coefficient and consequent high speed are the minimization of the number of wires and struts to support the wings, the smooth, highly streamlined semimonocoque wooden construction of the fuselage, the all-metal Curtiss Reed propeller, and the very interesting skin type radiators which were used to provide heat exchange surface for the water-cooled engine. The external surfaces of these radiators, which formed a part of the surface of the wing, were of corrugated skin with the corrugations aligned with the direction of air flow. The remainder of the wing surface was covered with plywood. The Curtiss PW-8 fighter of which about 30 were produced in the mid-1920's also employed the skin type surface radiator. Although the skin radiators contributed significantly to obtaining a low drag coefficient, and hence to improving performance, they were not practical for use on operational combat aircraft. In addition to being prone to leak as a result of flexing of the wings, they were extremely vulnerable to battle damage which was probably the deciding factor in their elimination from future combat aircraft.

The term "semimonocoque" which was used in describing the construction of the aircraft probably deserves some clarification. The word "monocoque" is French and means single shell. Thus, the true monocoque fuselage consists in an outside shell, usually constructed or formed from plywood, which is held in shape by a number of transverse bulkheads contained within the shell. The

strength and stiffness of such a fuselage is provided entirely by the outside shell. A semimonocoque fuselage has, in addition to the transverse bulkheads, several longitudinal members to enhance the stability, stiffness, and strength of the structure. A number of World War I German fighters, such as the famous Albatross series, employed semimonocoque fuselage construction. This type of construction was light in weight, provided a smooth streamline shape, was strong and rigid, and gave a large usable inside fuselage diameter for a given outside diameter. The semimonocoque type of construction will appear again in connection with the high performance Lockheed aircraft of the late twenties and thirties.

A number of racing aircraft were developed which employed the monoplane configuration. Some of these aircraft had cantilever wings; others employed strut braced wings, and such advanced concepts as the retractable landing gear were sometimes seen. For one reason or another, however, none of these monoplane racers were particularly successful. The Dayton Wright RB racer developed for the 1920 Gordon Bennett race was perhaps one of the most advanced concepts developed during the entire period. The aircraft is illustrated in figure 5.5,

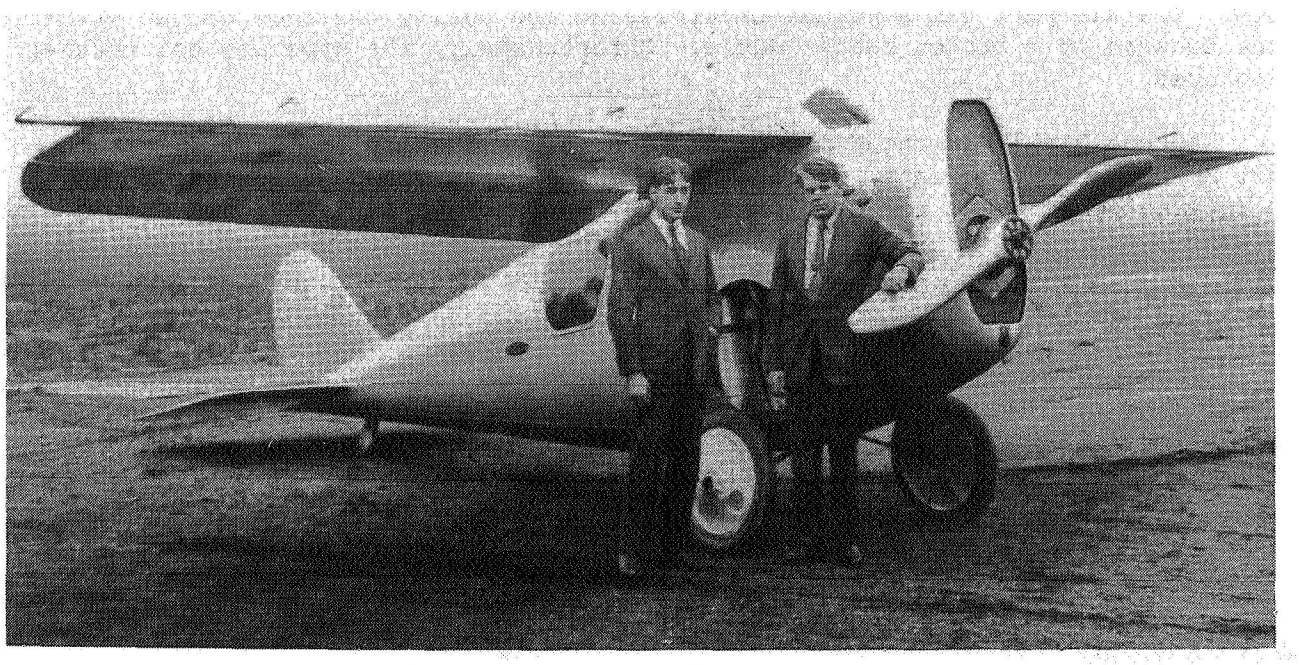


Figure 5.5.- Dayton Wright RB-1 racer; 1920.

and some of its characteristics are given in table 5.I. The pilot was entirely enclosed in the fuselage which was of wooden semimonocoque construction. The cantilever wing was constructed entirely of wood and employed leading- and trailing-edge flaps. These flaps in effect provided variable camber so that the airfoil section could be adjusted to its optimum shape for both high-speed and low-speed flight. This extremely advanced feature did not appear on production aircraft until the development of the jet transport in the 1950's. The

landing gear on the Dayton Wright racer retracted into the fuselage in very much the same way as that used in later Grumman fighters of the thirties and forties.

The drag coefficient at zero lift of the Dayton Wright racer was 0.0316 (table 5.I), which is considerably higher than the value of 0.0206 for the Curtiss R2C-1 but very much lower than the value of 0.0496 given in table 5.I for the DH-4B. A comparison of the skin friction parameter $\bar{C}_F$ for the Dayton Wright racer shows that this parameter is very low as compared to that for contemporary aircraft of the period, although again it is somewhat higher than the corresponding number for the Curtiss R2C-1. The skin friction parameter $\bar{C}_F$ is a drag coefficient based on the total wetted area of the aircraft and, hence, gives an indication of the relative aerodynamic refinement of different configurations. Comparisons of the zero-lift drag coefficient can sometimes be misleading because of large differences between the ratio of wing area to wetted area for different aircraft. The zero-lift drag coefficient $C_{D,0}$, however, is a parameter which is generally familiar to aeronautical engineers, and the wing area is the more usual basis for comparing the nondimensional aerodynamic characteristics of aircraft. The method utilized for estimating the value of the parameter $\bar{C}_F$ is described in appendix B. Although highly advanced for its time, the Dayton Wright racer was not successful in the Gordon Bennett race of 1920. The aircraft was somewhat underpowered and during the race had to withdraw because of a broken rudder cable. Unfortunately, the type was not further developed.

Another highly advanced monoplane racer, developed by the British for the 1925 Schneider Trophy race, was the Supermarine S-4. The Schneider race was an international event for seaplanes. The S-4 is shown in figure 5.6 and is

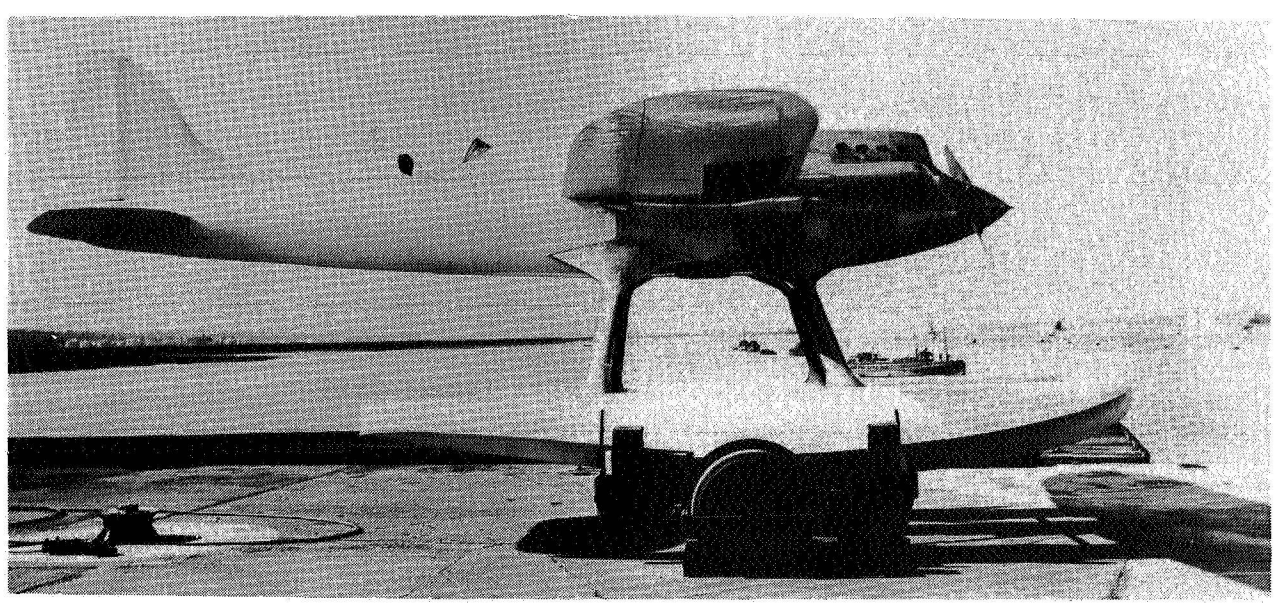


Figure 5.6.- Supermarine S-4 seaplane racer; 1925.

seen to be a beautiful, highly streamlined, cantilever monoplane mounted on twin floats. The wing was constructed of a wooden framework covered with plywood and employed flush radiators which, unlike the previously described Curtiss racer, however, were not of the skin type. The wings had landing flaps which could be geared to the ailerons. The rear of the fuselage was of wooden semi-monocoque construction, and the forward portion containing the engine was of metal. The engine had 12 cylinders arranged in three banks of four. A front view of the engine gave somewhat the appearance of the letter "W"; accordingly, this cylinder arrangement was referred to as a W-type engine. A glance at the characteristics of the aircraft contained in table 5.I indicates a drag coefficient of 0.0274, which must be considered quite low in view of the large amount of surface area of the exposed twin floats. The wing loading of about 23 lb/ft^2 was high for the period and accounts for the use of the wing trailing-edge flaps. Another important factor which allowed the use of such a high wing loading was the relatively long take-off and landing runs possible with the use of rivers and harbors, as compared to the confined land airfields of the day. The aircraft was destroyed by wing flutter before the 1925 Schneider Trophy race (ref. 5.74). The ailerons on the S-4, according to reference 5.72, were unbalanced which no doubt contributed to the onset of wing flutter at the high speeds of which the aircraft was capable. Flutter and divergence of cantilever monoplane wings were not understood at that period in the development of aeronautical technology. Later Supermarine racers, which were quite successful in subsequent Schneider Trophy competitions, employed the more predictable wire-braced monoplane wings. The designer of the Supermarine S-4, R. J. Mitchell, later designed the famous Spitfire fighter of World War II. For those familiar with the Spitfire, some resemblance between the S-4 and the famous fighter can be seen in figure 5.6.

5.3 Time of Revolution, 1926-1939

The pace of aircraft development began to accelerate as the decade of the 1920's reached midpoint. Policies were established within the United States which assured consistent, although somewhat small, yearly appropriations for the procurement and development of new military aircraft. In an attempt to improve the poor aviation safety record and thus enhance the image of aviation as a serious means of transportation, laws were enacted which required the licensing of civil aircraft and pilots. Airworthiness standards were developed for the aircraft, and proficiency requirements were established for the licensing of pilots. The aircraft airworthiness requirements opened a market for the development of new general aviation type aircraft. War surplus aircraft, such as the Jenny, could not meet the new requirements or either their certification would prove economically unfeasible. The airmail which had been carried by government aircraft for many years reverted to private contractors. Thus began the airline industry, albeit in a small way. Under the stimulus of these influences, the aircraft industry began to grow.

The pace at which advanced aircraft can be developed is closely coupled to the generation of new and advanced technology. The results of research investigations by the Langley Memorial Aeronautical Laboratory of the National Advisory Committee for Aeronautics (NACA) began to play an increasingly important part in providing the new technology necessary for the development of advanced aircraft.

Investigations in aerodynamics, stability and control, propulsion, loads, dynamics, and structures formed the research program of the NACA. Wind tunnels, laboratories, flight research, and analytical studies formed the means by which new technology was developed. The results of research investigations by the NACA were made available to the industry in the form of technical reports. Bound volumes of these reports, covering the entire lifespan of the NACA from 1915 to 1958, form a part of most good technical libraries. Indexes such as those cited in reference 5.48 give a complete bibliography of research publications by the NACA. Years subsequent to 1949 are covered in additional indexes. Brief accounts of the significant research activities of the NACA are contained in references 5.29, 5.34, and 5.47.

The universities played an important role in educating young aeronautical engineers and in various aspects of aeronautical research. Schools of aeronautical engineering sponsored by the Guggenheim Foundation were particularly important. These schools existed at the Massachusetts Institute of Technology, the California Institute of Technology, New York University, the University of Michigan, the Georgia Institute of Technology, Stanford University, and the University of Akron. The contributions of the Guggenheim Foundation to the development of aeronautics in the United States are described in reference 5.44.

The military services played an extremely important role not only in the generation of new technology but in sponsoring the application of that technology in the development of new and useful operating systems. Thus, the development and operation of new military equipment provided a highly significant foundation of proven components, such as engines, for use in new civil aircraft. A summary of the contributions of military aeronautical research and development to the development of advanced commercial aircraft throughout the thirties, forties, and fifties is contained in reference 5.63. A close relationship can frequently be found between the development of advanced military aircraft and new commercial aircraft which employed not only many of the design features of military aircraft but also hardware and concepts which had been proved in military aviation.

Another important ingredient in the formula for accelerated development and production of new aircraft were the many record-breaking flights which were extremely popular with the general public and which played an important role in popularizing aviation and its potentialities as a serious means of transportation. The nonstop solo flight of Charles A. Lindbergh from New York to Paris in May of 1927 had the most profound and lasting influence of any of the record-breaking flights. His magnificent flight thrilled and captured the imaginations of people all over the world and stimulated an interest and enthusiasm for aviation which had an almost incalculable effect on future aeronautical developments. As a result of his flight, a multitude of small companies dedicated to the manufacture of aircraft sprang up all over the United States. Most of these companies flourished for a few years and then quietly passed into bankruptcy as the country entered the great depression of the 1930's. Airline operations were given a tremendous boost as a result of the enthusiasm engendered by the Lindbergh flight.

The Ryan monoplane employed by Lindbergh on his historic flight, illustrated in figure 5.7, was of the strut-braced high-wing type which had a fixed landing

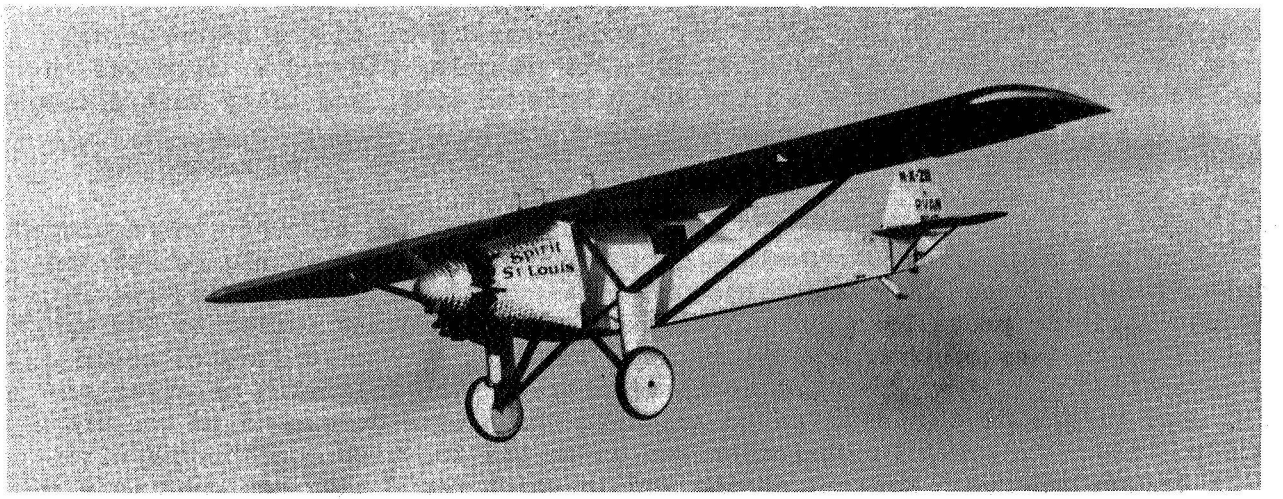


Figure 5.7.- Ryan NYP Spirit of St. Louis; 1927.

gear. The fuselage consisted of a welded steel tube frame, and the wings were of wooden frame construction. The entire aircraft was covered with cloth fabric. The pilot had no forward vision since the space immediately ahead of him was occupied by a large 360-gal fuel tank. The wheels incorporated no brakes, and the tail skid was of the fixed type. The aircraft utilized the relatively new Wright Whirlwind engine. This engine had nine cylinders radially disposed about the crankcase and crankshaft. In contrast to the rotary engine which was described earlier, however, the cylinders and crankcase of the radial engine were fixed and the crankshaft with the propeller attached rotated. The engine developed 220 hp and, for its day, was considered to be light and highly reliable. The air-cooled feature resulted in the deletion of the radiator and associated plumbing which was always a source of maintenance and reliability problems on liquid-cooled engines. The maximum gross weight of the aircraft was 5135 lb, and the zero-fuel weight was 2415 lb. Thus, the fuel in the aircraft represented more than half of the gross weight and gave the Spirit of St. Louis airplane a zero-wind range of about 4200 statute miles. The cruising speed of the aircraft was about 95 mph, and the maximum speed, 124 mph. The zero-lift drag coefficient $C_{D,0}$, given in table 5.I, was 0.0379. This coefficient represents a considerable reduction over the value of 0.0496 given for the DeHavilland DH-4 but still indicates that the fixed landing gear and multiple wing struts were serious drag producing elements. The maximum lift-drag ratio of the aircraft was 10.1, which compares favorably with the value of 7.7 given for the DeHavilland 4. The higher effective aspect ratio of the monoplane, as compared to the biplane, is in large measure responsible for the increased lift-drag ratio of the Spirit of St. Louis as compared to the DH-4 and other typical contemporary biplane configurations. A complete description of the Spirit of St. Louis giving design and performance data is contained in the appendix of reference 5.55.

Record-breaking flights continued for many years to play an important role in the development of aviation, particularly as a means of focusing public attention on the possibilities of the aircraft as a safe and reliable means for travel. Long distance flights, flights around the world, flights of explora-

tion, and, of course, all sorts of air races formed part of the aeronautical scene in the late twenties and thirties. For example, Richard E. Byrd was in command of the first flight over the South Pole in 1929, and Wiley Post circled the globe alone in $7\frac{1}{2}$ days in 1933. The world's absolute speed record was increased to 440 mph in 1934 by an Italian seaplane. The aircraft was equipped with pontoons similar to those shown on the Supermarine S-4 in figure 5.6 and employed wire braced monoplane wings and a 24-cylinder engine driving two counter-rotating propellers. The absolute speed record was raised to 467 mph in 1938 by the Messerschmitt 209V1 racer. The list of record flights could go on endlessly, but will not be continued here. The following paragraphs will deal with some of the advanced aircraft which were developed in the era 1926 to 1939. This may be characterized as an era in which concepts of aircraft design underwent radical change and in which rapid advances were made in performance.

5.3.1 Monoplanes and Biplanes

The Ryan monoplane Spirit of St. Louis, pictured in figure 5.7, popularized the monoplane configuration in America and marked the beginning of the decline of the biplane. Another immortal high-wing monoplane, the Ford trimotor, formed the mainstay of the infant United States airline industry in the late 1920's and early 1930's. The aircraft, which is pictured in figure 5.8, featured an inter-

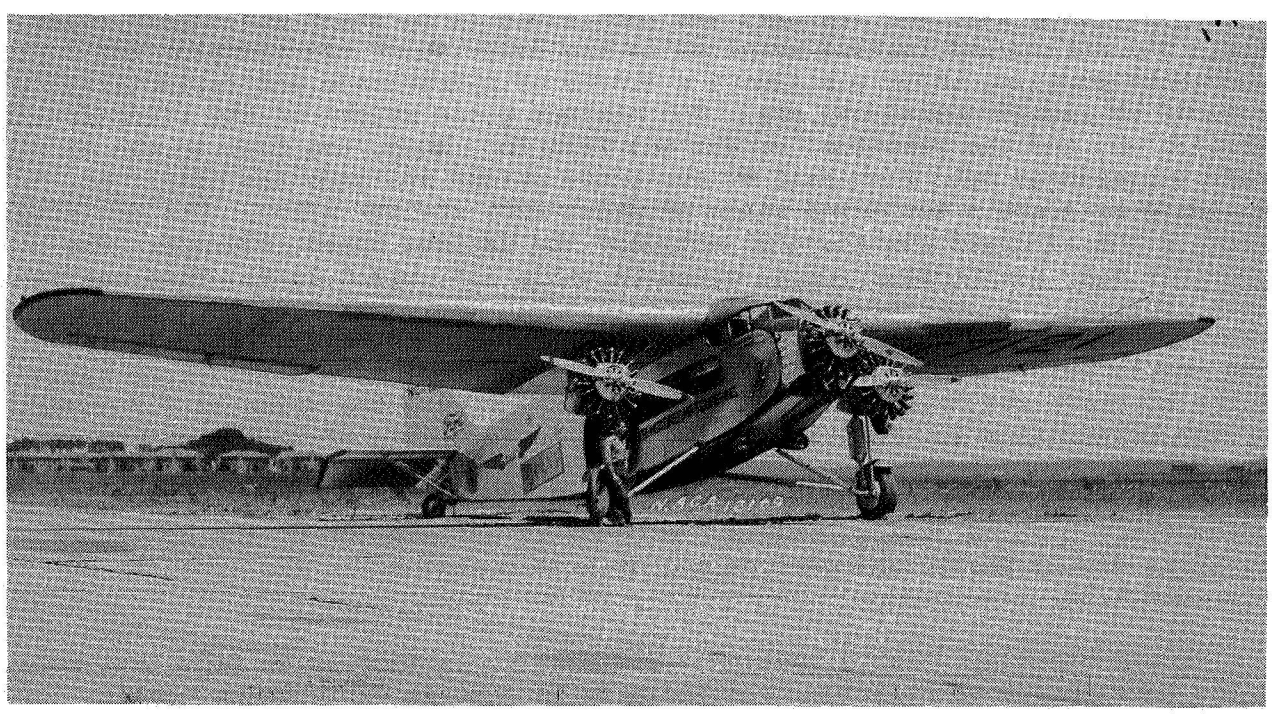


Figure 5.8.- Ford 4-AT 12-passenger trimotor transport; 1928.

nally braced wing, fixed landing gear, and three engines. The basic configuration was similar to the Fokker trimotor referred to earlier; however, the method of construction employed in the two aircraft was totally different. The Fokker had a structure consisting of a mixture of wood, metal, and fabric; whereas, the Ford was of all-metal construction. The internal structure of the aircraft was entirely of metal, and the skin was a corrugated aluminum alloy. The corrugations provided stiffness in the skin panels and were aligned with the direction of air flow in order to minimize the drag. This type of construction was pioneered by Hugo Junkers in Germany.

The aircraft was produced in two versions: the model 4-AT and the model 5-AT. These aircraft were similar in appearance, but the model 5-AT was slightly larger and employed somewhat more powerful engines than the model 4-AT. The photograph (fig. 5.8) depicts a model 4-AT, and the specifications given in table 5.I are for the model 5-AT. The model 5-AT carried from 13 to 15 passengers in an enclosed cabin, had a gross weight of 13 500 lb, and was equipped with three 420-hp Pratt & Whitney Wasp radial engines. The two pilots were, by this time, seated in an enclosed cockpit which was located ahead of the wing. Ground handling characteristics were enhanced by the provision of differential braking on the main landing gear wheels and a swiveling tail wheel. Cockpit instrumentation was primitive by modern standards, and some of the instruments for the outboard engines were actually located on the engine nacelles which required the pilots to look out of the side windows to read them. The large, powerful engines were equipped with an inertia starter; this type starter was much used for large engines beginning in the mid-1920's. A flywheel of large moment of inertia was brought to a high rotational speed through the use of either a geared hand crank or electrical power source. When the proper speed had been reached, a clutch was engaged and the angular momentum of the flywheel caused the engine to rotate and start.

The Ford trimotor was especially designed to maintain flight after the loss of one engine. Under full gross weight conditions, however, the aircraft was not able to climb after take-off following the loss of an engine, probably because of the excessive drag resulting from the windmilling propeller. Full feathering propellers had not been developed at that time. The top speed of 150 mph listed in table 5.I for the Ford trimotor may be excessive; cruising speeds somewhat less than 100 mph are indicated in reference 5.69 for a model 4-AT which is still flying today. Both the drag coefficient $C_{D,0}$ and the parameter $\bar{C}_F$ for the Ford are seen to be relatively high, as compared to corresponding values for the Ryan Spirit of St. Louis. The drag of the two outboard engines and the nacelles no doubt contribute significantly to the drag of the trimotor and, to some extent, nullify the advantages of the cantilever wing. Furthermore, according to reference 5.46, the wetted area of an aircraft may be increased by as much as 20 to 40 percent by corrugations in the metal covering. No account was taken of this increment in wetted area in calculating the coefficient $\bar{C}_F$ in table 5.I.

The prototype of the Ford trimotor flew in 1926 and the last production aircraft rolled off the line in 1933. A total of 116 models of the 5-AT and 84 models of the 4-AT were constructed. Some of these aircraft are still flying today, and one was flying in scheduled airline service with the remarkable

Island Airlines at Port Clinton, Ohio, into the 1970's. The longevity of these aircraft attests to their rugged construction and basic soundness of design.

The Lockheed Vega, shown in figure 5.9, was a very high-performance monoplane which first flew in 1927. The aircraft shown in the photograph is a fully

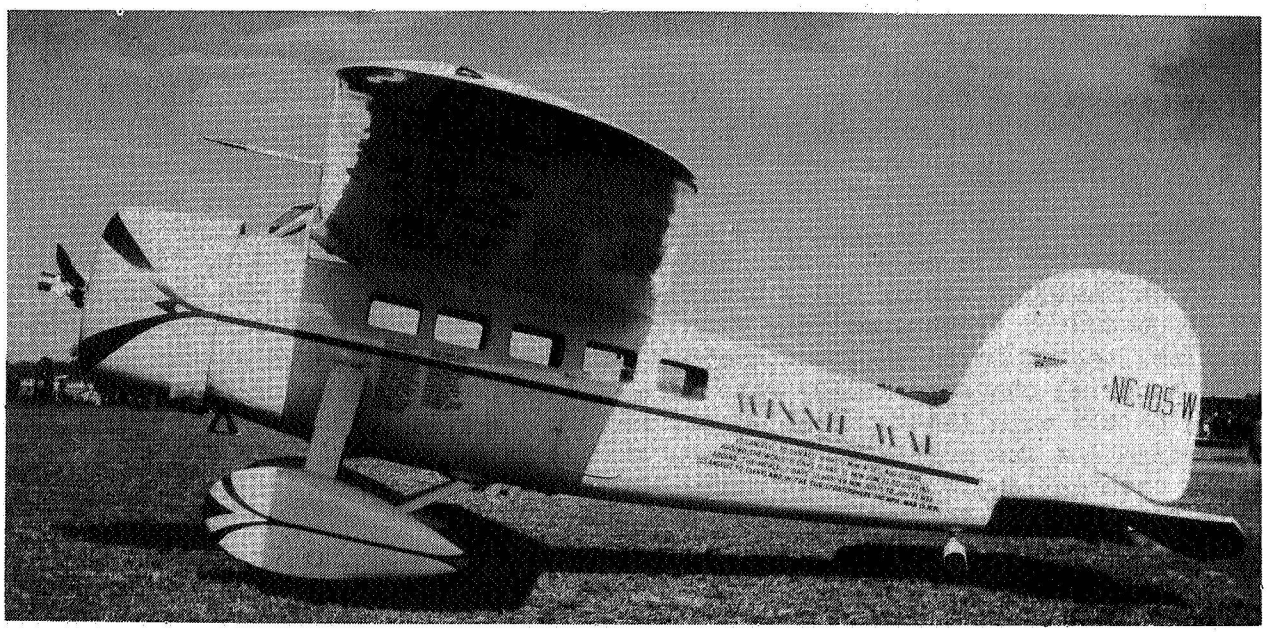


Figure 5.9.- Lockheed Vega 5C mail and passenger plane; 1929.

developed model 5C version. Both the internal structure and the outer covering of the aircraft were wood. The wing was of the internally braced, cantilever type, and the fuselage was of semimonocoque construction. A new feature, which appeared on this aircraft, was a circular cowling surrounding the 450-hp Pratt & Whitney Wasp air-cooled engine. This cowling concept was one of the early contributions of the NACA and provided substantial increases in the speed of aircraft employing radial engines but, at the same time, directed the cooling air through the engine in such a way as to provide adequate cooling. The maximum speed of the Lockheed Vega was increased from 165 mph to 190 mph by the addition of the NACA cowling. Fairings, called pants, around the wheels of the landing gear also reduced the drag and resulted in an increase in the speed of the aircraft. The Lockheed Vega had a very low zero-lift drag coefficient of 0.0278, as shown by the data in table 5.I. The low zero-lift drag coefficient was obtained through careful attention to detailed aerodynamic design of the aircraft and by the absence of drag producing struts, wires, and other external drag producing elements. The fixed landing gear, however, remained as a significant drag producing feature of the airplane. The maximum lift-drag ratio of the Vega was 11.4 which was unusually high for that time period. The Lockheed Vega was used in airline service (six passengers) and was also employed in many record-breaking flights. The aircraft in the photograph (fig. 5.9) is painted to represent the famous Winnie Mae, which Wiley Post flew around the world alone

in about 7½ days in the summer of 1933. The actual aircraft which Post flew on this remarkable flight is in the National Air and Space Museum in Washington, D.C. The Lockheed Vega was a highly advanced and refined design for its day, and, even now, the performance is very good for an aircraft with fixed landing gear.

The demise of the Jenny and its contemporaries opened the way for a new generation of general aviation aircraft for fixed base operators and barnstormers. Most of these new aircraft employed a welded steel tube fuselage and wooden wing structure and incorporated a fabric covering over the entire structure. The aircraft depicted in figures 5.10 and 5.11 are typical of the classes of aircraft which were produced during the latter part of the 1920's. The Curtiss Robin, shown in figure 5.10, was designed along the lines of the strut



Figure 5.10.- Curtiss Robin three-place-cabin monoplane; 1929.

braced monoplane formula popularized by Lindbergh's Spirit of St. Louis. The aircraft was ruggedly built with a view toward operation from poorly prepared airfields or pastures. The enclosed cabin provided seating for a pilot in the front and two passengers in the rear seat. The aircraft was usually equipped with either a Curtiss Challenger six-cylinder radial engine, or a Wright J6-5 five-cylinder radial engine. The specifications given in table 5.I are for the Challenger powered Robin which had 185 hp and was capable of a maximum speed of 115 mph. The aircraft was fitted with wheel brakes and a steerable tail wheel or skid. The drag coefficient of the Robin was a very high 0.0585 which probably resulted from the very large cylinders of the exposed radial engine, the many sharp corners of the forward facing windshield, and the relatively unfaired junctures between the multitude of struts supporting the wings and landing gear. The zero-lift drag coefficient of the Robin is seen to be more than 0.020 greater than that of the Ryan Spirit of St. Louis.

The biplane type was still popular and is illustrated by the Travelair 4000 of 1928 shown in figure 5.11. The aircraft was typical of a large number of three-place open biplanes in which the pilot sat alone in the rear cockpit, and

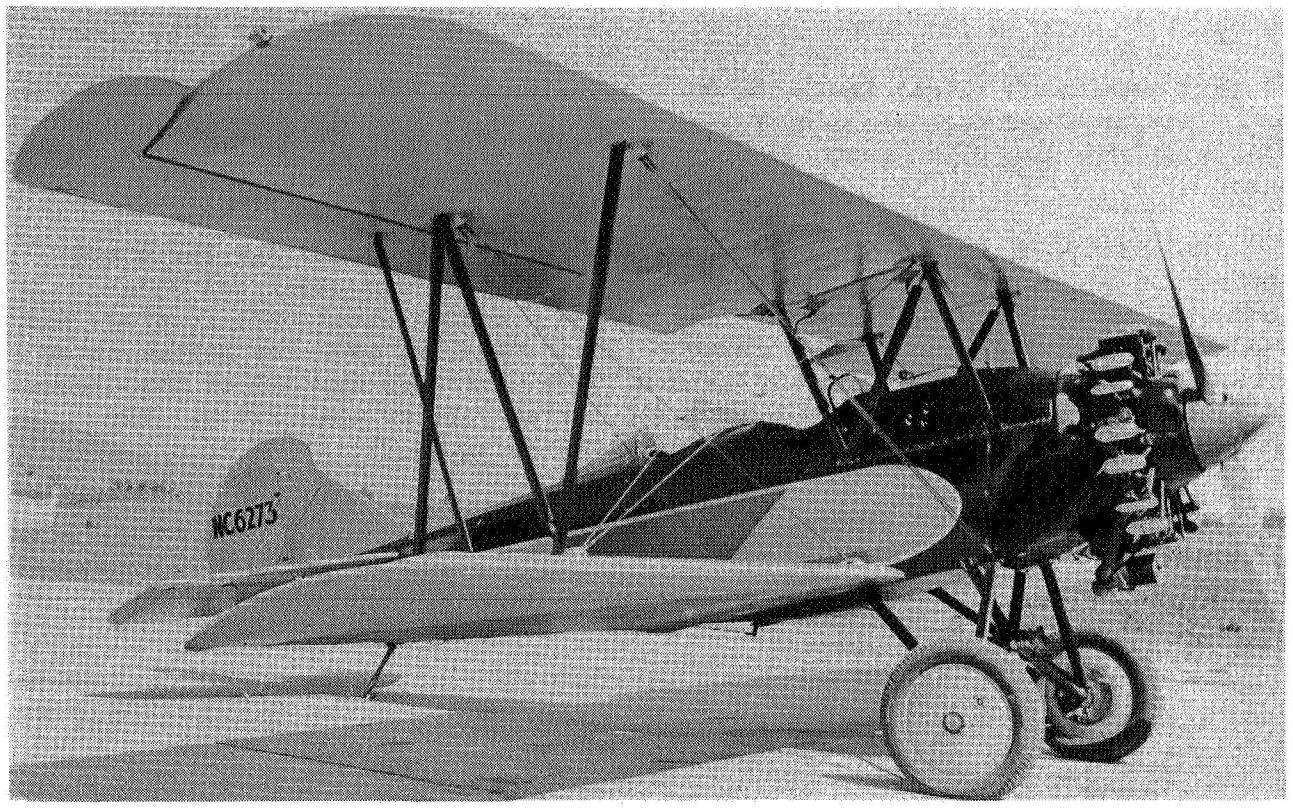


Figure 5.11.- Travelair 4000 three-place open-cockpit biplane; 1928.

two passengers were placed forward under the wing near the center of gravity in an open front cockpit. The aircraft is seen to employ struts and wires for bracing the wings, but they are far fewer in number than those used on the typical World War I biplane represented by the DH-4 pictured in figure 5.1. Many different powerplants were used in the various open cockpit biplanes produced in the late 1920's. The venerable Curtiss OX-5 water-cooled engine of World War I fame was still available in large numbers and formed a cheap source of powerplants for new aircraft. Engines of higher power and greater reliability, such as the Wright Whirlwind, were also available but these engines were considerably more costly than the surplus World War I engines. The Travelair 4000 shown in figure 5.11 has the Wright Whirlwind nine-cylinder radial engine. The large horn balanced ailerons and rudder on the Travelair are particularly noteworthy. Balanced controls of this type were used on the World War I German Fokker D-7 and formed a distinctive identifying feature of the aircraft. For this reason, the Travelair 4000, which was manufactured in Wichita, Kansas, is often referred to as the Wichita Fokker. Aircraft of the vintage of the Curtiss Robin and the Travelair 4000 are highly prized antiques today and are the subject of painstaking restoration. The Robin was used in the 1920's and 1930's in several record-breaking endurance flights, and in the late 1930's it was flown nonstop across the Atlantic by Douglas Corrigan.

Meanwhile, the military services remained wedded to the biplane concept for their fighters, observation planes, bombers, and other classes of aircraft. One of the last biplane fighters developed for the U.S. Army Air Corps, and

one of distinctly elegant design, was the Curtiss Hawk P-6E shown in figure 5.12. This aircraft traces its lineage back to the Curtiss Hawk P-1 of

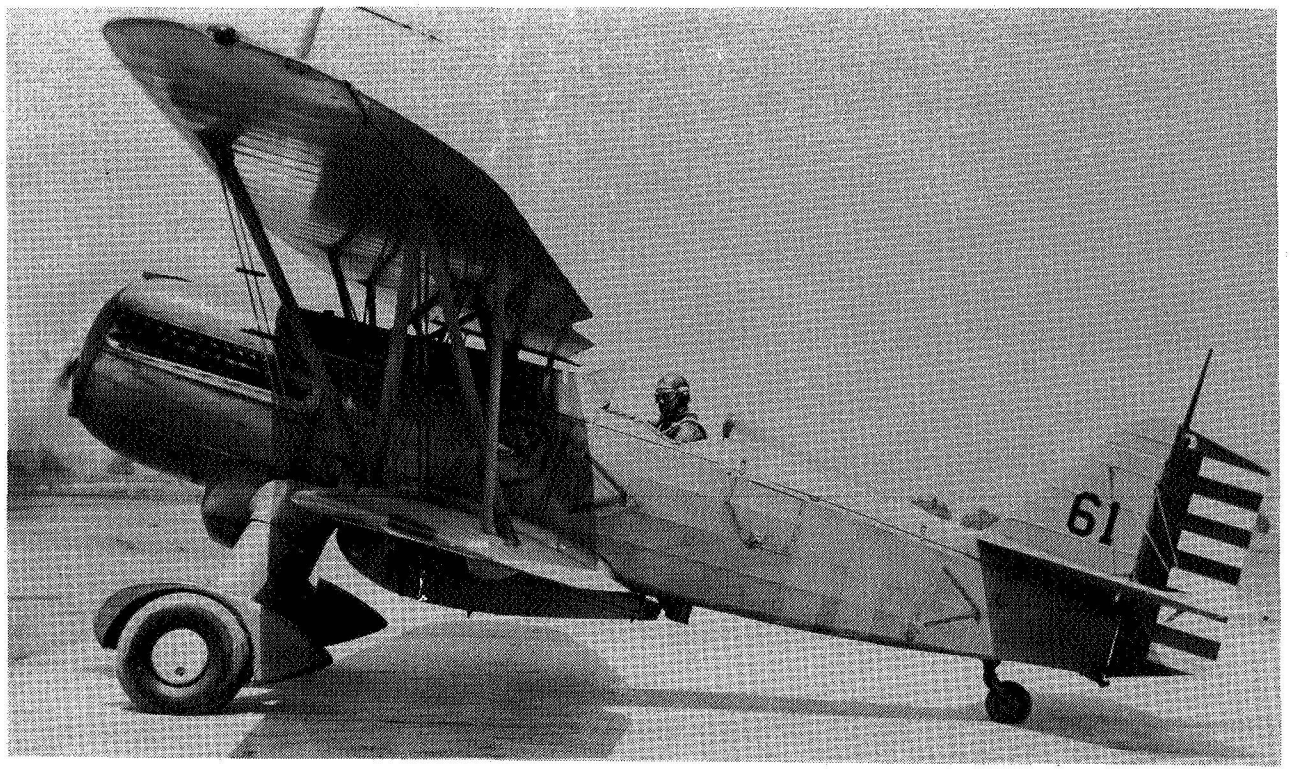


Figure 5.12.- Curtiss Hawk P-6E fighter; 1931.

1925 which in turn was derived, at least in part, from the Curtiss racing aircraft of that period. The P-6E was the last of the biplane line of Hawk fighters built for the U.S. Army Air Corps. Various versions of the Hawk were also procured for the U.S. Navy and a number of foreign countries. The entire Hawk series employed tapered wings, and the model P-6E featured a low drag, single-strut landing gear together with a carefully streamlined installation of the 650-hp Curtiss conquerer engine. The construction of the aircraft was conventional; the fuselage was of the welded steel tube type, and the wings were constructed of a wood framework. The entire aircraft except for the engine cowling, wing leading edges, and other special portions was covered with fabric. The P-6E was one of the first fighters to employ a droppable auxiliary fuel tank mounted under the fuselage and was equipped with wheel brakes and onboard oxygen equipment. The engine was liquid cooled and employed a chemical known as ethylene glycol rather than water as the coolant. This chemical is essentially the same as the antifreeze used in modern automobile engines. The drag coefficient of the Hawk was a relatively low 0.0371, and the value of the parameter $\bar{C}_F$ was 0.0098. A comparison of these coefficients and the corresponding values for the Ryan Spirit of St. Louis indicates that a well-designed biplane could be as efficient from the point of view of friction drag as a multistrutted monoplane. The lower effective aspect ratio of the biplane wing cell, however, gives a substantially lower maximum lift-drag ratio for the Hawk than for the Spirit of St. Louis.

The Hawk model P-6E made its first flight in 1931. A transitional monoplane fighter designed by Boeing was first flown in 1932. This aircraft, known as the P-26 or Pea Shooter, is shown in figure 5.13. The aircraft was a wire-

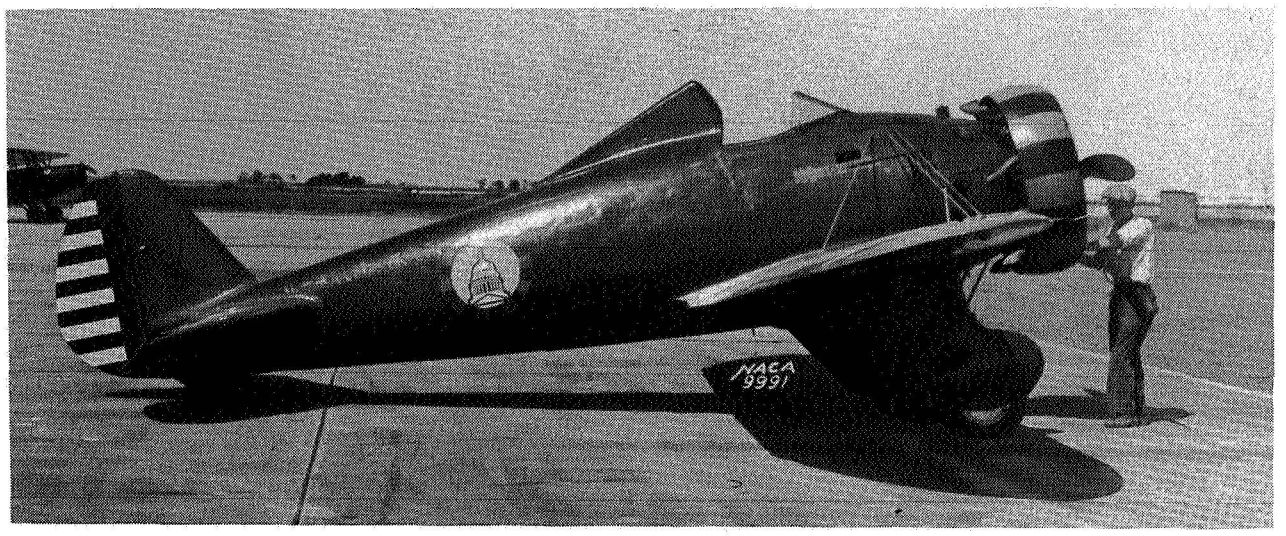


Figure 5.13.- Boeing P-26A fighter; 1932.

braced monoplane design which incorporated a fixed landing gear and open cockpit but was of all-metal construction, including the skin. The cowling around the engine, known as a Townend ring, reduced the drag of the radial engine but was not as effective as the full NACA type of cowling which was discussed in connection with the Lockheed Vega. The aircraft in its original form had a relatively high landing speed; consequently, all production versions were equipped with simple trailing-edge flaps to reduce the landing speed. This was the first fighter aircraft developed in the United States to employ landing flaps. Thus, the P-26 represented a strange collection of the old and the new in airplane design and was an anachronism when it went into production in 1934. The zero-lift drag coefficient of the Boeing P-26A, given in table 5.I, is seen to be higher than that of the Curtiss Hawk biplane fighter, although the values of the parameter $\bar{C}_F$ for the two aircraft are nearly the same. The P-26 was a transitional type of fighter and had a relatively short service life. Most of the P-26's had been recalled from first line service by the beginning of World War II, although at least one P-26 flown by a Philippine pilot is thought to have engaged a Japanese fighter in the early days of World War II.

5.3.2 Synergistic Developments

The Lockheed Vega, illustrated in figure 5.9, represented the highest level of aerodynamic efficiency to be achieved by a high-wing monoplane with fixed landing gear by the year 1930. Reduction in drag, and subsequent improvements in the performance of a monoplane such as the Lockheed Vega, could obviously be achieved by retracting the landing gear. Retraction of the landing gear on a high-drag aircraft, such as the DH-4, would result in very little improvement

in performance since the drag contribution of the landing gear was a relatively small percentage of the total drag coefficient. On an aircraft such as the Lockheed Vega, however, which was characterized by cantilever wings, highly streamlined fuselage, and efficiently cowled engine, the drag of the landing gear would be expected to be a significant portion of the total drag; hence, retraction of the gear would be expected to give a large increment in performance.

The Lockheed Orion, shown in figure 5.14, took this next step in improving aerodynamic efficiency. The Orion was a six-passenger low-wing monoplane, with



Figure 5.14.- Lockheed Orion 9D mail and passenger plane; 1931.

the pilot located in an enclosed cockpit forward of the wing. The method of construction employed in the Orion was the same as that utilized in the Vega. The low-wing configuration was particularly adaptable for the use of a retractable landing gear. The gear could be kept short and thus light, and the wing provided an ideal stowage space for the gear in the retracted position. The steerable tail wheel was also retractable in order to provide further increases in aerodynamic efficiency. The aircraft also utilized a rudimentary trailing-edge flap. The engine on this aircraft, as on the Vega, employed a single speed, geared blower to provide improved engine power output at the cruise altitudes of the aircraft. The data in table 5.I indicate that the Orion had a maximum speed of 226 mph at sea level and a cruising speed of 200 mph. The corresponding values of the zero-lift drag coefficient $C_{D,0}$ and the parameter $\bar{C}_F$ are 0.0210 and 0.0052. The values of these coefficients are seen to be remarkably low, even when compared with values for present-day aircraft; and a comparison with corresponding values for the Lockheed Vega gives a good indication

of the magnitude of the improvement in aerodynamic efficiency which was realized by retracting the landing gear. The retractable landing gear had been thought for many years to be too heavy for practical use in aircraft design; however, the spectacular reductions in drag associated with its use on an aerodynamically clean aircraft were found to far outweigh the relatively small increases in weight. The Orion first flew in mid-1931 and was produced in only limited quantities, perhaps because it was not really large enough for an airline transport; then too, there was a growing feeling that airline aircraft should be equipped with multiengines. Later in the 1930's, government regulations disallowed the use of single-engine aircraft for scheduled passenger-carrying operations.

The configuration and design details of the Lockheed Orion represented an extremely high level of aerodynamic efficiency, a level which has seldom been exceeded in the years since 1931. Yet, the Orion lacked several features which later became an integral part of the propeller-driven aircraft in its final definitive form. An aircraft with as broad a speed range as the Lockheed Orion requires some sort of variable pitch propeller in order that the desired amount of power may be efficiently extracted from the engine over a wide range of flight conditions. The full aerodynamic potential of a low-drag high-performance aircraft cannot be realized without the use of a variable pitch propeller. Such propellers became generally available and were in common use on high-performance aircraft by the mid-1930's. Another feature which the Orion lacked was an effective high-lift flap system for increasing the maximum lift coefficient and reducing the stalling speed. The aircraft had a rudimentary trailing-edge flap, but like most early flap systems, this was used primarily for increasing the drag in the approach and landing maneuver rather than increasing the maximum lift coefficient. Again, the use of effective high-lift flaps became standard practice on high-performance configurations later in the decade. Finally the use of wood as a primary material for construction had many disadvantages, and some form of light, stiff, all-metal monocoque or semimonocoque structure was desired.

One of the first aircraft developed in the United States to employ an all-metal stressed-skin semimonocoque type of structure was the Northrop Alpha, illustrated in figure 5.15. In this type of structure, the metal skin is smooth, not corrugated, and contributes significantly to the stiffness and load carrying capability of the structure. The stability of the thin metal skin is usually enhanced by numerous internal stringers attached to the skin. The Alpha employed a low wing of cantilever construction and a full NACA type cowling around the radial engine, but incorporated an anachronistic fixed landing gear together with an open cockpit for the pilot. The zero-lift drag coefficient for the aircraft is seen from Table 5.I to be about the same as that for the Lockheed Vega discussed earlier. The aircraft was used in limited numbers for mail and passenger operation, and the particular version shown in the photograph was employed for transportation of high ranking military officers. Various forms of stressed skin metal construction were destined to become the norm for propeller-driven aircraft in the years ahead.

The first aircraft which assembled most of the previously discussed desirable features in a single configuration was the Boeing 247 shown in figure 5.16. The first flight of the aircraft was in February of 1933, and airline operations were begun later that year. The enclosed cabin accommodated 10 passengers,

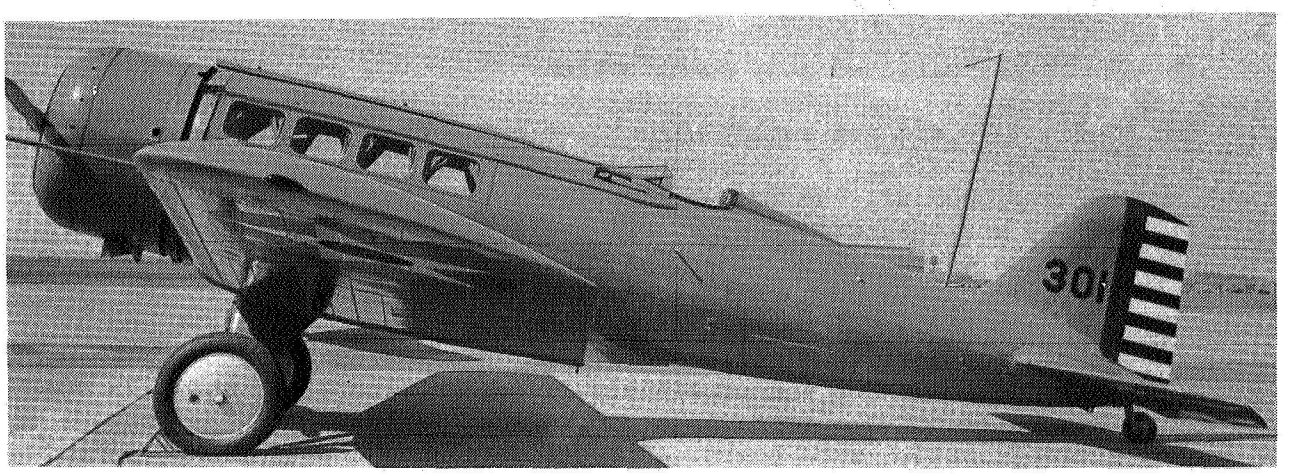


Figure 5.15.- Northrop Alpha mail and passenger plane; 1931.

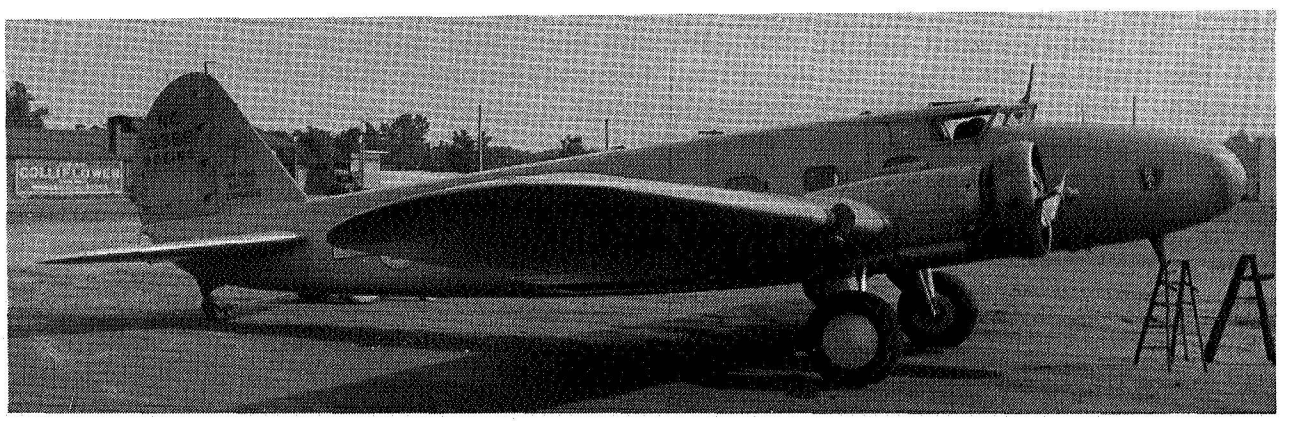


Figure 5.16.- Boeing 247 10-passenger twin-engine transport; 1933.

2 pilots, and 1 stewardess. Two 525-hp Pratt & Whitney Wasp engines were employed, and the aircraft could maintain an altitude of 6000 ft on one engine at full gross weight. The earlier models of the aircraft, such as the one shown in figure 5.16, had Townend rings on the engines and employed fixed pitch propellers. The definitive version of the aircraft, the model 247D, had both variable pitch propellers and full NACA type engine cowlings. All aircraft were later converted or retrofitted to the model 247D configuration. The synergistic design features of this aircraft are listed as follows:

(1) Cantilever wings

(2) Retractable landing gear

(3) Efficiently cowled, light radial engine

(4) Variable pitch, constant speed propellers

(5) Single speed geared supercharger

(6) All metal, stressed skin construction

The Boeing 247D did not employ wing flaps and had a relatively low, 16.3 lb/ft^2, wing loading. A contemporary and very similar aircraft, the Douglas DC-2, employed all the features mentioned for the Boeing machine and, in addition, had a higher wing loading and split type landing flaps. The model 247D was one of the first transport aircraft to employ rubber deicer boots and a significant amount of instrumentation for blind flying. The aircraft is seen from table 5.I to have a low zero-lift drag coefficient and a value of the maximum lift-drag ratio of 13.5 which compares favorably with the values of this parameter for the previously discussed aircraft. About 75 Boeing 247's were built but the type was not developed further, perhaps because of Boeing's preoccupation with bomber aircraft development during that period of time.

The Douglas DC-3 was developed from the DC-2 and is, by any measure, one of the best-known aircraft ever developed anywhere in the world. The aircraft first flew in December of 1935 and was in airline operation by the summer of 1936. It incorporated all of the advanced technical features of the Boeing 247 and the Douglas DC-2 but, in addition, was sufficiently large to carry 21 passengers. With this number of passengers and a cruising speed at 10 000 ft of 185 mph, the airlines for the first time had an aircraft with operating costs sufficiently low so that money could be made from carrying passengers without complete dependence on the revenue from airmail contracts.

A photograph of a DC-3 in flight is shown in figure 5.17. A distinctive identification feature of the aircraft is the sweptback wing which is clearly



Figure 5.17.- Douglas DC-3 21-passenger twin-engine transport; 1935.

shown in the photograph. The sweptback wing was inherited from the DC-2 and was used to position the aerodynamic center of the aircraft in the proper relationship to the center of gravity. The design of the wing of the DC-2 did not initially employ sweepback but had a highly tapered straight wing. As the design of the aircraft progressed, however, it became evident that the center of gravity was further aft than had been anticipated. Mounting the outer panels with sweepback offered a simple means for moving the aerodynamic center into the correct position. The Douglas DC-3 was powered either with two Wright Cyclone radial air-cooled engines of 1000 hp each, or two Pratt & Whitney R-1830 engines of 1200 hp each. Both the Wright and Pratt & Whitney engines had 14 cylinders arranged in two rows of seven, one behind the other. The double-row radial engine was extensively used throughout the subsequent development of large high-performance piston-engine aircraft. A comparison of the aerodynamic parameters for the Douglas DC-3 and the Boeing 247D, given in table 5.I indicates that the zero-lift drag coefficient of the DC-3 is about 17 percent higher than that for the Boeing aircraft; however, the values of the parameter $\bar{C}_F$ are quite close together. The larger zero-lift drag coefficient of the DC-3 results from the larger ratio of wetted area to wing area caused by the larger fuselage of the DC-3 which was designed to accommodate three-abreast seating as compared to two abreast for the Boeing aircraft. The value of the maximum lift-drag ratio for the Douglas DC-3, however, is 14.7 as compared to 13.5 for the Boeing machine; the higher aspect ratio of the DC-3 is responsible for the larger value of maximum lift-drag ratio. The wing loading of 25 lb/ft^2 for the DC-3, as compared to the 16 lb/ft^2 for the Boeing 247, reflects the use of split trailing-edge flaps on the DC-3 aircraft.

A total of 10 926 DC-3 type aircraft were built in the United States between 1936 and 1945. Of this total, about 10 000 aircraft were procured by the military services for their use, and many of these were later converted for various commercial activities following the end of World War II; today, 42 years after its first flight, there are still many hundreds of DC-3 aircraft in service throughout the world. The DC-3 has been used for every conceivable purpose to which an airplane can be put and surely must be considered as one of the truly outstanding aircraft developments of all time.

The Boeing B-17 bomber was a highly significant military aircraft which first flew in prototype form during July of 1935. A fully developed version of the aircraft, a Boeing B-17G utilized during World War II, is illustrated in figure 5.18. The aircraft incorporated all of the significant structural and aerodynamic design features discussed in connection with the Boeing 247D and the Douglas DC-3 but was equipped with four engines instead of two. The aircraft had a gross weight of 55 000 lb which was considered very heavy at the time of its introduction. The four engines developed 1200 hp each and were equipped with turbosuperchargers. In contrast to the gear driven, single-speed supercharger previously discussed, the turbosupercharger makes use of the energy in the exhaust gases from the engine. The supercharger blower is connected to a turbine which is driven by the exhaust gases. The fraction of the total exhaust gas which passes through the turbine can be varied by a valve in accordance with the altitude at which the aircraft is flying. Thus, the maximum rated power of the engine can be maintained up to an altitude at which all of the exhaust gases pass through the turbine; at higher altitudes, the power drops off with altitude in very much the same way as an unsupercharger engine at low



Figure 5.18.- Boeing B-17G; World War II U.S. four-engine heavy bomber; prototype first flown in 1935.

altitude. The critical altitude for the engines on the B-17, that is, the maximum altitude at which rated power could be maintained, was 25 000 ft. Experiments with turbosuperchargers had been underway for many years, but the B-17 was the first aircraft in large scale production to employ such a device. The turbosupercharged engines together with the relatively good aerodynamic parameters given in table 5.I for the B-17 gave the aircraft outstanding speed and range capability. The B-17 was used by the U.S. Army Air Forces throughout World War II as a heavy bomber. Nearly 13 000 of these aircraft were constructed, and a number of them are still employed today for various purposes.

The transformation of the military fighter aircraft into a thoroughly modern form had also taken place by 1936. The Seversky XP-35 shown in figure 5.19

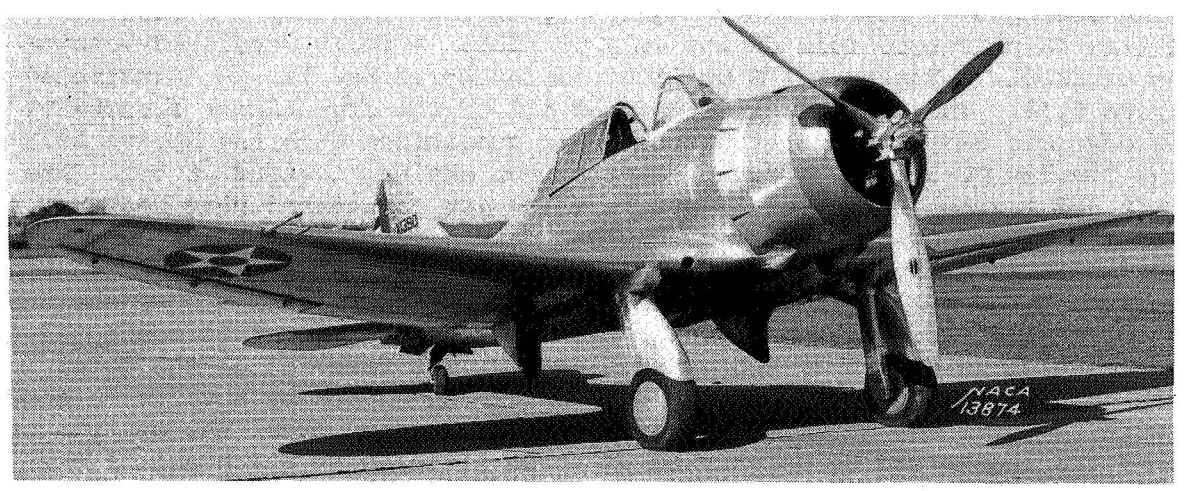


Figure 5.19.- Seversky XP-35 fighter; 1937.

was typical of the modern fighter aircraft developed in the mid to late 1930's. The XP-35 was a low-wing cantilever monoplane with a retractable landing gear, a fully cowled radial engine equipped with a geared single-speed supercharger, and a controllable pitch propeller; the enclosed cockpit was, at that time, quite an innovation in fighter design. The aircraft was of stressed skin metal construction and employed trailing-edge landing flaps. Wheel brakes and a tail wheel were also fitted. In 1939, the Seversky Aircraft Company changed its name to Republic Aviation Incorporated; thus, the XP-35 may be considered the progenitor of the famous P-47 Thunderbolt fighter of World War II. Only about 75 P-35 fighters were built in the time period between July 1937 and August 1938, at which time the aircraft was probably obsolete or obsolescent because of its relatively low horsepower. Refinements in fighter aircraft development were taking place at a rapid pace during this time although the basic configuration concept of the propeller-driven fighter aircraft changed very little from that of the P-35.

The Douglas DC-3, the Boeing B-17, and the Seversky XP-35 are seen to be representative of the definitive and final configuration of the propeller-driven aircraft concept as applied to transport aircraft, bombers, and fighters. Many aerodynamic and structural refinements lay in the future, and both radial and inline engines of ever increasing horsepower were employed, but the basic configuration of these aircraft may be thought of as something of an upper plateau in propeller-driven aircraft design.

5.3.3 General Aviation at End of Decade

As the 1930's drew to a close, the general aviation manufacturers offered the private owner and fixed base operator a variety of high priced luxurious aircraft, as well as a number of inexpensive, more austere models. Among the latter, the Piper J-3 Cub is without question the outstanding example. The prototype of the Cub which was first flown in 1931 during the early days of the great economic depression fostered the development of a number of light, low-powered, and above all, inexpensive aircraft. The aircraft was initially produced by the Taylor Aircraft Company, which was subsequently acquired by William T. Piper and became the Piper Aircraft Corporation. The original Cub was refined and improved through the years and appeared in the definitive model J-3 form in 1937. The aircraft is illustrated in figure 5.20 and is seen to be a conventional, strut-braced, high-wing monoplane equipped with a fixed landing gear. The Cub carried two people, seated one behind the other, in a small enclosed cabin, one side of which could be opened to provide cooling in warm weather. The aircraft was equipped with brakes and had a steerable tail wheel; but most of them had no electrical system, hence, no starter and, of course, no radio.

Power was supplied by a variety of engines ranging from 40 hp to 65 hp, with the 65-hp version being the most numerous. All of these engines were four-cylinder air-cooled types with the cylinders arranged so that two cylinders were oriented at 180° to the other two. This cylinder arrangement, known as a flat engine, is used almost exclusively today on modern general aviation aircraft equipped with reciprocating engines. The cylinders of the engines on the J-3 Cub protruded into the airstream to provide the necessary cooling.



Figure 5.20.- Piper J-3 Cub two-place training aircraft; 1938.

An adjustable stabilizer was provided for trimming the aircraft in flight. The Cub had no landing flaps, nor were any needed; the low wing loading of 6.8 lb/ft^2 together with the thick, high-lift airfoil section in the wing gave a stalling speed of just over 40 mph. The large air wheels on the landing gear allowed the aircraft to be safely operated from soft muddy fields. The internal structure of the aircraft was conventional and consisted of a welded steel tube fuselage, together with wings which incorporated metal spars and ribs (at least in the later models). The entire aircraft was covered with fabric. Most aircraft left the factory painted a distinctive yellow, which became almost a trademark for the Cub.

The first cost of the Cub was modest, the operating expenses were low, and maintenance was minimal. A glance at the specifications contained in table 5.I(b) shows that the performance was not spectacular, but the aircraft was completely viceless with respect to its flying and handling qualities. All of these factors made the Cub an ideal primary trainer. Thousands of pilots received their first dual instruction and made their first solo flight in the Cub during the explosive expansion of the U.S. Army and Navy Air Forces during World War II. In addition to training, the Cub was extensively used for liaison, observation, and other military duties during the conflict in Europe and Asia. About 20 000 of the J-3 type Cubs were produced, and a modernized, higher powered version, known as the Piper PA-18 Super Cub is still in production at this time. Today, the aircraft is used for crop spraying, glider towing, fish spotting, and various other utility tasks. Many thousands of these Super Cubs have also been built. Surely, the Cub and its descendants have had one of the longest production runs of any aircraft in history.

The larger, higher performance monoplane for the private owner and fixed base operator was typified by the Stinson Reliant SR-8B illustrated in figure 5.21. The Reliant represents the culmination of a large amount of expe-

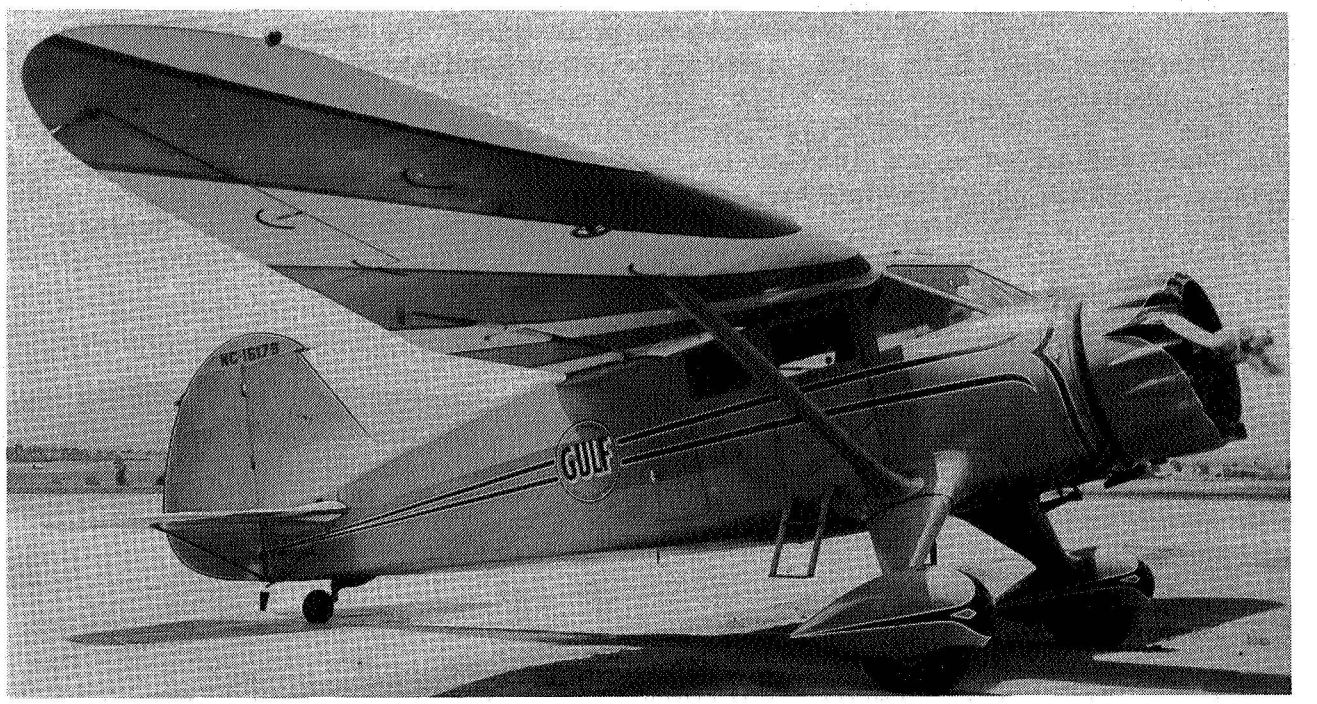


Figure 5.21.- Stinson Reliant SR-8B five-place-cabin monoplane; 1937.

rience accumulated by Stinson in the development of a long line of cabin monoplanes. The Stinson Reliant was a well-streamlined high-wing monoplane with a single strut supporting each wing and had a single strut type of landing gear with the wheels enclosed by pants. The radial engine was enclosed by a full NACA cowling and transmitted power to the air by means of a controllable pitch propeller. The luxuriously appointed cabin accommodated five people and included roll-down windows such as are used in automobiles. The aircraft had dual controls and a self-starter and was equipped with brakes, flaps, and all the latest flight instrumentation. The aircraft could be purchased with one of a number of different engines which varied in power from 245 to 450 hp. The aircraft illustrated in figure 5.21 and described in table 5.I was equipped with the Lycoming nine-cylinder radial engine of 245 hp. With this engine, the aircraft had a gross weight of 3650 lb and a cruising speed of 140 mph at 8000 ft. The performance of the Reliant is not particularly outstanding when compared with comparable general aviation aircraft today. However, the cabin of the Reliant was roomier and allowed elbow and leg room to a degree not usually available in modern single-engine general aviation aircraft. The entire structure of the aircraft was metal, with the exception of the skin which was the familiar doped fabric. During World War II, a version of the Reliant was built as a trainer for the Canadian government. Many of these aircraft reverted to

civilian status following the end of World War II. Production of the beautiful Reliant did not resume following the close of the war, and, today, examples of this aircraft are highly prized by collectors of antique aircraft.

Many biplanes manufactured during the late twenties and thirties were still in use in 1939, and several types were in production. Of these, two were high-performance, high priced, cabin aircraft. The most distinctive, and the one which represented the highest level of technology ever achieved in a biplane design, was the Beechcraft D-17. The prototype of the D-17 was first flown in 1932, and the type was continually refined and developed for many years. Production of the D-17 ended in 1948 after a total of 784 models had been produced. The aircraft is illustrated in figure 5.22 and is seen to be a highly stream-



Figure 5.22.- Beechcraft D17S four-place-cabin biplane; 1938.

lined biplane equipped with retractable landing gear, full NACA cowling around its radial engine, and only a single I-type of interplane strut between the two wings on either side of the fuselage. A minimum of wire bracing was employed between the wings. A distinctive feature of the aircraft is the negative stagger, that is, the upper wing was mounted behind the lower wing. This particular arrangement was not unique with the Beech but had been employed on such aircraft as the DeHavilland 5 and Sopwith Dolphin in World War I. However, the arrangement was rarely seen. The wing arrangement is responsible for the term "Stagger Wing Beech" by which the type is almost universally identified today. The term is not definitive, however, since most biplanes have the wings staggered, with the upper wing usually being forward of the lower wing; this arrangement is referred to as positive stagger. One may speculate on the reasons why the negative stagger wing arrangement was used in the design of the

Beech. If the landing gear is to be retracted into the lower wing, a most desirable feature, then the wing must be placed sufficiently far forward so that the landing gear is well ahead of the center of gravity of the aircraft; this location is necessary for ground stability. (The prototype and the first few aircraft produced had a short, highly streamlined, fixed gear attached to the lower wing.) To place the aerodynamic center of the aircraft in the proper relationship to the center of gravity, the upper wing must then be mounted behind the lower wing.

The Beech D-17 could be purchased with any one of a number of engines, ranging from about 200 to 450 hp. The particular version shown in figure 5.22 is the model D17S of about 1938 and was equipped with the 450-hp Pratt & Whitney Wasp Jr. engine. The aircraft was fully equipped with all of the latest innovations, including constant speed propeller, self starter, full instrument panel, and, or course, brakes. Plain flaps were also employed on the upper wing. Four passengers were accommodated in the luxuriously appointed cabin. The fuselage of the aircraft was constructed of welded steel tubing and employed wooden formers and stringers to provide the necessary streamlined shape. The wings were constructed entirely of wood, and the entire aircraft was covered with fabric. According to table 5.I, the cruising speed of the aircraft was 202 mph at 9700 ft, and the stalling speed was a relatively low 50 mph. The zero-lift drag coefficient was a very low 0.0182, and the value of the skin friction parameter C_F was 0.0050. The Beech D-17 can truly be said to represent the ultimate in biplane development.

5.4 Time of World War II, 1939-1945

The years of World War II saw extensive manufacturing, engineering, and research and development activity in the aviation industry. A similar explosive growth in aeronautical activity occurred during World War I; yet, there was a difference. World War I, as discussed in section 5.1, was characterized by experimentation of all types; different configurations, different materials and types of construction, and radically different types of engines were investigated and tested under actual combat conditions.

The final form of the propeller-driven aircraft had crystallized by the beginning of World War II, as discussed in section 5.3. All high-performance military aircraft used in World War II were designed to the same basic formula: internally braced, all metal monoplane, equipped with retractable landing gear, wing flaps, controllable pitch propeller, and enclosed compartment for the crew. This design concept was successfully applied to fighters, bombers, observation aircraft, and various other types of aircraft utilized during the war. The emphasis on research, development, and engineering was on achieving higher performance with this standard design formula. The quest was for higher speeds and altitudes, more maneuverability, longer range, better handling characteristics, and means for maintaining the landing speed within acceptable limits. These demands called for lighter weight, stronger structures, higher powered engines, and detailed aerodynamic refinement. The following section describes briefly a few representative areas of aerodynamic refinement.

5.4.1 Aerodynamic Problems and Refinements

A vast amount of aerodynamic research was conducted in the United States, Great Britain, Germany, and Italy during the years of World War II. No attempt will be made to give a complete summary or abstract of this work; however, a few examples taken from NACA research may serve to indicate the flavor of the activity. More detailed accounts of the research in aerodynamics may be found in references 5.29, 5.63, and 5.34.

5.4.1.1 Airfoils and High-Lift Devices

The low drag coefficients achieved by internally braced monoplanes equipped with retractable landing gears suggested that any further large reductions in drag could only be achieved through the maintenance of extensive laminar flow over the surfaces of the aircraft. The boundary-layer flow of contemporary aircraft was essentially all turbulent, and since the skin friction coefficients for turbulent flow are much higher than those for laminar flow, the achievement of laminar flow on the surface of the aircraft might be expected to yield large reductions in drag. For example, the skin friction coefficient on a flat plate is reduced by a factor of almost 2 as the point of transition from laminar to turbulent flow is moved from the leading edge to the 50-percent-chord location. In the late 1930's, the Langley Memorial Aeronautical Laboratory of the National Advisory Committee for Aeronautics undertook the development of special airfoils designed to achieve extensive regions of laminar flow. The problem involved extensive theoretical and experimental investigations and the development of an entirely new low-turbulence wind tunnel. The early work on laminar-flow airfoils is described by Jacobs in reference 5.50, which was originally published in June 1939. The development of laminar-flow airfoils continued throughout the years of World War II and for several years thereafter. Over 100 different airfoils were derived. The characteristics of these airfoils were published in summary form in reference 5.14, and a complete exposition of airfoil theory and presentation of airfoil aerodynamic characteristics are given in reference 5.13.

The profile shapes of two NACA low-drag airfoil sections compared with a conventional airfoil are shown in figure 5.23. The airfoils designated as NACA 66_1-212 and NACA 63_1-412 are the laminar-flow, or low-drag, sections; and the airfoil designated as NACA 23012 is a conventional airfoil designed during the 1930's. The 66_1-212 airfoil was designed to maintain laminar flow to the 60-percent-chord point, and the 63_1-412 was designed to maintain laminar flow to the 30-percent-chord point. The designation system used for these airfoils, as well as older conventional NACA airfoil sections, is described in reference 5.13. The laminar-flow sections are seen to have the point of maximum thickness located farther aft along the chord of the airfoil, as compared to the conventional section. The aft location of the maximum thickness point is associated with the need to achieve a particular type of airfoil-surface pressure distribution and is also desirable from the point of view of structural design. A comparison of the section drag characteristics of the NACA 63_1-412 airfoil and the NACA 23012 airfoil is shown in figure 5.24 in which the drag coefficient is plotted as a function of the lift coefficient for the two airfoils in both the smooth and rough condition.

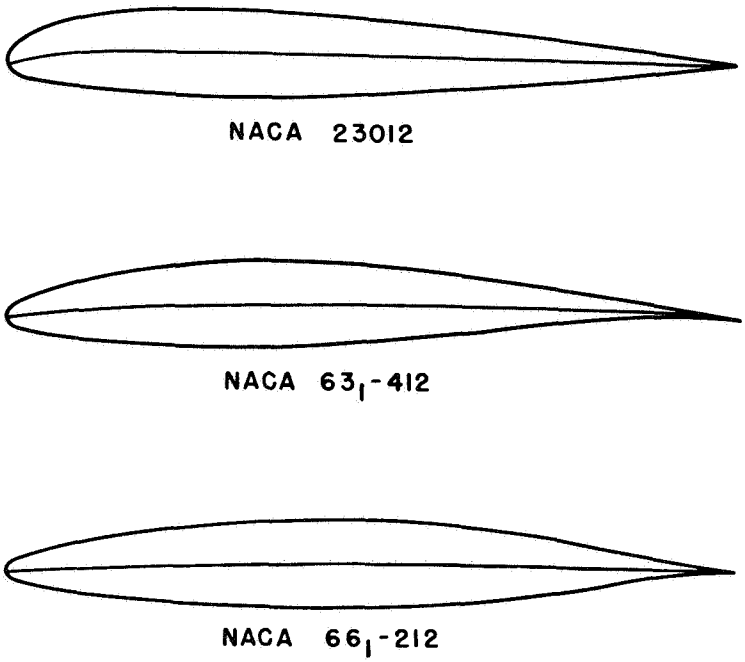


Figure 5.23.- Shapes of two NACA low-drag airfoil sections compared with the NACA 23012 airfoil section.

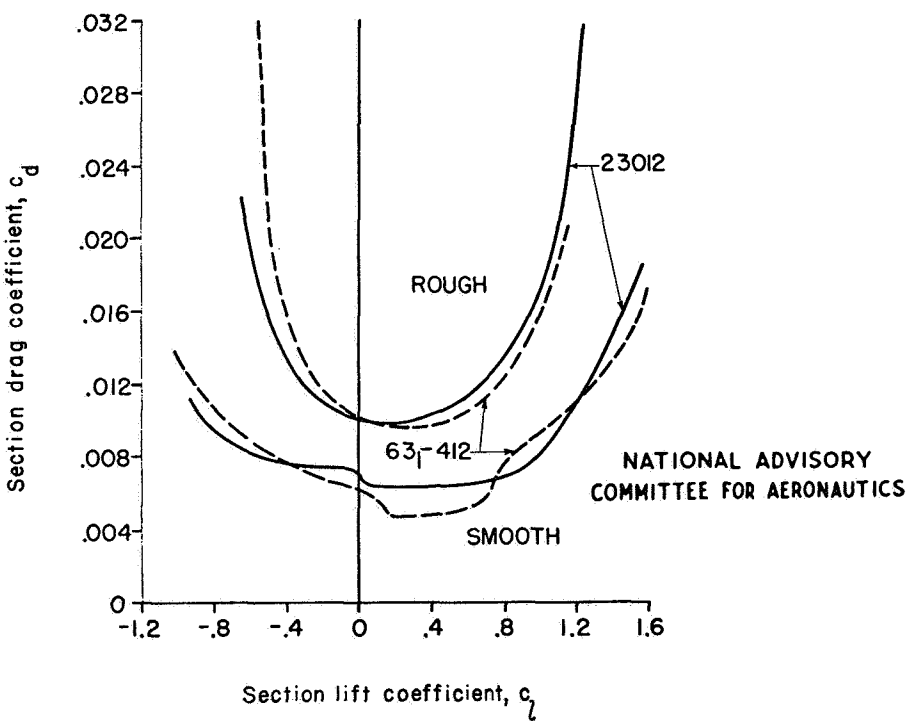


Figure 5.24.- Drag characteristics of NACA low-drag and conventional airfoil sections with both smooth and rough leading edges.

The bucket in the drag curve for the 63_1-412 airfoil corresponds to the lift coefficient range in which laminar flow is achieved. In the rough condition, the drag characteristics of the conventional and laminar-flow airfoils are very similar. The roughness employed in the test was a sand-like material which was intended to fix transition near the leading edge in a manner corresponding to a rough and poorly maintained airplane wing. The North American XP-51, which flew in prototype form in 1940, was the first aircraft to employ a laminar-flow-type airfoil section, and most subsequent high-performance aircraft designs utilized these airfoils. One of the essential requirements for achieving laminar flow is that the surface of the wings be manufactured and maintained in an extremely smooth and fair condition. (The term "fair" means that the wing surfaces must be essentially free from waves, that is, ripples, and must conform very closely to the specified contour shape.) This requirement could be met with highly accurate wind-tunnel models. Unfortunately, methods of aircraft manufacture and maintenance during World War II, and even today, were such that only very small regions of laminar flow located near the leading edge of the wing could be achieved on practical operational aircraft. As a consequence, the use of NACA laminar-flow airfoil sections has never resulted in any significant reduction in the drag as a result of the achievement of laminar flow. A practical means for achieving extensive regions of laminar flow under every-day operating conditions remains today and is one of the great challenges in aeronautical research. The NACA low-drag airfoils have seen extensive use and continue to be used on high-performance aircraft because they have better characteristics at high subsonic Mach numbers than conventional airfoil sections. (See section 5.4.1.3.) The effectiveness of the NACA laminar-flow airfoils as a means for delaying the adverse effects of compressibility at high subsonic Mach numbers is a classic example of a new technical concept developed to solve one problem, but proving highly useful in the practical solution of an entirely different one. Figures 5.23, 5.24, and 5.25 (to be discussed next) were taken from the unpublished proceedings of an NACA conference held in September 1946 for the purpose of informing representatives of the general aviation industry with the results of previously classified technical data generated during the World War II years.

As the wing loadings of high-performance military aircraft steadily increased, the desirability of maintaining the stalling speed within acceptable limits dictated the need for extensive work on high-lift devices to increase the maximum lift coefficients of aircraft. The types of trailing-edge flaps used in the mid to late 1930's were usually of the simple plain or split type. For example, the Douglas DC-3 employed simple split type flaps. Extensive studies were made of more complex high-lift devices during World War II. A summary of the state of the art of high-lift device design at the end of World War II is indicated in figure 5.25 in which the maximum lift capabilities of airfoils equipped with various types of leading- and trailing-edge high-lift devices are shown. The maximum lift coefficient of an airfoil equipped with a plain flap, split flap, single-slotted flap, double-slotted flap, and double-slotted flap in combination with a leading-edge slat are shown in figure 5.25. The use of a double-slotted flap and leading-edge slat increases the maximum lift coefficient from about 1.4 for the plain airfoil to a value slightly over 3.2. The Douglas A-26 was the first aircraft to employ a double-slotted flap, and the combination of double-slotted flap and slat was not used to any great extent until well after World War II. Many of today's jet transports employ

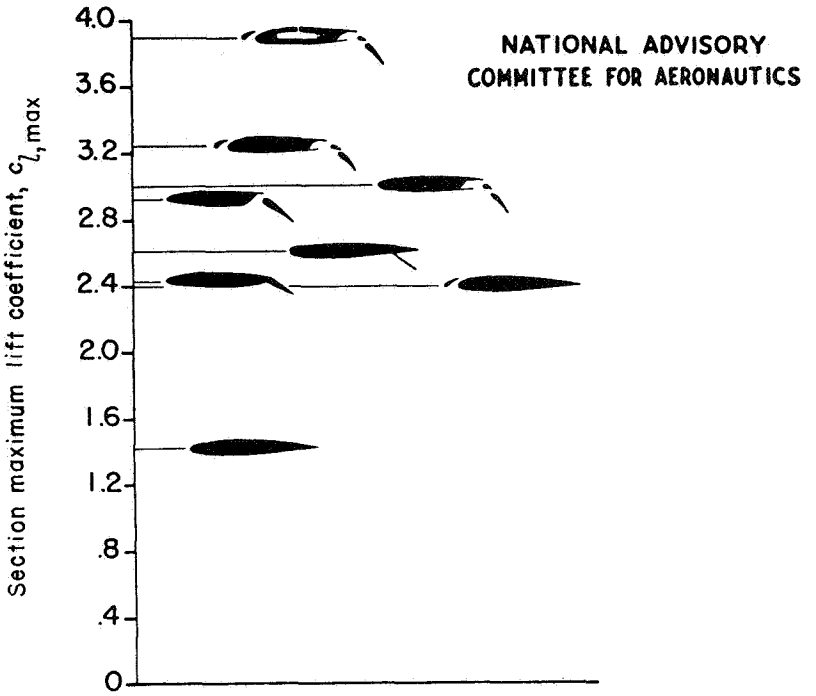


Figure 5.25.- Effect of various types of high-lift devices on airfoil section maximum lift coefficient.

double-slotted flaps or even triple-slotted flaps, in combination with leading-edge slats and flaps. The leading-edge flap is not shown in figure 5.25 since it was a German development and was not known in this country until German data became available following the end of World War II. Many general aviation aircraft of today employ either plain flaps or single-slotted flaps. The airfoil with double-slotted flaps and slats shown at the top of figure 5.25 with a maximum lift coefficient of about 3.8 employed boundary-layer suction through a single midchord slot to delay separation of the boundary layer and thus increase the maximum lift coefficient. This concept was the subject of numerous experiments in wind tunnels but has never been utilized on a production aircraft. Various types of boundary-layer blowing have been employed for improving the maximum lift coefficient. This type of boundary-layer control became practical, however, only after the development of the turbine engine.

5.4.1.2 Drag Cleanup

The internally braced monoplane with retractable landing gear, typified by the Douglas DC-3 shown in figure 5.17, would ideally be expected to have a zero-lift drag coefficient only slightly in excess of that which would be calculated with the use of the total wetted area of the airplane and a skin friction coefficient corresponding to a turbulent boundary layer. Such an ideal drag coefficient, however, is seldom achieved in actual service aircraft. The German Messerschmidt 109 fighter, for example, is shown in reference 5.46 to have a zero-lift drag coefficient which is about twice the value corresponding

to the ideal based on wetted area and a turbulent skin friction coefficient. The increases in drag above the ideal value result from one or more of the following:

(1) Projection of various items outside of the smooth basic contour of the aircraft

(2) Roughness or unevenness in the aircraft surface

(3) Unintentional leakage of air through the aircraft structure

(4) The use of large quantities of excess air for various cooling functions

Experience gained from the investigation of full-scale aircraft in the Langley Full-Scale Tunnel, a 30- by 60-foot wind tunnel, during the 1930's had given an indication of the importance of detailed design in the achievement of low drag coefficients on actual full-scale aircraft. Thus, during World War II, some 23 military aircraft were the subject of drag cleanup investigations in the Langley Full-Scale Tunnel. Individual reports were issued following the investigation of each aircraft, and two separate summary reports covering the drag cleanup work were issued by the close of World War II. Recently, the data obtained during these various investigations have been summarized again and issued as a new NASA publication, reference 5.23. The data obtained in the drag cleanup tests during World War II have been reissued in a modern report in order that they may be more available to the designers of modern general aviation aircraft.

A full-size aircraft installed in the Langley Full-Scale Tunnel for a drag cleanup investigation is shown in figure 5.26. In this case, the aircraft is

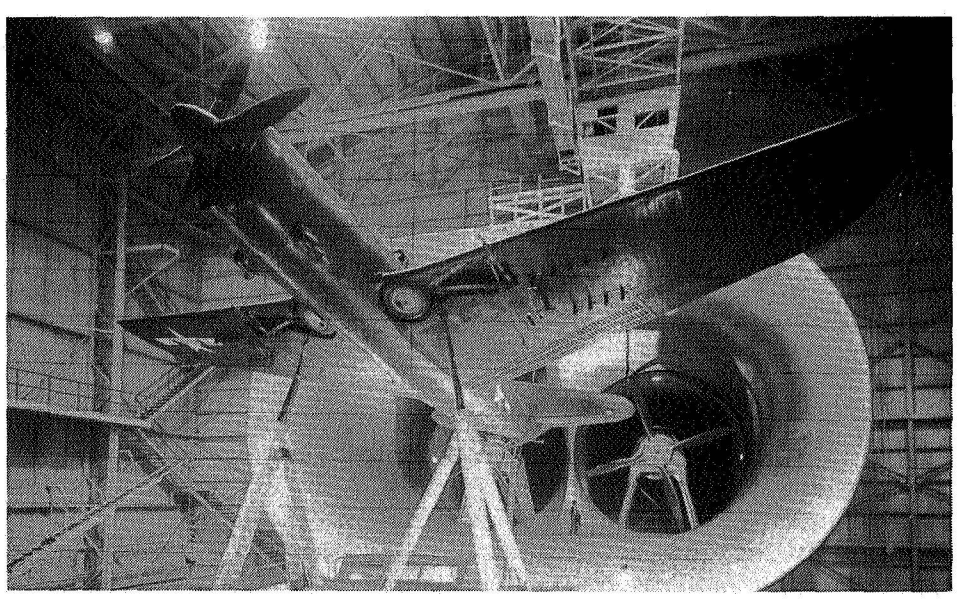


Figure 5.26.- Curtiss SB2C-4 mounted in Langley Full-Scale Tunnel for drag cleanup investigation.

a Curtiss SB2C-4 Navy dive bomber which was popularly known as the Helldiver. The aircraft is mounted on three struts, two of which are located near the longitudinal center of gravity on either side of the aircraft center line and the third is located near the tail of the aircraft. These struts are attached to scales from which the lift, drag, and pitching moment can be measured. The two large four-bladed fans visible in the background of the photograph are connected to 4000 hp electric motors which provide the power necessary to drive the tunnel. The top speed of the tunnel is about 100 mph. An indication of the size of the tunnel is shown by the two men standing on the lip of the exit bell of the open throat test section of the tunnel. The Langley Full-Scale Tunnel was first put into operation in 1931, has been continually used through the years since that date, and is still in use at this time.

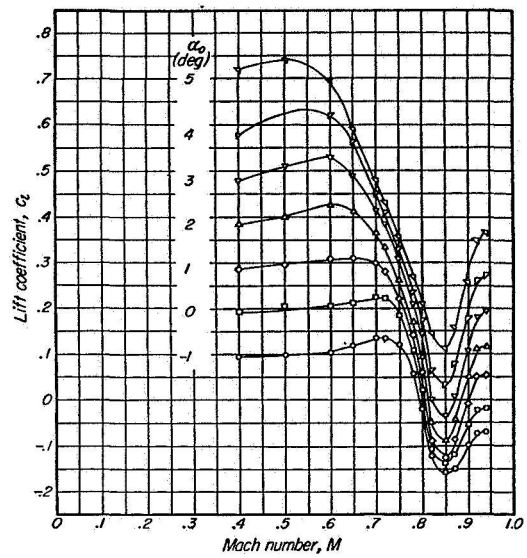
Drag cleanup investigations are still performed even today. A modern twin-engine general aviation aircraft is the most recent example of such an investigation. The procedure followed in a wartime drag cleanup study consisted of the following steps: First, the aircraft was examined in detail, those features suspected of causing unnecessary drag were identified, and necessary changes to eliminate the suspected unnecessary drag were planned. The airplane was then put in a faired and sealed condition in which all protrusions were either removed or carefully faired, all openings were closed, and all external leaks were sealed. The airplane was then returned to its service condition, item by item, and the drag was evaluated for each step. The procedure is illustrated by the results contained in table 5.III, taken from reference 5.23, which shows the sources of drag for the Seversky XP-41 aircraft. The XP-41 airplane was very similar in appearance to the Seversky XP-35 shown in figure 5.19. Table 5.III shows that the aircraft drag was evaluated for 18 different conditions, which are indicated by sketches on the left-hand side of the page and described on the right-hand side of the page. The drag coefficient of the clean airplane was 0.0166 as compared to 0.0275 for the aircraft in the service condition. In order to convert the clean configuration into a useful practical aircraft, the drag was increased by about 65 percent of the value obtained for the clean aircraft. All of the additional drag, however, was found to be unnecessary. Further tests and analyses showed that the additional drag could be reduced by more than one-half through careful tailoring of various aspects of the design. The drag coefficient of a practical service aircraft of the XP-41 type was accordingly reduced from 0.0275 to 0.0226. The data in table 5.III indicate that the increments in drag coefficient corresponding to the 18 steps of the cleanup process are generally rather small and, in many cases, only a few percent of the total drag coefficient. Yet, taken all together, these increments add up to an impressive total. Important performance improvements resulted from the drag cleanup of the 23 military aircraft in the Langley Full-Scale Tunnel. In many cases, the gains associated with care and attention to detailed design were found to be greater than the differences in drag between airplanes of different configurations. The drag cleanup work made an important contribution to the refinement of high-performance propeller-driven aircraft during World War II, and the gains resulting from the program often spelled the difference in performance between victory and defeat in the air.

5.4.1.3 Compressibility Effects

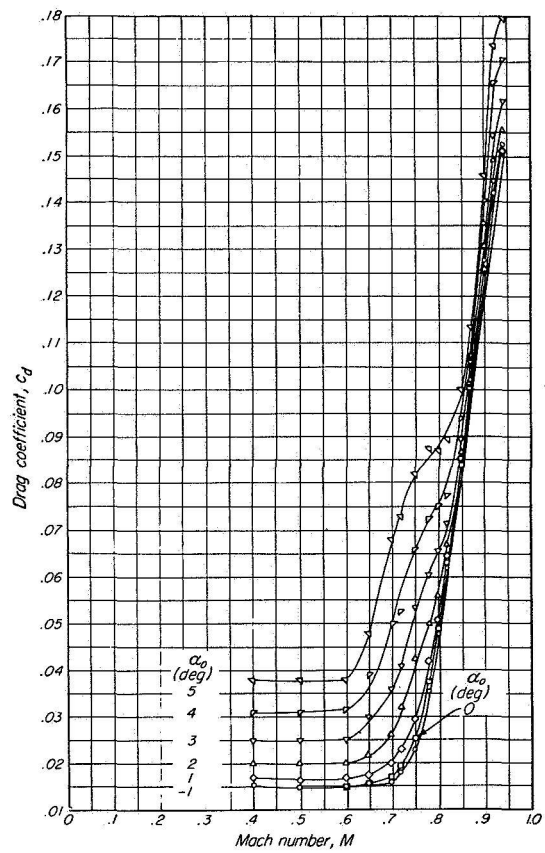
Until the late 1930's, aircraft were designed on the assumption that the air flowing over the wings and other surfaces was essentially incompressible, like water. As speeds and altitudes increased, however, the effects of compressibility on the flow over the aircraft began to assume increased importance. The ratio of the aircraft speed to the speed of sound provides a useful index for gaging the speed at which significant compressible effects begin to manifest themselves on a particular aircraft. This ratio is called the Mach number, in honor of the famous Austrian physicist Ernst Mach. The critical Mach number is defined as the aircraft flight Mach number at which the local Mach number over some portion of the aircraft, such as the upper surface of the wing for example, equals unity; that is, the flow at this point has reached sonic velocity.

Large changes in the pressures, forces, and moments acting on a wing or body occur at Mach numbers somewhat in excess of the critical value. These changes in aerodynamic characteristics result from the formation of shock waves and attendant flow separation behind the shock wave. An example of the effects of compressibility on the lift and drag characteristics of a 15-percent-thick airfoil section are shown in figure 5.27 (ref. 5.28). The section lift coefficient and the section drag coefficient are shown as a function of Mach number in figure 5.27(a) and figure 5.27(b), respectively. Precipitous reductions in lift coefficient occur with increases in Mach number beyond the critical value. The Mach number at which the lift begins to show a sharp decrease becomes smaller as the angle of attack is increased since the critical Mach number decreases with increasing angle of attack. Apparent also is the large reduction in lift-curve slope at the higher Mach numbers. For example, at a Mach number of 0.4, the lift coefficient increases from 0.2 to about 0.72 as the angle of attack varies from 0° to 5°; whereas, at a Mach number of 0.8, increasing the angle of attack from 0° to 5° results in an increment in lift coefficient of only about 0.2. The drag coefficient shows a large increase with Mach number as the Mach number is increased beyond the critical value. For example, at an angle of attack of -1°, the drag coefficient increases from about 0.015 at a Mach number of 0.65 to 0.13 at a Mach number of 0.9.

Engine cowlings, canopies, propellers, fuselages, and other aircraft components were also found to be subject to large compressibility effects. Although not shown by the data in figure 5.27, large Mach number effects were found in the pitching-moment characteristic of the airfoil and in the effectiveness of various types of trailing-edge control surfaces. The effect on the airplane of these various changes in aerodynamic coefficients manifested themselves in the form of a limiting speed, large changes in stability and trim characteristics of the aircraft, important reductions in the control power of the control surfaces, buffeting, loss in propulsive efficiency and various types of aircraft oscillation, and unintended maneuvers. In some cases, aircraft flown deep into the compressible regime became completely uncontrollable and could not be recovered. Loss of the aircraft and pilot frequently occurred under these circumstances. The state of understanding of compressibility effects in 1941 is outlined in reference 5.64 which was initially issued as a Confidential Report; a broader survey of knowledge in the field of compressibility aerodynamics is given in the Wright Brothers lecture for 1944, which is cited as reference 5.65.



(a) Section lift coefficient.



(b) Section drag coefficient.

Figure 5.27.- Lift and drag characteristics of NACA 2315 airfoil section as function of Mach number for several angles of attack. (Data from ref. 5.28.)

Extensive investigations were undertaken in the United States and Europe in an effort to better understand compressibility phenomena and, in particular, to devise design methods for increasing the value of the critical Mach number and reducing the adverse effects of compressibility which occur beyond this Mach number. These efforts were hampered by fundamental difficulties in both theoretical and experimental methods of investigation. The governing equations for flows near Mach number 1.0 proved intractable to closed form solution. Adequate solutions to these nonlinear equations were not possible until the advent of the large capacity, high-speed digital computer in the late 1960's and 1970's. Practical theoretical approaches to the compressibility problem during the war years usually involved the application of relatively simple correction factors to results obtained under the assumption of incompressible flow. These correction factors worked fairly well up to Mach numbers relatively close to the critical value but broke down completely at higher Mach numbers. The wind tunnel which had proved so useful in past aerodynamic investigations also became of questionable value at Mach numbers somewhat in excess of the critical value. At some Mach number, not too much higher than the critical value for the airfoil or body, the tunnel "choked," which meant that no higher free-stream Mach numbers could be obtained. A Mach number range between the subsonic choking value and some supersonic value, such as 1.2 or 1.3, was not available for wind-tunnel investigations. Supersonic tunnels operating beyond a Mach number of 1.2 or 1.3 were possible but were of little practical interest during the World War II time period. The solution to the problem of wind-tunnel choking was not found until the advent of the slotted and perforated throat wind tunnel in the early 1950's.

In spite of these experimental and theoretical difficulties, a good deal of progress was made in devising improved configuration concepts for high-speed flight. The laminar-flow airfoil sections which were described in section 5.4.1.1 did not achieve the desired objective of extensive laminar flow in flight; however, the pressure distributions of these airfoil shapes resulted in critical Mach numbers which were significantly higher for these sections than for other airfoil sections having the same thickness ratios. Most aircraft designed in the United States after 1940 employed the NACA laminar-flow airfoil sections or some modification of these sections, primarily because of the advantages which they offered as a means for increasing the critical Mach number. The original NACA cowling, which was developed before aircraft speeds reached high enough values for compressibility effects to be important, had a critical speed of only about 300 mph at 25 000 ft. New cowling shapes were developed which ultimately raised the critical speed to almost 600 mph. Studies of various wing body combinations led to configuration concepts which resulted in reduced interference effects and, hence, higher critical Mach numbers.

Propellers usually encounter the adverse effects of compressibility at flight Mach numbers below that at which the aircraft configuration itself penetrates the critical region because portions of the blades of the propeller, particularly near the tip, are traveling at a higher speed relative to the air than the aircraft itself. Compressibility problems on aircraft propellers were first encountered during the 1930's, and research studies were made in those years in an effort to improve propeller design. This work continued on through World War II. One major investigation which gives an indication of the type of research undertaken in the development of improved propellers is described

in reference 5.67. New planform shapes, new twist distributions, and new airfoil sections designed especially for propellers all combined to result in significant increases in the stream Mach number at which the propeller showed serious losses in efficiency. It seemed clear, however, that the propeller was likely to constitute the ultimate limitation on the speeds which could be reached with aircraft employing this means of propulsion.

The basic principles underlying the proper design of aircraft configurations intended for flight at high subsonic and transonic Mach numbers were fairly clear by the end of World War II. The need for small thickness ratios on wings and tail surfaces and high fineness ratios on bodies became increasingly evident by 1945. The P-51D airplane, one of the best of the United States fighter aircraft of World War II, employed a wing of about 15-percent thickness ratio; by contrast, the wings of transonic and supersonic aircraft of today are more likely to be of the order of 4 to 5 percent in thickness ratio. The use of wing sweepback as a means for increasing the critical Mach number and reducing the adverse effects of compressibility beyond the critical Mach number was first proposed in the United States in 1945. (See ref. 5.51.) The advantages of sweepback had been recognized in Germany at an earlier date, and the Messerschmidt ME-163 tailless rocket fighter employed a sweptback wing. This aircraft saw limited operational use toward the end of World War II but was not particularly effective as a fighter because of the capricious nature of the rocket propulsion system employed. The use of wing sweepback, together with small thickness ratios and high fineness ratios, and later combined with the transonic area rule, provided the basic configuration elements needed for successful high subsonic and transonic speed aircraft. The loss in propulsion efficiency at high subsonic Mach number remained the stumbling block to the development of successful aircraft for use at high subsonic and transonic speeds. The advent of jet propulsion solved this problem and, in addition, was capable of producing the large powers required for flight at these high speeds with a simple and light type of propulsion system. The large power producing characteristics of the turbine engine is related directly to the large air handling capability of this engine as compared to the reciprocating engine. The jet engine then became the basis for all high-performance aircraft developed after about 1945. This propulsion system when used in combination with the configuration concepts just discussed resulted in the high-performance subsonic and supersonic aircraft which are in operation today.

5.4.1.4 Flying and Handling Qualities

The stability, control, and flying qualities of aircraft were extensively studied and refined during the course of World War II. The flying qualities of an aircraft may be defined as the stability and control characteristics that have an important bearing on the safety of flight and on the pilots' impressions of the ease and precision with which the aircraft may be flown and maneuvered. For many years, there was considerable speculation as to what flying characteristics were desired in an airplane, and the entire subject was discussed in terms of the qualitative opinions of various pilots. Several years prior to World War II, a flight research program was undertaken in which the response characteristics of the aircraft following known control inputs were measured and correlated with the pilots' opinion of the behavior of the aircraft, and

finally related to the engineering parameters employed in the design of aircraft. The NACA continued the investigation of flying and handling qualities of various aircraft and, by the beginning of World War II, had assembled complete qualitative information on 12 different aircraft. From the fund of information accumulated in these tests, it was possible, in 1941, for the NACA to prepare a set of requirements (ref. 5.32) for satisfactory flying qualities in terms of qualities that had been measured in flight and could be estimated by engineers during the design of a new aircraft.

Flying qualities requirements may be listed under the broad headings of longitudinal stability and control characteristics, lateral stability and control characteristics, and stalling characteristics. The scope of flying qualities specification at that time is indicated in the following list of categories in which criteria were developed:

A. Requirements for longitudinal stability and control:

(1) Elevator control and take-off

(2) Elevator control in steady flight

(3) Longitudinal trimming device

(4) Elevator control in accelerated flight

(5) Uncontrolled longitudinal motion

(6) Limits of trim which are due to power and flaps

(7) Elevator control and landing

B. Requirements for lateral stability and control:

(1) Aileron control characteristics

(2) Yaw due to ailerons

(3) Rudder and aileron trim devices

(4) Limits of rolling moment due to sideslip

(5) Rudder control characteristics

(6) Yawing moment due to sideslip

(7) Cross wind force characteristics

(8) Pitching moment due to sideslip

(9) Uncontrolled lateral and directional motion

C. Stalling characteristics:

(1) Pitching-moment characteristics

(2) Rolling- and yawing-moment characteristics

(3) Control forces

(4) Recovery

These various categories will not be discussed in detail and are only given to indicate the extent of design criteria available at that time. Most of the control criteria involved specification of the control power, that is, the ability of the control to cause the aircraft to respond in the desired manner and control force and control force gradients which relate to the physical effort the pilot must exert in order to actuate the controls by an amount needed to give the desired response. For example, the elevator control in accelerated flight is expressed in terms of the pounds of force which the pilot must exert on the control column in order to produce an acceleration of 1g.

The U.S. Army and Navy revised the general NACA flying qualities specifications to their immediate specific requirements and looked to the NACA to continue its investigations and refinement of existing and new military aircraft. By the end of World War II, the total number of airplanes which had been studied in flight increased from 12 to 60. A good discussion of the state of understanding of aircraft stability and flying qualities at the close of World War II is given in reference 5.61. The study and refinement of aircraft flying and handling qualities has continued through the years as aircraft speeds, size, and configuration have changed and today forms a highly sophisticated branch of aeronautical engineering.

Although not a specific part of the flying qualities requirements as defined in reference 5.32, aircraft spinning and spin recovery might be briefly mentioned under category C above, designated as stalling characteristics. In 1936, the NACA put into operation at the Langley Memorial Aeronautical Laboratory the world's first vertical free-spinning wind tunnel. This tunnel (the Langley Spin Tunnel) was developed for the purpose of studying the control motions required to permit rapid and desirable recovery of an aircraft once it was in a spin and for developing stability and control criteria to be utilized in the design of aircraft so that the aircraft would have desirable spin recovery characteristics. During the war years, spin investigations were conducted in the free-spinning tunnel on approximately 150 different military airplane designs to determine recovery characteristics from developed spins. From the results of these investigations, criteria were developed for selection of proper design parameters so as to insure good spin recovery during the design process.

5.4.1.5 Summary Comments

The preceding paragraphs have described four different aspects of aerodynamic technology which were the subject of intensive research and refinement

during World War II. These are intended to serve only as typical examples of the type of detailed research and refinement which took place in all technical areas involved in aeronautical engineering. Many other aspects of the science of aerodynamics were under intensive investigation. Structures and materials were advanced and methods of mass production were developed which resulted in the output of over 95 000 airplanes in the United States during one year of World War II. Propulsion technology, including engines, superchargers, fuels, and so forth, was the subject of intensive research and development. As an example, the magnificent Rolls-Royce Merlin engine developed about 970 hp as installed in the original prototype of the Hurricane fighter; by the end of World War II, some versions of the Merlin engine developed 1600 to 1700 hp. The appearance of military aircraft changed very little in the time period between 1935 and 1945; however, the combat aircraft which existed in 1945 was far superior to its 1935 progenitor because of intensive work aimed at detailed refinement of all aspects of aeronautical design.

5.4.2 Examples of World War II Aircraft

Aircraft employed in World War II were usually designed to fill mission requirements in one or more of the following broad categories:

(1) Heavy bombers

(2) Attack and light bombers

(3) Fighters and interceptors

(4) Patrol and reconnaissance

(5) Transport and utility

(6) Training

Many aircraft specifically designed for use in one of these categories were later found to be useful in other categories with only minor modifications. There is no feasible way of describing all of the truly outstanding World War II aircraft in a short descriptive chapter such as this one. A number of the books listed in the references at the end of the chapter contain excellent detailed descriptions of the various aircraft used by the different warring powers during the period of World War II. For those particularly interested in U.S. combat aircraft, reference 5.75 is highly recommended. Fighters and bombers of World War II are described in great detail in references 5.35 to 5.40. Combat aircraft of all the nations, which saw operational service, are described in reference 5.70.

A few examples of much used United States bomber and fighter aircraft will be illustrated and described. These aircraft are representative of a vast array of very good aircraft produced by both Allied and Axis countries of World War II. The aircraft of no one country held a clear and continuing technical advantage over those of another country for very long. United States, British, and German aircraft were usually of about the same state of the art from a

technological viewpoint. Detailed refinements as discussed in the preceding paragraphs frequently spelled the difference between success and failure in combat operations. Essentially, all combat aircraft utilized in the World War II period were, as previously described, designed to the same cantilever monoplane formula with retractable landing gear, variable pitch propeller, and metal construction.

5.4.2.1 Bomber Aircraft

The Boeing B-17 Flying Fortress, which first flew in prototype form in 1935, was described in section 5.3.2 and illustrated in figure 5.18. The B-17 was one of a pair of heavy bomber types which carried out the U.S. strategic bombing offensive against Germany. The counterpart of the B-17 in this offensive was the Consolidated B-24 Liberator bomber. The B-24 was designed several years later than the B-17 and first flew as a prototype in December of 1939. The first production aircraft was delivered to the U.S. Army Air Force in 1941. The B-24 was a four-engine bomber of roughly the same gross weight as the B-17 and designed essentially for the same mission, but differed radically in appearance and design concept from the Boeing aircraft. The B-24 bomber is illustrated in figure 5.28, and the characteristics of the aircraft are given

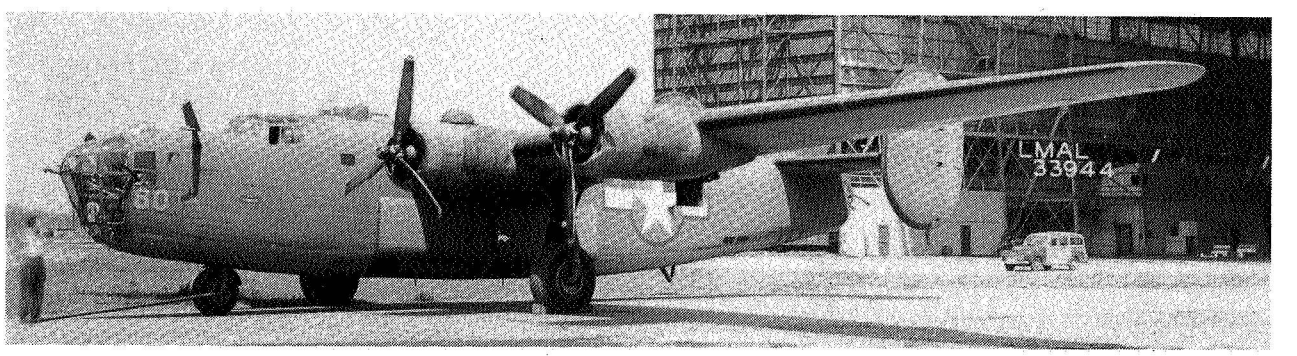


Figure 5.28.- Consolidated B-24 heavy bomber.

in table 5.I. The most distinguishing features of the B-24 as contrasted to the B-17 were the high-aspect-ratio wing mounted at the top of the fuselage, the tricycle landing gear, and the two fins and rudders. The wing of the B-24 had a very high aspect ratio of 11.55 and employed the much-publicized Davis airfoil section which, according to the popular aviation literature of the day, was supposed to provide the aircraft with unusually efficient aerodynamic characteristics. Later, wind-tunnel tests showed that while the Davis airfoil had reasonably good aerodynamic characteristics, they offered no marked superiority as compared to contemporary airfoils of that time period. The high-wing position employed on the B-24 offered the distinct advantage of allowing the bomb bay, including bomb-bay doors, to be housed directly beneath the wing which thus permitted the bomb load to be located in the optimum position with respect to the aircraft center of gravity. The high wing, however, had the disadvantage of requiring the use of relatively long heavy landing gear struts. An examination of the data given in table 5.I shows that the zero-lift drag

coefficient of the B-24 was 0.0406 as compared to 0.0236 for the B-17. Although the zero-lift drag coefficient of the B-24 was quite high as compared to that of the B-17, the maximum lift-drag ratio of the B-24 was only about 7 percent lower than that of the B-17 because of the high-aspect-ratio wing used on the B-24. The B-24 had four 14-cylinder Pratt & Whitney engines of 1200 hp each. These engines employed turbosuperchargers, just as did the Wright Cyclone engines used on the Boeing B-17. The critical altitude of the engines on the B-24 was nearly 32 000 ft. Somewhat over 18 000 B-24's were produced, and it was used as a bomber in all theatres of operation. A cargo version of the aircraft, known as the C-87, was also produced, as was a Navy patrol version known as the PB4Y.

The gross weights of the B-17 and B-24 were about 50 000 lb, and they were considered to be heavy bombers. Medium bombers and attack aircraft comprised another class of vehicle which usually had two engines and were considerably lighter than the heavy, strategic type of aircraft. They were employed for short-range bombing missions and various types of ground support activities. The United States used a number of aircraft types in the short-range bombing and ground support missions. Perhaps the best known of these aircraft was the North American B-25, known as the Mitchell, and the Martin B-26, known as the Marauder. The Martin B-26 is illustrated in figure 5.29, and some of the impor-

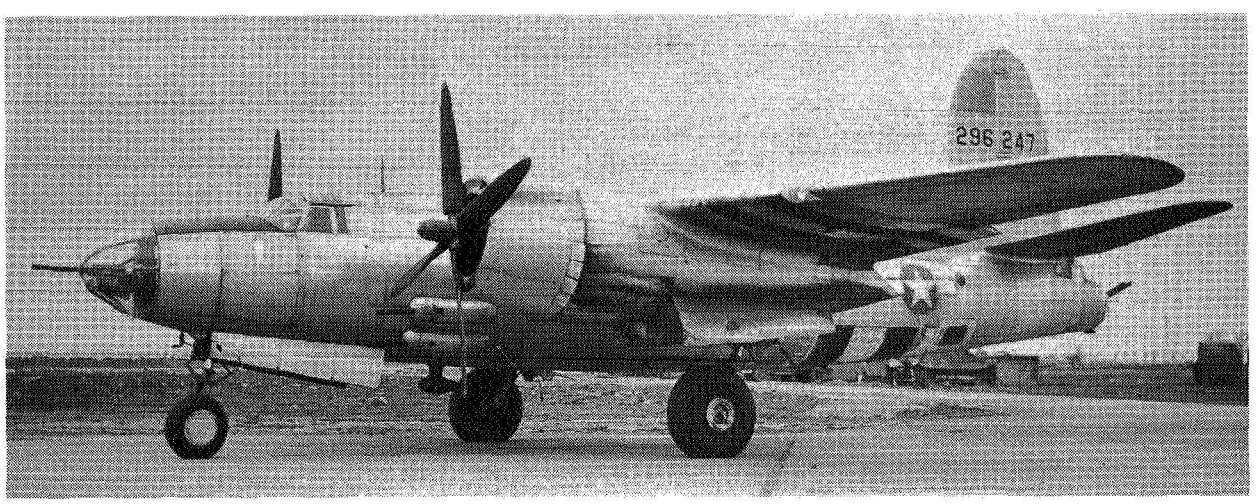


Figure 5.29.- Martin B-26F medium bomber.

tant characteristics of the aircraft are given in table 5.I. The twin-engine B-26 follows the same high-wing monoplane formula as the Consolidated B-24 just discussed and had the same type of tricycle landing gear. Both the B-25 and the B-26 had the tricycle gear, and these aircraft, together with the B-24, set the precedent for landing gear design in future Air Force bomber aircraft. The B-26 was equipped with two of the new 18-cylinder Pratt & Whitney twin-row radial engines of 2000 hp each. Since the aircraft was intended to operate at medium to low altitudes, these engines were only mildly supercharged and developed 1490 hp each at 14 300 ft. The aircraft weighed 37 000 lb fully

loaded and had, for that day, the exceedingly high-wing loading of 56.2 lb/ft^2. By comparison, the B-17 had a wing loading of 38.7 lb/ft^2, and the Seversky P-35 fighter had a wing loading of 25.5 lb/ft^2. As a result of the high-wing loading, the stalling speed of the B-26 was a very high 122 mph. The high landing speed together with certain other characteristics, made the B-26 a demanding airplane for the pilot, and many accidents occurred in training with this aircraft. As a result, the B-26 was frequently referred to by such unflattering names as "widow maker" and "the flying prostitute" (no visible means of support). The zero-lift drag coefficient of the B-26 was 0.0314 which is considerably lower than the 0.0406 of the B-24 but is about 30 percent higher than the value of 0.0236 for the B-17; the value of the skin friction parameter $\bar{C}_F$ for the B-26 is only about 20 percent higher than that for the B-17; hence, the high zero-lift drag coefficient of the B-26 is to some extent a result of the small wing area as compared to the relatively large fuselage area.

The Martin B-26 was ordered into production directly from the drawing board in September 1940, and a total of 5157 were built. The aircraft was used in both the European and Pacific theatres of operation, but was little used in the peacetime Air Force following the cessation of hostilities in 1945. The North American B-25, counterpart of the B-26, was produced in greater numbers than the B-26 and is perhaps better known today because it was the aircraft used by James H. Doolittle in the famous Tokyo Raid of April 1942. About 9800 models of the B-25 were constructed, and they served with the Air Force following World War II in a variety of training and support roles. In other countries, they remained as a primary bomber aircraft until comparatively recent years.

5.4.2.2 Fighter Aircraft

Each of the major Allied and Axis powers engaged in World War II developed a series of effective fighter aircraft. The British Hawker Hurricane and Supermarine Spitfire will long be remembered, particularly as being responsible for the air victory in the critical Battle of Britain in 1940. The famous German Messerschmitt 109 was the principal antagonist of the Spitfire and Hurricane during the battle of Britain and like these two aircraft was, together with the Focke-Wulf 190, to be the mainstay of the Luftwaffe fighter forces until the end of World War II. The Japanese Mitsubishi Zero probably is the best-remembered Japanese fighter in this country because of the role it played in the attack on Pearl Harbor in December of 1941. The North American P-51 Mustang and the Republic P-47 Thunderbolt are the best known of the U.S. Army Air Force fighters employed in World War II; the Grumman F6F Hellcat and the Vought F4U Corsair are equally well remembered for the outstanding role which they played as Navy fighters during the fierce conflicts in the Pacific area. A brief description will be given in the following paragraphs of the North American P-51 and the Grumman F6F. These aircraft are considered as typical of World War II land-based and carrier-based fighter aircraft as employed by the United States armed forces.

The North American P-51 Mustang is considered by many to represent the highest level of technical refinement ever achieved in a propeller-driven fighter aircraft. The P-51 was originally designed to a British specification for use by the Royal Air Force and was later adopted by the U.S. Army Air

Forces. The aircraft was ordered by a British purchasing commission during the hectic days of April 1940, with the understanding that the prototype was to be completed within 120 days. The prototype was completed on schedule; however, first flight was delayed until October of 1940. The aircraft first saw combat service with the RAF in July of 1942. At first, the aircraft was equipped with a 12-cylinder Allison inline engine of about 1200 hp. With this engine, the aircraft was intended as a low altitude fighter and ground attack machine. Later, the North American airframe was mated with the Britisth Rolls-Royce Merlin engine, and this combination resulted in one of the outstanding fighter aircraft of World War II. The Merlin was a liquid-cooled engine which employed 12 cylinders arranged in a V-configuration and was equipped with a two-speed two-stage gear-driven supercharger. The engine developed 1490 hp at take-off and was capable of producing 1505 hp under war emergency conditions at the critical altitude of 19 300 ft. The Merlin engine was produced under license in the United States by the Packard Motor Car Company.

The P-51 Mustang was produced in many variants of which the most numerous and best known was the P-51D which is illustrated in figure 5.30. Specifications

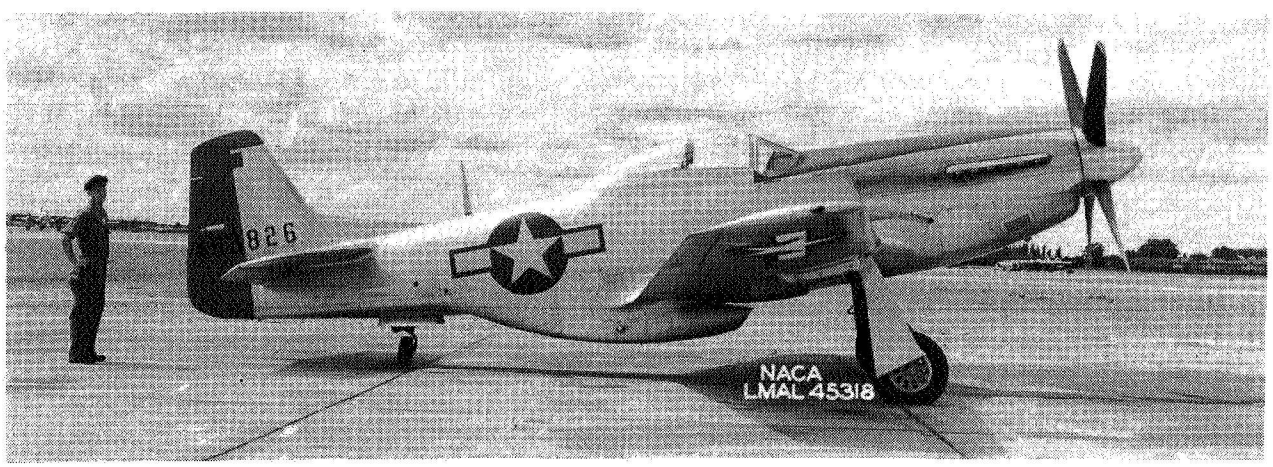


Figure 5.30.- North American P-51D fighter.

for the aircraft are given in table 5.I. The photograph shows the aircraft to be equipped with a low wing which was a highly favored wing position for fighter aircraft during World War II. The use of the inline engine of low frontal area resulted in a fuselage of relatively low total wetted area and gave the aircraft a lean streamlined appearance. The low frontal area of the inline engine was one of the chief advantages cited for this type of power plant; the disadvantage was the vulnerability of the cooling system to enemy fire. The aft location of the cooling radiator and its associated inlet and internal flow system is of interest. The system was designed with the objective of obtaining a net thrust from the cooling air as a result of heat addition from the engine coolant. This feature no doubt contributed to the very low drag coefficient of this aircraft. The P-51 was also the first aircraft to utilize the NACA laminar-flow airfoil sections which were discussed in an earlier section of this chapter. Although

it is doubtful that any significant laminar flow was achieved on production versions of the Mustang, the low-drag airfoils did provide improved characteristics at high subsonic Mach numbers.

A typical value of maximum gross weight for the P-51D was 10 100 lb, although this value varied to some extent depending upon the external armament and fuel load. The wing loading corresponding to the 10 100-lb gross weight was 43 lb/ft^2 and the power loading was 6.4 lb/hp. A typical maximum speed was 437 mph at 25 000 ft, and the stalling speed was 100 mph. The zero-lift drag coefficient of 0.0161 was the lowest of any of the aircraft analyzed herein. The corresponding value of the skin friction parameter $\bar{C}_F$ was 0.0034, and the value of the maximum lift-drag ratio was 14. The Mustang was therefore an extremely clean airplane. The aerodynamic cleanness of the aircraft was due, in large measure, to careful attention to detailed design and continued refinement of the aircraft during its production lifetime.

A total of 14 490 aircraft of the P-51 series were constructed. The aircraft was used in all theatres of operation during World War II, was called into use by the U.S. Air Force again during the Korean War, and was used by a number of foreign air forces for many years. Many P-51 aircraft are flying in the United States today as unlimited racing aircraft and even for executive transport use. A turboprop version of the Mustang has recently been proposed as a cheap, close air support aircraft for use by small, undeveloped countries in various parts of the world. An interesting history of the P-51 aircraft is given in reference 5.41.

Navy fighter aircraft are intended primarily for operations from the short decks of aircraft carriers. Operation from an aircraft carrier poses certain constraints during the design of the aircraft. For example, the relatively short length of the flight deck (about 700 ft for the larger carriers employed during World War II) imposed restrictions on the stalling speed of the aircraft and thus required that Navy fighters have somewhat lower wing loadings than their counterparts in the U.S. Army Air Forces. A tail hook must be provided to give rapid deceleration of the aircraft on touchdown, and this in turn required special strengthening of the rear portion of the fuselage. Furthermore, a carrier-based aircraft must be designed for higher landing sink rates than normally encountered in land-based aircraft; this higher sink rate requires a heavier landing gear and attachment structure. Since storage space both on the flight and hangar decks is at a premium on an aircraft carrier, provision must also be made for folding the wings so that the required parking space is reduced. A number of aircraft companies specialized in the design and production of fighters for use on aircraft carriers. The Grumman Aircraft Engineering Company was one of the leading producers of Navy fighter aircraft during the 1930's (as it still is today), and the Navy entered World War II with the Grumman F4F Wildcat as its first-line fighter.

Early in 1941, Grumman began the design of a new fighter as a replacement for the Wildcat. Much combat experience had been obtained in the European conflict and was utilized in the design of the new aircraft. Following entry of the United States in World War II in December of 1941, the Wildcat saw extensive service in combat against the Japanese. Although the Wildcat was a good air-

craft, it was not really competitive with the Japanese Zero shipboard fighter. The lessons learned in action with the Zero were also incorporated in the design of the new Grumman fighter. The prototype of this aircraft, known as the F6F Hellcat, first flew in June 1942, and deliveries of combat aircraft were made to the Navy in early 1943. The first operational use of the Hellcat was in the attack on Marcus Island from carrier USS Yorktown in August 1943. It is indeed remarkable that the aircraft could be developed from a prototype to combat status in little more than a year.

The Hellcat is illustrated in figure 5.31, and some of its characteristics are listed in table 5.I. The aircraft was a rather bulky looking low-wing mono-

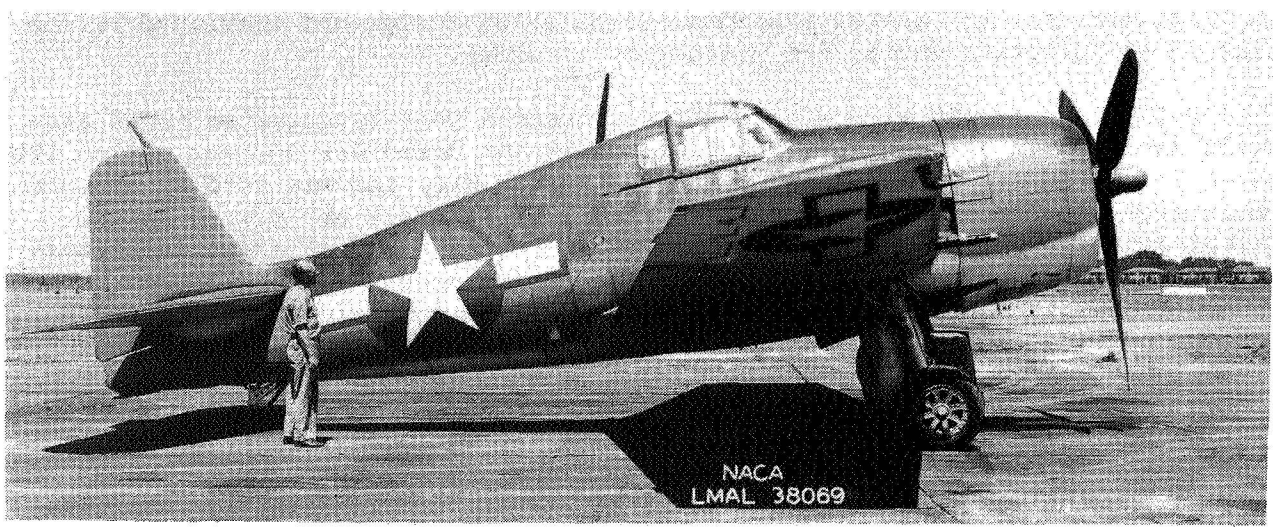


Figure 5.31.- Grumman F6F-3 fighter.

plane equipped with an 18-cylinder Pratt & Whitney twin-row radial engine of 2000 hp. The engine was equipped with a geared supercharger and gave 1970 hp at 16 900 ft. Although the U.S. Army Air Force deployed highly successful fighters with both air-cooled radial and liquid-cooled inline engines, the U.S. Navy had employed air-cooled radial engines exclusively since the mid-1920's. Apparently, the Navy felt that the advantages of simplicity and reduced vulnerability to gun fire offered by the radial engine more than offset the disadvantages of increased frontal area. Although not evident in the photograph shown in figure 5.31, the landing gear of the F6F retracted rearward and was enclosed within the wing root stubs. Outboard of the landing gear the wing could be rotated and folded aft so as to lie essentially flush along the sides of the fuselage to minimize the deck area required for storage.

The Grumman F6F was, for its day, a relatively large aircraft which had a fully loaded weight of 12 441 lb. The wing loading, however, was only 37.2 lb/ft^2 which gave a relatively modest stalling speed of 84 mph. The aircraft had a maximum speed of 375 mph at 17 300 ft. In spite of its bulky appearance, the Hellcat was a clean aircraft having a zero-lift drag coefficient of 0.0211 and a value of the skin friction parameter of only 0.0049.

The Grumman F6F Hellcat, of which 12 274 were produced, is considered by many to be the outstanding shipboard fighter of World War II. It was the standard carrier-based fighter employed by the U.S. Navy from mid-1943 until the end of World War II and accounted for the destruction of nearly 5000 enemy aircraft in air-to-air combat. The British Royal Navy took delivery of over 1100 Hellcats which were used in operations from their carriers. The Hellcat was unusual, as compared to other combat aircraft employed in World War II, in that very few modifications were made to the aircraft during its service life. The F6F served for several years in the U.S. Navy following the close of the war.

5.4.3 Summary Comments

The propeller-driven combat aircraft powered with reciprocating engines played a decisive role in World War II and reached a high level of perfection during that conflict. The revolutionary jet engine shaped the course of development of high-performance military aircraft in the post World War II period. The propeller continued, of course, to be employed on various types of utility, transport, and patrol aircraft, but the development of the jet engine spelled the end for the high-performance propeller-driven fighter, bomber, and attack aircraft. The postwar development of the propeller-driven aircraft has been primarily concerned with commercial and general aviation operations and will be considered in the next section.

5.5 Time of Maturity, 1945-1977

In the years since the end of World War II, turbojet- and turbofan-powered aircraft have come to dominate an increasingly large segment of aeronautical activity. The propeller-driven aircraft, however, continues to remain an important part of aviation, both in this country and in various parts of the world. The new propeller-driven aircraft which have appeared since 1945 differ little in configuration from those seen in the years immediately before and during World War II, nor has the level of aerodynamic refinement exceeded that of the earlier aircraft. The turboprop propulsion system is probably the most significant technical advancement to be incorporated in propeller-driven aircraft. In the realm of reciprocating engines, the supercharger has come into widespread use both in commercial transport aircraft, and in contemporary general aviation aircraft. The supercharger, together with the advent of cabin pressurization, has resulted in highly efficient cruising flight at high altitudes. High altitude operation also offers the passengers freedom from the discomfort of rough air to a degree which was not possible in unpressurized aircraft.

A few examples of propeller-driven transports of the post World War II period will be described and discussed, as will a number of contemporary general aviation aircraft.

5.5.1 Transport Aircraft

Two families of large, long-range, propeller-driven transports dominated U.S. airlines, as well as many foreign airlines, until the jet transport began

to appear in significant numbers toward the end of the 1950's. These families of aircraft, which served on both long-range domestic and international routes, were the Douglas DC-6 and DC-7 series and the Lockheed Constellation series. Both of these series of transports were derived from aircraft developed during World War II, had four supercharged engines and pressurized cabins, and both underwent large increases in size, power, and weight during their development history.

Representative of the long-range four-engine transport is the Lockheed L.1049G Super Constellation illustrated in figure 5.32; characteristics of the



Figure 5.32.- Lockheed L.1049G Super Constellation 91-passenger four-engine airliner; 1954.

aircraft are given in table 5.I. The prototype Constellation, known by its U.S. Army Air Force designation of C-69, first flew on January 9, 1943, and the model L.1049G first flew on December 12, 1954. The total number of all models of the Constellation constructed was 856.

The Lockheed L.1049G was powered by four Wright turbocompound engines of about 3250 hp each. The Wright 3350 turbocompound engine employed a two-speed gear-driven supercharger, and in addition, was equipped with three exhaust-driven turbines. The three turbines were geared to a single shaft which in turn was hydraulically coupled to the engine crankshaft. Each turbine was driven by the exhaust of six cylinders. About 15 percent of the total power of the engine was obtained from reclamation of exhaust gas energy. The specific fuel consumption was probably the lowest ever achieved in a reciprocating aircraft engine.

The gross weight of the aircraft was 133 000 lb which was more than twice that of the Boeing B-17 "heavy" bomber of World War II fame. The wing loading was 80.6 lb/ft^2, and the corresponding stalling speed was 100 mph. The wings employed very powerful Fowler type extensible slotted flaps to maintain the landing speed within acceptable limits. The landing gear was of the tricycle type which was standard on most post World War II transports. The maximum speed

of the aircraft was 352 mph, and the normal cruising speed was 331 mph at 23 000 ft. The pressurized cabin was capable of seating 71 first-class passengers or 91 coach passengers. Some versions of the aircraft were capable of carrying an acceptable payload nonstop from the East Coast of the United States to the West Coast. The zero-lift drag coefficient of 0.0211 together with the maximum lift-drag ratio of 16 indicate a highly refined and efficient aerodynamic design.

At this time, many Constellations and their Douglas counterparts are in operation in nonscheduled activities in different parts of the world. The use of these aircraft in long-range scheduled operations, however, terminated in this country during the 1960's.

The turbopropeller, or turboprop engine, is basically derived by gearing a conventional propeller to the shaft of a gas generator composed of a compressor, burner, and turbine. The turboprop engine may therefore be thought of as a turbojet engine which transmits power to the air by means of a propeller rather than through the jet exhaust. The turboprop engine is light and relatively simple, as compared to the large high-power reciprocating engines. For example, a modern turboprop engine may develop between 2 and 3 hp per pound of weight, as compared to a maximum of about 1 hp per pound for a reciprocating engine, and has been made in sizes of up to 15 000 hp. The specific fuel consumption of the turboprop engine, however, is somewhat higher than that of the best reciprocating engines. The turboprop engine has been used in a number of highly successful transport aircraft and is still in fairly widespread use.

The first civil airliner to be equipped with turboprop engines was the Vickers Viscount depicted in figure 5.33. The specifications of the



Figure 5.33.- Vickers Viscount 810 40-passenger turboprop airliner; 1948.

Viscount 700 series are given in table 5.I. The aircraft employed four Rolls-Royce Dart engines of 1600 hp each and had a gross weight of about 60 000 lb. Depending upon the configuration, 40 to 59 passengers could be carried in the pressurized cabin. The cruising speed of the Viscount was 334 mph at 25 000 ft. The aircraft employed double-slotted flaps and was equipped with a tricycle landing gear. The Viscount made its first flight in July of 1948 and subse-

quently was used by airlines all over the world. A total of 441 Viscounts were built and many are still in use.

Two turboprop aircraft of much larger size were also constructed in the United Kingdom. These were the Vickers Vanguard which had a gross weight of 146 500 lb and the Bristol Britannia which had a gross weight of 185 000 lb. Many types of turboprop transport aircraft have been designed and built in Russia. The largest passenger carrying turboprop ever built anywhere in the world was the Tupolev Tu-114. This aircraft has a gross weight of 377 000 lb and is equipped with four 14 795 equivalent shaft hp turboprop engines. Each of these engines drives two counterrotating propellers. The wings are swept-back, which is unusual for propeller-driven aircraft; the amount of sweep is 34°. The aircraft carries 220 passengers and cruises at a speed of 478 mph at an altitude of 29 500 ft. The Tu-114 is no longer in airline use, but a version known as the Bear is employed by the Soviet military forces as a reconnaissance aircraft. The Lockheed Electra is the only large turboprop airliner to be developed in the United States. Although the Electra was an efficient high-performance aircraft, it was never produced in large numbers because it was introduced at about the same time as the Boeing 707 jet airliner and could not compete with this aircraft. A few Electras are still in service with the scheduled airlines, and a number are employed in nonscheduled activities. The Naval version of the aircraft, known as the P-3 Orion, is employed by the U.S. Navy for antisubmarine patrol work.

A number of highly successful turboprop aircraft have been developed for use as cargo carriers. The largest of these aircraft is the Russian Antonov AN-22 which weighs over 550 000 lb and is equipped with four 15 000 hp engines. The Lockheed C-130 is perhaps the best known of the turboprop-powered cargo aircraft and the one which has been produced in the greatest numbers. The C-130 is used by all branches of the United States military forces and by the military forces of over 20 foreign governments. A commercial cargo version of the aircraft is also available. The first production contract for the aircraft was placed in 1952; over 1500 models of the C-130 have been built, and the aircraft is still in production.

A photograph of the Lockheed C-130 is shown in figure 5.34 and specifications are given in table 5.I. Many variations of the C-130 have been produced, and engines of slightly different power ratings have been employed. The specifications in table 5.I are for the C-130E. The aircraft has an unswept wing mounted in the high position at the top of the fuselage and is equipped with four Allison T-56 turboprop engines of 4910 equivalent shaft horsepower each at take-off. In order to minimize weight and complexity, the landing gear is retracted into blisters located on either side of the fuselage, rather than into the wing or engine nacelles. The high wing position is advantageous for a cargo aircraft because it allows trucks and other types of equipment to move beneath the wing, and the fuselage can be brought close to the ground without causing interference with the engines and propellers. A rear loading door may be deployed from the bottom of the upswept, aft portion of the under side of the fuselage. The proximity of the forward portion of the fuselage to the ground results in a loading door, with only a small inclination to the ground so that vehicles can be readily driven or pushed into the aircraft. The Lockheed

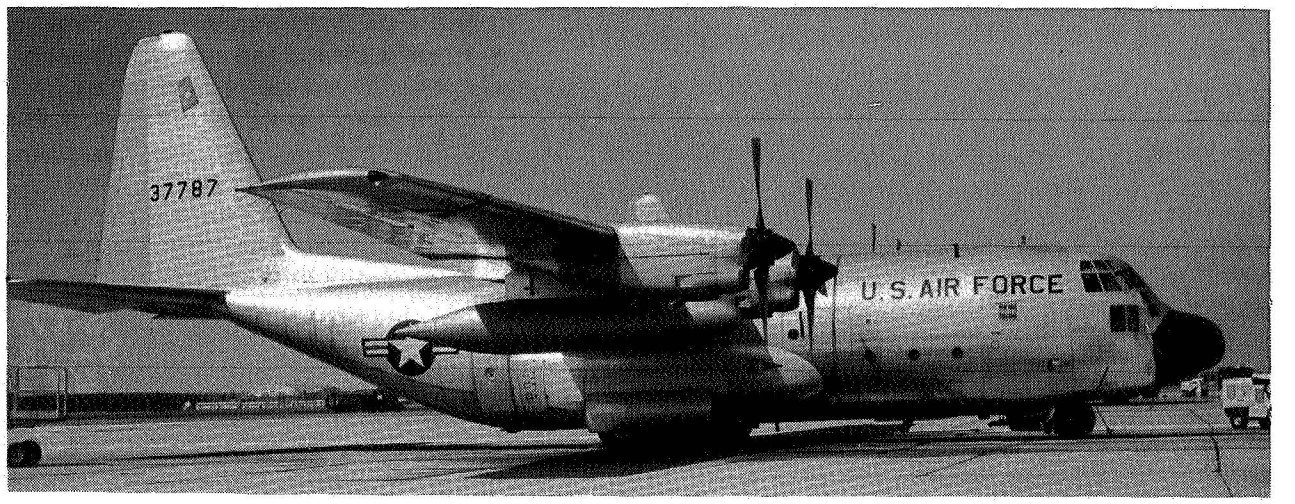


Figure 5.34.- Lockheed C-130 turboprop cargo transport; 1955.

C-130 has a gross weight of 155 000 lb and cruises at a speed of 386 mph at 20 000 ft. The wing loading is about 80 lb/ft^2, and the landing speed is 115 mph.

A great variety of twin-engine airliners have been developed both in the United States and abroad during the postwar years. These aircraft are smaller than the large, long-range, four-engine aircraft which have been described and are employed on short-haul types of operations. Twin-engine airliners have been developed with both reciprocating and turboprop engines. The twin-engine Martin 404 and Convair 440 aircraft, and earlier versions of these machines, were perhaps the most used postwar twin-engine transports powered with reciprocating engines. These aircraft are similar in configuration to the Douglas DC-3 but are larger, faster, and are equipped with pressurized cabins; in addition, they both employ the tricycle type of landing gear. The Fairchild F-27 (a Dutch Fokker design built under license by Fairchild in this country) and the Japanese YS-11A are probably the best known turboprop twins in the United States. The British Hawker Siddeley 748 turboprop-powered twin-engine airliner is widely used in many countries of the world.

5.5.2 General Aviation Aircraft

The term "general aviation" covers all types of flying except military and airline operations. Only contemporary aircraft designed for business and pleasure will be considered here. General aviation aircraft, designed for business and pleasure, are available in both single-engine and twin-engine models; most models are equipped with horizontally opposed reciprocating engines. However, several high-performance turboprop types are offered. Single-engine types may be had, with high- or low-wing location, retractable or fixed landing gear, constant speed or fixed pitch propeller, and in sizes varying from two place to seven place. The twin-engine aircraft usually employ the low-wing location

and have retractable landing gear and constant speed propellers. The twins may be had with or without turbosupercharging, with or without pressurized cabins, and with varying seating capacities. The modern aircraft designed for business or pleasure is almost invariably of all-metal construction, as contrasted to the metal, wood, and fabric construction typical of the pre-World War II general aviation aircraft. Reliability of the internal systems employed in the aircraft and the precision of the radio and navigational equipment have greatly improved as compared to the pre-World War II standards. The general aviation aircraft of today is almost universally equipped with an electrical system to power the radios and other types of equipment installed in the aircraft and to operate the self-starter. Hand starting of production aircraft is a thing of the past. The cabins of these aircraft are generally relatively comfortable, are equipped with heaters for wintertime and high altitude use, and are sometimes equipped with air conditioning for use on the ground and at low altitudes in the summer. The open cockpit is a thing of the past in production aircraft, except for special sport and aerobatic aircraft. Many aircraft employ complete instrumentation and communication equipment for flight under IFR conditions. Most contemporary aircraft employ a tricycle gear which greatly eases the problem of aircraft handling on the ground. The basic aerodynamic configuration of contemporary general aviation aircraft, however, differs little from those in use in 1939.

5.5.2.1 Contemporary Types

General aviation aircraft are manufactured in a number of different countries; however, the majority of these aircraft are produced within the United States. The major producers in the United States are the Cessna Aircraft Company, the Piper Aircraft Corporation, and the Beech Aircraft Corporation. Each of these major producers offers a wide variety of aircraft designed for various needs and markets. Six aircraft of different levels of performance, size, and price, offered by these manufacturers for different segments of the market, will be briefly described.

Two single-engine aircraft representative of the lower performance and price spectrum are shown in figures 5.35 and 5.36. The Piper Cherokee 180, shown in figure 5.35, is an all-metal aircraft having an internally braced, cantilever wing mounted in the low position. The aircraft shown has four seats and is equipped with a 180-hp four-cylinder Lycoming engine of the opposed type. The engine drives a fixed pitch propeller. The landing gear on the aircraft is fixed, and although not visible in the photograph, the horizontal tail employed on the Cherokee is of the all-moving type equipped with a geared tab. The Cherokee 180 has a maximum speed of 148 mph at sea level and cruises at 141 mph at 7000 ft. The stalling speed with the split flaps deflected is 61 mph. The gross weight of the aircraft is indicated in table 5.I to be 2450 lb. The Cherokee 180 is representative of one of the lower cost members of a complete family of Piper aircraft which carry the Cherokee name. Some of these aircraft have six or seven seats and more powerful engines which drive constant-speed propellers. Other versions of the Cherokee employ a retractable landing gear. The flight of the first production aircraft was made in February of 1961, and well over 25 000 Cherokees of all types have now been produced.

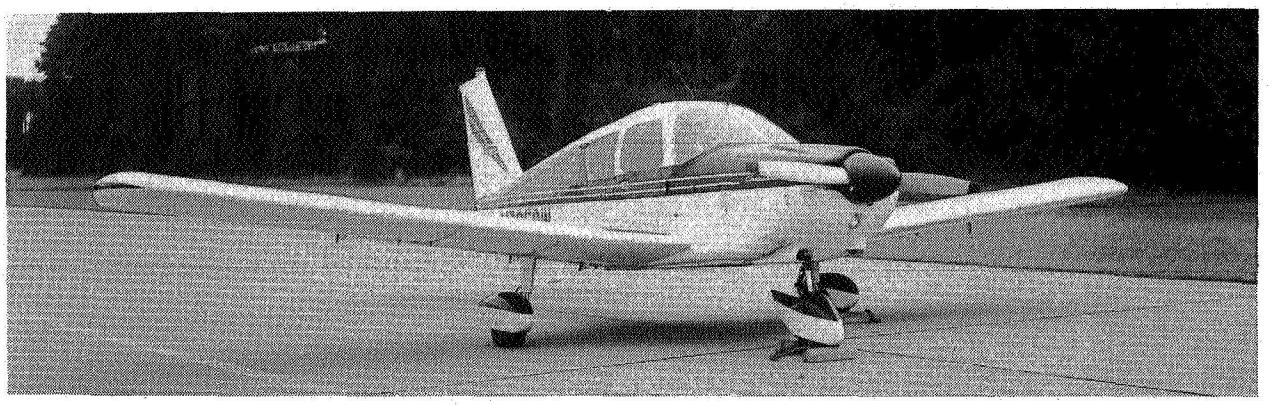


Figure 5.35.- Piper Cherokee 180 contemporary general aviation aircraft.

The Cessna Skyhawk, shown in figure 5.36, is one of the lower cost members of an entire series of Cessna aircraft of the same basic configuration. The



Figure 5.36.- Cessna Skyhawk contemporary general aviation aircraft.

Skyhawk, like the Cherokee 180, is equipped with a fixed tricycle landing gear and has a four-cylinder, horizontally opposed engine driving a fixed pitch propeller. Unlike the Cherokee 180, however, the Cessna Skyhawk is a high-wing configuration with a single wing strut on either side of the fuselage to brace the wing. The Skyhawk has a maximum speed of 144 mph and cruises at 138 mph at 8000 ft. The stalling speed with the flaps deflected is 49 mph. The gross weight of the Cessna Skyhawk is 2300 lb, and the wing loading and power loading are 13.1 lb/ft^2 and 15.33 lb/hp, respectively. These values are in the same order as those shown in table 5.I for the Piper Cherokee. The zero-lift drag

coefficient of the Skyhawk is 0.0319 as compared to 0.0358 for the Cherokee, and the maximum lift-drag ratios for the two aircraft are 11.6 and 10.0, respectively.

Two representative high-performance single-engine general aviation aircraft are shown in figures 5.37 and 5.38. The Beech Bonanza V-35, shown in figure 5.37, is of all-metal construction, has an internally braced wing mounted



Figure 5.37.- Beech Bonanza V-35B contemporary general aviation aircraft.

in the low position, has single-slotted flaps, and is equipped with a fully retractable tricycle landing gear. The aircraft is equipped with a six-cylinder, horizontally opposed, Continental engine of 285 hp which drives a constant-speed propeller. The aircraft can be configured for four, five, or six seats. Data for the Bonanza are given in table 5.I. The unique Butterfly tail combines the stability and control functions of both the conventional vertical and horizontal tails. The gross weight of the aircraft is 3400 lb. The aircraft has a maximum speed of 210 mph at sea level, cruises at 203 mph at 6500 ft, and has a stalling speed of 63 mph. The zero-lift drag coefficient is a very low 0.0192, and the corresponding maximum lift-drag ratio is 13.81. The prototype of the Bonanza first flew in December of 1945, and the aircraft has been continuously in production since 1947. Approximately 10 000 Beech Bonanzas have been built.

The Cessna Cardinal RG II, shown in figure 5.38, is a high-performance aircraft which has an internally braced wing mounted in the high position. The aircraft is equipped with a fully retractable tricycle landing gear and is equipped with a four-cylinder, horizontally opposed, Lycoming engine of 200 hp which drives a constant speed propeller. The Cardinal is of all-metal construction and is equipped with trailing-edge flaps and an all-moving horizontal tail employing a geared trim tab. The aircraft has a maximum speed of 180 mph at sea level, cruises at 171 mph at 7000 ft, and has a stalling speed of 57 mph. The aircraft weighs 2800 lb. The zero-lift drag coefficient of the Cardinal is 0.0223, and the corresponding maximum lift-drag ratio is 14.22.



Figure 5.38.- Cessna Cardinal RG II contemporary general aviation aircraft.

The first twin-engine aircraft designed specifically for business use was probably the Beech Model D-18 which was first produced in 1937. This aircraft was similar to the Douglas DC-3 in general appearance, although much smaller, and was in continuous production from 1937 until the early 1970's. A wide variety of twin-engine aircraft of various sizes and with different levels of performance are now offered for business use. Two contemporary twin-engine aircraft are shown in figures 5.39 and 5.40.

The Cessna 310 shown in figure 5.39 is representative of one of the smaller contemporary twin-engine aircraft offered for business use. The aircraft is a



Figure 5.39.- Cessna 310 contemporary twin-engine general aviation aircraft.

low-wing configuration with an engine mounted in each wing on either side of the fuselage. The aircraft can be had with both normally aspirated engines or with turbosuperchargers. The specifications and performance given in table 5.I are for the aircraft without turbosupercharging. The engines are six-cylinder, horizontally opposed, Continental engines of 285 hp each which drive constant-speed, full feathering propellers. The aircraft normally has a seating capacity of five but can be configured for six. Maximum speed is 238 mph at sea level, and cruising speed is 223 mph at 7500 ft. The wings are equipped with split flaps which with a wing loading of 30.7 lb/ft^2 result in a landing speed of 77 mph. The gross weight of the aircraft is 5500 lb. The Cessna 310 has a zero-lift drag coefficient of 0.0267 and a maximum lift-drag ratio of 12.95. The Cessna 310 was first flown in January of 1953 and has been in continuous production ever since that time. The aircraft is unpressurized and may be thought of as the smallest of a whole line of Cessna twins, both pressurized and unpressurized.

The Beech King Air 200, shown in figure 5.40, is an example of a new, relatively large, high-performance twin-engine business aircraft. Provision



Figure 5.40.- Beech Super King Air 200 contemporary twin-engine turboprop general aviation aircraft.

is provided for 2 pilots and 6 to 13 passengers, depending on the configuration. The cabin is pressurized to permit comfortable cruising flight at high altitudes. Power is provided by two Pratt & Whitney PT6A-41 turboprop engines of 850 shaft hp each. The engines drive constant-speed, full feathering, reversible propellers. The low-wing configuration of the aircraft is conventional although the use of a T-tail on a straight-wing propeller-driven aircraft is somewhat unusual. The use of this tail arrangement is said to reduce both vibration resulting from the slipstream of the engines and trim changes with flap deflection. The aspect ratio of the wing is 9.8 which must be considered as relatively high for any aircraft. The King Air 200 has a maximum speed of 333 mph at 15 000 ft and a maximum cruising speed of 320 mph at 25 000 ft. The aircraft is equipped with single-slotted flaps which together with a wing loading of 41.32 lb/ft^2 give a stalling speed of 92 mph. The gross weight of the

aircraft is 12 500 lb. The Beech King Air 200 was certified in December of 1973 and is now in series production.

5.5.2.2 Other Types of General Aviation Aircraft

The six aircraft just described may be considered as representative of generic classes of aircraft designed for business and pleasure use. In order to gain a true appreciation of the wide variety of such aircraft offered today, the reader is referred to the current year's issue of Jane's All The World's Aircraft. Other types of aircraft of interest and not described here are specially designed agricultural aircraft intended for spraying and dusting crops. These aircraft will also be found in Jane's, as will many types of sport and aerobatic aircraft. Another segment of general aviation aircraft is made up of the so-called home builts. These aircraft, where are built by individuals or clubs at home, are gaining in popularity and are flown in relatively large numbers in this country. They are usually not certified under any of the pertinent Federal Air Regulations, but rather, operate in an experimental category. Many of the more popular types of home-built designs are also described in Jane's All The World's Aircraft.

5.6 Design Trends

To summarize briefly the progress in aircraft design since 1918, the variation with years of a number of important aircraft design and performance parameters will be discussed in the following paragraphs. Parameters to be discussed are:

(1) Maximum speed, V_{max}

(2) Stalling speed, V_S

(3) Wing loading, W/S

(4) Maximum lift coefficient, $C_{L,max}$

(5) Power loading, W/P

(6) Zero-lift drag coefficient, $C_{D,0}$

(7) Skin friction parameter, $\bar{C}_F$

(8) Maximum lift-drag ratio, $(L/D)_{max}$

The values of each of these parameters, obtained from table 5.I are plotted against the appropriate year in figures 5.42 to 5.49. All of the parameters could not be obtained for some of the aircraft; in particular, the zero-lift drag coefficient, skin friction parameter, and the maximum lift-drag ratio could not be determined for a number of the aircraft because of insufficient performance data from which to make the desired calculation. The symbols identifying each aircraft are given in figure 5.41 and have been used through-

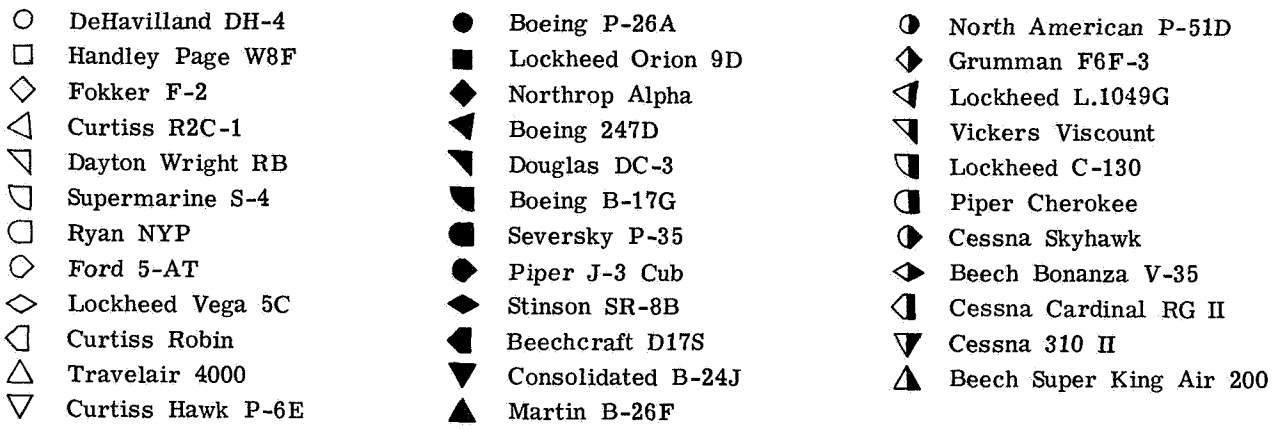


Figure 5.41.- Symbols used in figures 5.42 to 5.49.

out the subsequent figures. The order in which the aircraft are listed in figure 5.41 follows the order in which the characteristics were given in table 5.I. The year for which the characteristics of a given aircraft are plotted is in some degree arbitrary. For example, most of the World War II aircraft characteristics are plotted for the year 1942. In other cases, aircraft which were used for a number of years are shown at a year corresponding to the first year of production, or after the aircraft had achieved a fully developed status. The points for the different aircraft show a large spread in the different figures; hence, lines representing an upper and lower bound are shown on each figure. (The shape of these bound lines may be varied according to the manner in which the data are interpreted. The lines shown are only suggested fairings of the data points presented.) One of these bounds corresponds to aircraft developed with the highest technology available at a particular time, and the other is for aircraft of a relatively low and slow changing level of technology. Neither of these bounds represents boundaries of maximum and minimum values but, rather, corresponds to higher and lower levels of technology for operational aircraft of a particular time period. No data for racing or special performance aircraft are given.

5.6.1 Maximum Speed

Trends in maximum speed of propeller-driven aircraft are shown as a function of time in figure 5.42. The maximum speeds of high-technology operational aircraft are seen to increase steadily from about 125 mph in 1920 to nearly 450 mph in the World War II years. The maximum speed shown is for the P-51D aircraft which achieved a speed of 437 mph at 25 000 ft. Late in the war, a Republic P-47J achieved a speed in level flight of 507 mph at 34 000 ft. The upper bound through the years follows closely the advancement of fighter type aircraft. No increases in speed of operational propeller-driven aircraft have been achieved since the end of World War II, nor are any significantly increased speeds likely to be achieved in the future because of the inherent limitations imposed by the effects of compressibility on the efficiency of conventional propellers. The lower bound in figure 5.42 shows an increase in speed from about 80 mph to about 130 mph from 1920 to 1976. This bound indicates a continued

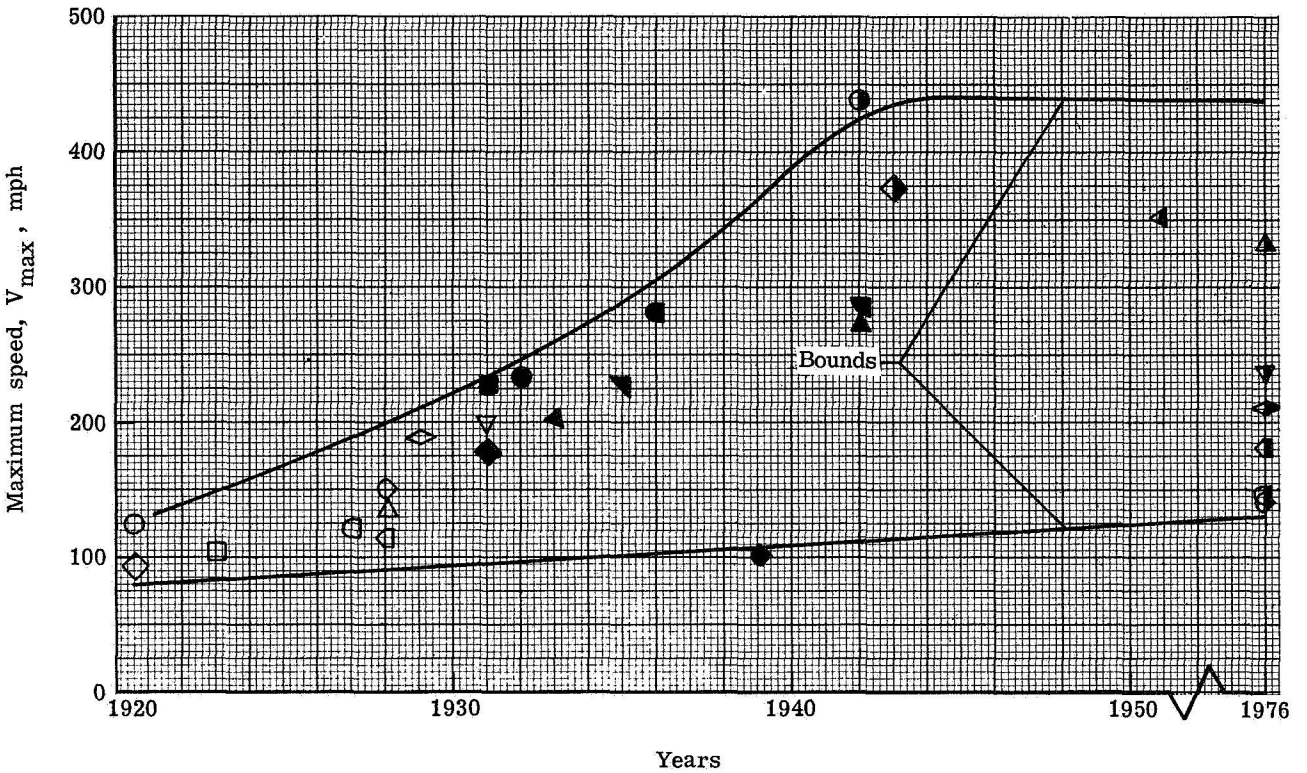


Figure 5.42.- Trends in maximum speed of propeller-driven aircraft.

desire for low-performance aircraft throughout the years. The general aviation aircraft of today are seen to encompass a range of maximum speed from about 130 mph to almost 350 mph, which indicates the wide range of technical sophistication in contemporary propeller-driven aircraft.

Although not shown in the data presented in figure 5.42, the performance of specially built racing aircraft through the years may be of some interest and is indicated as follows:

(1) 1931 seaplane speed record of 407 mph established by British Supermarine S-6B racer

(2) 1932 land plane speed record of 294.38 mph established by American Gee Bee model R-1 racer

(3) 1934 seaplane speed record of 440.7 mph established by Italian Macchi-Castoldi MC-72 racer

(4) 1938 land plane speed record of 469.22 mph established by German Messerschmitt 209V1 racer

(5) 1969 land plane speed record of 483.041 mph established by highly modified American Grumman F8F fighter aircraft

5.6.2 Stalling Speed, Wing Loading, and Maximum Lift Coefficient

The stalling speed, wing loading, and maximum lift coefficient are shown as a function of years for the various aircraft in figures 5.43, 5.44, and 5.45.

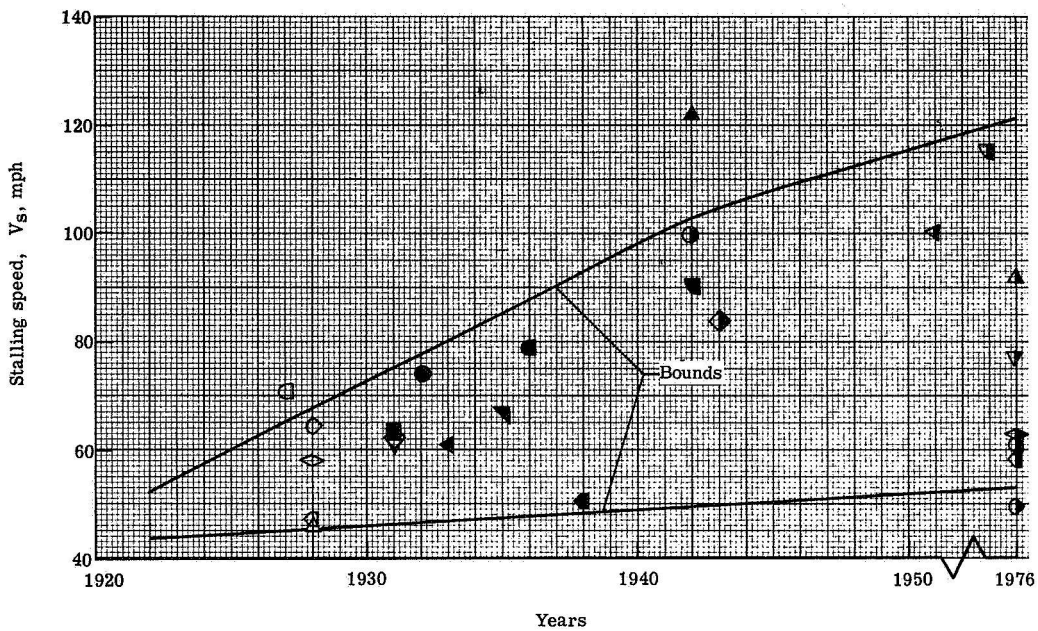


Figure 5.43.- Trends in stalling speed of propeller-driven aircraft.

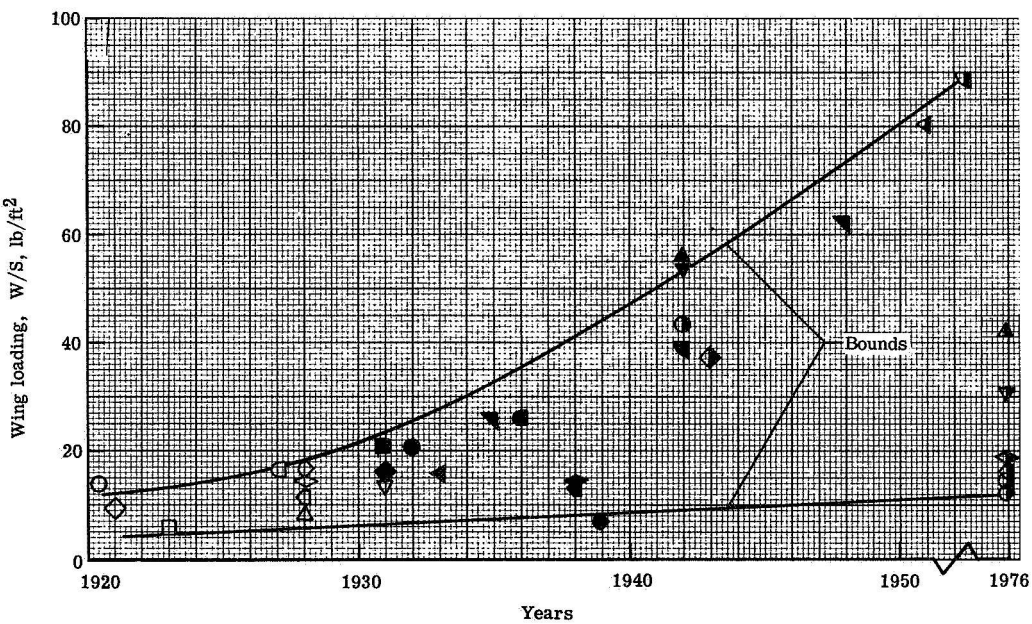


Figure 5.44.- Trends in wing loading of propeller-driven aircraft.

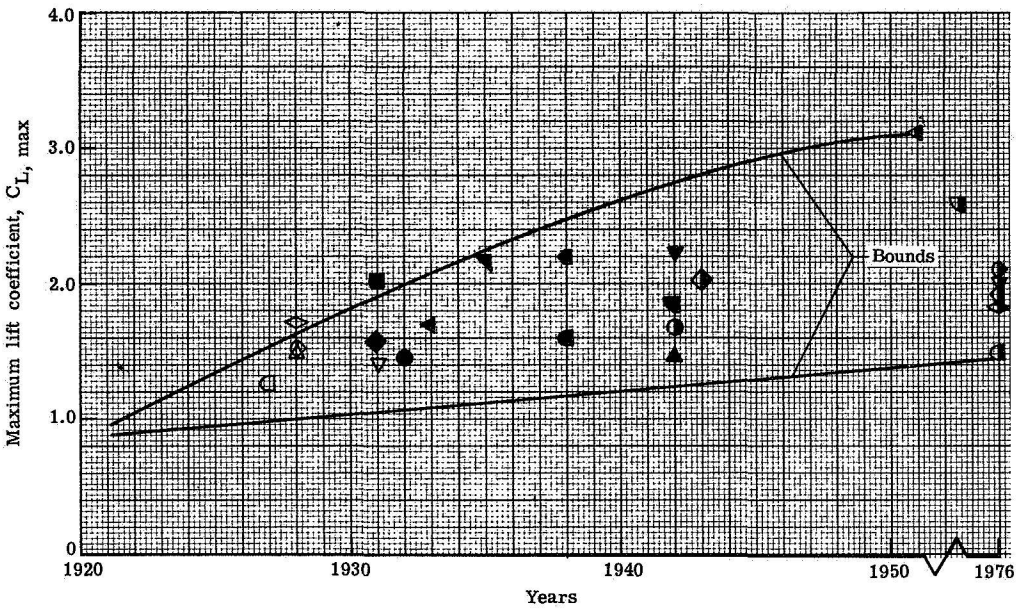


Figure 5.45.- Trends in maximum lift coefficient of propeller-driven aircraft.

The short, unpaved fields which served as airports in the early 1920's, together with the relatively poor flying characteristics of aircraft of that period, dictated the necessity for low values of the stalling speed. Values of the stalling speed of 35 to 40 mph were not unusual although precise data are not shown in figure 5.43 for the year 1920. High-lift devices were essentially unknown at that time; hence, the wing loadings needed to give the low values of the stalling speed were correspondingly low, as shown in figure 5.44. Values of the wing loading from 5 to 10 lb/ft^2 were typical, and the 14-lb wing loading of the DH-4 was considered high in 1920. For a given atmospheric density, the wing loading is, of course, related to the square of the stalling speed by the value of the wing maximum lift coefficient. Values of the maximum lift coefficient slightly in excess of a value of 1 were typical of unflapped aircraft in 1920, as shown in figure 5.45. The demands for increased high-speed performance resulted in increases in wing loading and, hence, increases in the stalling speed. By the time of World War II, the stalling speeds of high-performance military aircraft were in the range of 80 to 100 mph; wing loadings were in the range of 40 to 60 lb/ft^2. The development and the associated use of powerful high-lift devices, such as previously described in section 5.4.1.1, resulted in aircraft maximum lift coefficients of the order of 2.0 to 2.5 for high-performance aircraft in the World War II period. These high-lift devices, and consequent high maximum lift coefficient, prevented the stalling speed from increasing to an even greater extent than that shown in figure 5.43. Since World War II, the stalling speed of high-performance aircraft has continued to increase and is seen in figure 5.43 to be 115 mph for the contemporary Lockheed C-130 cargo transport. The wing loading for this aircraft is about 90 lb/ft^2, as shown in figure 5.44, and the maximum lift coefficient is about 2.75. The highest maximum lift coefficient of any of the aircraft for which data are shown in figure 5.45 is about 3.0 and was obtained by the Lockheed

Model 1049G Constellation. The corresponding wing loading for this aircraft is about 80 lb/ft^2. The high maximum lift coefficient of the Constellation gave a relatively slow landing speed of about 100 mph.

The lower bounds in figures 5.43, 5.44, and 5.45 show modest increases in stalling speed, wing loading, and maximum lift coefficient for aircraft of relatively low performance. The data for current general aviation aircraft show a wide spread in level of technology, insofar as maximum lift coefficients are concerned, and a wide range of values of stalling speed and wing loading. Values of maximum lift coefficient for these aircraft vary from about 1.3 to about 2.2. The higher values of maximum lift coefficient achieved by current high-technology general aviation aircraft are about the same as those achieved by military aircraft of World War II. The wing loading and stalling speeds of the high-performance general aviation aircraft of today are also seen to be in the same order as those of World War II military aircraft.

5.6.3 Power Loading

The power loading data shown in figure 5.46 appeared to have nearly constant values for the upper and lower bounds. Within these bounds, the transport

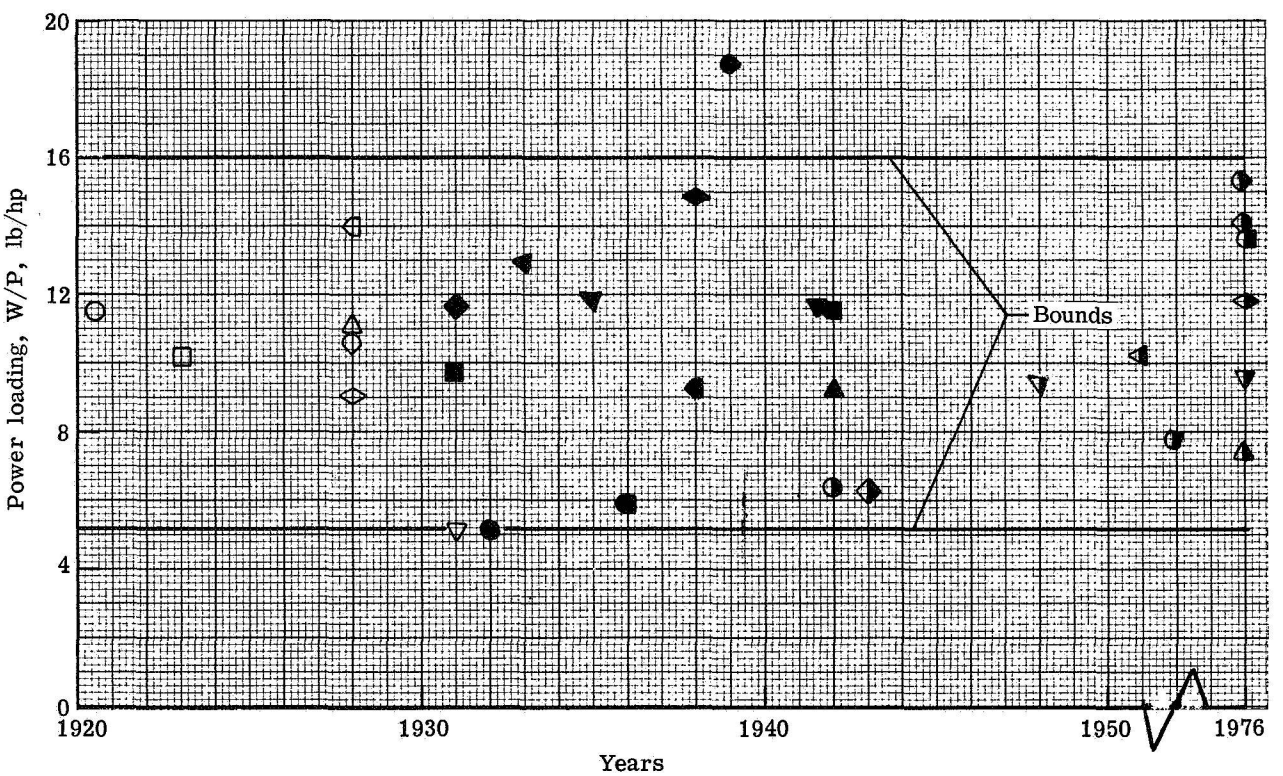


Figure 5.46.- Trends in power loading of propeller-driven aircraft.

and bomber type aircraft have power loadings which vary from about 12 lb/hp in 1928 to 8 to 10 lb/hp by the 1950's. Low-performance aircraft have a higher upper bound value of the power loading of about 16 lb/hp although the venerable

Piper Cub J-3 had a value of the power loading of about 19 lb/hp. The lower bound of the power loading is formed by fighter aircraft which tend to have power loadings in the range from 5 to 6 lb/hp. These low values of power loadings have, through the years, been dictated by the rate of climb and maneuvering performance characteristics required in fighter type aircraft. Present-day general aviation aircraft have power loadings which vary from nearly 16 lb/hp for the very low-performance type of pleasure or training aircraft to about 8 lb/hp for the high-performance Beech King Air 200.

5.6.4 Zero-Lift Drag Coefficient and Skin Friction Parameter

The value of the zero-lift drag coefficient $C_{D,0}$ is often used as an indicator of the aerodynamic cleanness or refinement of an aircraft. Values of $C_{D,0}$ calculated according to the methods of appendix B for the various aircraft described in this chapter are shown as a function of years in figure 5.47.

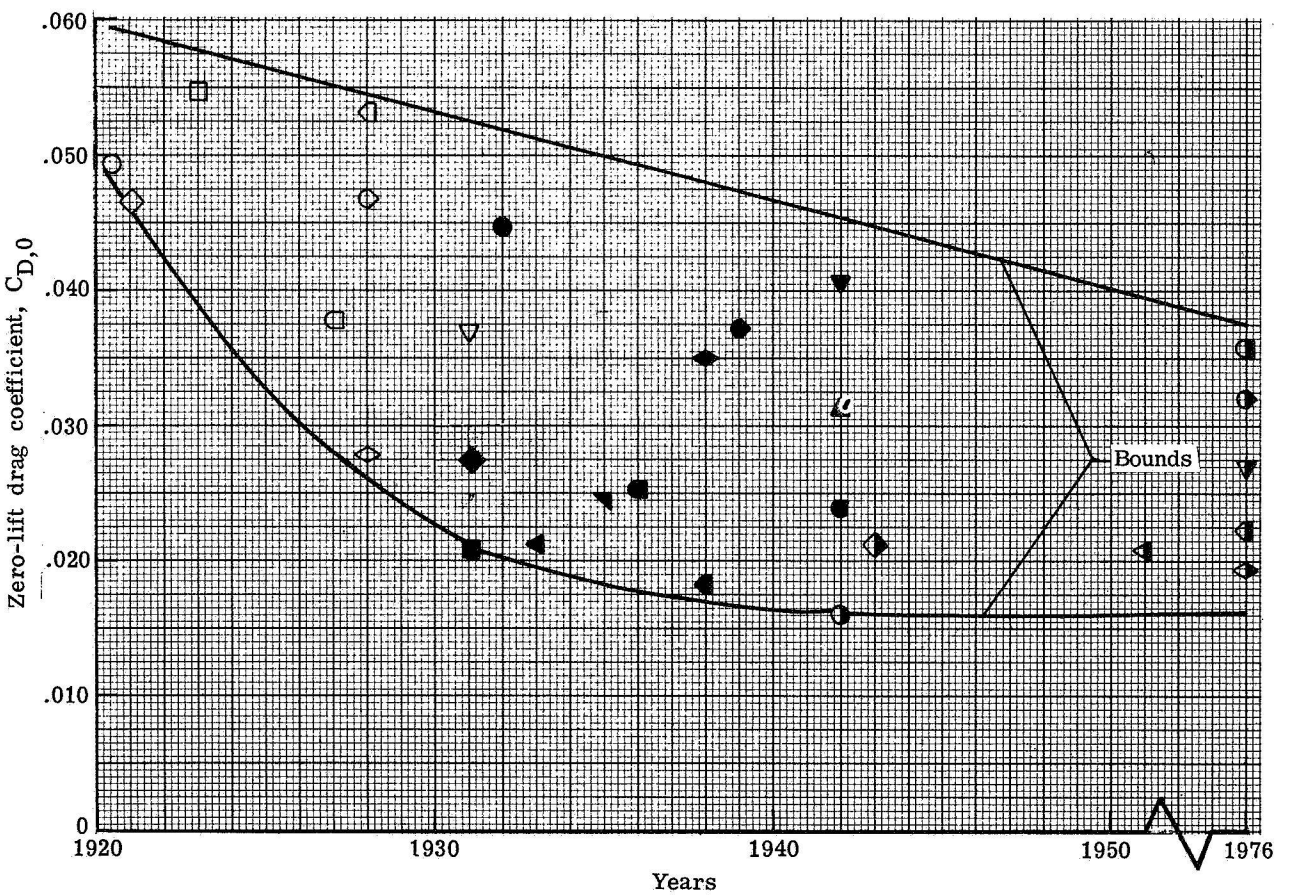


Figure 5.47.- Trends in zero-lift drag coefficient of propeller-driven aircraft.

The lower bound of $C_{D,0}$ drops sharply from a value of about 0.05 in 1920 to a value of about 0.021 in the early 1930's. A relatively small reduction in the lower bound value of $C_{D,0}$ took place in the years between the early 1930's

and the years of World War II. The general aviation aircraft of today show a spread in the values of $C_{D,0}$ from near the upper bound to near the lower bound. The lower bound curve shows the dramatic reduction in $C_{D,0}$ which accompanied the basic change in airplane configuration from a strut and wire braced biplane with a fixed landing gear to the highly streamlined, internally braced monoplane with retractable landing gear. As indicated in section 5.3, this transformation had largely taken place for high-performance operational aircraft by the early 1930's. Detailed aerodynamic refinements such as described in section 5.4.1 were responsible for some further improvements in aerodynamic efficiency as indicated by the lower bound curve.

The zero-lift drag coefficient, although useful as a measure of comparative aerodynamic refinement, has a basic limitation because the coefficient is based on wing area; and for a given wing area, many different fuselage sizes may be employed. Thus, differences in zero-lift drag coefficients may be interpreted as a difference in aerodynamic refinement when the difference may result from a significant difference in the ratio of wetted area to wing area.

In order to remove the effects of differences in the ratio of fuselage size to wing size, a drag coefficient, designated the skin friction parameter $\bar{C}_F$ was estimated for each of the aircraft and is shown as a function of years in figure 5.48. The upper and lower bounds of the data show the same trends

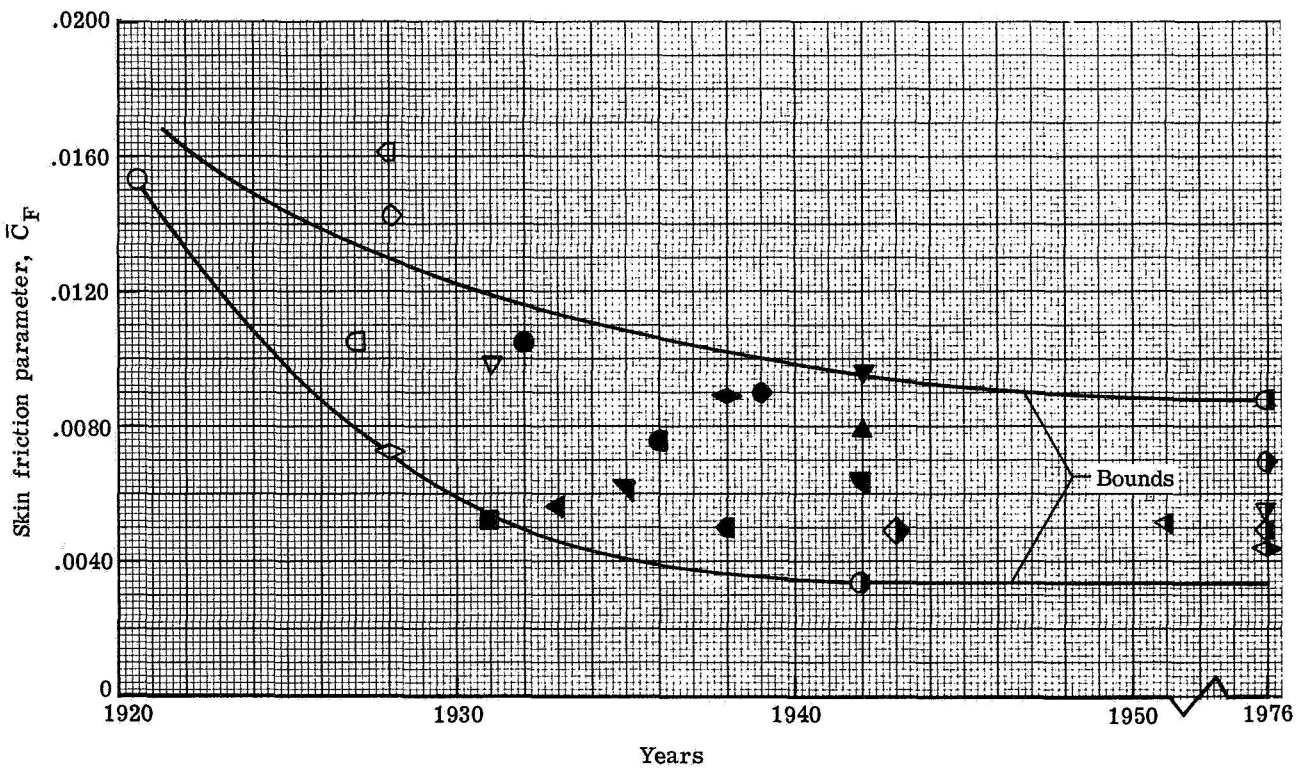


Figure 5.48.- Trends in skin friction parameter $\bar{C}_F$ of propeller-driven aircraft.

as do those for the zero-lift drag coefficient shown in figure 5.47. The lower bounds of the skin friction parameter indicate that essentially no progress has been made in reducing $\bar{C}_F$ since World War II, and little progress has been made since the early 1930's. The data for the current general aviation aircraft fall generally between the upper and lower bounds but do not reach as low a value as that of the lower bound curve. This suggests that these aircraft can be refined to a value at least as low as that achieved during World War II. There is little likelihood, however, that values of $\bar{C}_F$ significantly lower than the lower bound shown in figure 5.48 can be achieved unless some breakthrough is made which permits the achievement of a significant extent of laminar flow on the aircraft. Past experience with laminar-flow airfoils and laminar-flow control (briefly described in section 5.4.1.1), however, do not hold out much promise for the practical achievement of laminar flow on operational aircraft by any methods now known.

5.6.5 Maximum Lift-Drag Ratio

The maximum lift-drag ratio of the various aircraft was calculated according to the methods described in appendix B and is shown as a function of years in figure 5.49. The value of the maximum lift-drag ratio $(L/D)_{max}$ is a mea-

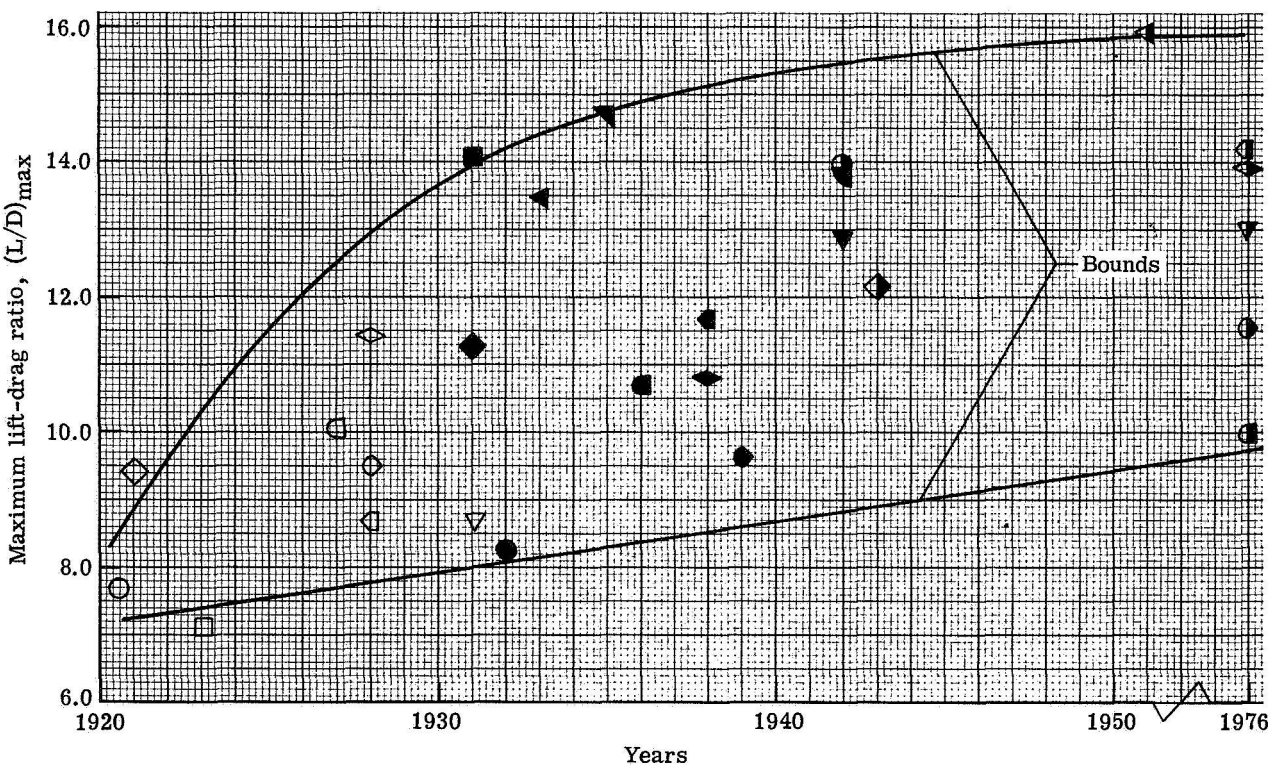


Figure 5.49.- Trends in maximum lift-drag ratio of propeller-driven aircraft.

sure of the aerodynamic efficiency of the aircraft. The upper bound of $(L/D)_{max}$ varies from a value near 8 for the DH-4 in 1920 to a value of about 16 achieved for the Lockheed 1049G in 1952. An upper bound of the curve of $(L/D)_{max}$ shows

a sharp rise between 1920 and the early 1930's, which corresponds to the reduction in zero-lift drag coefficient shown in figure 5.47 and to the emergence of the monoplane with its higher aspect ratio as compared to the biplane. Little change in maximum L/D has taken place since the end of World War II, and little further increases can be expected as a result of reduction in zero-lift drag, as has already been discussed. Increases in maximum lift-drag ratio may, however, result from future increases in aspect ratio which may perhaps be possible as a result of improved structural materials. Unconventional aircraft configurations which result in a reduction in the size of the fuselage relative to the wing or a reduction in tail size may also cause reductions in zero-lift drag and increases in maximum lift-drag ratio.

SYMBOLS

C_D drag coefficient

$C_{D,0}$ zero-lift drag coefficient

$\bar{C}_F$ skin friction parameter (see appendix B)

C_L lift coefficient

$C_{L,max}$ maximum lift coefficient

c_d section drag coefficient

c_l section lift coefficient

$c_{l,max}$ maximum section lift coefficient

$(L/D)_{max}$ maximum lift-drag ratio

M Mach number

W/P power loading, lb/hp

W/S wing loading, lb/ft^2

V_{max} maximum speed, mph (statute miles)

V_S stalling speed, mph (statute miles)

α_0 section angle of attack (fig. 5.27), deg

The symbols in column headings ① to ⑮ of table 5.I are defined sequentially as follows:

P_0 engine power for sea-level standard day, hp

W_g aircraft gross weight, lb

W_e aircraft empty weight, lb

b aircraft wing span (span of upper wing is given for biplane configurations), ft

l aircraft length, ft

S wing area (includes both wings for biplanes), ft^2

W_g/S wing loading obtained by dividing ② by ⑥, lb/ft^2

W_g/P_0 power loading obtained by dividing ② by ①, lb/hp

V_{max} maximum speed for sea-level conditions unless otherwise indicated, mph (statute miles)

V_c cruising speed for sea-level conditions unless otherwise indicated, mph (statute miles)

V_S stalling speed, mph (statute miles)

$C_{D,0}$ zero-lift drag coefficient determined by method described in appendix B

$\bar{C}_F$ skin friction parameter determined by method described in appendix B

A aspect ratio, b^2/S for monoplanes, and $(Kb)^2/S$ for biplanes (where K is Munk's span factor, having a value of 1.1 for all biplanes)

$(L/D)_{max}$ maximum value of lift-drag ratio determined by method described in appendix B

REFERENCES

5.1 Grey, C. G., ed.: All the World's Aircraft. Sampson Low, Marston & Co., Ltd. (London), 1922.

5.2 Grey, C. G.; and Bridgman, Leonard, eds.: All the World's Aircraft. Sampson Low, Martson & Co., Ltd. (London), 1928.

5.3 Grey, C. G.; and Bridgman, Leonard, eds.: Jane's All the World's Aircraft, 1931. Sampson Low, Marston & Co., Ltd. (London).

5.4 Grey, C. G.; and Bridgman, Leonard, eds.: Jane's All the World's Aircraft of 1933. Sampson Low, Marston & Co., Ltd. (London), 1933.

5.5 Grey, C. G.; and Bridgman, Leonard, eds.: Jane's All the World's Aircraft, 1934. Sampson Low, Marston & Co., Ltd. (London).

5.6 Grey, C. G.; and Bridgman, Leonard, eds.: Jane's All the World's Aircraft, 1936. Sampson Low, Martson & Co., Ltd. (London).

5.7 Grey, C. G.; and Bridgman, Leonard, eds.: Jane's All the World's Aircraft, 1937. Sampson Low, Marston & Co., Ltd. (London).

5.8 Grey, C. G.; and Bridgman, Leonard, eds.: Jane's All the World's Aircraft, 1939. Sampson Low, Marston & Co., Ltd. (London).

5.9 Bridgman, Leonard, ed.: Jane's All the World's Aircraft, 1945-46. Macmillan Co., c.1946.

5.10 Bridgman, Leonard, ed.: Jane's All the World's Aircraft, 1955-56. McGraw-Hill Book Co., Inc.

5.11 Taylor, John W. R., ed.: Jane's All the World's Aircraft, 1973-74. McGraw-Hill Book Co., c.1973.

5.12 Taylor, John W. R., ed.: Jane's All the World's Aircraft, 1975-76. Franklin Watts, Inc., c.1975.

5.13 Abbott, Ira H.; and Von Doenhoff, Albert E.: Theory of Wing Sections. Dover Publ., Inc., c.1959.

5.14 Abbott, Ira H.; Von Doenhoff, Albert E.; and Stivers, Louis S., Jr.: Summary of Airfoil Data. NACA Rep. 824, 1945. (Supersedes NACA WR L-560.)

5.15 The Aircraft of the World. Doubleday & Co., Inc., 1965.

5.16 Aeronautical Chamber of Commerce of America, Inc.: The Aircraft Year Book - For 1932. Volume 14. D. Van Nostrand Co., Inc., c.1932.

5.17 Allen, Richard Sanders: Revolution in the Sky - Those Fabulous Lockheeds, the Pilots Who Flew Them. Stephen Green Press, 1964.

5.18 Angle, Glenn D., ed.: Aerosphere - 1939. Aircraft Publ., c.1940.

5.19 Babington-Smith, Constance: Testing Time: The Story of British Test Pilots and Their Aircraft. Harper & Bro., 1961.

5.20 Bruce, J. M.: The de Havilland D.H.4. No. 26, Profile Publ., Ltd. (Surrey, England), c.1965.

5.21 Christy, Joe: Racing Planes Guide. Sports Car Press, Ltd., 1963.

5.22 Clarke, D. H.: What Were They Like to Fly? Ian Allen, Ltd. (London), 1964.

5.23 Coe, Paul L., Jr.: Review of Drag Cleanup Tests in Langley Full-Scale Tunnel (From 1935 to 1945) Applicable to Current General Aviation Airplanes. NASA TN D-8206, 1976.

5.24 Courtney, Frank T.: The Eighth Sea. Doubleday & Co., Inc., 1972.

5.25 Davies, R. E. G.: Airlines of the United States - Since 1914. Putnam & Co., Ltd. (London), 1972.

5.26 Diehl, Walter Stuart: Engineering Aerodynamics. Rev. ed. Ronald Press Co., c.1936.

5.27 Duval, G. R.: British Flying-Boats and Amphibians - 1909-1952. Aero Pub., Inc., c.1966.

5.28 Ferri, Antonio: Completed Tabulation in the United States of Tests of 24 Airfoils at High Mach Numbers (Derived From Interrupted Work at Guidonia, Italy, in the 1.31- by 1.74-Foot High-Speed Tunnel). NACA WR L-143, 1945. (Formerly NACA ACR L5E21.)

5.29 Fifty Years of Aeronautical Research. NASA EP-45, 1967.

5.30 Fokker, Anthony H. G.; and Gould, Bruce: Flying Dutchman - The Life of Anthony Fokker. Henry Holt & Co., c.1931.

5.31 Gibbs-Smith, Charles H.: The Aeroplane - An Historical Survey of Its Origins and Development. HMSO (London), 1960.

5.32 Gilruth, R. R.: Requirements for Satisfactory Flying Qualities of Airplanes. NACA Rep. 755, 1943. (Supersedes NACA ACR, Apr. 1941.)

5.33 A Glimpse of Scientific Research on Fundamental Problems of Military and Civil Aircraft. NACA, 1936.

5.34 Gray, George W.: Frontiers of Flight - The Story of NACA Research. Alfred A. Knopf, Inc., 1948.

5.35 Green, William: Famous Bombers of the Second World War. Volume I. Doubleday & Co., Inc., 1959.

5.36 Green, William: Famous Bombers of the Second World War. Volume II. Hanover House, 1960.

5.37 Green, William: War Planes of the Second World War, Fighters. Volume I. Hanover House, 1960.

5.38 Green, William: War Planes of the Second World War, Fighters. Volume II. Hanover House, 1961.

5.39 Green, William: War Planes of the Second World War, Fighters. Volume III. Doubleday & Co., Inc., 1962.

5.40 Green, William: War Planes of the Second World War, Fighters. Volume IV. Doubleday & Co., Inc., 1960.

5.41 Gruenhagen, Robert W.: Mustang - The Story of the P-51 Fighter. Rev. ed. Arco Pub. Co., Inc., c.1976.

5.42 Haddow, G. W.; and Grosz, Peter M.: The German Giants - The Story of the R-Planes, 1914-1918. Second ed., Funk & Wagnalls, 1969.

5.43 Hadingham, Evan: The Fighting Triplanes. Macmillan Co., 1969.

5.44 Hallion, Richard P.: Legacy of Flight - The Guggenheim Contribution to American Aviation. Univ. Washington Press, c.1977.

5.45 Hegener, Henri: Fokker - The Man and The Aircraft. Harleyford Publ., Ltd. (Letchworth, Herts, England), 1961.

5.46 Hoerner, Sighard F.: Fluid-Dynamic Drag. Hoerner Fluid Dynamics (Brick Town, N.J.), c.1965.

5.47 Hunsaker, J. C.: Forty Years of Aeronautical Research. Publ. 4237, Smithsonian Inst., 1956.

5.48 Index of NACA Technical Publications - 1915-1949. NACA, 1949.

5.49 Jackson, A. J.: British Civil Aircraft - 1919-59. Volume II. Putnam & Co., Ltd. (London), 1960.

5.50 Jacobs, Eastman, N.: Preliminary Report on Laminar-Flow Airfoils and New Methods Adopted for Airfoil and Boundary-Layer Investigations. NACA WR L-345, 1939.

5.51 Jones, Robert T.: Wing Plan Forms for High Speed Flight. NACA Rep. 863, 1947. (Supersedes NACA TN 1033.)

5.52 Juptner, Joseph P.: U.S. Civil Aircraft. Vol. 2 - (ATC 101 - ATC 200). Aero Pub., Inc., c.1964.

5.53 Lamberton, W. M., compiler: Fighter Aircraft of the 1914-1918 War. Harleyford Publ., Ltd. (Letchworth, Herts, England), 1960.

5.54 Larkins, William T.: The Ford Tri-Motor. No. 156. Profile Publ., Ltd. (Surrey, England), c.1967.

5.55 Lindbergh, Charles A.: The Spirit of St. Louis. Charles Schribner's Sons, 1953.

5.56 Loening, Grover: Our Wings Grow Faster. Doubleday, Doran & Co., Inc., 1935.

5.57 Miller, Ronald; and Sawers, David: The Technical Development of Modern Aviation. Praeger Publ., Inc., c.1968.

5.58 Nelson, Wilbur C.: Airplane Propeller Principles. John Wiley & Sons, Inc., 1944.

5.59 Penrose, Harald: British Aviation. The Great War and Armistice - 1915-1919. Putnam & Co., Ltd. (London), 1969.

5.60 Perkins, Courtland D.: The Development of Airplane Stability and Control Technology - 1969 Von Karman Lecture. AIAA Paper No. 69-1137, Oct. 1969.

5.61 Phillips, William H.: Appreciation and Prediction of Flying Qualities. NACA Rep. 927, 1949. (Supersedes NACA TN 1670.)

5.62 Reid, Elliott G.: Applied Wing Theory. First ed., McGraw-Hill Book Co., Inc., 1932.

5.63 Research and Development Contributions to Aviation Progress (RADCAP) - Executive Summary. U.S. Air Force, Aug. 1972. (Available as NASA CR-129574.)

5.64 Stack, John: Compressibility Effects in Aeronautical Engineering. NACA ACR, Aug. 1941.

5.65 Stack, John: Compressible Flows in Aeronautics. J. Aero. Sci., vol. 12, no. 2, Apr. 1945, pp. 127-143.

5.66 Stack, John; Lindsey, W. F.; and Littell, Robert E.: The Compressibility Burble and the Effect of Compressibility on Pressures and Forces Acting on an Airfoil. NACA Rep. 646, 1938.

5.67 Stack, John; Draley, Eugene C.; Delano, James B.; and Feldman, Lewis: Investigation of the NACA 4-(3)(08)-03 and NACA 4-(3)(08)-045 Two-Blade Propellers at Forward Mach Numbers to 0.725 To Determine the Effects of Compressibility and Solidity on Performance. NACA Rep. 999, 1950.

5.68 Swanborough, Gordon; and Bowers, Peter M.: United States Navy Aircraft Since 1911. Funk & Wagnalls, c.1968.

5.69 Tallman, Frank: Flying the Old Planes. Doubleday & Co., Inc., 1973.

5.70 Taylor, John W. R., ed.: Combat Aircraft of the World - From 1909 to the Present. G. P. Putnam's Sons, c.1969.

5.71 Taylor, John W. R.: Flight - A Pictorial History From the Wright Brothers to Supersonic. Peebles Press International, Inc., 1974.

5.72 Taylor, John W. R., ed.: Jane's 100 Significant Aircraft, 1909-1969. McGraw-Hill Book Co., 1969.

5.73 Taylor, John W. R., ed.: The Lore of Flight. Crescent Books, 1976.

5.74 Vorderman, Don: The Great Air Races. Doubleday & Company, Inc., 1969.

5.75 Wagner, Ray: American Combat Planes. Hanover House, 1960.

5.76 Wagner, Ray; and Nowarra, Heinz: German Combat Planes. Doubleday & Co., Inc., 1971.

5.77 Weick, Fred E.: Aircraft Propeller Design. McGraw-Hill Book Co., Inc., 1930.

5.78 Wigton, Don, compiler: From Jenny to Jet - Pictorial Histories of the World's Great Airlines. Bonanza Books, c.1963.

TABLE 5.I.- CHARACTERISTICS OF ILLUSTRATIVE AIRCRAFT

(a) Physical characteristics

Aircraft	Engine	①	②	③	④	⑤	⑥	⑦	⑧
		P_0	W_g	W_e	b	l	S	W_g/S	W_g/P_0
DeHavilland DH-4	Liberty	400	4 595	------	42.5	30.6	440	10.4	11.5
Handley Page W8F	Rolls-Royce Eagle IX, 360 hp (nose) Siddeley Puma, 240 hp (each side)	840	13 000	8 600	75.2	60.1	1456	8.9	15.5
Fokker F-2	BMW	185	4 180	2 640	56.6	33.8	452	9.3	22.6
Curtiss R2C-1	Curtiss D-12 (modified)	500	2 071	------	22.0	19.7	140	14.8	4.2
Dayton Wright RB	Hall Scott L-62	250	1 850	1 400	21.2	22.7	102	18.1	7.4
Supermarine S-4	Napier Lion	450	3 150	------	30.5	27.0	136	23.1	7.0
Ryan NYP	Wright J-5C Whirlwind	220	5 135	2 150	46.0	27.7	319	16.4	23.3
Ford 5-AT	Pratt & Whitney R-1340 Wasp (3 engines)	420	13 500	------	77.8	50.3	835	16.2	10.7
Lockheed Vega 5C	Pratt & Whitney R-1340 Wasp	450	4 033	2 465	41.0	27.5	275	14.7	9.0
Curtiss Robin	Curtiss Challenger	185	2 600	1 648	41.0	25.1	223	11.7	14.1
Travelair 4000	Wright J-5 Whirlwind	220	2 450	------	34.7	24.2	297	8.3	11.1
Curtiss Hawk P-6E	Curtiss V-1570	650	3 392	2 699	31.5	23.2	252	13.5	5.2
Boeing P-26A	Pratt & Whitney R-1340 Wasp	600 (h = 6000 ft)	3 012	2 271	27.9	23.6	149	20.2	5.0
Lockheed Orion 9D	Pratt & Whitney R-1340 Wasp	550	5 400	3 325	42.8	27.8	262	20.6	9.8
Northrop Alpha	Pratt & Whitney R-1340 Wasp	420	4 856	------	43.8	28.3	312	15.6	11.6
Boeing 247D	Pratt & Whitney R-1340 Wasp (2 engines)	525	13 650	8 940	74.0	51.3	836	16.3	13.0
Douglas DC-3	Pratt & Whitney R-1830 (2 engines)	1200	25 000	17 720	95	64.5	987	25.3	10.4
Boeing B-17G	Wright R-1820 Cyclone (4 engines)	1200	55 000	36 135	103.8	74.3	1420	38.7	11.5

TABLE 5.I.- Continued

(a) Concluded

Aircraft	Engine	①	②	③	④	⑤	⑥	⑦	⑧
		P_0	W_g	W_e	b	l	S	W_g/S	W_g/P_0
Seversky P-35	Pratt & Whitney R-1830	850 (h = 8000 ft)	5 599	4 315	36.0	26.8	220	25.5	6.6
Piper J-3 Cub	Continental A-65	65	1 220	730	32.2	22.4	178	6.9	18.8
Stinson SR-8B	Lycoming R-680	245	3 650	2 310	41.8	27.5	256	14.3	14.9
Beechcraft D17S	Pratt & Whitney R-985 Wasp Jr.	450	4 200	2 460	32.0	26.0	296	14.2	9.3
Consolidated B-24J	Pratt & Whitney R-1830-65 (4 engines)	1200	56 000	38 000	110.0	67.2	1048	53.4	11.7
Martin B-26F	Pratt & Whitney R-2800 (2 engines)	2000	37 000	23 700	71.0	56.0	658	56.2	9.3
North American P-51D	Rolls-Royce V-1650	1490	10 100	7 125	37.0	32.3	233	43.4	6.8
Grumman F6F-3	Pratt & Whitney R-2800	2000	12 441	9 101	42.8	33.6	334	37.3	6.2
Lockheed L.1049G	Wright R-3350 (4 engines)	3250	133 000	------	123.0	113.5	1650	80.6	10.2
Vickers Viscount (700 series)	Rolls-Royce Dart 506 (4 engines)	1600	60 000	36 776	93.8	81.2	963	62.3	9.4
Lockheed C-130	Allison T-56 (4 engines)	4910	155 000	75 331	132.6	97.7	1745	88.8	7.9
Piper Cherokee	Lycoming O-360	180	2 450	1 386	32.0	24.0	170	14.4	13.6
Cessna Skyhawk	Lycoming O-320	150	2 300	1 350	35.0	26.9	175	13.1	15.3
Beech Bonanza V-35	Continental IO-520	285	3 400	2 051	33.5	26.4	181	18.8	11.9
Cessna Cardinal RG II	Lycoming O-360	200	2 800	1 750	36.5	27.3	174	16.1	14.0
Cessna 310 II	Continental IO-520 (2 engines)	285	5 500	3 417	36.9	29.3	179	30.7	9.7
Beech Super King Air 200	Pratt & Whitney (Canada) PT6A-41 (2 engines)	850	12 500	7 315	54.5	43.8	303	41.3	6.9

TABLE 5.I.- Continued

(b) Performance characteristics

Aircraft	Reference	⑨ V_{max}	⑩ V_c	⑪ V_S	⑫ $C_{D,0}$	⑬ $\bar{C}_F$	⑭ A	⑮ $(L/D)_{max}$
DeHavilland DH-4	5.20	124	---	---	0.0496	0.0153	4.97	7.7
Handley Page W8F	5.49	103	85	---	.0549	------	4.67	7.1
Fokker F-2	5.1 & 5.45	93	---	---	.0466	------	7.1	9.4
Curtiss R2C-1	5.72	267	---	74	.0206	.0052	4.18	10.9
Dayton Wright RB	5.72 & 5.74	200	---	64	.0316	.0068	4.38	9.0
Supermarine S-4	5.72 & 5.74	239	---	90	.0274	------	6.84	12.1
Ryan NYP	5.55	120	95	71	.0379	.0106	6.63	10.1
Ford 5-AT	5.16 & 5.54	150	---	64	.0471	.0142	7.26	9.5
Lockheed Vega 5C	5.4 & 5.17	190	150	58	.0278	.0072	6.11	11.4
Curtiss Robin	5.16 & 5.52	115	102	47	.0585	.0161	7.54	8.7
Travelair 4000	5.2	135	110	46	------	------	4.80	-----
Curtiss Hawk P-6E	5.5 & 5.75	198	175	61	.0371	.0098	4.76	8.7
Boeing P-26A	5.5 & 5.75	234 (h = 7 500 ft)	211	74	.0448	.0105	5.24	8.3
Lockheed Orion 9D	5.4 & 5.17	226	200	63	.0210	.0052	7.01	14.1
Northrop Alpha	5.16	177	150	62	.0274	------	5.93	11.29
Boeing 247D	5.4 & 5.5	202 (h = 7 500 ft)	184 (h = 7 500 ft)	61	.0212	.0057	6.55	13.5
Douglas DC-3	5.9	229 (h = 7 500 ft)	185 (h = 10 000 ft)	67	.0249	.0062	9.14	14.7
Boeing B-17G	5.9 & 5.75	287 (h = 25 000 ft)	[a]182	90	.0236	.0064	7.58	13.8
Seversky P-35	5.7 & 5.75	282 (h = 10 000 ft)	[a]260	79	.0251	.0076	5.89	10.7
Piper J-3 Cub	5.9 & 5.15	100	87	---	.0373	.0090	5.81	9.6

[a]Altitude unknown.

TABLE 5.I.- Concluded

(b) Concluded

Aircraft	Reference	⑨	⑩	⑪	⑫	⑬	⑭	⑮
		V_{max}	V_c	V_S	$C_{D,0}$	$\bar{C}_F$	A	$(L/D)_{max}$
Stinson SR-8B	5.6	---	140 (h = 8 000 ft)	---	0.0348	0.0089	6.84	10.8
Beechcraft D17S	5.8 & 5.18	---	202 (h = 9 700 ft)	50	.0182	.0050	4.18	11.7
Consolidated B-24J	5.35 & 5.75	290 (h = 25 000 ft)	[a]215	95	.0406	.0096	11.55	12.9
Martin B-26F	5.35 & 5.75	274 (h = 15 000 ft)	[a]225	122	.0314	.0078	7.66	12.0
North American P-51D	5.40, 5.41, & 5.75	437 (h = 25 000 ft)	[a]362	100	.0161	.0034	5.86	14.0
Grumman F6F-3	5.40 & 5.75	375 (h = 17 300 ft)	[a]160	84	.0211	.0049	5.34	12.2
Lockheed L.1049G	5.10	352 (h = 10 500 ft)	331 (h = 23 000 ft)	100	.0211	.0042	9.17	16.0
Vickers Viscount (700 series)	5.10	---	334 (h = 25 000 ft)	---	------	------	9.14	-----
Lockheed C-130	5.12	---	386 (h = 20 000 ft)	115	------	------	10.08	-----
Piper Cherokee	5.11	148	141 (h = 7 000 ft)	61	.0358	.0088	6.02	10.0
Cessna Skyhawk	5.12	144	138 (h = 8 000 ft)	49	.0319	.0070	7.32	11.6
Beech Bonanza V-35	5.12	210	203 (h = 6 500 ft)	63	.0192	.0045	6.20	13.8
Cessna Cardinal RG II	5.12	180	171 (h = 7 000 ft)	57	.0223	.0049	7.66	14.2
Cessna 310 II	5.12	238	223 (h = 7 500 ft)	77	.0267	.0056	7.61	13.0
Beech Super King Air 200	5.12	333 (h = 15 000 ft)	320 (h = 25 000 ft)	92	------	------	9.80	-----

[a]Altitude unknown.

TABLE 5.II.- PHOTOGRAPH CREDITS

Figure	Photograph	Source
5.1	DeHavilland DH-4B	U.S. Air Force
5.2	Handley Page W8F	Flight International, London
5.3	Fokker F-2	Flight International, London
5.4	Curtiss R2C-1	National Air and Space Museum, Smithsonian Institution
5.5	Dayton Wright RB-1	National Air and Space Museum, Smithsonian Institution
5.6	Supermarine S-4	National Air and Space Museum, Smithsonian Institution
5.7	Ryan NYP	Ryan Aeronautical Library
5.8	Ford 5-AT	NASA Langley Research Center
5.9	Lockheed Vega 5C	Peter C. Boisseau
5.10	Curtiss Robin	Peter C. Boisseau
5.11	Travelair 4000	Peter C. Boisseau
5.12	Curtiss Hawk P-6E	Peter C. Boisseau
5.13	Boeing P-26A	NASA Langley Research Center
5.14	Lockheed Orion 9D	Lockheed Aircraft Corporation
5.15	Northrop Alpha	Peter C. Boisseau
5.16	Boeing 247	Peter C. Boisseau
5.17	Douglas DC-3	McDonnell Douglas Corporation

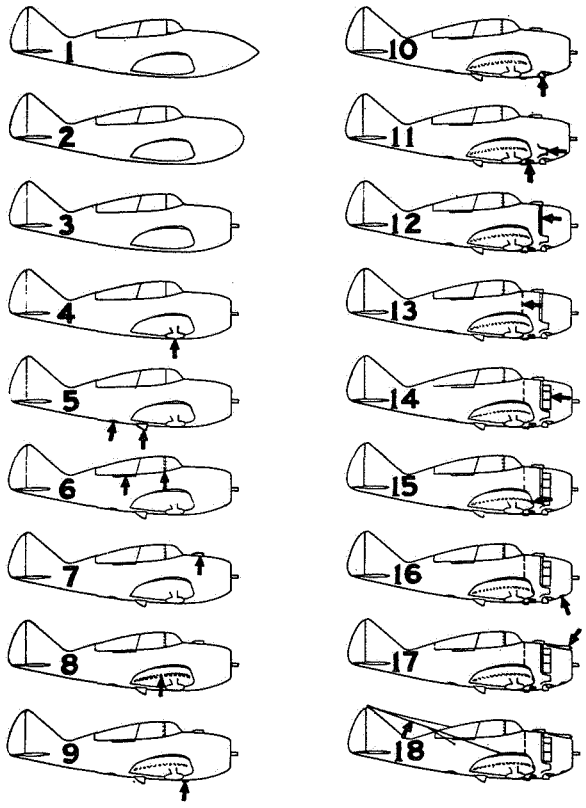
TABLE 5.II.- Concluded

Figure	Photograph	Source
5.18	Boeing B-17G	Peter C. Boisseau
5.19	Seversky XP-35	NASA Langley Research Center
5.20	Piper J-3 Cub	Peter C. Boisseau
5.21	Stinson SR-8B	Peter C. Boisseau
5.22	Beechcraft D17S	Peter C. Boisseau
5.26	Curtiss SB2C-4	NASA Langley Research Center
5.28	Consolidated B-24	NASA Langley Research Center
5.29	Martin B-26F	Peter C. Boisseau
5.30	North American P-51D	NASA Langley Research Center
5.31	Grumman F6F-3	NASA Langley Research Center
5.32	Lockheed L.1049G	Lockheed Aircraft Corporation
5.33	Vickers Viscount 810	Peter C. Boisseau
5.34	Lockheed C-130	Peter C. Boisseau
5.35	Piper Cherokee 180	NASA Langley Research Center
5.36	Cessna Skyhawk	Cessna Aircraft Corporation
5.37	Beech Bonanza V-35B	Beech Aircraft Corporation
5.38	Cessna Cardinal RG II	Cessna Aircraft Corporation
5.39	Cessna 310	Cessna Aircraft Corporation
5.40	Beech Super King Air 200	Beech Aircraft Corporation

TABLE 5.III.- EXPERIMENTAL STUDY OF DRAG SOURCES ON SEVERSKY XP-41

[From reference 5.23]

Airplane Condition



Condition number	Description	C_D (C_L = 0.15)	ΔC_D	ΔC_D, percent[a]
1	Completely faired condition, long nose fairing	0.0166		
2	Completely faired condition, blunt nose fairing	.0169		
3	Original cowling added, no airflow through cowling	.0186	0.0020	12.0
4	Landing-gear seals and fairing removed	.0188	.0002	1.2
5	Oil cooler installed	.0205	.0017	10.2
6	Canopy fairing removed	.0203	-.0002	-1.2
7	Carburetor air scoop added	.0209	.0006	3.6
8	Sanded walkway added	.0216	.0007	4.2
9	Ejector chute added	.0219	.0003	1.8
10	Exhaust stacks added	.0225	.0006	3.6
11	Intercooler added	.0236	.0011	6.6
12	Cowling exit opened	.0247	.0011	6.6
13	Accessory exit opened	.0252	.0005	3.0
14	Cowling fairing and seals removed	.0261	.0009	5.4
15	Cockpit ventilator opened	.0262	.0001	.6
16	Cowling venturi installed	.0264	.0002	1.2
17	Blast tubes added	.0267	.0003	1.8
18	Antenna installed	.0275	.0008	4.8
	Total		0.0109	

[a] Percentages based on completely faired condition with long nose fairing.

VI - SIZING OF PROPELLER-DRIVEN AIRCRAFT

CONTENTS

		Page
6.0	Introduction	317
6.1	Scope of Data	317
6.2	Performance Objectives	318
6.3	Sizing Procedure	320
6.4	Aircraft Speed Prediction	323
	6.4.1 The Three Classes of Aircraft Configuration	324
	6.4.2 Speed Analysis of the Three Classes of Aircraft Configuration	325
	6.4.2.1 Dispersion of Data	328
	6.4.2.2 Approximate Aerodynamic Parameters	329
	6.4.2.3 Use of Speed Curves	330
6.5	Airport Performance	333
	6.5.1 Stalling Speed	333
	6.5.2 Landing Field Performance	335
	6.5.3 Take-Off Field Performance	335
6.6	Climb Performance	340
	6.6.1 Rate of Climb Analysis	340
	6.6.2 Estimation of $C_L^{3/2}/C_D$	342
	6.6.3 Aircraft Rate-of-Climb Characteristics	345
	6.6.4 FAR Climb Criteria	347
	6.6.4.1 Aircraft Under 6000 lb Gross Weight	348
	6.6.4.2 Aircraft With One Engine Inoperative	351
	6.6.4.3 Climb Gradient Criteria	353
6.7	Matching Procedure	358
6.8	Aircraft Weight Relationships	361
	6.8.1 Useful Load Fraction	361
	6.8.2 Aircraft Gross Weight Estimation	364
6.9	Aircraft Range and Fuel Fraction	364
	6.9.1 Generalized Range Relationships	365
	6.9.2 Generalized Power Relationships	367
	6.9.3 Determination of Fuel Fraction	370
	6.9.4 Range and Power for Different Speeds and Altitudes	373
	6.9.5 Engine Characteristics	373

Page

6.10 Aircraft Sizing 376

SYMBOLS 377

REFERENCES 380

TABLES 382

6.0 Introduction

Rapid methods for estimating the size, weight, and power of propeller-driven aircraft intended to meet specified performance objectives are developed and discussed in chapter 6. The approach employed in developing a sizing procedure for propeller-driven aircraft is essentially similar to the one described in chapter 3 for jet-powered cruising aircraft in that extensive use is made of correlations of the characteristics of present and past aircraft. The parameters utilized in the correlations, however, as well as the detailed manner in which the sizing procedure is formulated, are slightly different for the two classes of aircraft primarily because the performance objectives are usually emphasized in a somewhat different manner.

6.1 Scope of Data

The characteristics of over 140 aircraft were examined in developing the correlations to be presented. The gross weights of these aircraft extended from approximately 1000 lb to over 100 000 lb, and the maximum speeds covered a range from about 100 mph to over 500 mph. The most modern general aviation aircraft were considered, as were older machines developed over a time period extending from World War I to the present. The aircraft are listed in tables 6.I(a) to 6.I(e) and are categorized as follows:

Table 6.I(a) - Modern General Aviation Aircraft

Table 6.I(b) - World War II Fighter Aircraft

Table 6.I(c) - Civil and Military Monoplanes

Table 6.I(d) - Biplanes

Table 6.I(e) - Turboprop-Powered Aircraft

The tables cite the references (refs. 6.1 to 6.18) from which data for each aircraft were taken and contain a brief code describing the basic configuration of each aircraft. The notations utilized in identifying the configurations are indicated as follows:

IB internally braced wing

EB externally strut-braced wing

WB externally wire-braced wing

RG retractable landing gear

FG fixed landing gear

C landing gear with tail wheel or skid (tricycle landing gear is implied if C is not used)

A numeral indicates the number of engines on multiengine aircraft. Thus, for example,

EB FGC 3

indicates an aircraft with externally strut-braced wings, a fixed landing gear with tail wheel, and three engines.

The modern general aviation aircraft of table 6.I(a) are all currently in production or have been produced since the end of World War II; whereas, the aircraft of table 6.I(c) were, in most cases, produced in the time period between World War I and World War II. Biplane production ended in World War II with the Boeing-Stearman Kaydet series of training planes. Accordingly, the biplanes of table 6.I(d) were all produced prior to World War II with the exception of a few modern home-built aircraft which have been included for completeness.

A number of important performance parameters have been analyzed and correlated utilizing data for the aircraft listed in the tables. All of the performance parameters for a particular aircraft were not necessarily employed in developing the various correlations because of incompleteness in the data for a particular aircraft, or because of inexplicable inconsistencies with well-defined trends. The published data on some of the older aircraft (pre-World War II), for example, frequently do not contain all the desired performance parameters and sometimes show large deviations in some performance characteristics from the expected trends. Only those data were used which appeared credible when considered in relation to the particular aircraft being examined and the trends shown by data for similar aircraft.

The aircraft listed in tables 6.I(a) to 6.I(e) do not necessarily include all the important aircraft developed in the United States from 1917 until the present time, nor has any attempt been made to examine in a complete way the characteristics of the many fine aircraft developed in other countries during this time period. Nevertheless, the aircraft contained in the tables are thought to represent a fair cross section of the design state of the art in any particular time period.

6.2 Performance Objectives

Modern propeller-driven aircraft are usually designed to meet one or more of the following performance objectives:

- Airport Performance
  - Stalling speed
  - Landing field length

- Take-off field length

- Climb performance

- Cruise Performance

  - Maximum or cruising speed usually at a specified altitude and power setting

  - Range at a specified altitude and speed or power setting

  - Payload

The specification of these performance objectives together with the use of the analyses and data developed herein permit the rapid estimation of the following important aircraft characteristics:

(1) Gross weight

(2) Empty weight

(3) Fuel weight

(4) Wing area and wing loading

(5) Power and power loading

(6) Performance characteristics at values of altitude and power other than those specified

Some important differences exist in the definition of parameters and the manner of optimization employed for propeller-driven aircraft and the jet-powered transport aircraft considered in chapter 3. Most propeller-driven aircraft being designed and developed today fall into the general aviation category, and this is the class of aircraft toward which the present analysis is directed. These aircraft are usually relatively small and carry fewer than 10 passengers. Such aircraft are designed to the airworthiness requirements of part 23 of the Federal Air Regulations (FAR). The regulations of FAR part 23 differ in many significant respects from those of FAR part 25 which govern the standards to which transport category aircraft must be designed. For example, the FAR landing and take-off field lengths discussed in chapter 3 for jet-powered transports (FAR part 25) are defined in such a way as to contain certain inherent safety margins. These margins are not present in the landing and take-off field lengths specified for aircraft designed to FAR part 23; hence, the field lengths which appear in chapter 6 are not comparable to those of chapter 3 for jet-powered transport aircraft. The exact definitions of the field lengths utilized for propeller-driven aircraft are given in section 6.5 which discusses airport performance in some detail. The climb criteria which govern aircraft performance with one engine inoperative are also greatly different for aircraft designed to FAR part 23 as compared to FAR part 25. These criteria will be discussed in section 6.6.4.

Another criterion which has a profound effect on the design of the aircraft relates to the stalling speed. The stalling speed of all single-engine aircraft and certain classes of multiengine aircraft is limited by the regulations of FAR part 23 to a value not to exceed 70 mph. This limitation on stalling speed, when considered in relation to the relatively simple high-lift systems employed on most propeller-driven aircraft presently being designed and produced, results in wing loadings which are very much lower than those characteristic of current jet-powered transports. These low wing loadings exert a significant influence on the efficiency of cruising flight.

In order to maximize efficiency in cruising flight, jet-powered transport aircraft are usually sized in such a way that they may be operated at the design cruise Mach number at a lift coefficient very close to that for maximum lift-drag ratio. (See chapter 3.) Some of the older propeller-driven aircraft (such as the Lockheed Electra and the Douglas DC-7) for which highly efficient, long-range cruising flight was a primary performance objective were sized in much the same way. Modern, propeller-driven general aviation aircraft, which form the subject of the present discussion, however, are usually sized in a somewhat different fashion. Typically, such aircraft have a specified maximum speed at sea level and/or cruising speeds corresponding to one or more combinations of power setting and altitude. For example, as a design condition for an unsupercharged aircraft, a cruising speed at 75 percent power at an altitude of 7500 ft might be specified along with a corresponding range. These performance objectives, when considered in combination with the low wing loadings previously discussed, usually result in operation at a lift coefficient well below that corresponding to the maximum lift-drag ratio. Flight at lower power settings and higher altitudes with supercharged engines results in operation at higher lift coefficients and lift-drag ratios; however, propeller-driven aircraft of this type are usually not operated at the maximum lift-drag ratio. As a consequence of these considerations, the method of cruise matching employed herein for sizing propeller-driven aircraft is somewhat different from that utilized in chapter 3 for jet-powered aircraft. Combinations of speed, range, and altitude are specified, and operation at the maximum lift-drag ratio is not considered as a design point. The following section describes the sizing procedure in terms of a flow diagram linking the various steps in the process.

6.3 Sizing Procedure

The procedure to be utilized in sizing a propeller-driven aircraft to meet a given set of performance objectives is illustrated in approximate form by the flow diagram shown in figure 6.1. The procedure will now be briefly described.

Block 1 of figure 6.1 implies a general knowledge of a number of pertinent aircraft design parameters, such as aspect ratio and propulsive efficiency, as well as the general type of configuration under consideration. The blocks in the first column represent analysis and prediction methods for different flight conditions or performance objectives, to be developed herein, which are utilized in the first steps toward sizing the aircraft. Block 2 yields a curve of power loading as a function of wing loading. Any point along this curve defines a combination of wing loading and power loading which will satisfy an input maximum speed, or 75-percent-power cruising speed, requirement at a given altitude

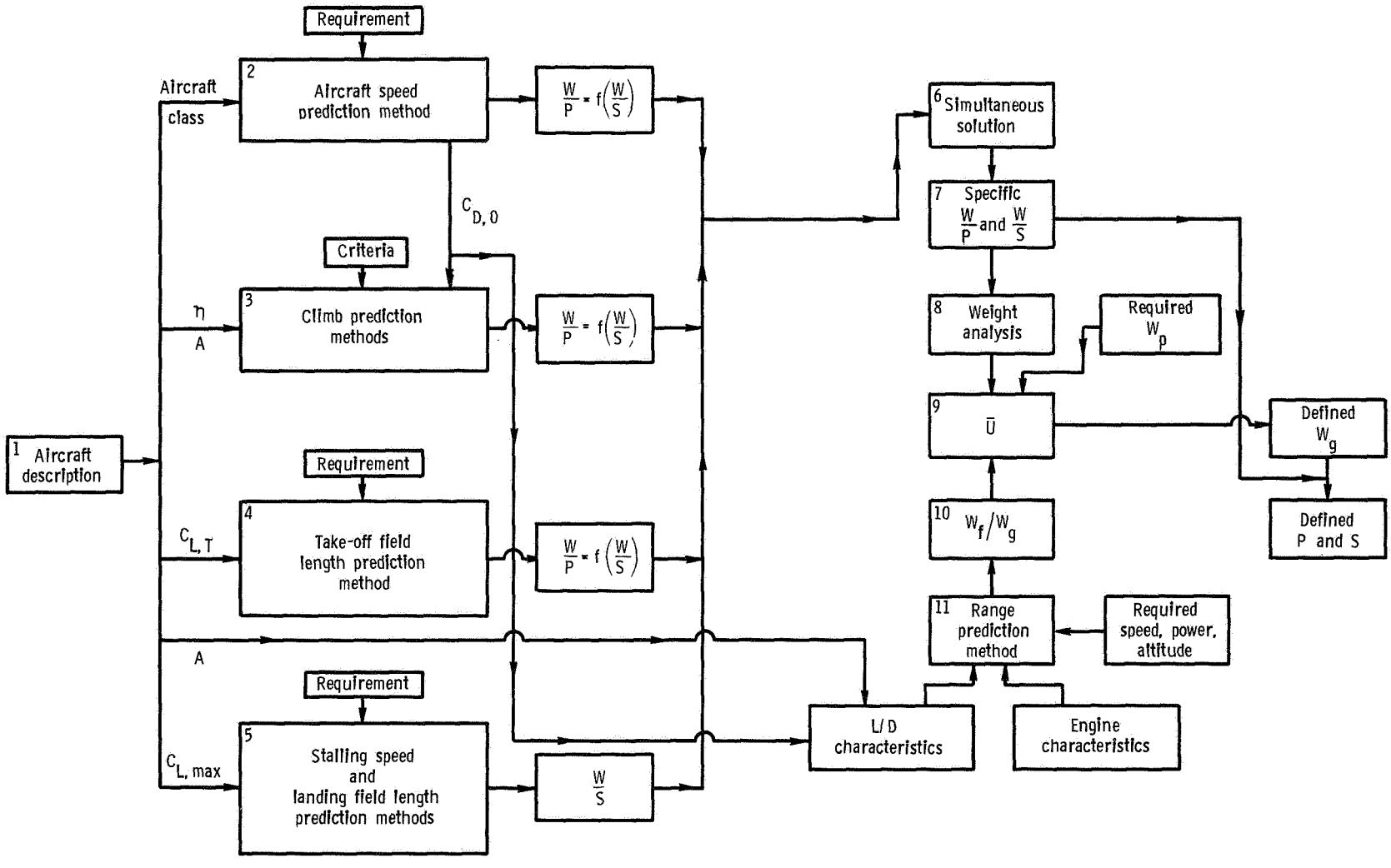


Figure 6.1.- Aircraft-sizing flow diagram for propeller-driven aircraft.

for a specified class of aircraft. The manner in which the classes of aircraft are defined is discussed in section 6.4.1. The speed prediction analysis also yields an average zero-lift drag coefficient $C_{D,0}$ which is employed in the estimation of several other performance parameters. Block 3 of figure 6.1 defines a functional relationship between power loading and wing loading which permits satisfaction of input climb requirements or criteria. The wing aspect ratio and the propulsive efficiency are necessary inputs for the estimation of the climb performance, as is the zero-lift drag coefficient determined from the speed analysis.

Blocks 4 and 5 of figure 6.1 relate to airport performance. Block 4 yields a curve of power loading as a function of wing loading necessary to meet a required take-off field length objective. The value of the lift coefficient in the take-off configuration $C_{L,T}$ is a necessary input parameter for the take-off field length prediction. Block 5 defines the wing loading necessary to meet a specified stalling speed and/or landing field length. The value of the maximum lift coefficient in the landing configuration $C_{L,max}$ is a necessary input parameter in the prediction of stall speed and landing field length. Both $C_{L,T}$ and $C_{L,max}$ are estimated from analysis of performance data for a large number of aircraft.

The outputs of the analyses represented by the first column in figure 6.1 constitute a set of relationships which, when considered simultaneously, yield unique values of wing loading and power loading required to meet the specified set of performance objectives. This step is depicted by blocks 6 and 7. The graphical procedure for determining the desired values of wing loading and power loading is similar to that used for jet-driven aircraft in chapter 3 and is described in section 6.7. The output values of wing loading and power loading are utilized in the weight analysis, block 8 of figure 6.1, to yield a specific value of the ratio of payload weight W_p plus fuel weight W_f to aircraft gross weight; that is, $(W_p + W_f)/W_g$ or $1 - (W_e/W_g)$. The payload weight is, of course, a specified quantity and the fuel weight may be determined from the desired range performance.

The range is usually specified at some altitude and speed or power setting. The range specification is shown as an input to block 11 of figure 6.1. The lift-drag ratio characteristics of the aircraft and certain engine and propulsive characteristics are also shown as inputs to the range prediction method. The determination of the necessary lift-drag ratio information requires the wing aspect ratio and zero-lift drag coefficient as inputs. The range prediction method itself is a rapid, generalized procedure which permits estimation of the fuel fraction required for a given range at any altitude and power setting.

With the values of fuel fraction W_f/W_g, payload W_p, and $1 - (W_e/W_g)$ known, the gross weight of the aircraft can be immediately determined, as can the fuel weight and aircraft empty weight. Since wing loading and power loading are known, the wing area and engine horsepower are also known. Thus, the aircraft has been grossly sized to meet the desired performance objectives. The prediction methods represented by the various blocks in figure 6.1 are developed in some detail in the remaining portions of this chapter, and application of the procedure to a specific design problem is described in chapter 7.

6.4 Aircraft Speed Prediction

The power required to fly at a particular speed is given by the following well-known relation:

$$550P\eta = C_D\left(\frac{\rho_i}{2}\right)SV^3 \tag{6.1}$$

where

P engine power, hp

η propulsive efficiency

C_D drag coefficient

ρ_i air density at given altitude, slugs/ft^3

S wing area, ft^2

V speed, ft/sec

The drag coefficient C_D employed in equation (6.1) includes all elements of the drag such as profile, induced, trim and cooling drag. Equation (6.1) may be rewritten in the form

$$V = 77.3\sqrt[3]{\left(\frac{P}{S}\right)\frac{\eta}{\sigma C_D}} \tag{6.2}$$

where σ is the ratio of the density at the given altitude to the density at sea level. The density at sea level for standard-day conditions was taken as 0.002378 slug/ft^3. The speed is seen to be proportional to the cube root of the product of the power per square foot of wing area and the ratio of propulsive efficiency to density ratio multiplied by drag coefficient. A form of equation (6.2) which utilizes more familiar and useful airplane design parameters is

$$V = 77.3\sqrt[3]{\left(\frac{W/S}{W/P}\right)\frac{\eta}{\sigma C_D}} \tag{6.3}$$

where W/S is the wing loading in pounds per square foot and W/P is the power loading in pounds per horsepower.

The direct application of equation (6.3) to the prediction of aircraft speed requires a knowledge of the drag coefficient. The determination of the drag coefficient by conventional methods, however, can be a tedious calculation involving a fairly detailed knowledge of the design of the aircraft. An examination of the characteristics of a large number of propeller-driven aircraft indicates that for the maximum speed condition, and in many cases for the cruising speed at 75 percent power, the induced drag coefficient averages about 10 percent of the total drag coefficient. Thus, a proportionality based on equation (6.3) can be written in the following form:

$$V \propto \sqrt[3]{\left(\frac{W/S}{W/P}\right)\frac{\eta}{\sigma C_{D,0}}} \tag{6.4}$$

where $C_{D,0}$ is the drag coefficient at zero lift. Then, if the zero-lift drag coefficients of aircraft of a given configuration class designed to a given level of technical sophistication are assumed to be of the same order, a simple correlation should exist between the speed of the aircraft and the parameter

$$\sqrt[3]{\left(\frac{W/S}{W/P}\right)\frac{1}{\sigma}}$$

This parameter is called the power index I_p thus

$$V \propto I_p \tag{6.5}$$

The expression (6.5) assumes the propulsive efficiency is not greatly different for aircraft of a given class. An empirical correlation between the power index I_p and the speed, as determined from the characteristics of present and past aircraft, suggests itself as a means for relating speed to important physical parameters of the aircraft without explicitly knowing the drag coefficient. Such correlations will provide a rapid means for determining the physical parameters of an aircraft necessary in order to provide a given speed.

6.4.1 The Three Classes of Aircraft Configuration

The photographs and descriptions of chapter 5 depict the development of the propeller-driven aircraft from the strut- and wire-braced biplanes of World War I to the highly streamlined internally braced monoplanes with retractable landing gear which represent the final aerodynamic form of propeller-driven aircraft. An examination of the aircraft described in chapter 5 suggests the following three classes into which aircraft configurations may be divided for the purpose of classification according to the level of zero-lift drag coefficient:

I Internally braced monoplanes with retractable landing gear.

II Monoplanes with fixed landing gear and (1) internally braced wings, (2) wings with a single strut on each side, or (3) wire-braced wings. The landing gear is usually of the single strut type but may have either nosewheel or tailwheel.

III Biplanes and multistrut monoplanes. Multistrut monoplanes are those with two or more wing struts on each side and several landing gear struts which are typically integrated with the wing struts.

This method of classification is admittedly an oversimplification but, as will be seen subsequently, provides an acceptable basis for correlating aircraft speed with the power index.

6.4.2 Speed Analysis of the Three Classes of Aircraft Configuration

The maximum speed and, in a number of cases, the cruising speed at 75 percent power have been plotted as a function of the power index in figure 6.2 for

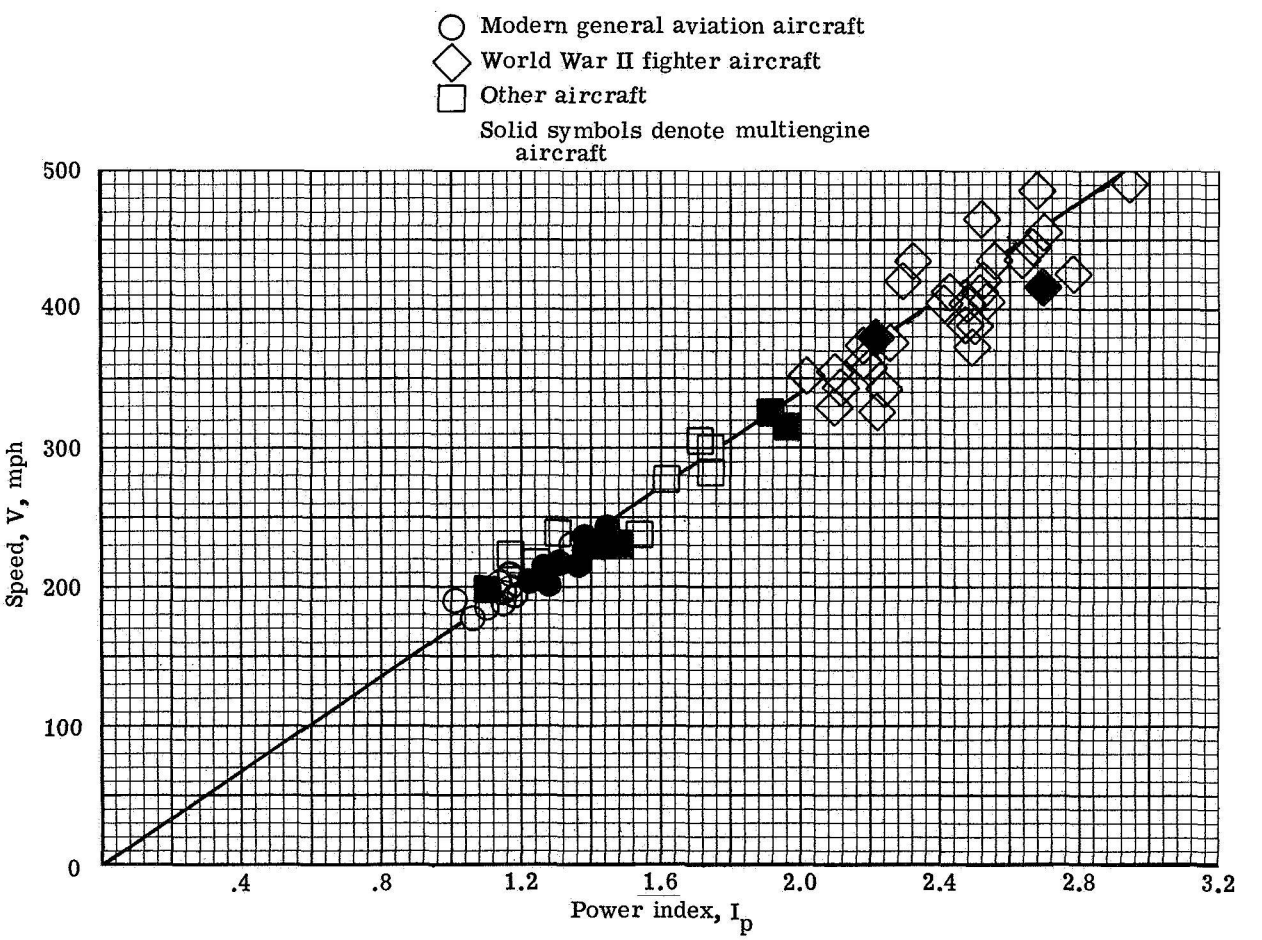


Figure 6.2.- Variation of aircraft speed with power index for internally braced monoplanes with retractable landing gear (class I).

aircraft of class I (that is, aircraft with internally braced wings and retractable landing gears). The values of the wing loading and power loading used in computing the power index were based on maximum gross weight. The value of the power loading utilized the power corresponding to the altitude at which the speed was specified. The circle symbols in figure 6.2 are for modern general aviation aircraft, the diamond symbols are for World War II fighter aircraft, and the square symbols are for other class I aircraft which, in most cases, were developed in the time period between World War I and World War II. Single-engine aircraft are indicated by the open symbols, and multiengine aircraft are indicated by the solid symbols. The speed range of the aircraft for which data are presented in figure 6.2 extends from about 175 mph to 500 mph, and the corresponding range of power index is from about 1 to 3. An examination of tables 6.I(a), (b), and (c) indicates that data are contained in figure 6.2 for such diverse aircraft as the Beech Bonanza, the Supermarine Spitfire, the Douglas DC-3 transport, the 1930 Lockheed Orion, and the 1935 Hughes racer. Although some scatter is present in the data, as would be expected, a well-defined trend of speed with power index is evident. The line shown in figure 6.2 is suggested as a reasonable fairing of the data points. For a given value of the power index, the maximum spread in speed shown by the data is about ±10 percent around the faired line. Thus, specification of a maximum speed at a given altitude yields a value of the power index which, in turn, gives the power loading as a linear function of the wing loading required to meet the desired speed objective.

Data for class II monoplanes, that is monoplanes equipped with fixed landing gear, are presented in figure 6.3 in a format similar to that of figure 6.2.

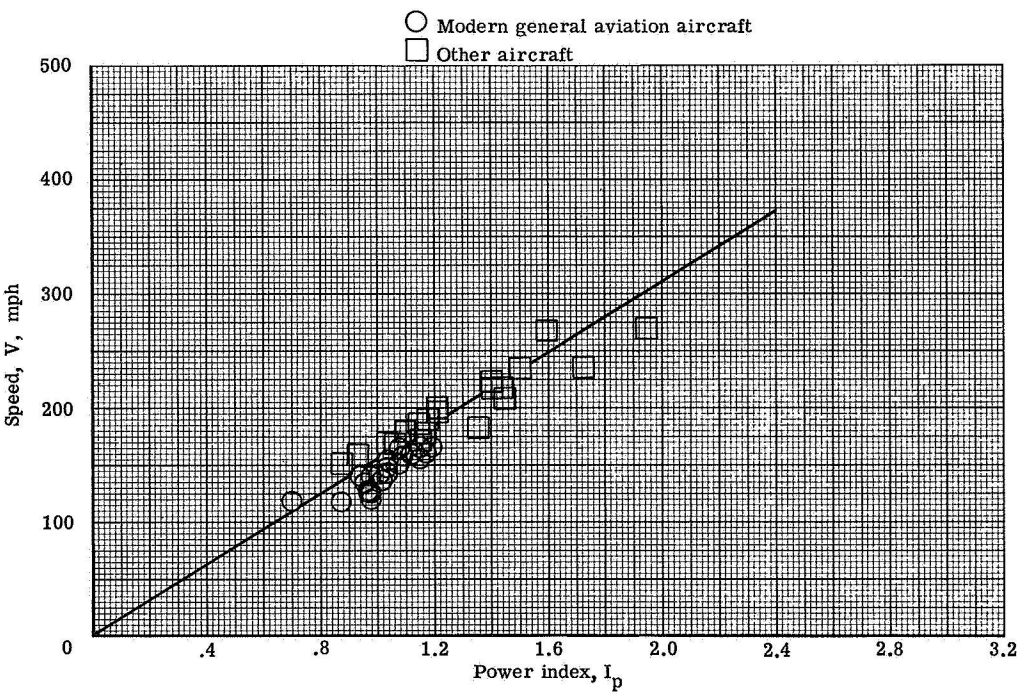


Figure 6.3.- Variation of aircraft speed with power index for monoplanes with fixed landing gear (class II).

The circle symbols are for modern general aviation aircraft and the square symbols are for both civil and military aircraft developed prior to World War II. As previously noted, aircraft with both internally and externally braced wings are included in class II. The externally braced aircraft, however, are limited to those with simple struts or wire bracing. The square point at $I_p = 1.95$ and 270 mph, for example, represents the wire-braced Gee Bee Model Z racer of 1931. Many of the points for modern general aviation aircraft (circle symbols) are seen to form a trend which falls below the faired line, whereas a number of the aircraft in the period between the two wars lie above the faired line. Some of this difference may result from less precise and more optimistic specification of the speeds of the older aircraft, as compared to more definitive data on present-day machines. Another possible explanation may lie in differences in the landing-gear configuration. Most modern general aviation aircraft employ a tricycle landing gear in contrast to the pre-World War II aircraft of figure 6.3 which, without exception, employed a conventional landing gear with tail wheel or skid. The added drag of the third landing gear strut and wheel on the modern aircraft, as well as the possible effect of the gear location immediately behind the propeller on the propulsive efficiency, may be partly responsible for the trends shown in figure 6.3. Again, however, as in the case for the class I aircraft of figure 6.2, the variation in speed from the faired line is no more than 10 percent for a given value of the power index.

Data for a number of class III aircraft are presented in figure 6.4. The circle symbols are for biplanes of the 1920's and 1930's as well as for several

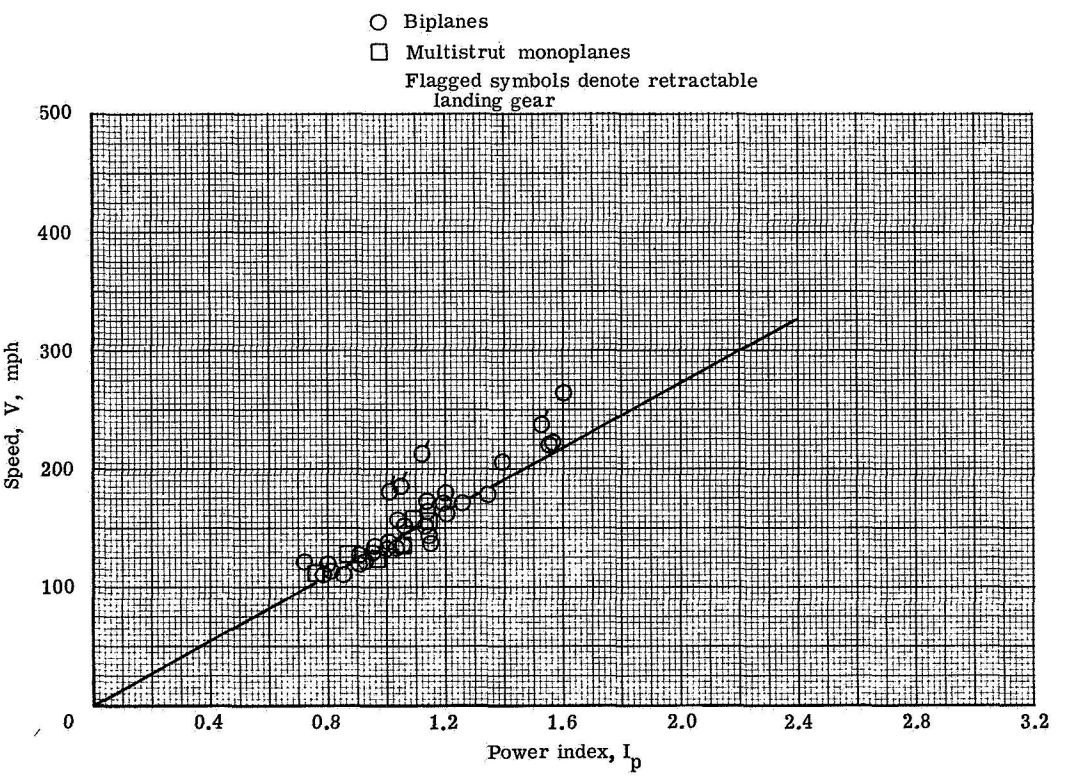


Figure 6.4.- Variation of aircraft speed with power index for biplanes and multistrut monoplanes with fixed landing gear (class III).

modern home-built midget biplanes. The biplanes for which data are given in figure 6.4, and listed in table 6.I(d), include fighters, observation planes, trainers, and sport planes. Two outstanding fighters of the World War I period, the Spad 13 and the SE-5, are also included. The flagged symbols are for biplanes with retractable landing gears. The highest point in figure 6.4 is for the very clean 1925 Curtiss R3C-1 racer which had a speed of 265 mph at a power index of 1.6. The square symbols in figure 6.4 represent monoplanes with a multiplicity of bracing struts. Examples of such aircraft are the Curtiss Robin and the Spirit of St. Louis which were depicted in chapter 5. A comparison of the circle and square symbols indicates that the maximum speed to be expected from a multistrut monoplane is about the same as that for a biplane with the same power index. This implies that the zero-lift drag coefficients of the two types of aircraft are about the same. The flagged circles indicate the dramatic effect of retracting the landing gear on very clean biplanes. The three flagged circles at the lower values of the power index are different variants of the Beech D-17, which is notable for the use of negative stagger as well as retractable landing gear and overall attention to aerodynamic cleanness. (See fig. 5.22 of chapter 5.)

6.4.2.1 Dispersion of Data

An examination of the data of figures 6.2, 6.3, and 6.4 discloses a close correlation between the speed and the power index. In most cases, the data are seen to fall within a range of speeds of ±10 percent of the mean line values. Much of the data show a closer relationship with the mean lines. Some of the scatter in the data no doubt results from differences in the accuracy of the specifications given for the various aircraft in the reference documents or to improper interpretation of these specifications. Some of the scatter also results from variations in the induced drag coefficient for the different aircraft at the speed conditions corresponding to the data. The induced drag effects have been examined in detail for all the aircraft for which data are presented in figures 6.2, 6.3, and 6.4. The induced drag coefficient was found to average about 10 percent of the total drag coefficient, although values as low as 5 percent and as high as 20 percent of the total drag were found in some instances. Thus, variations in induced drag account for no more than ±2 to 3 percent variation in speed around the faired lines in the figures.

Variations in the ratio of wing area to wetted area and in propulsive efficiency no doubt play a large part in the scatter shown by the data for aircraft of a given configuration class. Differences in aerodynamic efficiency are also responsible for a significant part of the scatter in the data of the figures. A point which falls above the appropriate mean line is indicative of an aircraft which is of higher aerodynamic efficiency than one represented by a point which falls below the line. The presence of bombs, bomb racks, guns, external tanks, rocket launchers, etc., for example, is certainly responsible for the relatively poor aerodynamic efficiency of some of the World War II fighters for which data are presented in figure 6.2. As indicated previously, the use of a tricycle landing gear, as compared to a tail wheel landing gear, may be responsible for many of the low points for the monoplanes in figure 6.3. Some of the variations in the data for the biplanes in figure 6.4 are probably associated with the power plant and its installation. Aircraft with both cowled

and uncowled radial air-cooled engines, in-line air-cooled engines, and in-line liquid-cooled engines are all represented by the data in figure 6.4. Variations in trim drag, cooling drag, and attention to aerodynamic detail such as surface finish, protuberances, gaps, and leaks all contribute in some degree to the scatter in the data for all three configuration classes.

6.4.2.2 Approximate Aerodynamic Parameters

Zero-lift drag coefficients may be extracted from the data for the three classes of aircraft presented in figures 6.2., 6.3, and 6.4. An average value of $C_{D,0}$ corresponding to the faired lines in the three figures as well as maximum and minimum values for the upper and lower edges of the scatter band may be determined. A knowledge of the zero-lift drag coefficient is needed in the analyses contained in later parts of this chapter. For purposes of estimating the zero-lift drag coefficient, equation (6.3) may be rewritten in the following form:

$$C_D = \eta(77.3)^3\left(\frac{I_p}{V}\right)^3 \tag{6.6}$$

If it is assumed that $C_{D,0} = 0.9C_D$ and $\eta = 0.85$ and if the velocity is expressed in terms of miles per hour rather than feet per second, equation (6.6) takes the form

$$C_{D,0} = 0.85(0.90)\left(\frac{77.3}{1.47}\right)^3\left(\frac{I_p}{V}\right)^3 \tag{6.7a}$$

or

$$C_{D,0} = (1.1140 \times 10^5)\left(\frac{I_p}{V}\right)^3 \tag{6.7b}$$

With the use of equations (6.7) and the data of the figures, the average, minimum, and maximum zero-lift drag coefficients have been determined for the three classes of aircraft and are given in table 6.II. These drag coefficients may be usefully employed in making quick estimates of such important aerodynamic parameters as the maximum lift-drag ratio. Some comments regarding the use of average, minimum, and maximum values of the zero-lift drag coefficient are contained in the next section.

6.4.2.3 Use of Speed Curves

The three faired lines in figures 6.2, 6.3, and 6.4 are representative of the application of good, average, state-of-the-art design practice. Performance significantly higher than that indicated by the faired lines will probably require unusual attention to design detail, whereas poor aerodynamic design or lack of attention to detail may easily result in performance lower than that predicted by the lines. The use of the mean lines of the three figures is therefore suggested for the rapid estimation of the power index required to provide a given maximum speed, or for comparing the performance of different aircraft, unless there are reasons to suggest the use of the data nearer the top or bottom of the scatter band. Similarly, the use of the average values of the zero-lift drag coefficient given in table 6.II are suggested unless more definitive information on the drag coefficient is available.

If the power index for a given maximum speed is known, the cruising speed at some power setting, such as 75 percent, may be roughly estimated by finding the speed corresponding to the power index reduced by $\sqrt{0.75}$. The comparison of the cruising speed with the maximum speed will not be quite correct, however, because of differences in the induced drag coefficient for the two cases. The curves in figures 6.2, 6.3, and 6.4 should not be used for low power settings. No data are included in the figures for power settings below 75 percent. An accurate method for obtaining the cruising speed at any power setting is given in section 6.9.2.

In order to facilitate the use of the data in figures 6.2, 6.3, and 6.4, portions of the faired lines of these figures have been replotted in figure 6.5

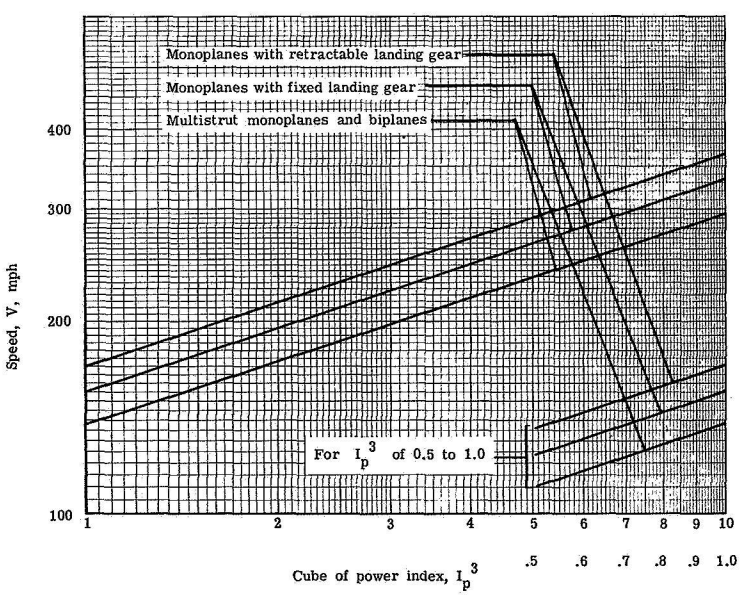


Figure 6.5.- Variation of aircraft speed with the cube of power index for aircraft of three different configuration classes.

on logarithmic paper. For convenience, the speed in this figure is plotted against the cube of the power index, that is

$$\left(\frac{W/S}{W/P}\right)\frac{1}{\sigma}$$

rather than the cube root of this quantity. In order to facilitate further the use of the speed curves, the atmospheric density ratio $1/\sigma$ (taken from table 1.I of chapter 1) is presented in figure 6.6 as a function of altitude.

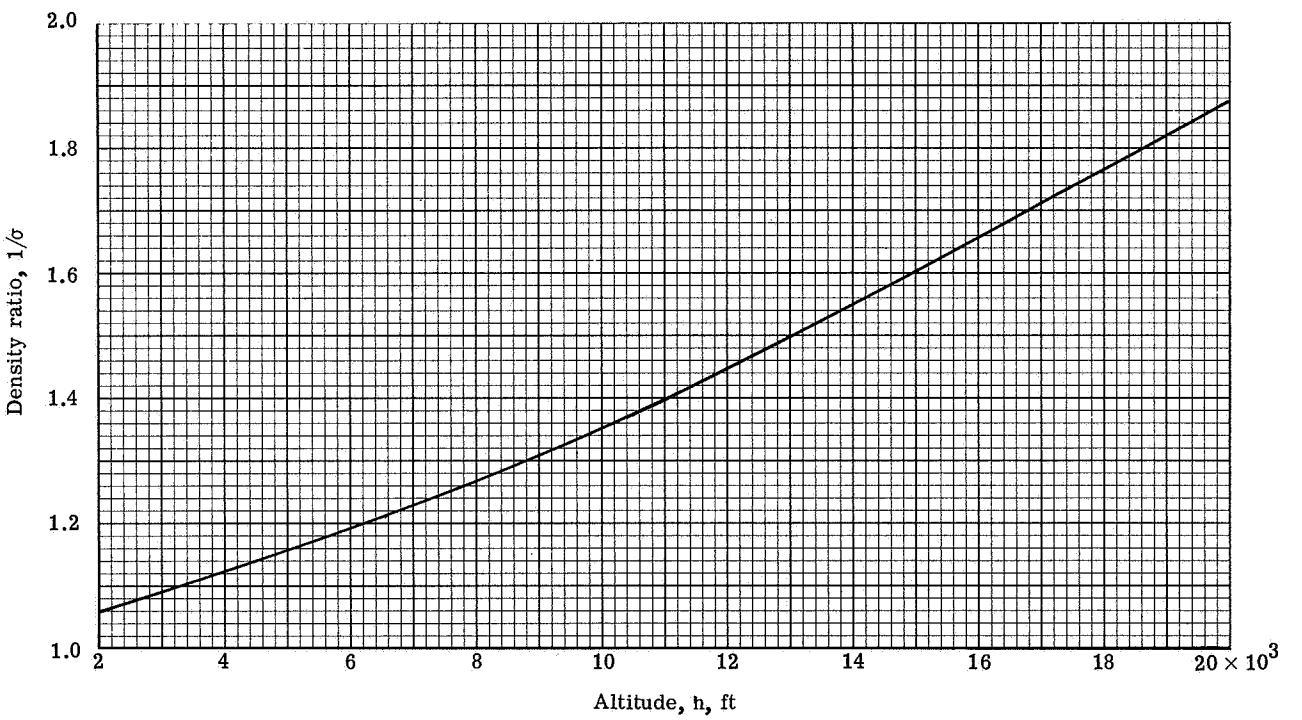


Figure 6.6.- Variation of atmosphere density ratio with altitude.

A guide is shown in figure 6.7 which may be utilized to determine the applicability of the speed curves in any given case. The aircraft speed is plotted against a wing loading parameter

$$\sqrt{\frac{W/S}{\sigma}}$$

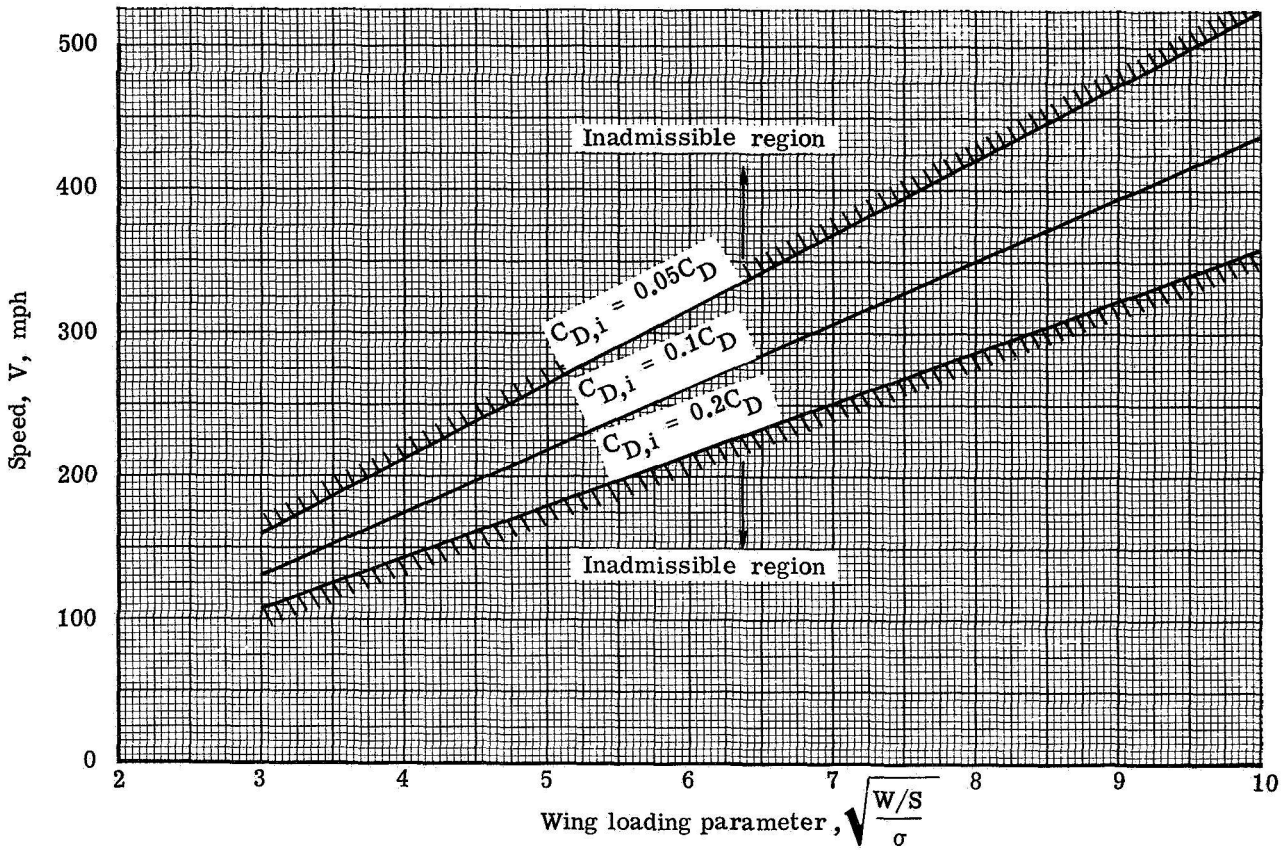


Figure 6.7.- Boundaries of speed and wing loading parameter corresponding to data of figures 6.2, 6.3, and 6.4.

for induced drag coefficients corresponding to 5, 10, and 20 percent of the total drag coefficient. The induced drag coefficient was calculated using the well-known expression

$$C_{D,i} = \frac{C_L^2}{\pi A \varepsilon}$$

where the average aspect ratio was taken to be 7 and an airplane efficiency factor of 0.7 was used. This value of efficiency factor was based on the wind-tunnel studies reported in references 6.19, 6.20, 6.21, and 6.22. An average value of the zero-lift drag coefficient of 0.0230 for class I aircraft was employed (table 6.II) in developing figure 6.7. If the performance of an aircraft is to be compared against the data of figures 6.2, 6.3, or 6.4, the speed and wing loading parameter should fall between the upper and lower boundaries of figure 6.7, preferably near the line $C_{D,i} = 0.1C_D$, *in order to be compatible* with the data contained in the figures which show speed against power index. The boundaries of figure 6.7 are specifically for class I aircraft but may be used as a rough guide for the other classes of aircraft.

6.5 Airport Performance

Methods for estimating the stalling speed, the landing field length, and the take-off field length are described in this section. The methods to be discussed relate to propeller-driven aircraft designed to meet the criteria of FAR part 23. The stalling speed, under these regulations (ref. 6.23), may not exceed 70 mph for single-engine aircraft and multiengine aircraft of less than 6000 lb gross weight which do not meet certain climb criteria. This speed of 70 mph corresponds to the maximum gross weight condition. As indicated previously, this limitation on stalling speed, when considered in relation to the relatively simple high-lift systems employed on most propeller-driven aircraft presently being designed and produced, results in wing loadings which are much lower than those characteristic of the jet-powered transports considered in chapter 3. These low wing loadings have an important effect on aircraft efficiency in cruising flight.

6.5.1 Stalling Speed

The stalling speed is related to the wing loading through the following well-known relation:

$$V_S = 29\sqrt{(W/S)\frac{1}{\sigma}\left(\frac{1}{C_{L,max}}\right)} \tag{6.8}$$

where

V_S stalling speed, ft/sec

W/S wing loading, lb/ft^2

σ density ratio

$C_{L,max}$ aircraft maximum lift coefficient

The value of the maximum lift coefficient is, in general, dependent upon the airfoil-section shape, the type of flap system, the wing-planform shape, the degree of wing surface roughness, and the Reynolds number. A correlation of the stalling speed V_S with the wing loading parameter $\sqrt{\frac{W/S}{\sigma}}$ suggests itself for wings of the same generic class. For example, a meaningful correlation should be possible for wings with little or no sweepback and moderate taper ratios, employing airfoils of moderate thickness and conventional design and equipped with relatively simple trailing-edge flap systems. The value of the stalling speed, in miles per hour, is plotted against the wing loading parameter in figure 6.8 for about 40 aircraft, including both modern general aviation aircraft and military aircraft of the World War II and prewar time periods. The points with circles are for the flags up and the points with squares are for

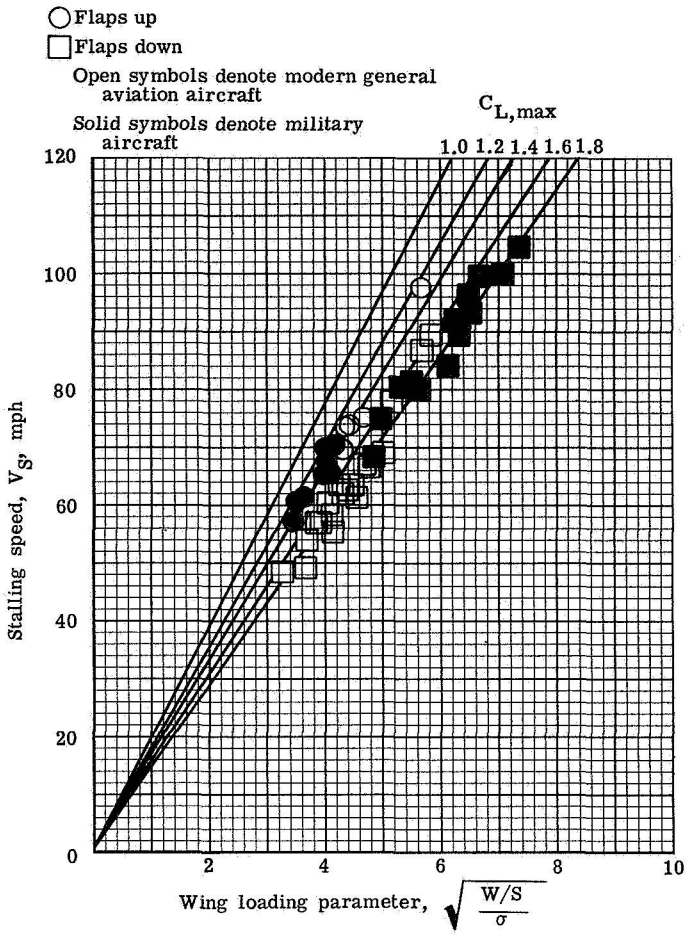


Figure 6.8.- Variation of aircraft stalling speed with wing loading parameter for flaps-up and flaps-down configurations.

flaps down. The solid symbols are for military aircraft and the open symbols are for general aviation aircraft. Only a few points are shown for the flaps-up case since stalling speeds are frequently not given for this condition in the reference documents for modern aircraft. A large number of pre-World War II aircraft specifications were examined since the use of flaps was relatively limited in that time period. Much of the data analyzed, however, were erratic and, in many cases, indicated unbelievably high values of maximum lift coefficient. Accordingly, only limited use has been made of these data. Also shown in figure 6.8 are straight lines corresponding to several values of the maximum lift coefficient. An examination of figure 6.8 indicates a close correlation of the data for the flaps-down case, with the points falling on or between the lines for maximum lift coefficients of 1.6 and 1.8. The points for the flaps-up case lie between the lines for maximum lift coefficients of 1.2 and 1.4. The results in figure 6.8 therefore suggest values of the maximum lift coefficient of 1.3 and 1.7 for the flaps-up case and flaps-down case, respec-

tively, as a basis for determining the wing loading required to give a desired value of the stalling speed.

The data in figure 6.8 for the flaps-down case correspond, of course, to split, plain, or simple single-slotted trailing-edge flaps without the use of leading-edge high-lift devices. Should a more sophisticated high-lift system be used, for example, double-slotted trailing-edge flaps together with leading-edge slats or flaps, some indication of the magnitude of the achievable maximum lift coefficient may be obtained from figure 3.4 of chapter 3. The approach lift coefficients $C_{L,A}$ given in figure 3.4, must be multiplied by the factor 1.69 in order to obtain corresponding values of maximum lift coefficients which may be compared with the data of figure 6.8. The data of figure 3.4, however, are for aircraft with relatively thin, moderately swept wings and, hence, will yield values of the maximum lift coefficient somewhat lower than would be expected from the application of the same powerful high-lift devices to straight wings of greater thickness ratio.

6.5.2 Landing Field Performance

The landing field performance which usually appears in specifications for modern, propeller-driven, general aviation aircraft designed to the airworthiness criteria of FAR part 23 consists in a ground run distance and a landing field length. The landing field length is defined as the horizontal distance from the point at which the aircraft is 50 feet above the ground to the point on the runway at which the aircraft is brought to a stop. An approach speed of at least 1.3 times the stalling speed, in miles per hour, must be maintained to the point at which the aircraft is 50 ft above the ground for aircraft of over 6000 lb gross weight. No minimum approach speed is specified for aircraft of less than 6000 lb gross weight. The landing field length is not divided by the factor 0.6 as was the case for the transport aircraft discussed in section 3.4 of chapter 3.

The landing ground run distance is shown as a function of the square of the stalling speed, in miles per hour, for about 20 modern general aviation aircraft in figure 6.9. The correlation shown by the data is seen to be reasonably good and provides a means for rapidly estimating the ground run for a given stalling speed or, conversely, the stalling speed required in order to achieve a given ground run. The landing field length is plotted in figure 6.10 as a function of the landing ground run distance for the same aircraft for which data are given in figure 6.9. The correlation of the data in figure 6.10 provides a means for determining the landing field length and, together with the data of figure 6.8, yields a limiting wing loading for a specified landing performance.

6.5.3 Take-Off Field Performance

The take-off field performance for modern, propeller-driven general aviation aircraft is usually specified in two parts, as was the case for the landing field performance. A ground run distance to lift-off is given, as is a

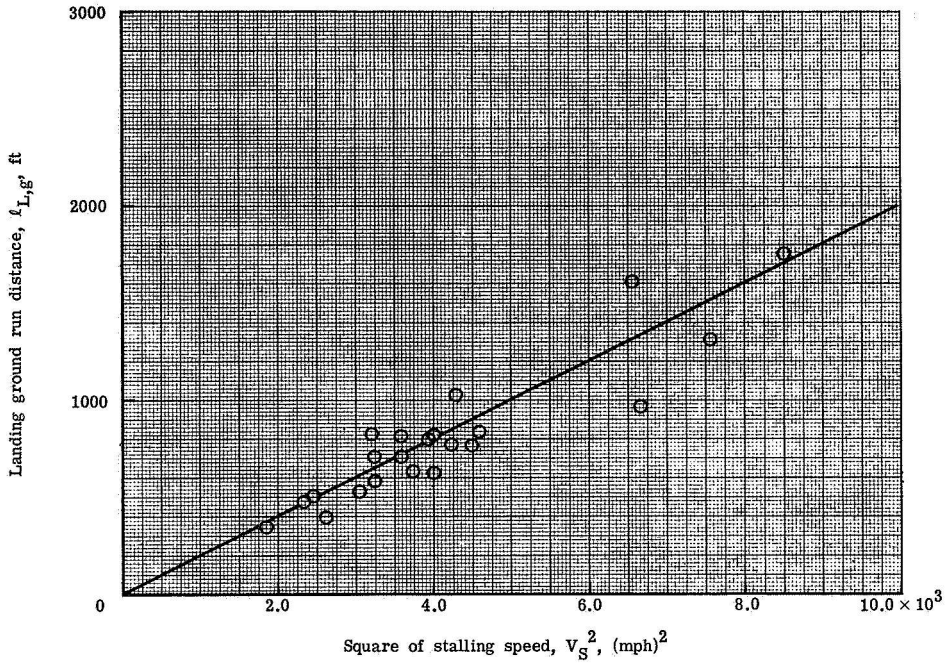


Figure 6.9.- Landing ground run distance as function of the square of stalling speed for a number of propeller-driven aircraft.

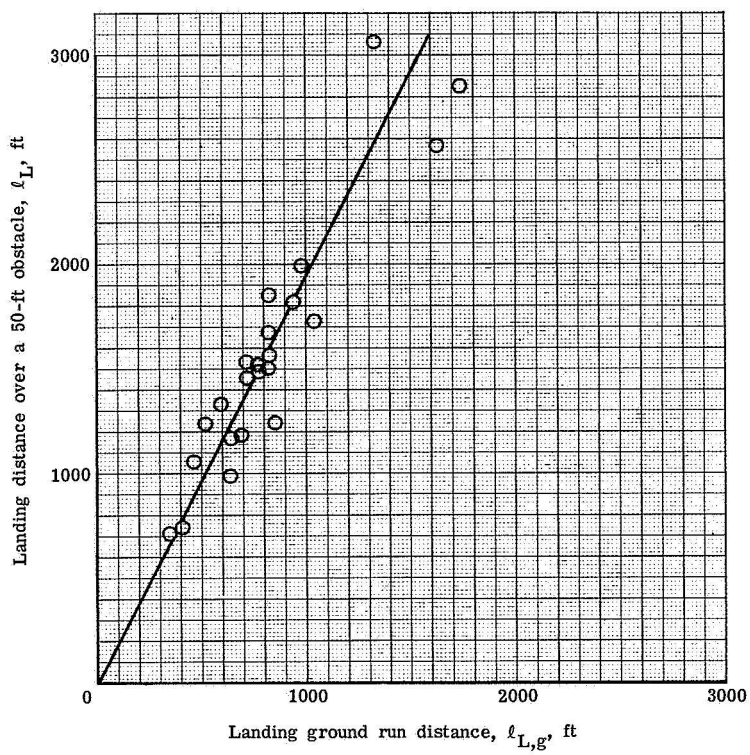


Figure 6.10.- Relationship between landing distance over a 50-ft obstacle and landing ground run distance for a number of propeller-driven aircraft.

total take-off distance. The total take-off distance is defined as the horizontal distance from the beginning of ground roll to the point at which the aircraft reaches an altitude of 50 ft. The take-off field length as used here is seen to be quite different from the FAR balanced field length concept described in chapter 3 for transport category aircraft.

A correlating parameter was developed in chapter 3 for use in estimating the take-off field length of jet-powered aircraft. For such aircraft, the take-off field length was found to be proportional to the take-off parameter as follows:

$$\ell_{T,g} \propto \frac{W/S}{\sigma C_{L,T}(T/W)} \tag{6.9}$$

where

$\ell_{T,g}$ take-off ground run distance

W/S wing loading

T/W thrust-to-weight ratio

$C_{L,T}$ take-off lift coefficient

σ density ratio

If the average thrust-to-weight ratio during the take-off of a propeller-driven aircraft is assumed to be proportional to the horsepower to weight ratio of the aircraft, then equation (6.9) takes the following form for the propeller-driven case:

$$\ell_{T,g} \propto \frac{(W/S)(W/P)}{\sigma C_{L,T}} \tag{6.10}$$

where W/P is the power loading. Curves for estimating the take-off ground run distance and take-off field length are given in terms of the parameter

$$\frac{(W/S)(W/P)}{\sigma C_{L,T}}$$

in a number of publications dealing with aircraft performance (ref. 6.24, for example).

The take-off ground run distance has been plotted against the parameter $\frac{(W/S)(W/P)}{\sigma}$ in figure 6.11 for a number of contemporary general aviation air-

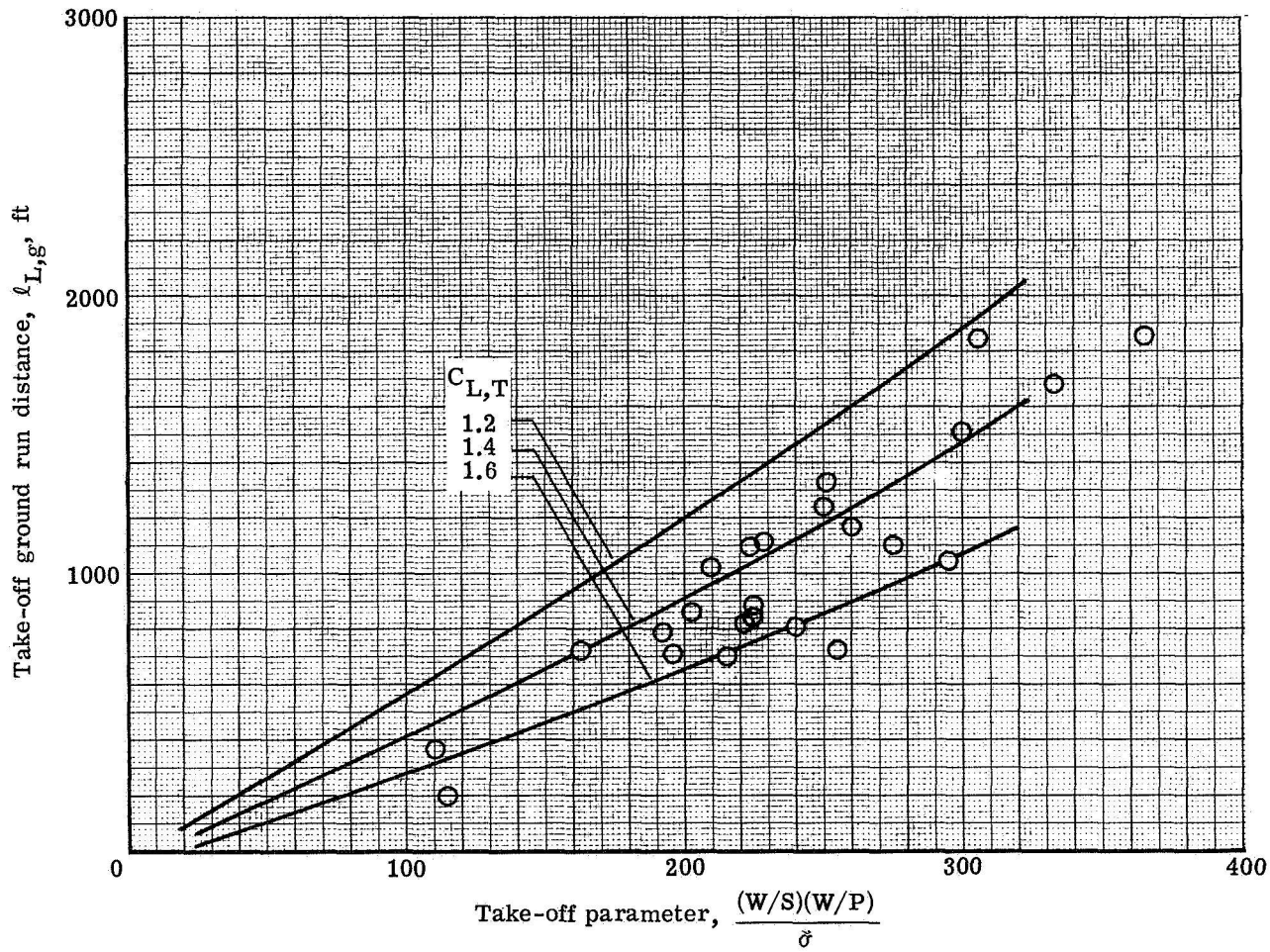


Figure 6.11.- Variation of take-off ground run distance with take-off parameter for a number of propeller-driven aircraft.

craft. The solid lines in the figure correspond to three different values of the lift coefficient $C_{L,T}$ and were calculated from the curves given in reference 6.24. The take-off lift coefficient is usually assumed to be somewhat lower than the maximum lift coefficient with flaps in the take-off configuration. This increment in lift coefficient provides a safety margin between the lift-off speed and the stalling speed. A 10-percent margin between the lift-off and stalling speeds is often used as a criterion in establishing the take-off lift coefficient. The data and curves given in figure 6.11 suggest that a take-off lift coefficient of about 1.5 corresponds to a reasonable mean of the data and, as indicated by the stalling speed trends in figure 6.8, corre-

sponds to the use of wings equipped with simple trailing-edge flaps. Thus, the information in figure 6.11 provides a means for estimating the take-off ground run distance. The take-off distance required to clear a 50-ft obstacle is shown in figure 6.12 plotted against take-off ground run distance for the same

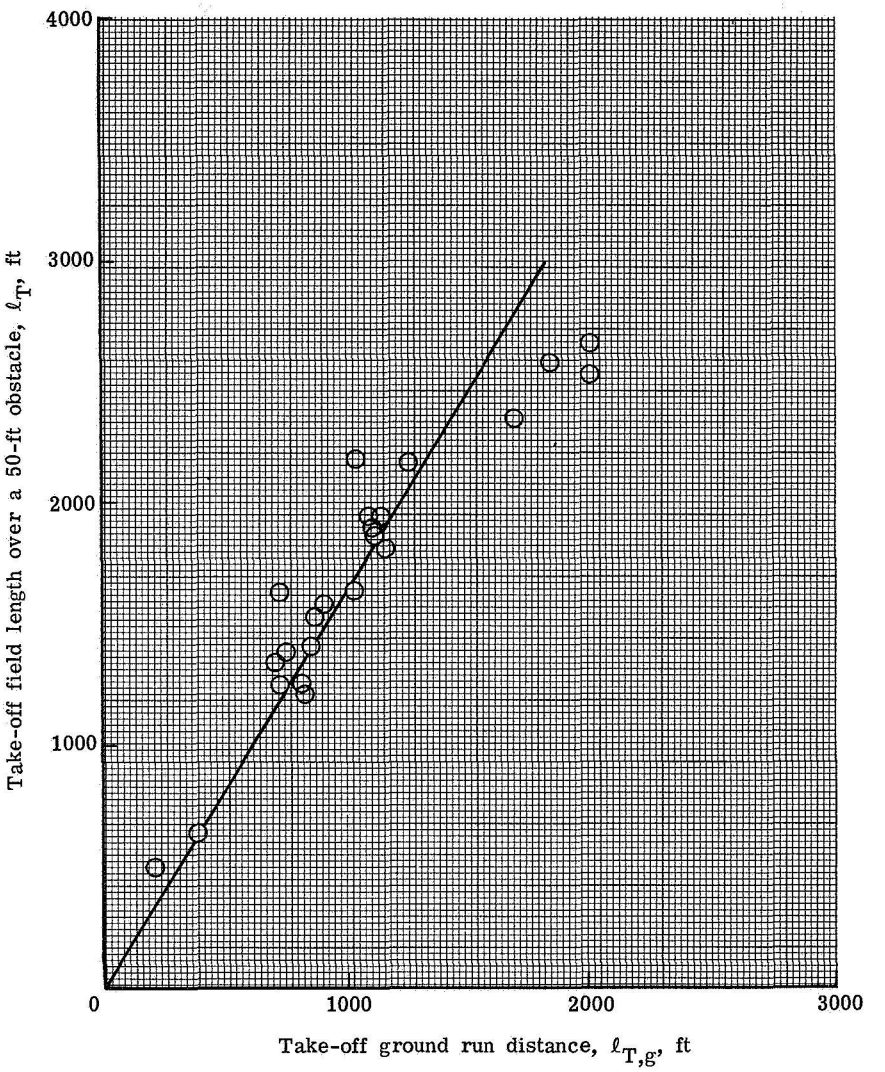


Figure 6.12.- Relationship between take-off field length over a 50-ft obstacle and take-off ground run distance for a number of propeller-driven aircraft.

aircraft for which data are given in figure 6.11. A reasonable correlation of the take-off field length with the take-off ground run distance is evident in figure 6.12. Thus, estimation of the total take-off distance and the ground run distance are possible with the use of figures 6.11 and 6.12, and a curve of power loading against wing loading required to meet a specified take-off performance may be developed.

6.6 Climb Performance

The development of a rapid method for estimating the rate of climb, including simple means for calculating certain of the necessary aerodynamic parameters, will first be discussed. FAR climb criteria will then be described, and the method for estimating the rate of climb will be utilized to develop design curves for insuring satisfaction of the relevant FAR climb criteria.

6.6.1 Rate of Climb Analysis

The aircraft rate of climb may be expressed in terms of the power available, the power required for level, unaccelerated flight at the flight condition of interest, and the aircraft weight. The relationship is given by the following well-known expression:

$$\dot{h} = \frac{33\ 000(P_a - P_r)}{W} \tag{6.11}$$

where

$\dot{h}$ rate of climb, ft/min

P_a power available, hp

P_r power required for level flight at a given speed, hp

W aircraft weight, lb

The power available may be expressed in the form

$$\frac{P_a}{W} = \frac{\eta P}{W} \tag{6.12}$$

where P is the maximum shaft horsepower available in the engine for the altitude of interest and η is the appropriate propulsive efficiency. A convenient expression for the power required may be developed as follows:

$$\frac{P_r}{W} = \frac{DV}{550W} \tag{6.13}$$

where D is the drag in pounds, V is the velocity in feet per second, and the conversion constant 550 is used so that the power required, like the power available, is expressed in horsepower. The weight, drag, and velocity may, of course, be expressed in terms of aircraft design parameters in the following way:

$$V = \sqrt{\frac{W/S}{C_L}\frac{2}{\rho}}$$

$$W = C_L(\rho/2)SV^2$$

$$D = C_D(\rho/2)SV^2$$

where S is the wing area and ρ is the atmospheric density. If these expressions for velocity, drag, and weight are substituted into equation (6.13), the following relation emerges:

$$\frac{P_r}{W} = \frac{\sqrt{W/S}}{19\left(C_L^{3/2}/C_D\right)\sqrt{\sigma}} \tag{6.14}$$

With the use of equations (6.11), (6.12), and (6.14), the rate of climb may be expressed as

$$\dot{h} = 33\ 000\left[\eta\frac{P}{W} - \frac{\sqrt{W/S}}{19\left(C_L^{3/2}/C_D\right)\sqrt{\sigma}}\right] \tag{6.15}$$

or

$$\dot{h} = 33\ 000\bar{P} \tag{6.16}$$

where $\bar{P}$ is the expression contained within the brackets of equation (6.15) and is designated the "climb parameter." Equation (6.16) provides a means for calculating the rate of climb and suggests that $\bar{P}$ be used as a parameter against which to plot the measured rates of climb of various aircraft. Before presenting such a correlation, however, methods will be developed in the next section for quickly estimating the aerodynamic parameter $C_L^{3/2}/C_D$.

6.6.2 Estimation of $C_L^{3/2}/C_D$

Equation (6.15) indicates that, for a constant value of η, the power for unaccelerated, level flight is a minimum and, hence, the rate of climb is a maximum when the aircraft is flown at a speed so that the aerodynamic parameter $C_L^{3/2}/C_D$ is a maximum. Parenthetically, unaccelerated, level flight at this speed results in maximum flight duration for a given amount of fuel. Attention will, therefore, be focused on the development of simple expressions for calculating $\left(C_L^{3/2}/C_D\right)_{max}$ and the lift coefficient corresponding to this condition, and for the variation of $C_L^{3/2}/C_D$ with lift coefficient.

The drag polar of the aircraft is assumed to be symmetrical about zero lift so that it may be represented by the equation

$$C_D = C_{D,0} + KC_L^2 \tag{6.17}$$

where C_D is the total drag coefficient, $C_{D,0}$ is the zero-lift drag coefficient, and KC_L^2 is the induced drag coefficient. The coefficient K is defined as

$$K = \frac{1}{\pi A \epsilon}$$

where

A wing aspect ratio

ϵ airplane efficiency factor

With the use of equation (6.17), the parameter $C_L^{3/2}/C_D$ may be written

$$\left(C_L^{3/2}/C_D\right) = \frac{C_L^{3/2}}{C_{D,0} + KC_L^2} \tag{6.18}$$

The maximum value of the parameter $C_L^{3/2}/C_D$ is determined through the process of taking the first derivative of $C_L^{3/2}/C_D$ (eq. (6.18)) with respect to C_L and equating the resulting equation to zero. Thus,

$$\frac{d\left(C_L^{3/2}/C_D\right)}{dC_L} = \frac{\frac{3}{2} C_{D,0}\sqrt{C_L} + \frac{3}{2} KC_L^{5/2} - 2KC_L^{5/2}}{\left(C_{D,0} + KC_L^2\right)^2}$$

Setting this expression equal to zero, cancelling $\sqrt{C_L}$, and rearranging terms yields the following:

$$\frac{3}{2} C_{D,0} - \frac{1}{2} KC_L^2 = 0 \tag{6.19}$$

or

$$C_{L,c} = \sqrt{\frac{3C_{D,0}}{K}} = \sqrt{3C_{D,0}\pi A\varepsilon} \tag{6.20}$$

Equation (6.20) provides a means for calculating the lift coefficient $C_{L,c}$ corresponding to the maximum value of $C_L^{3/2}/C_D$. Note also from equation (6.19) that the induced drag coefficient is three times the zero-lift drag coefficient at $C_L^{3/2}/C_{D\ max}$. In contrast, the induced drag coefficient is equal to the zero-lift drag coefficient for the condition of maximum C_L/C_D. The maximum value of the parameter $C_L^{3/2}/C_D$ is obtained in the following way:

$$C_{L,c}^{3/2} = \left(\sqrt{3C_{D,0}\pi A\varepsilon}\right)^{3/2}$$

$$C_D = 4C_{D,0}$$

where C_D denotes total drag coefficient. Hence,

$$\left(C_L^{3/2}/C_D\right)_{max} = \frac{(3C_{D,0}\pi A\varepsilon)^{3/4}}{4C_{D,0}}$$

$$\left(C_L^{3/2}/C_D\right)_{max} = \frac{1.345(A\varepsilon)^{3/4}}{(C_{D,0})^{1/4}} \tag{6.21}$$

Equations (6.20) and (6.21) have been used to construct the chart presented in figures 6.13 in which the maximum value of the parameter $\left(C_L^{3/2}/C_D\right)_{max}$ has been plotted against the zero-lift drag coefficient for different aspect ratios. The solid lines in the figure are for the different aspect ratios and the dashed lines represent constant values of the lift coefficient $C_{L,c}$ corresponding to $\left(C_L^{3/2}/C_D\right)_{max}$. A value of 0.7 of the airplane efficiency factor ε was used in calculating the curves of figure 6.13. The curves in figure 6.13 pro-

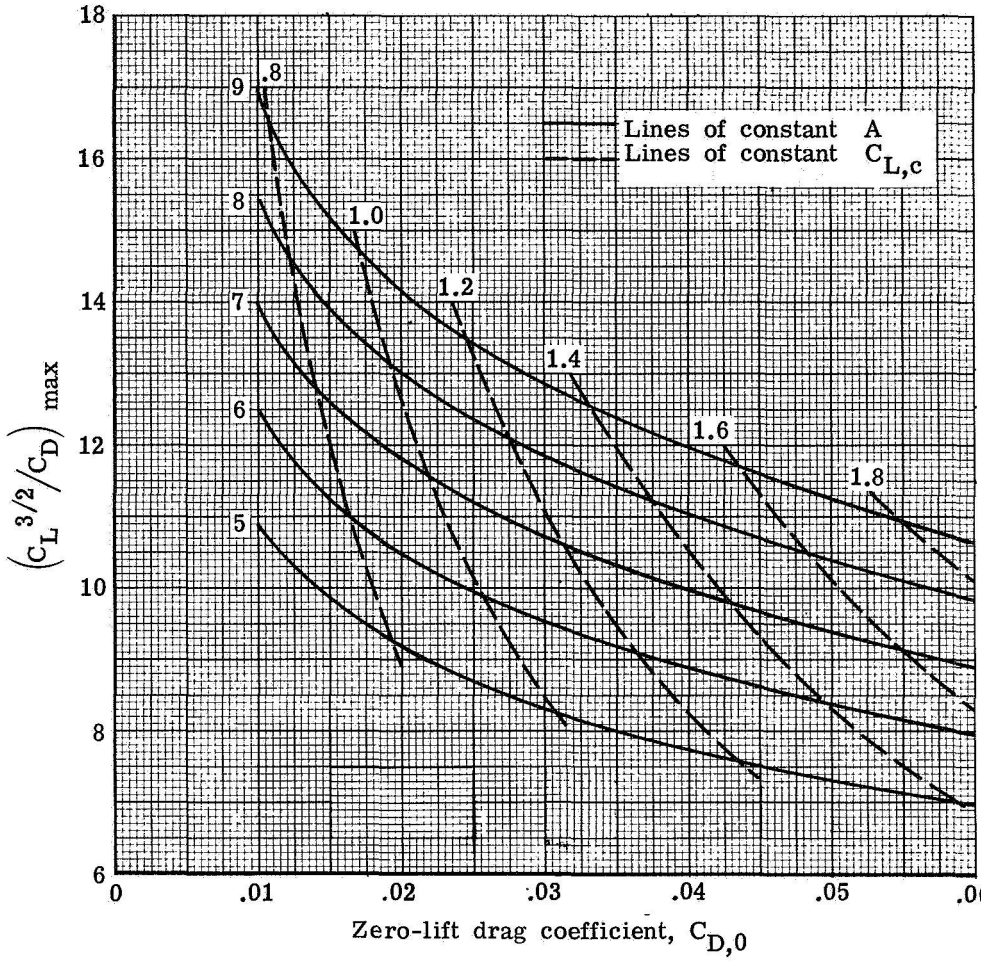


Figure 6.13.- Chart for estimating the parameter $\left(C_L^{3/2}/C_D\right)_{max}$. $\varepsilon = 0.7$.

vide a rapid means for obtaining the aerodynamic information needed to determine the climb parameter $\bar{P}$ given by equations (6.15) and (6.16).

The manner in which the parameter $C_L^{3/2}/C_D$ varies with lift coefficient is of interest for the prediction of rate of climb at lift coefficients other than that for maximum climb rate. A generalized relationship which permits the determination of $C_L^{3/2}/C_D$ at any lift coefficient in terms of $\left(C_L^{3/2}/C_D\right)_{max}$ and $C_{L,c}$ is easily derived. The value of the zero-lift drag coefficient was shown by equation (6.19) to be one-fourth that of the total drag coefficient at $\left(C_L^{3/2}/C_D\right)_{max}$. Thus,

$$C_D = 4C_{D,0}$$

and

$$C_D = \frac{4}{3} C_{D,i}$$

where $C_{D,i}$ is the induced drag coefficient. Then the ratio of the total drag coefficient at any lift coefficient to that at the lift coefficient for $\left(C_L^{3/2}/C_D\right)_{max}$ is

$$\frac{C_D}{C_{D,c}} = \frac{C_{D,0} + KC_L^2}{C_D} = \frac{C_{D,0}}{4C_{D,0}} + \frac{KC_L^2}{\frac{4}{3} K(C_{L,c})^2}$$

or

$$\frac{C_D}{C_{D,c}} = \frac{1}{4} + \frac{3}{4} \bar{C}_L^2 \tag{6.22}$$

where $\bar{C}_L = \frac{C_L}{C_{L,c}}$ and $C_{D,c}$ is the total drag coefficient corresponding to the lift coefficient for $\left(C_L^{3/2}/C_D\right)_{max}$.

If equation (6.22) is inverted and multiplied on both sides by $(\bar{C}_L)^{3/2}$, the following relation is obtained:

$$\frac{C_L^{3/2}/C_D}{\left(C_L^{3/2}/C_D\right)_{max}} = \frac{4(\bar{C}_L)^{3/2}}{1 + 3(\bar{C}_L)^2} \tag{6.23}$$

Equation (6.23) is plotted in figure 6.14 and permits the rapid determination of $C_L^{3/2}/C_D$ at any lift coefficient if $\left(C_L^{3/2}/C_D\right)_{max}$ and $C_{L,c}$ are known.

The data in figures 6.13 and 6.14 are, as previously noted, based on the assumption of a symmetrical drag polar; however, reasonably accurate results may be obtained from these figures for values of the design lift coefficient in the range from 0 to 0.4.

6.6.3 Aircraft Rate-of-Climb Characteristics

The measured rate of climb, as determined from the reference documents, is presented in figure 6.15 as a function of the climb parameter $\bar{P}$ for a

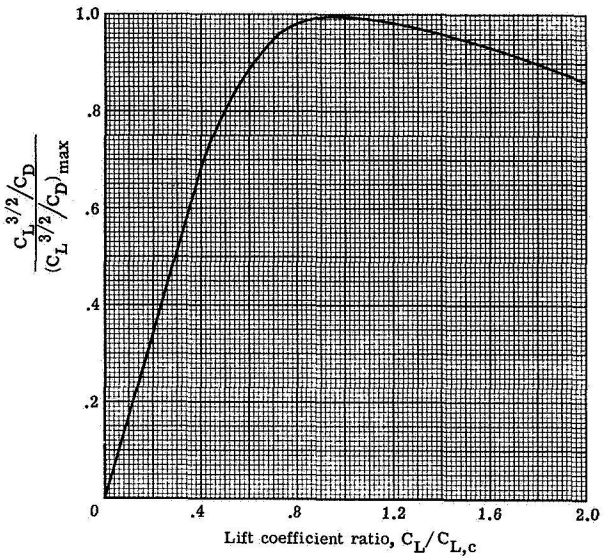


Figure 6.14.- Variation of normalized parameter with lift coefficient ratio.

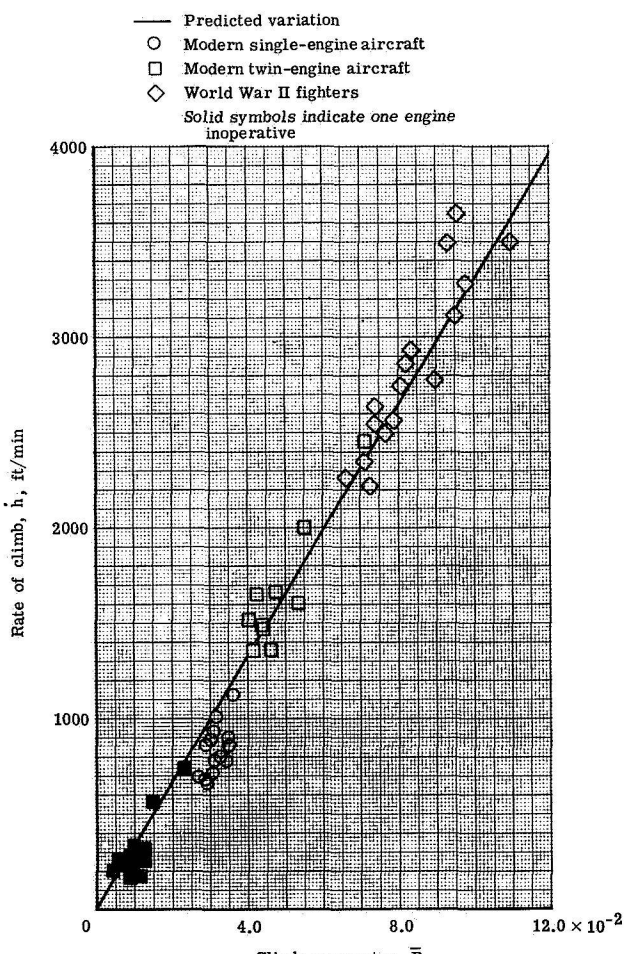


Figure 6.15.- Rate of climb as function of climb parameter for a number of propeller-driven aircraft.

number of modern general aviation aircraft and World War II fighter aircraft. The circles represent modern single-engine aircraft, the squares represent modern twin-engine aircraft, and the diamonds represent World War II fighter aircraft. The solid symbols are for twin-engine aircraft with one engine inoperative.

Equation (6.15) together with the curves of figure 6.13 were used to determine the value of $\bar{P}$ for the various aircraft. The average values of zero-lift drag coefficient, as given in table 6.II for class I and class II aircraft, were utilized together with $\varepsilon = 0.7$ in determining the value of the climb parameter $\bar{P}$. The aspect ratio of each individual aircraft was employed in the calculations. A study of reference 6.25 suggested that a value of the propulsive efficiency of 0.7 would be appropriate for the high propeller rotational speed and relatively low forward speed conditions typical of an aircraft flying at its maximum rate of climb. The value of η was accordingly taken to be 0.7 in all cases. The predicted variation line in figure 6.15 merely represents the rate of climb as given by equation (6.16) for arbitrarily assumed values of the climb parameter $\bar{P}$.

The experimental points for the various aircraft are seen to form a close, linear correlation with the climb parameter $\bar{P}$. A good fairing of the points is represented by the solid line which gives the predicted variation of rate of climb with the climb parameter. The experimental rates of climb for a number of the modern single-engine aircraft are seen to fall below the predicted line. Many of these low points are for aircraft with fixed tricycle landing gear. Similarly, the maximum speeds of such aircraft were seen to fall below the mean line values in figure 6.3; and as pointed out in section 6.4.2, the zero-lift drag coefficients of these aircraft may be higher than the average values as a result of the tricycle landing gear. The use of a value of $C_{D,0}$ closer to the maximum value, as given in table 6.II for Class II aircraft, would bring the points closer to the line representing the predicted variation. In any case, the predicted line in figure 6.15 would appear to be a good basis for estimating aircraft rate of climb. In the absence of more definitive information, values of ε and η as used herein and average values of $C_{D,0}$ from table 6.II are recommended in the determination of $\bar{P}$.

6.6.4 FAR Climb Criteria

The climb criteria for propeller-driven aircraft designed to meet the airworthiness standards of FAR part 23 are described in detail in reference 6.23. The most significant aspects of these criteria are briefly summarized as follows:

For aircraft under 6000 lb gross weight with all engines operating:

(1) The rate of climb in the take-off configuration must be at least $10V_S$ where V_S is the stalling speed in miles per hour with the flaps in the take-off position and the rate of climb is expressed in feet per minute. The aircraft in this case is at maximum gross weight, sea-level standard conditions are specified, and the landing gear is extended.

(2) The rate of climb in the landing configuration must be at least $5V_S$ where V_S now corresponds to that for the flaps in the landing position. All other conditions are the same as for the take-off case.

For aircraft over 6000 lb gross weight, and aircraft under 6000 lb gross weight which have a stalling speed greater than 70 mph, and one engine inoperative:

(1) The rate of climb in feet per minute must be $0.02V_S^2$ where V_S is in miles per hour and the flaps are in the landing position. Maximum gross weight and sea-level standard conditions are specified in determining V_S. The rate of climb is that for an altitude of 5000 ft with the landing gear retracted and the flaps in the most favorable position.

For aircraft over 6000 lb gross weight with all engines operating:

(1) The climb gradient in the take-off configuration must be at least 8.33 percent. The flaps in this case are in the take-off position, the landing gear is retracted, the aircraft is at maximum gross weight, and sea-level standard conditions prevail.

(2) The climb gradient in the landing configuration must be at least 3.33 percent. The flaps for this case are in the landing position, and the landing gear is extended. Other conditions are the same as for the take-off case.

The above brief statements summarizing the climb criteria will be used as a basis for developing analytical methods for insuring compliance and for generating a group of charts which can be used as a rough guide in determining compliance with the regulations.

6.6.4.1 Aircraft Under 6000 lb Gross Weight

The required climb rate for aircraft under 6000 lb gross weight can be expressed in the form

$$\dot{h} = K_1 V_S \tag{6.24}$$

where $\dot{h}$ is in feet per minute and V_S is in miles per hour. For the take-off configuration, $K_1 = 10$; for the landing configuration, $K_1 = 5$. The values of V_S used in the two cases differ according to the two different flap deflections and associated airplane maximum lift coefficients. If the expression for the rate-of-climb requirement given by equation (6.24) is inserted into equation (6.15) and the stalling speed is expressed in terms of the wing loading, maximum lift coefficient, and sea-level density, the following equation is obtained:

$$\frac{P}{W} = \frac{\sqrt{\frac{W/S}{\sigma}}\left[\frac{19.73K_1}{\sqrt{C_{L,max}}} + \frac{1736.8}{\left(C_L^{3/2}/C_D\right)_{max}}\right]}{33\ 000\eta} \tag{6.25}$$

The ratio of horsepower to weight required to meet the climb criteria may be plotted as a function of wing loading for aircraft having a given value of $\left(C_L^{3/2}/C_D\right)_{max}$, $C_{L,max}$, and propulsive efficiency η. Such plots are shown in figures 6.16 and 6.17 for aircraft in the take-off and landing configurations, respectively. Curves for aspect ratios of 6, 7, 8, and 9 are presented for each case. The values of $\left(C_L^{3/2}/C_D\right)_{max}$ used in deriving the curves of figures 6.16 and 6.17 were obtained from figure 6.13 with the use of zero-lift drag

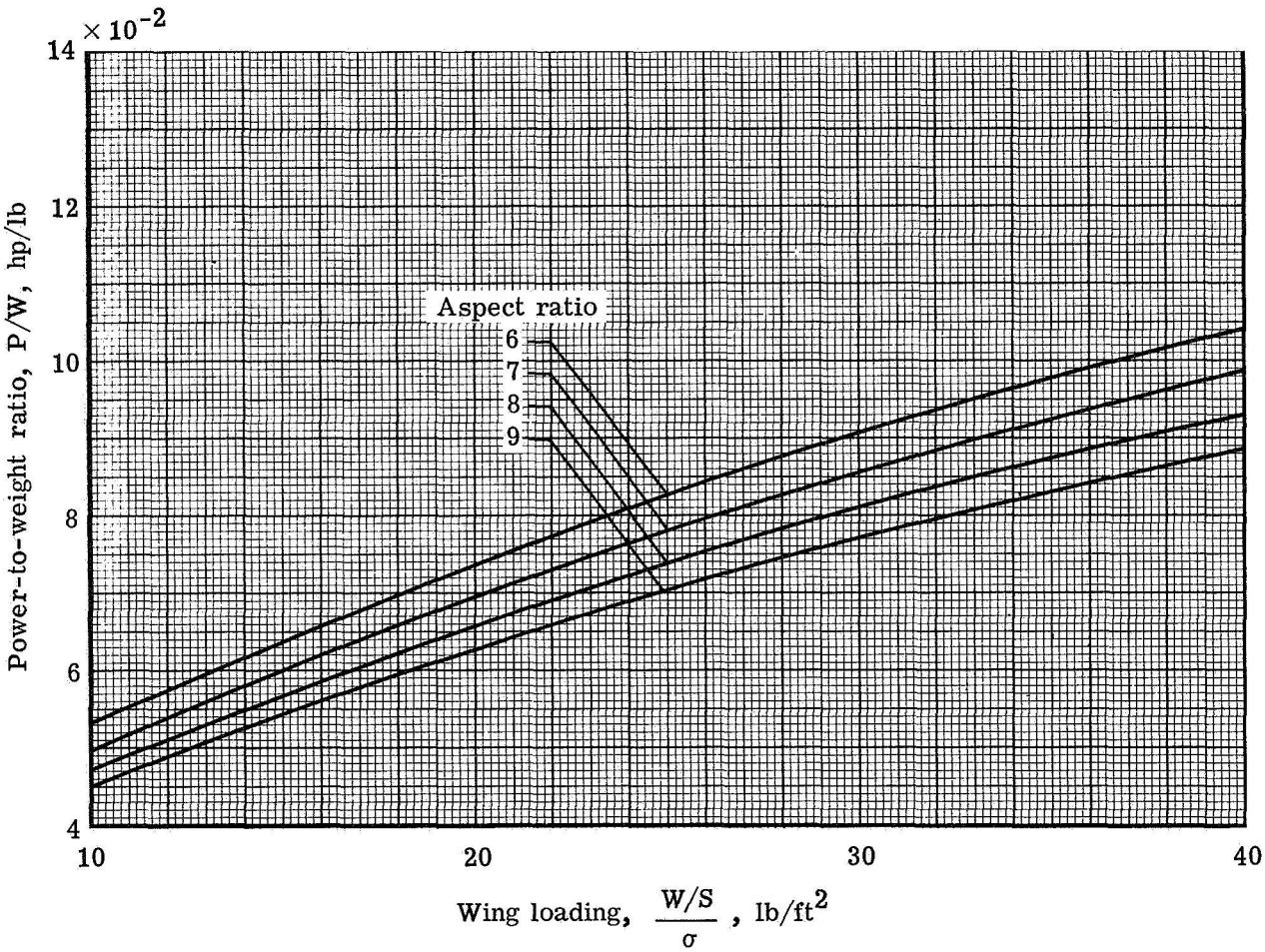


Figure 6.16.- Power-to-weight ratio, all engines operating, required to meet climb rate criterion for propeller-driven aircraft in take-off configuration. FAR part 23 for aircraft under 6000 lb gross weight; $C_{L,T} = 1.5$.

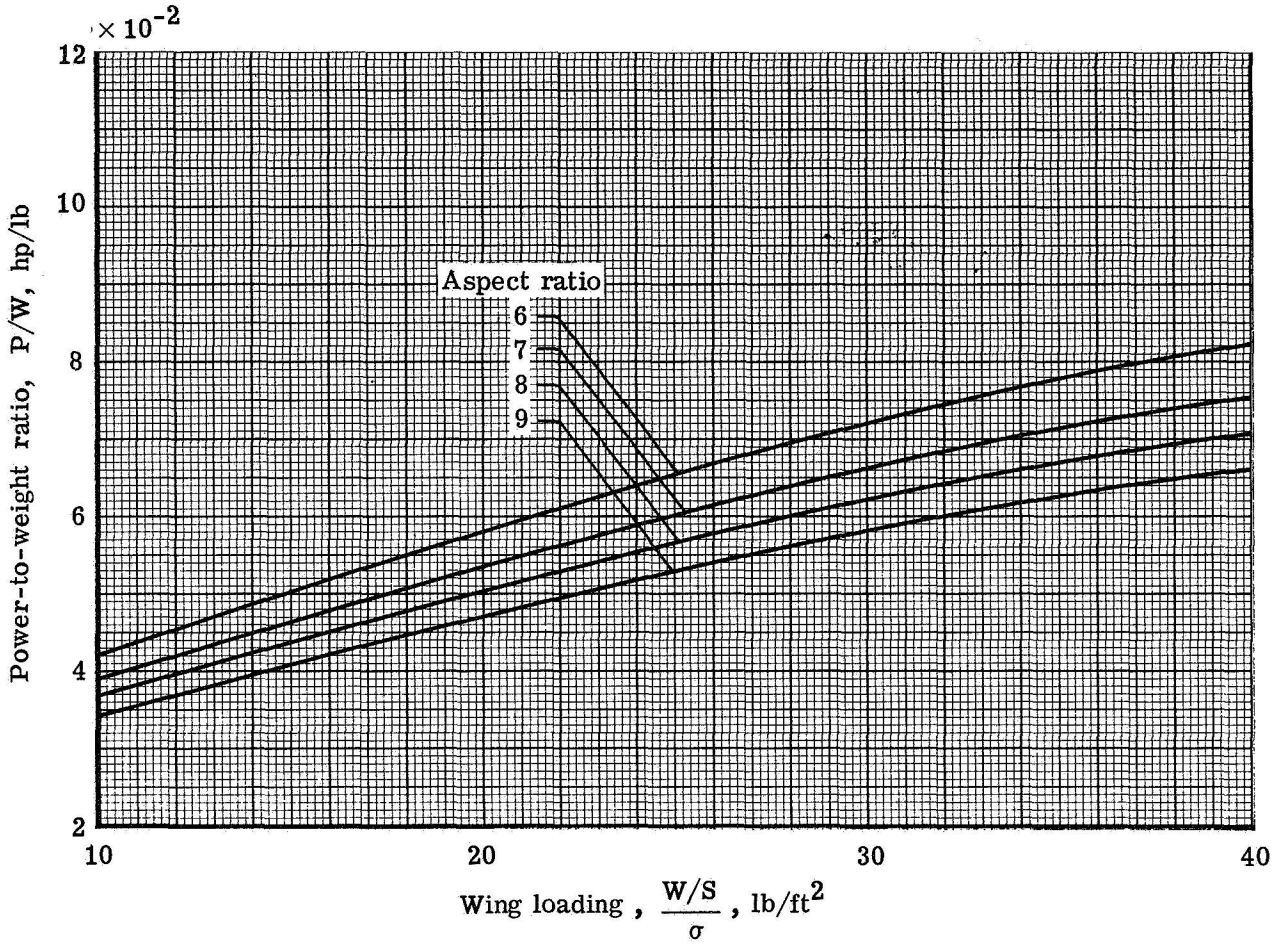


Figure 6.17.- Power-to-weight ratio, all engines operating, required to meet climb rate criterion for propeller-driven aircraft in landing configuration. FAR part 23 for aircraft under 6000 lb gross weight; $C_{L,max} = 1.7$.

coefficients of 0.043 and 0.038 corresponding to the aircraft in the landing and take-off configurations, respectively. These drag coefficients contain the following elements:

$C_{D,0} = 0.0230$ for clean, class I aircraft

$\Delta C_{D,0} = 0.010$ for the landing gear

$\Delta C_{D,0} = 0.010$ for the flaps in the landing configuration

$\Delta C_{D,0} = 0.005$ for the flaps in the take-off configuration

The drag increment attributable to the landing gear was obtained from the difference between the average zero-lift drag coefficients of class I and class II aircraft as given in table 6.II. The actual increment of 0.0066 was increased to 0.010 to account for the drag of open wheel well doors, exposed wheels, and

other drag producing elements of a retractable landing gear in the extended position. The drag increments associated with flap deflection were estimated by the method of reference 6.26. The flaps were assumed to be of the single-slotted type, to influence 65 percent of the wing area, and to have a chord of 20 percent of the wing chord. The maximum lift coefficients for the landing and take-off configurations were taken to be 1.7 and 1.5, respectively, and a value of propulsive efficiency of 70 percent was used in all calculations.

The curves in figure 6.16 and 6.17 may be used for quickly estimating the power-to-weight ratio required to meet the FAR climb criteria for aircraft weighing less than 6000 lb. The curves were developed for aircraft with retractable landing gear and wing flaps, but may be used with some conservatism for aircraft with fixed landing gear and wing flaps. For aircraft without flaps, or aerodynamic parameters significantly different from those employed in constructing figures 6.17 and 6.18, additional curves must be calculated with the use of equation (6.25).

6.6.4.2 Aircraft With One Engine Inoperative

The required climb rate with one engine inoperative for aircraft of over 6000 lb gross weight and lighter aircraft with a stalling speed of over 70 mph, may be expressed in the form

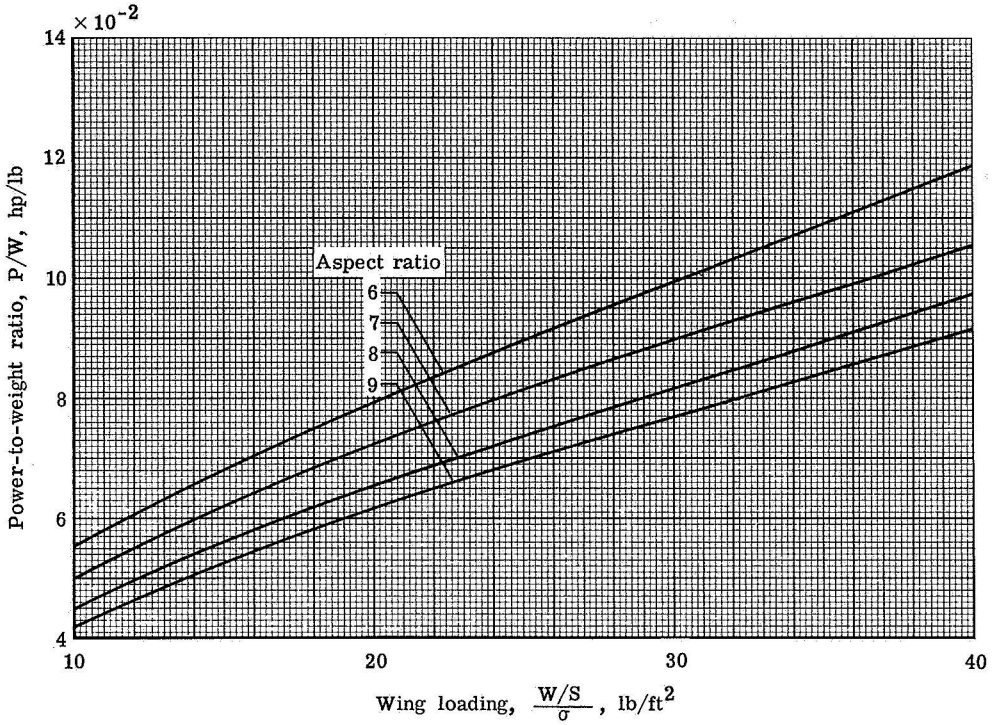
$$\dot{h} = 0.02 V_S^2 \tag{6.26}$$

where $\dot{h}$ is in feet per minute and V_S is the stalling speed at sea level in miles per hour for wing flaps in the landing position. The climb rate, however, is measured with the flaps in the most favorable position, the landing gear retracted, and at an altitude of 5000 ft. If the expression for the rate of climb given by equation (6.26) is introduced into equation (6.15) and the stalling speed is expressed in terms of the wing loading, the maximum lift coefficient and the density at sea level, the following equation is obtained:

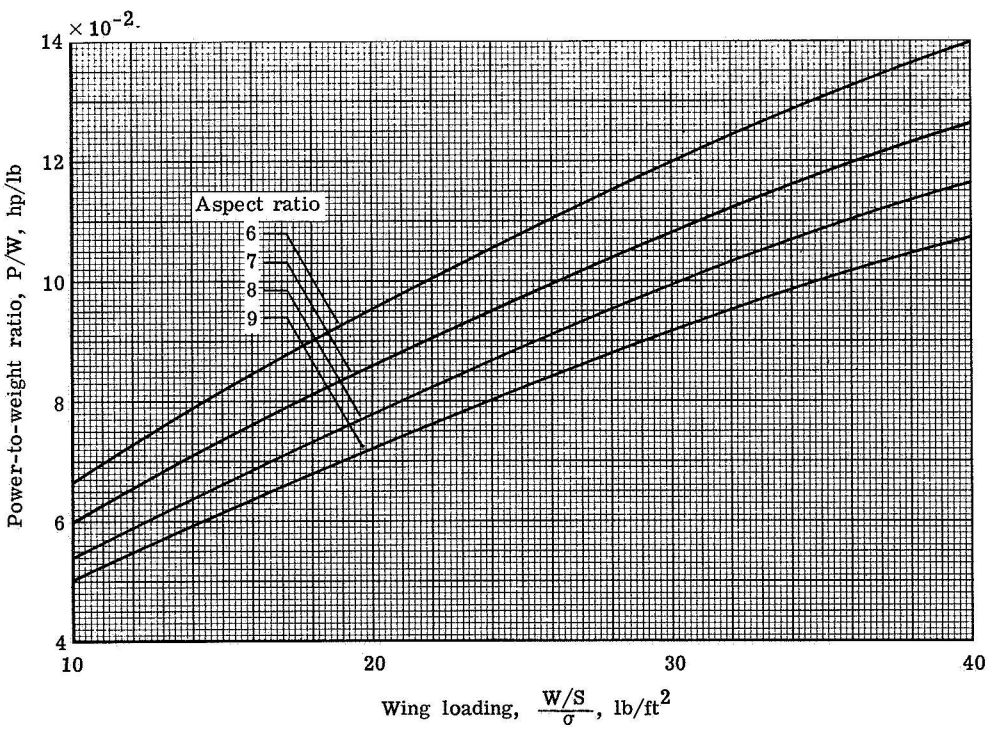
$$\frac{P}{W} = \frac{\dfrac{7.784\ W/S}{C_{L,max}\sqrt{\sigma}} + \dfrac{1736.8\sqrt{W/S}}{\left(C_L^{3/2}/C_D\right)_{max}\sqrt{\sigma}}}{33\ 000\eta} \tag{6.27}$$

where P/W is the power-to-weight ratio with one engine inoperative.

The power-to-weight ratio, all engines operating, required to meet the one-engine inoperative climb criteria may be plotted as a function of wing loading for aircraft having a given value of $C_L^{3/2}/C_D$, $C_{L,max}$, and propulsive efficiency η. Such plots for twin-engine aircraft, constructed with the use of equation (6.27), are shown in figure 6.18(a) for aircraft with supercharged engines and in figure 6.18(b) for aircraft with unsupercharged engines. Curves



(a) Supercharged twin-engine aircraft.



(b) Unsupercharged twin-engine aircraft.

Figure 6.18.- Power-to-weight ratio, all engines operating, required to meet climb criterion for propeller-driven aircraft with one engine inoperative. FAR part 23 for aircraft over 6000 lb gross weight.

are presented in each figure for aspect ratios of 6, 7, 8, and 9. For unsupercharged aircraft (fig. 6.18(b)), the power-to-weight ratio as determined by equation (6.27) must be divided by the factor 0.852 to account for the reduction in power with altitude. The power at 5000-ft altitude is found in figure 6.28 (fig. 6.28 will be discussed in section 6.9) to be 0.852 times the power at sea level for an unsupercharged engine. The values of maximum lift coefficient $C_{L,max}$ and propulsive efficiency η were assumed to be 1.7 and 0.70, respectively. The value of σ for 5000-ft altitude is found from figure 6.6 to be 0.862. The values of $\left(C_L^{3/2}/C_D\right)_{max}$ were determined from figure 6.13 for class I aircraft in the clean condition, that is, the zero-lift drag coefficient $C_{D,0}$ was taken to be 0.0230. The curves in figure 6.18 may be used for quickly estimating the power-to-weight ratio, all engines operating, required to meet the one-engine-inoperative climb requirement.

6.6.4.3 Climb Gradient Criteria

The climb gradient criteria apply to aircraft having a gross weight of 6000 lb or more. The criteria may be expressed in the following form:

$$K_2 = \frac{\dot{h}}{V} \tag{6.28}$$

where K_2 is the climb gradient criterion which is 8.33 percent and 3.33 percent for aircraft in the take-off configuration and landing configuration, respectively. The climb rate $\dot{h}$ and velocity in equation (6.28) must, of course, be expressed in consistent units. An expression for the climb gradient may be obtained by dividing equation (6.15) by the velocity

$$\frac{\dot{h}}{V} = K_2 = \frac{550\left[\eta(P/W) - \dfrac{\sqrt{W/S}}{19\left(C_L^{3/2}/C_D\right)\sqrt{\sigma}}\right]}{29\sqrt{\dfrac{W/S}{C_L\sigma}}} \tag{6.29}$$

where the quantity $29\sqrt{\dfrac{W/S}{C_L\sigma}}$ expresses the aircraft velocity in feet per second and the constant 550 appears outside the brackets, rather than 33 000 as in equation (6.15), in order that the rate of climb will also be in feet per second. This equation may be simplified and rearranged in the following form:

$$\bar{\theta} = \frac{K_2 + \dfrac{1}{L/D}}{\sqrt{C_L}} \tag{6.30}$$

where the parameter $\bar{\theta}$ is defined as

$$\bar{\theta} = 18.97\eta(P/W)\sqrt{\frac{\sigma}{W/S}} \tag{6.31}$$

and L/D is the aircraft lift-drag ratio and C_L is the corresponding lift coefficient. Thus, with the use of equation (6.30), $\bar{\theta}$ may be determined as a function of lift coefficient and associated lift-drag ratio for a given value of K_2. The minimum value of $\bar{\theta}$ determined in this fashion may then be used with equation (6.31) to generate a curve of power-to-weight ratio required to meet the climb gradient criteria, against wing loading. This procedure will be utilized to construct curves of power-to-weight ratio versus wing loading for wings of different aspect ratio and aircraft in both the take-off and landing configurations.

In order to simplify the calculations, equation (6.30) is rewritten in the form:

$$\bar{\theta} = \frac{K_2 + \dfrac{1}{(L/D)_{max}\dfrac{L/D}{(L/D)_{max}}}}{\sqrt{C_{L,m}}\sqrt{\bar{C}_L}} \tag{6.32}$$

where $C_{L,m}$ is the lift coefficient for maximum lift-drag ratio $(L/D)_{max}$, and $\bar{C}_L$ is the ratio $C_L/C_{L,m}$. Equation (3.27) of chapter 3 gives the following important expression for $(L/D)/(L/D)_{max}$:

$$\frac{L/D}{(L/D)_{max}} = \frac{2\bar{C}_L}{1 + \bar{C}_L{}^2} \tag{6.33}$$

Substitution of equation (6.33) into equation (6.32) yields

$$\bar{\theta} = \frac{K_2 + \dfrac{1 + \bar{C}_L^2}{2(L/D)_{max}\bar{C}_L}}{\sqrt{C_{L,m}}\sqrt{\bar{C}_L}} \tag{6.34}$$

The values of $(L/D)_{max}$ and $C_{L,m}$ may be determined from the expressions given in chapter 3 and repeated here as follows:

$$(L/D)_{max} = \frac{1}{2}\sqrt{\frac{\pi A \epsilon}{C_{D,0}}} \tag{6.35}$$

$$C_{L,m} = \sqrt{\pi A \epsilon C_{D,0}} \tag{6.36}$$

Equations (6.34), (6.35), and (6.36) have been used to calculate $\bar{\theta}$ as a function of lift coefficient for aspect ratios of 6, 7, 8, and 9 for aircraft in the take-off and landing configurations. Both flaps and landing gear retracted were assumed for the take-off configuration with a resulting zero-lift drag coefficient $C_{D,0}$ for class I aircraft of 0.0230. The value of the airplane efficiency factor ϵ was taken to be 0.7. Curves of $\bar{\theta}$ are shown as a function of C_L for the different aspect ratios in figure 6.19 for the take-off

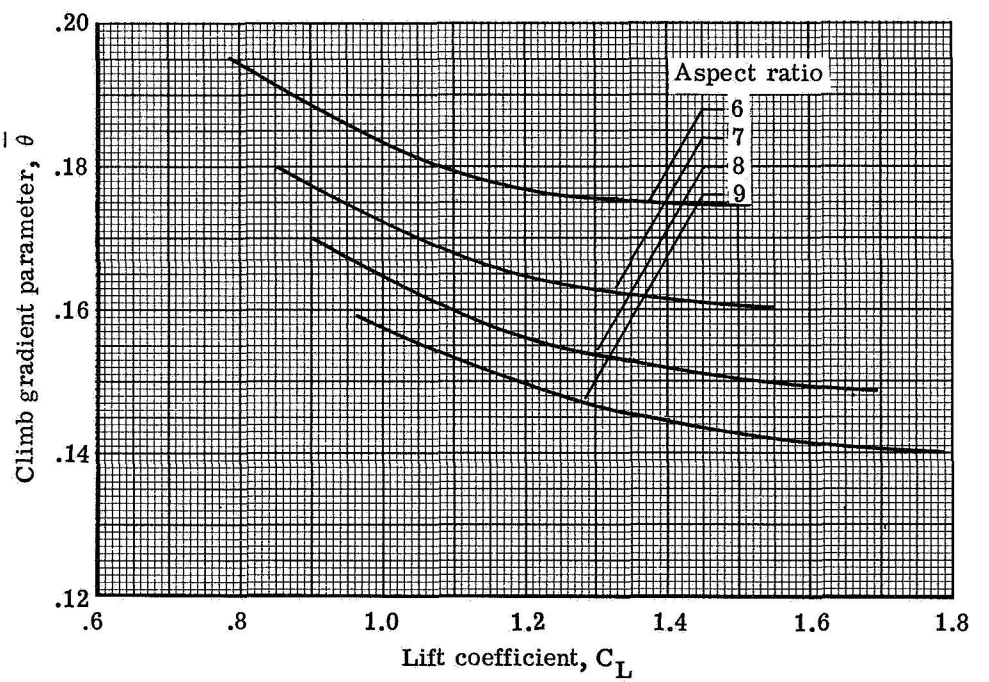


Figure 6.19.- Climb gradient parameter as function of lift coefficient for aircraft in take-off configuration. 8.3 percent climb gradient.

configuration. The minimum value of $\bar{\theta}$ is seen to occur at a lift coefficient which varies from 1.4 for aspect ratio 6 to a value above 1.8 for aspect ratio 9.

A minimum value of $\bar{\theta}$ is, of course, desired in order to minimize the power-to-weight ratio for a given wing loading. The value of the maximum lift coefficient for unflapped wings is about 1.3 according to the trends shown in figure 6.8. The climb lift coefficient must be less than the maximum lift coefficient to allow for speed excursions, turbulence, maneuvers, etc. Part 23 of the Federal Air Regulations does not specify a relationship between stalling speed and the speed at which the angle of climb is determined. A lift coefficient of 1.1 was therefore chosen as the climbing lift coefficient for the take-off configuration. The values of $\bar{\theta}$ corresponding to this lift coefficient for the different aspect ratios were used in calculating the variation of power-to-weight ratio with wing loading.

The margin between the climbing lift coefficient and the maximum lift coefficient may, from safety considerations, be too small and probably should only be used for demonstration purposes. The important effects of power in increasing the maximum lift coefficient, however, result in a larger difference between maximum and climbing lift coefficients than is indicated by the power-off values. Higher climbing lift coefficients would be possible with the use of small flap deflections; however, the value of $\bar{\theta}$ at a given lift coefficient would be increased somewhat by the reduction in $(L/D)_{max}$ resulting from deflection of the flaps. Further calculations would be required in order to determine the desirability of deflecting flaps as a means for obtaining a net reduction in $\bar{\theta}$ for a given wing loading.

The use of equation (6.31) together with the values of $\bar{\theta}$ found in figure 6.19 for a lift coefficient of 1.1 and a propulsive efficiency of 70 percent have been used to construct the curves of figure 6.20 which give the required power-to-weight ratio against wing loading for different aspect ratios. These curves may be used to obtain a rough estimate of the power required to meet the FAR climb gradient requirement for aircraft of over 6000 lb gross weight in the take-off configuration.

The same procedure as that just described was used in calculating the curves of power-to-weight ratio as a function of wing loading for aircraft in the landing configuration. The zero-lift drag coefficient in this case was 0.0430 and included increments, as described in section 6.6.4, for the flaps and extended landing gear. The parameter $\bar{\theta}$ is plotted against C_L for aspect ratios of 6, 7, 8, and 9 in figure 6.21 for aircraft in the landing configuration. Values of $\bar{\theta}$ corresponding to a lift coefficient of 1.5 were chosen as a basis for calculating the power-required curves. The climbing lift coefficient of 1.5 compares to an average power-off maximum lift coefficient for the flaps-deflected configuration of about 1.7 as shown by figure 6.8. Curves of required power-to-weight ratio plotted against wing loading are presented in figure 6.22 for aircraft in the landing configuration and may be used for estimation purposes.

Comparison of the curves of figures 6.20 and 6.22 with those of figure 6.18 indicates that the one-engine inoperative criterion usually yields a higher

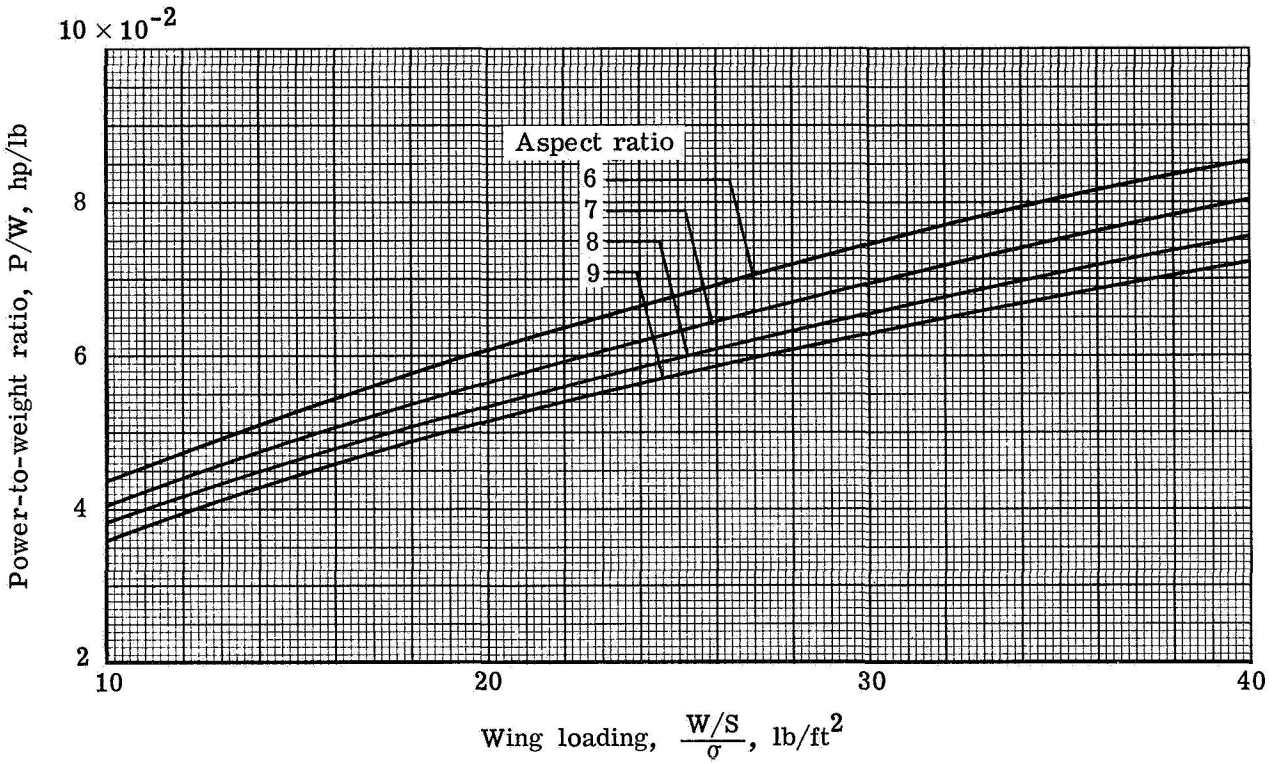


Figure 6.20.- Power-to-weight ratio, all engines operating, required to meet climb gradient requirement for propeller-driven aircraft in take-off configuration. FAR part 23 for aircraft over 6000 lb gross weight.

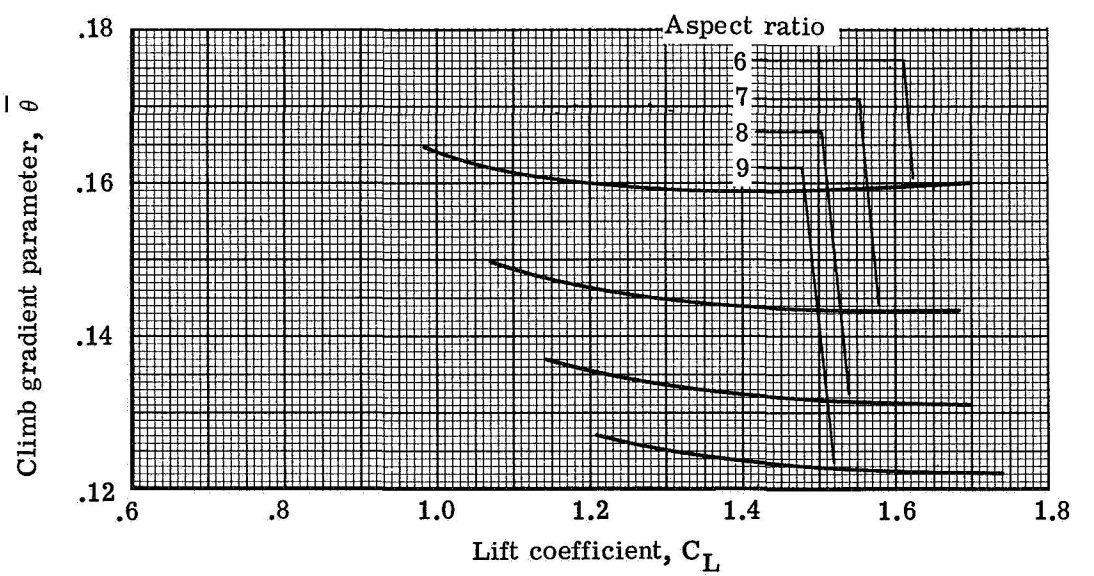


Figure 6.21.- Climb gradient parameter as function of lift coefficient for aircraft in landing configuration. 3.3 percent climb gradient.

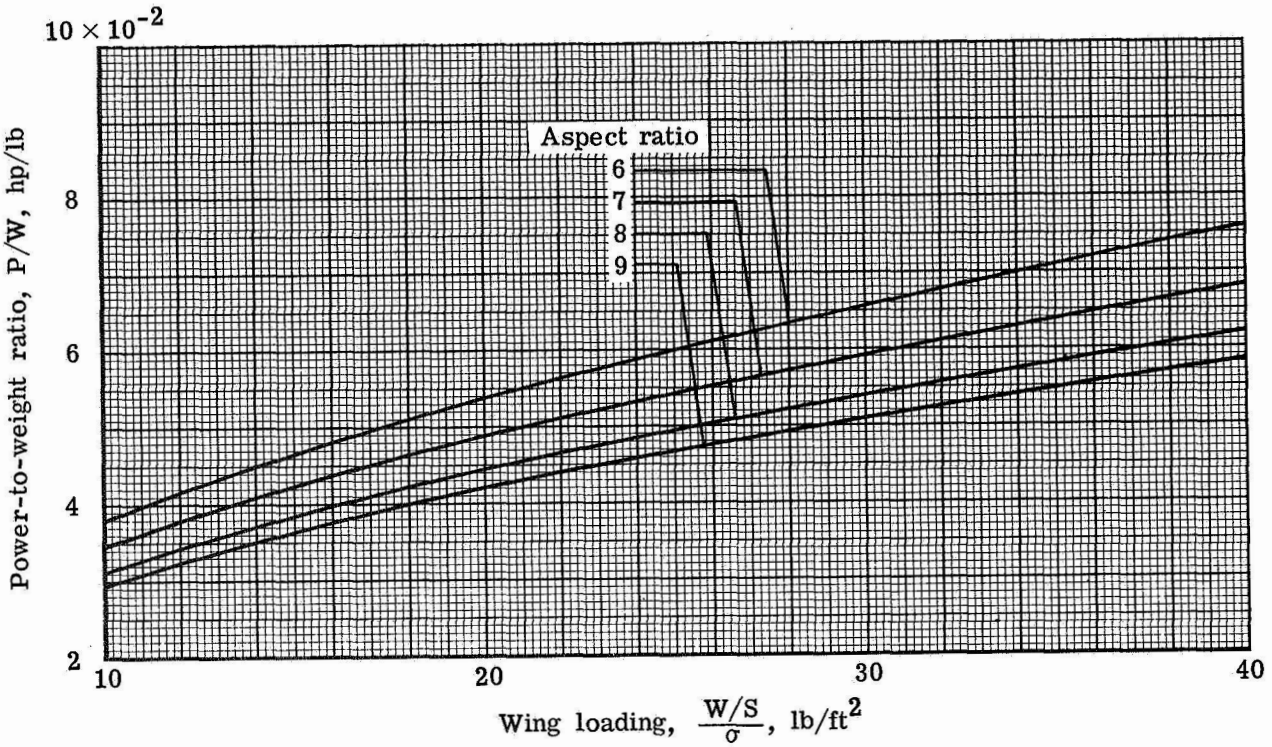


Figure 6.22.- Power-to-weight ratio, all engines operating, required to meet climb gradient requirement for propeller-driven aircraft in landing configuration. FAR part 23 for aircraft over 6000 lb gross weight.

required power-to-weight ratio than does the climb gradient criterion. It must be stressed, however, that such comparisons are dependent upon the aerodynamic parameters assumed.

6.7 Matching Procedure

Analyses and procedures have been described in sections 6.4, 6.5, and 6.6 which permit the determination of the relationships between wing loading and power loading required to meet several specified performance objectives. The process was described in section 6.3 and is illustrated schematically by the outputs of blocks 2 to 5 in figure 6.1. Block 6 in the third column of figure 6.1 shows a simultaneous solution of the outputs from the blocks in the first column. This solution yields unique values of wing loading and power loading necessary to meet the desired performance objectives.

A simultaneous solution of the type described is illustrated graphically in figure 6.23. The power loading W/P is plotted as a function of the wing loading $\frac{W/S}{\sigma}$ for the various performance parameters. Combinations of wing loading and power loading which fall on the hatched side of a curve do not satisfy the performance objective represented by that particular curve. Lines

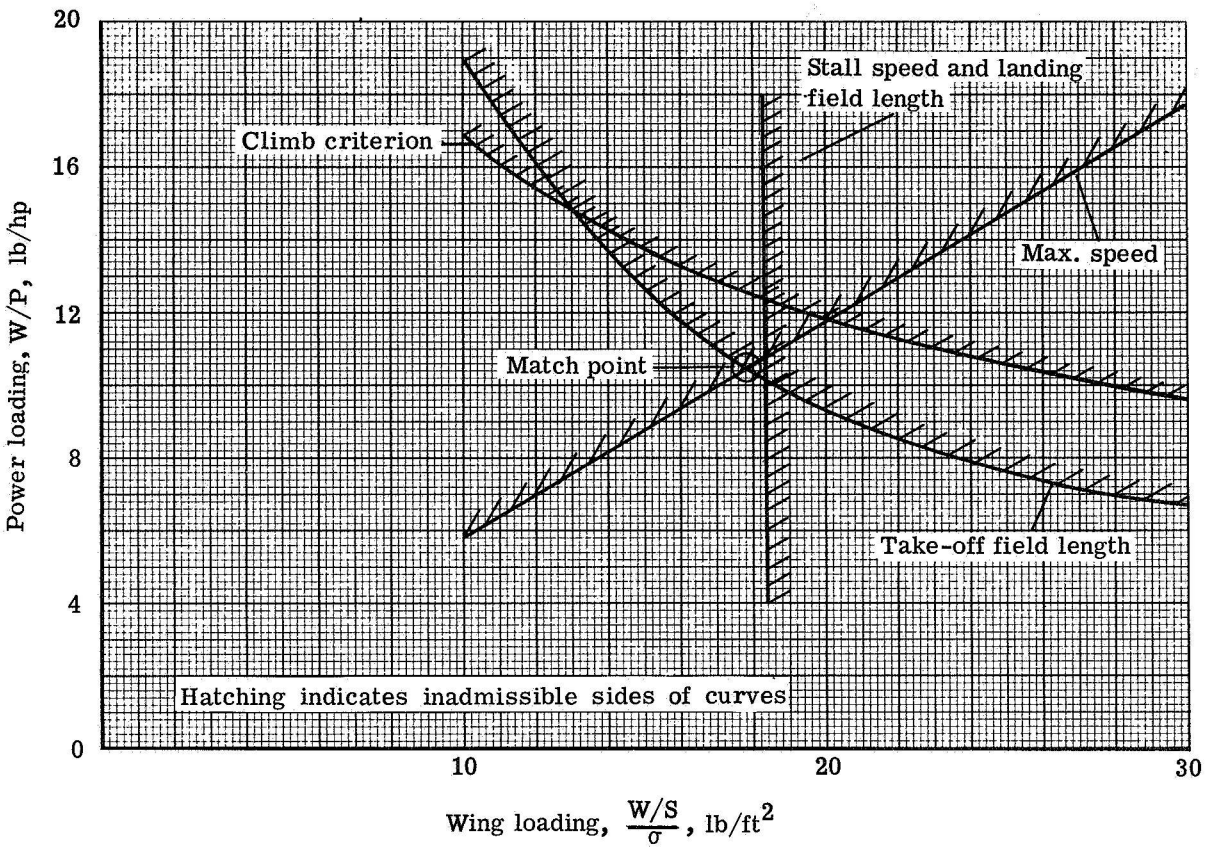


Figure 6.23.- Illustrative matching chart for propeller-driven aircraft.

are shown for specified values of maximum speed, take-off field length, climb rate, and stalling speed. For illustrative purposes, the following performance objectives were chosen:

V_{max} 200 mph at sea level

V_S 65 mph, flaps extended, with an associated landing field length of 1640 ft

ℓ_T 1550 ft over a 50-ft obstacle

$\dot{h}$ 1100 ft/min

The aircraft was assumed to have an internally braced wing and retractable landing gear. The line in figure 6.23 labeled "maximum speed" was determined with the use of a value of the power index I_p of 1.19 which was found from figure 6.2 for a maximum speed of 200 mph. The stalling speed line was determined from figure 6.8 for a maximum lift coefficient of 1.7 and a stalling speed of 65 mph. The corresponding landing field length over a 50-ft obstacle is found from figures 6.9 and 6.10 to be 1640 ft. The take-off field length line was found from figures 6.11 and 6.12 with an assumed take-off lift coefficient of 1.4. The climb rate line was found from figure 6.16.

The intersection of the take-off field length and maximum speed lines, labeled "match point," represents the unique values of wing loading and power loading required to meet the desired speed and take-off field length objectives. The stall speed and landing field length line also passes essentially through the circled match point. Thus, a wing loading of 18 lb/ft^2 and a power loading of 10.4 lb/hp will result in an aircraft which yields the desired maximum speed and take-off and landing performance. This combination of wing loading and power loading is seen in figure 6.23 to provide a rate of climb which exceeds the minimum FAR requirement.

Sometimes the procedure for determining the required wing loading and power loading is simplified by a reduction in the number of specified performance parameters. For example, if the maximum speed and stalling speeds are the only specified performance objectives, the values of W/S and W/P may be determined directly with the use of the high-speed charts, figures 6.2, 6.3, and 6.4, and the stalling speed chart, figure 6.8 without the need for a graphical solution such as that presented in figure 6.23. For example, for the aircraft just considered (class I) with a maximum speed of 200 mph and a stalling speed of 65 mph but no requirement on take-off distance or climb rate, the values of wing loading and power loading are determined as follows:

From figure 6.2,

$$I_p = 1.19$$

and

$$I_p{}^3 = \frac{W/S}{W/P} = 1.69$$

From figure 6.8,

$$(W/S) = 18.4$$

Thus,

$$(W/P) = \frac{18.4}{1.69} = 10.9$$

The wing loading and power loading necessary to provide a maximum speed of 200 mph and a stalling speed of 65 mph are, therefore, 18.4 lb/ft^2 and 10.9 lb/hp, respectively.

The values of W/S and W/P needed to meet specified performance objectives will be utilized in the next section in the final steps in sizing the aircraft as indicated by the flow diagram of figure 6.1.

6.8 Aircraft Weight Relationships

The approach taken to the estimation of aircraft weights for propeller-driven aircraft is the same as that described in chapter 3 for jet-propelled aircraft. For completeness, the process will be repeated here. The estimation of the useful load fraction will be considered first, after which a method of determining aircraft gross weight will be described.

6.8.1 Useful Load Fraction

In reference 6.27 Wilson describes a method of weight estimation which suggests a relationship between the power loading W/P and the physical characteristics of the aircraft. From an analysis of a large number of aircraft, the gross weight is shown in reference 6.27 to be related to the fuel weight, propulsion system weight, and payload weight in the following way:

$$W_f + W_t + W_p = 0.6W_g \tag{6.37}$$

where

W_g gross weight, lb

W_f fuel weight, lb

W_t propulsion system weight, lb

W_p payload weight, lb

An examination of a number of comtemporary propeller-driven aircraft equipped with reciprocating engines indicates that equation (6.37) still provides a reasonable approximation to current weight relationships. Equation (6.37) can be rewritten in the following useful form:

$$\frac{W_p + W_f}{W_g} - C = -\frac{W_t/P}{W_g/P}$$

or

$$\left(1 - \frac{W_e}{W_g}\right) - C = -\frac{W_t/P}{W_g/P} \tag{6.38}$$

where P is the engine power in horsepower, W_t/P is the weight in pounds per horsepower of the propulsion system, W_g/P is the power loading, and W_e is the aircraft empty weight. The parameter $1 - (W_e/W_g)$ is termed the useful load fraction. The constant 0.6 which appears in equation (6.37) is not used in the present analysis and has simply been replaced by a constant C of undefined magnitude. If the assumption is made that the weight per unit horsepower of the propulsion system is relatively constant for a given level of propulsion system technology, equation (6.38) suggests that a correlation should exist between the useful load fraction $1 - (W_e/W_g)$ and the power loading of the aircraft.

The weight characteristics of some 38 aircraft have accordingly been analyzed and the results are presented in figure 6.24 in the form of a plot of

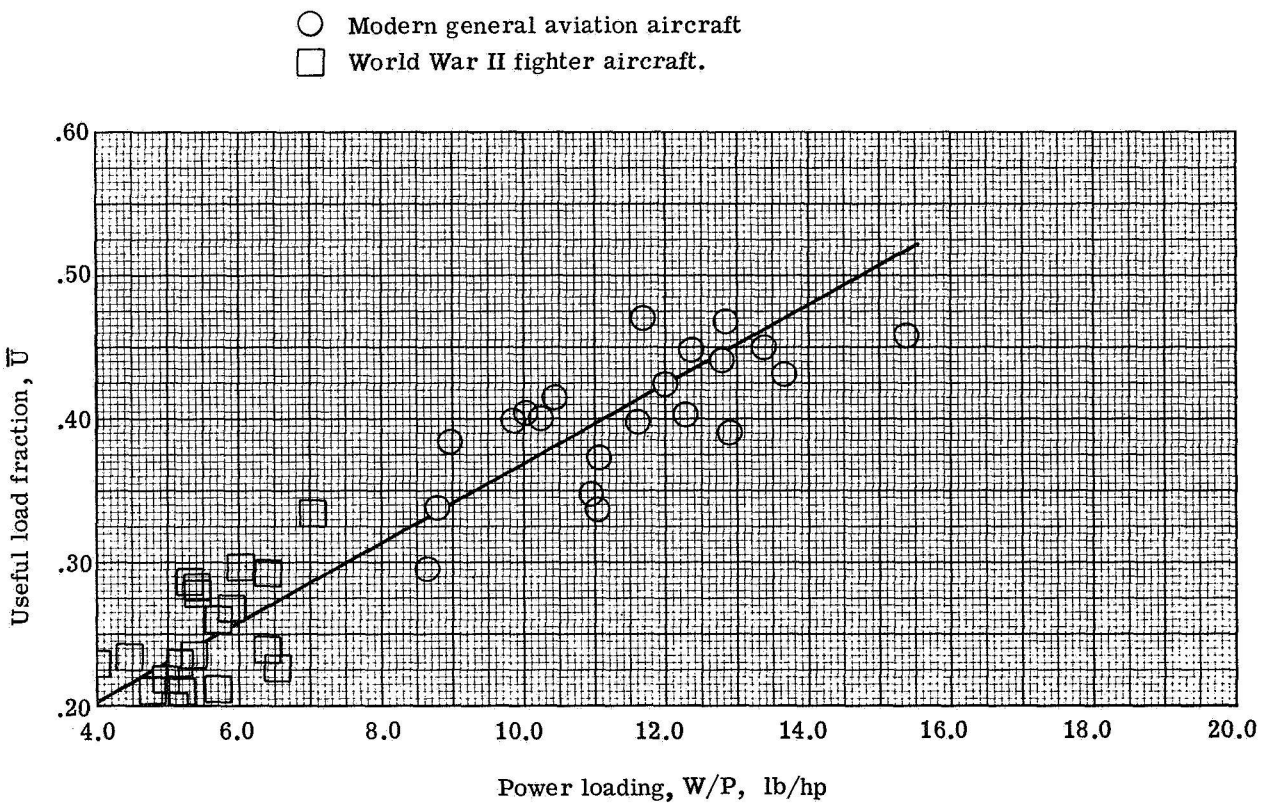


Figure 6.24.- Useful load fraction as function of power loading for a number of propeller-driven aircraft with reciprocating engines.

useful load fraction $1 - (W_e/W_g)$ as a function of aircraft power loading W_g/P, where W_g implies aircraft gross weight in all cases. The circle points are primarily for modern general aviation aircraft, and the square points are for World War II fighters. The gross weights of the aircraft for which data are presented in figure 6.24 varied from 1000 to 100 000 lb. The aircraft analyzed were generally taken from those listed in tables 6.I(a) and 6.I(b), although a few others were examined and are included in figure 6.24 from which

a suggested mean line fairing of the data is given in figure 6.24. A meaningful correlation between the useful load fraction and the aircraft power loading is seen to exist, with the majority of the points falling within a ±10 percent scatter band.

The faired line of figure 6.24 may be used for estimating the useful load fraction in terms of the power loading for propeller-driven aircraft equipped with reciprocating engines. A similar correlation was attempted for propeller-driven aircraft with turbine engines, and the results are presented in figure 6.25 for 13 different aircraft. The aircraft for which data are presented

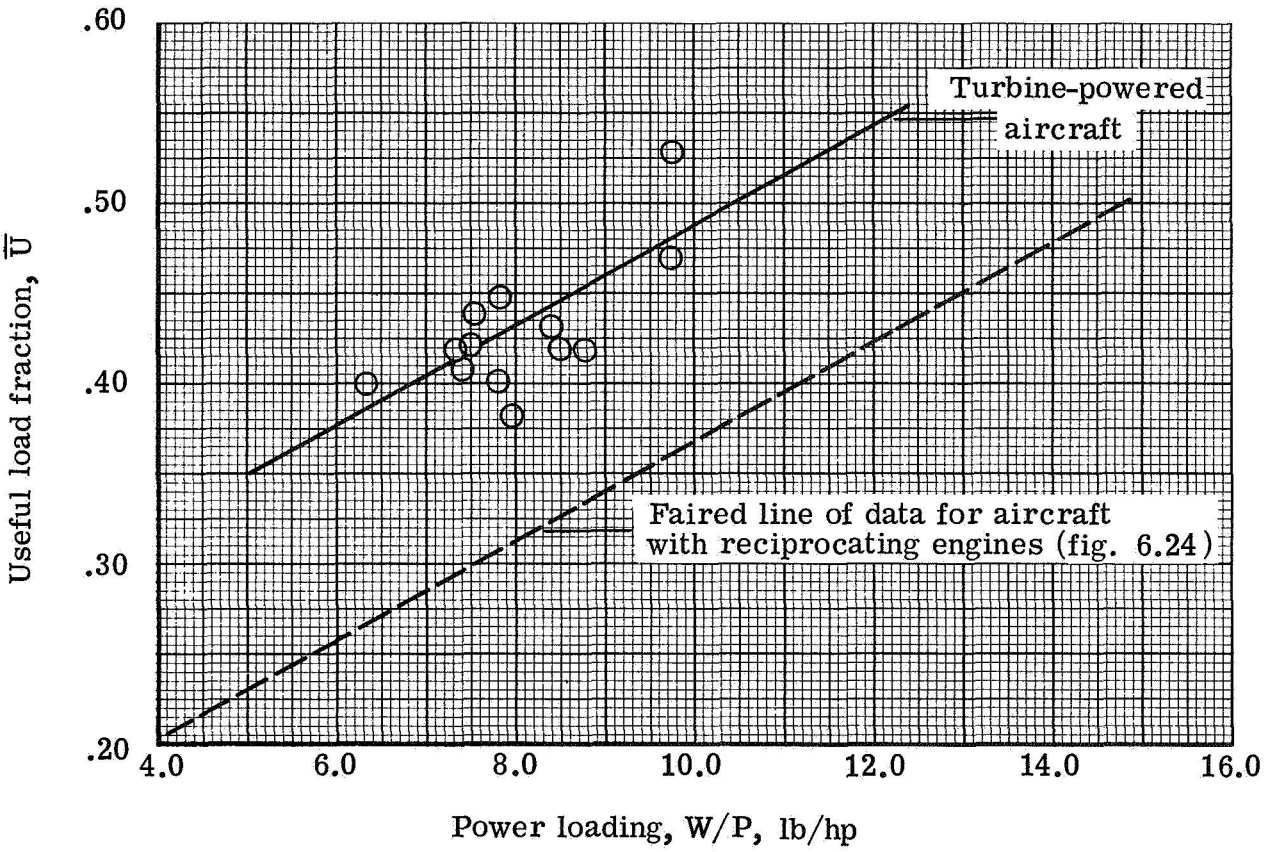


Figure 6.25.- Useful load fraction as function of power loading for a number of propeller-driven aircraft with turbine engines.

are listed in table 6.I(e). The majority of the aircraft are of the general aviation type and weigh less than 10 000 lb although the Lockheed C-130E, the Fairchild Hiller F-227, and the Grumman Gulfstream I are exceptions which weigh in the range from 155 000 to 35 000 lb. The correlation of the data in figure 6.25 seems reasonable, and, as would be expected, the useful load fraction for a given power loading is seen to be significantly higher for the aircraft with turbine engines than for those with reciprocating engines. The range of power loadings for which data were available, however, was relatively narrow

for the aircraft with turbine power plants so that the trend of weight ratio with power loading is not too well defined. Furthermore, the data for some aircraft examined were not consistent with the trend shown in figure 6.25. Thus, the faired line given in figure 6.25 for turbine-powered aircraft may be tentatively used for estimating the weight fraction but is considered less reliable than the curve for aircraft with reciprocating engines given in figure 6.24.

6.8.2 Aircraft Gross Weight Estimation

If the useful load fraction $1 - (W_e/W_g)$ corresponding to a given value of power loading is denoted by $\bar{U}$, then

$$1 - \frac{W_e}{W_g} = \bar{U} = \frac{W_p + W_f}{W_g}$$

or

$$\frac{W_p}{W_g} = \bar{U} - \frac{W_f}{W_g}$$

and

$$W_g = \frac{W_p}{\bar{U} - (W_f/W_g)} \tag{6.39}$$

Equation (6.39) indicates that the gross weight of the aircraft can be determined if the payload weight and the fuel fraction along with the useful load fraction $\bar{U}$ are known. The value of the aircraft power loading W/P, and hence the useful load fraction $\bar{U}$, are known from the matching process described in section 6.7. The payload weight is usually a specified quantity. The fuel fraction may be determined in terms of the specified range and the lift-drag ratio at which the aircraft flies. The determination of the fuel fraction will be considered in the next section.

6.9 Aircraft Range and Fuel Fraction

The Breguet range equation for propeller-driven aircraft takes the following form:

$$R = 375 \frac{\eta (L/D)}{c} \log_e \frac{1}{1 - (W_f/W_g)} \tag{6.40}$$

and the fuel fraction may be expressed explicitly as

$$\frac{W_f}{W_g} = 1 - \frac{1}{e^{R/B}} \tag{6.41}$$

where

R	range, statute miles
η	propulsive efficiency
L/D	aircraft lift-drag ratio
c	specific fuel consumption, pounds of fuel per horsepower per hour
W_f	fuel weight, lb
W_g	gross weight, lb
B	Breguet factor, $\frac{375\eta(L/D)}{c}$

Jet-powered transports, as described in chapter 3, are usually designed so that they can cruise at or near maximum lift-drag ratio at a specified high value of cruise Mach number. The high wing loadings of these aircraft together with the high altitudes at which they are flown make high-speed flight at or near maximum lift-drag ratio a practical reality. The fuel fraction for these aircraft may therefore be immediately determined with the use of equation (6.41). The majority of contemporary propeller-driven general aviation aircraft, however, are usually not flown in cruise flight at or near the maximum lift-drag ratio because the low wing loadings of these aircraft and the relatively low altitudes at which they are flown would result in unacceptably low cruising speeds. The range of such propeller-driven aircraft is usually given for a specified altitude and power setting or several combinations of altitude and power setting. The corresponding speeds for the different power settings are also given. Generalized relationships between speed, range, and power are developed in the next sections. These relationships will be used in determining the fuel fraction necessary for a given range.

6.9.1 Generalized Range Relationships

Equation (6.40) shows that the range, for a given fuel fraction, is a direct function of the Breguet factor B where B is defined as $\frac{375\eta(L/D)}{c}$. The Breguet factor varies with speed and altitude primarily through changes in the lift-drag ratio which result from changes in the required lift coefficient. The specific fuel consumption of reciprocating engines varies by only a small

amount with power, and consequently with speed, and will be neglected in the present analysis. Values of the specific fuel consumption c may be estimated with the use of the data in table 6.III. (See ref. 6.28.) The propulsive efficiency does not change by a large amount with cruising speed in this case because the propeller rotational speed may be reduced along with the aircraft cruising speed so as to minimize the loss in propulsive efficiency. This is different from the maximum rate of climb problem considered in section 6.6. The propeller rotational speed in the climb case must be kept at a high value in order to generate maximum engine power. The resultant reduced values of the propeller advance ratio give values of the propulsive efficiency significantly below cruise values.

If the specific fuel consumption and propulsive efficiency are constant, the range for a given value of the fuel fraction may be expressed in terms of the range at maximum lift-drag ratio as follows:

$$\frac{R}{R_m} = \frac{L/D}{(L/D)_{max}} \tag{6.42}$$

where

R range at some value of lift-drag ratio L/D

R_m range at maximum lift-drag ratio $(L/D)_{max}$

The ratio $\frac{L/D}{(L/D)_{max}}$ may be expressed in the following form:

$$\frac{L/D}{(L/D)_{max}} = \frac{2}{(1/\bar{C}_L) + \bar{C}_L} \tag{6.43}$$

where

$\bar{C}_L$ $\frac{C_L}{C_{L,m}}$

C_L lift coefficient corresponding to L/D

$C_{L,m}$ lift coefficient for $(L/D)_{max}$

Equation (6.43) was developed in section 3.5.1.3 of chapter 3. The lift coefficient $C_{L,m}$ may be determined from the following expression which is developed in section 3.5.1 of chapter 3:

$$C_{L,m} = \sqrt{C_{D,0}\pi A\epsilon} \tag{6.44}$$

The lift coefficient ratio for constant altitude may be expressed as

$$\frac{C_L}{C_{L,m}} = \frac{V_m^2}{V^2} \tag{6.45}$$

where

V_m speed at $(L/D)_{max}$

V speed at L/D

Substitution of equation (6.45) into equations (6.42) and (6.43) yields

$$\frac{R}{R_m} = \frac{2}{\frac{1}{(V_m/V)^2} + (V_m/V)^2} \tag{6.46}$$

The value of V_m is given by the equation

$$V_m = 29\sqrt{\frac{W/S}{\sigma C_{L,m}}} \tag{6.47}$$

where the constant 29 is the reciprocal of the square root of one-half the atmospheric density at sea level and V_m is in feet per second. The constant becomes 19.73 if V_m is desired in miles per hour. Equation (6.46) gives the desired generalized relationship between aircraft range and speed. The values of V_m and V, as previously noted, are for the same altitude; however, any number of different altitudes for V_m may be chosen by selecting the proper value of density ratio σ. The range ratio R/R_m, calculated by equation (6.46), is plotted as a function of speed ratio V/V_m in figure 6.26.

6.9.2 Generalized Power Relationships

The drag coefficient at any value of lift-drag ratio is related to that at the maximum value of lift-drag ratio by the following relation which is developed in section 3.5.1.3 of chapter 3:

$$\frac{C_D}{C_{D,m}} = \frac{1}{2}\left(1 + \bar{C}_L^2\right) \tag{6.48}$$

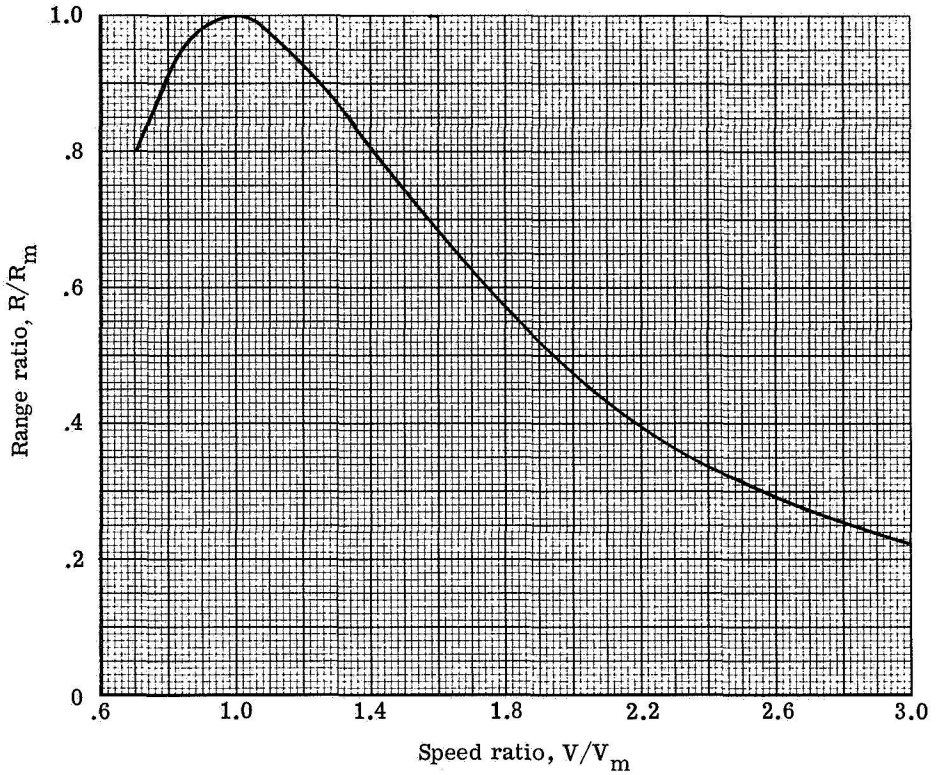


Figure 6.26.- Variation of range ratio with speed ratio for propeller-driven aircraft.

where

C_D drag coefficient corresponding to arbitrary value of L/D

$C_{D,m}$ drag coefficient at $(L/D)_{max}$

If P/P_m is defined as the ratio of power at any arbitrary lift-drag ratio P to the power at the maximum lift-drag ratio P_m, then

$$\frac{P}{P_m} = \frac{1}{2}\left(\frac{V}{V_m}\right)^3\left(1 + \bar{C}_L{}^2\right) \tag{6.49}$$

where V and V_m are as previously defined in equation (6.45) and are for the same altitude. If the lift coefficient ratio is expressed as

$$\frac{C_L}{C_{L,m}} = \left(\frac{V_m}{V}\right)^2 \tag{6.50}$$

equation (6.49) takes the form

$$\frac{P}{P_m} = \frac{1}{2}\left[\left(\frac{V}{V_m}\right)^3 + \frac{1}{\frac{V}{V_m}}\right] \tag{6.51}$$

An expression for the power required at maximum lift-drag ratio may be developed from equation (6.14), repeated here as

$$\frac{P_r}{W} = \frac{\sqrt{W/S}}{19\left(C_L^{3/2}/C_D\right)\sqrt{\sigma}} \tag{6.52}$$

Equation (6.52) is for the power-to-weight ratio; however, the numerator and denominator of equation (6.51) may be multiplied by the weight without causing any change in the relationship. Thus,

$$\frac{P}{P_m} = \frac{P/W}{(P/W)_m}$$

According to section 3.5.1 of chapter 3, the zero-lift drag coefficient is equal to the induced drag coefficient at the maximum lift-drag ratio. This is strictly true only for drag polars which are symmetrical about zero lift coefficient, but the approximation is reasonably good up to design lift coefficients of about 0.4 and will be accepted for use herein. Since the total drag coefficient is twice the zero-lift drag coefficient at maximum lift-drag ratio, equation (6.52) may be written for the power-to-weight ratio at maximum lift-drag ratio as

$$\frac{P_m}{W} = \frac{C_{D,0}\sqrt{W/S}}{9.5\left(C_{L,m}^{3/2}\right)\sqrt{\sigma}} \tag{6.53}$$

The power ratio P/P_m, or $\dfrac{P/W}{(P/W)_m}$, calculated from equation (6.51) is plotted as a function of the speed ratio V/V_m in figure 6.27. The curve shown in figure 6.27 is a generalized, nondimensional, power-required curve for propeller-driven aircraft expressed in terms of the power required and the speed at the maximum value of lift-drag ratio. As was the case with the gener-

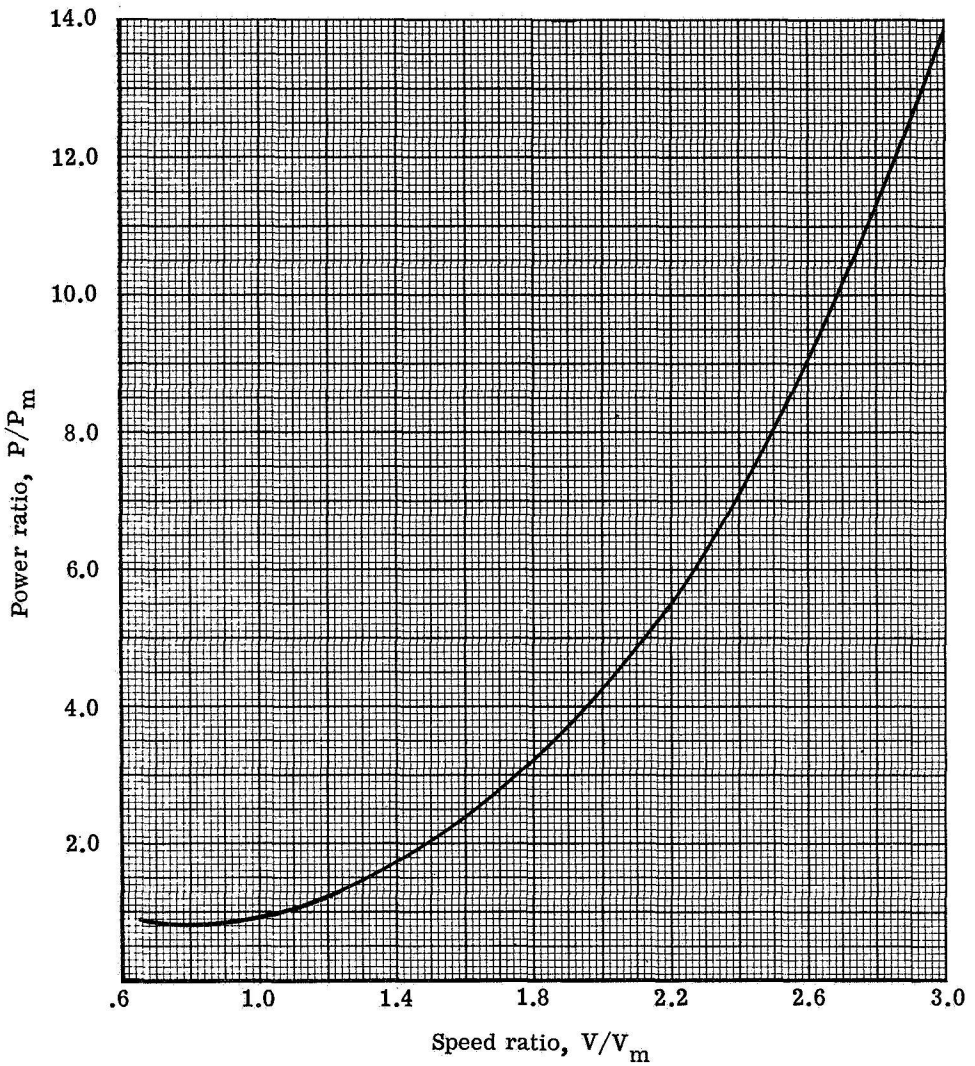


Figure 6.27.- Variation of power ratio with speed ratio for propeller-driven aircraft.

alized range curve given in figure 6.26, V and V_m, as well as P and P_m, must be evaluated at the same altitude.

6.9.3 Determination of Fuel Fraction

The generalized range and power curves presented in figures 6.26 and 6.27 provide the means for determining the fuel fraction necessary to meet a given range requirement at a specified percentage of maximum power or at a specified speed.

The information contained in the following items is necessary in order to use these curves:

(1) The values of wing loading W/S and power loading W/P as determined from the matching process described in section 6.7.

(2) The value of the zero-lift drag coefficient $C_{D,0}$ determined from table 6.II for the class of aircraft under consideration.

(3) The values of wing aspect ratio A and airplane efficiency factor ϵ. A value of ϵ of 0.7 is typical of contemporary general aviation aircraft.

(4) The value of the propulsive efficiency η. A cruising value of η of 85 percent is representative of current designs.

(5) The value of the engine specific fuel consumption c. Values of the specific fuel consumption for a number of present-day, horizontally opposed, reciprocating engines are given in table 6.III.

The following parameters, listed in four steps, can now be calculated:

(a) Lift coefficient for $(L/D)_{max}$ (See eq. (6.44).)

$$C_{L,m} = \sqrt{C_{D,0}\pi A\epsilon}$$

(b) Maximum lift-drag ratio (See eq. (3.20) of chapter 3.)

$$(L/D)_{max} = \frac{1}{2}\sqrt{\frac{\pi A\epsilon}{C_{D,0}}}$$

(c) Speed at $(L/D)_{max}$ in miles per hour at the specified altitude (See eq. (6.47) corrected to read in miles per hour.)

$$V_m = 19.73\sqrt{\frac{W/S}{\sigma C_{L,m}}}$$

(d) Power-to-weight ratio, expressed in horsepower per pound, required to fly at $(L/D)_{max}$ at the specified altitude (See eq. (6.53).)

$$\frac{P_m}{W} = \frac{C_{D,0}\sqrt{W/S}}{9.5\left(C_{L,m}^{3/2}\right)\sqrt{\sigma}}$$

The case of a specified range at a given altitude and percentage of maximum power is to be considered here; however, the generalized range and power curves of figures 6.26 and 6.27 can be used equally well for the case of range at a given speed. If γ is the percentage power at which the range R_s is specified, then the power ratio to be used with figure 6.27 for this power setting may be written as

$$\left(\frac{P}{P_m}\right)_\gamma = \frac{\gamma\eta(P/W)}{(P/W)_m}$$

where P/W is the reciprocal of the power loading corresponding to maximum power and weight as determined from the matching procedure (section 6.7) and $(P/W)_m$ is found in step (d) just outlined. The ratio P/W is in terms of shaft horsepower and must be converted to thrust horsepower through multiplication by the propulsive efficiency η. The ratio $(P/W)_m$ is calculated in terms of thrust horsepower. The value of the velocity ratio corresponding to the desired power setting $(V/V_m)_\gamma$ may be read from figure 6.27, and the actual speed is determined from $(V/V_m)_\gamma$ and the known value of V_m as determined from step (c).

The value of the range ratio R/R_m corresponding to the velocity ratio $(V/V_m)_\gamma$ may now be determined from figure 6.26 and is designated as $(R/R_m)_\gamma$. The specified range R_s can then be written in the form

$$R_m\left(\frac{R}{R_m}\right)_\gamma = R_s$$

and the maximum range R_m necessary in order for the specified range to be achieved at the desired power setting is

$$R_m = \frac{R_s}{(R/R_m)_\gamma}$$

Finally, the fuel fraction necessary to achieve the specified range may now be determined in terms of the maximum range R_m with the use of equation (6.41), which is repeated here for convenience

$$\frac{W_f}{W_g} = 1 - \frac{1}{e^{R_m/B}}$$

The value of the Brequet factor $B = \frac{375\eta(L/D)_{max}}{c}$ is determined from the information given in items (4) and (5) and step (b) of this section.

6.9.4 Range and Power for Different Speeds and Altitudes

The generalized range relationship of figure 6.26 may be used, together with values of R_m and V_m, to construct a series of curves of actual ranges in miles against speed in miles per hour for different altitudes. The range R_m does not change with altitude; however, the speed V_m increases with altitude. Consequently, the values of R_m, and all other range values, occur at successively higher speeds as the altitude is increased. The speed V_m is given by equation (6.47), and the reciprocal of the density ratio is given in figure 6.6 as a function of altitude.

The actual horsepower, or the percentage of maximum power, may also be plotted as a function either of speed in miles per hour or range in miles for different altitudes with the use of figure 6.26, figure 6.27, equation (6.47), and equation (6.53). In this case, both P_m and V_m vary with altitude.

6.9.5 Engine Characteristics

A knowledge of the manner in which the horsepower of actual engines varies with speed and altitude is necessary in order to establish meaningful limits on the power available and thus make the range, power, and speed curves just discussed compatible with the characteristics of the propulsion system. The horsepower delivered by an unsupercharged reciprocating engine does not vary to any significant extent with speed but does decrease with altitude. The ratio of the horsepower available at some altitude to that at sea level, P_h/P_0, is plotted as a function of altitude in figure 6.28 for unsupercharged engines. The curve of figure 6.28 is based on information contained in reference 6.25 which has been found to be a reasonable representation of the behavior of those modern, horizontally opposed engines for which data were available. This curve may be used with that of figure 6.27 to limit the maximum speeds and power in constructing the curves of actual power and range as a function of speed.

The variation of power ratio with altitude for a typical modern, supercharged engine is illustrated schematically in figure 6.29. The maximum rated power is seen to remain constant with altitude until a "critical altitude" is reached, after which the power decreases in a manner somewhat similar to that shown in figure 6.28 for unsuperchared engines. The critical altitude for maximum rated power is 18 000 ft in this case. The critical altitude for maximum cruise power, 75 percent of maximum rated power, is seen to be 25 000 ft. The critical altitude varies with different engines although 18 000 ft for maximum rated power is typical of contemporary designs. At the upper left-hand side of figure 6.29 is a mark, slightly above maximum rated power, which is labeled maximum take-off power. The maximum take-off power is frequently the same as

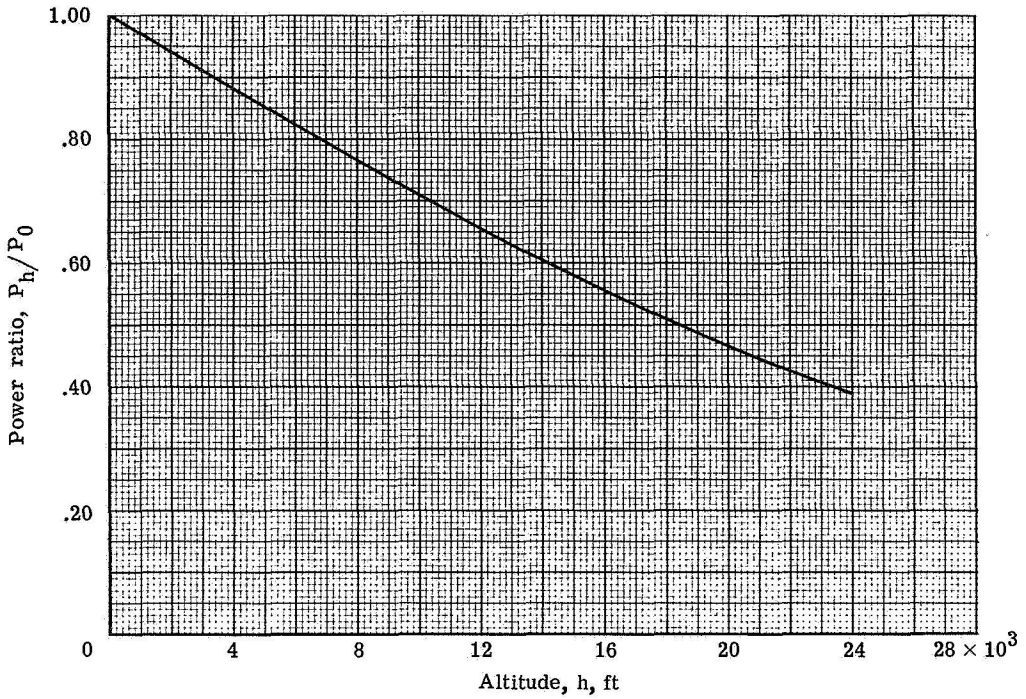


Figure 6.28.- Variation of power ratio with altitude for a typical unsupercharged reciprocating engine.

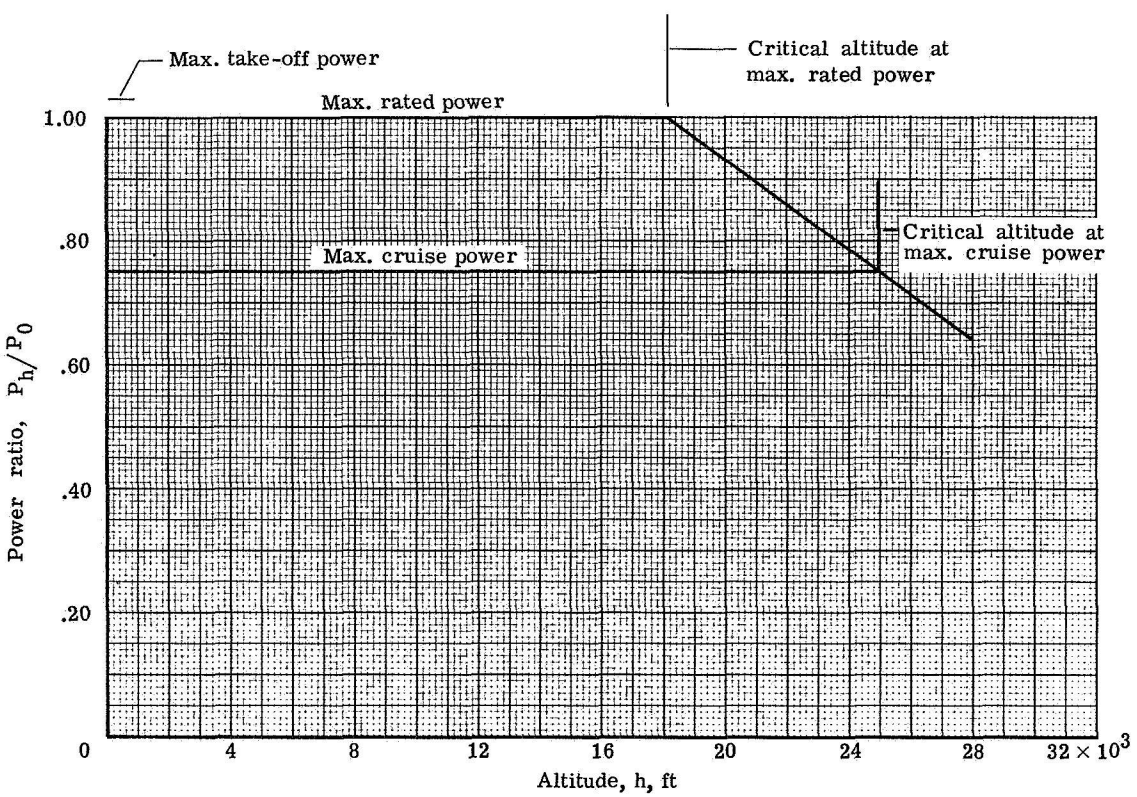


Figure 6.29.- Typical power characteristics of a modern supercharged reciprocating engine.

maximum rated power although the take-off power is sometimes higher, as in the illustrative case shown in figure 6.29. The power characteristic shown in figure 6.29 is only intended to illustrate the behavior of a supercharged engine. The characteristics of an actual specific engine should be used, if possible, in the construction of curves of speed, range, and power.

The variation of the power ratio with speed and altitude of a typical small turboprop engine is shown in figure 6.30. The ordinate is the ratio of the max-

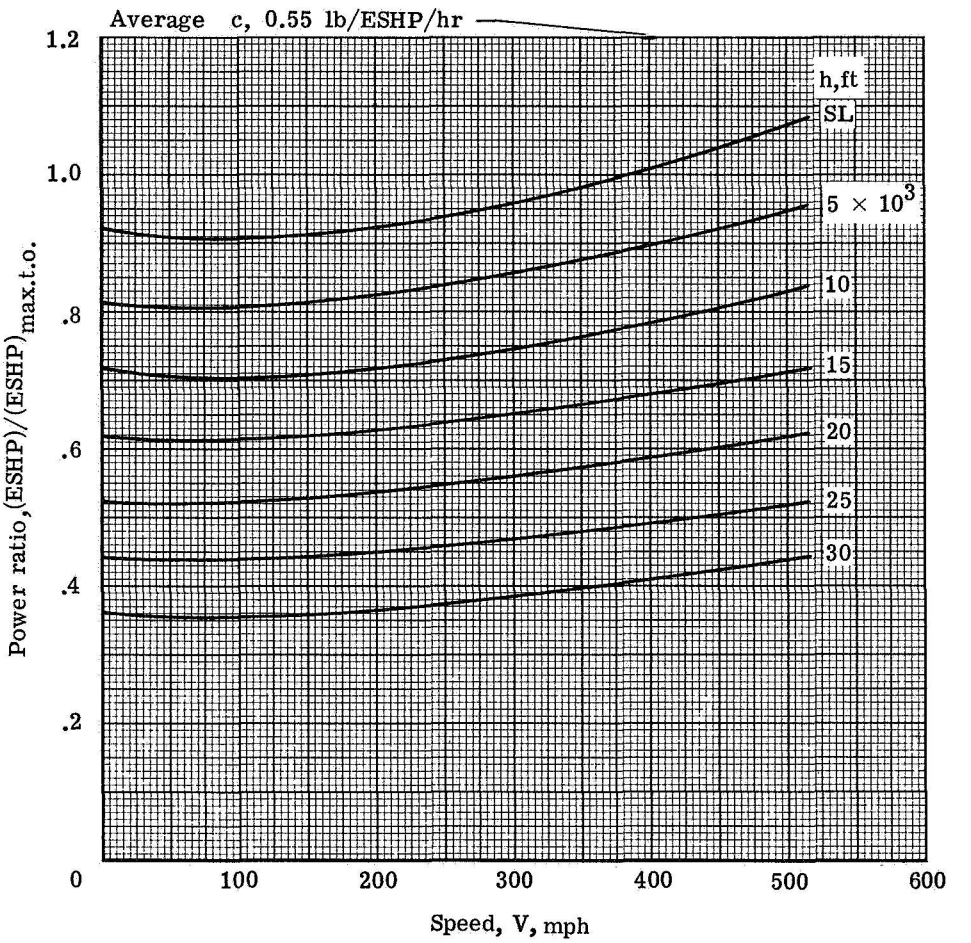


Figure 6.30.- Power characteristics of a typical turboprop engine as function of speed and altitude. Standard day.

imum continuous equivalent shaft horsepower to the maximum take-off value, and the speed is on the abscissa. Curves are shown for altitudes which vary from sea level to 30 000 ft. The power ratio at zero speed and sea-level altitude is seen to be about 0.93 which means that the maximum continuous power is less than the take-off power in this case. The term equivalent shaft horsepower (ESHP) perhaps warrants some explanation. According to reference 6.29, the equivalent shaft horsepower is the actual shaft horsepower plus the horsepower equivalent of the jet thrust from the engine exhaust. The horsepower of the

jet for static conditions is defined as the jet thrust divided by 2.5; and in forward flight, the jet thrust is multiplied by the flight velocity and converted to horsepower. At the top of figure 6.30 is given a value of specific fuel consumption which may be considered as an average value corresponding to maximum continuous power for the altitude and speed ranges given in the figure. The specific fuel consumption, however, varies significantly as the power is varied from the maximum continuous value. Reference should be made to detailed data for a specific engine to determine the manner in which specific fuel consumption varies with different operating conditions.

6.10 Aircraft Sizing

All the procedures have now been developed which permit the sizing, outlined in the flow diagram of figure 6.1, of a propeller-driven aircraft to meet a prescribed set of performance objectives.

The matching procedure described in section 6.7 gives values of the wing loading and power loading needed to meet high-speed, airport-performance, and climb-performance objectives. The useful load fraction is determined according to the method described in section 6.8, and determination of the fuel fraction necessary to meet the desired range is described in section 6.9. The gross weight can be calculated by the expression given in equation (6.39) which, for convenience, is repeated here as

$$W_g = \frac{W_p}{\bar{U} - (W_f/W_g)}$$

With the gross weight and payload weight known, the fuel weight and empty weight can be calculated since the fuel fraction and useful load fractions are known. The wing loading, power loading, and gross weight are known; consequently, the wing area and engine power can be calculated. The basic physical characteristics of size, weight, and power of the aircraft have now been completely determined. In the next chapter (chapter 7) an illustrative example of the sizing of a propeller-driven aircraft according to the methods described in this chapter (chapter 6) will be considered in detail.

SYMBOLS

A	aspect ratio, b^2/S
B	Breguet factor, $\dfrac{375\eta(L/D)}{c}$
b	wing span, ft
C	constant defined by equation (6.38)
C_D	total drag coefficient
$C_{D,i}$	induced drag coefficient, $C_L^2/\pi A\epsilon$ or KC_L^2 $\left(\text{where } K = \dfrac{1}{\pi A\epsilon}\right)$
$C_{D,0}$	drag coefficient at zero lift
C_L	lift coefficient
$\bar{C}_L$	lift coefficient ratio, $C_L/C_{L,m}$ or $C_L/C_{L,c}$
$C_{L,c}$	lift coefficient for $\left(C_L^{3/2}/C_D\right)_{max}$
$C_{L,m}$	lift coefficient for $(L/D)_{max}$
$C_{L,max}$	maximum lift coefficient
$C_{L,T}$	take-off lift coefficient
c	specific fuel consumption, pounds of fuel per horsepower per hour
D	drag, lb
$(ESHP)/(ESHP)_{max.t.o.}$	ratio of maximum continuous equivalent shaft horsepower to maximum take-off value (see fig. 6.30)
h	altitude, ft
$\dot{h}$	rate of climb, ft/min
I_p	power index, $\sqrt[3]{\left(\dfrac{W/S}{W/P}\right)\dfrac{1}{\sigma}}$
K_1	constant, $\dot{h}/V_S$
K_2	specified climb gradient, percent
L	lift, lb

L/D	lift-drag ratio
$(L/D)_{max}$	maximum lift-drag ratio
ℓ_L	landing distance over a 50-ft obstacle
$\ell_{L,g}$	landing ground run, ft
ℓ_T	take-off distance over a 50-ft obstacle
$\ell_{T,g}$	take-off ground run distance, ft
P	engine power, shaft hp
$\bar{P}$	climb parameter (see eq. (6.15))
P_a	maximum power available at some flight condition
P_h	engine power at some altitude h
P_m	power required at $(L/D)_{max}$
P_r	power required at some flight condition
P_0	engine power at sea level
R	range, statute miles
R_m	range for $(L/D)_{max}$, statute miles
R_s	design range, statute miles
S	wing area, ft^2
$\bar{U}$	useful load fraction, $1 - (W_e/W_g)$
V	speed, statute mph or ft/sec
V_m	speed at $(L/D)_{max}$
V_S	stalling speed for aircraft in landing configuration
W	weight, lb
W_e	empty weight, lb
W_f	fuel weight, lb
W_g	gross weight, lb
W_p	payload weight, lb

W_t propulsion system weight, lb

γ percentage of maximum power

ε Oswald's airplane efficiency factor (see chapter 3)

η propulsive efficiency

$\bar{\theta}$ climb parameter (see eq. (6.30))

ρ atmospheric density at some altitude other than sea level, slugs/ft^3

ρ_0 atmospheric density at sea level

σ density ratio ρ/ρ_0

Configurations:

IB internally braced wing

EB externally strut-braced wing

WB externally wire-braced wing

RG retractable landing gear

FG fixed landing gear

C landing gear with tail wheel or skid (tricycle landing gear implied if C is not used)

A numeral in the configuration indicates the number of engines on multi-engine aircraft.

REFERENCES

6.1 Grey, C. G.; and Bridgman, Leonard, eds.: Jane's All the World's Aircraft, 1931. Sampson Low, Marston & Co., Ltd. (London).

6.2 Grey, C. G.; and Bridgman, Leonard, eds.: Jane's All the World's Aircraft, 1936. Sampson Low, Marston & Co., Ltd. (London).

6.3 Grey, C. G.; and Bridgman, Leonard, eds.: Jane's All the World's Aircraft, 1940. Sampson Low, Marston & Co., Ltd. (London).

6.4 Bridgman, Leonard, ed.: Jane's All the World's Aircraft, 1950-51. Sampson Low, Marston & Co., Ltd. (London).

6.5 Taylor, John W. R., ed.: Jane's All the World's Aircraft, 1969-70. McGraw-Hill Book Co., Inc., c.1969.

6.6 Taylor, John W. R., ed.: Jane's All the World's Aircraft, 1971-72. McGraw-Hill Book Co., c.1971.

6.7 Taylor, John W. R., ed.: Jane's All the World's Aircraft, 1973-74. McGraw-Hill Book Co., c.1973.

6.8 Taylor, John W. R., ed.: Jane's All the World's Aircraft, 1974-75. Franklin Watts, Inc., c.1974.

6.9 Green, William: War Planes of the Second World War, Fighters. Volume I, Hanover House, 1960.

6.10 Green, William: War Planes of the Second World War, Fighters. Volume II, Hanover House, 1961.

6.11 Green, William: War Planes of the Second World War, Fighters. Volume III, Doubleday & Co., Inc., 1962.

6.12 Green, William: War Planes of the Second World War, Fighters. Volume IV, Doubleday & Co., Inc., 1960.

6.13 Swanborough, Gordon; and Bowers, Peter M.: United States Navy Aircraft Since 1911. Funk & Wagnalls, c.1968.

6.14 Wagner, Ray: American Combat Planes. Hanover House, 1960.

6.15 Wagner, Ray; and Nowarra, Heinz: German Combat Planes. Doubleday & Co., Inc., 1971.

6.16 Smith, Robert T.: Staggerwing! Story of the Classic Beechcraft Biplane. Cody Publ., Inc., c.1979.

6.17 Allen, Richard Sanders: Revolution in the Sky - Those Fabulous Lockheeds, the Pilots Who Flew Them. Stephen Green Press, 1964.

6.18 Mandrake, Charles G.: The Gee Bee Story. Robert R. Longo Co., Inc., 1957.

6.19 Fink, Marvin P.; and Freeman, Delma C., Jr.: Full-Scale Wind-Tunnel Investigation of Static Longitudinal and Lateral Characteristics of a Light Twin-Engine Airplane. NASA TN D-4983, 1969.

6.20 Fink, Marvin P.; Freeman, Delma C., Jr.; and Greer, H. Douglas: Full-Scale Wind-Tunnel Investigation of the Static Longitudinal and Lateral Characteristics of a Light Single-Engine Airplane. NASA TN D-5700, 1970.

6.21 Fink, Marvin P.; Shivers, James P.; Greer, H. Douglas; and Megrail, James L.: The Effects of Configuration Changes on the Aerodynamic Characteristics of a Full-Scale Mockup of a Light Twin-Engine Airplane. NASA TN D-6896, 1972.

6.22 Greer, H. Douglas; Shivers, James P.; Fink, Marvin P.; and Carter, C. Robert: Wind-Tunnel Investigation of Static Longitudinal and Lateral Characteristics of a Full-Scale Mockup of a Light Single-Engine High-Wing Airplane. NASA TN D-7149, 1973.

6.23 Airworthiness Standards: Normal, Utility, and Aerobatic Category Airplanes. Federal Aviation Regulations, vol. III, pt. 23, FAA, June 1974.

6.24 Smith, C. W., ed.: Aerospace Handbook. Second ed. FZA-381-II, Convair Aerosp. Div., General Dynamics, Oct. 1972; Rev. A., Nov. 1973.

6.25 Diehl, Walter Stuart: Engineering Aerodynamics. Revised ed. Ronald Press Co., c.1936, pp. 312-361.

6.26 Roskam, Jan: Methods for Estimating Drag Polars of Subsonic Airplanes. Pub. by author (519 Boulder, Lawrence, Kansas 66044), c.1971.

6.27 Wilson, R. C.: Preliminary Airplane Design. Pitman Pub. Co., c.1941.

6.28 Wilkinson, Paul H.: Aircraft Engines of the World - 1970. Pub. by author (5900 Kingswood Road, N.W., Washington, D.C. 20014), c.1970.

6.29 The Aircraft Gas Turbine Engine and Its Operation. Part No. PWA 182408, PWA Oper. Instr. 200, Pratt & Whitney Aircraft, June 1952. Reprinted with revisions May 1974.

TABLE 6.I.- BASIC CONFIGURATIONS OF ILLUSTRATIVE AIRCRAFT

(a) Modern general aviation aircraft

Aircraft	Configuration (a)	Reference
Piper PA-24G Comanche	IB RG	6.5
Piper PA-28-180 Cherokee	IB FG	6.5
Piper PA-28-140 Cherokee	IB FG	6.5
Piper PA-28-235C Cherokee	IB FG	6.5
Piper PA-32-260 Cherokee Six	IB FG	6.5
Piper PA-32-300 Cherokee Six	IB FG	6.5
Piper PA-28-180 Arrow	IB RG	6.5
Piper PA-30 Twin Comanche	IB RG 2	6.5
Piper PA-31 Navajo	IB RG 2	6.5
Piper PA-23-25 Aztec D	IB RG 2	6.5
Piper PA-18 Super Cub	EB FGC	6.5
Beech Musketeer Standard	IB FG	6.5
Beech Bonanza V-35A	IB RG	6.5
Beech Baron B-55	IB RG 2	6.5
Beech Baron D-55	IB RG 2	6.5
Cessna 150	EB FG	6.5
Cessna 172 Skyhawk	EB FG	6.5
Cessna 180 Skywagon	EB FGC	6.5
Cessna 207 Skywagon	EB FG	6.5
Cessna 210 Centurian	IB RG	6.5
Cessna 310P	IB RG 2	6.5
Cessna 337D Super Skymaster	{ IB RG 2 Push-Pull }	6.5
Cessna 401	IB RG 2	6.5
Bellanca Viking	IB RG	6.5
Citabria (two versions)	EB FGC	6.5

[a]See section 6.1.

TABLE 6.I.- Continued

(b) World War II fighter aircraft

Aircraft	Configuration (a)	Reference
Curtis P-40B	IB RGC	6.12 and 6.14
Curtis P-40F	IB RGC	6.12 and 6.14
Grumman F4F	IB RGC	6.12 and 6.14
Grumman F6F	IB RGC	6.12 and 6.14
Grumman F7F	IB RG2	6.12 and 6.14
Grumman F8F	IB RGC	6.12 and 6.14
Lockheed P-38J	IB RG2	6.12 and 6.14
North American P-51D	IB RGC	6.12 and 6.14
Republic P-47D	IB RGC	6.12 and 6.14
Republic P-47J	IB RGC	6.12 and 6.14
Republic XP-72	IB RGC	6.12 and 6.14
Vought F4U-4	IB RGC	6.12 and 6.14
Hawker Hurricane I	IB RGC	6.10 and 6.14
Hawker Hurricane IIB	IB RGC	6.10 and 6.14
Hawker Tempest I	IB RGC	6.10
Hawker Tempest V	IB RGC	6.10
Hawker Typhoon	IB RGC	6.10
Hawker Sea Fury	IB RGC	6.10
DeHaviland Mosquito	IB RGC2	6.10
Supermarine Spitfire IIA	IB RGC	6.10
Supermarine Spitfire VII	IB RGC	6.10
Messerschmidt Bf 109E	IB RGC	6.9 and 6.15
Messerschmidt Bf 109F	IB RGC	6.9 and 6.15
Focke-Wulf 190A-8	IB RGC	6.9 and 6.15
Focke-Wulf 190D-9	IB RGC	6.9 and 6.15
Mitsubishi A6M5-8 Zero-Zen	IB RGC	6.11
Mitsubishi JM2-7 Raiden	IB RGC	6.11

[a]See section 6.1.

TABLE 6.I.- Continued

(c) Civil and military monoplanes

Aircraft	Configuration (a)	Reference
Lockheed Vega 5C	IB FGC	6.17
Lockheed Sirius 8	IB FGC	6.17
Lockheed Air Express	IB FGC	6.17
Lockheed Altair	IB RGC	6.17
Lockheed Orion 9 & 9F	IB RGC	6.17
Douglas DC-3	IB RGC 2	6.2
Ford 5-AT	IB FGC 3	6.1
Fokker F-10A	IB FGC 3	6.1
Cessna Airmaster	IB FGC	6.2
Cessna 190 and 195	IB FGC	6.4
Boeing 247D	IB RGC 2	6.2
Monocoupe 110	EB FGC	6.4
Monocoupe 90AL	EB FGC	6.4
Brown B-3 racer	WB FGC	6.2
Curtiss Wright 19R	IB FGC	6.2
Kinner Envoy	WB FGC	6.2
Luscomb Phantom	EB FGC	6.2
Hughes Racer	IB RGC	6.2
Howard "Mister Mulligan"	EB FGC	6.2
Bellanca Skyrocket	EB FGC	6.2
Gee Bee model Z	WB FGC	6.18
Boeing P-26A	WB FGC	6.14
Curtiss XP-31	EB FGC	6.14
Boeing YP-29A	IB RGC	6.12
Consolidated P-30	IB RGC	6.12
Bellanca Flash	WB RGC	6.12
Republic P-35	IB RGC	6.12
Curtiss P-36A	IB RGC	6.12
Boeing B-17E	IB RGC 4	6.12
North American B-25	IB RG 2	6.12
Curtiss A-8	WB FGC	6.12
Howard DGA-8	EB FGC	6.3
Fairchild 22	EB FGC	6.1
Ryan B-5	EB FGC	6.1
Stinson Jr.	EB FGC	6.1
Fairchild 24	EB FGC	6.2
Travelair model R	WB FGC	6.1
Northrop Gamma	IB FGC	6.2
Northrop Delta	IB FGC	6.2

[a]See section 6.1.

TABLE 6.I.- Continued

(d) Biplanes

Aircraft	Configuration (a)	Reference
Curtiss P-1B	EB FGC	6.14
Curtiss PW-8	EB FGC	6.14
Curtiss P-6E	EB FGC	6.14
Curtiss O-39	EB FGC	6.1
Curtiss F11C-2	EB FGC	6.14
Curtiss F8C	EB FGC	6.1
Curtiss BF2C-1	EB RGC	6.14
Curtiss XP-22	EB FGC	6.1
Curtiss YP-23	EB FGC	6.14
Curtiss F9C-2	EB FGC	6.14
Curtiss R3C-1 racer	EB FGC	6.13
Boeing P-12B	EB FGC	6.1
Boeing P-12E	EB FGC	6.12
Boeing 40B	EB FGC	6.1
SPAD 13	EB FGC	6.14
SE-5	EB FGC	6.14
Douglas 02	EB FGC	6.1
Great Lakes trainer	EB FGC	6.1
Stearman C-3R	EB FGC	6.1
Stearman PT-17	EB FGC	6.3
DeHaviland Tiger Moth	EB FGC	6.2
Hawker Fury	EB FGC	6.2
Grumman F2F-1	EB RGC	6.3 and 6.14
Grumman F3F-1	EB RGC	6.3 and 6.14
Waco Taperwing	EB FGC	6.1
Eaglerock	EB FGC	6.1
Beech D17R	EB RGC	6.16
Beech E17B	EB RGC	6.16
Beech F17B	EB RGC	6.16
Pitts Special	EB FGC	6.6
D'Apuzzo P-260-2	EB FGC	6.5
EAA Biplane	EB FGC	6.5
Baby Great Lakes	EB FGC	6.5
Mong Sport	EB FGC	6.5
Knight Twister KT-85	EB FGC	6.5
Smith Miniplane DSA-1	EB FGC	6.5
Starduster SA300	EB FGC	6.5

[a]See section 6.1.

TABLE 6.I.- Concluded

(e) Turboprop-powered aircraft

Aircraft	Configuration (a)	Reference
Beech King Air (five versions)	IB RG 2	6.7 and 6.8
Fairchild Hiller F-227E	IB RG 2	6.7
Fairchild Hiller Turbo Porter	EB FGC	6.7
Helio H-550A	EB FGC	6.7
Lockheed C-130E	IB RG 4	6.7
Rockwell Turbo Commander	IB RG 2	6.7
Swearingen Merlin III	IB RG 2	6.7
Swearingen Metro	IB RG 2	6.7
Scottish Aviation Jetstream	IB RG 2	6.7 and 6.8
Grumman Gulfstream I	IB RG 2	6.5

[a]See section 6.1.

TABLE 6.II.- ESTIMATED ZERO-LIFT DRAG COEFFICIENT

Aircraft (a)	$C_{D,0}$		
	Average	Minimum	Maximum
Class I	0.0230	0.0173	0.0330
Class II	.0296	.0230	.0360
Class III	.0430	.0330	.0610

[a]See section 6.4.1.

TABLE 6.III.- FUEL CONSUMPTION OF CURRENT RECIPROCATING ENGINES AT CRUISE POWER

Engine	Take-off horsepower	Compression ratio	c, lb/hp/hr	Turbo-charged
1	65	6.30	0.50	No
2	115	6.78	.47	No
3	150	7.0	.45	No
4	180	8.50	.43	No
5	295	8.70	.46	No
6	340	7.30	.48	No
7	285	7.50	.50	Yes 19 000 ft
8	310	7.30	.55	Yes 15 000 ft
9	400	7.30	.50	Yes 15 000 ft

VII - APPLICATION OF SIZING METHOD FOR PROPELLER-DRIVEN AIRCRAFT

CONTENTS

		Page
7.0	Introduction	390
7.1	Performance Objectives	390
7.2	Aircraft Description	390
7.3	Scope of Studies	392
7.4	Aircraft Cruising Speed	393
7.5	Airport Performance	396
	7.5.1 Take-Off Field Length	396
	7.5.2 Stalling Speed and Landing Field Length	397
7.6	Aircraft Climb Performance	398
7.7	Aircraft Matching	399
	7.7.1 Match Point Parameters	400
	7.7.2 Comparative Aircraft Performance	402
7.8	Aircraft Sizing	404
	7.8.1 Aircraft Fuel Fraction	404
	7.8.2 Aircraft Weights and Sizes	407
7.9	Design Trends	409
7.10	Speed, Range, and Power Relationships	411
	7.10.1 Unsupercharged Aircraft	413
	7.10.2 Supercharged Aircraft	415
	7.10.3 Aircraft Performance Map	416
7.11	Altitude Effects on Rate of Climb	418
7.12	Comparative Climb Performance	420
7.13	Summary	421
SYMBOLS		422
TABLES		424

7.0 Introduction

The methods for sizing propeller-driven aircraft described in chapter 6 are illustrated in chapter 7 by application to a specific design problem. A light, twin-engine aircraft capable of carrying four to six people for a range of 1260 statute miles is studied. The aircraft is to be sized for three different cruising speeds; and for each speed, the effect on the size, weight, and power of three different design values of single-engine rate of climb is to be studied. The single-engine rate of climb has been chosen as a primary design variable because of its importance in flight safety. In addition, the effects of two different field lengths and stalling speeds on the physical characteristics of the aircraft are to be studied.

7.1 Performance Objectives

The light, twin-engine aircraft is intended to have a design range of 1260 statute miles with no fuel reserves and to carry four persons with their baggage over this distance. The design range is to be achieved at a cruising speed corresponding to 75 percent power and 8000-ft altitude. The average person is assumed to weigh 175 lb; baggage and other articles are assumed to weigh 400 lb. The total payload weight is thus:

Four persons at 175 lb each, lb	700
Baggage and other articles, lb	400
Total payload weight, lb	1100

The cabin volume is intended to be sufficiently large to carry six persons with reduced baggage weight and/or reduced range.

As indicated in section 7.0, aircraft are to be studied for three different cruising speeds. These specified speeds are 200, 225, and 250 statute mph at 8000-ft altitude and 75 percent of maximum sea-level power. For each of these speeds, aircraft are to be sized for single-engine rates of climb at sea level of 300, 400, and 500 ft/min. The resulting aircraft are to be examined in relation to take-off field lengths of 2000 and 1600 ft and stalling speeds of 70 and 75 statute mph. The landing field lengths corresponding to these speeds of 70 and 75 mph are 1910 and 2204 ft, respectively. All take-off, landing, and rate-of-climb specifications are for sea-level standard-day atmospheric conditions.

7.2 Aircraft Description

The configuration of the aircraft to be analyzed is similar to contemporary light twins. The wing is internally braced, is mounted on the bottom of the fuselage, and is equipped with partial span, single-slotted flaps. The power is supplied by two unsupercharged engines. In one special case, to be discussed later, the effect of supercharging is considered. One engine is mounted in each

wing on either side of the fuselage. The engines are assumed to be equipped with constant speed, full feathering propellers. The tricycle landing gear is fully retractable.

The configuration of the aircraft is denoted as class I. (See section 6.4.1 of chapter 6.) The average zero-lift drag coefficient for this class of aircraft is 0.023, as shown in table 6.II of chapter 6. The wing aspect ratio A and the airplane efficiency factor ε are assumed to be 7.0 and 0.7, respectively. The maximum lift-drag ratio $(L/D)_{max}$ and the corresponding lift coefficient $C_{L,m}$ may now be calculated from equations (3.19) and (3.20) which, for convenience, are repeated here

$$(L/D)_{max} = \frac{1}{2}\sqrt{\frac{\pi A \varepsilon}{C_{D,0}}} \tag{7.1}$$

or

$$(L/D)_{max} = \frac{1}{2}\sqrt{\frac{\pi (7)(0.7)}{0.023}} = 12.9$$

$$C_{L,m} = \sqrt{\pi A \varepsilon C_{D,0}} \tag{7.2}$$

or

$$C_{L,m} = \sqrt{\pi (7)(0.7)(0.023)} = 0.60$$

The minimum power required parameter $(C_L^{3/2}/C_D)_{max}$ and the corresponding value of the lift coefficient $C_{L,c}$ may be calculated from equations (6.20) and (6.21) which are repeated here

$$(C_L^{3/2}/C_D)_{max} = \frac{1.345(A\varepsilon)^{3/4}}{(C_{D,0})^{1/4}} \tag{7.3}$$

or

$$(C_L^{3/2}/C_D)_{max} = \frac{1.345\,[(7.0)(0.7)]^{3/4}}{(0.023)^{1/4}} = 11.4$$

$$C_{L,c} = \sqrt{3C_{D,0}\pi A\epsilon} \tag{7.4}$$

or

$$C_{L,c} = \sqrt{3(0.023)\pi(7.0)(0.7)} = 1.03$$

The parameter $(C_L^{3/2}/C_D)_{max}$ is necessary for estimating the rate of climb by the methods of chapter 6.

The take-off calculations are to be made with the use of the curve in figure 6.11, together with an assumed value of 1.6 for the maximum lift coefficient in the take-off configuration $C_{L,T}$. The maximum lift coefficient in the landing configuration, used for determination of the stalling speed, is assumed to be 2.2. A study of the data in figure 6.8 (chapter 6) shows that this value of $C_{L,max}$ is slightly higher than the values achieved in contemporary practice; however, the value of 2.2 is thought to be reasonable. The values of the propulsive efficiency to be used for the cruise and climb calculations, η_c and η_h', are assumed to be 0.85 and 0.70, respectively.

The quantitative characteristics of the aircraft which have just been discussed are summarized as follows:

$A = 7.0$	$C_{L,c} = 1.03$
$\epsilon = 0.70$	$C_{L,T} = 1.6$
$C_{D,0} = 0.023$	$C_{L,max} = 2.2$
$(L/D)_{max} = 12.9$	$\eta_c = 0.85$
$C_{L,m} = 0.60$	$\eta_h' = 0.70$
$(C_L^{3/2}/C_D)_{max} = 11.4$	$c = 0.50$

7.3 Scope of Studies

A matching chart similar to that illustrated in figure 6.23 of chapter 6 is to be constructed with the use of the various design constraints and aircraft parameters discussed in sections 7.1 and 7.2. Match points defining the wing loading and power loading of various aircraft which satisfy some or all of the different performance objectives are to be obtained from the intersections of different constraint lines. The following aircraft characteristics are to be calculated for each match point:

(1) Gross weight

(2) Empty weight

(3) Fuel weight

(4) Wing area

(5) Engine power

In addition, the rate of climb with both engines operating is to be calculated for the aircraft corresponding to each match point; and the take-off and landing field lengths, the stalling speed, and the single-engine rate of climb are to be determined for those cases in which these quantities are different from the specified values.

In order to illustrate the effect of changes in specified performance objectives on the aircraft physical characteristics, gross weight, wing area, and engine power are to be shown graphically as a function of single-engine rate of climb for the three different cruising speeds. One of the aircraft which appears to have an attractive combination of physical and performance characteristics will then be chosen for additional performance calculations. The range at different speeds and altitudes together with the required percentage of power will be determined for this aircraft. The range of speeds to be studied will extend from that for maximum lift-drag ratio to the maximum speed achievable at each altitude. The altitude range to be studied will extend from sea level to 18 000 ft. The effect of supercharging on the speed, range, and altitude relationships of this aircraft will also be studied. The supercharged aircraft is assumed to have a critical altitude of 18 000 ft. The maximum altitude for which performance calculations are to be made is 25 000 ft in this case. The effect of altitude on the rate of climb will also be determined for both the unsupercharged and supercharged aircraft. The gross weight of the supercharged aircraft is assumed to be the same as that of the unsupercharged aircraft. This assumption means that the payload or fuel weight would be reduced somewhat to account for the weight associated with the engine superchargers, cabin oxygen equipment, etc. The cabin is assumed to be unpressurized.

The following sections describe and discuss the detailed calculations involved in the design study.

7.4 Aircraft Cruising Speed

Aircraft with design cruising speeds of 200, 225, and 250 mph at 75 percent power and an altitude of 8000 ft are to be sized. A curve of power loading as a function of wing loading will be obtained for each of the three different specified cruising speeds. These curves are similar in nature to the curve labeled "maximum speed" in figure 6.23.

The speed constraint curves are obtained with the use of the data contained in figure 6.2 of chapter 6 for class I aircraft. Figure 6.2 indicates a linear variation of speed with power index as follows:

$$V = KI_p \tag{7.5}$$

and

$$I_p = \sqrt[3]{\frac{W/S}{(W/P)\sigma}} \tag{7.6}$$

where

W/S wing loading

W/P power loading

σ density ratio, ρ/ρ_0

K = 170 for class I aircraft (slope of curve of fig. 6.2)

If the wing loading and power loading are based on maximum gross weight and maximum power at sea level, respectively, then the expression for the power index for a given percentage of power takes the form

$$I_p = \sqrt[3]{\frac{(W_g/S)\gamma}{(W_g/P_0)\sigma}} \tag{7.7}$$

where

γ percentage of maximum sea-level power at which speed V (eq. (7.5)) is to be obtained

W_g maximum gross weight

P_0 maximum sea-level power

With the use of the definition of the power index I_p given by equation (7.7), the relationship for the speed (eq. (7.5)) may be rewritten in the following useful computational form:

$$W_g/P_0 = \left(\frac{K}{V}\right)^3 (W_g/S)\,(\gamma/\sigma) \tag{7.8}$$

or

$$W_g/P_0 = \frac{4.913 \times 10^6}{V^3}(W_g/S)\frac{\gamma}{\sigma} \tag{7.9}$$

Equation (7.8) or (7.9) may be used to obtain the power loading corresponding to a range of values of the wing loading for each of the three different specified cruising speeds. The detailed calculations of the power loading corresponding to the three different cruising speeds and aircraft variants 1, 2, and 3 are contained in table 7.I. The calculations are perhaps best understood by identifying each of the columns in table 7.I as follows:

① V_c, design cruising speed.

② γ, percentage of maximum sea-level power at which the design cruising speed is specified.

③ σ, value of the density ratio corresponding to the design cruising altitude of 8000 ft. The value of σ may be obtained from figure 6.6 of chapter 6 or from a table of atmospheric data such as table 1.I of chapter 1.

④ K, slope of the straight line through the data points of figure 6.2.

⑤ $(K/V_c)^3$, cube of the ratio of the value of ④ divided by ①.

⑥ γ/σ, ② divided ③.

⑦ W_g/S, assumed values of wing loading for which values of power loading are desired.

⑧ W_g/P_0, power loading, based on maximum gross weight and maximum sea-level power, corresponding to the values of wing loading given in ⑦. The values of power loading were obtained by multiplication of ⑤, ⑥, and ⑦ according to equation (7.8), that is, ⑧ = ⑤ × ⑦ × ⑥.

Columns ⑦ and ⑧ give pairs of values of power loading and wing loading which, within the accuracy of the method, will yield the desired speeds given in column ①. A curve of power loading against wing loading may therefore be plotted for each of the three design values of cruising speed.

The method just described for calculating the required power loading as a function of wing loading for a specified speed contains certain inherent inaccuracies which should be clearly recognized. The linear relationship between power loading and wing loading shown by equations (7.8) and (7.9) implies a constant drag coefficient. As the wing loading is varied for constant velocity, however, the induced drag coefficient must obviously vary also. Hence, the linear relationship between wing loading and power loading upon which the data of table 7.I are based is not strictly true. The magnitude of the error resulting from the linear assumption, however, depends upon the extent of the differences in wing loading considered for a given assumed velocity. The differences in induced drag coefficient corresponding to wing loadings of 40 and 15 lb/ft^2 are significant for a given speed. As will be seen later, however, the differences in wing loading for different matching points at a given speed are not very large. Significant differences in induced drag coefficient would not,

therefore, be expected. The magnitude and importance of the difference in induced drag coefficient corresponding to different wing loadings at a given speed and altitude may be quickly estimated with the use of the boundary curves contained in figure 6.7 and discussed in section 6.4.2.3 of chapter 6. In any case, values of power loading and wing loading which give approximately the desired speed may be obtained with the use of equations (7.8) and (7.9) together with the exercise of good judgment in their application. A more precise method for the determination of the speed corresponding to a given wing loading and power loading is described in section 6.9 of chapter 6 and will be applied in setion 7.10 to one of the aircraft being studied herein.

Another assumption implicit in the linear relationship between W/S and W/P for a given speed is that the zero-lift drag coefficient $C_{D,0}$ is invariant with wing loading. This assumption means that the ratio of total wetted area to wing area remains constant as the wing loading varies. This assumption may be invalid in many practical cases because of limitations imposed by such factors as cabin and engine size. Again, however, for the range of wing loadings corresponding to the matching points which will subsequently be found in section 7.7, the effect of variations in the ratio of total wetted area to wing area is well within the scatter of the data in figure 6.2 upon which the linearized equations (7.8) and (7.9) are based.

7.5 Airport Performance

Definitions of airport performance parameters for aircraft designed to meet part 23 of the Federal Air Regulations (FAR) are discussed in section 6.5 of chapter 6. The airport performance objectives in the present study include the take-off field length, landing field length, and stalling speed. Methods for calculating these parameters are described in sections 6.5.1, 6.5.2, and 6.5.3 of chapter 6.

7.5.1 Take-Off Field Length

The performance objectives discussed in section 7.1 require that the aircraft be examined in relation to take-off field lengths of 1600 and 2000 ft. The field length is the total horizontal distance from the point on the runway at which the aircraft begins to move to the point at which an altitude of 50 ft is reached. The curves given in figures 6.11 and 6.12 are used to compute the values of necessary power loading corresponding to various assumed values of wing loading for each of the two take-off field lengths. These two figures were used to develop the take-off performance data given in table 7.II. The calculations are perhaps best understood by identifying each of the columns in table 7.II as follows:

① ℓ_T, take-off field length.

② $C_{L,T}$, take-off lift coefficient obtained from aircraft characteristics given in section 7.2.

③ σ, density ratio which is assumed to be 1.0.

④ $\frac{(W_g/S)(W_g/P_0)}{\sigma}$, take-off parameter corresponding to a ground run distance (fig. 6.11) which when multiplied by the ratio of take-off length to ground run distance of 1.65 (fig. 6.12) gives the desired field length specified in ①.

⑤ W_g/S, assumed values of the wing loading for which the corresponding values of power loading are desired.

⑥ W_g/P_0, power loading which is obtained by dividing ④ by ⑤.

Columns ⑤ and ⑥ give pairs of values of wing loading and power loading which give the desired take-off field lengths specified in column ①.

7.5.2 Stalling Speed and Landing Field Length

Stalling speeds less than 70, or at most 75 mph, are specified in the performance objectives described in section 7.1. The wing loadings for these two stalling speeds may be estimated from the curves given in figure 6.8 of chapter 6 or may be calculated directly from the following equation:

$$W_g/S = 0.00257 C_{L,max} \sigma V_S^2 \qquad (7.10)$$

where

W_g/S wing loading for maximum gross weight

$C_{L,max}$ maximum lift coefficient in landing configuration (2.2 specified in section 7.2)

σ atmospheric density ratio

V_S stalling speed, mph

The values of the wing loading corresponding to the two stalling speeds are found to be: $V_S = 70$ for $W_g/S = 27.7$ and $V_S = 75$ for $W_g/S = 31.8$.

The landing field length is defined as the horizontal distance from the point at which the aircraft is 50 ft above the ground on final approach to the point at which the aircraft is brought to a stop on the runway. The landing field length may be calculated from the specified stalling speeds with the use of the curves of figures 6.9 and 6.10. The values of field length determined by this method are: $V_S = 70$ for $\ell_T = 1910$ and $V_S = 75$ for $\ell_T = 2204$.

7.6 Aircraft Climb Performance

The performance objectives (section 7.1) specify that aircraft are to be sized for single engine rates of climb of 300, 400, and 500 ft/min. The estimation of aircraft rate of climb is discussed in detail in section 6.6 of chapter 6. A convenient expression for calculating the rate of climb is given by equation (6.15) which is repeated here as

$$\dot{h} = 33\ 000\left[\eta \frac{P}{W} - \frac{\sqrt{W/S}}{19\left(C_L^{3/2}/C_D\right)\sqrt{\sigma}}\right] \tag{7.11}$$

where

$\dot{h}$ rate of climb, ft/min

η propulsive efficiency

P/W reciprocal of power loading

W/S wing loading

C_L lift coefficient

C_D drag coefficient

σ density ratio

For use in calculating the boundary curve to be employed in developing a matching chart, equation (7.11) can be rewritten in the following form:

$$\frac{P}{W} = \frac{1}{\eta}\left[\frac{\dot{h}}{33\ 000} + \frac{\sqrt{W/S}}{19\left(C_L^{3/2}/C_D\right)\sqrt{\sigma}}\right] \tag{7.12}$$

If W_g/P_0 is defined as the power loading required, with both engines operating, in order that a specified single-engine rate of climb, $\dot{h}_{1/2}$, may be achieved with one engine inoperative, then equation (7.12) takes the form

$$\frac{P_0}{W_g} = \frac{2}{\eta}\left[\frac{\dot{h}_{1/2}}{33\ 000} + \frac{\sqrt{W_g/S}}{19\left(C_L^{3/2}/C_D\right)_{max}\sqrt{\sigma}}\right] \tag{7.13}$$

where $\left(C_L^{3/2}/C_D\right)_{max}$ is the maximum value of the parameter $C_L^{3/2}/C_D$ achievable with a particular aircraft. The calculation of $\left(C_L^{3/2}/C_D\right)_{max}$ is discusse in section 6.6.2 of chapter 6.

Equation (7.13) provides a convenient means for calculating the power loading as a function of wing loading for each of the three specified values of rate of climb. The detailed calculations are contained in table 7.III. The calculations are perhaps best understood by identifying each of the columns in table 7.III as follows:

① $\dot{h}_{1/2}$, specified single-engine rate of climb.

② W/S, assumed values of wing loading for which power loading is desired.

③ $(C_L^{3/2}/C_D)_{max}$, value obtained from aircraft description contained in section 7.2.

④ σ, density ratio assumed to be 1.0.

⑤ $\dfrac{\sqrt{W/S}}{19(C_L^{3/2}/C_D)_{max}\sqrt{\sigma}}$, parameter obtained by the operation $\dfrac{\sqrt{②}}{19 \times ③ \times \sqrt{④}}$.

⑥ $\dfrac{\dot{h}_{1/2}}{33\ 000}$, single-engine rate of climb obtained by dividing ① by horsepower conversion factor 33 000.

⑦ $\eta_{\dot{h}}$, propulsive efficiency in the climb configuration which was specified as 0.7 in section 7.2.

⑧ W_g/P_0, required power loading obtained as follows:

$$⑧ = \frac{1}{\frac{2}{⑦}\left(⑥ + ⑤\right)}$$

7.7 Aircraft Matching

An aircraft matching chart similar in form to that shown conceptually in figure 6.23 of chapter 6 has been constructed from the data contained in tables 7.I, 7.II, and 7.III and is presented in figure 7.1. The power loading is shown on the ordinate, and the wing loading is on the abscissa. The constraint lines for the different cruising speeds, single-engine climb rates, take-off field lengths, and stalling speeds are shown with the inadmissible sides of the curves denoted by the hatching. For example, any combination of wing loading and power loading which falls above the 225 mph cruising speed line will give a speed less than the desired value. The constant speed lines show a linear increase in power loading (that is, a reduction in required power for a given weight) as the wing loading is increased. This trend results from the reduction in wing area, and hence total wetted area, which accompanies an increase in wing loading. The curves of constant rate of climb and take-off

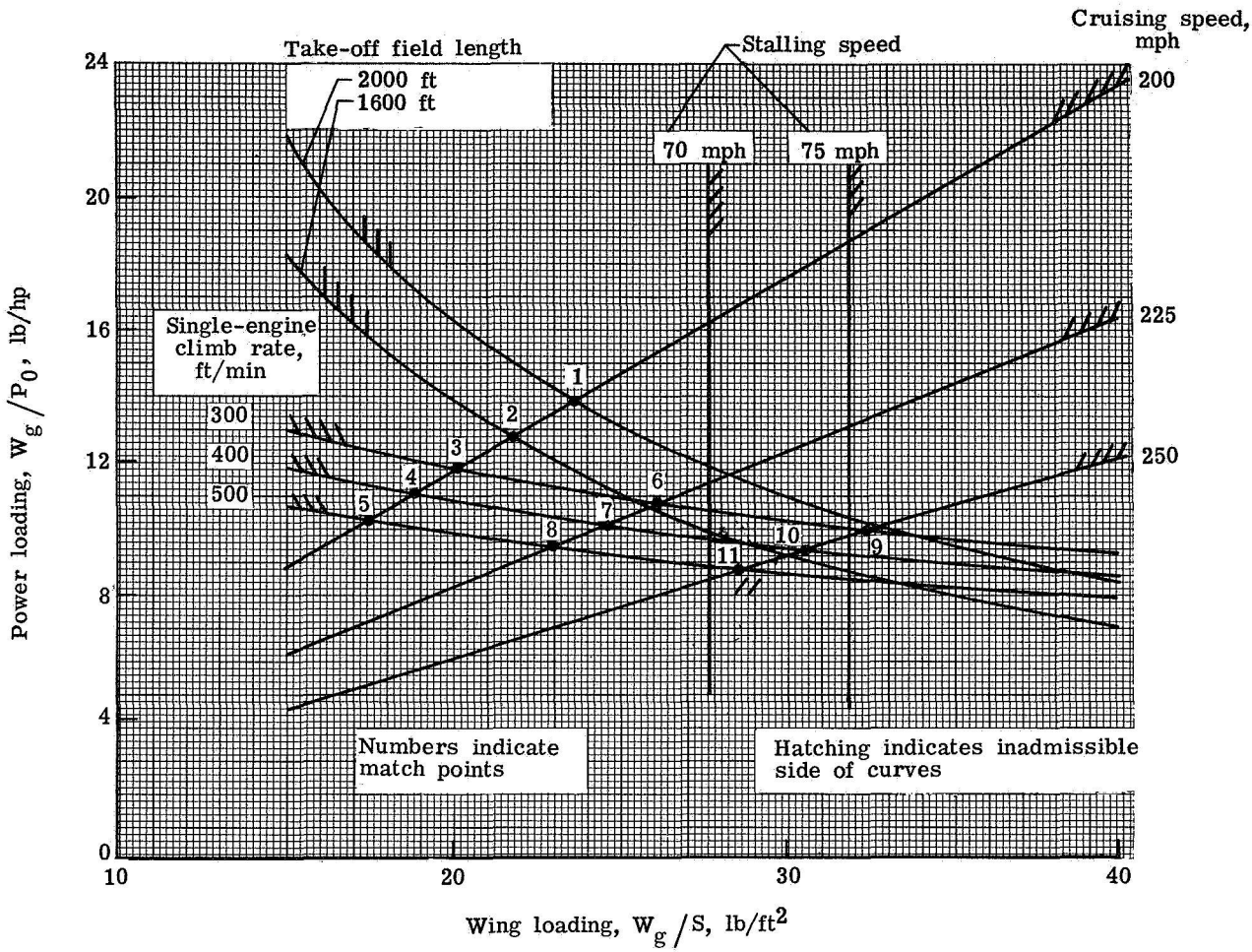


Figure 7.1.- Aircraft matching chart.

field length show a reduction in power loading with increasing wing loading. The increase in speed at which the aircraft takes off and climbs for specified values of field length and climb rate causes the observed trends.

7.7.1 Match Point Parameters

The match points are indicated by the numbers shown in figure 7.1 adjacent to the intersections of the various constraint lines. The match points are taken at the intersections of the constant speed and rate of climb lines except for points 1 and 2 which correspond to the 200 mph cruising speed line and take-off field lengths of 2000 and 1600 ft, respectively.

The effect of differences in induced drag coefficient on the comparative characteristics of the aircraft corresponding to the different match points may be evaluated with the use of the boundaries given in figure 6.7 of chapter 6. These boundaries are given in figure 7.2 along with points corresponding to the

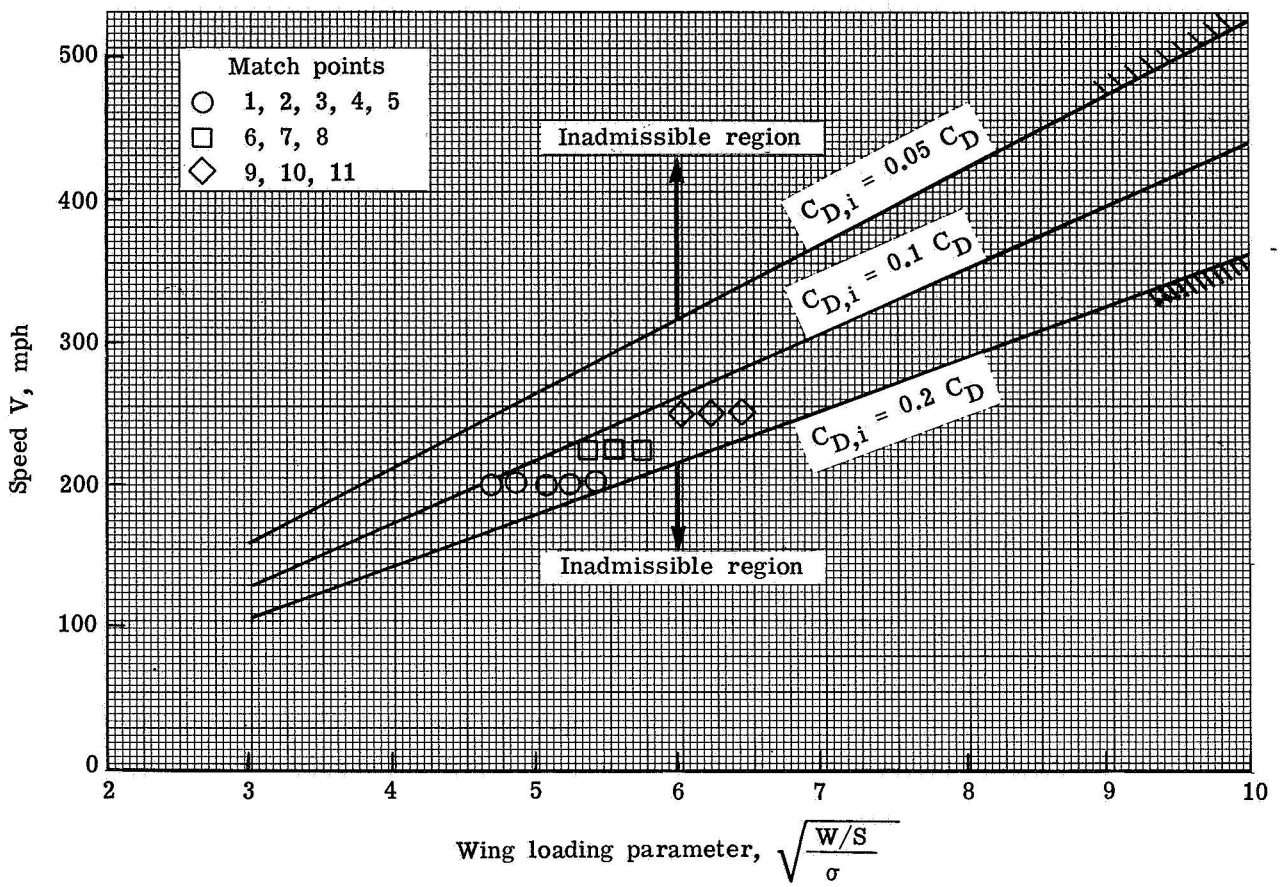


Figure 7.2.- Matching point parameters in relation to boundaries of figure 6.7.

values of speed V and wing loading parameter $\sqrt{\frac{W/S}{\sigma}}$ for each of the numbered match points in figure 7.1. The average induced drag coefficient for each of the three values of cruising speed is seen to be about 15 percent of the total drag coefficient. The variation in induced drag coefficient for the different points is approximately 3 percent on either side of the mean value for cruising speeds of 225 and 250 mph and about 5 percent on either side of the mean value for a cruising speed of 200 mph. The larger variation for the 200 mph case is attributable to the wider range of wing loadings covered by the five match points for this speed. Accordingly, variations in induced drag coefficient would be expected to have only a relatively small effect on the comparative characteristics of the aircraft corresponding to the various match points.

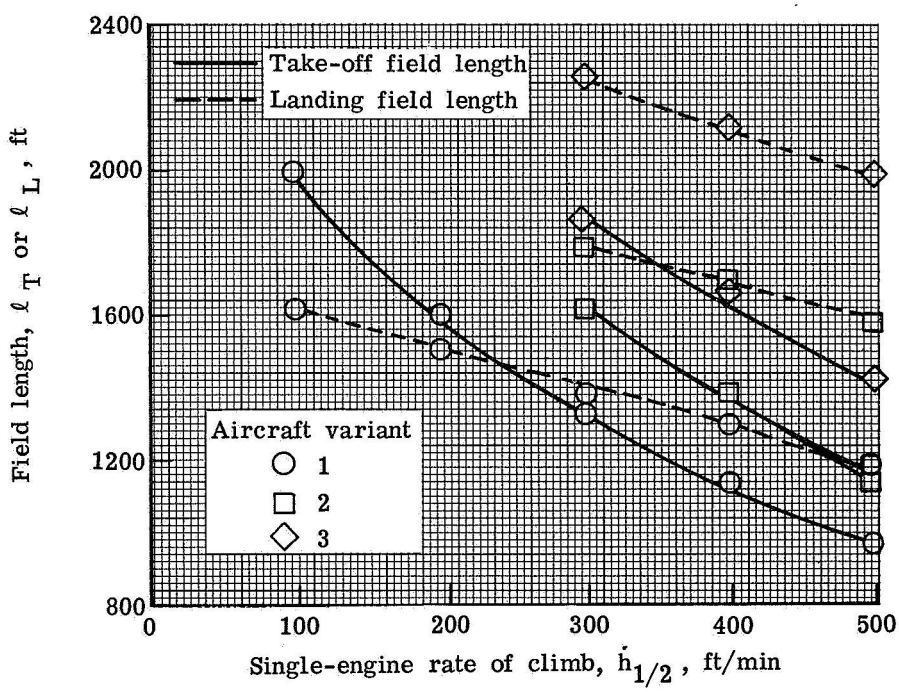
An examination of figure 7.1 indicates that any one of the specified single-engine climb rates calls for significantly lower power and wing loadings than are required to meet either of the take-off field length requirements for a cruising speed of 200 mph. Thus, satisfaction of any of the climb rates for this speed would result in take-off field lengths significantly less than either of the specified values. Match point 6 for 225 mph simultaneously satisfies

the cruising speed, take-off field length of 1600 ft and single-engine rate of climb of 30 ft/min. Match point 9 for 250 mph is a close approximation to a simultaneous satisfaction of the cruising speed, take-off field length of 2000 ft, and single-engine rate of climb of 300 ft per minute; match point 10 for the same speed is a near simultaneous satisfaction of speed, take-off field length of 1600 ft, and single-engine rate of climb of 400 ft/min. Stalling speeds less than 70 mph are associated with match points 1 to 6, whereas these speeds fall between 70 and 75 mph for match points 9, 10, and 11.

7.7.2 Comparative Aircraft Performance

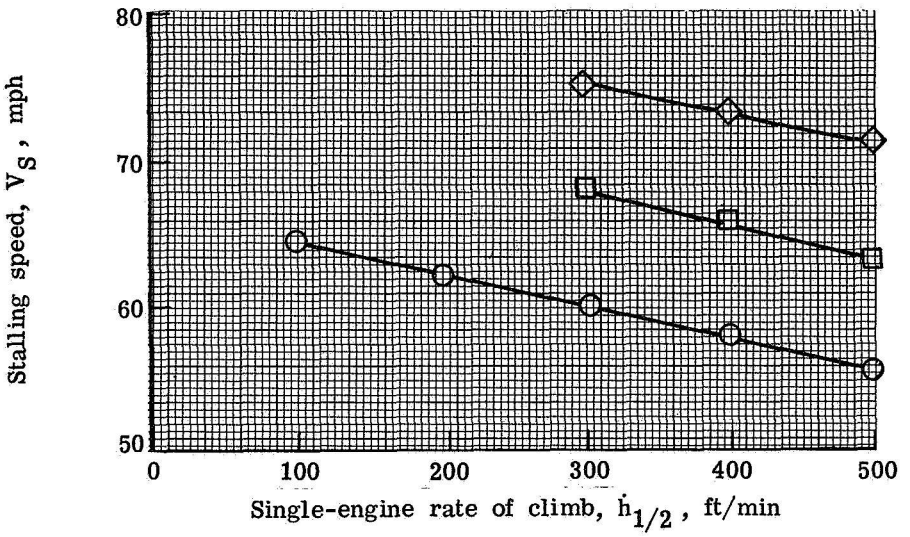
The wing loading, power loading, and some of the pertinent performance characteristics of the aircraft are given for each match point in table 7.IV. The climb rate given in column (9) is for both engines operating and was calculated by equation (7.11). The stalling speeds and landing and take-off field lengths were calculated by the methods of chapter 6 which were described in section 7.5.

In order to show more clearly the relationship between the various performance parameters, some of the data of table 7.IV have been plotted against single-engine rate of climb in figure 7.3. The manner in which take-off and

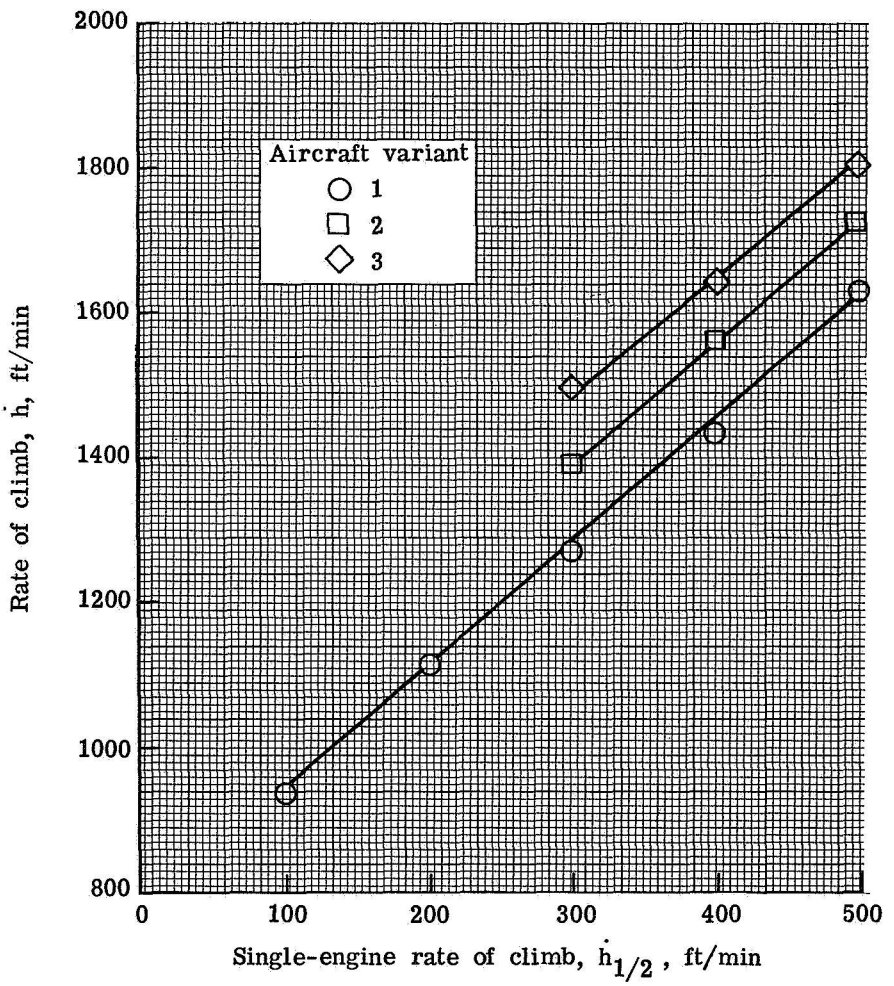


(a) Field length.

Figure 7.3.- Variation of performance parameters with single-engine rate of climb for aircraft variants 1, 2, and 3.



(b) Stalling speed.



(c) Rate of climb, both engines operating.

Figure 7.3.- Concluded.

landing field length vary with the climb rate is shown in figure 7.3(a). For example, for a cruising speed of 200 mph (aircraft variant 1), match point 1 gives a take-off field length of 2000 feet with a single-engine climb rate of slightly less than 100 ft/min, whereas match point 5 gives a take-off distance of less than 1000 ft and a climb rate of 500 ft/min. Similar trends are shown by the data for aircraft variants 2 and 3. The conclusion can be reached that the single-engine rate of climb for a given take-off field length increases as the specified cruising speed increases; or the take-off field length for a constant single-engine rate of climb increases as the specified cruising speed increases.

The stalling speeds are shown as a function of single-engine rate of climb in figure 7.3(b). As previously indicated, the stalling speeds of aircraft variants 1 and 2 fall below 70 mph and those for aircraft variant 3 are between 70 and 75 mph. The landing field lengths corresponding to these speeds are seen in figure 7.3(a) to be greater than the take-off field lengths for single-engine climb rates of 300, 400, and 500 ft/min. The difference is inconsequential in some cases but may be significant in others. The larger differences occur for the higher cruising speeds and climb rates. For example, aircraft variant 3 indicates a take-off field length of about 1400 ft, as compared to a landing field length of 2000 ft for a single-engine climb rate of 500 ft/min. A more sophisticated high-lift system might be desirable for cases such as this in order to make the landing and take-off field lengths more compatible.

The rate of climb with both engines operating is shown as a function of single-engine rate of climb in figure 7.3(c). These data indicate that the rate of climb with all engines operating is from three to five times the single-engin rate of climb. The magnitude of the factor depends upon the particular aircraft being considered. The large difference in the one-engine and two-engine rates of climb results from the high percentage of the total power of one engine which is required just to maintain level flight at the speed for best climb. In this connection, extrapolation of any of the curves of figure 7.3(c) to a zero value of single-engine rate of climb gives a positive two-engine rate of climb. This corresponds to the case in which all of the power in one engine is needed to maintain level flight at the climb speed.

7.8 Aircraft Sizing

Estimation of the various aircraft weights and sizes with the use of relationships which utilize the match point parameters, payload, and design range is discussed in section 6.8 of chapter 6. The method requires the determinatior of the fuel fraction corresponding to the design range. Calculation of the fuel fraction is discussed in section 6.9 of chapter 6; the procedure described therein will now be applied to the determination of the fuel fraction corresponding to the 11 match points and for the design range of 1260 n. mi.

7.8.1 Aircraft Fuel Fraction

The fuel fraction necessary for a specified range is given by equation (6.41) of chapter 6 and is repeated here for convenience

$$W_f/W_g = 1 - \frac{1}{e^{R/B}} \tag{7.15}$$

where

W_f fuel weight, lb

W_g aircraft gross weight, lb

R range, statute miles

B Breguet factor, $\frac{375\eta_c(L/D)}{c}$

and

L/D lift-drag ratio

c specific fuel consumption, pounds of fuel per horsepower per hour

η_c propulsive efficiency in cruising flight

The range which appears in equation (7.15) is not the design range of 1260 miles but is the range corresponding to the maximum value of the lift-drag ratio. Thus, equation (7.15) becomes

$$W_f/W_g = 1 - \frac{1}{e^{R_m/B}} \tag{7.16}$$

The design range R_s is related to the maximum range R_m by equation (6.46) of chapter 6 which is repeated here in slightly altered form as follows:

$$R/R_m = \frac{2}{(V/V_m)^2 + \frac{1}{(V/V_m)^2}} \tag{7.17}$$

where V and V_m are the speeds corresponding to the ranges R and R_m, respectively, and the speed V_m is given by equation (6.47) which is repeated here as

$$V_m = 19.73\sqrt{\frac{W/S}{C_{L,m}\sigma}} \tag{7.18}$$

where V_m is in statute miles per hour and $C_{L,m}$ is the lift coefficient.

If the design range is designated by R_S and the specified cruising speed is denoted by V_C, equation (7.17) becomes

$$R_S/R_m = \frac{2}{(V_C/V_m)^2 + \frac{1}{(V_C/V_m)^2}} \tag{7.19}$$

Equations (7.16), (7.18), and (7.19) have been used to determine the fuel fraction required to give the design range, R_S for each of the 11 match points found in figure 7.1. The value of wing loading used in determining the speed V_m was assumed to be that for maximum gross weight. No allowance was made for the reduction in wing loading associated with the consumption of fuel during the course of the flight. This assumption means that, for a given altitude, cruising speed must be reduced slightly during the course of the flight to maintain a constant value of L/D. The design range is exactly achieved in this case. Other cruise alternatives exist which may result in some small variations in range.

The detailed calculations of the fuel fraction corresponding to each of the 11 match points are given in table 7.V. The calculations are perhaps best understood by identifying each of the columns in table 7.V as follows:

① Match point, corresponding to the match points of figure 7.1.

② W_g/S, wing loading corresponding to the match points of ①.

③ σ, density ratio for an altitude of 8000 ft. The value can be obtained from figure 6.6 of chapter 6 or table 1.I given in chapter 1.

④ $C_{L,m}$, value of lift coefficient for $(L/D)_{max}$ given in section 7.2.

⑤ V_m, value of speed for $(L/D)_{max}$ calculated from equation (7.18) as follows:

$$⑤ = 19.73\sqrt{\frac{②}{④ \times ③}}$$

⑥ V_c, design cruising speed.

⑦ V_c/V_m, ratio of cruising speed to speed at $(L/D)_{max}$.

⑧ R_s/R_m, ratio calculated by equation (7.19) as follows:

$$⑧ = \frac{2}{⑦^2 + \frac{1}{⑦^2}}$$

⑨ R_m, value of range at $(L/D)_{max}$ obtained by dividing design range of 1260 miles by ⑧.

⑩ $(L/D)_{max}$, value given in section 7.2.

⑪ c, specific fuel consumption given in section 7.2.

⑫ η_c, propulsive efficiency for cruising flight as given in section 7.2.

⑬ B, Breguet factor calculated as follows:

$$⑬ = \frac{375 \times ⑩ \times ⑫}{⑪}$$

⑭ W_f/W_g, fuel fraction determined with the use of equation (7.16) as follows:

$$⑭ = 1 - \frac{1}{e^{⑨/⑬}}$$

7.8.2 Aircraft Weights and Sizes

The aircraft gross weight may be determined with the use of equation (6.39) of chapter 6 and from known values of fuel fraction, power loading, and design payload. Equation (6.39) is repeated here for convenience as follows:

$$W_g = \frac{W_p}{\bar{U} - (W_f/W_g)} \qquad (7.20)$$

where

W_g gross weight, lb

W_p payload weight, lb

$\bar{U}$ useful load fraction obtained from figure 6.24 of chapter 6, together with value of power loading at a particular match point

W_f/W_g fuel fraction corresponding to particular match point

Sufficient information is now available to calculate the desired gross physical characteristics of the aircraft.

The detailed calculations of the characteristics of the aircraft corresponding to each of the 11 match points are given in table 7.VI. The calculations are perhaps best understood by identifying each of the columns in table 7.VI as follows:

① Match point, corresponding to match points of figure 7.1.

② W_g/S, wing loading corresponding to match points of ①.

③ W_g/P_0, power loading corresponding to match points of ①.

④ W_f/W_g, fuel fraction taken from column ⑭ of table 7.V.

⑤ W_p, design payload of 1100 lb given in section 7.1.

⑥ $\bar{U}$, useful load fraction taken from figure 6.24 of chapter 6 for power loading in ③.

⑦ W_g, gross weight determined from equation (7.20) as follows:

$$⑦ = \frac{⑤}{⑥ - ④}$$

⑧ W_e, empty weight determined as follows:

$$⑧ = ⑦\ (1 - ④) - ⑤$$

⑨ W_f, fuel weight determined as follows:

$$⑨ = ④ \times ⑦$$

⑩ S, wing area determined as follows:

$$⑩ = ⑦ \div ②$$

⑪ P_0, maximum engine power determined as follows:

$$⑪ = ⑦ \div ③$$

7.9 Design Trends

Several of the important physical characteristics found for the different aircraft by the calculations contained in table 7.VI are plotted against the single-engine rate of climb in figures 7.4., 7.5, and 7.6. The gross weight, maximum installed power, and wing area are given in these figures for aircraft variants 1, 2, and 3.

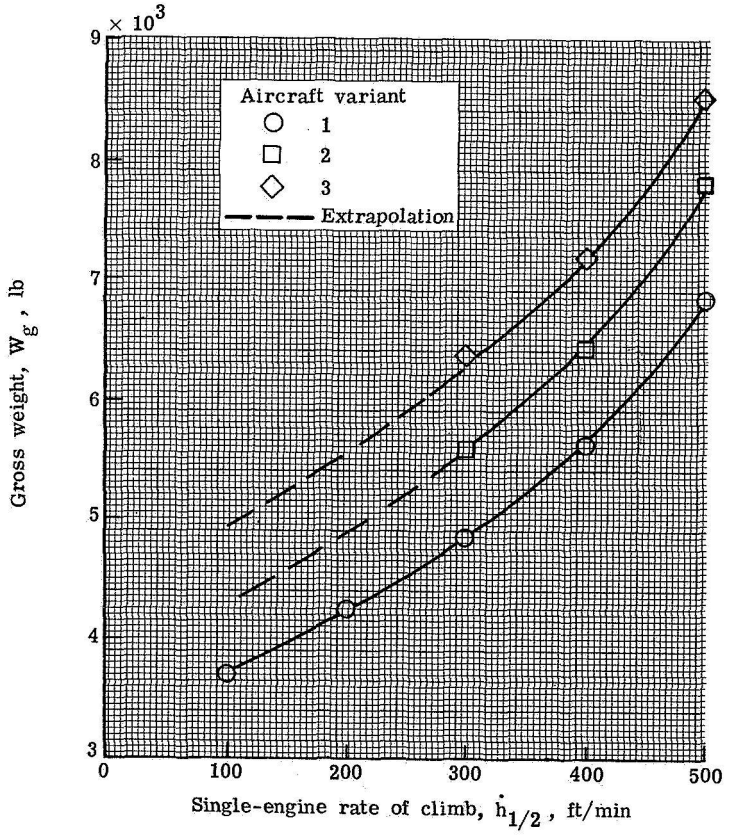


Figure 7.4.- Variation of aircraft gross weight with single-engine rate of climb for aircraft variants 1, 2, and 3.

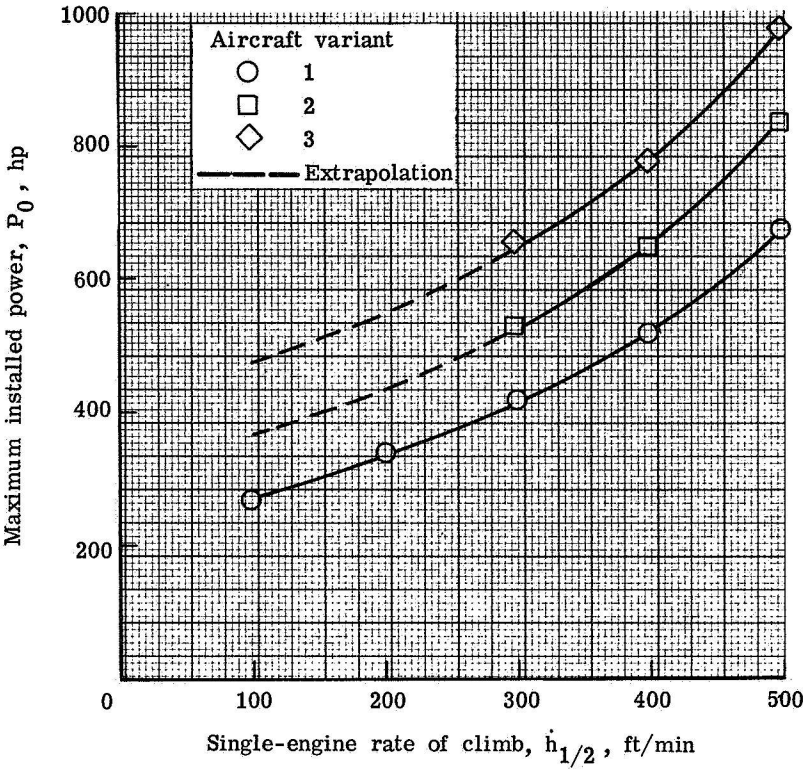


Figure 7.5.- Variation of maximum installed power with single-engine rate of climb for aircraft variants 1, 2, and 3.

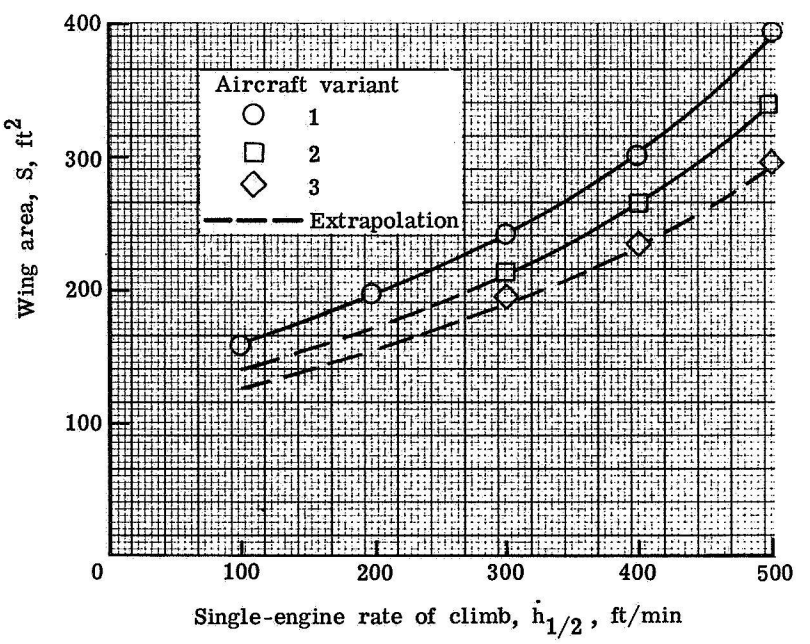


Figure 7.6.- Variation of wing area with single-engine rate of climb for aircraft variants 1, 2, and 3.

A study of the data in figures 7.4, 7.5, and 7.6 indicates a large increase in weight, size, and power for a given aircraft variant as the design single-engine rate of climb is increased. For example, the gross weight of aircraft variant 1, which has a design cruising speed of 200 mph, increases from about 3700 lb to about 6800 lb as the climb rate is increased from 100 to 500 ft/min; the corresponding total engine power increases from 235 to 635 hp. Increases in the weight and power also accompany an increase in design cruising speed for a given value of single-engine rate of climb. For example, the gross weight increases from about 4700 lb to about 6350 lb as the design cruising speed is increased from 200 mph (aircraft variant 1) to 250 mph (aircraft variant 3) at a climb rate of 300 ft/min; the corresponding increase in engine power is from 410 to 625 hp. The wing area is seen to decrease with increasing speed for a given single engine rate of climb.

The trends shown are attributable to the reduction in power loading dictated by an increase in cruising speed for a given single-engine rate of climb, or an increase in climb rate for a given cruising speed. These reductions in power loading are clearly seen in the matching chart presented in figure 7.1. The weight correlation, given in figure 6.24 of chapter 6, indicates a reduction in the useful load fraction as the value of the power loading is decreased. Thus, for a given payload and fuel fraction, the gross weight must increase. The increases in power and wing area are related to the increase in gross weight by the power loading and wing loading, respectively.

An examination of the performance and physical characteristics given in figures 7.3, 7.4, 7.5, and 7.6 indicates that aircraft variant 2 with a design single-engine climb rate of 300 ft/min and a cruising speed of 225 mph seems to represent a good compromise between performance, size, weight, and power. This aircraft will accordingly be chosen for more detailed performance study. The aircraft corresponds to match point 6 of figure 7.1 and is designated aircraft variant 2-6. A supercharged version of this aircraft will also be studied and is designated aircraft variant 2-6S.

7.10 Speed, Range, and Power Relationships

A map is to be generated for aircraft variants 2-6 and 2-6S which presents the range as a function of speed for different altitudes and includes lines of constant percentage of maximum sea-level power. Generalized range and power relationships are discussed in sections 6.9.1, 6.9.2, and 6.9.4 of chapter 6. The range relationship was employed in section 7.8.1 of the present chapter to compute the fuel fraction and was given in equation (7.17), repeated here as follows:

$$R/R_m = \frac{2}{(V/V_m)^2 + \frac{1}{(V/V_m)^2}}$$

where the subscript m refers to conditions at the maximum value of the lift-drag ratio , and the speed V_m is (eq. (7.18))

$$V_m = 19.73\sqrt{\frac{W/S}{\sigma C_{L,m}}}$$

The necessary power relationships are given by equations (6.51) and (6.53) of chapter 6 which are repeated here for convenience as

$$P/P_m = \frac{1}{2}\left[(V/V_m)^3 + \frac{1}{(V/V_m)}\right] \tag{7.21}$$

and

$$P_m/W = \frac{C_{D,0}\sqrt{W/S}}{9.5\left(C_{L,m}{}^{3/2}\right)\sqrt{\sigma}} \tag{7.22}$$

where the subscript m again refers to conditions at $(L/D)_{max}$. The value of the weight W employed in equation (7.22) is the maximum gross weight, just as in the calculations of the fuel fraction discussed in section 7.8.1.

The method of calculation involves determination of the speed and range corresponding to different power settings and altitudes. If the percentage of maximum sea-level power (power setting) is denoted by γ, then

$$\frac{\eta_c \gamma (P_0/W_g)}{P_m/W_g} = \frac{\gamma \eta_c P_0}{P_m} \tag{7.23}$$

where P_0/W_g is the reciprocal of the power loading corresponding to maximum sea-level power and maximum gross weight and P_m/W_g is determined from equation (7.22) for the specified altitude. Since P_m is expressed in terms of thrust horsepower, the cruising propulsive efficiency η_c is employed in equation (7.23) to convert the shaft horsepower P_0 to thrust horsepower. The parameter $\gamma\eta_c P_0/P_m$, called the power ratio, is related to the velocity ratio V/V_m by equation (7.21), and the value of V_m is determined for the desired

altitude by equation (7.18). The speed for any specified power setting and altitude can then be found. The corresponding value of the range is found from equation (7.17) for the known value of V/V_m. The determination of the speed ratio V/V_m for a given value of the power ratio P/P_m is most easily accomplished from a graphical representation of equation (7.21.) Such a graph is presented in figure 6.27 of chapter 6. The scales employed in figure 6.27, however, are not sufficiently large for the present calculations. Equation (7.21) has accordingly been replotted to an enlarged scale in figure 7.7 of the present chapter. The procedure just described has been used in the calculations to be discussed in the next two sections for unsupercharged and supercharged aircraft.

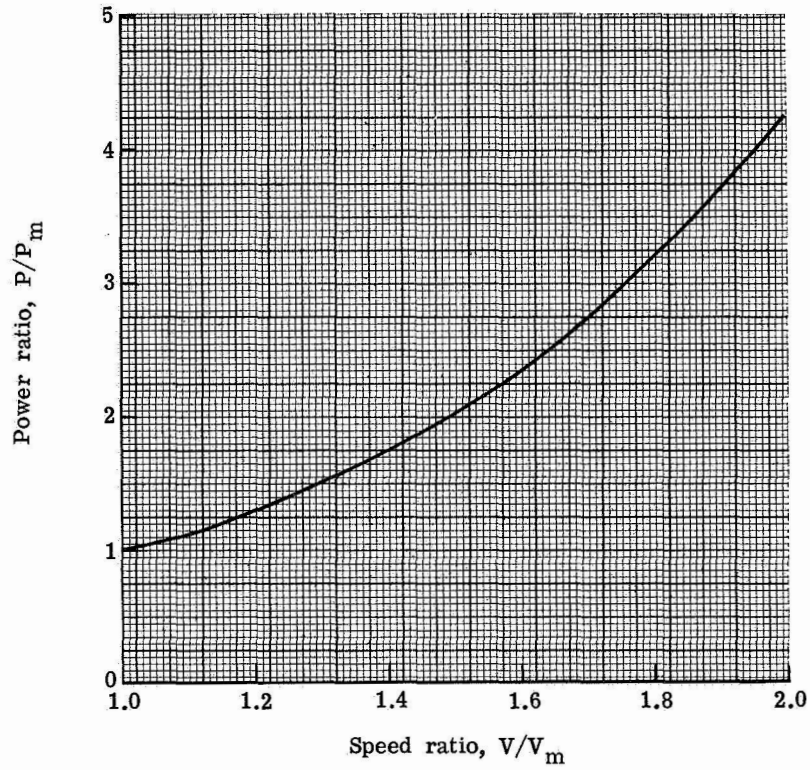


Figure 7.7.- Variation of power ratio with speed ratio.

7.10.1 Unsupercharged Aircraft

The range for aircraft variant 2-6 has been determined as a function of speed at sea level and for altitudes of 8000 ft and 12 000 ft. The power settings for which calculations were made at the different altitudes were as follows:

h	γ
0	1.00
	.75
	.65
	.55
	.45
	.34
8 000	.77
	.75
	.65
	.55
	.45
	.38
12 000	.65
	.55
	.45
	.40

The maximum value of the power setting γ for which the speed and range are determined at each altitude is the maximum value of the power obtainable from the unsupercharged engine at that altitude. The characteristic curve of engine power against altitude given in figure 6.28 of chapter 6 was employed for determining the maximum power. The minimum value of the power setting γ considered at each altitude was that corresponding to flight at the maximum value of the lift-drag ratio. The detailed calculations of speed and range are given in table 7.VII. The calculations are perhaps best understood by identifying each of the columns in table 7.VII as follows:

(1) h, altitude for which speed and range are to be determined.

(2) σ, density ratio, corresponding to the altitude given in (1), obtained from figure 6.6 of chapter 6 or from table 1.I of chapter 1.

(3) V_m, speed determined from equation (7.18) with the use of the values of σ in (2), a value of 26.0 for W_g/S given for aircraft variant 2 in table 7.IV, and a value of 0.60 for $C_{L,m}$ given in section 7.2.

(4) P_m/W_g, the parameter determined from equation (7.22) with use of the density ratio given in (2), a wing loading W_g/S of 26.0, a value of $C_{L,m}$ of 0.60, and a value of drag coefficient $C_{D,0}$ of 0.023 as given in section 7.2.

(5) W_g/P_0, power loading for aircraft variant 2 as given in table 7.IV.

(6) η_c, propulsive efficiency for cruising flight given in section 7.2.

(7) γ, percentage of maximum sea-level power.

⑧ $\frac{P_0 \gamma \eta_c}{W_g}$, the parameter determined as follows:

$$⑧ = \frac{⑥ \times ⑦}{⑤}$$

⑨ $\frac{P_0 \gamma \eta_c}{P_m}$, power ratio determined as follows:

$$⑨ = \frac{⑧}{④}$$

⑩ V/V_m, speed ratio determined from figure 7.7 for value of power ratio given in ⑨.

⑪ V, speed for power setting in ⑦ and altitude in ① determined as follows:

$$⑪ = ⑩ \times ③$$

⑫ R_m, range for cruising at maximum lift-drag ratio given in table 7.V.

⑬ R/R_m, range ratio corresponding to speed ratio given in ⑩, determined from equation (7.17).

⑭ R, range for power setting given in ⑦ and altitude in ① determined as follows:

$$⑭ = ⑬ \times ⑫$$

A map which gives the range as a function of speed for different altitudes and which includes lines of constant power setting can now be constructed from the information given in columns ①, ⑦, ⑪, and ⑭ of table 7.VII.

7.10.2 Supercharged Aircraft

Aircraft variant 2-6S is the same as aircraft variant 2-6 except that the engines are assumed to be equipped with superchargers which provide for the maintenance of maximum sea-level power up to a critical altitude of 18 000 ft. The power is assumed to decrease with altitude above 18 000 ft in the manner shown in figure 6.29 of chapter 6. The power settings for which calculations

of speed and range were made for aircraft variant 2-6S at different altitudes were as follows:

h	γ
8 000	1.00
12 000	1.00
	.75
18 000	1.00
	.75
	.65
	.55
	.46
25 000	.75
	.65
	.55
	.51

The power settings for which calculations were made at 8000 and 12 000 ft are complimentary to those given in table 7.VII for aircraft variant 2-6 but could not be achieved with the unsupercharged engines. The minimum power settings at 18 000 and 25 000 ft correspond to flight at the maximum value of the lift-drag ratio. The procedures employed in making the calculations contained in table 7.VIII are the same as those described for table 7.VII and, consequently, will not be discussed further.

7.10.3 Aircraft Performance Map

The data contained in tables 7.VII and 7.VIII have been used to construct the performance map presented in figure 7.8 for aircraft variants 2-6 and 2-6S. Cruising range is shown on the ordinate and speed is on the abscissa. Lines of constant altitude and power setting are shown, as are the lines of maximum available power for both the unsupercharged and supercharged aircraft. The broken line portions of the constant altitude lines represent speed and range capabilities which are achievable only with the supercharged aircraft.

The cruising speed at 75 percent power and an altitude of 8000 ft is 218 mph as compared to the specified value of 225 mph. The corresponding range is about 55 miles greater than the design value of 1260 miles. These values of the speed and range are correct ones for the given values of W_g/S, W_g/P_0, $C_{D,0}$, $C_{L,m}$, and R_m. The small (3 percent) difference in cruising speed is within the accuracy of the method by which the power loading and the wing loading were estimated. The increase in range is caused by the smaller value of speed ratio V/V_m found for the cruising speed of 218 mph as compared

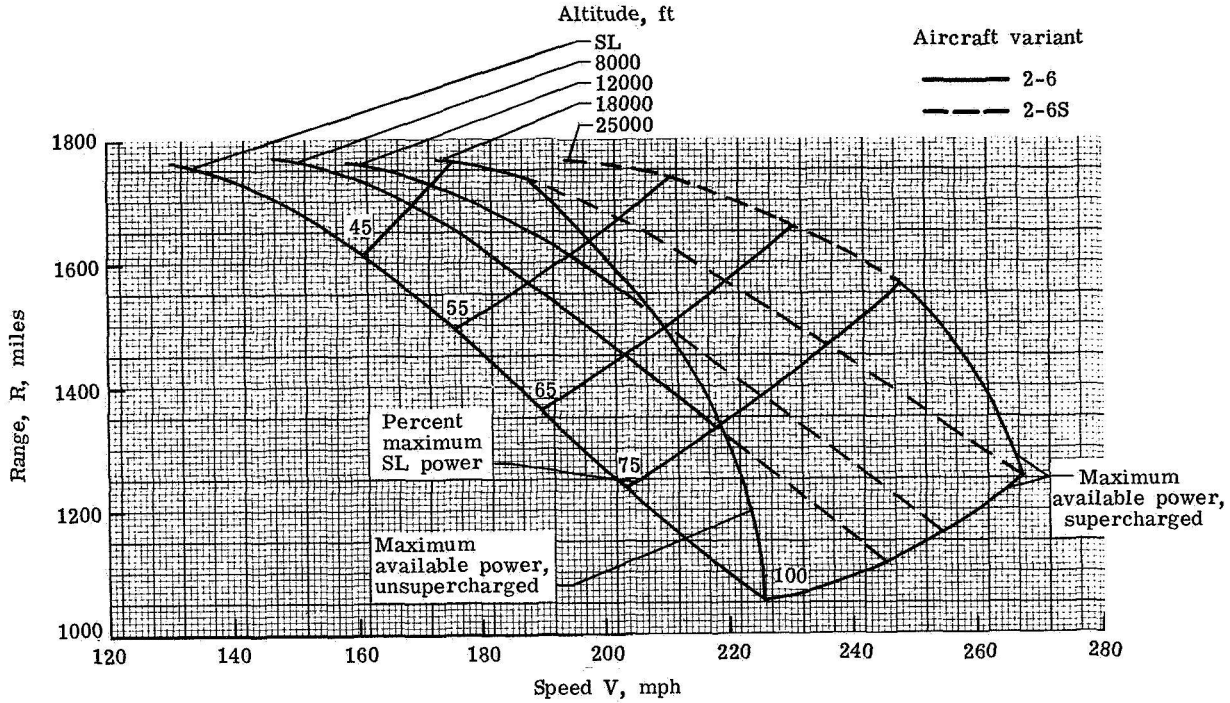


Figure 7.8.- Speed, range, and power relationships of aircraft variants 2-6 and 2-6S.

to 225 mph. A value of V/V_m of 1.54, based on the specified cruising speed of 225 mph, was used in table 7.V for calculating the fuel fraction. The value of V/V_m for a power ratio $P_0\gamma\eta_c/P_m$ corresponding to 75 percent of maximum power was found to be 1.49 in table 7.VII. This value of V/V_m, according to equation (7.17), gives a larger range than does 1.54 for a given range, R_m. The fuel fraction can be recomputed with a speed ratio of 1.49 and a design range of 1260 miles and new weights, sizes, and powers determined. Although the calculations are not included here, a new gross weight and engine power were calculated and found to be 5360 lb and 501 hp, as compared to 5584 lb and 520 hp for a range of 1325 miles. The new value of the range R_m was found to be 1680 miles, as compared to 1760 miles used in table 7.V and 7.VII. The revised value of the fuel fraction was 0.185, as compared to 0.193 given in table 7.V.

The effects of altitude and supercharging on the speed and range at a given power setting are clearly shown in figure 7.8. For example, the speed for 75 percent power increases from 203 to 248 mph as the altitude is increased from sea level to 25 000 ft. The corresponding range increases from 1230 to 1560 miles. The range at the maximum value of the lift-drag ratio does not, of course, vary with speed and is 1760 miles. The speed at $(L/D)_{max}$, however, varies from 130 to 194 mph as the altitude increases from sea level to 25 000 ft. The maximum speed is attained at 18 000 ft with aircraft variant 2-6S and is 267 mph.

The curves in figure 7.8 are a comprehensive representation of the performance capabilities of aircraft variants 2-6 and 2-6S. The amount of computation

required to obtain the data upon which the curves of figure 7.8 are based was relatively small and quickly accomplished. Curves for other altitudes and power settings may be easily calculated.

7.11 Altitude Effects on Rate of Climb

The effect of altitude on the rate of climb has been estimated with the use of equation (7.11) which is written here in a slightly modified form as follows:

$$\dot{h} = 33\ 000 \left[\frac{\gamma \eta_h \dot{P}_0}{W_g} - \frac{\sqrt{W_g/S}}{19\left(C_L^{3/2}/C_D\right)_{max}\sqrt{\sigma}} \right] \tag{7.24}$$

where γ is the percentage of maximum sea-level power available at the different altitudes. The value of γ is found from figure 6.28 for aircraft variant 2-6 and from figure 6.29 for aircraft variant 2-6S. The values of the altitude and power setting for which the rate of climb was calculated are given for the unsupercharged aircraft variant 2-6 as follows:

h	γ
0	1.00
8 000	.77
12 000	.65
18 000	.51

The rates of climb for the supercharged aircraft variant 2-6S were calculated for an altitude of 25 000 ft as well as for the same altitudes as aircraft variant 2-6. The rates of climb were calculated with both engines operating and with one engine inoperative. The aircraft with one engine inoperative are designated in the subsequent tables as aircraft variants 2-6-$\frac{1}{2}$ and 2-6S-$\frac{1}{2}$. The parameter $\left(C_L^{3/2}/C_D\right)_{max}$ in equation (7.24) was assumed to have a value of 11.4 in all of the subsequent calculations. (See section 7.2.)

The detailed calculations of the rate of climb for the various altitudes are contained in table 7.IX for aircraft variant 2-6. The calculations are perhaps best understood by identifying each of the columns in table 7.IX as follows:

① W_g/S, wing loading obtained from table 7.IV.

② W_g/P_0, power loading given in table 7.IV. The power loading is doubled in the calculations for aircraft variant 2-6-$\frac{1}{2}$.

③ h, altitude for which rate of climb is to be determined.

④ γ, percentage of maximum sea-level power available at altitude given in ③.

⑤ $\eta_{\dot{h}}$, propulsive efficiency for climbing flight given in section 7.2.

⑥ $\frac{P_0 \gamma \eta_{\dot{h}}}{W_g}$, power ratio determined as follows:

$$⑥ = \frac{④ \times ⑤}{②}$$

⑦ σ, density ratio, corresponding to altitude given in ③, obtained from figure 6.6 of chapter 6 or from table 1.I of chapter 1.

⑧ $\frac{\sqrt{W_g/S}}{19(C_L^{3/2}/C_D)_{max}\sqrt{\sigma}}$, value of the parameter obtained as follows:

$$⑧ = \frac{\sqrt{①}}{19 \times 11.4 \times \sqrt{⑦}}$$

⑨ $\dot{h}$, rate of climb obtained as follows:

$$⑨ = 33\ 000\left(⑥ - ⑧\right)$$

The calculations for the supercharged aircraft variant 2-6S are contained in table 7.X. The procedure employed in making the calculations given in table 7.X are the same as those described for table 7.IX and, consequently, will not be discussed further.

7.12 Comparative Climb Performance

The single and multiengine rates of climb are shown in figure 7.9 as a function of altitude for both the unsupercharged and supercharged aircraft.

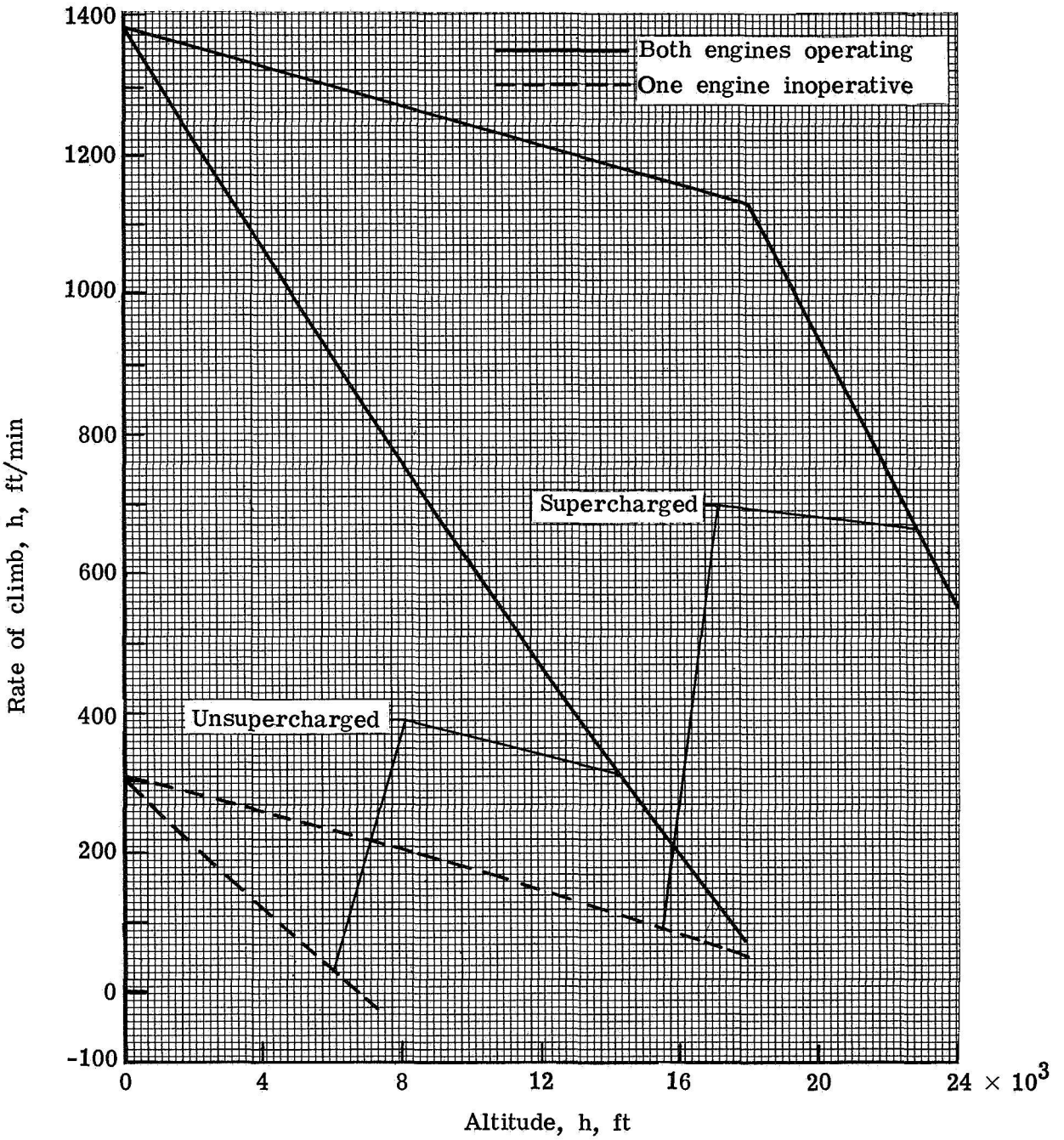


Figure 7.9.- Effect of altitude on rate of climb of aircraft variant 2-6.

The rate of climb of the unsupercharged aircraft variant 2-6 with both engines operating decreases rapidly and reaches a value of about half the sea-level value at 9000 ft. The absolute ceiling at which the rate of climb is zero is about 19 000 ft. The service ceiling, which corresponds to a rate of climb of 100 ft/min, is 17 500 ft. The loss of engine power with altitude is primarily responsible for the decrease in climb rate with altitude. Equation (7.24) shows that the reduction in density ratio σ is also involved. The reduction in σ can be thought of as increasing the effective wing loading $\sqrt{\frac{W/S}{\sigma}}$, which in turn reduces the rate of climb for a given power loading. The single-engine rate of climb for aircraft variant 2-6 reaches 100 ft/min at an altitude of 4500 ft and becomes zero at an altitude of about 7000 ft.

The supercharged aircraft with both engines operating shows only a small reduction in rate of climb up to the critical altitude of 18 000 ft. Further increases in altitude cause a characteristic reduction in rate of climb very similar in slope to that shown by aircraft variant 2-6. The magnitude of the effect of the density ratio in effectively increasing the wing loading is clearly shown by the reduction in rate of climb up to 18 000 ft. The ceiling of aircraft variant 2-6S with both engines operating is well above 25 000 ft. The single-engine rate of climb for this aircraft reaches 100 ft/min at 15 000 ft, and the absolute ceiling is in excess of 18 000 ft.

7.13 Summary

The sizing methods described in chapter 6 for propeller-driven aircraft have been applied in the analysis of a number of light, twin-engine aircraft equipped with retractable landing gear and having an internally braced wing. Eleven different aircraft having various combinations of cruising speed, rate of climb, and airport performance were analyzed. One of these aircraft which appeared to represent an attractive compromise between the various performance requirements was chosen for further study. The specifications and performance of unsupercharged and supercharged versions of this aircraft are given in table 7.XI. The two aircraft are designated by the numbers 2-6 and 2-6S, respectively. The data in table 7.XI indicate that the aircraft have weights, sizes, and power consistent with current, light, twin-engine aircraft having comparable performance.

Langley Research Center
National Aeronautics and Space Administration
Hampton, VA 23665
March 7, 1980

SYMBOLS

A	aspect ratio, b^2/S
B	Breguet factor, $\dfrac{375\eta(L/D)}{c}$
b	wing span, ft
C_D	total drag coefficient
$C_{D,i}$	induced drag coefficient, $C_L^2/\pi A\epsilon$
$C_{D,0}$	drag coefficient at zero lift
C_L	lift coefficient
$C_{L,c}$	lift coefficient for $\left(C_L^{3/2}/C_D\right)_{max}$
$C_{L,m}$	lift coefficient for $(L/D)_{max}$
$C_{L,max}$	maximum lift coefficient
$C_{L,T}$	take-off lift coefficient
c	specific fuel consumption, pounds of fuel per horsepower per hour
h	altitude, ft
$\dot{h}$	rate of climb, ft/min
$\dot{h}_{1/2}$	rate of climb with one engine inoperative, ft/min
I_p	power index, $\sqrt[3]{\left(\dfrac{W/S}{W/P}\right)\dfrac{1}{\sigma}}$
K	slope of curve of V against I_p
L/D	lift-drag ratio
$(L/D)_{max}$	maximum lift-drag ratio
ℓ_L	landing distance over a 50-ft obstacle
ℓ_T	take-off distance over a 50-ft obstacle
P	engine power, shaft hp
P_h	engine power at some altitude h, shaft hp

P_m power required at $(L/D)_{max}$, thrust hp

P_0 maximum engine power at sea level, shaft hp

R range, statute miles

R_m range for $(L/D)_{max}$, statute miles

R_s design range, statute miles

S wing area, ft^2

$\bar{U}$ useful load fraction, $1 - (W_e/W_g)$

V speed, statute mph

V_c cruising speed

V_m speed at $(L/D)_{max}$

V_S stalling speed for aircraft in landing configuration

W weight, lb

W_e empty weight, lb

W_f fuel weight, lb

W_g gross weight, lb

γ percentage of maximum sea-level power

ε Oswald's airplane efficiency factor

η propulsive efficiency

η_c propulsive efficiency in cruising flight

$\eta_h^{\cdot}$ propulsive efficiency in climbing flight

ρ atmospheric density at some altitude other than sea level, $slugs/ft^3$

ρ_0 atmospheric density at sea level

σ density ratio, ρ/ρ_0

TABLE 7.I.- POWER, LOADING, AND WING LOADING RELATIONSHIPS FOR THREE DIFFERENT CRUISING SPEEDS

①	②	③	④	⑤	⑥	⑦	⑧
V_c	γ	σ	K	$(K/V_c)^3$	γ/σ	W_g/S	W_g/P_0
Aircraft variant 1							
200	0.75	0.786	170.0	0.614	0.954	15 20 25 30 35 40	8.79 11.72 14.65 17.58 20.51 23.44
Aircraft variant 2							
225	0.75	0.786	170.0	0.431	0.954	15 20 25 30 35 40	6.17 8.23 10.29 12.35 14.40 16.46
Aircraft variant 3							
250	0.75	0.786	170.0	0.314	0.954	15 20 25 30 35 40	4.50 6.00 7.50 9.00 10.50 12.00

TABLE 7.II.- POWER LOADING AND WING LOADING RELATIONSHIPS FOR TWO TAKE-OFF FIELD LENGTHS

①	②	③	④	⑤	⑥
ℓ_T	$C_{L,T}$	σ	$\frac{(W/S)\,(W/P)}{\sigma}$	W_g/S	W_g/P_0
2000	1.6	1.0	330	15	22.00
				20	16.50
				25	13.20
				30	11.00
				35	9.43
				40	8.25
1600			276	15	18.40
				20	13.80
				25	11.04
				30	9.20
				35	7.89
				40	6.90

TABLE 7.III.- CLIMB PERFORMANCE

①	②	③	④	⑤	⑥	⑦	⑧
$\dot{h}_{1/2}$	W/S	$\left(C_L{}^{3/2}/C_D\right)_{max}$	σ	$\frac{\sqrt{W/S}}{19\left(C_L{}^{3/2}/C_D\right)_{max}\sqrt{\sigma}}$	$\frac{\dot{h}_{1/2}}{33\ 000}$	$\eta_{\dot{h}}$	W_g/P_0
300	15	11.4	1.0	0.0179	0.0091	0.7	12.98
	20			.0206			11.77
	25			.0231			10.88
	30			.0253			10.18
	35			.0273			9.61
	40			.0292			9.14
400	15			0.0179	0.0121		11.67
	20			.0206			10.68
	25			.0231			9.94
	30			.0253			9.36
	35			.0273			8.86
	40			.0292			8.47
500	15			0.0179	0.0152		10.60
	20			.0206			9.78
	25			.0231			9.15
	30			.0253			8.66
	35			.0273			8.24
	40			.0292			7.89

TABLE 7.IV.- COMPARATIVE AIRCRAFT PERFORMANCE

①	②	③	④	⑤	⑥	⑦	⑧	⑨
V_C	Match point (a)	W_g/S	W_g/P_0	$h_{1/2}$	ℓ_T	V_S	ℓ_L	$\dot{h}$
Aircraft variant 1								
200	1	23.5	13.8	98	2000	64.5	1623	935
	2	21.7	12.7	200	1600	62.0	1500	1109
	3	20.1	11.8	296	1320	59.6	1385	1275
	4	18.9	11.0	388	1139	57.8	1303	1438
	5	17.3	10.2	500	963	55.3	1193	1631
Aircraft variant 2								
• 225	6	26.0	10.7	303	1617	67.8	1793	1382
	7	24.4	10.0	400	1370	65.7	1683	1557
	8	22.9	9.4	500	1172	63.7	1583	1728
Aircraft variant 3								
250	9	32.1	9.8	300	1870	75.4	2242	1494
	10	30.6	9.3	400	1650	73.6	2113	1641
	11	28.7	8.8	500	1419	71.3	1983	1809

[a]See figure 7.1.

TABLE 7.V.- FUEL FRACTION CORRESPONDING TO 11 MATCH POINTS

[R_S = 1260 miles]

①	②	③	④	⑤	⑥	⑦	⑧	⑨	⑩	⑪	⑫	⑬	⑭
Match point (a)	W_g/S	σ (b)	$C_{L,m}$	V_m	V_c	V_c/V_m	R_S/R_m	R_m	$(L/D)_{max}$	c	η_c	B	W_f/W_g
Aircraft variant 1													
1	23.5	0.786	0.60	139.3	200	1.44	0.783	1610.2	12.9	0.50	0.85	8223.8	0.178
2	21.7			133.8		1.49	.749	1682.4					.185
3	20.1			128.8		1.55	.710	1775.8					.194
4	18.9			124.9		1.60	.678	1858.9					.202
5	17.3			119.5		1.67	.635	1982.9					.214
Aircraft variant 2													
6	26.0	0.786	0.60	146.5	225	1.54	0.716	1759.7	12.9	0.50	0.85	8223.8	0.193
7	24.6			142.5		1.58	.690	1825.1					.199
8	22.9			137.5		1.64	.653	1928.7					.209
Aircraft variant 3													
9	32.1	0.786	0.60	162.8	250	1.54	0.716	1759.7	12.9	0.50	0.85	8223.8	0.193
10	30.6			158.9		1.57	.697	1808.5					.197
11	28.7			153.9		1.62	.665	1893.4					.206

[a]See figure 7.1.
[b]For altitude of 8000 ft.

TABLE 7.VI.- AIRCRAFT CHARACTERISTICS CORRESPONDING TO 11 MATCH POINTS

①	②	③	④	⑤	⑥	⑦	⑧	⑨	⑩	⑪
Match point (a)	W_g/S	W_g/P_0	W_f/W_g	W_p	$\bar{U}$	W_g	W_e	W_f	S	P_0
Aircraft variant 1										
1	23.5	13.8	0.178	1100	0.475	3704	1944	659	158	268
2	21.7	12.7	.185		.444	4247	2361	786	196	334
3	20.1	11.8	.194		.420	4867	2823	944	242	413
4	18.9	11.0	.202		.397	5671	3401	1139	299	513
5	17.3	10.2	.214		.375	6832	4270	1462	395	670
Aircraft variant 2										
6	26.0	10.7	0.193	1100	0.390	5584	3406	1078	215	522
7	24.4	10.0	.199		.370	6433	4053	1280	264	643
8	22.9	9.4	.209		.350	7801	5071	1631	341	830
Aircraft variant 3										
9	32.1	9.8	0.193	1100	0.365	6395	4061	1234	199	653
10	30.6	9.3	.197		.350	7190	4673	1416	235	773
11	28.7	8.8	.206		.335	8527	5671	1757	297	969

[a]See figure 7.1.

TABLE 7.VII.- SPEED, RANGE, AND POWER RELATIONSHIPS FOR UNSUPERCHARGED AIRCRAFT VARIANT 2-6[a]

①	②	③	④	⑤	⑥	⑦	⑧	⑨	⑩	⑪	⑫	⑬	⑭
h	σ	V_m	P_m/W_g	W_g/P_0	η_c	γ	$\frac{P_0\gamma\eta_c}{W_g}$	$\frac{P_0\gamma\eta_c}{P_m}$	V/V_m	V	R_m	R/R_m	R
0	1	129.9	0.027	10.7	0.85	1.00	0.079	2.93	1.74	226	1760	0.60	1048
						.75	.060	2.21	1.56	203		.70	1237
						.65	.051	1.89	1.46	190		.78	1354
						.55	.044	1.63	1.35	175		.84	1484
						.45	.036	1.33	1.24	161		.91	1609
						.34	.027	1.00	1.00	130		1.00	1760
8 000	0.786	146.5	0.030	10.7	0.85	0.77	0.061	2.03	1.50	220	1760	0.74	1306
						.75	.060	2.00	1.49	218		.75	1320
						.65	.051	1.70	1.38	202		.82	1445
						.55	.044	1.45	1.28	187		.89	1565
						.45	.036	1.19	1.14	167		.97	1701
						.38	.030	1.00	1.00	147		1.00	1760
12 000	0.693	156.0	0.032	10.7	0.85	0.65	0.051	1.60	1.34	209	1760	0.85	1496
						.55	.044	1.38	1.24	193		.91	1609
						.45	.036	1.13	1.11	173		.98	1722
						.40	.031	1.00	1.00	156		1.00	1760

[a]See section 7.9 for designation.

TABLE 7.VIII.- SPEED, RANGE, AND POWER RELATIONSHIPS FOR SUPERCHARGED AIRCRAFT VARIANT 2-6S[a]

①	②	③	④	⑤	⑥	⑦	⑧	⑨	⑩	⑪	⑫	⑬	⑭
h	σ	V_m	P_m/W_g	W_g/P_0	η_c	γ	$\frac{P_0\gamma\eta_c}{W_g}$	$\frac{P_0\gamma\eta_c}{P_m}$	V/V_m	V	R_m	R/R_m	R
12 000	0.693	156.0	0.032	10.7	0.85	1.00	0.079	2.47	1.63	254	1760	0.66	1161
						.75	.059	1.85	1.44	225		.78	1377
						.65	.051	1.60	1.34	209		.85	1496
						.55	.044	1.38	1.24	193		.91	1609
						.45	.036	1.13	1.09	170		.99	1734
						.41	.032	1.00	1.00	156		1.00	1760
18 000	0.570	172.1	0.036	10.7	0.85	1.00	0.079	2.19	1.55	267	1760	0.71	1249
						.75	.059	1.64	1.36	234		.84	1473
						.65	.051	1.42	1.26	217		.90	1587
						.55	.044	1.22	1.16	200		.96	1685
						.46	.036	1.00	1.00	172		1.00	1760
25 000	0.448	194.1	0.0403	10.7	0.85	0.75	0.059	1.46	1.28	248	1760	0.89	1565
						.65	.051	1.27	1.19	231		.94	1657
						.55	.044	1.10	1.09	212		.99	1734
						.51	.040	1.00	1.00	194		1.00	1760

[a]See section 7.9 for designation.

TABLE 7.IX.- ALTITUDE EFFECT ON RATE OF CLIMB FOR UNSUPERCHARGED AIRCRAFT VARIANT 2-6

①	②	③	④	⑤	⑥	⑦	⑧	⑨
W_g/S	W_g/P_0	h	γ	$\eta_{\dot{h}}$	$\frac{P_0 \gamma \eta_{\dot{h}}}{W_g}$	σ	$\frac{\sqrt{W_g/S}}{19\left(C_L{}^{3/2}/C_D\right)_{max}\sqrt{\sigma}}$	$\dot{h}$
Aircraft variant 2-6								
26	10.7	0	1.00	0.70	0.0654	1.000	0.0235	1382
		8 000	.77		.0504	.786	.0266	786
		12 000	.65		.0425	.693	.0283	470
		18 000	.51		.0334	.570	.0312	72
Aircraft variant 2-6--$\frac{1}{2}$[a]								
26	21.4	0	0.50	0.70	0.0327	1.000	0.0235	303
		4 000	.44		.0288	.888	.0249	126
		8 000	.39		.0255	.786	.0266	-34

[a]One engine inoperative.

TABLE 7.X.- ALTITUDE EFFECT ON RATE OF CLIMB FOR SUPERCHARGED

AIRCRAFT VARIANT 2-6S

①	②	③	④	⑤	⑥	⑦	⑧	⑨
W_g/S	W_g/P_0	h	γ	$\eta_{\dot{h}}$	$\frac{P_0 \gamma \eta_{\dot{h}}}{W_g}$	σ	$\frac{\sqrt{W_g/S}}{19(C_L^{3/2}/C_D)_{max}\sqrt{\sigma}}$	$\dot{h}$
Aircraft variant 2-6S								
26	10.7	0	1.00	0.70	0.0654	1.000	0.0235	1382
		8 000	1.00		.0654	.786	.0266	1283
		12 000	1.00		.0654	.693	.0283	1226
		18 000	1.00		.0654	.570	.0312	1130
		25 000	.75		.0491	.448	.0352	459
Aircraft variant 2-6S--$\frac{1}{2}$[a]								
26	10.7	0	0.50	0.70	0.0327	1.000	0.0235	303
		8 000	.50		.0327	.786	.0266	203
		12 000	.50		.0327	.693	.0283	146
		18 000	.50		.0327	.570	.0312	51

[a]One engine inoperative.

TABLE 7.XI.- CHARACTERISTICS OF AIRCRAFT VARIANT 2-6

Physical characteristics:	
Wing area, ft^2	215
Wing span, ft	39
Wing aspect ratio	7.0
Wing loading, lb/ft^2	26
Power loading, lb/hp	10.7
Gross weight, lb	5584
Empty weight, lb	3406
Fuel weight (180 gal), lb	1078
Payload, lb	1100
Useful load, lb	2178
Power (each of two engines), hp	260
Performance characteristics:	
Maximum speed:	
Aircraft variant 2-6, mph	226 (h = 0)
Aircraft variant 2-6S, mph	267 (h = 18 000)
Cruising speed at 75 percent power:	
Aircraft variant 2-6, mph	218 (h = 8000)
Aircraft variant 2-6S, mph	248 (h = 25 000)
Range at 75 percent power:	
Aircraft variant 2-6, mi	1320 (h = 8000)
Aircraft variant 2-6S, mi	1565 (h = 25 000)
Maximum rate of climb at sea level -	
With both engines operative, ft/min	1382
With one engine inoperative, ft/min	300
Service ceiling with both engines operative, ft	17 500
Service ceiling with one engine inoperative, ft	4500
Stall speed, mph	68
Take-off distance over 50 ft, ft	1617
Landing distance over 50 ft, ft	1793

APPENDIX A

ESTIMATION OF OVERALL PROPULSION-SYSTEM EFFICIENCY

The overall propulsion-system efficiency, discussed in chapter 2, is the ratio of the power usefully expended in propelling the aircraft to the heating value of the fuel consumed per unit time. The overall propulsion-system efficiency η is the product of the cycle efficiency η_c and the propulsive efficiency η_p. A simple method for estimating the overall propulsion-system efficiency is developed in the following paragraphs for aircraft powered with either jet, turboprop, or reciprocating engines. The symbols used in appendix A are defined as follows:

c_p	specific fuel consumption, pounds of fuel per brake horsepower per hour
c_T	specific fuel consumption, pounds of fuel per pound of thrust per hour
H	heating value of fuel, Btu/lb
h	fuel-flow rate, lb/hr
J	Joule's constant, 778 ft-lb/Btu
M	Mach number
P	power usefully expended in propelling the aircraft, ft-lb/sec
P_e	power developed by engine, hp
Q	heat added by fuel, Btu/sec
T	thrust, lb
V	velocity, ft/sec

The jet propulsion system will be considered first. In such a system the heat added per unit time is given by the following expression:

$$Q = \frac{HhJ}{3600} \tag{A1}$$

and the power usefully expended in propelling the aircraft is

$$P = TV \tag{A2}$$

The overall propulsion-system efficiency is then given by

$$\eta = \frac{3600TV}{HhJ} \tag{A3}$$

If the heating value of the fuel is taken as 18 500 Btu/lb, the overall propulsion-system efficiency is given by the following simple expression:

$$\eta = \frac{0.00025V}{c_T} \tag{A4}$$

since

$$c_T = \frac{h}{T} \tag{A5}$$

Expressed as a percentage, equation (A4) becomes

$$\eta = \frac{0.025V}{c_T} \tag{A6}$$

Equation (A6) may also be expressed in terms of the Mach number as

$$\eta = \frac{24.3M}{c_T} \tag{A7}$$

where the speed of sound has been taken as 971 ft/sec (this value being for altitudes above the tropopause).

An expression for the overall propulsion-system efficiency of propeller-driven aircraft, powered with either reciprocating or turboprop engines, will now be developed. The capability of these types of engines is usually expressed in terms of the power which they develop rather than their thrust. Consequently, the expression for the overall propulsion-system efficiency is developed in a slightly different way than that used for jet-propelled aircraft. The amount of power developed by the engine will first be related to the engine cycle efficiency η_c. The amount of heat added to the engine per unit time, given by equation (A1), is also applicable to propeller-driven aircraft and is used in forming the following relationship:

$$550P_e = \frac{\eta_c HhJ}{3600} \tag{A8}$$

where the constant 550 converts the power P_e from horsepower to foot pounds per second. If the specific fuel consumption c_p is defined as the amount of fuel used per brake horsepower per hour, the cycle efficiency may then be expressed as follows:

$$\eta_c = \frac{550(3600)}{18\ 500(778)c_p} \tag{A9}$$

or

$$\eta_c = \frac{0.14}{c_p} \tag{A10}$$

Expressed as a percentage, equation (A10) for the cycle efficiency becomes

$$\eta_c = \frac{14}{c_p} \tag{A11}$$

If the propulsive efficiency η_p is taken as 86 percent, a reasonable average value, the overall propulsion-system efficiency becomes

$$\eta = \frac{12}{c_p} \tag{A12}$$

Equations (A7) and (A12) were used in the construction of figure 2.2 in chapter 2.

APPENDIX B

ESTIMATED AERODYNAMIC PARAMETERS

Appendix B presents the methods employed for estimating the aerodynamic parameters given in tables 5.I of chapter 5. The parameters were estimated from published performance data for the various aircraft. In most cases, the performance data in the tables formed the basis for the calculations. The methods are briefly described in the following paragraphs.

The zero-lift drag coefficient was determined from the equation

$$C_{D,0} = C_D - C_{D,i} \tag{B1}$$

where

$C_{D,0}$ zero-lift drag coefficient

C_D total drag coefficient for given combination of power, speed, and altitude

$C_{D,i}$ induced drag coefficient corresponding to same flight conditions as total drag coefficient

The total drag coefficient can be estimated from the following relationship:

$$C_D = \frac{550\eta P}{\frac{1}{2}\rho_0\left[\sigma S(1.47V)^3\right]} \tag{B2}$$

where

η propulsive efficiency

P engine power, hp

ρ_0 sea-level density, slugs/ft^3

σ atmospheric density ratio for some altitude other than sea level

S wing area, ft^2

V speed, statute mph

Equation (B2) can be put in the form

$$C_D = 1.456 \times 10^5 \left(\frac{\eta P}{\sigma S V^3} \right) \tag{B3}$$

by substituting a value of 0.002378 for the standard atmospheric density at sea level. Equation (B3) was used for estimating the value of the drag coefficient C_D. The values of propulsive efficiency η employed in equation (B3) varied between 0.77 and 0.85, depending on the aircraft, and were chosen on the basis of information contained in references B.1 and B.2.

The induced drag coefficient $C_{D,i}$ was obtained from

$$C_{D,i} = \frac{C_L{}^2}{\pi A \varepsilon}$$

and

$$C_L = \frac{W}{\frac{1}{2} \rho_0 \left[\sigma S (1.47V)^2 \right]}$$

which can be combined to give

$$C_{D,i} = \frac{4.822 \times 10^4}{A \varepsilon \sigma^2 V^4} (W/S)^2 \tag{B4}$$

where

W	weight, lb
W/S	wing loading, lb/ft^2
ε	airplane efficiency factor
A	aspect ratio, K^2b^2/S
b	wing span (upper wing span for biplanes), ft

S wing area (includes upper and lower wing area for biplanes), ft^2

K Munk's span factor (for biplanes)

Munk's span factor is a function of the geometry of the biplane wing arrangement and can be either less or greater than 1.0. On the basis of information given in references B.3 and B.4, an average value of the span factor of 1.1 was used for all of the biplane configurations. An average value of the airplane efficiency factor of 0.75 was used for all the aircraft.

The value of the maximum lift-drag ratio $(L/D)_{max}$ was computed by equation (3.20) of chapter 3 which is repeated here for convenience as

$$(L/D)_{max} = \frac{1}{2}\sqrt{\frac{\pi A \epsilon}{C_{D,0}}} \tag{B5}$$

The skin friction parameter $\bar{C}_F$ is a drag coefficient based on the total wetted area rather than the wing area. The value of $\bar{C}_F$ can be determined from the zero-lift drag coefficient $C_{D,0}$ by the following relationship:

$$\bar{C}_F A_t = C_{D,0} S$$

or

$$\bar{C}_F = C_{D,0}\left(\frac{S}{A_t}\right) \tag{B6}$$

where

S wing area, ft^2

A_t total wetted area, ft^2

The values of the ratio of wing area to wetted area for the different aircraft were estimated by means of simple geometric representations of the configurations in a manner somewhat similar to that given by equation (3.25) of chapter 3 for jet transport aircraft. The values of S/A_t could not be obtained very accurately in most instances because of the small scale and limited accuracy of the available drawings. For the same reason, nacelle areas were not included in the total wetted area of multiengine aircraft.

In addition to the assumptions described in the preceding paragraphs, the accuracy of the calculated aerodynamic parameters depends on two other important assumptions. First, the accuracy of the calculated results obviously depends

upon the accuracy of the published information on the various aircraft, and, second, the accuracy depends on the completeness of the performance information. For example, can the power be determined for a given combination of speed and altitude. No general assessment of either of these possible sources of error can be made. Aerodynamic parameters for those cases in which the performance data were incomplete, or could not be estimated with reasonable confidence, were not included in tables 5.I of chapter 5; and if comparative performance data for different aircraft showed unexplained anomalies, aerodynamic data were not presented for the aircraft whose published performance characteristics seemed questionable.

REFERENCES

B.1 Nelson, Wilbur C.: Airplane Propeller Principles. John Wiley & Sons, Inc., 1944.

B.2 Weick, Fred E.: Aircraft Propeller Design. McGraw-Hill Book Co., Inc., 1930.

B.3 Diehl, Walter Stuart: Engineering Aerodynamics. Rev. ed. Ronald Press Co., c.1936.

B.4 Reid, Elliott G.: Applied Wing Theory. First ed. McGraw-Hill Book Co., Inc., 1932.

1. Report No.	2. Government Accession No.	3. Recipient's Catalog No.
NASA RP-1060		

4. Title and Subtitle	5. Report Date
SUBSONIC AIRCRAFT: EVOLUTION AND THE MATCHING OF SIZE TO PERFORMANCE	August 1980
	6. Performing Organization Code
7. Author(s)	8. Performing Organization Report No.
Laurence K. Loftin, Jr.	L-13367
	10. Work Unit No.
9. Performing Organization Name and Address	023-10-01-02
NASA Langley Research Center Hampton, VA 23665	11. Contract or Grant No.
	13. Type of Report and Period Covered
12. Sponsoring Agency Name and Address	Reference Paper
National Aeronautics and Space Administration Washington, DC 20546	14. Sponsoring Agency Code

15. Supplementary Notes

Laurence K. Loftin, Jr.: Distinguished Research Associate
NASA Langley Research Center

16. Abstract

Methods for estimating the approximate size, weight, and power of aircraft intended to meet specified performance requirements are presented for both jet-powered and propeller-driven aircraft. The methods are simple and require only the use of a pocket computer for rapid application to specific sizing problems. Application of the methods is illustrated by means of sizing studies of a series of jet-powered and propeller-driven aircraft with varying design constraints. Some aspects of the technical evolution of the airplane from 1918 to the present are also briefly discussed.

17. Key Words (Suggested by Author(s))	18. Distribution Statement
Subsonic aircraft Aircraft performance Aircraft design Aircraft size Evolution of aircraft	Unclassified - Unlimited Subject Category 01

19. Security Classif. (of this report)	20. Security Classif. (of this page)	21. No. of Pages	22. Price*
Unclassified	Unclassified	443	A19

For sale by the National Technical Information Service, Springfield, Virginia 22161 NASA-Langley, 1980

National Aeronautics and Space Administration

Washington, D.C.
20546

Official Business
Penalty for Private Use, $300

SPECIAL FOURTH CLASS MAIL
BOOK

Postage and Fees Paid
National Aeronautics and
Space Administration
NASA-451



NASA

POSTMASTER: If Undeliverable (Section
Postal Manual) Do Not Re